GEOTECHNICAL ASPECTS OF
THE BANGKOK MRT BLUE LINE PROJECT

Chanaton Surarak
B. Sc, M. Eng

Griffith School of Engineering
Science, Environment, Engineering and Technology
Griffith University

Submitted in fulfilment of the requirements of the degree of
Doctor of Philosophy

September 2010

ABSTRACT

This dissertation is on the geotechnical aspects of the completed Bangkok MRT Blue Line Project and its extension which is currently under design. There were 18 cut and cover subway stations and nearly 22 km of tunnels constructed by the use of earth pressure balanced shield tunnel boring machines. The soil profile model up to depths of 60 to 65 m consists of seven layers: Weathered Crust and Backfill Material; Very Soft to Soft Bangkok Clay; Medium Stiff Clay; Stiff to Hard Clay; Medium Dense to Very Dense Sand; Very Stiff to Hard Clay; and Very Dense Sand.

The strength and deformation characteristics of the Bangkok subsoils are determined from laboratory tests (mainly oedometer and triaxial tests) and in-situ field tests (such as vane tests and pressuremeter tests). Additionally, the small strain behaviour is also investigated using Bender element tests in the laboratory and cross hole seismic tests in the field. The soil parameters needed for the deformation analyses are determined for the Mohr Coulomb Model, Soft Soil Model, Hardening Soil Model, and the Hardening Soil Model with Small Strain Stiffness.

Based on the review of the quality of field measurements (wall deflections and ground surface settlements), in 18 subway stations, the Sukhumvit Station is selected as the best one to perform a detail 2D finite element analysis using Plaxis. The ratio of the maximum ground surface settlement to the maximum horizontal wall movement is 0.75 as measured from four deep excavations. This ratio lies within the range as reported in the literature. Three empirical methods (i.e. Clough and O'Rourke, 1990; Hsieh and Ou, 1998; Ou and Hsieh, 2000) are adopted for surface settlement computations. It was found that all three methods provide similar magnitude of maximum surface settlement, which agrees well with the measured data. However, only the methods of Hsieh and Ou (1998) and Ou and Hsieh (2000) predicted well, the surface settlements in the Primary and Secondary Influence Zones. The lateral wall movements and the surface settlements predicted are very sensitive to the type of constitutive soil models used in the 2D Plaxis analysis: i.e. Mohr Coulomb Model, Soft Soil Model, Hardening Soil Model and Hardening Soil Model with Small Strain Stiffness. Realistic values

are obtained when the constlutive models are sophisticated and the accuracy is increased with the Soft Soil Model than with the Mohr Coulomb Model; also with the Hardening Soil Model with Small Strain Stiffness than with Soft Soil Model. The axial force, shear force and bending moment distributions from the Plaxis analyses are not sensitive to the type of soil model used in the analyses.

Back-calculated E_u/s_u ratios from the literature can be used for the prediction of the lateral movement of the retaining walls with Mohr Coulomb Model. However, accurate ground surface settlements cannot be obtained. For Soft Soil Model and Hardening Soil Model analyses, the soil parameters interpreted from laboratory and in-situ tests are sufficient to obtain good prediction of lateral wall movements and surface settlements. Results from the Hardening Soil Model with Small Strain analysis confirmed the values of $\gamma_{0.7}$ in Soft clay as predicted by Ishibashi and Zhang (1993) and Vucetic and Dobry (1991) methods. However, a higher value of $\gamma_{0.7}$ of 0.002% is necessary for better lateral wall movement and surface settlement predictions in stiff clay layer.

With the aim to find the best analytical method to predict the ground surface settlement induced by shield tunnelling, three analytical methods (i.e. Verruijt and Booker, 1996; Loganathan and Poulos, 1998; Bobet 2001) are examined in this study. Eight twin tunnels cross sections, which consist of both side-by-side and stack configurations, are selected. These sections cover various conditions of subsoils in which the shields were located during the tunnelling works. It is found that Loganathan and Poulos (1998) Method gave the best prediction of ground surface settlements induced by shield tunnelling compared to the other two analytical methods.

A total of 21 (7 locations with three methods of analysis in each case) twin side-by-side shield tunnelling cases are analysed with 2D finite element method. Three 2D approaches for shield tunnel modelling, namely the contraction method, the stress reduction method and the modified grout pressure method are used. All analyses are conducted using Hardening Soil Model. The back-calculated percentage of contraction and percentage of volume loss from Gaussian curve and super position techniques are comparable. The back-calculated face pressures from the modified grout pressure method are higher than the measured values. Inter-relationships among the contraction ratio, which is comparable to the volume loss ratio in the undrained condition, the unloading factor and the normalised face pressure are established.

These relationships can be used to approximate the values of unloading factor or face pressure with a given percentage of contraction or volume loss and vice versa.

STATEMENT OF ORIGINALITY

This work has not previously been submitted for a degree or diploma in any university. To the best of my knowledge and belief, the thesis contains no material previously published or written by another person except where due reference is made in the thesis itself.

_____

Capt. Chanaton Surarak

September 2010

TABLE OF CONTENTS

LIST OF FIGURES

LIST OF TABLES

NOTATIONS

Roman

a	Offset parameter (m)
a_v	Coefficient of compressibility (dimensionless)
c'	Cohesion (kN/m^2)
C	Depth to the tunnel crown (m)
C_c	Compression index (dimensionless)
d	Diameter of lining (m)
d	Distance from wall (m)
D	Tunnel diameter (m)
e	Void ratio (dimensionless)
E	Young's modulus (kN/m^2, MN/m^2)
E_{50}, E_{50}^{ref}	Secant elastic modulus at 50% peak strength and 50 % secant modulus at reference pressure, p^{ref} (kN/m^2, MN/m^2)
E_{oed}, E_{oed}^{ref}	Oedometer modulus and oedometer modulus at reference pressure, p^{ref} (kN/m^2, MN/m^2)
E_p	Modulus from lateral load test (kN/m^2, MN/m^2)
E_{ur}, E_{ur}^{ref}	Unloading/reloading modulus and unloading/reloading modulus at reference pressure, p^{ref} (kN/m^2, MN/m^2)
$E_{ur,oed}$, $E_{ur,oed}^{ref}$	Unloading/reloading oedometer modulus, unloading/reloading oedometer mosulus at reference pressure, p^{ref} (kN/m^2, MN/m^2)
g	Gap parameter (mm)
G	Shear modulus (kN/m^2, MN/m^2)
G_{eq}	Equivalent shear modulus (kN/m^2, MN/m^2)
G_{max}, G_{max}^{ref}	Small strain shear modulus and small strain shear modulus at reference pressure, p^{ref} (kN/m^2, MN/m^2)
G_P	Physical gap (mm)
G_s	Specific gravity (dimensionless)

H	Depth to the source (m)
H_e	Excavation depth (m)
H_g	Depth to hard stratum (m)
H_p	Embedded depth of wall (m)
i	Trough width parameter (m)
I	Moment of inertia (mm^4)
I_l	Liquidity index (dimensionless)
I_p	Plasticity index (dimensionless)
I_r	Rigidity index (dimensionless)
k	Modulus number (dimensionless)
K	Bulk modulus (kN/m^2, MN/m^2)
K	Empirical dimensionless constant (O'Rilly and New, 1982)
K_0	Coefficient of earth pressure at rest (dimensionless)
K_o^{nc}	Coefficient of earth pressure at rest for normally consolidated soil (dimensionless)
l	Length of mesh generation (m)
L_{exc}	Round length or excavation (delayed) length (m)
m	Power for stress level dependency stiffness (dimensionless)
M	Slope of critical state line (dimensionless)
N	Stability ratio (dimensionless)
N_p	Pressuremeter constant (dimensionless)
p'	Mean effective stress (kN/m^2)
p^{ref}	Reference pressure (kN/m^2)
p_0	Total stress removed at the tunnel face (kN/m^2)
p_e	Effective pressure in pressuremeter test (kN/m^2)
p_F	Shield face pressure (kN/m^2)
p_i	Tunnel support pressure (kN/m^2)
p_L	Limit pressure in pressuremeter test (kN/m^2)
p_L^*	Net limit pressure in pressuremeter test (kN/m^2)
p_p	Pre-consolidation pressure (kN/m^2)
p_v'	Vertical effective stress at tunnel springline (kN/m^2)

p_w	In-situ pore pressure at tunnel springline prior to tunnel construction (kN/m^2)
p_y	Yield pressure in pressuremeter test (kN/m^2)
q	Deviatoric stress (kN/m^2)
r_0	Inner tunnel radius (m)
R	Tunnel radius (m)
R_f	Failure ratio (dimensionless)
s_u	Undrained shear strength of soil (kN/m^2)
u	Water pressure (kN/m^2)
$ú$	Tunnel ovalisation (mm)
u^*_{3D}	Equivalent 3D elasto-plastic deformation at tunnel face (mm)
u_0	Uniform radius ground loss (mm)
u_r	Displacement in coordinate (r, θ) (mm)
u_x	Horizontal movement in transverse direction (mm)
u_y	Vertical movement in transverse direction (mm)
u_z	Downward vertical movement (mm)
u_θ	Displacement in coordinate (r, θ) (degree)
V	Cavity volume (mm^3)
V_s	Shear wave velocity (m/s)
V_L	Volume loss (%)
V_S	Volume of settlement trough per unit length
w	Gap between shield tail and lining (mm)
w	Width of mesh generation (m)
w, w_n	Water content (%)
w_l	Liquid limit (%)
w_p	Plastic limit (%)
x	Horizontal distance from tunnel centreline (m)
Z, Z_0	Depth to the tunnel axis (m)

Greek

β	Geometry correction factor (dimensionless)
β	Unloading factor (dimensionless)
δ	Long term ground deformation due to ovalisation (mm)
δ	Clearance required for lining erection (mm)
δ_f	Surface settlement due to face loss (mm)
δ_{hm}	Maximum lateral wall deflection (mm)
δ_s	Surface settlement due to shield loss (mm)
δ_t	Surface settlement due to tail loss (mm)
δ_v	Surface settlement at transverse distance x from tunnel centerline (mm)
δ_{vm}	Maximum ground surface settlement behind wall (mm)
δ_x	Maximum axial intrusion at tunnel face (mm)
Δ	Thickness of tail piece (mm)
ε	Uniform radius ground loss (mm)
ε_0	Equivalent ground loss (mm) (Loganathan and Poulos, 1998)
ε_a	Axial strain (dimensionless)
ε_c	Cavity strain (dimensionless)
ε_s	Shear strain (dimensionless)
ε_v^{pc}	Volumetric cap strain (dimensionless)
ϕ	Angle of internal friction (degree)
γ	Unit weight of soil (kN/m^2)
γ , γ_a	Shear strain amplitude (dimensionless)
$\gamma_{0.7}$	Shear strain amplitude at 0.7 G_{max} (dimensionless)
γ_c	Cyclic shear strain (dimensionless)
γ_{rf}	Reference threshold shear strain at failure (dimensionless)
γ_{tl}	Linear threshold shear strain (dimensionless)
γ_{tv}	Volumetric threshold shear strain (dimensionless)
κ^*	Modified swelling index (dimensionless)
λ^*	Modified compression index (dimensionless)

ν	Poisson's ratio (dimensionless)
ρ	Soil density (Mg/m^3)
ρ	Cavity radius (mm)
σ'_1, σ'_3	Major, minor effective principal stress (kN/m^2)
σ_h, σ'_h	Total, effective horizontal stress (kN/m^2)
σ_v, σ'_v	Total, effective vertical stress (kN/m^2)
τ	Shear stress (kN/m^2)
τ_f	Shear stress at failure (kN/m^2)
ω	Workmanship parameter (mm)
Ω	Displacement factor (dimensionless)
ψ	Dilatancy angle (degree)

ACKNOWLEDGEMENTS

CHAPTER 1

Introduction

1.1 Background

This dissertation is on the Geotechnical aspects of the completed Bangkok Mass Rapid Transit (MRT) Blue Line project and its extension currently under design. The Bangkok MRT Blue Line project was the first underground MRT in Bangkok. Indeed, it is the first phase of an integrated transportation plan for Bangkok; it will be implemented in conjunction with other schemes being undertaken by the Mass Rapid Transit Authority of Thailand (MRTA). The project was constructed along highly congested roads in the heart of Bangkok city. The tunnel, which is 22 km in length, included 18 underground cut and cover subway stations, and was divided into two major alignments; the North and South. The tunnels were constructed using eight Earth Pressure Balance shields. The major North and South alignments have been divided into 4 sub-sections, namely: Sections A and B for the North alignment, and Sections C and D for the South alignment. The underground stations are, typically, comprised of three levels of structures; with the Centre Platform, Side Platform and Stacked Platform. The stations are up to 230 m long and approximately 25 m wide, and are excavated up to a depth of 25 to 30 m below the ground surface. The station

perimeter was constructed of diaphragm walls, 1.0 to 1.2 m thick and up to 30 to 35 m deep. The tunnel lining is of twin bored single-track tunnels. Each tube has an outer diameter of 6.3 m, with an inner diameter of 5.7 m of concrete segmental lining.

The major emphasis of this thesis is on ground movements associated with the excavations for the stations and the construction of the tunnel. Bangkok city is located on the low flat Chao Praya Delta Plain. The terrestrial deposits in the city lie from 0 to about 4-5 m above the mean sea level, with the other soil layers being marine deposits, resulting from changes in sea levels during the Quaternary period. The deposit consists of an extensive overlay of Bangkok soft marine clay, which is of low strength and high compressibility. The upper soft clay layer is underlain with several aquifers inter-bedded with clay and sand. Over several decades extensive ground water pumping from the aquifers has caused large piezometric drawdowns and alarming subsidence. Generally, the Bangkok subsoils consist of several layers and a typical soil profile up to 60 m deep will indicate layers such as ; Made Ground, Bangkok Soft Clay, First Stiff Clay, Clayey Sand, Second Stiff Clay, Hard Clay and Dense Sand.

The major tasks in this thesis can be divided into four parts: (1) a critical literature review; (2) estimation of the geotechnical parameters for the constitutive soil models established for the soil profile which extends to 60 to 65 m with seven distinct layers; (3) the ground deformation associated with deep excavations with diaphragm walls and (4) the ground deformation associated with nearly 22 km of tunnels constructed with the use of earth pressure balanced shield tunnel boring machines. These works are first introduced in the latter part of this chapter.

1.2 Research Objectives

This dissertation is on the Geotechnical aspects of the completed Bangkok MRT project (Blue Line) and its extension currently under design. Main objectives are:

(1) To carry out a comprehensive literature review on

    (a) the estimation of the geotechnical parameters that govern the deformation behavior during excavations and tunneling works in sedimentary soils;

    (b) the critical evaluation of the empirical methods available in estimation of ground movements;

    (c) the analytical methods available in estimating ground movements and

    (d) the numerical analyses using 2D approaches for the estimation of ground deformations during MRT works with deep excavations and earth pressure balanced shield tunnels.

(2) To establish the best data bank on the geotechnical parameters from laboratory tests (triaxial and odeometer tests), field tests (pressuremeter tests, vane tests and standard penetration tests); and small strain behaviour using Bender elements in the laboratory tests and down hole seismic method in the field.

(3) To carry out a comprehensive study of the diaphragm wall movements during deep excavations and the associated ground surface settlements, at locations where the MRT stations are constructed. The measured movements are to be compared with the predicted values from empirical methods and numerical analyses using Plaxis software.

(4) To carry out a detailed study on the ground surface settlements as induced by the earth pressure balanced shield tunnelling works. The measured settlements are to be compared with the values estimated from analytical methods and numerical analyses using the Plaxis software.

1.3 Layout of this Thesis

Chapter one of this thesis gives a general introduction of the work contained in this thesis indicating that the emphasis of the thesis is a detail study of the ground deformation related to the excavation and tunnelling works on the Bangkok MRT projects. Following this chapter, is Chapter 2 which contains the literature review on soft ground tunnelling and the associated geotechnical problems, followed by various

empirical and analytical methods and the use of numerical analyses using the Plaxis software in estimating ground movements.

The MRT works and the Bangkok soil conditions are then summarised comprehensively in Chapter 3. The general background of the MRT projects in Bangkok subsoils is presented in the first part of this chapter. The main focus is on the completed MRT project (Blue Line), and its extension which is currently under design. Critical reviews of the geological and geotechnical backgrounds of Bangkok subsoils are given in the second part. Such input soil parameters are important factors in the finite element analysis of wall deflections and ground movements of deep excavations. The third part of the chapter then focuses on the back-analysed soil parameters (i.e. E_u/s_u ratios) of Bangkok Clays, based on the MRT station excavations and other building basement excavation case histories. For the finite element analysis of tunnelling works, the soil parameters, as well as other factors related to tunnelling sequences play a key role.

Chapter 4 focused on evaluation of geotechnical parameters from laboratory tests. The work contained herein is in three parts. The first one is related to undrained strength parameters of Bangkok Clays as interpreted from vane shear tests (Bangkok Soft Clay) and CK_oU triaxial tests (Stiff and Hard Clays). Path dependent drained strength parameters are also included in this section. The second part is the major one and it relates to interpretation of oedometer and triaxial deformation parameters for Hyperbolic and Hardening Soil Model analyses. Oedometer tests from Bangkok MRT Blue Line Extension project are examined. Also, large amount of undrained and drained triaxial test series conducted at Asian Institute of Technology under the supervision of Prof. A.S.Balasubramaniam (see Chaudhry, 1975; Ahmed, 1975; Hassan, 1976; Kim, 1991; Gurung, 1992) are re-analysed. In the last part of this chapter, an attempt is made on 2D finite element modelling of triaxial and oedometer tests using Plaxis. A series of parametric study is conducted to gain better understanding of the effects of input parameters. After that, soil model calibration is done by means of curve matching.

In Chapter 5, soil parameter interpretations from the LLT pressuremeter tests are discussed with the emphasis on their application in finite element analyses. The vital

idea is to find an alternative source of soil parameters to be adapted in higher order soil models, such as the Hardening Soil Model. Details of each method are summarised in subsequent sections.

The works in Chapter 6 are related to two small strain parameters, namely small strain shear modulus (G_{max}) and reference shear strain ($\gamma_{0.7}$) of Bangkok Clays. These two parameters are used to govern the small strain behaviours of soil in Hardening Soil Model with Small-Strain Stiffness. The area of research in small strain parameters is new and not familiar in Griffith University. Some basic concepts related to the subject are also included. The chapter starts with a brief summary of background knowledge of small strain stiffness followed by methods of measurement of small strain both in-situ and in laboratory. Next, empirical methods for small strain shear modulus are reviewed. These methods are then verified with small strain modulus measured from in-situ tests (Down hole and seismic cone methods) and laboratory tests (Bender element) in Bangkok areas. Small strain shear modulus (G_{max}) is also correlated with pressuremeter parameters. The following part deals with the concept of volumetric threshold shear strain (γ_{tv}) and its relationship with reference shear strain parameter ($\gamma_{0.7}$). Two approaches developed by Ishibashi and Zhang (1993) and Vucetic and Dobry (1991) are used to calculate reference shear strain parameter ($\gamma_{0.7}$). The results of this calculation are then compared with laboratory Bender element test results conducted in Bangkok Soft Clay samples (Teachavorasinskun *et al.*, 2002a). Validations of calculated $\gamma_{0.7}$ values for both Bangkok Soft and Stiff Clays are conducted by means of deep excavation finite element back-analyses in Chapter 7.

Based on the review of the quality of field measurements (wall deflections and ground surface settlements), in 18 subway stations, the Sukhumvit Station is selected as the best one to perform a detail study of deep excavations in Chapter 7. Various aspects of the estimation of deformations are discussed including empirical and numerical analyses. Studies on the relationships between the maximum lateral wall deflection (δ_{hm}) and the maximum ground surface settlement (δ_{vm}) are conducted. These studies are done to verify the ability of empirical methods in predicting ground surface settlements induced by excavations in Bangkok subsoils. For numerical aspects, various soil models are employed including Mohr Coulomb Model, Soft Soil Model,

Hardening Soil Model, and Harden Soil Model with Small Strain Stiffness. A Summary of each model is given in Chapter 2. Performances of these models are examined in terms of diaphragm wall movements and the ground surface settlement predictions. Extensive studies of geotechnical parameters were conducted on both laboratory and in-situ testing in Chapters 4, 5 and 6. Soil parameters from these studies are then used as input parameters in the above mentioned constitutive models. Three analytical methods were adopted for the ground response for eight different sections during shield tunnelling using the methods of Verruijt and Booker (1996); Loganathan and Poulos (1998); and Bobet (2001). The selection of the sections is based on the geometries of the section and the positions of the tunnels. Section CS-8 (Phra Ram 9 to Phetchaburi) is chosen representing the side by side twin tunnel located mainly in stiff clay layer; Section 26-001 (Lat Phrao to Ratchada) is selected as the representative of side by side twin tunnel located partly in soft clay layer and partly in stiff clay layer; Section 23-001 (Pracharat Bumphen to Thiam Ruam Mit) and Section 6D (Sirikit to Sukhumvit) are picked for the side by side twin tunnel partly located in dense sand layer and partly in the overlying stiff clay layer; Section 7C (Sukhumvit to Phetchaburi) is analysed for the case of side by side tunnel partly located in the clayey sand layer and in the stiff clay layer; and lastly, Sections CS-2A-1 (Silom to Samyan), CS-3 (Lumphini to Silom) and 4C (Lumphini to Bon Kai) are the choice of stack tunnels located in soft clay, stiff clay and dense sand layers.

These eight sections cover all the cases of the different location of tunnels and their relative positions side by side or stacked one above the other. Results obtained from these solutions are presented in the subsequent chapters. Both single tunnel and twin tunnel behaviours are studied in these selected sections.

Three, 2D finite element methods, namely the contraction method, the stress reduction method and the modified grout pressure method are used to model the shield tunnelling of the Bangkok MRT Blue Line project. General geological conditions of this project are discussed earlier in Chapter 3. Seven twin, side-by-side tunnelling sections are selected as case studies. Note that these sections are chosen in order to cover various combinations of soil profiles and shield operation factors encountered. An example is the tunnel cross section located entirely in stiff clay or partially in stiff clay and clayey sand. In terms of shield operation factors, four factors namely face

pressure, penetration rate, grout pressure and percentage of grout filling are the most influence ones during shield tunnelling. If sufficiently high face pressure, grout pressure, percentage grout filling are combined with fast penetration rate, the resulting surface settlement can be limited to an order of 10 to 15 mm. In the contrary, if one or more shield operation factors have failed to reach the required magnitude, higher magnitude of surface settlement is to be expected. The final part of Chapter 8 deals with the design currently in progress of the subway station in the MRT Blue Line Extension Project, using a combination of the "Cut and Cover and New Austrian Tunnelling Method (NATM)". Two dimensional finite element analyses are conducted on the critical cross sections using the Hardening Soil Model.

Finally in Chapter 9, concluding remarks and recommendations for future research are made.

CHAPTER 2

Literature Review

2.1 Introduction

The first part of this review is on tunnelling methods and tunnel boring machines. It also includes: a classification of mechanised tunnelling techniques; details of Slurry Pressure Balance (SPB) shield and Earth Pressure Balance (EPB) shield in soft ground tunnelling; tunnelling sequences using tunnel boring machines and tunnel lining. The first section is followed by the second one, on undrained component of volume loss, tunnel face stability and propagation of soil movements towards ground surface, as the topics relevant to soft ground response during tunnelling works.

Details of the survey on ground movements during excavations are not included in this chapter, but instead presented in Chapter 7 on deep excavations. The ground movements during tunnelling works in part three of this review is presented under the headings of empirical methods, analytical methods and numerical methods. Under the empirical method the classical work of Peck (1969), still widely used with a Gaussian distribution for ground settlement is presented. For the analytical methods using elastic approach the work of Sagaseta (1987), Verruijt and Booker (1996), Gonzalez and

Sagaseta (2001), Lee *et al.* (1992), Rowe and Lee (1992), Loganathan and Poulos (1998) and Bobet (2001) are reviewed in detail. The work of Verruijt and Booker (1996), Loganathan and Poulos (1998) and Bobet (2001) are used extensively in Chapter 8 for the ground movement during the tunnelling works of the Bangkok MRT works. The Plaxis software is used for the numerical analyses on ground movements during deep excavations and tunnelling works. While tunnel excavation can be considered as a 3D problem (Swoboda, 1979; Swoboda and Abu-Krisha, 1999), full 3D numerical analysis is time consuming and requires excessive computational resources. Consequently, 2D analysis is considered to be sufficiently flexible and economic, in terms of both person-hours and computer-hours, to find applications in practice. Therefore, the research work on various 2D methods is reviewed in detail. These methods have been proposed to take into account the change in stresses and strains owing to tunnelling when adopting plane strain analyses to simulate tunnel construction. The work of the following researchers are considered in detail; Rowe *et al.* (1983), Rowe and Kack (1983), Finno and Clough (1985), Addenbrooke *et al.* (1997), Lee and Rowe (1989), and Karakus and Fowell (2003; 2005).

The last part of the literature review is on constitutive equations to be used in the numerical analyses: the following models are reviewed and adopted: Mohr Coulomb Model (MCM); Soft Soil Model (SSM); Hardening Soil Model (HSM) and Hardening Soil Model with Small Strain Stiffness (HSS).

2.2 Tunnelling Methods and Tunnel Boring Machines

Over the last three decades, the demand in transportation infrastructure usage has increased dramatically due to limited spaces and growth of population. This has brought numerous technical innovations to underground construction including tunnelling works. In general, tunnelling methods can be broadly divided into four categories:

- Open-cut tunnelling method
- Cut and cover tunnelling method
- Mechanised tunnelling method

- Sprayed concrete tunnelling method

In tunnelling with the open-cut method, initially a trench is excavated vertically from ground surface to the required excavation depth. It is then followed by the construction of the actual tunnel structure; after that the excavated trench is back filled again. The cut and cover tunnelling method is normally a simple method for shallow tunnels where a trench is initially excavated and then roofed over. Strong overhead support systems are required to carry the load of the covering material. Two practical construction methods are available as follows (Ou, 2006):

- *Bottom-up construction method* where a trench is excavated with a necessary ground support system. Then, the tunnel of desired material will be constructed within the trench. After that, the trench is backfilled and the surface is reinstated.
- *Top-down construction method* where side walls (normally reinforced concrete diaphragm walls) and capping beams are constructed from the ground surface. An excavation is then made to allow the tunnel roof to be constructed using precast beams or in-situ concrete. The surface is reinstated except the access openings. This allows early reinstatement of roadways or other surface features. Excavation machinery is then lowered into the access openings, and the main excavation is carried out under the permanent tunnel roof, followed by constructing the base slab.

Mechanised tunnelling method has various applications due to a number of available excavators and Tunnel Boring Machines (TBM). The classification of the mechanised tunnel techniques and their method of construction are discussed in the following sections.

Sprayed concrete tunnelling methods, such as Sprayed Concrete Lining (SCL) or New Austrian Tunnelling Method (NATM) was originally developed for tunnelling in rock mass. However, in the last two decades these construction techniques were also applied successfully in soft ground tunnelling. Basic principle of SCL or NATM is to excavate the soil or the rock in small area of cross section then to immediately support

the excavation by a thin layer of shotcrete to form temporary support. The remaining cross sectional area will be excavated later on and again followed by immediate shotcreting. Finally the permanent tunnel lining is constructed. The tunnelling methods briefly described above are the methods now available for modern tunnel construction.

The following sections deals with further aspects of mechanised tunnelling technique; this is the main focus of this research.

2.2.1 Classification of Mechanised Tunnelling Techniques

According to AFTES (2000), mechanised tunnelling techniques can be classified in to groups, categories and types as shown in Figure 2.1. The first column in this figure refers to the type of support; "NONE" means there is no immediate support either peripherally or in the front. The remaining two types are described as "PERIPHERAL" and "PERIPHERAL AND FRONTAL". They refer to machines providing immediate peripheral and to machines providing both immediate peripheral and frontal support simultaneously.

When consideration is paid on excavation characteristics, the mechanised tunnelling can be broadly classified as partial-face boring and full-face boring. As the name implies, partial-face boring machines drive or construct the tunnel by digging, excavating or cutting the in-situ formation in parts, and not boring the full face at one time. In full-face boring machines, on the other hand, the full face is bored at one time. This equipment is also known as a Tunnel Boring Machine (TBM). There are various forms of TBM (AFTES, 2000):

- Open face without shield
- Open face with shield (single or double)
- Closed face with compressed air shield
- Closed face with slurry shield
- Closed face with earth pressure balance shield

The last two techniques are discussed further in the following sections.

TYPE OF SUPPORT	GROUP	CATEGORY	TYPE
NONE	Boom-type tunnelling machine	Roadheader	In line cutter / Transverse cutter
		Digger type	Backhoe bucket / Hydraulic impact breaker
	Hard rock TBM		
	Tunnel reaming machine		
PERIPHERAL	Open-face shield TBM	Gripper shield	Full face
		Segmental shield	Full face / Partial face
		Double shield (gripper and segmental)	Full face
PERIPHERAL AND FRONTAL	Closed-face shield TBM	Mechanical support	Full face / Partial face
		Compressed-air shield	Full face / Partial face
		Slurry shield	Full face
		Earth pressure balance machine	Full face
		Mixed face shield	Open mode and EPB — Full face / Open mode and slurry — Full face / EPB and slurry — Full face

Figure 2.1: Classification of Mechanised Tunnelling Techniques (AFTES, 2000)

2.2.2 Shield Tunnelling in Soft Ground

The demand of tunnelling in soft ground conditions is increasing. This demand resulted in two types of soft ground TBM, namely Slurry Pressure Balance (SPB) TBM; and Earth Pressure Balance (EPB) TBM which became more and more advanced. The basic design of SPB TBM and EPB TBM are quite similar. The overall appearance and many of the systems from one type are used directly on the other with limited or no change to design. When these two TBM were first introduced, they had

remarkable limitation in terms of ground conditions. Traditionally, the SPB machine has been selected for coarser grained soils and the EPB machine for fine grained soils. In recent years, the increased development of additives and its injection systems has allowed both types of machines to excavate a broader range of soil conditions to the point where the type of soil is no longer the most critical item in the decision making process in selecting a type of TBM.

2.2.2.1 Slurry Pressure Balance (SPB) Shield

A SPB machine is a machine which utilises fluid mixture to remove the cuttings, maintaining the front face and preventing settlement. This fluid mixture is also acting as part of the machine coolant and as lubricant. The fluid mixture in the SPB machine comprises a suspension of bentonite in water with appropriate additives. The excavation process starts by pumping bentonite suspension (having high pressure) into the cutting head chamber which is located in front of the tunnel face. When the pressurised slurry enters into the earth – mass (ground) in front of the face, a filter cake is formed very quickly. The water remains behind this cake. This cake is then excavated by tools in the chamber and mixed with supporting fluid. This is how slurry, consisting of excavated ground and supporting fluid, is formed. This slurry is transported to the surface through pipes and discharged into separation tanks. The fluid is separated form these tanks for recirculation. Figure 2.2 shows the schematic diagram of the SPB machine. The face loss (ground loss at the face of TBM during tunnel excavation) is minimized by controlling the slurry pressure, the flow and the density in the cutting- head chamber. The long term effect due to tunnelling process, which causes secondary settlement, must be controlled by good backfill grouting around the segments (EFNARC, 2005).

❶ Cutterhead	❹ Thrust arms	❼ Bentonite Slurry Feed
❷ Bentonite Slurry / Soil	❺ Segments	❽ Bentonite Slurry/ Soil Return
❸ Air Bubble	❻ Tail sealant	❾ Annulus Grout
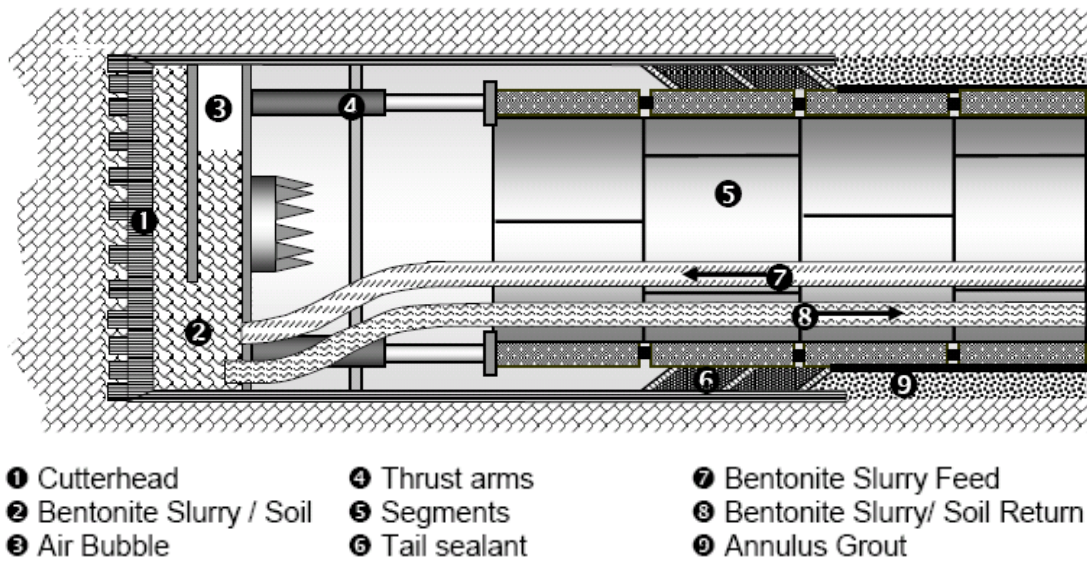
Figure 2.2: Slurry Pressure Balance Machine (EFNARC, 2005)

2.2.2.2 Earth Pressure Balance (EPB) Shield

The technique of balancing the earth pressure in EPB shield is similar to SPB shield. As can be seen in Figure 2.3 (a), the earth pressure and the water pressure (in case of tunnelling under ground water level) are supported by slurry pressure in the working chamber to prevent the loss of stability at the working face. In terms of environmental and sometime economical reasons, the EPB shield technique has some advantages over the SPB shield techniques due to the fact that use of a separate plant on the ground surface is not required. By using EPB shield method, a tunnel can be excavated by the cutting wheel (located in front of the cutter-head). The shield area in which the cutting wheel rotates (working chamber) is designated as the extraction chamber and is separated from the shield section, which is under atmospheric pressure, by the pressure wall. The spoil or excavated soil is loosened by the tools of the cutting wheel, drops through the working chamber and are taken out through the screw conveyor and belt conveyor as shown in Figure 2.3 (b).
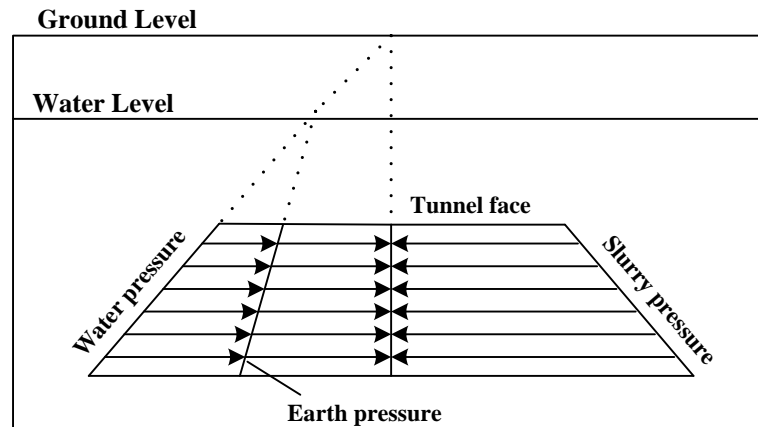
(a) Pressure Distribution in EPB Shield

❶ Cutterhead   ❹ Screw conveyor   ❼ Segments
❷ Working Chamber   ❺ Thrust Arm   ❽ Annulus Grout
❸ Pressure Wall   ❻ Tail sealant
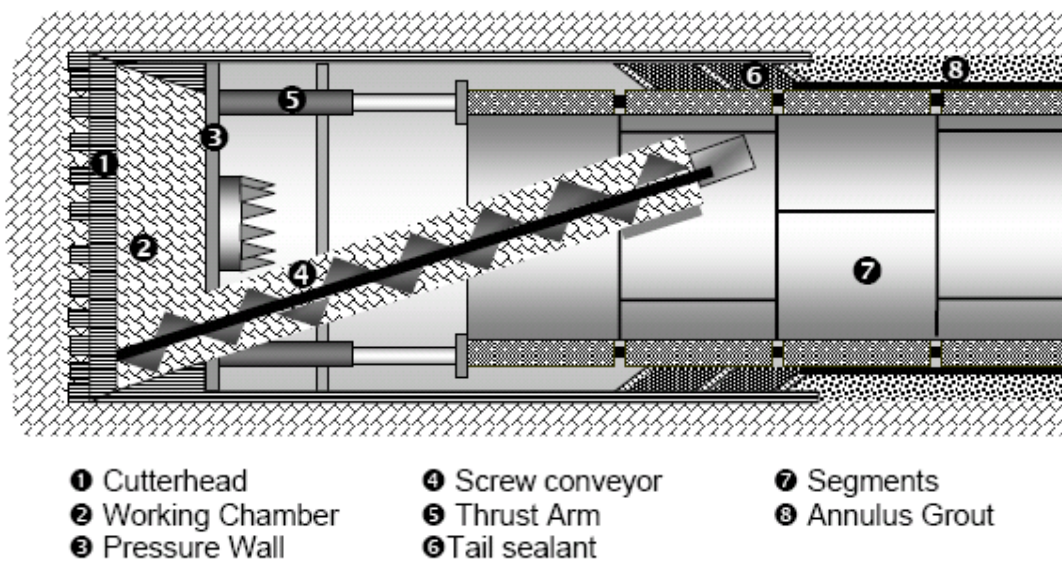
(b) Earth Pressure Balance Shield

Figure 2.3: Earth Pressure Balance Machine (EFNARC, 2005)

In general practice, the ground movement due to EPB shield tunnelling can be minimised using a control parameter, such as the target face pressure, which is calculated prior to the excavation. This target face pressure is dependent on the design alignment and subsurface ground conditions. During tunnel excavation, the actual face pressure has to be recorded for each of the excavated rings or each excavation cycle in order to be used as a reference in the future.

2.2.3 Tunnelling Sequences Using Tunnel Boring Machines

The construction sequences of tunnelling using TBM are commonly divided into four major stages as follows (Komiya *et al.*, 1999; Ding *et al,.* 2004)

Stage 1 – Shield Advancement and Balancing Pressure at the Face: This stage includes the process of cutting the soil at the face of the shield and advancing the shield towards the soil at the tunnel face. The advancing rate of a closed – face TBM depends on the effectiveness of a number of factors including the cutter-head design, the quality of spoil conditions and the uniformity of the ground condition, etc. The typical values of the shield advanced rate are ranging from 40 mm per minute to 100 mm per minute. The pressure from the existing soil at the cutting face is balanced by the pressure from the machine behind the cutter. Consequently, changes in stress due to the cutting process and the balancing pressure will not result in significant soil movements. Moreover, the surrounding soil outside the shield will not be able to release its stress due to the rigid support of the shield.

Stage 2 – Installation of Segmental Lining and Backfill Grouting: The second stage is to install the lining segments and backfill the gap at the shield tail with grout. Once the shield moves forward and the soil inside the shield is removed, the lining segment will be installed to form a circular ring within the shield tail cover plate. Simultaneously, a gap between the surrounding soil and the lining segment will be created as a result of the difference of shield and lining diameter. To prevent the immediate soil deformation, a grout must be injected to backfill the gap space. Furthermore, this grout is also functioning to improve the tunnel stabilisation and the water-proof performance.

Stage 3 – Grout Hardening: This is a transient stage. The grout will harden and consolidate and the soil deformation will also increase with time though its rate decrease. The lining segments and the surrounding soil interaction will increase with time until an equilibrium state is reached. It is, therefore, necessary to assess the effects of the grout hardening and the pressure distribution on the response of the lining structure at this stage.

Stage 4 – Harden grout: In the final stage, the grout becomes hardened and gains its full stiffness and strength. The settlement will be eliminated.

2.2.4 Tunnel Lining

The lining is a structure to secure a tunnel space by withstanding the earth and water pressures. In shield tunnelling, segmental linings are usually utilised. Generally, the segment is made of reinforced concrete or of steel. Several segments are assembled to form a circle, multi-circle or other required shapes.

These segmental linings can act as both a one-pass and two-pass system. In the one-pass system, the segmental linings are erected within the protection of a cylindrical tail shield. After erected, the segmental linings will provide both the stabilisation of the tunnel opening during construction and a permanent lining. In the two-pass system, temporary segments will be constructed to provide only the construction stabilisation in the first pass. Then, in a second pass, the case-in-place concrete lining is added for the permanent service. Typically, segmental linings are smaller in diameter than that of the excavated tunnel; because they are erected inside a cylindrical shield, they are in a sense, part of the excavating equipment. The resulting annular void space is usually filled with grout.

2.3 Review of Soft Ground Response Induced by Tunnelling

2.3.1 Characterisation of Soft Ground

The definition of soft ground in tunnelling may consists of both cohesive and/or cohesion materials. Previous researchers have recognised a difference in ground movements due to tunnelling in the two types of materials. The results from centrifuge tests revealed that the pattern of ground movement in cohesionless soil appear to be

restricted to a narrower region above the tunnel than the cohesive soil (Figures 2.4 and 2.5).
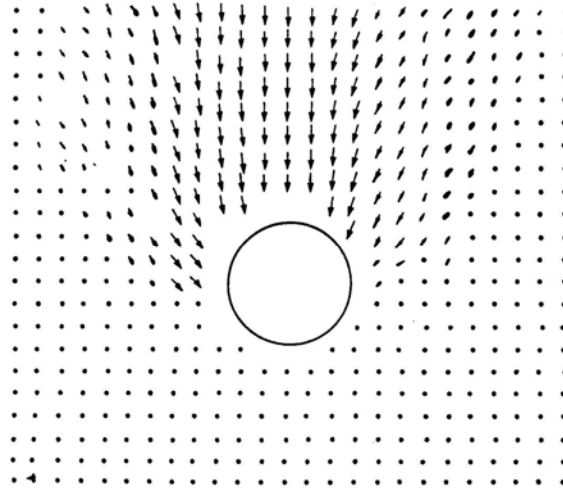
Figure 2.4: Soil Deformation Around Tunnel in Clay (after Kimura and Mair, 1981)
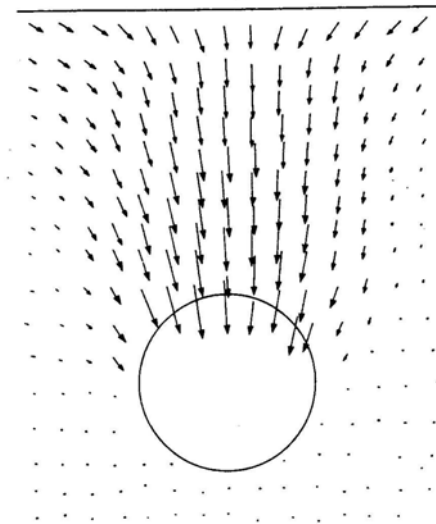
Figure 2.5: Soil Deformation Around Tunnel in Sand (after Potts, 1976)

2.3.2 Undrained Components of Volume Loss

The construction of a tunnel inevitably leads to a larger amount of soil to be excavated than to be replaced by the volume of the tunnel. The amount of this over excavation is quantified by the volume loss (V_L) which is the ratio of the difference between volume of excavated soil and tunnel volume (defined by the tunnel's outer diameter) over the tunnel volume, The volume loss is a measure of the total ground disturbance. It causes the settlement trough at the surface and in undrained conditions; the volume of this

settlement trough is equal to V_L. For shield tunnelling, Attewell (1978) divides the sources of volume loss into 4 categories, which are the face loss, the shield loss, the tail loss and the radial loss after grouting.
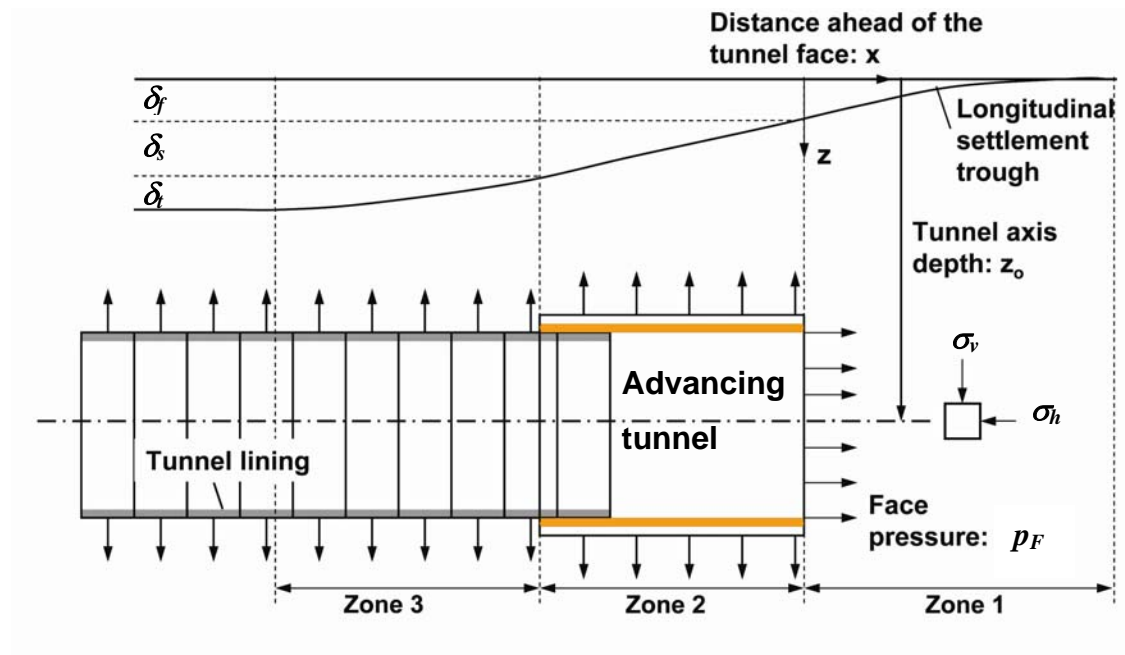
Figure 2.6: Definition of Volume Loss Components and Related Machine Parameters (Wongsaroj, 2005)

Figure 2.6 shows a schematic section of the advancing tunnel shield, which depicts the three components of volume loss due to soft ground shield tunnelling. The first component is called the "face loss". It is mainly due to the inward flow of ground from a zone of influence ahead and to the side of the face (Zone 1) into the shield. The settlement component caused by face loss is referred to as δ_f in Figure 2.6. To minimise the volume loss at the face, the shield advanced parameter must be controlled in the face pressure (p_F).

In order to advance the shield, it is necessary to excavate an oversize hole using over-cutter or copy cutter. After the copy cutter has passed, an annular void will be created and the surrounding soil will tend to move inward radially to fill the void. This movement of soil create a loss of ground namely "shield loss" which leads to the settlement component of δ_s in Zone 2. Due to the slightly smaller size of tunnel lining compared to the shield, there will be an annular which is normally filled with grout. Thus, there is an opportunity for the soil to displace radially onto the lining until the

19

grout has hardened and gain enough strength to resist the earth pressure. This soil movement cause the last component of volume loss "tail loss" which occurs in Zone 3. It should be noted that some authors (Bloodworth, 2002; Schroeder, 2002) have combined the loss of ground in Zone 2 together with Zone 3 and termed as "radial loss". The last component of volume loss is the radial loss which continues after grouting as the lining is deformed due to the transfer of overburden pressure to the new boundary.

2.3.3 Tunnel Face Stability

Analysing the tunnel face stability provides an indication of the most probable failure mechanism, as well as of parameters to be taken into consideration in the evaluation of ground movements induced by tunnelling. Based on the nature of the grounds encountered, two types of failure mechanisms may be observed.

In the case of cohesive soils, face failure involves a large volume of ground ahead of the working front. This mechanism leads to the formation of a sinkhole at the ground surface with a width larger than one tunnel diameter.

In the case of cohesionless soils, failure tends to propagate along a chimney like mechanism above the tunnel face (ITA/AITES, 2007). Both mechanisms have been evidenced in centrifuge tests carried out in clays and dry sand. (see Figures 2.4 and 2.5)

The conclusions from the two cases (cohesive and cohesionless soils) are consistent with extensive field observations (Clough and Leca, 1993). These are however based on the consideration of idealized conditions and should be adjusted to account for the actual conditions found on each individual worksite: non-homogeneous grounds and water inflows (ITA/AITES, 2007). In particular, in water-bearing sands, ground stability will be considerably influenced by hydraulic gradients induced by seepage towards the face. Further study on the seepage force acting on the tunnel face was conducted by Lee *et al.* (2003). It was found that the average seepage pressure acting on the tunnel face is proportional to the hydrostatic pressure at the same elevation, and

the magnitude is about 22% of the hydrostatic pressure for the drainage type tunnel and about 28% for the waterproof type tunnel.

2.3.4 Propagation of Movements towards the Surface

Ground movements initiated at the tunnel opening will tend to propagate towards the ground surface. The extent and time scale of this phenomenon will typically be dependent upon the geotechnical and geometrical conditions, as well as construction methods used on the site.

Two propagation modes have been identified, based on the conclusions of in situ measurements and observations. These modes can be used to evaluate, in a transverse plane, the degree of propagation of displacements initiated at the opening. They will be referred to, in the following, as primary mode and secondary mode (ITA/AITES, 2007).

The primary mode (Figure 2.7 (a)) occurs as ground stresses are released at the face. It is characterized by the formation of a zone of loosened ground above the excavation. The height of this zone (C) is typically 1-1.5 times the tunnel diameter (D) and about one diameter wide. Two compression zones develop laterally along the vertical direction. For deeper tunnels ($C/D > 2.5$), the observed tunnelling impact at the ground surface is generally limited. (Cording and Hansmire, 1975; Leblais and Bochon, 1991).

The secondary mode (Figure 2.7 (b)) may occur subsequently, when the tunnel is located close to the surface ($C/D < 2.5$) and insufficient confining support exists. These conditions result in the formation of a rigid ground block, bounded by two single or multiple shear planes extending from the tunnel to the surface. Displacements at the ground surface above the opening are of the same order of magnitude as those generated at the opening.
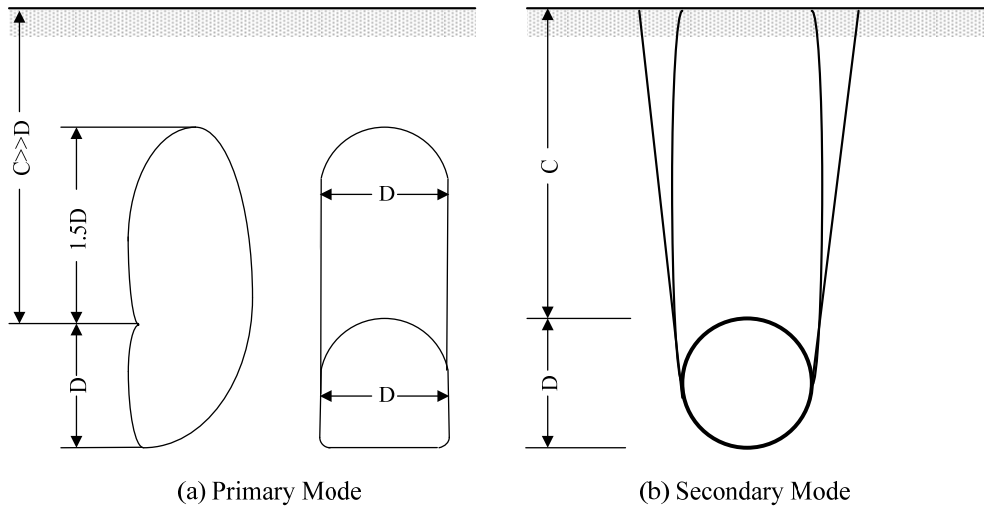
Figure 2.7: Propagation of Soil Movement in Primary and Secondary Mode
(ITA/AITES, 2007)

2.4 Prediction Methods for Ground Movements due to Tunnelling

The literature review in this section is on the empirical, analytical and numerical methods involved in ground movement prediction related to tunnelling works. In terms of the empirical methods, most of the research work has been developed from the pioneer work of Peck (1969). The appropriate analytical methods identified by this review allow the surface settlement profile to be estimated. Additionally, the components of ground loss (i.e. face, shield and tail loss) are assessed using a gap parameter. The numerical analysis focuses on both 2D tunnelling models. A range of numerical modelling techniques are also discussed.

2.4.1 Empirical Methods

2.4.1.1 Peck (1969)

Based on many tunnelling project case histories, Peck (1969) observed that the settlement profile of a single tunnel can be reasonably described using a normal

probability function curve, also known as the Gaussian or error function curve. Peck simplified the stochastic solution, first developed by Litwiniszyn (1956), to estimate the settlements at various distances from the tunnel centreline. The equation used in his proposed method was:

$$\delta_V = \delta_{V,\max} \exp\left(-\frac{x^2}{2\,i^2}\right)$$

Eq.2.1

where,

δ_V =   surface settlement at transverse distance x from the tunnel centreline

$\delta_{V,\,max}$ =   maximum settlement (at $x = 0$)

x =   horizontal distance from tunnel centreline

i =   distance from the tunnel centreline to the point of inflexion.

Figure 2.8 shows the surface settlement trough profile and other parameters, explained in Equation 2.1. As can be clearly seen, the trough has its maximum slope at the points of inflexion (i), which is located at the distance i and $-i$ from the tunnel centreline. According to the properties of the normal probability curve or the standard deviation curve, the value of i is equal to 0.61 $\delta_{V,\,max}$ (O'Reilly and New, 1982).
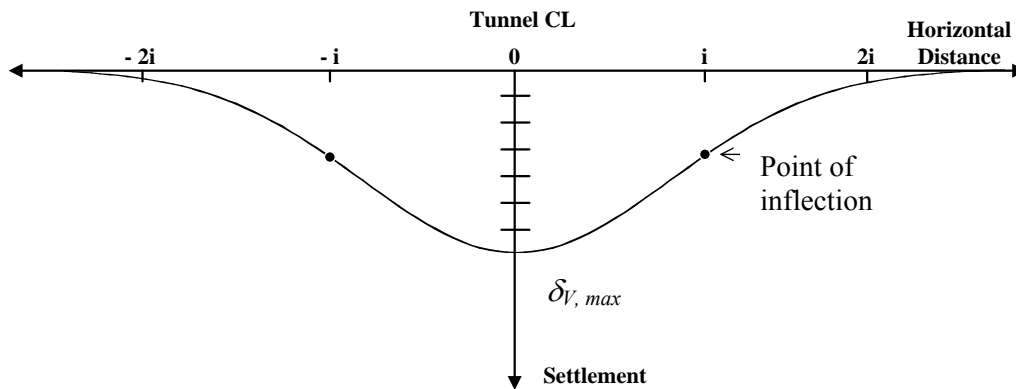
Figure 2.8: Transverse Settlement Trough Profile (Peck, 1969)

Peck (1969) proposed a plot of i versus depth from the ground surface to the tunnel axis (z), with both being normalised by the tunnel radius (R), as illustrated in Figure 2.9. This plot revealed the empirical trends of value i at various tunnel depths with regards to soil type.
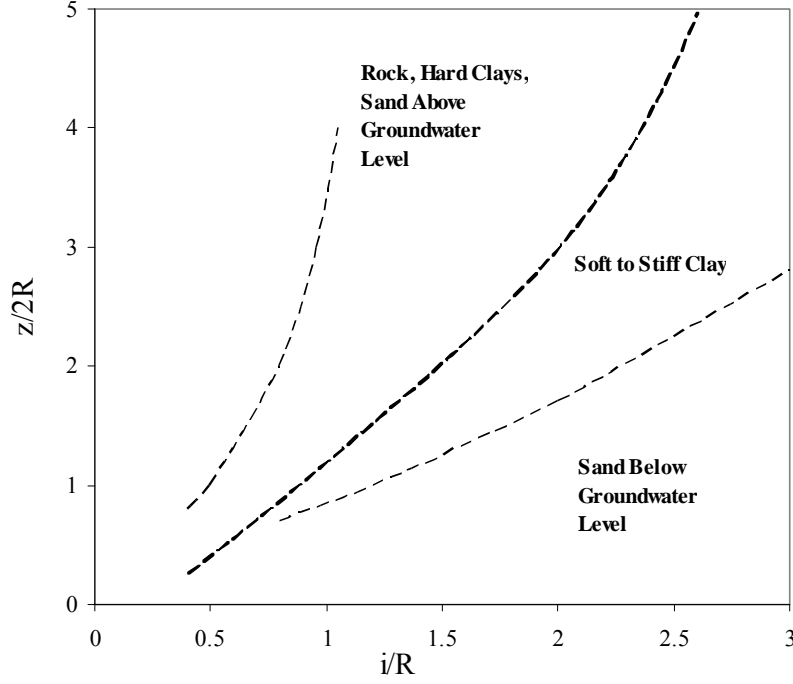
Figure 2.9: Plot of Settlement Trough Width Parameter versus Tunnel Depth
(Peck, 1969)

The area below the Gaussian error function is, by definition, equal to 1 as it represents the probability that the variable x has a value between $-\infty$ to ∞. However, the parameter $\delta_{V,\,max}$ and i in Equation 2.1 are mathematically independent. Consequently, the area enclosed by the settlement trough profile can be calculated by:

$$V_S = \int_{-\infty}^{\infty} \delta_V \, dv = \sqrt{2\pi} i \delta_{V,\max} \approx 2.5 i \delta_{V,\max}$$

Eq.2.2

where,

V_S =   volume of settlement trough per unit length.

In materials with a low permeability, such as stiff clay, the initial response of the ground to the tunnel construction can be considered to be undrained. The volume of the surface settlement trough, therefore, is equal to the volume of soil which is excavated in excess of the theoretical volume of the tunnel. It is common to specify this excess volume as a proportion of the theoretical tunnel volume (per unit length):

24

$$V_L = \frac{V_S}{0.25\pi D^2}$$

Eq.2.3

where, V_L is the volume loss and D is the outer tunnel diameter. It is normally expressed as a percentage. After combining Equations 2.1 to 2.2 the transverse settlement profile can be expressed in terms of volume loss:

$$\delta_V = \sqrt{\frac{\pi}{2}} \frac{V_L D^2}{4i} \exp\left(-\frac{x^2}{2i^2}\right)$$

Eq.2.4

In Equation 2.4, if the tunnel diameter D is known, the shape and magnitude of the transverse settlement curve will only depend on the volume loss V_L and trough width parameter i.

2.4.2 Analytical Methods

2.4.2.1 Sagaseta (1987), Verruijt and Booker (1996), Gonzalez and Sagaseta (2001)

A number of authors have provided the background research into the use of appropriate analytical methods. Sagaseta (1987) presented closed form solutions for obtaining undrained soil deformation, due to ground loss, in an initially isotropic and homogeneous soil. The soil was modelled as a linear-elastic material, with a virtual image technique and some results from the elastic half-space being utilised (Figure 2.10), to estimate the movements of soil surface in strain-controlled cases, such as soft ground tunnelling. The undrained ground loss at a finite depth in an infinite space was assessed in terms of reducing the tunnel to a point sink and neglecting the effect of the soil surface (Step 1), with the conditions of incompressibility and spherical symmetry determining a radial field of displacements, decreasing with the distance to the sink. Next, the ground surface was addressed using a virtual image technique (Step 2), combined with corrective surface tractions (Step 3), for which the elastic solutions for the half space were used.
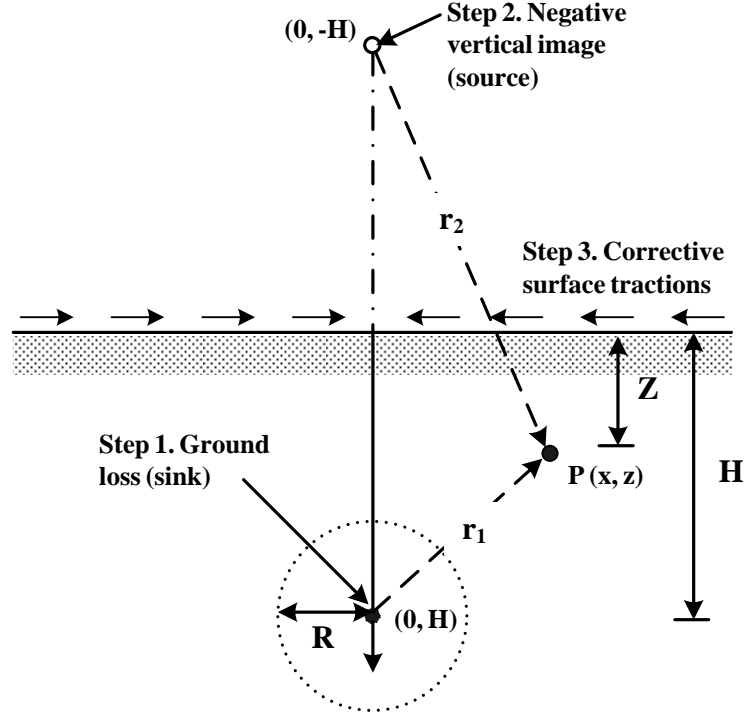
Figure 2.10: Virtual Image Technique

(Sagaseta, 1987; Gonzalez and Sagaseta, 2001)

Verruijt and Booker (1996) extended Sagaseta's solution by including the volumetric strain and the effects of ovalisation of the tunnel opening. The displacements are expressed as the sum of the effect of the uniform radial ground loss and the tunnel ovalisation (components a and b in Figure 2.11). To estimate the surface and subsurface ground deformation in vertical and horizontal directions, the authors presented the following equations (Eqs. 2.5 and 2.6):

$$
u_x = -\varepsilon R^2 \left(\frac{x}{r_1^2} + \frac{x}{r_2^2} \right) + \delta R^2 \left(\frac{x(x^2 - kz_1^2)}{r_1^4} + \frac{x(x^2 - kz_2^2)}{r_2^4} \right)
$$

$$
- \frac{2\varepsilon R^2 x}{m} \left(\frac{1}{r_2^2} - \frac{2mzz_2}{r_2^4} \right) - \frac{4\delta R^2 xh}{m+1} \left(\frac{z_2}{r_2^4} + \frac{mz(x^2 - 3z_2^2)}{r_2^6} \right) \qquad \text{Eq.2.5}
$$

$$u_z = -\varepsilon R^2\left(\frac{z_1}{r_1^2} + \frac{z_2}{r_2^2}\right) + \delta R^2\left(\frac{z_1(kx^2 - z_1^2)}{r_1^4} + \frac{z_2(kx^2 - z_2^2)}{r_2^4}\right) + \frac{2\varepsilon R^2}{m}\left(\frac{(m+1)z_2}{r_2^2}\right)$$

$$-\frac{mz(x^2 - z_2^2)}{r_2^4}\Bigg) - 2\delta R^2 h\left(\frac{x^2 - z_2^2}{r_2^4} + \frac{m}{m+1}\frac{2zz_2(3x^2 - z_2^2)}{r_2^6}\right) \qquad \text{Eq.2.6}$$

where,

ε	=	uniform radial ground loss (Figure 2.4 (a))
δ	=	long term ground deformation due to ovalisation of the tunnel lining, $\delta = 0$ represents short term undrained conditions
z_1	=	$z - H$
z_2	=	$z + H$
r_1^2	=	$x^2 + z_1^2$
r_2^2	=	$x^2 + z_2^2$
R	=	initial tunnel radius
H	=	depth to the source
m	=	$1/(1-2\upsilon)$
k	=	$\upsilon(1-\upsilon)$
υ	=	Poisson's ratio
u_x	=	horizontal movement in transverse direction
u_y	=	vertical movement in transverse direction
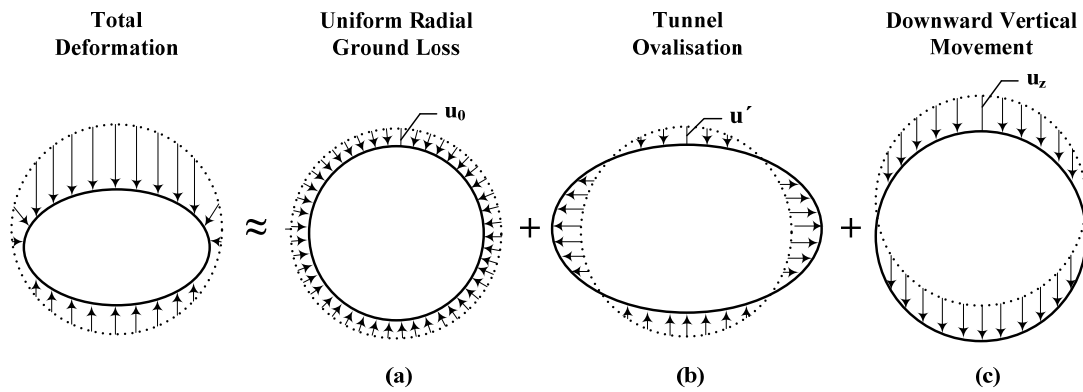
Figure 2.11: Components of Tunnel Deformation

(Gonzalez and Sagaseta, 2001)

2.4.2.2 Lee et al. (1992), Rowe and Lee (1992)

As noted above, Peck (1969) developed an empirical solution analysing tunnel trough, although it was based on statistics and judgement. Lo and Rowe (1982) and Rowe *et al.* (1983) introduced the important gap parameter, which addresses ground loss as a function of strength and deformation behaviour in the elastic and plastic state, the physical clearance between the excavated diameter and the lining, and workmanship.

The gap parameter was modified by Lee *et al.* (1992), and can be estimated as:

$$g = G_P + u_{3D}^* + \omega \qquad \text{Eq.2.7}$$

where,

G_p	=	physical gap ($G_p = 2\Delta + \delta$, as illustrated in Figure 2.12)
Δ	=	thickness of tail piece
δ	=	clearance required for lining erection
$u*_{3D}$	=	equivalent 3D elasto-plastic deformation at tunnel face
ω	=	value that takes into account the quality of workmanship

Figure 2.12 shows the simulation of ground loss proposed by Lee *et al.* (1992) for three different cases, represented by: (i) physical gap; (ii) 3D simulation of ground losses ahead of the tunnel faces; and (iii) ground losses over the shield.

a) Tunnel advances in perfect alignment and fully supported at the face

b) Tunnel advance in perfect alignment but allowing full stresses releases at the face

c) Tunnel advancement is subjected to all possible sources of "ground loss" including overexcavation due to workmanship problem
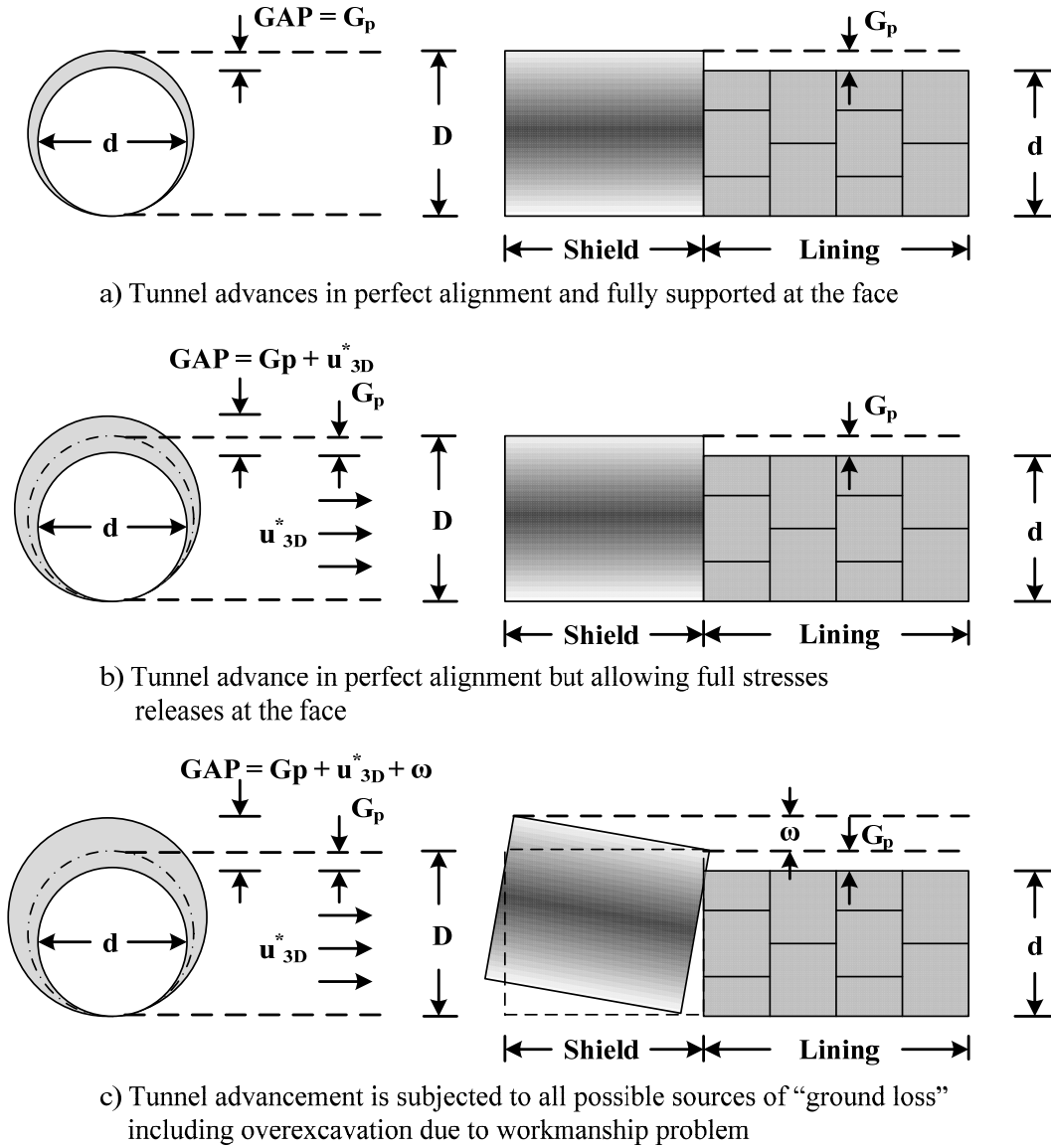
Figure 2.12: Simulation of Ground Loss (Total Gap Parameter) (Lee *et al.*, 1992)

(i) Physical Gap

The physical gap is defined as the difference between the diameter of Tunnel Boring Machine (TBM) and the diameter of the tunnel lining (Figure 2.12). Recently, jet grouting has been used in tunnelling practice, which effectively reduces the physical gap, with voids being created by over cutting during tunnel construction. In the laboratory there was a 7-10% time-dependent length reduction in the cement-soil mix samples. The value of the physical gap, therefore, can be considered to be:

G_p= 7 - 10% (2Δ + δ)   Eq.2.8

However, it should be noted that the values are different in soft clay and stiff clay, depending on the ground conditions. The value of the ratio relies on the effectiveness of the grouting. The effectiveness is estimated by the rate of soil movement into the void. In the case of soft clay, ground movements develop rapidly after the TBM advance; so the grouting is ineffective since it is injected after the shield advanced. In the case of stiff clay, the rate of development of the void near the crown is lower than the rate of advance of the tunnel shield; the grouting can be injected easily and effectively into the tailpieces.

(ii) 3D Simulation of Ground Losses Ahead of the Tunnel Face

Relief of the stresses around the tunnel face takes place during the process of excavation. Soil particles will intrude into the tunnel face, forming great pressure, as well as deformation, in the ground surface. Generally, the volume of the ground loss is equal to the amount of over-excavated or displaced material at the face. Thus, u^*_{3D} is the equivalent 3D elasto-plastic deformation at the tunnel face using a simulation in the plane strain finite element analysis, achieved by increasing the maximum allowable radial displacement at the tunnel crown. It can be approximately expressed as:

$$u^*_{3D} = \frac{k_1}{2}\delta_x$$ Eq.2.9

where, k_1 is a factor taking into account the doming effect across the tunnel face; it can be expressed as:

$$k_1 = \frac{\text{volume of nonuniform axial intrusion across the tunnel face determined by 3D analysis}}{\text{volume assuming uniform axial intrusion}}$$

The normal range of the k_1 value is 0.7-0.9 from stiff clay to soft clay. In a design

situation, the value of $k_l = 1$ would be considered as reasonable within a uniform intrusion at the tunnel face. In this case the equation can be simplified as:

$$u_{3D}^* = \frac{\delta_x}{2}$$
Eq.2.10

Meanwhile, the displacement δ_x can be calculated using:

$$\delta_x = \frac{\Omega \cdot a \cdot p_o}{E}$$
Eq.2.11

where,

$$p_o = (K_o p_v' + p_w) - p_i$$
Eq.2.12

K_o = the effective coefficient of earth pressure at rest

p_v' = the vertical effective stress at the tunnel springline

p_w = the initial in-situ pore pressure at the tunnel springline prior to tunnel construction

p_i = the tunnel support pressure (i.e. if there is no support at the tunnel face, then $P_i = 0$, and for the presence of compressed air or other means of face support $P_i > 0$)

Ω can be determined from Figures 2.14 and 2.15 (Lee et al., 1992).

All the pressures acting on the tunnel are shown in Figure 2.13.
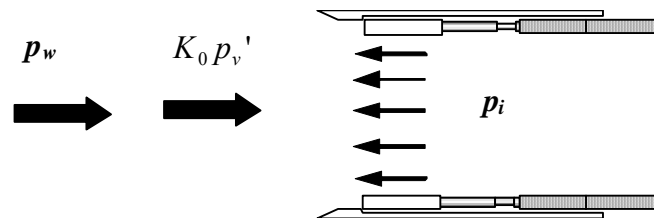
Figure 2.13: Pressures Acting on Tunnel During Excavation

Another non-dimensional parameter is used frequently in soft ground tunnel 'N', and is defined by the following equation.

$$N = \frac{\gamma H - p_i}{s_u}$$

Eq.2.13

N is the stability ratio related to the dimensionless parameter Ω. Lee *et al.* (1992) suggested that when δ_x is calculated in terms of Ω, it is extremely insensitive to the tunnel depth (*H/D*). For N less than 2.5, Ω can be considered as 1.12. However, when the N value is larger than 3, the soil mass in front of the shield face extents, from the elastic zone to the plastic zone, so δ_x increases sharply.

The relation of N and Ω are shown in graphical form for different conditions. Figure 2.14 shows the dimensionless axial displacement ahead of the tunnel face with various *H/D* conditions, while Figure 2.15 provides the dimensionless axial displacement ahead of the tunnel face with various K_0 conditions.
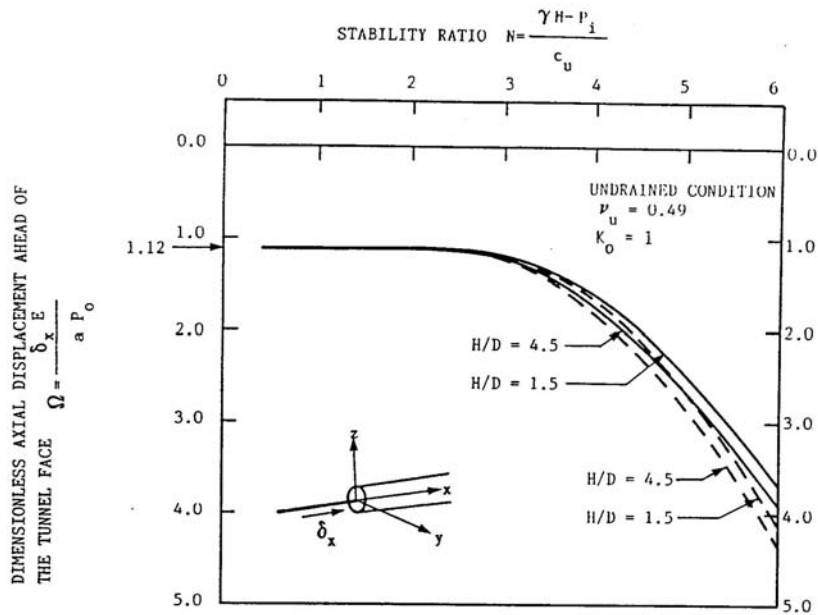
Figure 2.14: Dimensionless Axial Displacement Ahead of the Tunnel Face with Various *H/D* Conditions (Lee *et al.,* 1992)

STABILITY RATIO $N = \dfrac{\gamma H - P_i}{c_u}$

DIMENSIONLESS AXIAL DISPLACEMENT AHEAD OF THE TUNNEL FACE

$\Omega = \dfrac{\delta_x \, E}{a \, (K_o P'_v + P_w - P_i)}$

UNDRAINED CONDITION
$\nu_u = 0.49$
$H/D = 1.5$

$K'_o = 0.6$
$K'_o = 1.4$
$K'_o = 1.0$

$K'_o = 0.6$
$K'_o = 1.0$
$K'_o = 1.4$
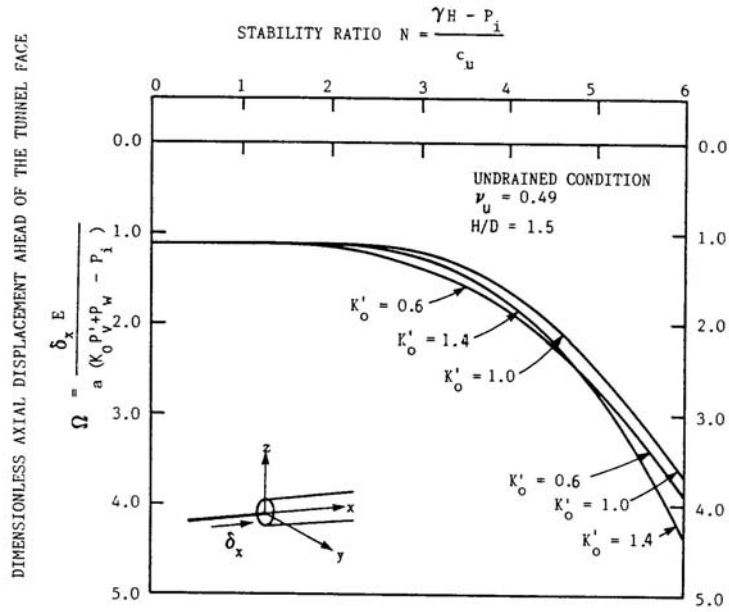
Figure 2.15: Dimensionless Axial Displacement Ahead of the Tunnel Face with Various K_0 Conditions (Lee *et al.,* 1992)

(iii) Ground Losses over the Shield

In practise, tunnel operators incorporate a small slightly elevated pitch angle to avoid the downward tendency of the shield due to its own weight. In some circumstances, the usage of the copy cutter enables the shield to turn around, while simultaneously causing over-excavation of the soil. These most common alignment problems over-cut the ground near the crown of the tunnel. Figure 2.16 further explains the ground losses over the shield due to workmanship.
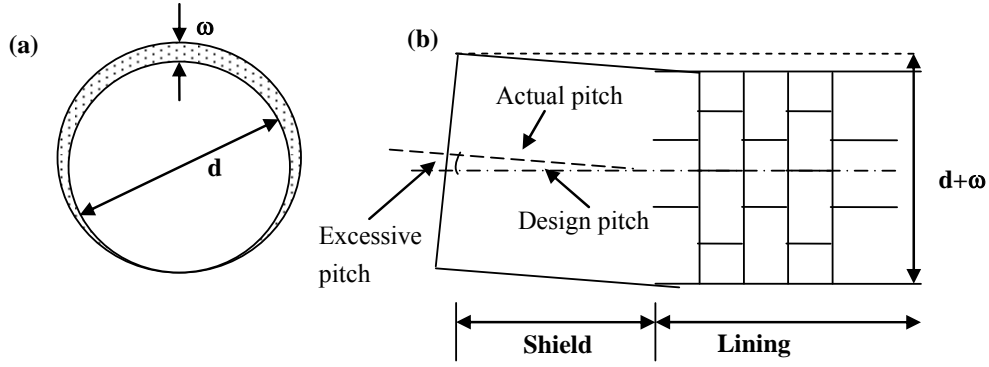
(a) Ground loss owing to pitching of tunnel shield, (b) equivalent transverse section

Figure 2.16: Ground losses over the shield (Lee *et al.*, 1992)

Lee *et al.* (1992) also developed a formula for estimating the possibility of workmanship (ω), which is

$$\omega = L \times (\text{Excessive pitch})$$

Eq.2.14

while, L is the length of the shield.

Since the intermittent alignment related to the experiences and quality of the operators and cannot be precisely estimated, Lee *et al.* (1992) defined a range of ω values as: $\omega = 0.6G_p$, when $\omega \leq \frac{1}{3}u_i$, and $\omega = \frac{1}{3}u_i$ in other circumstances. Thus, u_i is the elasto-plastic plane strain displacement at the crown (and is equal to the maximum displacement of the unlined condition of the tunnel).

2.4.2.3 Loganathan and Poulos (1998)

Loganathan and Poulos (1998) defined the equivalent ground loss ε_0 with respect to the gap parameter *g* as:

$$\varepsilon_0 = \frac{4gR + g^2}{4R^2} \times 100\%$$

Eq.2.15

where,

R   =   radius of the tunnel

g   =   gap parameter estimated using Equation 2.15

The ground loss and the ground deformation calculations proposed by Verruijt and Booker (1996) are based on uniform radial ground movement around the tunnel ovalisation (Figure 2.11, components a and b). However, as noted by Rowe and Kack (1983), the radial ground movement is not uniform, since the equivalent 2D gap around a tunnel is noncircular but oval-shaped, as shown in Figure 2.10. The reasons, given by Rowe and Kack (1983) for the formation of an oval-shaped gap around the tunnel are: (1) the tunnel operators advance the shield at a slightly upward pitch relative to the actual design grade to avoid the diving tendency of the shield; (2) the tunnel lining settles on the ground when the tail is removed; and (3) 3D elastoplastic movement of the soil occurs at the tunnel face.
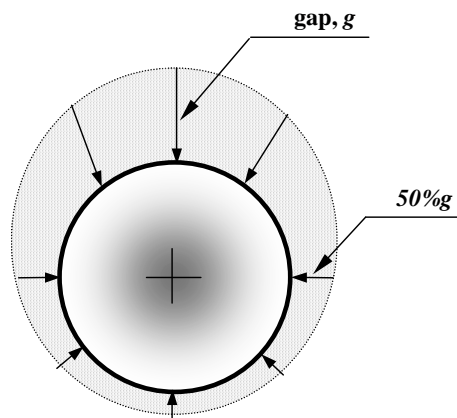
Figure 2.17: Oval-shape Ground Deformation Around Tunnel Section
(Loganathan and Poulos,1998)

As a consequence, the equivalent ground loss parameter obtained in Equation 2.15 is further modified to incorporate the non-uniform radial movement of the soil (due to the oval-shaped gap) around the tunnel, which basically influences the deformation pattern of the surrounding soil. The component of the equivalent ground loss parameter $\varepsilon_{x,z=0}$, which causes the surface settlement, may be assumed to be an exponential function that models the non-uniform movement of the soil around the tunnel, as follows:

35

$$\varepsilon_{x,z=0} \;=\; \varepsilon_0 B \cdot \exp(-Ax^2)$$

<div align="right">Eq.2.16</div>

where A, B = constants and ε_0 = equivalent ground loss, as obtained from Equation 2.23. Constants A and B can be derived, based on the boundary conditions as shown in Figure 2.18.
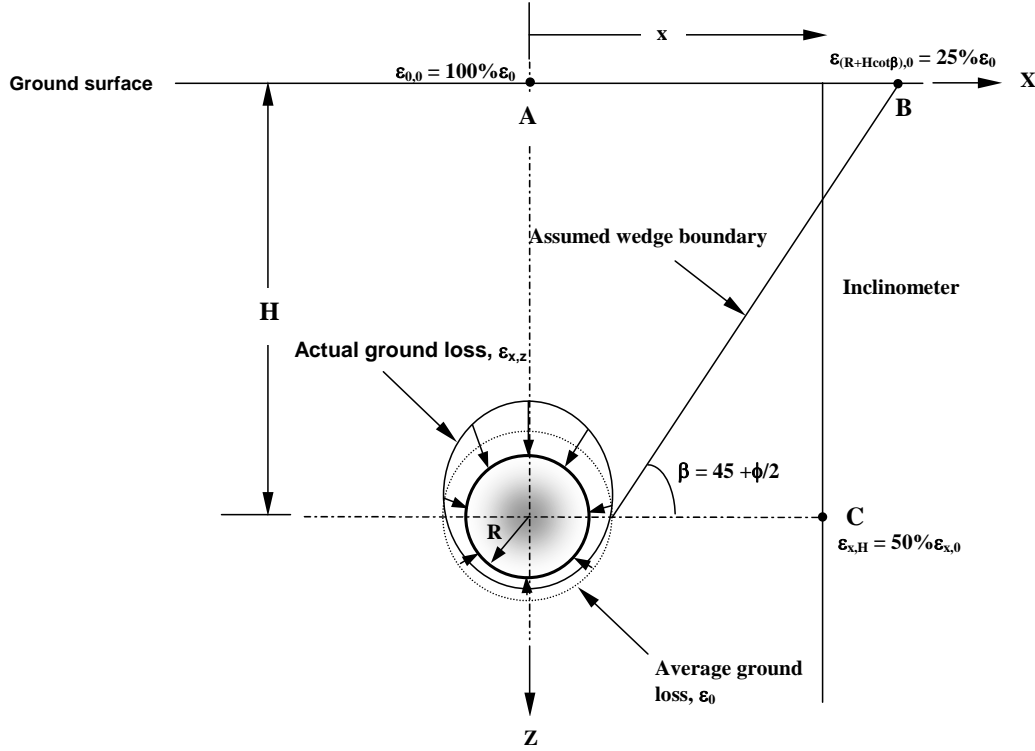
Figure 2.18: Ground Deformation Patterns and Ground Loss Boundary Conditions
(Loganathan and Poulos, 1998)

Further, when the portion of the soil above the tunnel crown touches the tunnel lining, the soil at the side of the tunnel displaces towards the bottom of the tunnel, as shown in Figure 2.19. Therefore, any upward movement of the soil below the tunnel is limited. Loganathan and Poulos (1998) assumed that, when the tunnel lining settles on the bottom of the annulus gap (due to its own-weight), the distance between the crown of the tunnel lining and the crown of the excavated surface become twice the thickness of the annulus gap (Figure 2.17). This conclusion is based on the simple geometric assumption that the void area above the tunnel springline is approximately 75% of the total void area. Thus, the authors postulated that 75% of the vertical ground movement occurs within the upper annulus of the gap around the tunnel, as shown in Figure 2.20.
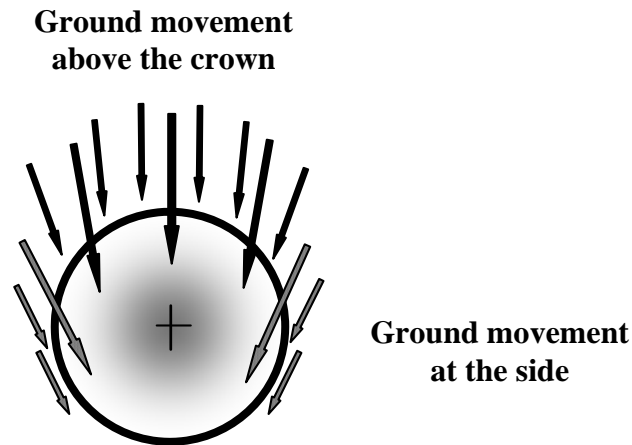
Figure 2.19: Ground Movement towards Tunnel

(Loganathan and Poulos, 1998)
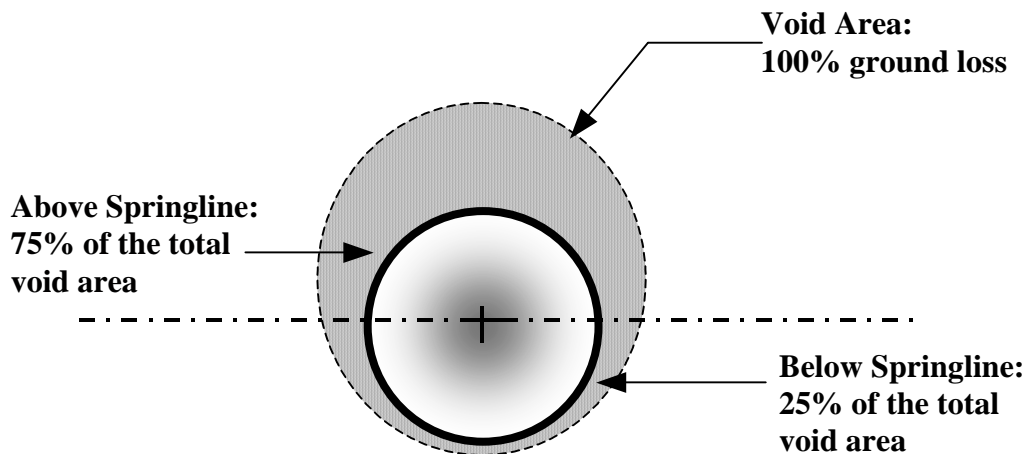
Figure 2.20: Void Areas Around Tunnel Section (Loganathan and Poulos, 1998)

The relationship between the surface deformation trough width, which is an indirect measure of the ground movement influence zone, and the tunnel depth can be expressed as a horizontal angle β drawn from the springline of the tunnel to the width of the surface deformation trough. From the observations made by Cording and Hansmire (1975), angle β can be defined as $45 + \phi/2$, where ϕ = friction angle. Therefore, for tunnelling in undrained conditions, the parameter $\beta = 45°$ and $cot\beta = 1$.

Based on the assumption stated above, the surface settlement above the tunnel axis is the complete cumulative equivalent ground loss ($100\%\varepsilon_0$) around the tunnel, as represented by point A in Figure 2.18. Furthermore, the surface settlement at the

horizontal distance ($R+Hcot\beta$), which is labelled as point B in Figure 2.18, is the partial cumulative equivalent ground loss (25% ε_0).

In the case of undrained conditions, where $\beta = 45°$, and applying the boundary conditions in Figure 2.18 on Equation 2.16, the equivalent ground loss component that models the non-uniform vertical movement can be derived as:

$$\varepsilon_{x,z} = \varepsilon_0 \exp\left[\frac{-1.38x^2}{(H+R)^2}\right]$$

Eq.2.17

Loganathan and Poulos (1998) posited that the horizontal ground movement into the tail void or gap is at its maximum at the springline of the tunnel, and is zero at the crown and the invert of the tunnel. Therefore, the lateral ground movement is symmetrical about the tunnel axis. The lateral movement component is incorporated into the ground loss as:

$$\varepsilon_{x,z} = \varepsilon_{x,z=0}C \cdot \exp\left(-Dz^2\right)$$

Eq.2.18

where C and D are constants that are derived, based on the boundary conditions described below.

Using oval-shaped gap geometry, the magnitude of the horizontal movement at the tunnel springline is approximately half of the vertical movement at the tunnel crown; this causes 75% of the ground movement into the upper annulus of the oval-shaped gap around the tunnel. Thus, the equivalent ground loss component, due to the horizontal movement at the horizontal distance x and the depth H ($\varepsilon_{x,H}$) designated as point C in Figure 2.18, is approximately 50% of the equivalent ground loss causing surface deformation ($\varepsilon_{x,z=0}$) at the horizontal distance x.

By applying these boundary conditions (Figure 2.18) and substituting Equation 2.17 into Equation 2.18, the modified equivalent ground loss parameter, incorporating the

nonlinear ground movement (due to the oval-shaped gap) around the tunnel-soil interface, can be written as:

$$\varepsilon_{x,z} = \frac{4gR + g^2}{4R^2} \exp\left\{-\left[\frac{1.38x^2}{(H+R)^2} + \frac{0.69z^2}{H^2}\right]\right\}$$
Eq.2.19

Note that if $\delta = 0$, the surface settlement troughs predicted using Verruijt and Booker's (1996) method are wider than the observed values. Therefore, Loganathan and Poulos (1998) modified the analytical solution proposed by Verruijt and Booker, as expressed in Equation 2.6, to accommodate the newly defined ground loss parameter shown in Equation 2.19. However, the ovalization of the tunnel lining is neglected ($\delta = 0$) in their study because they believed that ovalisation only occurs over the long-term, and it is very small. Therefore, by combining Equations 2.6 and 2.19, the modified equation for the prediction of the surface deformation can be expressed as:

$$U_{z=0} = 4(1-v)R^2 \frac{H}{\left(H^2 + x^2\right)} \frac{4gR + g^2}{R^2} \exp\left[-\frac{1.38x^2}{(H+R)^2}\right]$$
Eq.2.20

Loganathan and Poulos (1998) indicated that the modified analytical solution Equation 2.20 gives a narrower surface settlement trough than the original solution Equation 2.6, provided by Verruijt and Booker (1996).

2.4.2.4 Bobet (2001)

Bobet (2001) presented the analytical solution for a shallow tunnel, in saturated ground, by expanding the solution developed for deep tunnels in dry ground by Einstein and Schwartz (1979). In such a situation, the following assumptions are made (Figure 2.21):

- the circular cross section has a radius r_o
- the plane strain conditions are in a direction perpendicular to the cross section of the tunnel

- a gap between the tail of the shield and the liner is assumed to be constant, $w = \dfrac{ground\ loss(\%)}{100} \dfrac{\pi r_0^2}{2\pi r_0} = \dfrac{ground\ loss(\%)}{200} r_0$

- there is full slippage between the ground and the liner
- the depth to the radius ratio is larger than 1.5 (for smaller values, the solutions are not valid due to the effect of ground surface)
- the soil is assumed to be homogenous
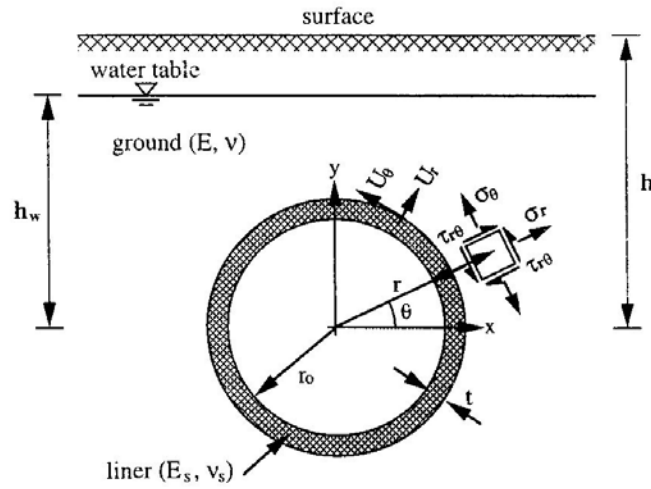
Figure 2.21: Shallow Tunnel Notations (Bobet, 2001)

Since the focus of this study is on the short-term ground movements of a tunnel in a saturated ground, with or without air pressure during construction, the relevant solutions are described here (Bobet, 2001).

The ground displacements of a tunnel in saturated ground without air pressure are obtained as:

$$u_r = \frac{1+v}{E}\left\{-\frac{a_0}{r} + \left[\frac{c'_1}{r^2} + \frac{1}{2}c_1 \ln r\right]\sin\theta + \left[2\frac{a'_2}{r^3} + a\frac{b'_2}{r}\right]\cos 2\theta + \left[3\frac{c'_3}{r^4} + 3\frac{d'_3}{r^2}\right]\sin 3\theta\right\}$$ Eq.2.21

$$u_\theta = \frac{1+v}{E}\left\{-\left[\frac{c'_1}{r^2} + \frac{1}{2}c_1(1+\ln r)\right]\cos\theta + 2\frac{a'_2}{r^3}\sin 2\theta - \left[3\frac{c'_3}{r^4} + 3\frac{d'_3}{r^2}\right]\cos 3\theta\right\}$$ Eq.2.22

where,

u_r and u_θ = displacements in coordinate (r, θ), in Figure 2.21

40

$$a_0 = \frac{1}{2} \frac{[\gamma_b h(1+K) + 2\gamma_w h_w](1-\nu^2)CF + 2E(C+F)(w/r_0)}{(C+F)(1+\nu) + (1-\nu^2)CF} r_0^2 \qquad \text{Eq.2.23}$$

$$c_1 = -(\gamma_b + \gamma_w)r_0^2 \qquad \text{Eq.2.24}$$

$$c_1' = -\frac{1}{8}\gamma_b(1-K)r_0^4 \qquad \text{Eq.2.25}$$

$$a_2' = -\frac{1}{4}\frac{(1-\nu)F+3}{(1-\nu)F+6}\gamma_b h(1-K)r_0^4 \qquad \text{Eq.2.26}$$

$$b_2' = \frac{1}{4}\frac{2(1-\nu)F+3}{(1-\nu)F+6}\gamma_b h(1-K)r_0^2 \qquad \text{Eq.2.27}$$

$$c_3' = \frac{1}{12}\frac{(1-\nu)F+12}{(1-\nu)F+24}\gamma_b(1-K)r_0^6 \qquad \text{Eq.2.28}$$

$$d_3' = -\frac{1}{8}\frac{(1-\nu)F+8}{(1-\nu)F+24}\gamma_b(1-K)r_0^4 \qquad \text{Eq.2.29}$$

ν = Poisson' ratio

E = Soil modulus of elastic

C and F are the compressibility and flexibility ratios, respectively, defined as:

$$C = \frac{Er_0(1-\nu_s^2)}{E_s A_s(1-\nu^2)} \qquad \text{Eq.2.30}$$

$$F = \frac{Er_0^3(1-\nu_s^2)}{E_s I_s(1-\nu^2)} \qquad \text{Eq.2.31}$$

A_s and I_s = the area and moment of inertia of the cross section of the liner per unit length of tunnel; γ_b and γ_w = the buoyant unit weight of the ground and the unit weight of water; K = the coefficient of the earth pressure at rest; h and h_w = the depth of the tunnel below the ground surface and below the water table, respectively.

The solution with air pressure is given by Equations 2.29 and 2.30 with:

$$a_0 = \left[\frac{1}{2}\gamma_b h(1+K) + \gamma_w h_w - p_a + \frac{(1-v^2)CFp_a + E(C+F)(w/r_0)}{(C+F)(1+v) + (1-v^2)CF}\right]r_0^2$$ Eq.2.32

$$c_1 = -(\gamma_b + \gamma_w)r_0^2$$ Eq.2.33

$$c_1' = -\frac{1}{8}\gamma_b(1-K)r_0^4$$ Eq.2.34

$$a_2' = -\frac{1}{4}\gamma_b h(1-K)r_0^4$$ Eq.2.35

$$b_2' = \frac{1}{2}\gamma_b h(1-K)r_0^2$$ Eq.2.36

$$c_3' = \frac{1}{12}\gamma_b h(1-K)r_0^6$$ Eq.2.37

$$d_3' = -\frac{1}{8}\gamma_b h(1-K)r_0^4$$ Eq.2.38

Since small variations of w may have a large effect on soil displacements, the estimation of w is important. The gap parameter g can be obtained from one of the following two methods (Chou and Bobet, 2002):

- Using the same definition of the gap parameter (g) from Equation 2.7 (Lee $et\ al.$, 1992), or
- Back-calculation from the estimated or measured ground loss:

$$ground\ loss = \frac{\pi(r_0+w)^2 - \pi r_0^2}{\pi r_0^2} \cong \frac{2w}{r_0}$$ Eq.2.39

However, it should be noted that the gap parameter w, used by Chou and Bobet (2002), is half of the gap parameter g, suggested by Lee $et\ al.$ (1992); this is because Bobet's solution assumes that there is a circular ground deformation pattern around the tunnel section, not an oval-shaped pattern.

2.4.3 Two Dimensional Numerical Methods

While tunnel excavation can be considered as a 3D problem (Swoboda, 1979; Swoboda and Abu-Krisha, 1999), full 3D numerical analysis is time consuming and requires excessive computational resources. Consequently, 2D analysis is considered to be sufficiently flexible and economic, in terms of both person-hours and computer-hours, to find application in practice. This section is, therefore, aimed at summarising various 2D methods. These methods have been proposed to take into account the change in stresses and strains owing to tunnelling when adopting plane strain analyses to simulate tunnel construction.

2.4.3.1 Rowe et al. (1983), Rowe and Kack (1983)

Rowe *et al.* (1983) proposed a 2D numerical method for estimating surface settlement owing to tunnelling. This method takes into account the soil-lining interaction, lining weight and plastic failure within the soil. The following key tunnelling factors are approximated by a so called "Gap parameter";

- volume decrease of soil in a remoulded zone due to shield advancement
- movement of soil in front of tunnel head, both radially and axially, towards the tunnel face (see Peck, 1969)
- loss of ground caused by the presence of an annular void, which is the difference between a mined diameter and an outer lining diameter.

As illustrated in Figure 2.22 (a), the annular void is equal to the difference between the diameter of the excavated surface (*D*) and the lining (*d*). While the shield advances, the weight of the lining will cause it to rest on the excavated surface, as shown in Figure 2.22 (b). In this case, the gap parameter can be determined as a vertical distance from the crown of the tunnel lining to the crown of the excavated surface.
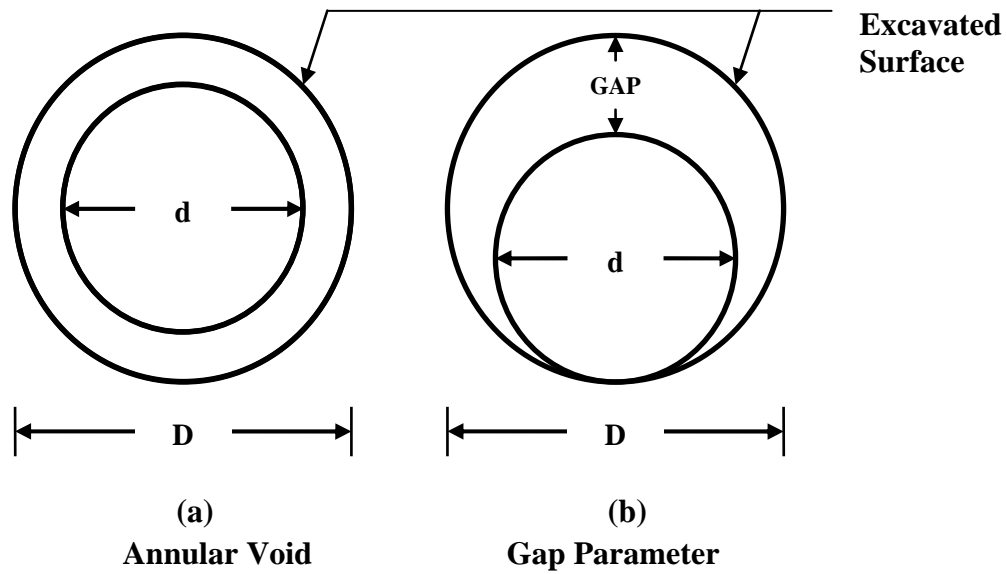
Figure 2.22: Definition of Annular Void and Gap Parameter
(Rowe and Kack, 1983)

In the method by Rowe *et al.'s* (1983), extensive parametric studies have been undertaken to identify the potentially significant factors that affect the prediction of settlement due to a soft ground tunnel. A total of six governing parameters, including gap parameter, anisotropic of soil elastic parameter, coefficient of earth pressure at rest (K_0), plasticity parameters, grouting pressure and soil unit weight, have been considered in their study. The results show that the gap parameter used in the plane strain analysis is the most critical governing parameter.

2.4.3.2 Finno and Clough (1985)

A technique for using 2D finite element analyses to simulate the actual process of the Earth Pressure Balance (EPB) shield tunnelling has been proposed by Finno and Clough (1985). This technique involves plane strain analyses of both longitudinal and transverse sections of the tunnel; it accounts for an initial soil heave away from the tunnel face caused by shield advancement.

The entire EPB tunnelling process is divided into five calculation stages. Material nonlinearity and time effects are accounted for by using an incremental procedure and by allowing for pore pressure dissipation in each stage. The longitudinal section

analysis was adopted in the first stage of loading to study the behaviour of soil ahead of the shield. The results in this stage provide significant information concerning the pressure distribution, which then will be used to simulate the heaving process in the transverse section analysis (in stages 2-5).

Importantly, the proposed longitudinal-transverse method of Finno and Clough (1985) involves a plane strain analysis of the longitudinal tunnel, to basically model an infinite slot cut in the soil at some depth below the ground. A series of 3D finite element analyses by Rowe and Lee (1992) showed that longitudinal settlement profiles, from such a plane strain approach, significantly overestimate the ground deformations and extend the plastic zone caused by the tunnelling process, when compared with the 3D results.

2.4.3.3 Addenbrooke et al. (1997)

Addenbrooke *et al.* (1997) carried out plane strain predictions of ground movement for both single and twin tunnel excavations in stiff clay. The analyses modelled the geometry of the twin Jubilee Line Extension Project tunnels; the field data were compared with the analytical results. In their method, volume loss (V_L) parameters were calculated from the settlement data and then were used as control parameters. The tunnel excavation process was simulated by the removal of material from the finite element mesh over a number of increments. After each increment had finished, the volume loss is calculated. As soon as the prescribed volume loss is reached the lining is placed. If the analysis only focuses on the ground displacement (and no results of the lining stresses and moment are required), the analysis can be terminated after the required volume loss has been achieved.

Parametric studies were performed to highlight the effect of isotropic and anisotropic parameters using a series of 2D tunnelling analyses. The models were used to investigate the effects of different pre-yield soil models, namely:

(1) linear elastic perfectly plastic, with Young's modulus increasing with depth

(2) isotropic non-linear elastic, based on the formulation by Jardine *et al.* (1986). The shear stiffness varies with the deviatoric strain and mean effective stress, while the bulk stiffness depends on the volumetric strain and the mean effective stress (referred to as J4 in the original publication).

(3) isotropic non-linear elastic analysis with shear and bulk stiffness, depending on the deviatoric strain and the mean effective level (referred to as L4 in Figure 2.23). This model also accounts for loading reversals.

(4) anisotropic non-linear elastic, which has been adapted from the J4 model (referred to as AJ4 in Figure 2.24).

The above models were combined with a Mohr-Coulomb yield surface. Figure 2.23 shows the surface settlement obtained from the pre-yield soil models described above. Addenbrook *et al.* (1997) stated that it is necessary to include small strain stiffness into the pre-yield model as the predictions of the linear elastic model are inadequate (see Figure 2.23). Some similar results, which have revealed an ineffectiveness in the linear elastic models for both isotropic and anisotropic, can also be found in the literature (Attewell and Farmer, 1974; Nyren, 1998). For the non-linear models of Addenbrooke *et al.* (1997), referred to as J4 and L4 in Figure 2.23, the results from non-linear analyses performed under volume loss control have improved in comparison to the linear analyses. However, both models predict similar settlement troughs which are too wide and too shallow, when compared to the filed data.
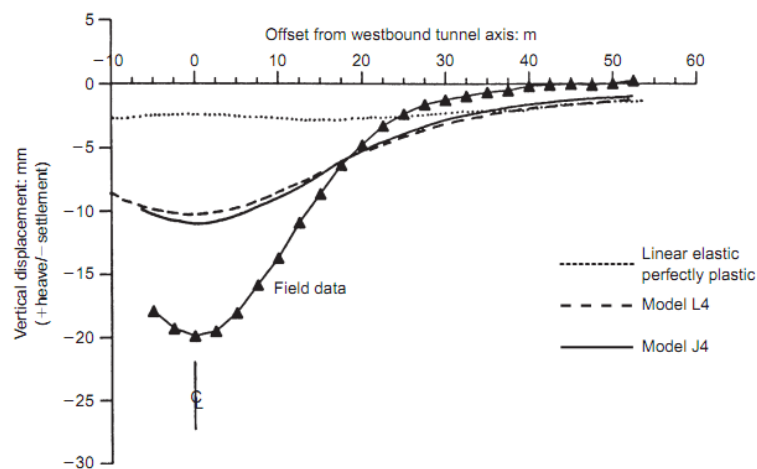
Figure 2.23: Surface Settlement Troughs Obtained from Different Isotropic Soil Models (L4 and J4) (Addenbrooke *et al.*, 1997)
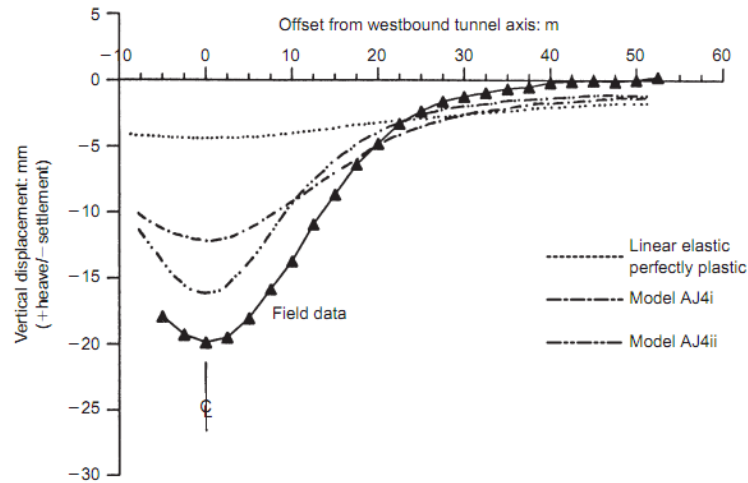
Figure 2.24: Surface Settlement Troughs Obtained from Difference Anisotropic Soil Models (AJ4i and AJ4ii) (Addenbrooke *et al.*, 1997)

Gens' (1995) research highlighted that K_0 plays a key role in the prediction of tunnel construction. He also stated that the importance of K_0 is often neglected in the published literature. Continuing in the same vein, Addenbrooke (1996) conducted a parametric study to investigate the effect of K_0 in a surface settlement trough by comparing both $K_0 = 1.5$ and 0.5 with the field measurements. He concluded that, with $K_0 = 1.5$, the surface settlement trough showed as too shallow and too wide a pattern, when compared with the field measurements. On the other hand, with a lesser K_0, better results were obtained from the analysis.

Further, the technique of introducing a reduced zone of K_0 to obtain improved surface settlement profiles has been proposed by Potts and Zdravković (2001). This method was adopted in the analyses of the Jubilee Line tunnel project. Basically, a local zone of reduced K_0 of 0.5 (reduced from the original K_0 (1.5) of London Clay) was assumed to extend horizontally between the crown and the invert of the tunnel, for a distance equal to three times the excavated radius (Figure d). As shown in the axisymmetric analysis of tunnel heading (Addenbrooke, 1996), the effective stress ratio reduced to the side and increased above and below the tunnel. Such a change in the stress state can be represented in a plane strain analysis by introducing the local zone of reduced K_0.
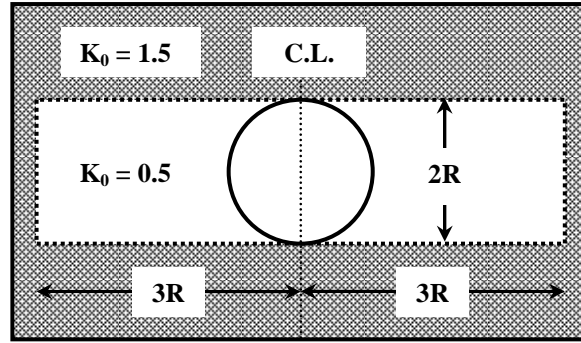
Figure 2.25: Layout of Zone of Reduced K_0 (after Potts and Zdravković, 2001)

Lee and Rowe (1989) also carried out linear elastic perfectly plastic finite element analyses of tunnelling, specifically to show the influence of cross-anisotropic parameters in pre-failure. Importantly, the terms cross-anisotropic or transversely anisotropic in the soil parameter mean that soil has the same material properties in any horizontal direction, but has different properties in the vertical direction.

Indeed, Lee and Rowe (1989) concluded that the finite element predicted better settlement profiles when the soil anisotropy has been included in the soil model. In particular, they suggested that more attention should be given to the ratio of the independent shear modulus to the vertical modulus. In Addenbrooke *et al.* (1997), the non-linear anisotropic pre-yield soil model (as listed above) had included the cross-anisotropic soil parameters, as derived from the small strain stiffness formulation of the original isotropic model. Two analyses were performed using the proposed model (AJ4). In the first analysis (referred to as AJ4i in Figure 2.24), anisotropic ratios from the observed field measurements data, reported by Burland and Kalra (1989), were adopted. The ratio of the vertical to the horizontal Young's modulus (E_v'/E_h') was kept as 0.625, while the ratio of the shear modulus to the vertical Young's modulus (G_{vh}/E_v') equalled 0.44. In the second analysis (referred to as AJ4ii in Figure 2.24), the clay was assumed to be very soft in the shear, with the G_{vh}/E_v' ratio was reduced to 0.2.

As illustrated in Figures 2.23 and 2.24, it appears that the first anisotropic analysis (AJi) yielded slightly better results for the settlement trough profile compared to the non-linear elastic isotropic soil parameter analysis (model L4 and J4). In contrast, the

second anisotropic analysis gave a significantly improved settlement profile, with the reduced ratio of G_{vh}/E_v'.

2.4.3.4 Karakus and Fowell (2003; 2005)

Karakus and Fowell (2003) studied the ability of the New Austrian tunnelling Method (NATM to control settlements in London Clay. Three different face advance techniques (Figure 2.26) were used for three trial tunnel constructions (namely the Heathrow Express Trial tunnel). The details of each advance techniques are as follows:

1. Twin sidewall excavation/drift (TS1): two shotcrete walls were constructed to separate the tunnel face into 3 partitions; 2 partitions at both edges were excavated first, followed by one in the middle.
2. Single side wall excavation/drift (TS2): one shotcrete wall was constructed to separate the tunnel face into 2 partitions.
3. Crown, Bench and Invert excavation (TS3): neither shotcrete walls nor excavations was undertaken from top to the bottom.

The results from the trial tunnel construction proved that the Single Side Wall excavation (TS2) produced the minimum settlement above tunnel CL, with only TS2 being subjected to the research.

| TS1 | TS2 | TS3 |
| Twin side wall drift | Single side wall drift | Crown, bench and invert |
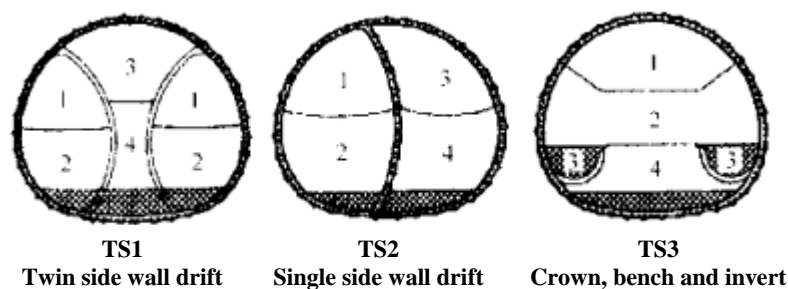
2.26: Heathrow Express Trial Tunnel (Bower, 1997)

The materials encountered at the site consisted of London Clay, at a depth of 4.2 m, overlain by coarse gravel, with 0.3 m of cement-stabilised material and, above this, a

bitumen-covered car park on made ground. The construction of the trial tunnel was carried out approximately 16.8 m below the surface.

The 2D finite element analyses were conducted using ABAQUS software. The undrained material properties of London Clay were used, as well as the Modified Cam Clay parameters (adopted from oedeometer tests and undrained triaxial test back analysis). For the shotcrete elements, an elastic beam element was used.

In the multi-stage excavation simulation, the Hypothetical Modulus of Elasticity (HME) soft lining approach was adopted, as well as its reduction parameter for the short-term elasticity modulus of the lining. Three models, namely sequential excavation model (SEM), two-stage excavation model (TSM), and the full-face excavation model (FFM), were carried out in the 2D plane strain FE analysis, with respect to the 3D tunnelling effects and the deformations prior to the shotcrete installation.

The results from this analysis showed that the Sequential excavation model (SEM), which has the most number of steps for its calculation, predicted the settlement profiles in close agreement with the field measurements, especially when compared with other models. However, the use of appropriate values for the HME is required. The analysis also showed that the actual NATM excavation process, which involves a 3D tunnelling effect, can be simulated effectively by modelling the excavation processes as closely as possible to the field sequence, using the 2D finite element analysis. The study also provided the relationship between the maximum surface settlement and the HME values, in accordance with the face advance sequence adopted.

Further study to confirm the HME approach has been undertaken by Karakus and Fowell (2005). Both the finite difference method (FDM) and the finite element method (FEM) were adopted in the 2D plane strain analyses. The isotropic soil parameters were used in the Mohr-Coulomb plasticity model to represent the stress-stain behaviour for the entire subsoils, including London Clay, Thames gravel, and made ground. The results of this study revealed that both FDM and FEM gave a reasonably close agreement with each other, as well as with field measurements for the tunnel enlargement. However, the FDM analysis produced better surface settlement

predictions for the sidewall excavation. The authors point out that this arises because of the variation of the London Clay elasticity modulus with depth, which was considered in the FDM analysis. They also suggested that, for further numerical study, soil anisotropy should be considered when tunnelling in London Clay.

In 2006, Karakus and Fowell conducted 3D numerical analysis with the same Heathrow Express Trial Tunnel case study. They concluded that the proposed method of using the HME approach in 2D analysis gave a good agreement, especially when compared with the 3D approach and the field measurements.

2.4.3.5 Summary of 2D Numerical Analysis

The details of the 2D numerical analyses, presented in the above literature review, are summarised in Table 2.4. Also, the following conclusions can be drawn:

- The process of tunnelling is clearly a 3D problem. When modelling the tunnel excavation process, using a 2D plane strain analysis, some approximate methods, as proposed by the above authors, are needed to take into account the stress redistribution ahead of the tunnel face.
- In a 2D plane strain analysis, small strain soil stiffness is an important factor when seeking to obtain a close agreement with the field monitoring. However, the influence of soil anisotropy in improving settlement trough predictions, due to tunnelling, is still in doubt.
- Different construction sequences and methods of advancing face will result in significantly diverse ground settlements when dealing with NATM tunnelling. As the lining is done by shotcreting, an appropriate approach, that assumes green and fully hardened lining stiffness need to be considered.

Table 2.1: Details of 2D Finite Element Analyses Reviewed in This Section

Author(s)	Project	Material	Soil Model	Method of Tunnelling	D (m)	Z_0 (m)	K_0	Program
Rowe *et al.* (1983)	Thunder Bay sewer tunnel	Isotropic/cross anisotropic	Linear elasto-plastic		2.38	10.5	0.6	EPTUN
Finno and Clough (1985)	N-2 tunnelling project	Isotropic	Modified Cam-Clay	EPB shield	2.9*	11.5*	-	-
Addenbrooke *et al.* (1997)	Jubilee Line Extension project	Isotropic/ anisotropic	Linear/non-linear elastic perfectly plastic	EPB shield	4.75	10/35	1.5	ICFEP
Karakus and Fowell (2003)	Heathrow Express Trial tunnels	Isotropic	Modified Cam-Clay	NATM	7.9 (h) 9.2 (w)	25	1.15	ABAQUS
Karakus and Fowell (2005)	Heathrow Express Trial tunnels	Isotropic	Linear elastic perfectly plastic	NATM	7.9 (h) 9.2 (w)	25	1.15	FLAC

*: The measurement was not specified in the text of publication. The given value was determined from plots, graphs, etc.

2.5 Constitutive Models of Soil Behaviour

In recent years, numerical methods have become standard tools in the analysis of geotechnical problems. This use is principally owed to the availability of sufficient computer capability to solving 2D and 3D analyses, as well as to the continuous achievements being made in the development of the constitutive soil models. Although a large number of constitutive models have been developed, the majority are predominantly used for research oriented proposes. Schweiger (2009) grouped practical oriented constitutive models into five categories:

1. Linear or non-linear elastic models
2. Elastic-perfectly plastic models
3. Isotropic hardening single surface plasticity models
4. Isotropic hardening double surface plasticity models
5. Kinematic hardening multi-surface plasticity models

In the first category, the elastic model, soil behaviour is said to be elastic, with one stiffness parameter used. In most cases, the results from the elastic model are unrealistic and, therefore, should not be adopted in practice. The second category, elastic-perfectly plastic (Mohr-Coulomb) model, is relatively simple, and is considered the most widely used model among practising engineers. The elastic-perfectly plastic model seems to be sufficient for some areas of geotechnical problems, especially when being used by experienced engineers. For example, the deformation of the diaphragm wall, induced by excavation, can be actually predicted when used in conjunction with a total stress analysis and a back analysed stiffness parameter (Phienwej, 2009; Lim *et al.*, 2010). However, care must be taken because the stress path predicted by this model can be misleading and results in an over-prediction of soil strength in the case of soft clays.

The isotropic hardening single surface plasticity model category (the third category) is the first step to modelling real soil behaviour. The principal soil model of this category is the Modified Cam-Clay (MCC) Model (Roscoe and Burland, 1968). The MCC Model introduced an elliptic yield surface which separates the elastic behaviour

from the plastic behaviour. The application of this mode has been widely accepted, especially for cases of embankments on soft clay modelling. Where there is an unloading problem, such as an excavation, the soil stress path remains generally inside the yield surface. Thus, the predicted deformations are governed by the elastic behaviour.

The forth category is the isotropic hardening double surface plasticity model. The predominant model in this category is the Hardening Soil Model (Schanz *et al.*, 1999), which was developed from the double hardening model, introduced by Vermeer (1978). It is believed that this type of model will replace the standard Mohr Coulomb Model in the future and, thus, has been the main focus of the current study.. This type of model gives more realistic displacement patterns for the working load conditions, especially in the case of an excavation. The predicted ground movement patterns induced by tunnelling are realistic and have no influence on the finite element boundary conditions (Schweiger, 2009). An extension of the Hardening Soil Model (HSM), to incorporate the small strain behaviour of soil, is also available in the Hardening Soil Model with Small Strain Stiffness: (HSS) Model (Benz, 2006).

The last category contains the kinematic hardening multi-surface plasticity models. These models are generally able to capture more complex soil behaviour, including softening, small strain, anisotropy, and structured soils. Examples of soil models in this category are the Kinematic Hardening Model or Bubble Model (Al Tabbaa and Wood, 1989; Wood, 1995), and the Three-Surface Kinematic Hardening (3-SKH) Model (Atkinson and Stallebrass, 1991). Such models have been developed from the Cam-Clay Model and, therefore, share the basic assumptions of linear behaviour within the elastic (recoverable) state, while the associated flow rule at the yield surface is applied. Other, more complex, soil models, such as the MIT-E3 Model (Whittle and Kavvadas, 1994), use different assumptions, for example, non-linear behaviour in recoverable state and non-associated flow rule. These models require large numbers of, and more complicated, input parameters. Further, they are not yet available in commercial softwares.

From all five categories of soil models mentioned above, four soil models (i.e. Mohr Coulomb Model, Soft Soil Model, Hardening Soil Model, and Hardening Soil Model

with Small Strain Stiffness) will be used in the current study. They are also discussed in the following subsections.

2.5.1 Mohr Coulomb Model

In 1773, the French engineer Coulomb introduced his analysis of the thrust acting on a retaining wall. Thus the soil failure condition in the analysis is now called the Mohr-Coulomb failure criterion. In the Mohr-Coulomb yield surface, the soil is assumed to behave as a linear elastic perfectly plastic material; thus no hardening/softening rules are required. The failure criterion for the model is shown in Figure 2.27 and can be expressed as:

$$\tau_f = \sigma_{nf}' \tan\phi' + c' \qquad \text{Eq.2.40}$$

where, τ_f and σ_{nf}' are the shear and the normal effective stresses on the failure plane, respectively. The Mohr-Coulomb yield function, when formulated in term of effective principal stress, is given as:

$$f = \frac{1}{2}(\sigma_1' - \sigma_3') + (\sigma_1' + \sigma_3')\sin\phi' - c'\cos\phi' \qquad \text{Eq.2.41}$$

where, σ_1' and σ_3' are the major and minor effective principal stresses, respectively.

The full Mohr-Coulomb yield from two plastic model parameters, friction angle (ϕ') and cohesion (c'), together represent a hexagonal cone in the principal stress space as, shown in Figure 2.28.
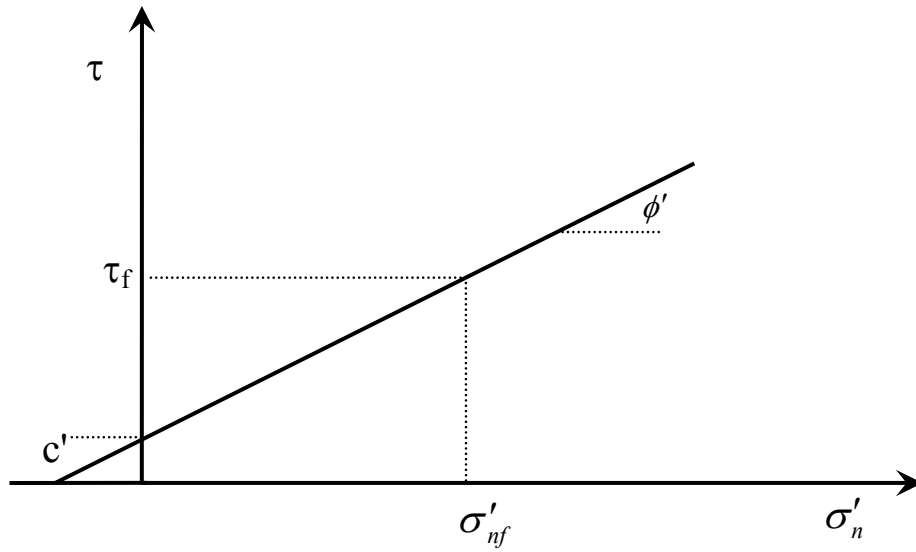
Figure 2.27: Mohr-Coulomb Failure Criterion
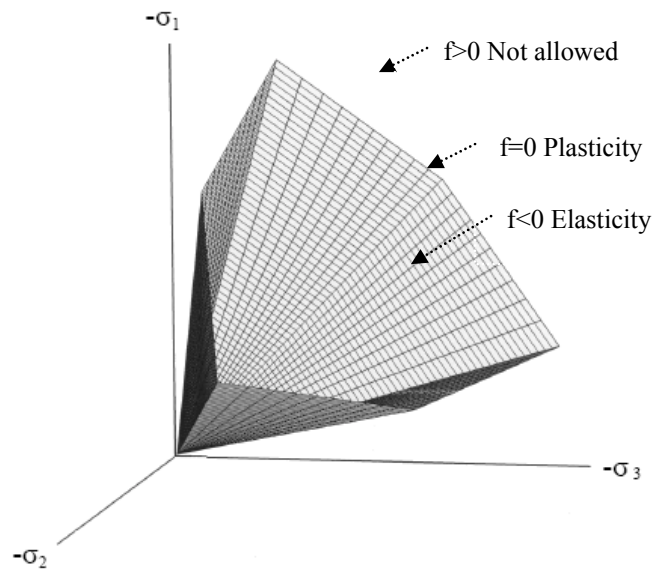
Figure 2.28: Mohr-Coulomb Yield Surface in Principal Stress Space ($c' = 0$)

The Mohr-Coulomb Model requires a total of five parameters (see Table 2.2). The following sections summarise the details of those parameters.

Table 2.2: Mohr Coulomb Model Input Parameters

Parameter	Description	Parameter evaluation
ϕ'	Internal friction angle	Slope of failure line from MC failure criterion
c'	Cohesion	y-intercept of failure line from MC failure criterion
ψ	Dilatancy angle	Function of ε_a and ε_v
E_{50}	Reference secant stiffness from drained triaxial test	y-intercept in $\log(\sigma_3/p^{ref})$-$\log(E_{50})$ space
v	Poisson's ratio	0.3-0.4 (drained), 0.5 (undrained)
K_o^{nc}	Coefficient of earth pressure at rest (NC state)	1-$\sin\phi'$ (default setting)

a) *Young's Modulus (E)*

The Young's modulus is a basic stiffness modulus which relates the soil stress and the strain. Generally, the secant modulus at 50% strength, denoted as E_{50}, is suitable for soil loading conditions, see Figure 2.29.
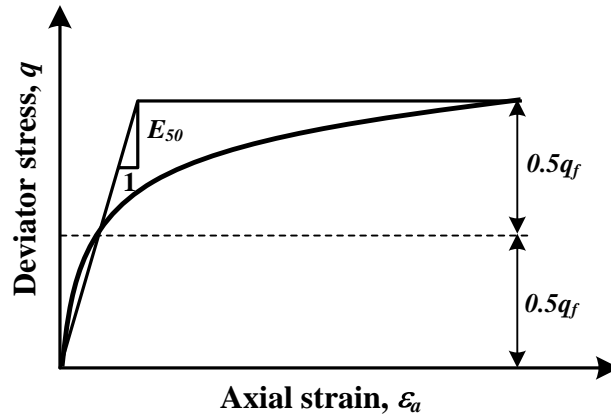
Figure 2.29: Definition of E_{50}

The relationship between Young's modulus (*E*) and other stiffness moduli, such as the shear modulus (*G*) and the bulk modulus (*K*), is given as:

$$\frac{1}{E} = \frac{1}{9K} + \frac{1}{3G}$$

Eq.2.42

$$\frac{-v}{E} = \frac{1}{9K} - \frac{1}{6G}$$

Eq.2.43

Equations 2.35 and 2.36 can be rearranged and give:

$$G = \frac{E}{2(1+\upsilon)}$$
Eq.2.44

$$K = \frac{E}{3(1-2\upsilon)}$$
Eq.2.45

$$E_{oed} = \frac{(1-\upsilon)E}{(1-2\upsilon)(1+\upsilon)}$$
Eq.2.46

where, E_{oed} refers to the Young's modulus in the oedometer test under constrained conditions.

b) *Poisson's Ratio (υ)*

The drained Poisson's ratio of soils in the loading condition ranges in a narrow band from 0.3 to 0.4 (Bowles, 1986). For an undrained condition, the undrained Poisson's ratio is 0.5. However, using the exact undrained Poisson's ratio of 0.5 leads to numerical difficulty, and so $v_u = 0.495$ is suggested.

c) *Cohesion (c′)*

The cohesion ($c′$) has the dimension of stress. In the Plaxis software, even for cohesionless materials ($c′ = 0$), it is advised to adopt a small value of cohesion (at least $c′ > 0.2$ kN/m^2) to avoid computational complications.

d) *Friction Angle (ϕ′)*

The friction angle ($\phi′$) is obtained from a plot of shear stress versus normal stress, as shown in Figure 2.27 (Mohr-Coulomb failure criterion). The unit of friction angle is in degrees.

e) *Dilatancy Angle (ψ)*

The dilatancy angle (ψ) is specified in degrees. Bolton (1986), in relation to Plaxis, recommended the correlation of the friction angle and the dilatancy

angle for cohesionless materials. For cohesive materials, which tend to have a small dilatancy, the value of $\psi = 0$ would be realistic for use in a general case.

2.5.2 Soft Soil Model

The Soft Soil Model (SSM) has been developed within the Critical State Soil Mechanics (CSSM) frameworks, which are similar to that of the Cam Clay (CCM) or Modified Cam Clay (MCC) Models. This section outlines the similarities and improvements of the SSM to the MCC. Table 2.3 tabulates seven input parameters for the SSM. Similar to the MCC, the modified compression and swelling indices (λ^* and κ^*), as shown in Figure 2.30, are used. To distinguish between recompression and the primary loading, a stress history parameter, namely pre-consolidation pressure (p_p), is required. This pre-consolidation pressure can be specified by the value of the over-consolidation ratio (OCR).

Table 2.3:Soft Soil Model Input Parameters

Parameter	Description	Parameter evaluation
ϕ'	Internal friction angle	Slope of failure line from MC failure criterion
c'	Cohesion	y-intercept of failure line from MC failure criterion
ψ	Dilatancy angle	Function of ε_a and ε_v
λ^*	Modified compression index	Slope of primary loading curve $\ln p'$ versus e_v space
κ^*	Modified swelling index	Slope of unloading/reloading curve $\ln p'$ versus e_v space
ν_{ur}	Unloading/reloading Poisson's ratio	0.2 (default setting)
K_o^{nc}	Coefficient of earth pressure at rest (NC state)	1-sinϕ' (default setting)
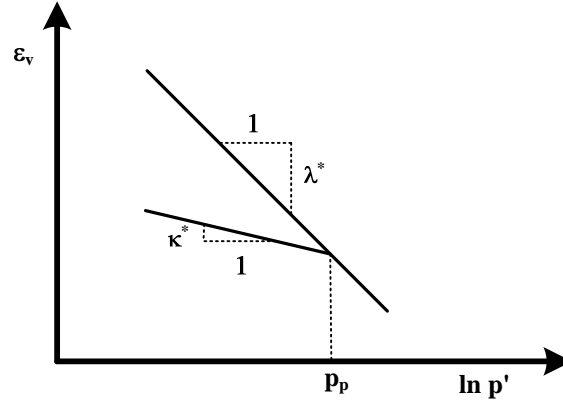
Figure 2.30: Compression and Swelling Indices and Preconsolidation Pressure

The Mohr-Coulomb failure criterion is adopted in the SSM, therefore the drained strength parameters, ϕ' and c', are required. The SSM utilises the ellipse shape yield surface, which is similar to the Modified Cam Clay Model.
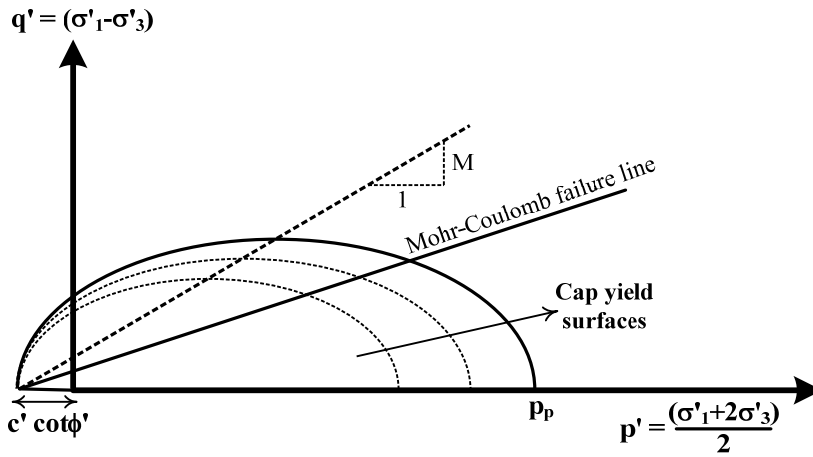
Figure 2.31: Yield Surfaces of Soft Soil Model in p'-q Space

Figure 2.31 illustrates the ellipse shape yield surfaces of the SSM. Unlike the Modified Cam Clay Model, the critical state parameter M does not govern the failure line. The Mohr-Coulomb failure criteria are used instead, while the parameter M is kept in the SSM to determine the height of the ellipses. Hence, failure line and the elliptical yield surfaces can be controlled separately. Significantly, the parameter M is not a direct input parameter in the SSM. In fact, it is calculated internally from the input parameters (K_o^{nc}, ν_{ur} and λ^*/κ^*). However, K_o^{nc} is a dominant parameter and parameter M can be approximated (Brinkgreve, 2002).

$$M \approx 2.8 - 3.0 K_o^{nc}$$

Eq.2.47

2.5.3 Hardening Soil Model

Initially the Hardening Soil Model was first introduced in the Plaxis program as an extension of the Mohr Coulomb Model (Nordal, 1999). Then, in Plaxis Version 7, an additional cap was added to the model to allow for the pre-consolidation pressure to be taken into account; at this point the soil model name was changed to the Hardening Soil Model. The change indicates that the model has the capacity to be used for softer soils, including soft clay, with the aid of the Mobilised Friction Function (Nordal, 1989).

Indeed, Hardening Soil model has developed under the framework of the theory of plasticity. In the model, the total strains are calculated using a stress-dependent stiffness, which is different for both loading and unloading/reloading. Hardening is assumed to be isotropic, depending on the plastic shear and volumetric strains. A non-associated flow rule is adopted when related to frictional hardening and an associated flow rule is assumed for the cap hardening.

Schanz *et al.* (1999) explained in detail, the formulation and verification of the Hardening Soil Model. The essential backgrounds of the model are summarised in this section. A total of 10 input parameters are required in the HSM, as tabulated in Table 2.4.

Unlike the Mohr Coulomb Model, the stress-strain relationship, due to the primary loading, is assumed to be a hyperbolic curve in the Hardening Soil Model. The hyperbolic function, as given by Kondner (1963), for the drained triaxial test can be formulated as:

$$\varepsilon_1 = \frac{q_a}{2E_{50}} \cdot \frac{q}{q_a - q}, \text{ for q < q}_f$$

Eq.2.48

61

Table 2.4: Hardening Soil Model Input Parameters

Parameter	Description	Parameter evaluation
ϕ'	Internal friction angle	Slope of failure line from MC failure criterion
c'	Cohesion	y-intercept of failure line from MC failure criterion
R_f	Failure ratio	$(\sigma_1-\sigma_3)_f / (\sigma_1-\sigma_3)_{ult}$
ψ	Dilatancy angle	Function of ε_a and ε_v
E_{50}^{ref}	Reference secant stiffness from drained triaxial test	y-intercept in $\log(\sigma_3/p^{ref})$-$\log(E_{50})$ space
E_{oed}^{ref}	Reference tangent stiffness for oedometer primary loading	y-intercept in $\log(\sigma_1/p^{ref})$-$\log(E_{oed})$ space
E_{ur}^{ref}	Reference unloading/reloading stiffness	y-intercept in $\log(\sigma_3/p^{ref})$-$\log(E_{ur})$ space
m	Exponential power	Slope of trend-line in $\log(\sigma_3/p^{ref})$-$\log(E_{50})$ space
v_{ur}	Unloading/reloading Poisson's ratio	0.2 (default setting)
K_o^{nc}	Coefficient of earth pressure at rest (NC state)	$1-\sin\phi'$ (default setting)

where, ε_1 is the axial strain, and q is the deviatoric stress. The ultimate deviatoric stress (q_f) is defined as:

$$q_f = \frac{6\sin\phi'}{3-\sin\phi'}\cdot(\sigma_3' + c'\cot\phi'),$$

Eq.2.49

and the quantity (q_a) is:

$$q_a = \frac{q_f}{R_f}$$

Eq.2.50

where, q_f is the ultimate deviatoric stress at failure, which is derived from the Mohr-Coulomb failure criterion involving the strength parameters c' and ϕ'. q_a is the asymptotic value of the shear strength. R_f is the failure ratio, if $q_f = q_a$ ($R_f = 1$), the failure criterion is satisfied and perfectly plastic yielding occurs. The failure ratio (R_f) in Plaxis is given as 0.9 for the standard default value. Figure 2.32 shows the hyperbolic relationship of stress and strain in primary loading.
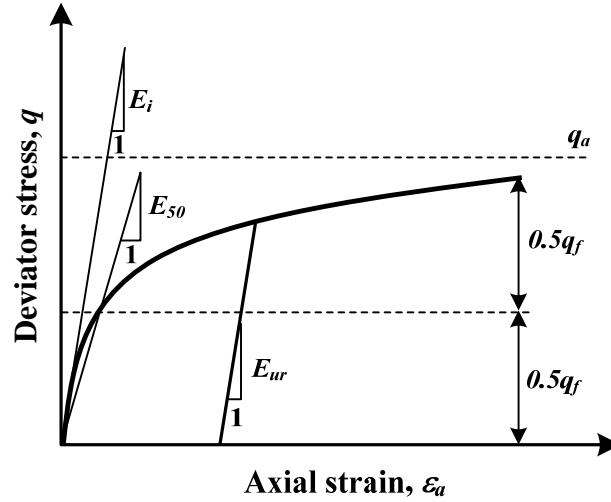
Figure 2.32: Hyperbolic Stress-Strain Relation in Primary Loading for a Standard Drained Triaxial Test (Schanz *et al.*, 1999)

The stress strain behaviour for primary loading is highly non-linear. The parameter E_{50} is a confining stress dependent stiffness modulus for primary loading. E_{50} is used instead of the initial modulus E_0 for small strain which, as a tangent modulus, is more difficult to determine experimentally, and is given as:

$$E_{50} = E_{50}^{ref} \left(\frac{c' \cos \phi' - \sigma_3' \sin \phi'}{c' \cos \phi' + p^{ref} \sin \phi'} \right)^m \qquad \text{Eq.2.51}$$

where, E_{50}^{ref} is a reference stiffness modulus corresponding to the reference stress p^{ref}. In Plaxis, a default setting $p^{ref} = 100$ kN/m^2, is used. The actual stiffness depends on the minor principal stress σ_3', which is the effective confining pressure in a triaxial test. Note that in Plaxis, σ_3' is negative in compression. The amount of stress dependency is given by the power *m*. In order to simulate a logarithmic stress dependency, as observed for soft clay, *m* should be taken as 1. Soos Von (2001) reported a range of *m* values from 0.5 to 1 in different soil types with the values of 0.9 to 1 for the clay soils.

The stress dependent stiffness modulus for unloading and reloading stress paths is calculated as:

$$E_{ur} = E_{ur}^{ref} \left(\frac{c' \cos\phi' - \sigma_3' \sin\phi'}{c' \cos\phi' + p^{ref} \sin\phi'} \right)^m$$
<div align="right">Eq.2.52</div>

where, E_{ur}^{ref} is the reference modulus for unloading and reloading, which corresponds to the reference pressure p^{ref} ($p^{ref} = 100$ kN/m^2 by default setting). For a practical case, Plaxis gives the default setting of E_{ur}^{ref} equal to $3E_{50}^{ref}$.

The shear hardening yield function (f_s) in the HSM is given as:

$$f_s = \bar{f} - \gamma^p,$$
<div align="right">Eq.2.53</div>

$$\bar{f} = \frac{q_a}{E_{50}} \frac{(\sigma_1' - \sigma_3')}{q_a - (\sigma_1' - \sigma_3')} - \frac{2(\sigma_1' - \sigma_2')}{E_{ur}},$$
<div align="right">Eq.2.54</div>

where, σ'_1 and σ'_3 are the major and minor principal stresses, E_{50} is 50 per cent secant stiffness modulus, q_a is the asymptotic value of the shear strength, and γ^p is the plastic shear strain, and can be approximated as:

$$\gamma^p \approx \varepsilon_1^p - \varepsilon_2^p - \varepsilon_3^p = 2\varepsilon_1^p - \varepsilon_v^p \approx 2\varepsilon_1^p,$$
<div align="right">Eq.2.55</div>

where, ε_1^p, ε_2^p, and ε_3^p are the plastic strains, and ε_v^p is the plastic volumetric strain.

From the formulations of the shear hardening yield function (Equations 2.53 to 2.55), it can be seen that the triaxial moduli (E_{50}^{ref} and E_{ur}^{ref}) are parameters that control the shear hardening yield surfaces. In addition to the shear hardening yield surfaces, the cap yield surfaces are also used in the HSM. These cap yield surfaces are related to the plastic volumetric strain measured in the isotropic compression condition. Figure 2.33 shows the shear hardening and the cap yield surfaces in the HSM for soil with no cohesion ($c' = 0$).
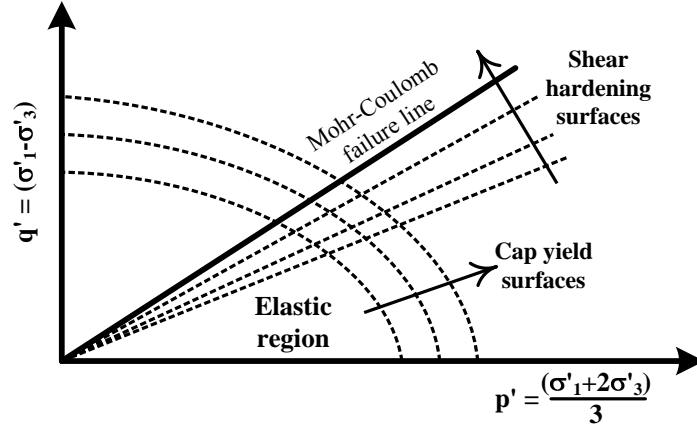
Figure 2.33: Shear Hardening and Cap Yield Surfaces in the Hardening Soil Model

The input parameter, the reference oedometer modulus (E_{oed}^{ref}), is used to control the magnitude of the plastic strains that originate from the yield cap (ε_v^{pc}). In a similar manner to the triaxial moduli, the oedometer modulus (E_{oed}) obeys the stress dependency law:

$$E_{oed} = E_{oed}^{ref} \left(\frac{c' \cos \phi' - \sigma_1' \sin \phi'}{c' \cos \phi' + p^{ref} \sin \phi'} \right)^m \qquad \text{Eq.2.56}$$

The definition of the cap yield surface can be given as:

$$f^c = \frac{\tilde{q}^2}{\alpha^2} + p^2 - p_p^2 \qquad \text{Eq.2.57}$$

where, α is an auxiliary model parameter related to K_o^{nc} (as described below). The parameters p and $\tilde{q}$ are expressed as:

$$p = \frac{-(\sigma_1 + \sigma_2 + \sigma_3)}{3} \qquad \text{Eq.2.58}$$

$$\tilde{q}^2 = \sigma_1 + (\delta - 1)\sigma_2 - \sigma_3 \qquad \text{Eq.2.59}$$

where,

$$\delta = \frac{(3+\sin\phi')}{(3-\sin\phi')}$$

Eq.2.60

$\tilde{q}$ is the special stress measure for deviatoric stresses. In the case of the triaxial compression $\tilde{q}$ reduces to $\tilde{q} = -\delta(\sigma_1 - \sigma_3)$.

The magnitude of the yield cap is determined by the isotropic pre-consolidation stress p_p. Importantly, the hardening law, which relates the pre-consolidation pressure (p_p) to the volumetric cap-strain (ε_v^{pc}), can be expressed as:

$$\varepsilon_v^{pc} = \frac{\beta}{1-m}\left(\frac{p_p}{p^{ref}}\right)^{1-m}$$

Eq.2.61

where, ε_v^{pc} is the volumetric cap strain, which represents the plastic volumetric strain in isotropic compression. In addition to the constants m and $p^{ref,}$ which have been discussed earlier, there is another model constant β. Both α and β are cap parameters, but Plaxis does not adopt them as input parameters. Instead, their relationships can be expressed as:

$$\alpha \leftrightarrow K_o^{nc} \qquad \text{(by default } K_o^{nc}=1\text{-}\sin\varphi) \qquad \text{Eq.2.62}$$

$$\beta \leftrightarrow E_{oed}^{ref} \qquad \text{(by default } E_{oed}^{ref} = E_{50}^{ref}) \qquad \text{Eq.2.63}$$

Such that K_o^{nc} and E_{oed}^{ref} can be used as input parameters that determine the magnitude of α and β, respectively. Figure 2.34 shows the ellipse shape cap surface in the $p - q$ plane.
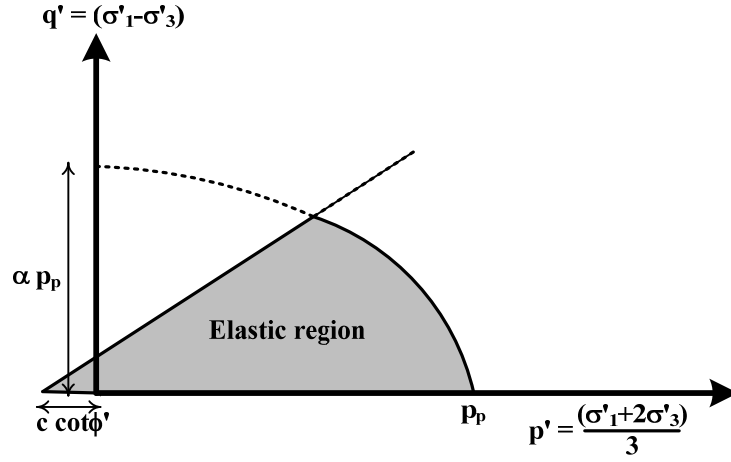
Figure 2.34: Yield Surface of the Hardening Soil Model in p - $\tilde{q}$ Plane

2.5.4 Hardening Soil Model with Small Strain Stiffness (HSS)

The Hardening Soil-Small (HSS) Model was developed by Benz (2006). It is an extension of the Hardening Soil Model (HSM) with the capability to model soil behaviour at a small strain. All input parameters of the HSM, as seen in Table 2.4, are carried over to the HSS model, with two additional parameters, namely G_{max} and $\gamma_{0.7}$ (see Table 2.5).

Table 2.5: Hardening Soil Model with Small Strain Stiffness Input Parameters

Parameter	Description	Parameter evaluation
All parameters of HSM (Table 2.4) are required for HSS		
G_{max}^{ref}	Reference small strain shear modulus	Equation 2.64
$\gamma_{0.7}$	Shear strain amplitude at $0.7G_{max}$	Figure 2.35

Janbu's (1963) hyperbolic law, which is similar to that of in parameters E_{50}, E_{ur} and E_{oed}, is applied to the shear modulus at a small strain (G_{max}) parameter. Therefore, G_{max} at any values of confining pressure can be calculated as:

$$G_{max} = G_{max}^{ref}\left(\frac{\sigma_3' + c'\cot\phi'}{p^{ref} + c'\cot\phi'}\right)^m \qquad \text{Eq.2.64}$$

Parameter $\gamma_{0.7}$ is the level of shear strain, where G_{max} reduces to 70 per cent of its initial value. This parameter is closely related to the volumetric threshold shear strain

(γ_{tv}), and is regarded as a soil parameter in the model. The background concept of parameter $\gamma_{0.7}$ is detailed in Chapter 6. The small strain shear modulus (G_{max}) and parameter $\gamma_{0.7}$ are shown in the stiffness degradation curve in Figure 2.35.
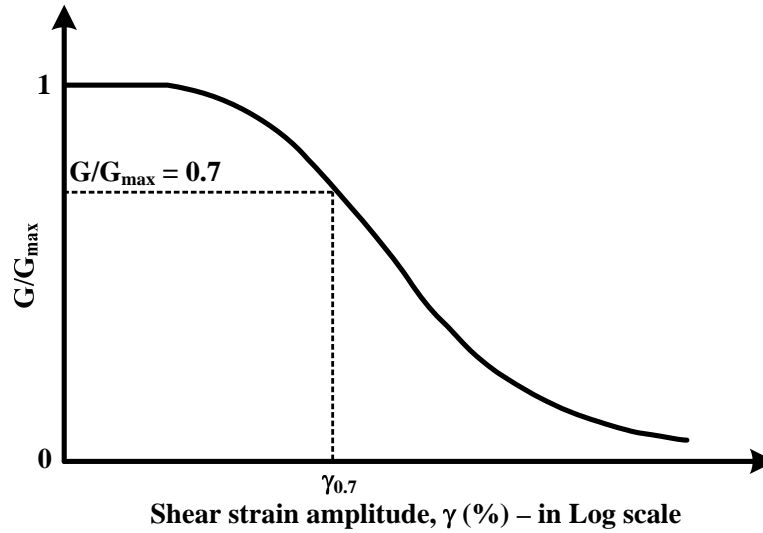
Figure 2.35: Definition of Parameter $\gamma_{0.7}$

The HSS used a modified hyperbolic law (developed by Hardin and Drnevich, 1972). The original hyperbolic law is given as.

$$\frac{G}{G_{max}} = \frac{1}{1 + \left| \dfrac{\gamma}{\gamma_{rf}} \right|}$$

Eq.2.65

where, γ is the shear strain amplitude from the cyclic triaxial test

γ_{rf} is the reference threshold shear strain at failure ($\gamma_{rf} = \tau_{max}/G_{max}$)

The reference threshold shear strain at failure relates to the large strain behaviour of soil. Using this parameter can be cumbersome in the cyclic triaxial test, especially where small strain behaviour is the main focus. However, Darendeli (2001) modified Equation 2.65 with the use of the reference threshold shear strain at a smaller strain, namely $\gamma_{0.5}$. This parameter refers to the level of shear strain amplitude, where G_{max} reduces to half. The constant curvature coefficient (α) is also introduced to adjust the shape of the stiffness degradation curve. The modified equation is given as:

$$\frac{G}{G_{max}} = \frac{1}{1 + \left(\dfrac{\gamma}{\gamma_{0.5}}\right)^{\alpha}}$$

Eq.2.66

Further development of Hardin and Drnevich's (1972) equation was proposed by Santos and Correia (2001). Basically, Santos and Correia utilised the parameter $\gamma_{0.7}$ instead of $\gamma_{0.5}$. The following equation is modified after Hardin and Drnevich's established relationship.

$$\frac{G}{G_{max}} = \frac{1}{1 + a\left(\dfrac{\gamma}{\gamma_{0.7}}\right)}$$

Eq.2.67

It should be noted that using Equation 2.67 will not give the exact results when compared to Equation 2.65 by Hardin and Drnevich (1972). This outcome occurs simply because the constant a of 0.385 was selected to obtain the best fit function with the test data of Santos and Correia (2001). Nevertheless, Benz (2006) pointed out that the difference between Equation 2.65 and 2.67 is less than 3 per cent.

2.5.5 Discussion on the Use of Soil Models in Tunnelling and Deep Excavation Problems

The Mohr Coulomb and Hardening Soil Models are outlined in the previous sections. In this section, the advantages and disadvantages of the two soil models, in regard to unloading problems, such as tunnelling and deep excavations, are discussed. Further, the new development in the advanced Hardening Soil Model, which takes into account the soil stiffness at a small strain, is also briefly described.

Although the Mohr Coulomb Model has been adopted successfully in many geotechnical engineering projects, the model still has some problems, due to the model's assumptions and limitations, which especially holds true in the unloading problems. The disadvantages of the Mohr Coulomb Model, which can be overcome in the Hardening Soil Model, are listed below:

- The Mohr Coulomb Soil Model cannot distinguish the differences among the primary loading, unloading and reloading problems. In fact, the only governing stiffness modulus for all types of problems is E_{50}.

- Unlike the Hardening Soil Model, the stress dependency stiffness is not available.

- Below the Mohr-Coulomb failure line, soil deviatoric and volumetric hardenings, due to plastic strains, cannot be taken into account.

- For unloading problems, the undrained behaviour of soil can be unrealistic (and thus the undrained shear strength of soil can be over-predicted).

The new developments in the Hardening Soil Model have added advantages through having the additional small strain stiffness of the soil. The original Hardening Soil Model assumed elastic material behaviour during the unloading and reloading. It is, however, the soil stiffness at the small strain which governs the purely elastic soil behaviour (see Figure 2.32). This phenomenon of soil stiffness at a small strain has been confirmed by many researchers (Burland, 1989; Atkinson and Sallfors, 1991; Mair, 1993). Importantly, in the Plaxis Hardening Soil Model with Small Strain Stiffness, two additional parameters are included:

- The initial or very small strain shear modulus (G_{max}), and
- The shear strain level $\gamma_{0.7}$ at which the secant shear modulus G is reduced to 70 percent of G_{max}.

2.6 Concluding Remarks

This chapter summarised the salient issues related to tunnelling methods and tunnel boring machines, undrained components of volume loss and soft ground tunnel face stability, empirical, analytical and numerical methods on soft ground movement owing to tunnelling works, and soil constitutive models for finite element analysis. The following points are discussed and conclusions made:

(1) The literatures related to the process of tunnel excavation, especially shield tunnels, are surveyed. A review of the components of ground loss in relation to each step of shield tunnel excavation is also given. These parts of the literature review reserves as fundamental elements for further study on tunnelling.

(2) The pioneering work of Peck (1969) benefited from the shape of the Gaussian curve to predict the ground settlement owing to tunnelling. An empirical base solution is necessary to estimate the trough width parameter (i) and the maximum surface settlement ($\delta_{v,max}$) prior to the use of Gaussian function. These methods (i.e. O'Reilly and New (1982), Peck (1969); Figure 2.9) are often correlate the trough width parameter with soil type, tunnel diameter, dept from the tunnel centreline to the ground surface, etc. In the subsequent analysis in Chapter 8, it will be shown that tunnelling components (i.e. face pressure, grout pressure, penetration rate and percentage of grout filling) are of important factors for the prediction of ground movement induced by shield tunnelling. Nonetheless, the Gaussian curve can be matched with the measured settlement trough very well. Consequently, it could be used for back-analysis.

(3) With the aim to find the best analytical method to predict the ground surface settlement induced by shield tunnelling, three analytical methods (i.e. Verruijt and Booker, 1996; Loganathan and Poulos, 1998; Bobet 2001) are examined in this study. Their major differences, such as the assumptions on soil behaviour, shape of ground loss, are pointed out. The comparisons of computed settlement trough, as compared to the field measured data, are shown in Chapter 8.

(4) The final part of this chapter provides a critical review of literatures on 2D numerical analyses of both shield and NATM tunnelling. A brief summary of related constitutive soil models (i.e. Mohr Coulomb Model, Soft Soil Model, Hardening Soil Model and Hardening Soil Model with Small Strain Stiffness) is also included. These models are used in the analyses of the deep excavation and EPB shield tunnelling with Plaxis software.

CHAPTER 3

MRT Works and
Subsoil Conditions in Bangkok

3.1 Introduction

The general background of the MRT (Mass Rapid Transit) projects on Bangkok subsoils is presented in the first part of this chapter. The main focus is on the completed Bangkok MRT project (Blue Line), and the extension project (Blue Line Extension), currently under design. Critical reviews of the geological and geotechnical backgrounds of Bangkok subsoils are given in the second part. Such input soil parameters are important factors in the finite element analysis of wall deflections and ground movements of deep excavations. The third part of the chapter focuses on the back-analysed soil parameters (i.e. E_u/s_u ratios) of Bangkok Clays, based on the MRT station excavations and other building basement excavation case histories. For the finite element analysis of tunnelling works, the soil parameters, as well as other factors related to tunnelling sequences play a key role (as discussed in more detail in the previous chapter, Chapter 2). In 2D finite element analysis of tunnelling problems, the factors related to tunnelling sequences are simplified as

ground (volume) loss ratio, stress relaxation ratio, stiffness deduction ratio, etc. These simplified factors, as related to the tunnelling works in Bangkok subsoils, are briefly summarised in the final part of this chapter.

3.1.1 History of Development of Soft Ground Tunnelling in Bangkok

The Bangkok soft ground tunnelling history dates back to as early as the 1970s. The first soft ground tunnel project (a storm drainage tunnel for the Bangkok Metropolitan Administration (BMA)) was 3.3 m in diameter and 1.8 km in length. At the beginning of the project, an open-face shield with compressed air was used; however, later, it was changed to a blind shield type, due to a number of serious difficulties. From the late 1970s to the 1990s, major concerns were raised in relation to the water supply transmission tunnels, which come under the governance under the governance of the Metropolitan Water Works Authority (MWA). Various types of tunnelling methods, such as cut-and-cover tunnels, mechanised shield with compressed air tunnels, Slurry Pressure Balance (SPB) shield tunnels, and Earth Pressure Balance (EPB) shield tunnels, had been used to construct water supply transmission tunnels for smaller diameters, raging from 2.0-3.5 m (Phienwej, 1997).

The EPB shield technique was considered a suitable method for the Bangkok subsoils (especially the stiff clay layer), as proved by the many water transmission, and storm drain and waste water tunnelling projects that were successfully constructed. Consequently, the EPB shield technique was selected for the larger diameter (5.7 m) Bangkok MRT Blue Line tunnelling project, which will be discussed further in the following sections. A summary of completed shield tunnelling projects in Bangkok is given in Table 3.1.

Table 3.1: Summary of Completed Shield Tunnels in Bangkok (Phienwej, 1997)

Year	Purpose of Tunnel Usage	Geometry (Diameter (m); Length (km))	Soil Type	Construction Method
1970-1974	Strom drain	3.3; 1.8	Soft clay of 5-8 m	Blind shield
1975-1979	Water transmission	2.0-3.4; 24.5	Stiff clay of 17-20 m deep, some portion in sand River undercross	Mechanical and semi-mechanical shields with compressed air Slurry shield for sand sections and river crossing
1981-1983	Water transmission	2.0-2.5; 7.1	Stiff clay of 17-20 m deep	Semi-mechanical shield with compressed air
1986-1988	Water transmission	2.0-3.2; 34	Soft clay up to 9 m deep	Cut-and-cover Pipe jacking with blind shields
1990-1991	Water transmission	2.0; 2.2	Stiff clay of 18 m deep	Semi-mechanical shield
1994-1997	Stage 1 waste water tunnel	2.5 & 3.2; 10	Soft and stiff clay of 10-18 m deep	EPB shield
1995-1997	Water transmission Srinakarin-Romklao	2.0; 10.5	Stiff clay of 16-18 m deep	EPB shield
1999-2000	Klong Premprachakorn storm drain	3.4; 1.8	Stiff clay	EPB shield
1999-2000	Ratburana waste water	2.3; 1	Stiff clay	EPB shield
1998-2001	MRT Blue Line	5.7; 18	Stiff clay, sand and soft clay of 12-25 m deep	EPB shield

3.2 Bangkok MRT Projects

In the past three decades the population of Bangkok has increased, exponentially, with now over ten million people. Indeed, it is common for Bangkok residents to travel by their own cars, especially as owning an automobile is considered to be a prestigious status symbol among the Thai Society. Thus, almost all the major and minor roads are completely blocked with traffic during peak hour. In order to ease the traffic, elevated roads were constructed in the city; these roads have virtually spoiled the beauty of the city. Further road developments were undertaken with the inclusion of the North and South Bangkok into the MRT Blue Line project. In August 1999, the official name of the Bangkok MRT Blue Line project was retitled, by His Majesty the King of Thailand, as "*The Chaleom Ratchamongkhon Line*". After the completion of the project in July 2003, the project was hailed as a most successful project by the Bangkok Mass Rapid Transit Authority of Thailand (MRTA). As a result of this success, the Bangkok MRTA is to launch an extension project, the Bangkok MRT Blue Line Extension, which is now in the design stage.

3.2.1 Background of Bangkok MRT Blue Line Project

The Bangkok MRT Blue Line project was the first underground MRT in Bangkok. Indeed, it is the first phase of an integrated transportation plan for Bangkok; it will be implemented in conjunction with other schemes being undertaken by the Mass Rapid Transit Authority of Thailand (MRTA). The project was constructed along highly congested roads in the heart of Bangkok city. The tunnel alignment, which is 22 km in length, included 18 underground cut-and-cover subway stations, and was divided into two major sections (the North and South sections (see Figure 3.1)). The underground stations are, typically, comprised of three levels of structure; with the Centre Platform, Side Platform and Stacked Platform (as shown in Figure 3.2). The stations are up to 230 m long and approximately 25 m wide, and are excavated up to a depth of 25 m to 30 m below the ground surface. The station perimeter was constructed of diaphragm walls, 1.0 – 1.2 m thick and up to 30 – 35 m deep. The tunnel lining is of twin bored

single-track tunnels. Each tube has an outer diameter of 6.3 m, with an inner diameter of 5.7 m of concrete segmental lining.
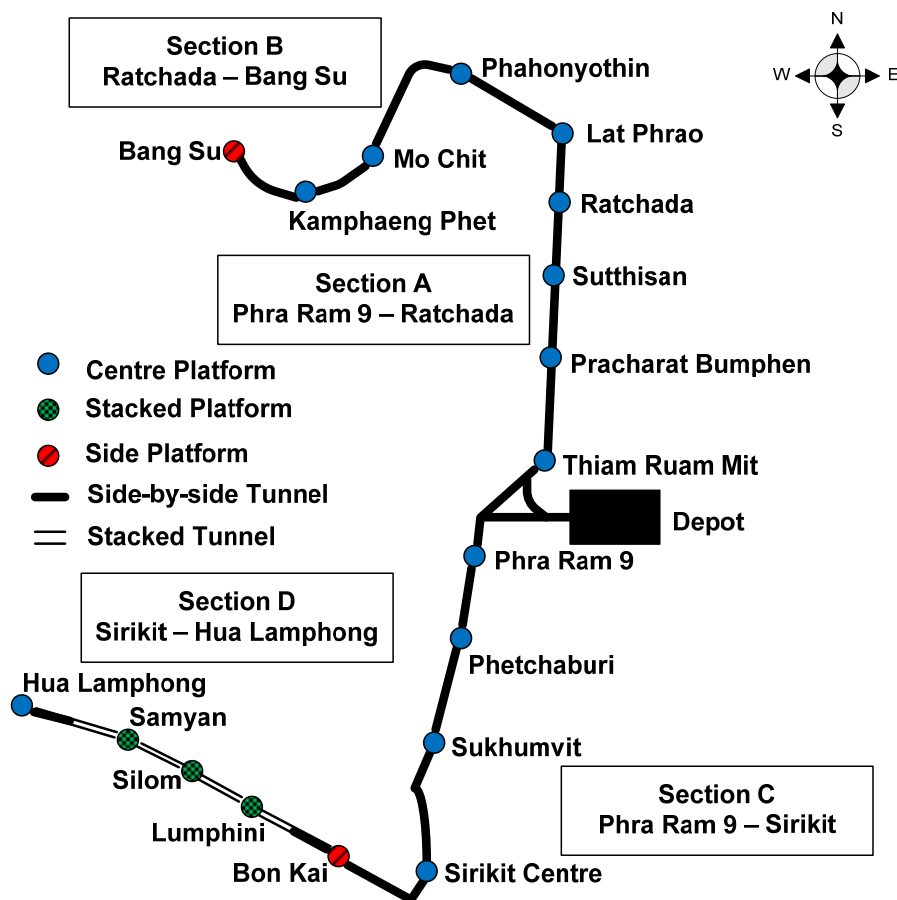
Figure 3.1: Bangkok MRT Blue Line Project
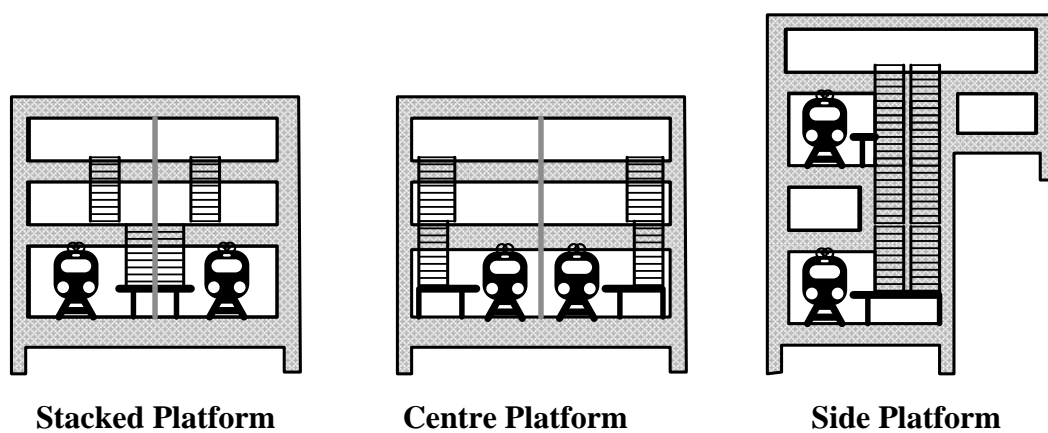
Figure 3.2: Types of Underground Stations

3.2.2 Station Excavation Works of Bangkok MRT Blue Line Project

A total of 18 underground stations were constructed using the Top-Down construction technique, together with diaphragm walls and concrete slabs as excavation supports. Table 3.2 summarises the MRT station dimensions, excavation depth, and diaphragm wall (D-wall) length for all 18 stations. Nine stations from the South contract were designated as S1 to S9, while N1 to N9 notations were used for the North side contract. The excavation depth and D-wall lengths are plotted in Figure 3.3. The stacked platform stations (S2, S3 and S4) had a greater excavation depth and D-wall length compared to the centre and side-by-side platform stations. The majority of the centre and side-by-side platform stations (except stations S1 and N9) have similar depths of excavation (about 21 – 22 m). However, the embedded depth of the D-wall differed among the South and North contracts due to the difference in design criteria.

Table 3.2: Summary of MRT Station Dimensions, Excavation Depths
and D-wall Lengths

| Notation | Station | Station Dimension | | Excavation Depth, H_e (m) | D-wall Length, L (m) |
		Length (m)	Width (m)		
S1	Hua Lamphong	211	22	15.5	20.1
S2	Samyan	178	20	27.1	39.7
S3	Silom	154	28	32.6	46.2
S4	Lumphini	230	25	29.6	39.5
S5	Bon Kai	230	25	21.1	28.6
S6	Sirikit Center	230	25	23.6	31.6
S7	Sukhumvit	200	23	20.9	27.9
S8	Phetcaburi	199	23	22.4	28.9
S9	Phra Ram 9	400	26	20.9	25.6
N1	Thiam Ruam Mit	358	29	22.4	32.7
N2	Pracharat Bamphen	228	25	21.7	32.2
N3	Sutthisan	228	25	21.7	32.2
N4	Ratchada	228	25	21.6	34.5
N5	Lad Phrao	293	25	22.0	37.4
N6	Phahonyothin	228	25	22.0	33.6
N7	Mo Chit	364	32	21.8	33.5
N8	Kamphaeng Phet	228	25	22.1	38.5
N9	Bang Su	228	32	15.8	29.5
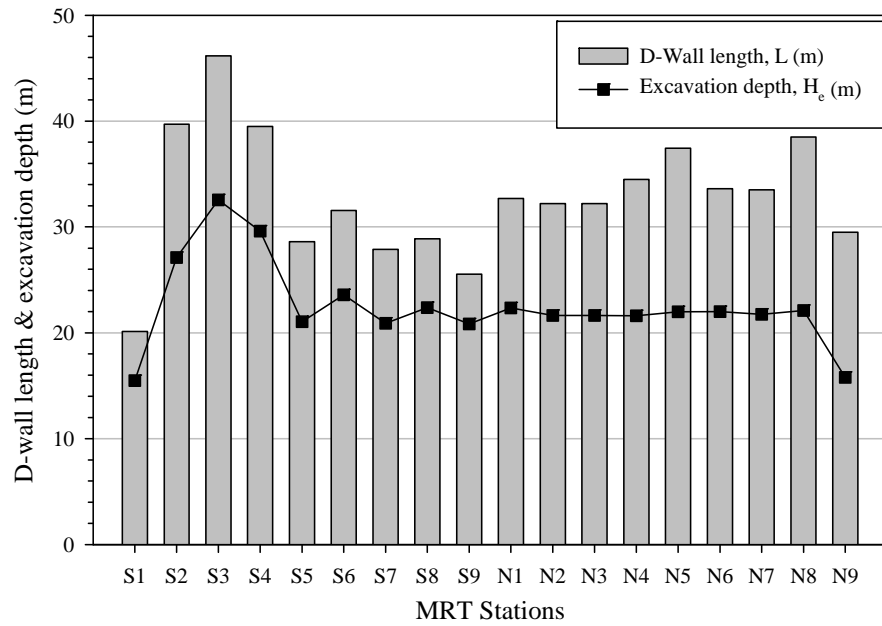
Figure 3.3: Excavation Depth and D-wall Length of Bangkok MRT Blue Line Stations (after Phienwej, 2008)

3.2.3 Earth Pressure Balance Shields (EPB) Tunnelling Works of Bangkok MRT Blue Line Project

A total tunnel length of 20 km (excluding underground stations) was constructed using eight Earth Pressure Balance (EPB) shields (6 Kawasaki and 2 Herrenknecht machines). A comparison of the EPB shield used in the project, as listed by Suwansawat (2002) and Timpong (2002), has been modified and presented in Table 3.3. The sequences of the EPB shield drives are presented in Table 3.4. As seen in Figure 3.1, the major North and South alignments have been divided into 4 sub-sections, namely: Sections A and B for the North alignment, and Sections C and D for the South alignment.

Table 3.3: Comparison of EPB Shields Used in Bangkok MRT Blue Line Project

EPB Shield	1 &2	3 &4	5 &6	7 & 8
Section Route	**A North** TRM—Ratchada TRM—Rama IX, Depot	**B North** Ratchada—Bang Sue	**C South** Rama IX—Sirikit	**D South** Sirikit—Hua Lampong
Operator	**Nishimatsu**	**Obayashi**	**Kumagai Gumi**	**Bilfinger & Berger**
Specification				
Manufacturer	**Kawasaki**	**Kawasaki**	**Kawasaki**	**Herrenknecht**
Shield Diameter	**6.43 m**	**6.43 m**	**6.43 m**	**6.46 m**
Typical Face Pressure	**50 kPa**	**180 kPa**	**200 kPa**	**180 kPa**
Cutting wheel dia. Not including copy cutter	6.43 m	6.43 m	6.43 m	6.48 m
Over-excavation Gap	**6.5 cm**	**6.5 cm**	**6.5 cm**	**9 cm**
Max. Copy Cutter Stroke	10 cm	10 cm	10 cm	N.A.
Overall Length	**8.35 m**	**8.35 m**	**8.33 m**	**6.19 m**
Articulation Number	1 (4.39/3.94)	1 (4.39/3.94)	1 (4.39/3.94)	1 (3.275/2.915)
Number of Jacks	20 x 200 tonne	20 x 200 tonne	40 x 100 tonne	40 x 100 tonne
Total Thrust Force	35630 kN	35630 kN	35630 kN	28300 kN
Cutter head drive	4 x 180 Kw electric motors	4 x 180 Kw electric motors	4 x 180 Kw electric motors	8 hydraulic motors powered by 4 x 160 Kw electric pumps
Opening Ratio of cutter face	60 %	60 %	60 %	42 %
Grouting				
Type of Grouting	Thixotropic cement / bentonite	Thixotropic cement / bentonite	Thixotropic cement / bentonite	Bentonite, cement + Fly Ash
Typical Pressure	**2.5 bar**	**2 bar**	**2 bar**	**>3 bar**
Typical Quantities	1.8 m^3/m	1.8 m^3/m	2.2 m^3/m	N.A.
Typical Grout Filling Ratio	120 %	120 %	120 %	150%
Muck Removal				
Operation	**Screw Conveyor, Belt Conveyor & Muck Car**	**Screw Conveyor & Pumping**	**Screw Conveyor, Belt Conveyor & Muck Car**	**Screw Conveyor, Belt Conveyor & Muck Car**
Max. Screw Conveyor	312 m^3 / hr	312 m^3 / hr	312 m^3 / hr	200 m^3 / hr
Max. Belt Conveyor	150.0 m^3 / hr	-		
Max. Pumping Rate	-	150.0 m^3/hr	-	-
Typical Slurry Additive Volume	2.5 m^3 / m	13.0 m^3 / m	N.A.	11.0 m^3 / m
Typical Excavated Soil Volume	45.0 m^3 / m	55.0 m^3 / m	N.A.	51.0 m^3 / m

Table 3.4: Driving Sequences of the EPB Shields

EPB Shield	1 & 2	3 & 4	5 & 6	7 & 8
Section **Route**	**A North** Thiam Ruam Mit – Ratchada TRM – Rama IX TRM – Depot	**B North** Ratchada – Bang Sue	**C South** Rama IX - Sirikit	**D South** Sirikit - Hua Lampong
Operator	**Nishimatsu**	**Obayashi**	**Kumagai Gumi**	**Bilfinger & Berger**
Tunnelling Start Date	SB 23-Apr-99 NB 30-Apr-99	SB 16-Feb-99 NB 19-Mar-99	NB 9-Jun-99 SB 25-Jun-99	SB 24 July 99 NB late August 1999
Section Length (SB & NB)	6871 m, 1290 m, 631	4292 m, 2819 m, 2459 m	7466 m	9888 m
TBM / Station interface	Station excavation incomplete, move TBM between drives except as noted	Station excavation incomplete, move TBM between drives except as noted	Skid TBM thru completed station boxes S8, S7	Skid TBM thru completed station boxes S5, S4, S3, S2
Driving Sequence Refer Figure 1	**NB**:- TRM→Ratchada drive thru PRA, SUT TRM→DEPOT Rama IX→TRM **SB**:- TRM→Ratchada TRM→Rama IX	RAT→Phahonyothin drive thru Lat Phoa Bang S→KamPP Mo C→Pahonyothin Mo C→KamPP	Rama IX→Sirikit	Sirikit→Hua Lumphong
Best week	199 rings from both machines	231 rings from both machines	164 rings from both machines	167 rings from one machine
Best Day	41 rings	43 rings	35 rings	33 rings
Alignment	Twin Tunnels 18 m apart	Twin Tunnels 18 m apart	Twin Tunnels 12-18 m apart (<2 m in Asoke Rd.)	Twin & Stacked Tunnels
Maximum Cover	22 m	22 m	20 m	27 (SB), 22 (NB)
Minimum Cover	15 m	8 m	13 m	8 m
Minimum horizontal Curve Radius	200 m	190 m	300 m	200 m
Maximum Gradient	+ /- 4 %	+ /- 2 %	+ /- 2 %	+ / -3 %
Geological Conditions	Stiff Clay & dense fine sand	Stiff Clay & dense fine sand	Mostly in Stiff Clay Layer	SB:-Stiff—Clay & sand NB:-Soft—Stiff Clay
Max. Water Level above Invert	7 m	7 m	10 m	9 m
Location of highest Water pressures	Thiam Ruam Mit - Pracharat Bumphen	Lat Phrao – Phahonyothin	Sukhumvit – Sirikit	Silom—Sam Yan

3.2.4 Construction Methods for Tunnelling and Underground Stations

The construction methods used for the tunnelling and the underground stations of the North and South sections had different sequences. The contractors for the North sections (i.e. Sections A and B) were to start their tunnelling works as soon as possible, with the launching of the station to be prior to their excavation.

In contrast, the EPB shields of the North section commenced work from the Thiam Ruam Mit Station, with a launch shaft located at the north end of the station towards Pracharat Bamphen and Sutthisan Stations, and arrived at the Ratchada Station, which was already fully excavated and with the base slab construction completed. Then, the shield was driven from the north end of Ratchada Station to Phahonyothin Station, and involved tunnelling through the incomplete Lad Phrao Station. An illustration of the North section construction method is presented in Figure 3.4.
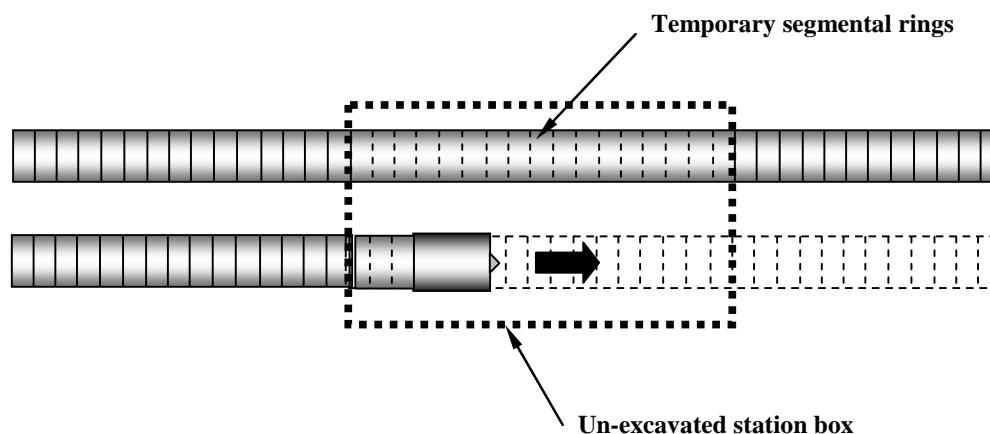
Figure 3.4: Construction Method of the North Section (Suwansawat, 2002)

For the South section (i.e. Sections C and D), on the other hand, the underground station boxes were excavated and constructed prior to the tunnelling. Hence, the South contractor avoided the extra length of temporary tunnel, which was approximately equal to the length of the underground station box. In Section C (see Figure 3.5), the shield cut through the diaphragm wall at the approaching end, and then was shifted to the far end of station box. After that, the shield was re-assembled and the tunnelling re-commenced.

**Shift the shield to
the far end of station box**

Completed station box
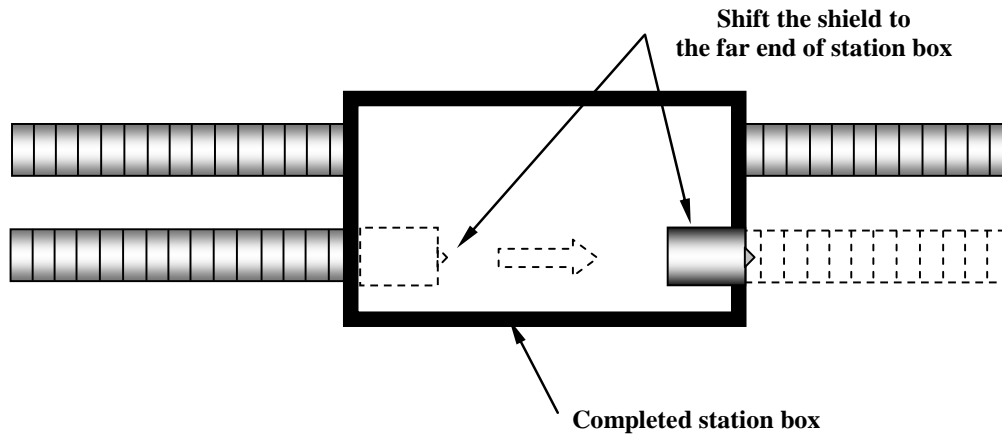
Figure 3.5: Construction Method of the South Section (Suwansawat, 2002)

3.2.5 Bangkok MRT Blue Line Extension Project

The MRT Blue Line Extension project is the second phase of an integrated transportation plan of Bangkok to moderate the traffic congestion in the southern part of Bangkok city. The project comprises a total length of 14 km (9 km elevated and 5 km underground), including 7 elevated and 4 underground stations. It is to connect the initial MRT route at Hua Lamphong cut-and-cover station, then continues along the underground route along the Rama 4 Road to Charoen Krung Road, Wat Mangkon, Wang Burapha, turning left to Sanam Chai Road passing the Royal Palace, and crossing under the Chao Phraya River at Pak Khlong Talat area. The line also passes through Khlong Bangkok Yai, Itsaraphap Road, Bang Phai, Bang Wa, Phasi Charoen, and Bang Khae before ending at Lak Song. The alignment of this project is presented in Figures 3.6 and 3.7.
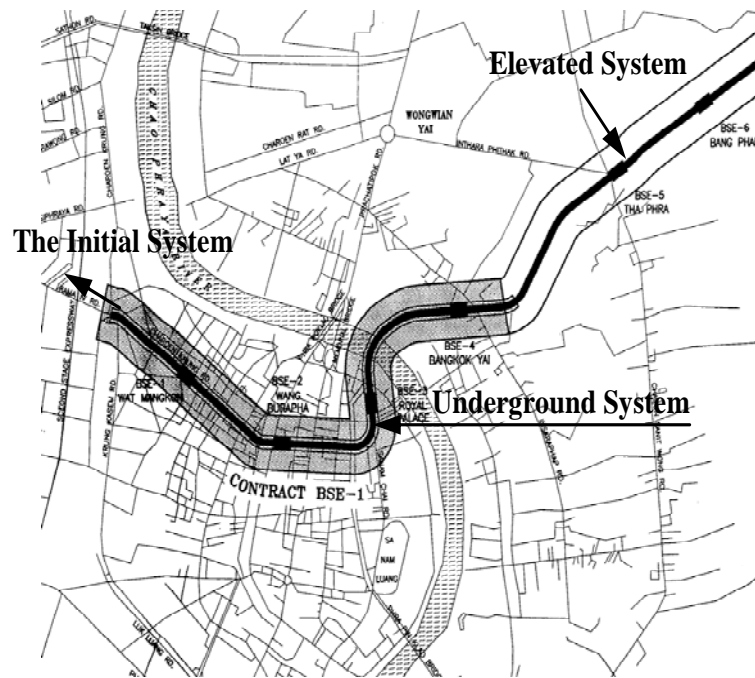
Figure 3.6: Bangkok MRT Blue Line Extension Project
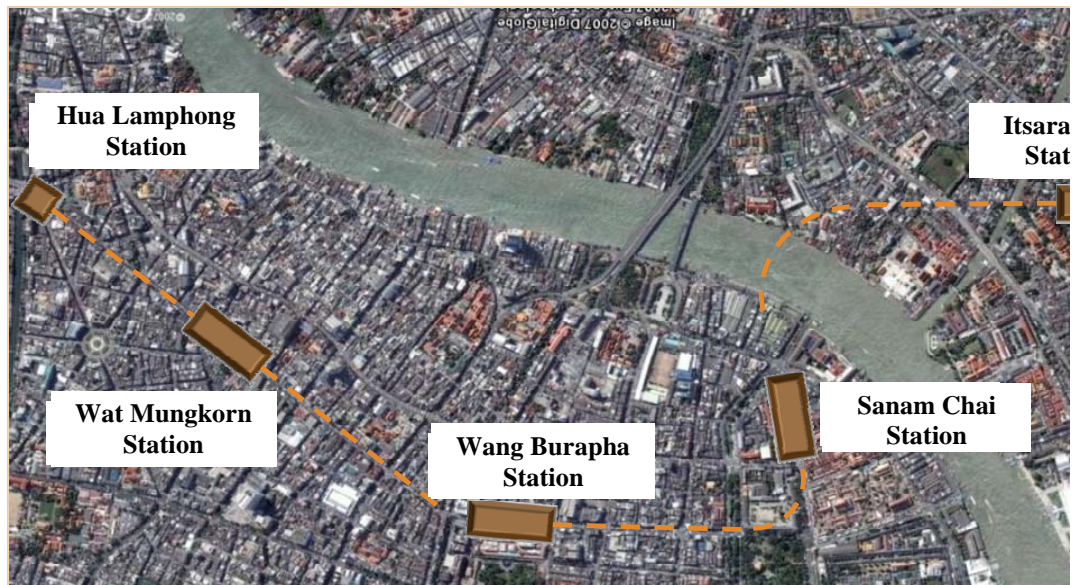
Figure 3.7: Locations of Subway Stations in the Bangkok
MRT Blue Line Extension Project

In the current research, only the underground route will be assessed; it will be referred to as the Blue Line Extension project. As shown in Figure 3.7, the underground alignment connected the existing MRT route at Hua Lamphong station and extended it to the east towards Chao Phraya River. There are four underground stations: Wat Mungkorn Station, Wang Burapha Station, Sanam Chai Station, and Itsaraphap Stataion. The Wat Mungkorn and Itsaraphap stations will be constructed using the cut-and-cover method. The remaining two stations are located in the old historical area of Rattanokosin Island. The route also passes through an area of Bangkok's China Town and the Royal Grand Palace. Consequently, the proposed construction method needs to minimise the environmental impact.

Further details of the design aspects for the underground station excavation methods, for the Bangkok Blue Line Extension Project, can be found in Suwansawat *et al.* (2007). A method has been proposed by Surarak *et al.* (2007), which will utilise the advantages of both the conventional cut-and-cover method, and the New Austrian Tunnelling Method (NATM). A typical cross section of the Wang Burapha Station is illustrated in Figure 3.8.
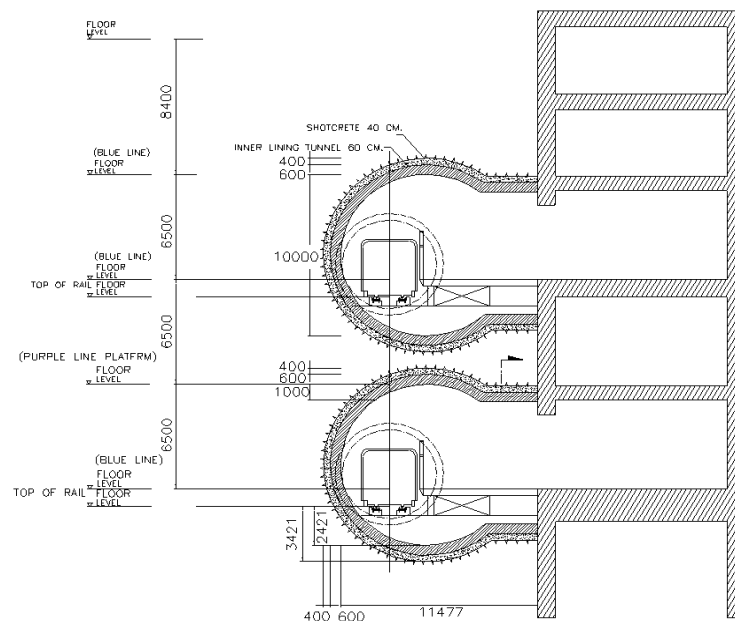
Figure 3.8: Wang Burapha Station Cross Section

3.3 Bangkok Subsoil Conditions

3.3.1 Introduction

Bangkok city is located on the low flat Chao Praya Delta Plain (see the geomorphological map in Figure 3.9). The terrestrial deposits in the city lie from 0 to about 4-5 m above the mean sea level, with the other soil layers being marine deposits, resulting from changes in sea levels during the Quaternary period. A multitude of construction activities, including deep excavations, high rise buildings, elevated expressways, a new airport, and even subway tunnels, have taken place or are taking place in this sedimentary marine deposit. The deposit consists of an extensive overlay of Bangkok soft marine clay, which is of low strength and high compressibility. The upper soft clay layer is underlain with several aquifers inter-bedded with clay and sand. Over several decades extensive ground water pumping from the aquifers has caused large piezometric drawdowns and alarming subsidence.

In this section, a critical review is given of the Bangkok subsoil conditions and the studies related to the subsidence (due to the deep well pumping). The available and extensive laboratory and field testing results are addressed to obtain meaningful geotechnical soil properties. In addition, back-analyses and parametric studies, as described in the literature (to obtain geotechnical soil parameters suitable for advanced soil models) are reviewed.
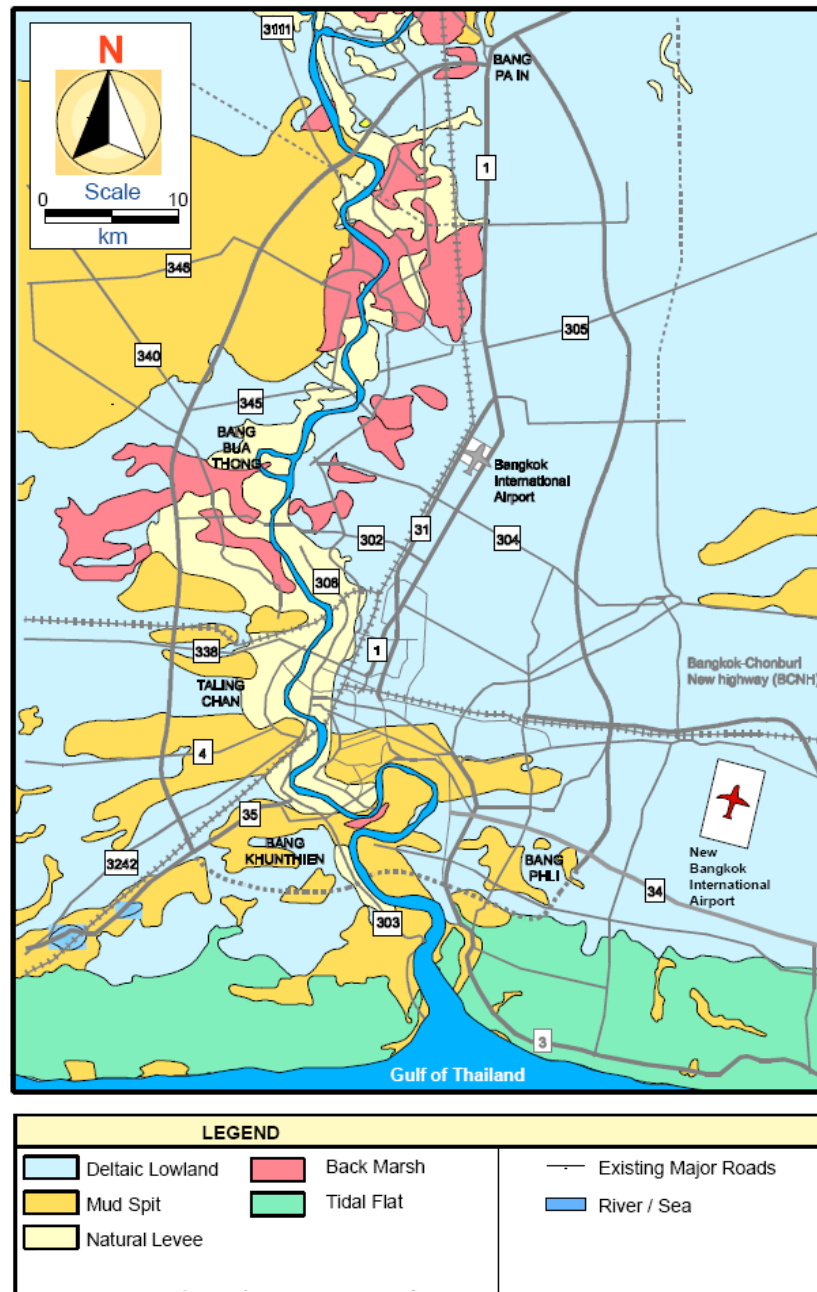
Figure 3.9: Geomorphological Map of Bangkok Metropolitan Area
(BMTDC, 2002)

3.3.2 Geotechnical Environment

The Bangkok subsoil, which forms a part of the larger Chao Phraya Plain, consists of a broad basin filled with sedimentary soil deposits (Figure 3.10). These deposits form alternate layers of sand, gravel and clay. While the depth of the bedrock is still

undetermined, its level in the Bangkok area is known to vary between 400 m to 1800 m in depth. The aquifer system beneath the city area is very complex and the deep well pumping from the aquifers, over the last fifty years or so, has caused substantial piezometric drawdown in the upper soft and highly compressible clay layer (Figure 3.11). According to early researchers (e.g. Cox, 1968; Piancharoen, 1976), there are eight artesian aquifers in the upper 600 m, separated from each other by thick layers of clay or sandy clay. The aquifers are located at depths of 50, 100, 150, 200, 300, 350, 450, and 550 m. The records indicate that the deep well pumping in 1954 was only about 8,360 m^3/day; however, this increased to 371,000 m^3/day in 1974 and to some 1.4 million m3 in 1983. Strict ground water control measures have made the withdrawal drop between 1983 and 1987. Since 1988 the pumped quantities have begun to rise.
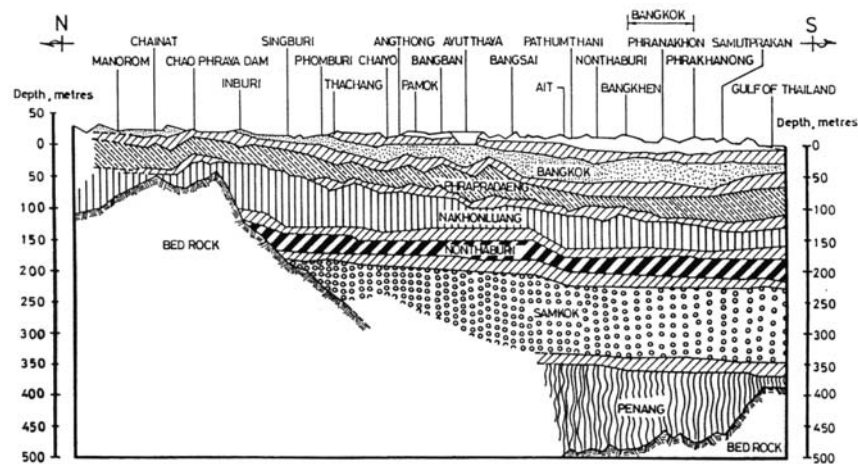
Figure 3.10: Bangkok Aquifer System (Balasubramaniam *et al.*, 2005)

Studies into Bangkok's subsidence problems, related to deep well pumping, started as early as 1968. The early studies addressed the ultimate settlement in three parts: due to the compression of the aquifers, the soft clay, and the stiff clay; they also included a mathematical model for the simulation of the phenomenon of land subsidence. These pioneering works revealed that 40 percent of the subsidence was due to the compression in the upper 50 m of soil, while the rest was due to the soils below. Additionally, the maximum subsidence was of the order of 0.05 to 0.10 m/year. However, after control measures for the ground water pumping were reinstated, the subsidence rate appears to have been reduced, from 1988 to 1990 the rate declined from 0.03 to 0.05 m/year (Nguyen, 1999; Phienwej *et al.*, 2006). Of importance,

therefore, is the apparent shift of the subsidence bowl, on the Bangkok plain, from location to location, depending on the pattern and the extent of ground water withdrawal.
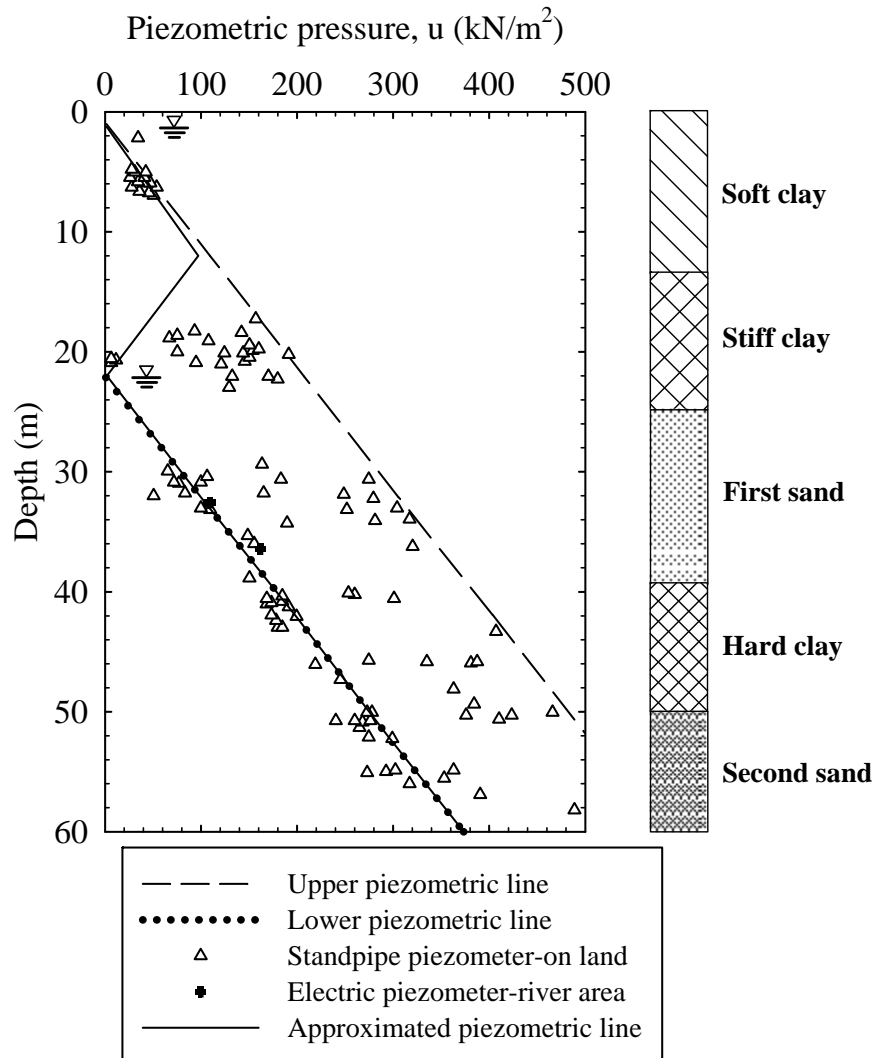
Figure 3.11: Piezometric Pressure in Bangkok Subsoils

3.3.3 Subsurface Conditions

Field exploration and laboratory tests from both the Bangkok Blue Line and the Bangkok Blue Line Extension projects show that the subsoils, down to a maximum drilling depth of approximately 60 to 65 m, can be divided into seven distinct layers. The basic soil properties are plotted in Figure 3.12. The typical soil profiles from both projects are shown in Figures 3.13 to 3.15.
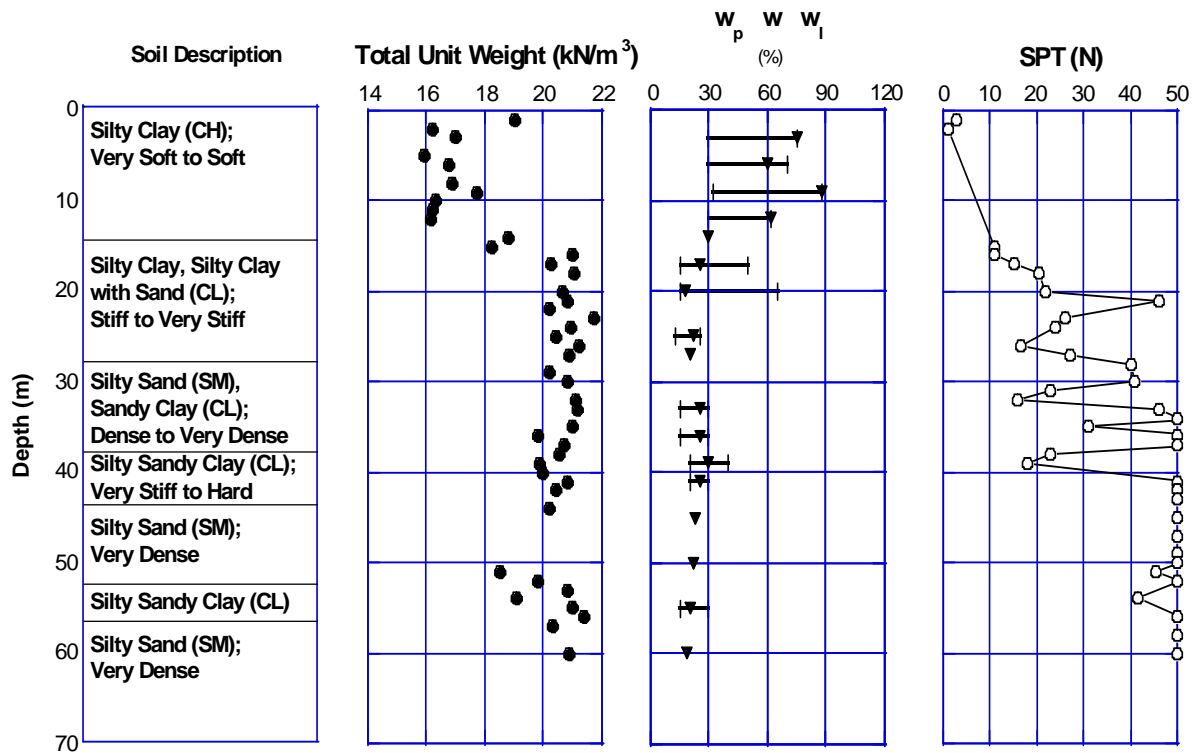
Figure 3.12: Soil Profile and Soil Properties for Bangkok MRT Blue Line Extension Project
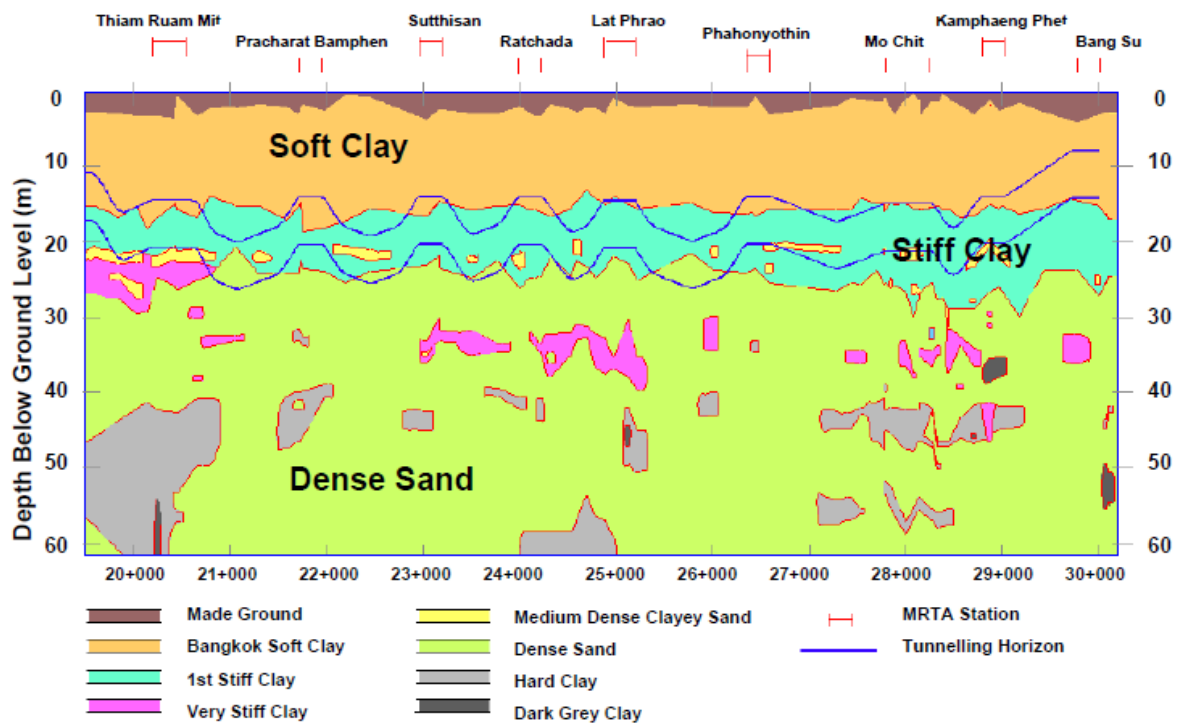
Figure 3.13: Soil Profile of Bangkok MRT Blue Line North Tunnel Section

89
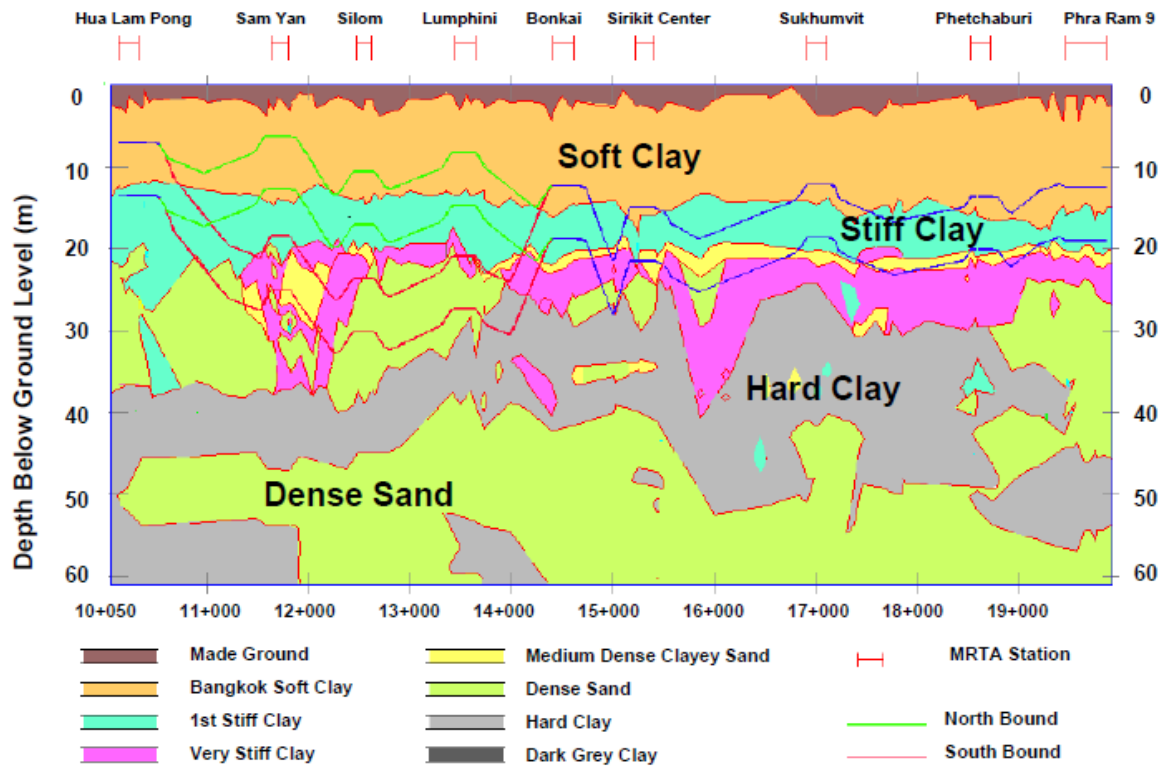
Figure 3.14: Soil Profile of Bangkok MRT Blue Line South Tunnel Section
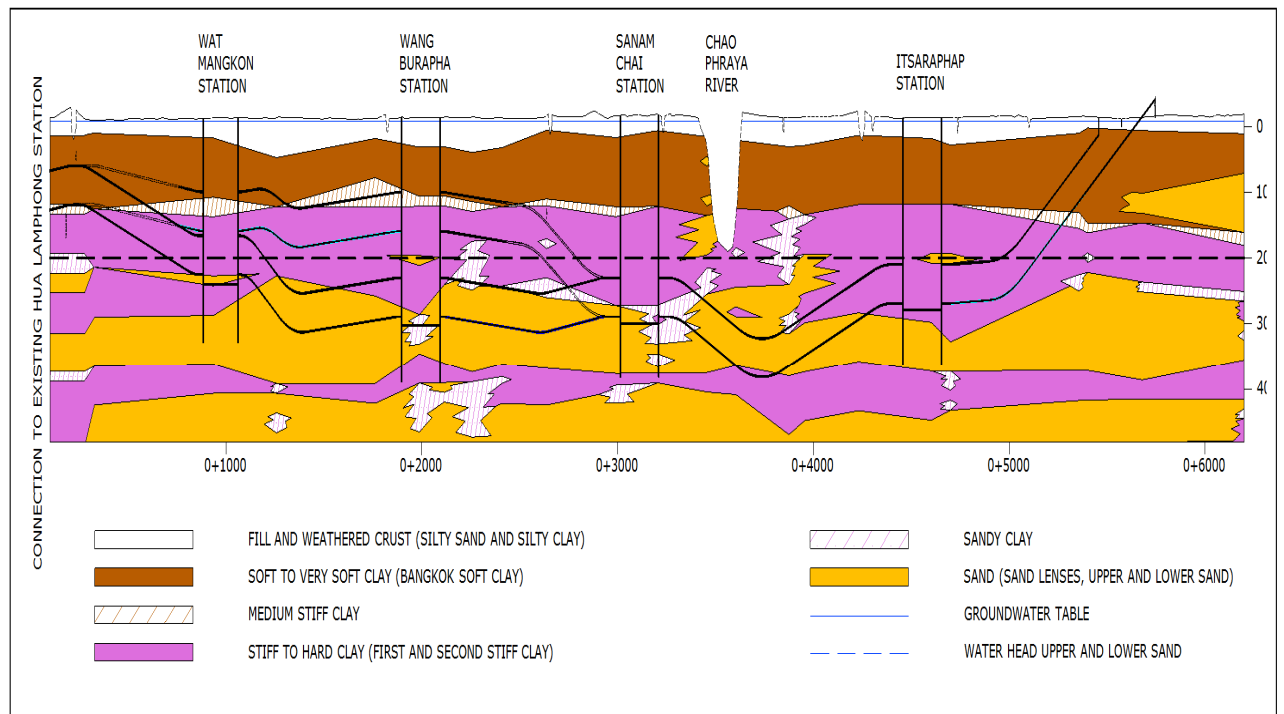
Figure 3.15: Soil Profile along Bangkok MRT Blue Line Extension Project

(Suwansawat *et al.*, 2007)

The following sections outline the general descriptions of Bangkok subsoils.

(a) First Soil Layer: Weathered Crust and Backfill Material

The uppermost layer is weathered crust (medium to stiff silty clay) and backfill material, (very loose to medium density, silty sand) light to yellowish in colour. The average thickness ranges from 2 to 5 m in most areas, with the SPT N value ranging from 2 to 21. The water content in this layer of soil varies from 10 to 35%; the groundwater table is within this layer.

(b) Second Soil Layer: Very Soft to Soft Bangkok Clay

This very soft to soft Bangkok clay layer is present between the depths of 3 to 12 m; it consists of medium gray to dark gray clay. The undrained shear strength varies from 10 to 25 kN/m^2, except for samples with a strength less than 10 kN/m^2 (probably due to sample disturbance). The natural water content of this layer ranges from 60 to 105%.

(c) Third Soil Layer: Medium Stiff Clay

A layer of dark gray to brownish gray, medium stiff clay is found below the soft clay layer, with thickness of about 2 to 3 m, along the Bangkok MRT Blue Line North, and 3 to 4 m, along Bangkok MRT Blue Line South. However, some areas of the Blue Line South can have a thickness of about 6 m. The clay's undrained shear strength is about 26 to 47 kN/m^{2,} with the natural water content ranging from 31 to 62%.

(d) Fourth Soil Layer: Stiff to Hard Clay

A layer of yellowish to light grayish brown, stiff to very stiff (or hard) clay is present between depths of 15 to 33 m. Generally, some spots of sandy soil are present in this

layer. The SPT *N* values vary from 9 to 35, with undrained shear strength of 75 to 162 kN/m^2. The water content is relatively low, with values of 15 to 32%.

(e) Fifth Soil Layer: Medium Dense to Very Dense Sand

First layer of the medium to very dense clayey and silty sand, with a yellowish to grayish brown in colour, is present below the stiff clay layer, down to depths of 35 to 40 m. This sand is fine to medium grained, with fine contents from 17 to 29%. The water content varies from 12 to 25%, with the SPT *N* values being greater than 20.

(f) Sixth Soil Layer: Very Stiff to Hard Clay

The very stiff to hard clay layer is found below the medium to dense sandy layer, with a thickness of 10 to 12 m, and its colour varies from light gray to grayish brown. It should be noted that this hard clay is absent at some locations. The SPT *N* value is greater than 30, with water content ranging from 15 to 22%.

(g) Seventh Soil Layer: Very Dense Sand

The very dense layer is found below the hard clay layer, and all the way down to the end of the borehole, at about 60 to 65 m. The sand is silty and poorly graded with silt, being yellowish brown to brownish gray in colour. The SPT *N* values, in general, exceed 50 blows. Most of the large bored piles require pile tips to be situated in this layer to yield their maximum capacities.

3.4　Related Works on Deep Excavation and Tunnelling Projects in Bangkok

3.4.1 Related Works on Deep Excavation Projects

The Bangkok MRT works are the main concern of this research, especially those related to deep excavations for the MRT stations and shield tunnelling. This section summarises the literature related to deep excavation projects in Bangkok subsoils. Further, since the MRT station excavations are braced excavations with diaphragm wall types, the summary will also include a review of the literature related to similar works on building basements.

Field monitoring data of diaphragm wall Top-Down construction of building basements are reported in the early work of Chaiseri and Parkinson (1989). The authors found that braced excavations with diaphragm walls were a competitive solution to conventional sheet piled walls. Their success was due to their excellent ground support available during the excavations and the minimised effects of the post construction movement.

Balasubramaniam *et al.* (1994) analysed six deep basement excavations for high rise buildings wherein the support systems had different rigidities. The finite element method was employed to investigate the effects of preloading, the use of barrette piles for support of columns, and the depth of retaining walls embedment and surcharge. The ground movements were observed and calculated, and indicated that retaining wall stiffness and the spacing of braced systems controlled the ground deformations. In general, then, the ground deformations in diaphragm wall cases were less than the cases of sheet piled wall excavations. The embedded depth of the retaining wall was more effective in the case of sheet piled walls than in the diaphragm wall excavations.

The analyses of the deep excavation problems are often conducted using finite element software with the Mohr Coulomb Model. Many researchers (e.g. Teparaksa *et al.*, 1999; Phienwej and Gan, 2003; Hooi, 2003; Phienwej, 2009; Mirjalili, 2009)

concentrated their work on back calculating the ratio of undrained elastic modulus and undrained shear strength (E_u/s_u). However, undrained shear strength, determined from vane shear (in soft clay) and triaxial (in stiffer clays) tests, were normally adopted in the back analyses of E_u/s_u ratio. Teparaksa *et al.* (1999) conducted 2D finite element back analysis on diaphragm wall braced excavations of the Sathorn Complex building. E_u/s_u ratios of 500 and 2000 were found to give reasonable wall deflections compared to field observations. The authors further concluded that the back calculated E_u/s_u ratios were comparable with the same ratios resulting from the self-boring pressuremeter tests ($E_u/s_u = 480$ and 1020 from soft and stiff clays, respectively). Note that the E_u/s_u ratios of their pressuremeter test were calculated from G/s_u ratios at a shear strain level of 0.1 to 0.2 %, and 0.05 to 0.1 % from soft and stiff clays.

Gan (1997), and Phienwej and Gan (2003) studied the behaviour of concrete diaphragm wall deflections for 12 cases in Bangkok. Typically, the excavation depths of the case histories ranged from 8 to 20 m. The authors observed that the maximum lateral wall movements were approximately 0.3 to 1.0 % of the excavation depth. The 2D finite element back analyses were conducted using CRISP and Plaxis software. The E_u/s_u ratios of 500, 700 and 1200 were obtained for soft clay, medium clay, and stiff clay, respectively.

Similar back analyses were performed by Hooi (2003) and Phienwej (2009). Three subway stations (Silom, Sirikit and Thiam Ruam Mit) were utilised in the case studies. Hooi (2003) found the same values for the E_u/s_u ratio of 500 and 1200, for soft and stiff clays, respectively. Mirjalili (2009) refined the work of Hooi (2003) by performing back analyses using both the Mohr Coulomb and Soft Soil Models. Indeed, Mirjalili's Mohr Coulomb Model back analysis confirmed the E_u/s_u ratio of 500 in soft clay. However, slightly lower values of $E_u/s_u = 500$ and 1000 were found to be suitable for the stiff clay and the hard clay layers. From the Soft Soil Model back analysis, a ratio of λ^*/κ^* of 0.5 was obtained. The E_u/s_u ratios, as discussed above, are summarised in Table 3.5.

Table 3.5: E_u/s_u Ratios Resulted from Finite Element Back Analyses

of Previous Works

Soil layer	E_u/s_u ratio			
	Teparaksa *et al.* (1999)	Phienwej and Gan (2003)	Phienwej (2009)	Mirjalili (2009)
Soft Clay	500	500	500	500
Medium Clay	-	700	-	500
Stiff Clay	2000	1200	1200	500
Hard Clay	-	-	-	1000

3.4.2 Related Works on Tunnelling Projects

Throughout the construction of the Bangkok MRT Blue Line project, comprehensive instrumentation measurements were used to visualise the behaviour of the Tunnel Boring Machine (TBM), as well as the response of the soil during the tunnelling process. Particular attention was paid to the surface and subsurface ground deformations with regard to the tunnelling effect along the tunnel alignment. Based on the available data, different research methodologies were used to study the behaviour of the Bangkok subsoil during shield tunnelling works, including empirical, analytical and numerical methods. This section presents a review of the literature related to tunnelling research in Bangkok subsoils.

3.4.2.1 Empirical Methods

The Gaussian Error function, as proposed by Peck (1969), has been used successfully to describe the settlement trough in the Bangkok MRT Blue Line project (Timpong, 2002; Suwansawat, 2002). The back calculated trough width parameters (i) for a single tunnel ranged from 8 to 16 m. Suwansawat (2002) plotted the calculated parameter (i) in Peck's (1969) empirical curve (Figure 2.9); most of the data fell within the sand below the ground water level rather than below the soft to stiff clay zone, in which most of the tunnel was located. Figure 3.16 shows the empirical relationship of the trough width parameter (i) to the tunnel depth (z) m as taken from

O'Reilly and New (1982). The back calculated parameters (*i*) from Bangkok's MRT Blue Line project are plotted, together with the case history data collected by Mair and Taylor (1997). It can be seen that most of the data are enclosed by the empirical line of *i* = 0.4*z* and *i* = 0.6*z*. This result confirmed the works of O'Reilly and New (1982), that for most cases, *i* = 0.5*z,* irrespective of the condition of the (soft or stiff) clays within which the tunnels are located.

Chanchaya (2000) also conducted a similar study on the same project using Peck's (1969) empirical approaches. He concluded that the overall trough width parameter (*i*), for single and twin tunnels, was about 8-13 m and 9-19 m, respectively. The constants *K* from O'Reilly and New (1982) were of the order of 0.45-0.55 and 0.70-0.80, for single and twin tunnels, bored in first stiff clay layer. The *K* values for the first sand layer ranged from 0.35-0.40 and 0.42-0.48 for single and twin tunnels, respectively.
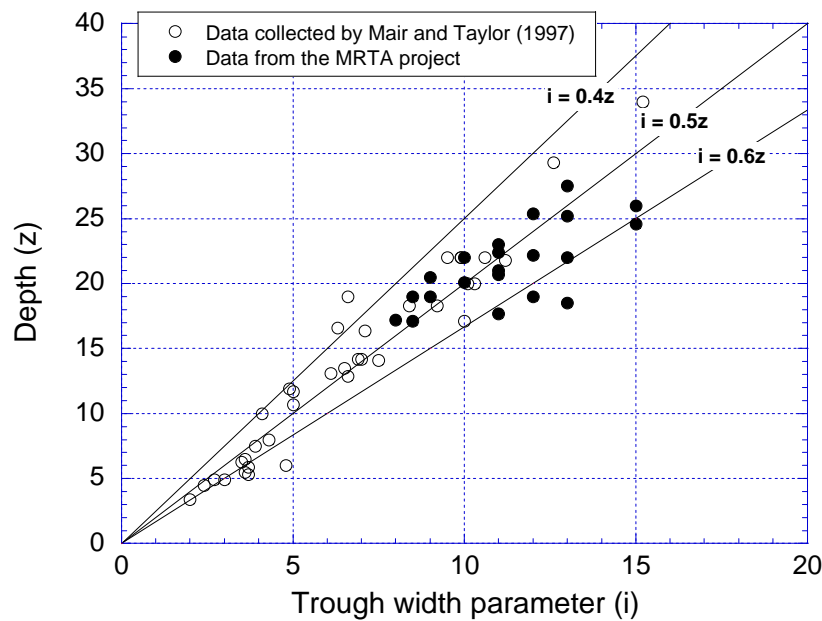
Figure 3.16: Observed Trough Parameters from the Blue Line Project
(Only Tunnelling in Clays) Together with Case History Data, (Suwansawat, 2002)

Peck (1969) also recommended applying the Gaussian function to twin tunnels, by assuming that the maximum settlement ($\delta_{v, max}$) occurs over the middle of the two tunnels. If Peck's empirical curve (*i/R* versus *z/2R*) is adopted in twin tunnels, one

would follow the adjusted parameter R' (which should be used instead of R in this plot) and can be calculated using:

$$R' = D + c/2 \qquad\qquad \text{Eq.3.1}$$

where, D is the tunnel diameter, and c is the tunnel clearance (which is equal to the distance between the two tunnel axis). According to Timpong (2002), most of the back calculated parameters (i) for the twin tunnels in the Blue Line project (which are located in the stiff clay layer) fall within the sand below the ground water zone.

Timpong (2002) proposed a new adjusted parameter (R''), which yields a better agreement with Peck's empirical chart, and is given as:

$$R'' = (D + c)/2 \qquad\qquad \text{Eq.3.2}$$

The assumption that the maximum surface settlement of twin tunnels is located in the middle of the two tunnels cannot hold true for the Bangkok MRT Blue Line case. Peck (1969) also pointed that a larger settlement is likely to occur towards the first tunnel, and that this will cause the Gaussian curve to shift to the side of the larger settlement tunnel. The shifted Gaussian curve is called the "Offset Gaussian Curve"; its calculation was suggested by New and Bowers (1993). They introduced the offset parameter (a) into the Gaussian functions, as:

$$\delta_V = \delta_{V,\max} \exp\left(-\frac{(x-a)^2}{2\,i^2} \right) \qquad\qquad \text{Eq.3.3}$$

This new offset parameter (a) allows one to fit the new Gaussian functions with the field measurements, where the value of the offset parameter equals the offset distance (distance toward the first tunnel). The offset parameter (a) is obtained by trial and error, in order to fit the plots from Equation 3.3 to the field measurements. Further, the shape of the new Gaussian curve is always symmetrical.

An improved Gaussian function based empirical technique for twin tunnels, namely the "Superposition Technique", was given by Suwansawat and Einstein (2007). They found that the results from laboratory experiments and field observations demonstrated different ground loss between the first and second tunnel. Thus, the total surface settlement trough, measured after the second tunnel was excavated, tended to be asymmetric. The proposed technique, from which the asymmetrical curves can be gained, was divided into two steps. First, the ground response by the second tunnel was investigated by introducing the additional surface settlements, developed after the first shield had passed. This additional settlement was calculated by subtracting the settlements measured after the first shield passed from the one, after the second shield passed (Figure 3.17). For the majority of the Bangkok MRT Blue Line data, the additional settlements were less than the ones induced by the first shield. After obtaining the additional settlements, the final surface settlements can be obtained by superimposing the additional settlements and the settlements induced by the first shield. The final results for the Gaussian curves and the superposition curves, when they are compared to the field measurements between the Thiam Ruam Mit and Phaecharat Bumphen Stations, are illustrated in Figure 3.18. Suwansawat and Einstein (2007) also successfully adopted the superposition technique with the twin stacked tunnels in the Blue Line project; however, the sections, where a heave has occurred, are not suitable for this technique.
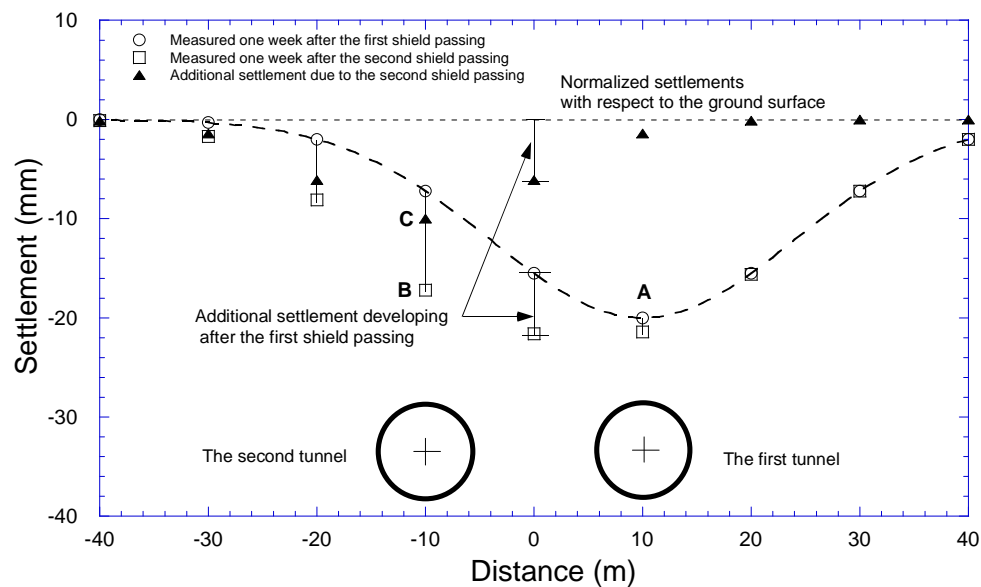
Figure 3.17: Additional Settlement Development after the First Shield Passed
(Suwansawat and Einstein, 2007)
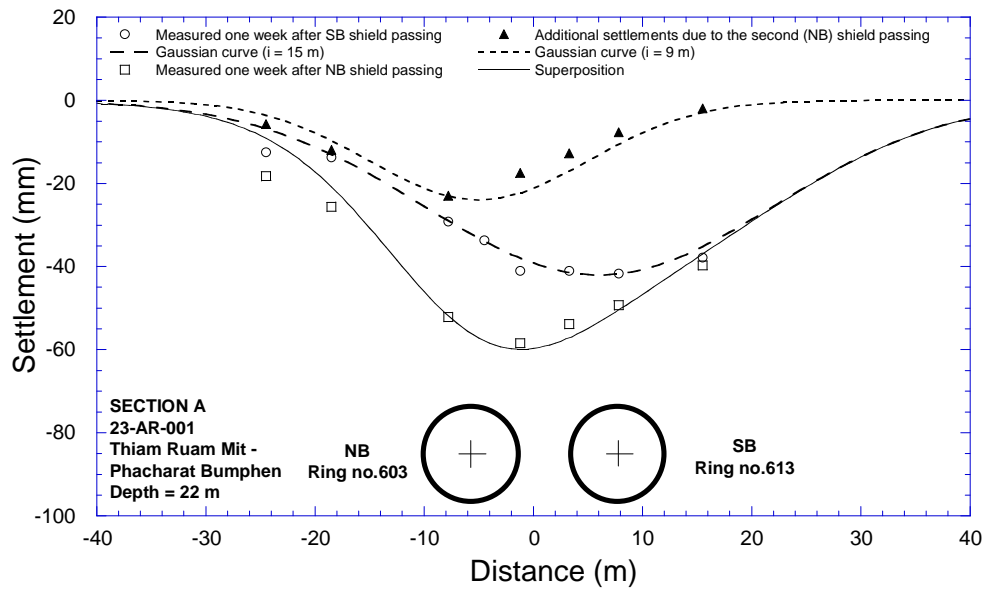
Figure 3.18: Surface Settlements Measured in Section A, Settlement Troughs
Described by Gaussian Curves and Superposition Curve

(Suwansawat and Einstein, 2007)

3.4.2.2 Numerical Methods

Many researchers (Chanchaya, 2000; Timpong, 2002; Du, 2003; Tavaranun 2004)
have conducted numerical analyses on the Bangkok MRT Blue Line project using
both Finite Element Method, FEM (using Plaxis software) and Finite Difference
Method, FDM (using Flac software). All these analyses have been undertaken in the
2D plane strain with the elastic perfectly plastic Mohr Coulomb model. The soil
parameters were obtained from the laboratory and field testing in the site investigation
reports. The main findings from each researcher are summarised in Table 3.6.

Table 3.6: Summary of Related Literature on the Bangkok MRT Blue Line Project

Author	Main Findings
Chanchaya (2000) *(Plaxis 2D)*	▪ Back calculation using 2D FE analysis has been conducted. ▪ The parameters E_u/s_u from back calculations suitable for soft and first stiff Bangkok clay layers are 240 and 480, respectively; these values are comparable to the pressuremeter test results from Teparaksa (1999).
Timpong (2002) *(Flac 2D)*	▪ Reasonable agreement between 2D finite element analysis and field observations can be obtained if the appropriated ground loss, expressed in percent relaxation, is adopted. ▪ The values of the percent relaxation range from 30 to 80 per cent.
Du (2003) *(Plaxis 2D)*	▪ Plaxis interface element is used to simulate the redial contraction between the shield and surrounding soil. ▪ The reduction factor (R) for the interface element property varies from 0.5-0.9, with the average being 0.7.
Tavaranum (2004) *(Plaxis 2D)*	▪ Back calculated percentage ground loss from the Plaxis analysis and analytical solution by Loganathan and Poulos (1998) are compared. ▪ Generally, good agreements are obtained from the two methods, with the values varying from 0.3-2.9%.

The 3D Finite Difference Analysis, using $FLAC^{3D}$, was conducted on the Bangkok Blue Line project by Hong (2005) and Phienwej *et al.* (2006). The Mohr-Coulomb failure criterion was used throughout the analysis. The undrained condition was assumed to be valid due to the very low permeability of the first Bangkok stiff clay and the impervious tunnel lining. The analysis investigated the effect of the influencing parameters on the ground deformations. The parameters included in the parametric study were: shield face pressure; coefficient of earth pressure at rest (K_o); variation of soil type, where the shield was located; initial ground pore pressure; and soil strength.

A part of the Bangkok Blue Line project, Section A (referred to in Figure 3.1), from the Thiam Ruam Mit Station to the Pracharat Bumphen Station was selected for the study. The dimensions in the finite element mesh were set in such a way that the boundary had no vital effect on the results of the analysis. As the tunnel shape is circular, only half of the tunnel was modelled. The typical model geometry and mesh generation is depicted in Figure 3.19, while the typical soil profile of Section A is shown in Figure 3.20.
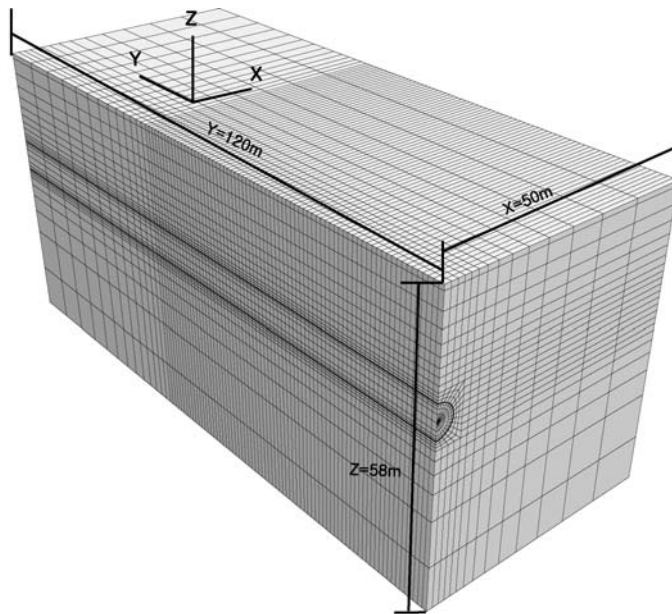
Figure 3.19: Three Dimensional FD Mesh for Tunnel Excavation (Hong, 2005)

Figure 3.20: Soil Profile in Section A (Hong, 2005)

Comparisons have been made in the results of uniform and non-uniform stress conditions (with $K_o = 1$ and K_o less than 1, respectively). The major governing parameter, face pressure, was set in the range from 50 to 400 kN/m^2, and was recorded for the upper and lower bound of the shield operation. As one would expect, a small surface settlement occurred when a high face pressure was applied. However, at the upper bound of the face pressure of the order of 400 and 350 kN/m^2 for the cases with uniform and non-uniform stress conditions, surface heaves were reported. As can be seen in Figure 3.21, the settlement in front of the shield is larger in the case of uniform stress conditions.
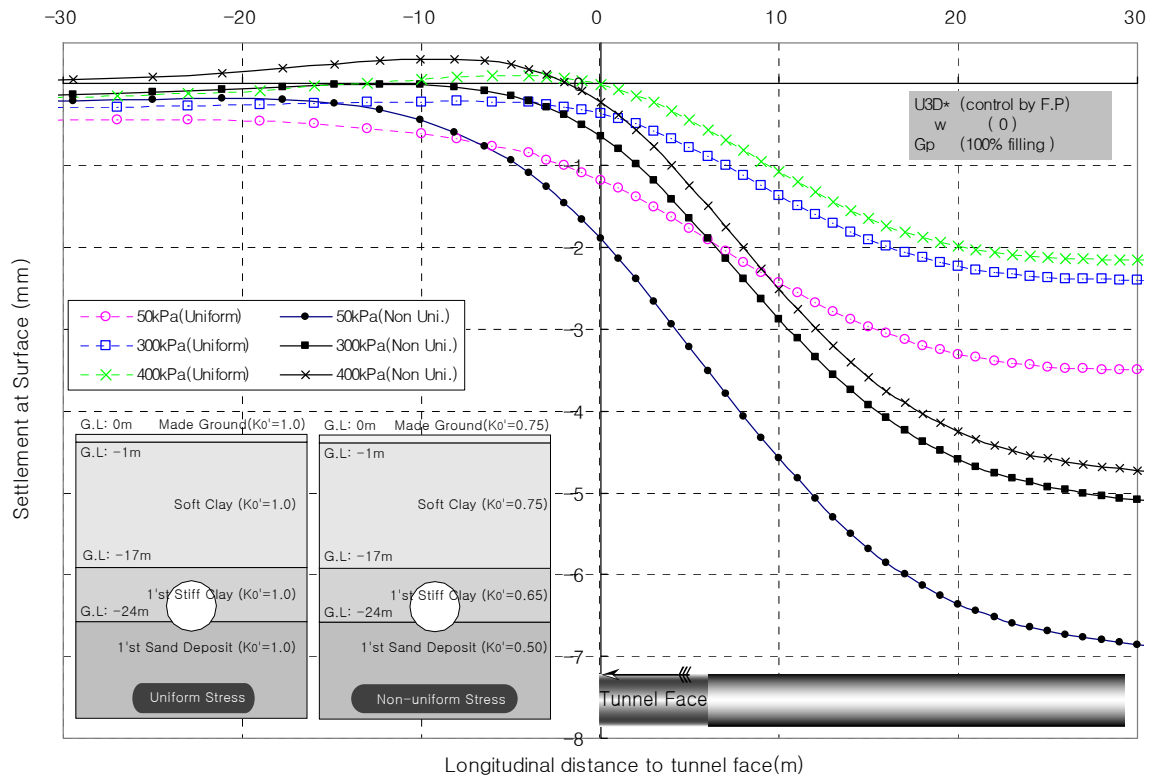
Figure 3.21: Comparison of Longitudinal Surface Settlement between Uniform and Non-Uniform Stress Analysis with Various TBM Face Pressures (Hong, 2005)

In contrast, the maximum surface settlement after the shield passed is larger in the case of the non-uniform stress conditions. An influenced zone of approximately four times the tunnel diameter was observed in each analysis.

To study the influence of the initial piezometric condition on the ground movement of the Bangkok subsoil, two sets of analyses were performed by Hong (2005). First, the initial pore pressure was assumed to be hydrostatic for the constant ground water level, at 1 m below the ground surface. Second, the pore pressure after the influence of the deep well pumping (referred to in Section 3.3.2) was assumed. The results reveal similar surface settlement in front and over the shield, but tend to be larger after shield passing in the case of the Bangkok piezometric pressure conditions as the initial pore pressures.

3.5 Concluding Remarks

This section   provides a summary of the work contained in this chapter. Firstly, the MRT works, including station excavations and the EPB shield tunnelling, were reviewed; vital construction techniques and design philosophies were discussed. Secondly, the Bangkok subsoil conditions were explained. The general consensus is that the MRT projects in Bangkok have encountered similar soil conditions, thus the Bangkok subsoils appear to be fairly uniform. Importantly, deep well pumping from Bangkok's aquifer has created long term ground subsidence, while also affecting the piezometric drawdown and the pore water pressures. The influences of this drawdown piezometric pressure, which differs from the hydrostatic condition, on soil parameter interpretations and finite element analyses, will be studied in subsequence chapters. Thirdly, the soil parameters were back-calculated from the deep excavation projects in Bangkok's subsoils. These studies pinpoint the E_u/s_u ratios as being back-calculated from the finite element analysis, with a basic linear elastic Mohr Coulomb Model. The results from literature review showed that the E_u/s_u ratio of 500 is suitable for soft to medium clays. For stiff to hard clays, a wider range of E_u/s_u ratios of 500 to 2000 were used. The review of the empirical methods revealed that trough width parameter (*i*) in Bangkok MRT projects fell within the range, as presented in Mair and Taylor (1997). The back-calculated stress relaxation ratios were within the wide range of 0.3 to 0.8. Finally, the back-calculated volume loss ratios, from 2D finite element analysis, were similar to the back-calculated values from Loganathan and Poulos (1998).

CHAPTER 4

Geotechnical Parameters Evaluated from Laboratory Tests

4.1 Introduction

The use of laboratory and in-situ tests, that help to determine the soil parameters in elastic or elastic perfectly plastic finite element analyses, has been widely developed and accepted, in part due to its simplicity. However, the soil behaviour is highly non-elastic in most instances. Over the past decades, enormous efforts have been made to further develop elasto-plastic finite element constitutive models. Nevertheless, the use of these constitutive models in engineering practice is still very limited, especially in South East Asian region. The reason for this lack of is higher degree constitutive models normally require additional parameters (i.e. advance laboratory or in-situ test results are required). These parameters are often costly and time consuming to evaluate. For this reason, the major aim of the current study (presented in this chapter) was to conduct an extensive study of the finite element parameters evaluation from conventional laboratory tests (i.e. triaxial and oedometer tests). Chapter 5 presents the finite element parameters evaluation from in-situ tests. The constitutive models related to this study are the Mohr Coulomb Model (MCM), the Hyperbolic Model (Duncan and Chang, 1970), the Hardening Soil Model (HSM), and the Hardening Soil Model with Small Strain Stiffness (HSS).

The work contained herein is in three parts. The first part relates to the undrained strength parameters of Bangkok Clays, as interpreted from the vane shear test (Bangkok Soft Clay) and CK_oU triaxial test (Stiff and Hard Clays). Path dependent drained strength parameters are also included in this section. The second one, which is the major part, relates to the interpretation of the oedometer and triaxial deformation parameters for the Hyperbolic and Hardening Soil Model analysis. The oedometer tests from the Bangkok MRT Blue Line Extension project are used in this work. A large number of the undrained and drained triaxial test series, conducted at Asian Institute of Technology, under the supervision of Prof. A. S. Balasubramaniam (Chaudhry, 1975; Ahmed, 1975; Hassan, 1976; Kim, 1991; Gurung, 1992), are also re-analysed. Table 4.1 summarised the sources and subsoil conditions of the oedometer and triaxial test series analysed in the current study. The third part presents an attempt to make a 2D finite element modelling of the triaxial and oedometer tests using Plaxis software. A series of parametric studies is undertaken to gain a better understanding of the effects of the input parameters. After that, a soil model calibration is completed using the curve matching process.

Table 4.1: Summary of Oedometer and Triaxial Tests Series Analysed in the Current Study

Type of test	Source	Related section	Subsoils tested
Oedometer	Feasibility study of Bangkok MRT Blue Line Extension project	4.5	Soft, medium, stiff and hard clays
CIU test Series I (Table 4.14)	Gurung (1992)	4.7	Normally consolidated soft clay (OCR = 1)
CIU, CK_oU and CK_oUE: Series II, III and IV (Table 4.14)	Kim (1991)	4.7	Lightly overconsolidated soft clay (OCR = 1 to 2.75)
CID, CK_oD and CK_oDE: Series V, VI and VII (Tables 4.19 to 4.21)	Kim (1991)	4.7	Lightly overconsolidated soft clay (OCR = 1 to 2.75)
CIU, CID (Tables 4.24 and 4.25)	Chaudhry (1975)	4.8	Soft clay (σ'_3 = 138 to 414 kN/m^2)
CIU, CID (Tables 4.27 and 4.28)	Hassan (1976)	4.8	Stiff clay (σ'_3 = 17 to 620 kN/m^2)

4.2 Types of Finite Element Analysis in Geotechnical Engineering

In conventional triaxial tests, undrained tests are applied to only clay soils, whereas drained tests are conducted in both clayey and sandy soils. Correspondingly, in finite element analysis, effective stress analysis is applied to drained materials, while both effective and total stress analyses are adopted for undrained materials (see Figure 4.1 and Table 4.2). An analysis of drained materials is relatively straightforward, as only the effective stress analysis (using effective strength and stiffness parameters) are used. An undrained material analysis is, on the other hand, complex and requires an understanding of the calculation methods and the constitutive models to be used. Further details of the undrained material analyses are summarised in Appendix A.
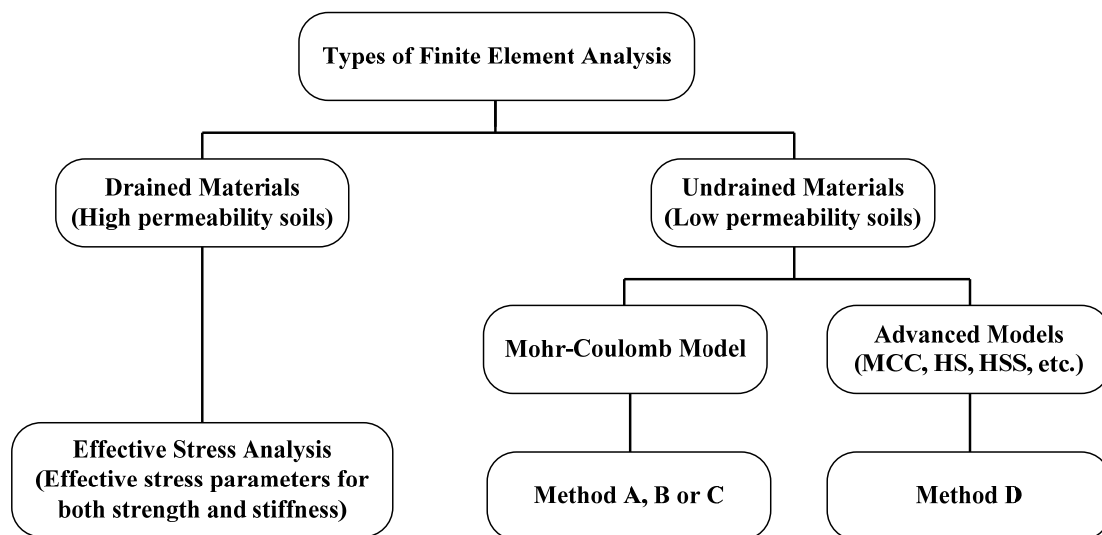
Figure 4.1: Types of Finite Element Analysis in Geotechnical Engineering

Table 4.2 (a): Summary of Analyses for Drained Materials

Material type	Material model	Computed stresses	Parameters	
			Stiffness	Strength
Drained	All soil models	Effective stress & pore pressure	Effective parameters depending on soil model selected	

106

Table 4.2 (b): Summary of Analyses for Undrained Materials

Method	Material type	Material model	Computed stresses	Parameters	
				Stiffness	Strength
A	Undrained (MC)	Mohr-Coulomb	Effective stress & pore pressure	Effective (E', v')	Effective (ϕ', c')
B	Undrained (MC)	Mohr-Coulomb	Effective stress & pore pressure	Effective (E', v')	Total (ϕ_u, c_u)
C1	Non-porous (MC)	Mohr-Coulomb	Total stress	Total (E_u, v_u)	Total (ϕ_u, c_u)
C2	Drained (MC)	Mohr-Coulomb	Total stress	Total (E_u, v_u)	Total (ϕ_u, c_u)
D	Undrained (MCC, SS, HS, HSS)	Hardening Soil or Soft Soil	Effective stress & pore pressure	Effective parameters depending on soil model selected	

NOTE: MC = Mohr-Coulomb Model, MCC = Modified Cam Clay Model, SS = Soft Soil Model, HS = Hardening Soil Model, and HSS = Hardening Soil Model with Small Strain

4.3 Strength Characteristics of Bangkok Clays

A discussion of the undrained and drained strength parameters of the Bangkok subsoils is presented in this section. As mentioned in Section 4.2, undrained shear strength is used in Method B and Method C analyses using the Mohr Coulomb Model. Using the advanced model analysis (Method D), the drained strength parameters (c' and ϕ') are used to govern the failure criteria. It is, however, necessary to perform some laboratory simulations to ensure that the undrained shear strength computed by the advanced model will not exceed the value of the in-situ undrained shear strength.

4.3.1 Undrained Shear Strength

The undrained shear strength of Bangkok Soft and Stiff clays are discussed in this section. To identify the undrained shear strength, the field vane shear and the CK_oU triaxial tests are utilised for the soft to medium stiff and the stiff to hard clays, respectively. Both the field vane shear and the CK_oU triaxial tests were conducted

along the alignment of the Bangkok MRT Blue Line Extension project. The field vane shear tests were conducted at 1.5 m intervals, until the approximate limit of 70 kN/m^2 was reached. A correction factor of 0.8 was applied to the vane shear strength, as per the work of Bjerrum (1973).

The CK$_o$U triaxial tests were carried out on 38 mm samples of the stiff to hard clays. A confining pressure of 0.7 times in-situ effective overburden pressure was applied at the consolidation stage. Then, the samples were sheared under undrained conditions. Figure 4.2 shows the undrained shear strength of the Bangkok clays from the field vane shear and the CK$_o$U triaxial tests.
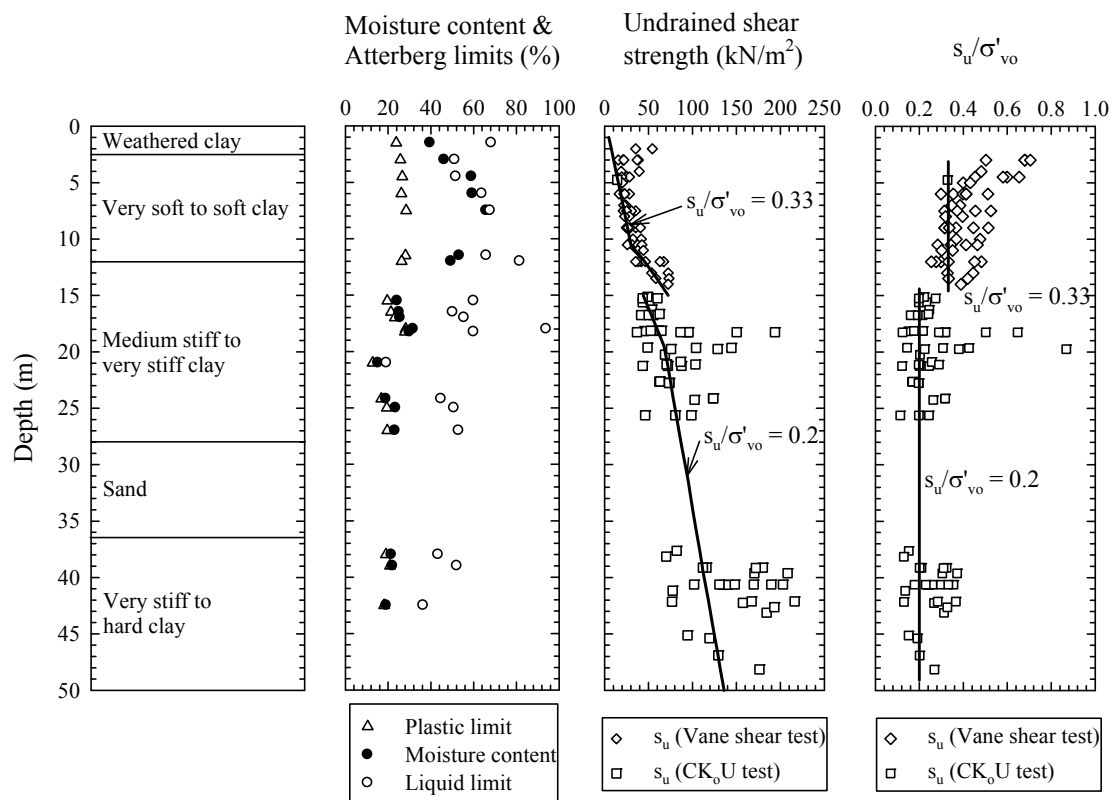
Figure 4.2: Undrained Shear Strength of Bangkok Clays Resulting from Vane Shear and CK$_o$U Triaxial Tests

The classical relations of the undrained shear strength-effective stress ratio (s_u/σ'_{vo}) and the plasticity index (I_p) are summarised in Table 4.3 and plotted in Figure 4.3. As seen from Figure 4.3, all three empirical methods give very close predictions, particularly within the range of I_p of 20 to 60. The ratio of s_u/σ'_{vo}, as predicted by the empirical methods for soft to medium stiff clay and stiff to hard clay, are summarised

in Table 4.3. s_u/σ'_{vo} ratio of 0.33 and 0.2 are selected as the average measured values for soft to medium stiff clay (3 to 15 m depth) and stiff to hard clay (15 to 50 m depth), respectively. These selected values of 0.33 and 0.2 also fall within the predicted range of s_u/σ'_{vo} ratio using Eqs. 4.1 to 4.3 (see Table 4.4 (a)).

Table 4.3: Undrained Shear Strength from Plasticity Index

Reference	Formulae	Eqs.
Skempton and Henkel (1953)	$s_u/\sigma'_{vo} = 0.0037 I_P + 0.11$	4.1
Osterman (1959)	$s_u/\sigma'_{vo} = 5 \times 10^{-7} I_P^3 - 8 \times 10^{-5} I_P^2$ $+ 6.8 \times 10^{-3} I_P + 0.08$	4.2
Bjerrum and Simons (1960)	$s_u/\sigma'_{vo} = 5 \times 10^{-7} I_P^3 - 8 \times 10^{-5} I_P^2$ $+ 7.4 \times 10^{-3} I_P + 0.06$	4.3
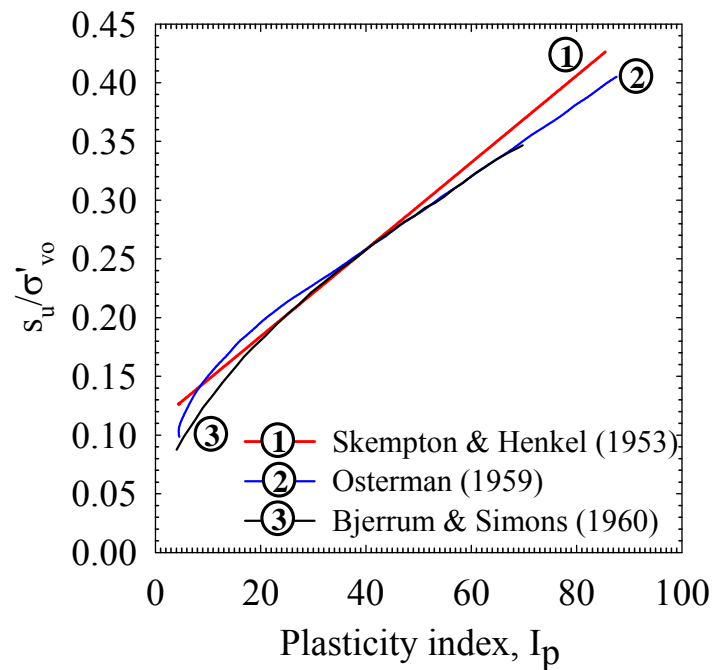
Figure 4.3: Relationships between s_u/σ'_{vo} and Plasticity Index

An alternative method used to estimate s_u/σ'_{vo} ratio is the SHANSEP technique (Ladd, 1991), developed at Massachusetts Institute of Technology (MIT). This method allows s_u/σ'_{vo} for the overconsolidated soil to be estimated. The relationship between s_u/σ'_{vo} and the overconsolidation ratio (OCR) is given by:

$$\frac{s_u}{\sigma'_{vo}} = S(OCR)^m \qquad \qquad \text{Eq. 4.4}$$

where, S is the normally consolidated value of s_u/σ'_{vo}, and m is the strength increase exponent. The values of S and m for homogeneous CL and CH sedimentary clays, for low to moderate sensitivity with I_p of 20 to 80, were suggested as 0.22 and 0.8, respectively (Ladd, 1991). These values were confirmed from the in-situ undrained shear strength a case study of the new Bangkok International Airport project in the Nong Ngoo Hao project (Bergado *et al.*, 2002). The OCR values resulting from the oedometer maximum past pressure (Figure 4.12, Section 4.5) and the s_u/σ'_{vo} ratios, calculated from Equation 4.4, are tabulated in Table 4.4 (b).

Table 4.4 (a): Measured and Predicted s_u/σ'_{vo} for Bangkok Subsoils

Clay types	Depth	I_p	s_u/σ'_{vo}	
			Eqs. 4.1 – 4.3	Average measured
Soft to medium	3 – 15	40 – 60	0.26 – 0.33	0.33
Stiff to hard	15 – 50	20 – 30	0.2 – 0.23	0.2

Table 4.4 (b): Measured and Predicted s_u/σ'_{vo} for Bangkok Subsoils

Clay types	Depth	OCR	s_u/σ'_{vo} (Eq. 4.4)
Soft	3 – 12	1.21 – 1.87	0.26 – 0.36
Stiff to very stiff	12 – 28	1.31 – 1.86	0.27 – 0.36
Very stiff to hard	37 – 45	1[*]	0.22

Note: [*] is assumed value

4.3.2 Drained Strength Parameters

The drained (effective) strength parameters, ϕ' and c', are important parameters in the geotechnical analysis and design stages. Indeed, drained strength parameters are used in effective stress analyses of drained material (sand) and undrained material (clays), using Methods A and D (see Table 4.2). In engineering practice, drained parameters

are often obtained from the results of triaxial tests. It is important, however, to recognise how the applied stress paths can influence the drained strength parameters. The second part of this section summarises the drained strength parameters of Bangkok subsoils, as identified in the literature, as well as the values obtained from this study.

The influence of an applied stress path on the strength parameter of soil has been studied through a comparison of the drained angle of internal friction (ϕ') as sheared in compression and in extension. The results from the triaxial compression and the extension tests, conducted at various consolidation stresses, are presented in Table 4.5. As seen in the figure, the difference between the drained angle of internal friction in compression and extension is more obvious in the case of the anisotropic (K_o) consolidated samples. The ratios of drained angle of internal friction in compression to extension (ϕ'_c / ϕ'_e) in the anisotropic (K_o) case are of the order of $0.7 - 0.76$ compared to $0.78 - 1.10$ in isotropic condition. Kulhawy and Mayne (1990) presented the ϕ'_c / ϕ'_e ratio of 0.82 in general case considering both isotropic and anisotropic samples. This ratio of 0.82 is close to the average of value of 0.83 according to the values given in Table 4.5.

Table 4.5: Comparison of Drained Angle of Internal Friction as Sheared in Compression and Extension

Reference	Soil Type	Consolidation Stage	ϕ'_c (degrees)	ϕ'_e (degrees)	ϕ'_c / ϕ'_e
Parry (1960)	Weald clay	Isotropic	21.0	22.3	0.94
Parry and Nadarajah (1973)	Kaolin clay	Isotropic	22.6	20.5	1.10
		Anisotropic (K_o)	20.8	28.0	0.74
Parry and Nadarajah (1974)	Fulford clay	Isotropic	26.6	34.0	0.78
		Isotropic (H*)	27.5	34.4	0.80
		Isotropic (I$^\Delta$)	29.2	35.0	0.83
Atkinson et al. (1987)	Kaolin clay	Isotropic	24.0	27.0	0.89
		1-D then K_o	22.0	29.0	0.76
Balasubramaniam et al. (1978)	Weathered Bangkok clay	Isotropic	22.2	29.0	0.77
Kim (1991)	Soft Bangkok clay	Isotropic	22.2	-	-
		Anisotropic (K_o)	23.0	33.1	0.70

Note: H* and I$^\Delta$ mean that the soil specimens have been collected horizontally and at a 45 degree incline, respectively

Table 4.6 (a) presents a summary of the drained strength parameters of the Bangkok subsoils (namely, weathered clay, soft clay, stiff clay and hard clay), from the literature. The notations for the triaxial tests identified in Table 4.6 (a) are explained in Table 4.6 (b). It can be seen that the differences in the applied stress path have the most effect on the drained strength parameters. Initial conditions at the consolidation state (i.e. isotropic or anisotropic), as well as the drainage conditions during shear (i.e. drained or undrained), also have an effect on the drained strength parameter, but in a lesser magnitude. As a result, the drained strength parameters should be carefully selected according to the applied stress path, resulting from the construction sequences.

Table 4.6 (a): Summary of Drained Strength Parameter of Bangkok Subsoils

Reference	Location	Depth (m)	Test type	ϕ' (degrees)	c' (kN/m^2)
Weathered Clay					
Balasubramaniam and Uddin (1977)	Nong Ngoo Hao	2.5 to 3.0	CIUE$_U$	28.9	0
Balasubramaniam *et al.* (1978)	Nong Ngoo Hao	2.5 to 3.0	CIU	22.2	0
			CID	23.5	0
			CIUE$_U$	29	0
Bangkok Soft Clay					
Balasubramaniam and Chaudhry (1978)	Nong Ngoo Hao	5.5 to 6.0	CIU	26	0
			CID	21.7	0
Balasubramaniam *et al.* (1978)	Nong Ngoo Hao	5.5 to 6.0	CIU	24	38
			CID	23.5	0
			CIDP	23.7	0
			CIUE^L	26	0
			CIUE^U	21.1	58.7
			CIDE^L	26.2	0
			CIDE^U	23.5	31.8
Kim (1991)	AIT campus	3.0 to 4.0	CIU	22.2	0
			CK$_o$U	23	0
			CK$_o$UE^U	33.1	0
			CK$_o$D	21.4	20
			CK$_o$DE^U	35.5	16.5
Stiff Clay					
Ahmed (1975), Balasubramaniam *et al.* (1978)	Nong Ngoo Hao	16.0 to 16.6	CID	26	30
			CIUE^L	18	54
			CIUE^U	25	54
			CIDE^U	16.6	11
Hassan (1976)	Nong Ngoo Hao	17.0 to 18.0	CIU	28.1	11.4
			CID	26.3	32.8
The current study	MRT Blue Line Extension	15.0 to 25.0	CK$_o$U	26.1[*]	26.9[*]
Hard Clay					
The current study	MRT Blue Line Extension	39 to 43	CK$_o$U	23.4[*]	41.9[*]

Note: [*] represents average values over the length as shown.

Table 4.6 (b): Descriptions for Triaxial Test Notations

Notations	Descriptions
CIU	Isotropically consolidated undrained triaxial compression test
CID	Isotropically consolidated drained triaxial compression test
CIDP	Isotropically consolidated drained triaxial test with constant p'
CK_oU	Anisotropically (K_o) consolidated undrained triaxial compression test
CK_oD	Anisotropically (K_o) consolidated drained triaxial compression test
$CIUE^L$	Isotropically consolidated undrained triaxial extension (loading) test
$CIUE^U$	Isotropically consolidated undrained triaxial extension (unloading) test

It should be pointed out that, some test results of Bangkok soft clay (from Table 4.6 (a)) showed unrealistically high values of drained cohesion (c'). These high magnitudes of the cohesion were of the order of 32 to 59 kN/m^2. The possible reasons of this, in the case of CIUE test is that, incorrect values of membrane correction may have been applied (using the compression correction for the extension one). Further, the pre-failure (i.e. necking failure) may have occurred during the extension test process. In the case of CIU test, the high value of c' could be the result of personal judgement on the p - q' curve fitting (to obtain ϕ' and c' parameters). A combination of low ϕ' and high c' can result in the shear strength values being similar when the ϕ' is higher with little or no cohesion.

4.4 Stiffness Moduli in Triaxial and Oedometer Tests

Janbu (1963) studied the relationship between tangent modulus of elasticity (E_t) and stress based on a range of soil types of the oedometer and triaxial tests results. His empirically based tangent modulus can be defined as:

$$E_t = \frac{d\sigma_1'}{d\varepsilon_1} = \frac{E}{1 - 2\upsilon K} \qquad \text{Eq. 4.5}$$

where E = Elastic modulus

        υ = Poisson's ratio

        K = Coefficient of earth pressure = σ_3'/σ_1'

        σ_1' = Effective major principle stress

$$\sigma'_3 = \text{Effective minor principle stress}$$

$$\varepsilon_1 = \text{Axial strain}$$

A simple empirical equation has been purposed to adequately take into account the relationship of the tangent modulus and stress by:

$$E_t = k \cdot p^{ref} \left(\frac{\sigma'}{p^{ref}} \right)^m$$ Eq. 4.6

where k = Dimensionless modulus number

m = Modulus exponential for stress dependency

p^{ref} = Atmospheric (reference) pressure $\approx 100 \text{ kN/m}^2$

Further, the exponential (m) can vary from zero to unity. The value of the power $m = 1$ represents normally consolidated clay, where the relationship of the tangent modulus and stress is linear; whereas, the power m of zero reveals perfectly elastic material behaviour with the constant E_t. The corresponding value of 0.5 is typically found for medium dense sand.

The modified Janbu (1963) equations are given by Brinkgreve (2002), with applications to both the constrained modulus (E_{oed}) and the drained triaxial modulus, at 50 per cent shear strength (E_{50}).

$$E_{oed} = E_{oed}^{ref} \left(\frac{c' \cdot \cot \phi' + \sigma'_1}{c' \cdot \cot \phi' + p^{ref}} \right)^m$$ Eq. 4.7

$$E_{50} = E_{50}^{ref} \left(\frac{c' \cdot \cot \phi' + \sigma'_3}{c' \cdot \cot \phi' + p^{ref}} \right)^m$$ Eq. 4.8

Where, E_{oed}^{ref} & E_{50}^{ref} are the reference moduli for the primary loading in the oedometer and the drained triaxial tests, respectively. It should be noted that, Eqs. 4.7 and 4.8

are identical to Eq. 4.6, when the term $c' \cdot \cot \phi'$ in Eqs. 1 and 2 is zero, and $E_{oed}^{ref}, E_{50}^{ref} = k \cdot p^{ref}$.

The hyperbolic stress-strain function, such as the one developed by Kondner (1963), and later formalised by Duncan and Chang (1970), can be used mathematically to express the relationship between the axial strain and the deviator stress in the triaxial compression test. The hyperbolic stress-strain function is widely accepted because it is applicable for both effective and total stress analyses.

The hyperbolic relation is given in the form of an equation as:

$$(\sigma_1 - \sigma_3) = \frac{\varepsilon}{a + b \cdot \varepsilon} \qquad \text{Eq. 4.9}$$

Where, a and b are constant parameters of the hyperbolae. Figure 4.4 (b) shows the determination of a and b in $\frac{\varepsilon}{(\sigma_1 - \sigma_3)}$ vs ε space. From Eq. 4.9 it can be seen that with a very small strain, the initial tangent elastic modulus (E_i) is equal to $1/a$. For large strains, where $(\sigma_1 - \sigma_3) = q_{ult}$, i.e. the ultimate asymptotic value of the deviator stress, the relationship becomes $q_{ult} = 1/b$.
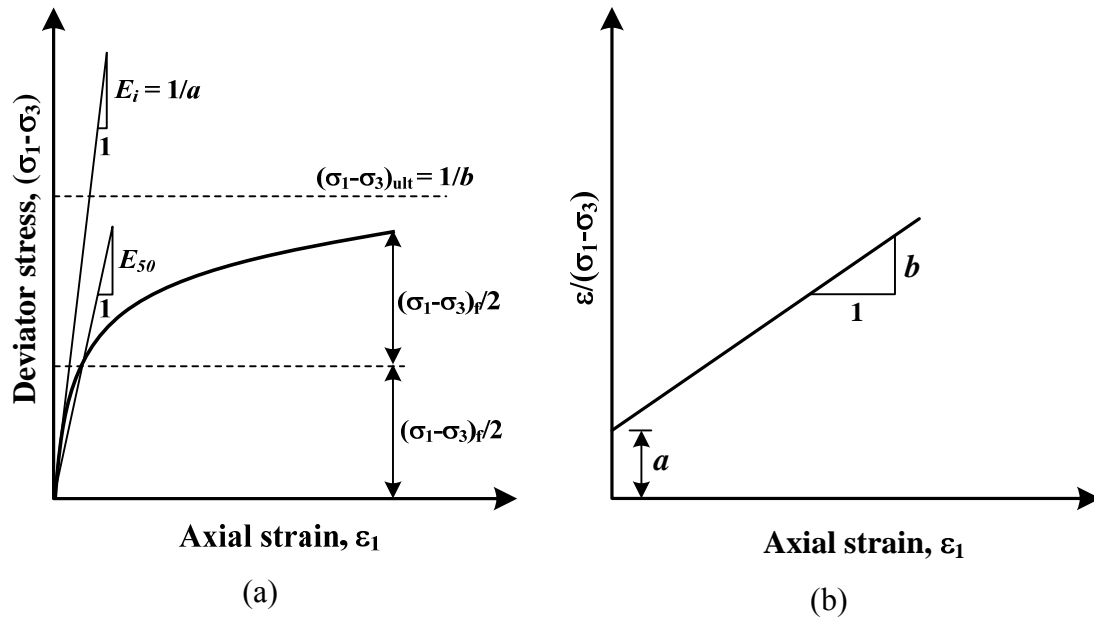
Figure 4.4: (a) Hyperbolic Stress-strain Curve,

(b) Transformed Hyperbolic Stress-strain Curve

116

From Eq. 4.9 and Figure 4.4 (a), with the secant modulus at 50 per cent shear strength, E_{50} is related to the initial stiffness modulus, E_i by:

$$E_{50} = E_i \left(1 - \frac{R_f}{2} \right)$$ Eq. 4.10

where, R_f is the failure ratio = q_f / q_{ult}. If the failure of the deviatoric stress is assumed to be a function of the confining pressure, σ'_3, the relationship between the compressive strength and the confining pressure maybe expressed in terms of the Mohr Coulomb failure criterion as:

$$(\sigma_1 - \sigma_3)_f = \frac{2c' \cdot \cos \phi' + 2\sigma'_3 \sin \phi'}{1 - \sin \phi'}$$ Eq. 4.11

where, c' and ϕ' are the soil cohesion and the angle of internal friction, respectively.

4.5 Consolidation Characteristics of Bangkok Clays

The aim of this section was to investigate the consolidation characteristics of Bangkok clays, based on the concept of Janbu (1963), see also Section 4.4 for stiffness moduli in triaxial and oedometer tests. The primary loading oedometer modulus (E_{oed}) and the unloading/reloading oedometer modulus ($E_{ur,oed}$) of the Bangkok soft clay, stiff and hard clays, are examined by means of both graphical and empirical methods.

The oedometer test results of the Bangkok clays from the site of the MRT Blue Line South Extension project, located on the eastern side of the Chao Phraya River, are analysed in this section. Further, the oedometer test results, from various depths, are divided into four groups, according to soil type and depth of undisturbed sampling. These groups are: soft clay at 6 to 8 m depths; medium clay at 12 to 14 m depths; stiff clay at 15.5 to 18 m depths; and very stiff to hard clay at 37.5 to 40.5 m depths. The resulting reference oedometer moduli (E_{oed}^{ref}, $E_{ur,oed}^{ref}$), the modulus exponential (m; from Eq. 4.6), Cam clay primary loading, and unloading/reloading parameter (λ^*, κ^*)

are presented in Tables 4.7 to 4.10. The reference moduli E_{oed}^{ref} and $E_{ur,oed}^{ref}$ are found by plotting normalised E_{oed} and $E_{ur,oed}$ versus normalised σ'_1 in double log scale plots (see Figures 4.5 to 4.8). In this plot, the reference loading and unloading/reloading constrained moduli (E_{oed}^{ref} & $E_{ur,oed}^{ref}$) can be found from the y-intercept of their linear trend lines; while the modulus exponential power (m) is the slope of the same lines. Figures 4.5 to 4.8 show the average values of E_{oed}^{ref}, $E_{ur,oed}^{ref}$ and their modulus exponential power (m) for soft clay layer (6 to 8 m), medium clay (12 to 14 m), stiff clay (15.5 to 18 m), and very stiff to hard clay (37.5 to 40.5 m), respectively.

Table 4.7: Consolidation Parameters Resulting from Oedometer Tests
on Soft Clay at 6 to 8 m

Test	Loading		Un/re-loading		$E_{ur,oed}^{ref} \Big/ E_{oed}^{ref}$	λ^*	κ^*
	E_{oed}^{ref} (kN/m^2)	m	$E_{ur,oed}^{ref}$ (kN/m^2)	m			
1	901	0.9	7679	1.1	8.5	0.115	0.009
2	1068	1.0	4310	1.5	4.0	0.094	0.008
3	858	0.9	7546	1.1	8.8	0.122	0.010
4	1105	0.7	4532	1.2	4.1	0.111	0.013
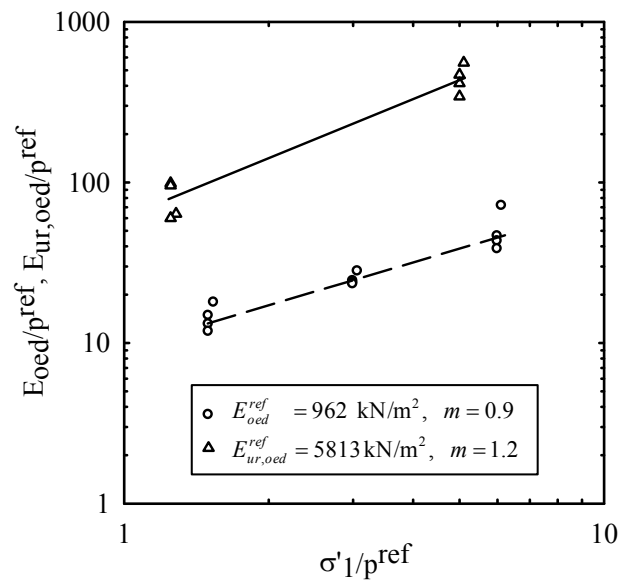
Figure 4.5: Variation of Oedometer Moduli with Consolidation Pressure
Resulting from Soft Clay at 6 to 8 m

Table 4.8: Consolidation Parameters Resulting from Oedometer Tests
on Medium Stiff Clay at 12 to 14 m

| Test | Loading | | Un/re-loading | | $E_{ur,oed}^{ref} \big/ E_{oed}^{ref}$ | λ^* | κ^* |
	E_{oed}^{ref} (kN/m²)	m	$E_{ur,oed}^{ref}$ (kN/m²)	m			
5	2282	0.6	8989	1.2	3.9	0.073	0.006
6	1429	0.6	2903	0.6	2.0	0.110	0.023
7	1749	0.5	7663	1.0	4.4	0.099	0.012
8	1288	0.6	4126	1.2	3.2	0.113	0.015
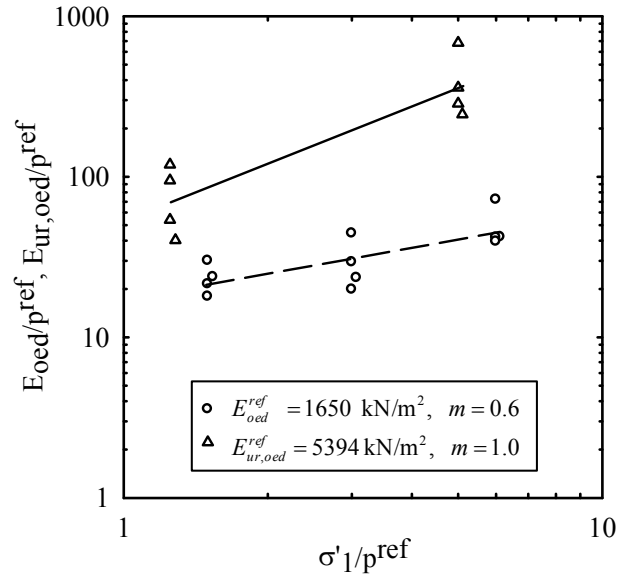
Figure 4.6: Variation of Oedometer Moduli with Consolidation Pressure
Resulting from Medium Clay at 12 to 14m

Table 4.9: Consolidation Parameters Resulting from Oedometer Tests
on Stiff Clay at 15.5 to 18 m

| Test | Loading | | Un/re-loading | | $E_{ur,oed}^{ref} / E_{oed}^{ref}$ | λ^* | κ^* |
| | E_{oed}^{ref} | m | $E_{ur,oed}^{ref}$ | m | | | |
	(kN/m^2)		(kN/m^2)				
9	5548	0.6	8670	1.1	1.6	0.033	0.009
10	5187	0.7	12451	1.0	2.4	0.032	0.007
11	3736	0.6	8241	1.0	2.2	0.049	0.012
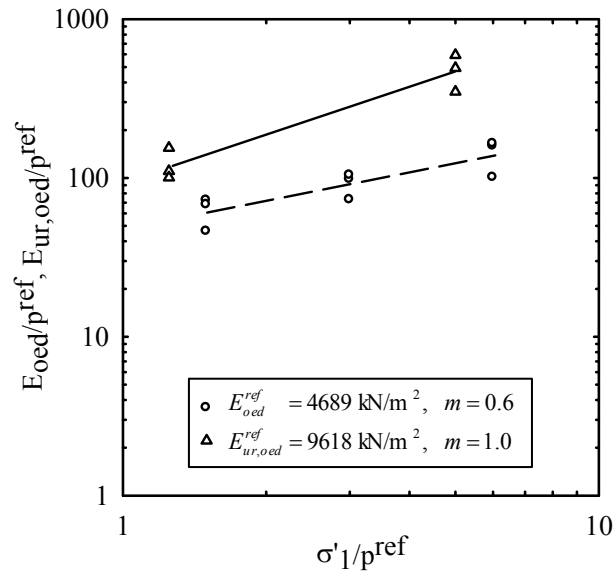
Figure 4.7: Variation of Oedometer Moduli with Consolidation Pressure
Resulting from Stiff Clay at 15.5 to 18 m

Table 4.10: Consolidation Parameters Resulting from Oedometer Tests
on Stiff to Hard Clay at 37.5 to 40.5 m

Test	Loading		Un/re-loading		$E_{ur,oed}^{ref} \big/ E_{oed}^{ref}$	$\lambda*$	$\kappa*$
	E_{oed}^{ref}	m	$E_{ur,oed}^{ref}$	m			
	(kN/m^2)		(kN/m^2)				
12	6262	0.4	8888	1.0	1.4	0.060	0.010
13	2598	0.7	11275	1.0	4.3	0.056	0.008
14	5082	0.5	6714	1.1	1.3	0.059	0.009
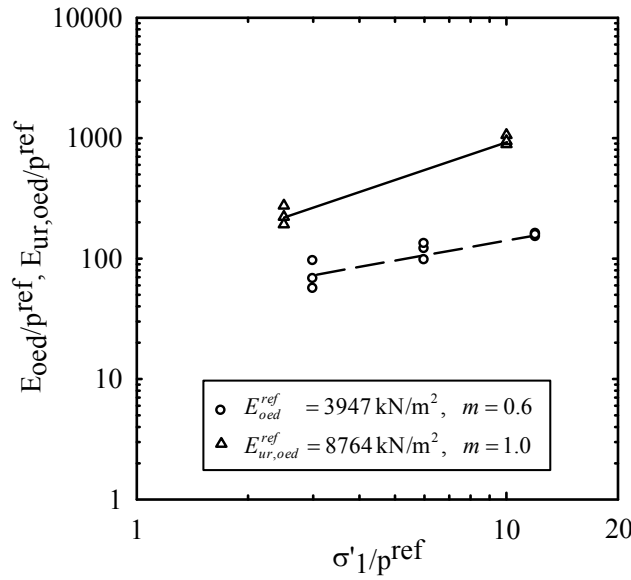
Figure 4.8: Variation of Oedometer Moduli with Consolidation Pressure
Resulting from Stiff to Hard Clay at 37.5 to 40.5 m

The averaged values of E_{oed}^{ref} for each subsoil layer are in the order of 926, 1650, 4689 and 3947 kN/m^2 for soft, medium, stiff and very stiff to hard clays, respectively. For $E_{ur,oed}^{ref}$, these average values are 5813, 5394, 9618 and 8764 kN/m^2 for soft, medium, stiff and very stiff to hard clays, respectively. The values of the exponential power (m) are close to unity for E_{oed}^{ref} in soft clay and for $E_{ur,oed}^{ref}$ in all layers. This finding is in agreement with the power m of 1 for normally consolidated clay (Janbu, 1963). The values of power m for E_{oed}^{ref} in medium, stiff and very stiff to hard clays are, however, reducing to 0.6. The ratios of $E_{ur,oed}^{ref} / E_{oed}^{ref}$ in the soft clay layer generally range from 2

to 4. These ratios tend to reduce with depth as the soil strength increases. The lower and upper bound values are 1.3 (hard clay) and 8.8 (very soft clay).These average values are also summarised in Table 4.11.

Table 4.11: Summary of Averaged E_{oed}^{ref}, $E_{ur,oed}^{ref}$ and m from Figures 4.5 to 4.8

Subsoils	Depth (m)	Loading		Un/re-loading	
		E_{oed}^{ref} (kN/m^2)	m	$E_{ur,oed}^{ref}$ (kN/m^2)	m
Soft clay	6 - 8	962	0.9	5813	1.2
Medium clay	12 - 14	1650	0.6	5394	1.0
Stiff clay	15.5 - 18	4689	0.6	9618	1.0
Very stiff to hard clay	37.5 - 40.5	3947	0.6	8764	1.0

Liquidity index (I_l), E_{oed}^{ref}, $E_{ur,oed}^{ref}$, λ^* and κ^* according to Figure 4.5 to 4.8, are plotted with depth in Figure 4.9. The liquidity index is defined as:

$$I_l = \frac{w_n - w_p}{I_p}$$

Eq. 4.12

where, w_n = Natural moisture content

w_p = Plastic limit

I_p = Plastic index

In the soft clay layer up to about 12 m depth, the liquidity index values are high and close to unity. This outcome indicates that the in-situ natural moisture content of soft clay is approaching its liquid limit. The soil liquidity indices gradually reduce with depth to small values of close to zero in the stiff to very stiff and hard clay layers. The values of the liquidity index close to zero indicate that stiff to very stiff and hard clays are within their plastic stage. Indeed, the tendency of the liquidity index to reduce with depth is similar to that of the Cam clay primary loading parameter (λ^*). A similar, but reverse, relationship is found for I_l and E_{oed}^{ref}. These tends have led to the establishment of simple correlations, as shown in Figures 4.10 and 4.11. Further, the

following equations can be used to estimate λ^* and E_{oed}^{ref} from I_l with a reasonable R^2 of 0.8545 and 0.9311, respectively.

$$\lambda^* = 0.0239\ln(I_l) + 0.117 \qquad\qquad \text{Eq. 4.13}$$

$$E_{ref}^{oed} = 9238(I_l)^{-0.5643} \qquad\qquad \text{Eq. 4.14}$$
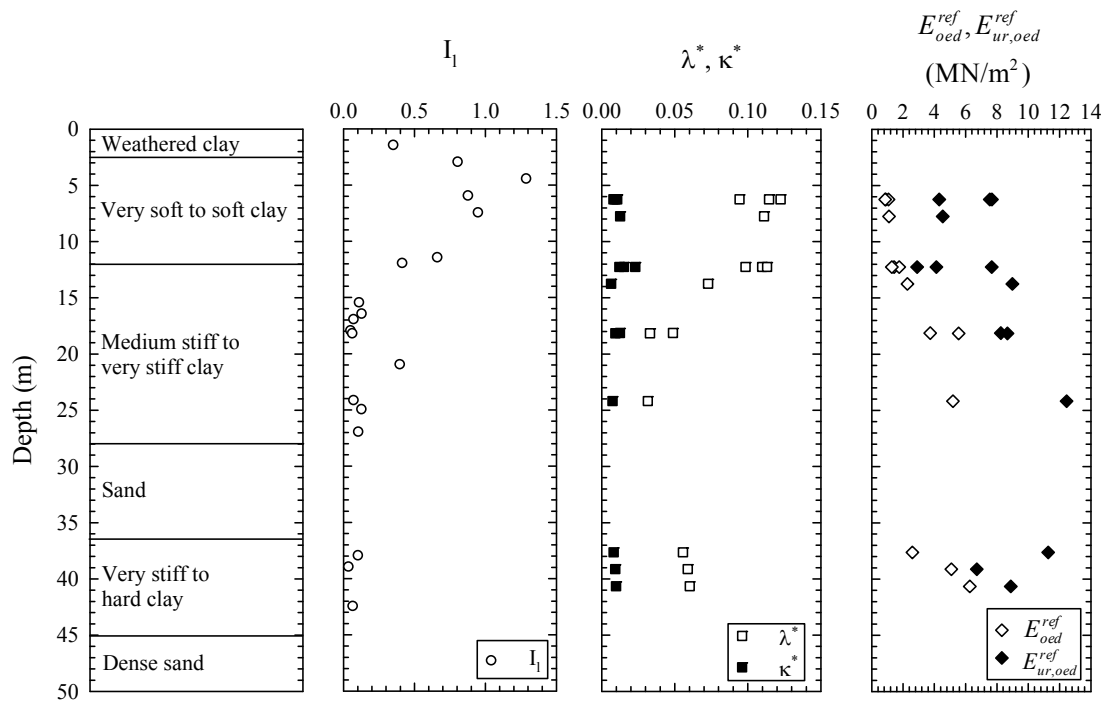
Figure 4.9: Consolidation Parameters and Liquidity Index of Bangkok Subsoils
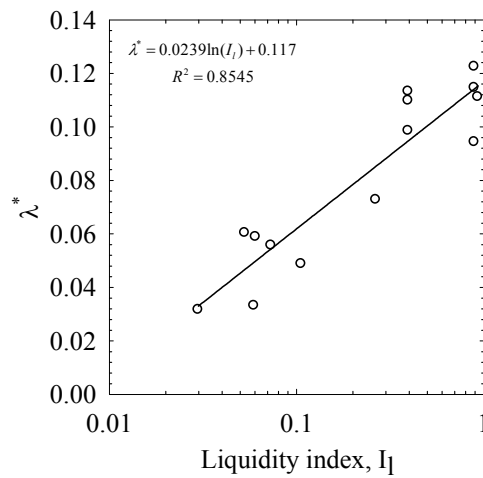
Figure 4.10: Regression Analysis of λ^* and I_l

123
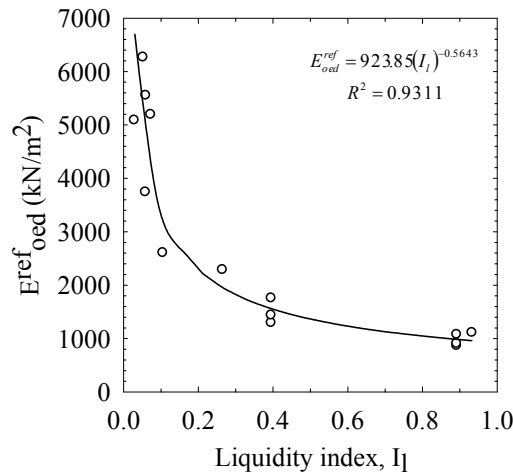
Figure 4.11: Regression Analysis of E_{oed}^{ref} and I_l

Figure 4.12 shows the plot of the overconsolidation Ratio (OCR) resulting from the maximum past pressure (oedometer test) with depth. The OCR in the soft clay layer ranges from 1.21 to 1.87. In the medium to stiff clay, with a depth from12 to 16 m, the OCR values are within the range of 1.31 to 1.86. At a deeper depth, the resulting OCRs are less than one. This outcome may be due to the disturbance of the soil sampling.
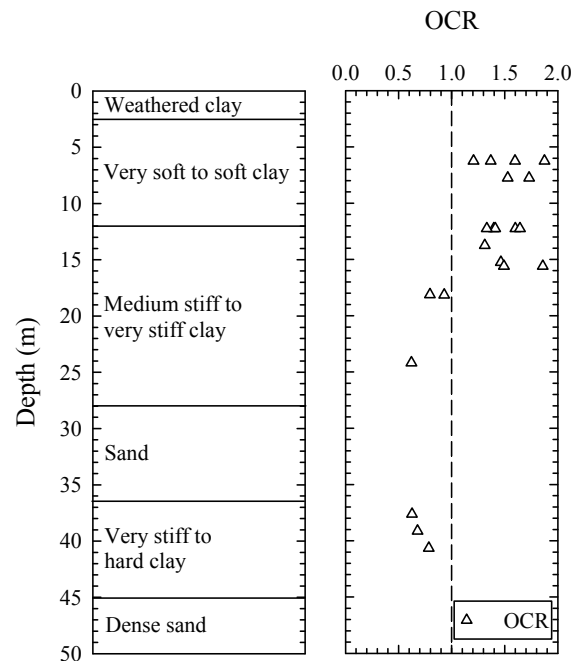
Figure 4.12: Overconsolidation Ratio (OCR) of Bangkok Subsoils

4.6 Undrained Modulus of Cohesive Soils

The stiffness of the cohesive soils in the undrained condition is characterised by the undrained elastic modulus applicable to the elastic response before the plastic yielding. Of importance are such factors as soil anisotropy, stress history, difference types of testing, and their test conditions, which can result in variations of the undrained modulus. Kulhawy and Mayne (1991) have summarised the literature on the typical ranges of undrained modulus for the clay, as shown in Table 4.12.

Table 4.12: Typical Ranges of Undrained Modulus for Clays

Clay types	Undrained modulus, E_u (kN/m^2)
Soft	1500 to 4000
Medium	4000 to 8000
Stiff	8000 to 20000

The undrained modulus, E_u is commonly normalised by the undrained shear strength, s_u, as E_u/s_u ratio. Based on the data from the direct simple shear (CK$_o$UDSS) test on seven normally consolidated soil samples, Ladd et $al.$ (1977) concluded that E_u/s_u ratios decrease substantially with the increase in plasticity, organic content, applied shear stress ratio (τ_h/s_u), and OCR. The broad and more general forms of E_u/s_u, OCR and I_p relationships are shown in Figure 4.13 (Duncan and Buchignani, 1976).
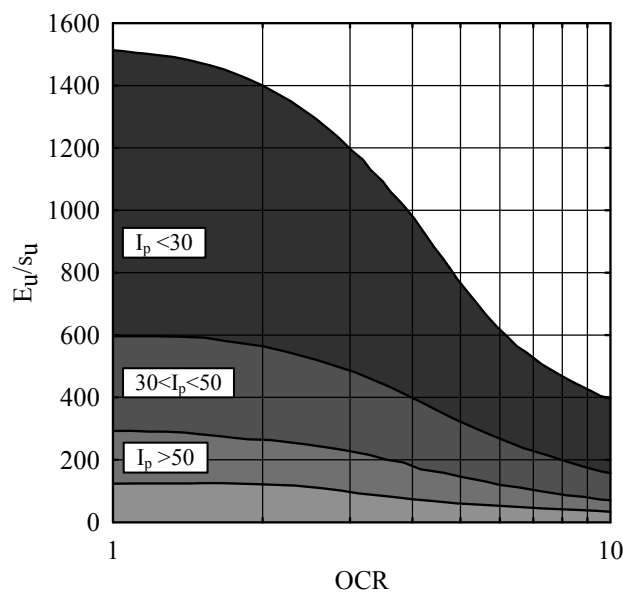
Figure 4.13: E_u/s_u, OCR and I_p Relationships (Duncan and Buchignani, 1976)

An alternative way of considering the E_u/s_u and OCR relationship is to utilise the Cam clay based model. Mayne and Swanson (1981) gave the normalised relationship for the normally consolidated clay $(E_{u,i}/s_u)_{nc}$ as:

$$(E_{u,i}/s_u)_{nc} = \frac{2M(1+e_o)\ln(10)}{C_c \cdot \Lambda(1-\Lambda)\exp(-\Lambda)}$$

Eq. 4.15

where, C_c is the virgin compression index, e_o is the initial void ratio, M is the slope of critical state line, and $\Lambda = 1 - (\kappa/\lambda)$. This equation corresponds to the CIU triaxial compression condition. The Modified Cam Clay model, proposed by Wroth *et al.* (1979), can be used to estimate the undrained modulus ratio of the overconsolidated clay as:

$$(E_{u,i}/s_u)_{oc} = (E_{u,i}/s_u)_{nc}(1+C\ln(OCR))\cdot OCR^{-\Lambda}$$

Eq. 4.16

where, C is an experimentally based constant which is likely to be between 0 and 2. A value of C equal to one is suggested for the laboratory test data.

4.7 Stress-strain Characteristics of Bangkok Clays

This section consists of two parts. The first one (Sections 4.7.1 to 4.7.6) deals with the effects of the applied stress paths on the deformation moduli of Bangkok soft clays, in the normally to lightly overconsolidated states (OCR of 1 to 2.75). The second part (Sections 4.7.7 to 4.7.9) considers the stress-strain characteristics of both soft and stiff clays under various applied confining pressures. The drained and undrained soil parameters to be used in the Hyperbolic Soil Model (Duncan and Chang, 1970) and the Hardening Soil Model were determined from the isotropic and K_o-consolidation triaxial test series. The results were compared with the values from previous studies reported in the literature review, and the Cam Clay based method.

4.7.1 Basic Soil Properties and Testing Programmes of Lightly Overconsolidated Bangkok Soft Clay

The undrained and drained, compression and extension tests were performed on Bangkok soft clay. The undisturbed clay samples were taken from a site located within the Asian Institute of Technology campus. Thin-walled piston samplers, with a 75 mm diameter and 90 mm long, were used to collected the samples from a depth of 3 to 4 m. The basic engineering properties of the tested soil are summarised in Table 4.13.

Table 4.13: Basic Engineering Properties of Bangkok Soft Clay (Kim, 1991)

Natural water content, w_n (%)	81 ± 5
Liquid limit, w_l (%)	98
Plastic limit, w_p (%)	37
Plasticity index, I_p	61
Liquidity index, I_l	0.73
Average unit weight, γ (kN/m^3)	14.8
Specific gravity, G_s	2.69
Clay content (%)	70
Silt content (%)	24
Sand content (%)	6

The testing programme comprised of seven series of tests (4 undrained and 3 drained tests). Series I, II, II, V and VI were compression tests, where the cell pressure was kept constant while the axial stress increased until failure. Series IV and VII were tested in a standard extension mode. All the triaxial tests were conducted by Kim (1991) and Gurung (1992). Details of all the test series are summarised in Tables 4.14 and 4.15.

Table 4.14: Summary of Undrained Test Series

Series	Test Type	OCR	p_0 (kN/m^2)	q_0 (kN/m^2)	K_o	p_f (kN/m^2)	q_f (kN/m^2)	ε_{af} %
I	CIU 1.1	1.00	150	0	1	94	62	6.6
	CIU 1.2	1.00	300	0	1	207	157	6.9
	CIU 1.3	1.00	586	0	1	328	267	9.9
	CIU 1.4	1.00	635	0	1	366	301	9.2
II	CIU 1	1.00	635	0	1	366	301	9.2
	CIU 2	1.24	539	0	1	377	313	9.8
	CIU 3	1.50	466	0	1	341	311	8.0
	CIU 4	1.78	408	0	1	328	298	9.6
	CIU 5	2.15	353	0	1	334	295	7.1
	CIU 6	2.75	295	0	1	331	271	5.7
III	CK$_o$U 1	1.00	439	216	0.63	361	293	2.9
	CK$_o$U 2	1.24	382	163	0.67	348	291	3.5
	CK$_o$U 3	1.50	339	124	0.71	333	291	3.7
	CK$_o$U 4	1.78	305	88	0.76	302	290	3.1
	CK$_o$U 5	2.15	273	59	0.81	282	277	3.1
	CK$_o$U 6	2.75	238	25	0.90	263	255	4.9
IV	CK$_o$UE 1	1.00	439	216	0.63	358	-348	-19
	CK$_o$UE 2	1.24	382	163	0.67	338	-350	-18
	CK$_o$UE 3	1.50	339	124	0.71	348	-278	-9
	CK$_o$UE 4	1.78	305	88	0.76	349	-318	-14
	CK$_o$UE 5	2.15	273	59	0.81	341	-312	-16
	CK$_o$UE 6	2.75	238	25	0.90	341	-320	-13

Table 4.15: Summary of Drained Test Series

Series	Test Type	OCR	p_0 (kN/m^2)	q_0 (kN/m^2)	K_o	p_f (kN/m^2)	q_f (kN/m^2)	ε_{af} (%)
V	CID 1	1.00	632	0	1	831	594	26.1
	CID 2	1.24	537	0	1	713	539	23.7
	CID 3	1.50	462	0	1	630	512	24.9
	CID 4	1.78	406	0	1	558	482	24.6
	CID 5	2.15	347	0	1	494	456	26.8
	CID 6	2.75	293	0	1	407	378	19.1
VI	CK$_o$D 1	1.00	441	217	0.63	509	420	21.3
	CK$_o$D 2	1.24	382	164	0.67	451	369	21.3
	CK$_o$D 3	1.50	339	124	0.71	411	339	20.1
	CK$_o$D 4	1.78	306	90	0.75	375	296	10.0
	CK$_o$D 5	2.15	272	58	0.81	355	308	10.7
	CK$_o$D 6	2.75	238	26	0.90	323	286	7.7
VII	CK$_o$DE 1	1.00	439	219	0.63	271	-291	-18.4
	CK$_o$DE 2	1.24	381	171	0.65	239	-260	-20.4
	CK$_o$DE 3	1.50	341	128	0.70	225	-223	-20.7
	CK$_o$DE 4	1.78	304	91	0.75	204	-223	-22.1
	CK$_o$DE 5	2.15	273	66	0.79	184	-212	-12.3
	CK$_o$DE 6	2.75	238	32	0.88	170	-183	-11.8

4.7.2 Undrained Triaxial Test on Normally Consolidated Clay (Series I)

The first series of tests (Series I) were carried out on a normally consolidated sample, with a consolidation pressure that ranged from 150 to 635 kN/m^2. Two of the undrained deformation parameters, namely the initial undrained tangent modulus ($E_{u,i}$) and the undrained tangent modulus at 50 per cent shear strength ($E_{u,50}$), were determined from the hyperbolic stress-strain curve and the transformed hyperbolic stress-strain curve (as shown in Figure 4.14 (a and b)). It can be seen from Figure 4.14 (a) that the stress-strain curves for all the CIU tests were fairly hyperbolic in shape,

except for a number of small parts at the axial strain of more than 10%; these parts showed some strain softening. The transformed hyperbolic test data in Figure 4.14 (b) agrees well with the linear trend lines revealing that the stress-strain curves were fairly hyperbolic in shape. The reference moduli, $E_{u,i}^{ref}$ and $E_{u,50}^{ref}$, and the corresponding exponential power (m) can be determined using Eq. 4.6; the values of the tangent moduli are plotted at different confining pressures in a double logarithmic scale. From Figure 4.14 (c), the reference moduli of $E_{u,i}^{ref}$ is 61334 kN/m^2, $E_{u,50}^{ref}$ is 5717 kN/m^2, and the corresponding m of 0.65 and 0.77 were obtained.
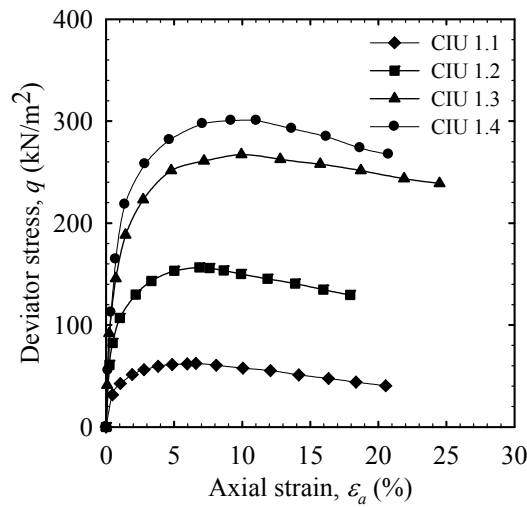
Figure 4.14 (a): q versus ε_a Plot of CIU Test Series I
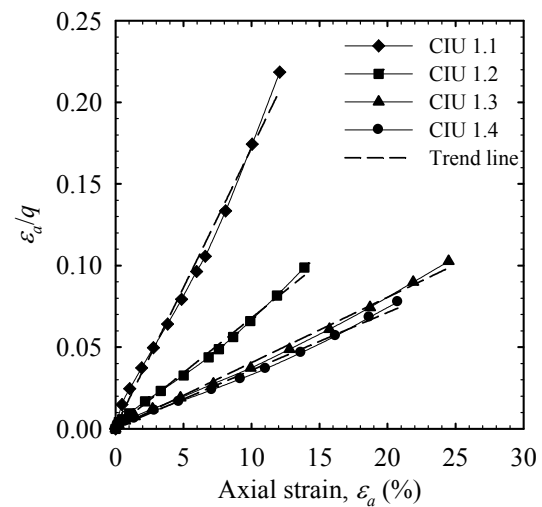
Figure 4.14 (b): Transformed Hyperbolic Stress-Strain Curve of CIU Test Series I
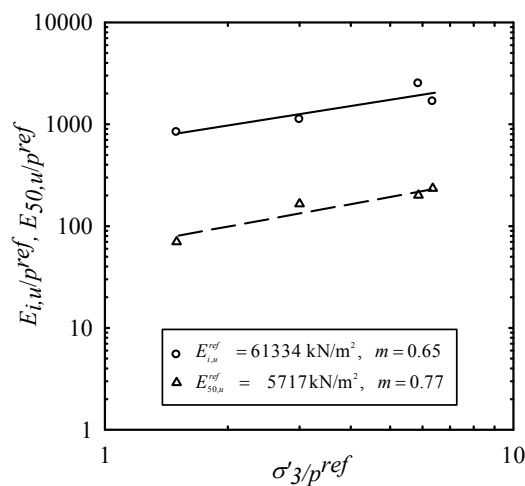
Figure 4.14 (c): Variations of $E_{u,i}$ and $E_{u,50}$ with Confining Pressure of CIU Test Series I

4.7.3 Undrained Triaxial Test on Lightly Overconsolidated Clay (Series II, III and IV)

Tests series II, III and IV were conducted on lightly overconsolidated clay, with the OCR ranging from 1.0 to 2.7. The deviator stress and pore pressure were recorded against the axial strain. The undrained test results for all three series (CIU, CK_oU and CK_oUE) are shown in Figures 4.15 to 4.17, respectively. The deviator stress–axial strain relationships of all the specimens were roughly the same, except for CIU 6, CK_oU 5 and CK_oU 6. In the CK_oUE test series all the (q, ε_a) relationships were nearly identical. Most of the q–ε_a curves depict a normally to lightly overconsolidated clay behaviour with strain hardening, except for CIU 6 (OCR of 2.75), which shows brittle failure behaviour with clear peak deviator stress at 5.7 per cent axial strain.
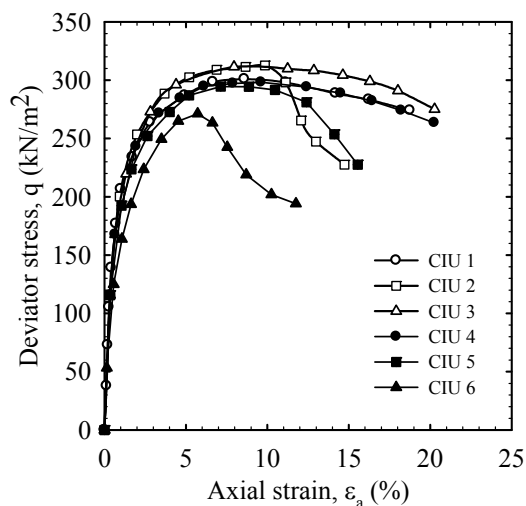
Figure 4.15 (a): q versus ε_a Plot of CIU Test Series II
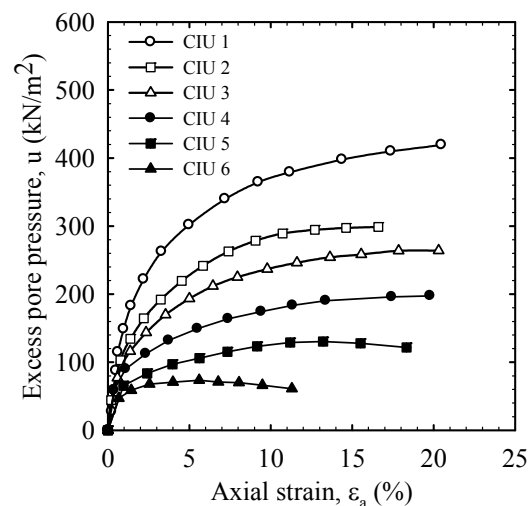
Figure 4.15 (b): u versus ε_a Plot of CIU Test Series II
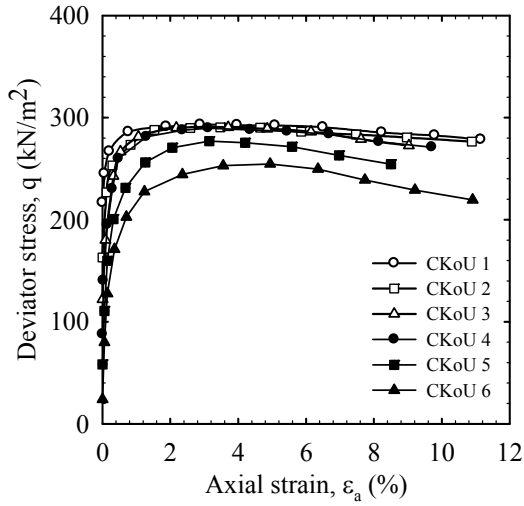
Figure 4.16 (a): q versus ε_a Plot of
CK$_o$U Test Series III
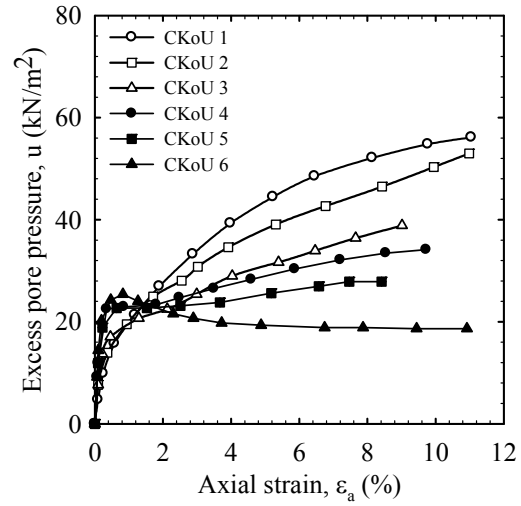
Figure 4.16 (b): u versus ε_a Plot of
CK$_o$U Test Series III
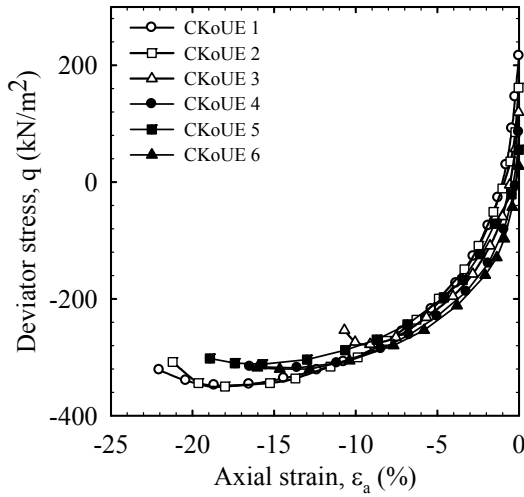
Figure 4.17 (a): q versus ε_a Plot of
CK$_o$UE Test Series IV
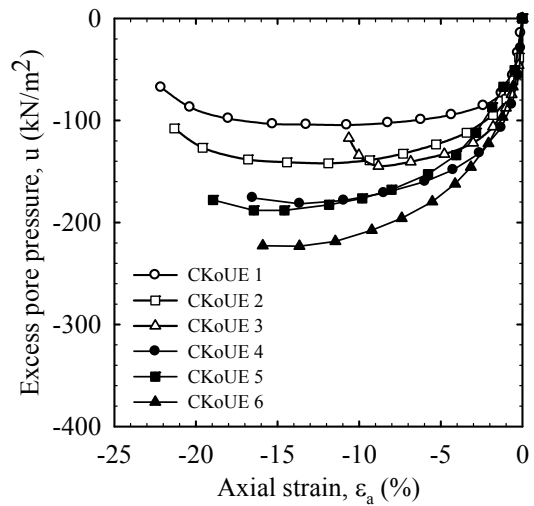
Figure 4.17 (b): u versus ε_a Plot of
CK$_o$UE Test Series IV

Figure 4.15 (b) illustrates the (u, ε_a) relationship for the overconsolidated samples sheared from the isotropic stress state (CIU). Consistent trends in the continuous development of the smaller excess pore pressures, with increasing OCR at all strain levels, were observed. Similar trends are shown in Figure 4.16 (b) for the CK$_o$U samples, with OCR values of 1.00, 1.24, and 1.50. The samples with the OCR values of 1.78, 2,15, and 2.75, a higher pore pressure is developed, initially at a low strain up

to ε_a of about 1%, and then the (u, ε_a) relationship seems to rise at a lower rate. However, beyond the axial strain of 1.5% the trend in excess pore pressure that was developed reduced with the increase in the OCR values. Figure 4.17 (b) shows a steady reduction in the pore water pressure, with an increase in the axial strain for all the samples sheared, in extension, under unloading conditions. Except for samples CK_oUE 3 and CK_oUE 5, all the other samples had a reduction in the excess pore pressure, which consistently increased with the OCR values.

4.7.4 Drained Triaxial test on Lightly Overconsolidated Clay (Series V, VI and VII)

As with the undrained test series, the drained behaviour of the lightly overconsolidated Bangkok clay was studied comprehensively using the conventional CID, CK_oD and CK_oDE tests. All the tested specimens had the same pre-shear void ratio, with the OCR values being 1.00, 1.24, 1.50, 1.78, 2.15, and 2.75. The deviator stress and volumetric strain, plotted with the axial strain, are shown in Figures 4.18 to 4.20. The initial deviator stress–axial strain relationships of all the test series were roughly the same up to the deviator stresses of 320, 300 and -120 kN/m^2 for CID, CK_oD and CK_oDE, respectively. Beyond these values of the deviator stress, the samples were each found to have different stress–strain curves.

As can be seen in Figures 4.18 (b) and 4.19 (b), the $(\varepsilon_v, \varepsilon_a)$ relationships of drained compression test series (CID and CK_oD), for all the tested samples, coincided with the contraction zone (positive ε_v), up to the axial strain of 2%. Beyond this axial strain all the curves started to diverge and the $(\varepsilon_v, \varepsilon_a)$ relationships tended to reduce with the increasing of OCR values. For the extension test series (CK_oDE) in Figure 4.20, all the $(\varepsilon_v, \varepsilon_a)$ curves fell into the dilation zone (negative ε_v). However, a clear relationship between $(\varepsilon_v, \varepsilon_a)$ and a variation in the OCR values could not be observed.
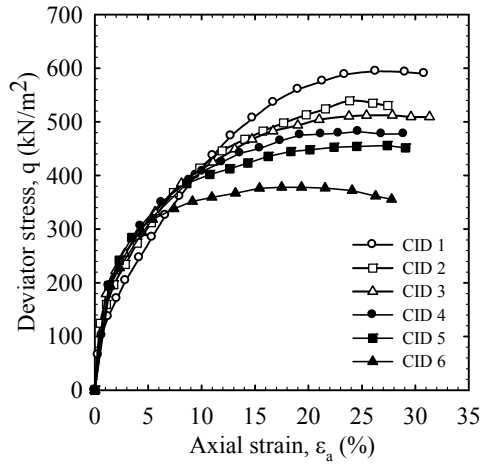
Figure 4.18 (a): q versus ε_a Plot of
CID Test Series V
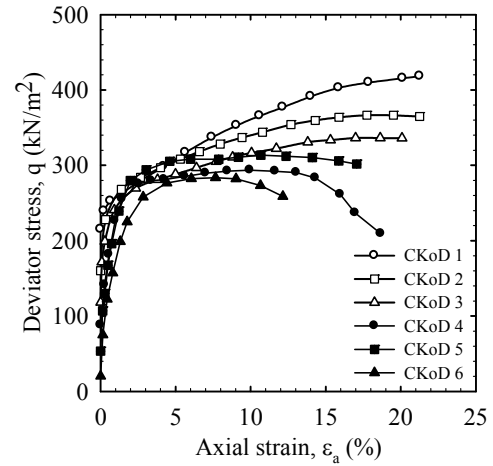
Figure 4.19 (a): q versus ε_a Plot of
CK$_o$D Test Series VI
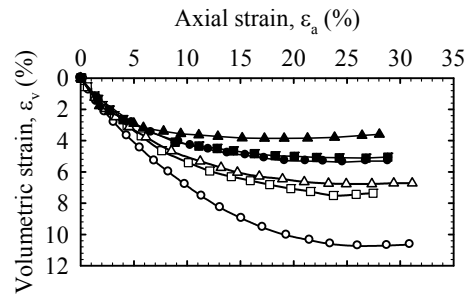
Figure 4.18 (b): ε_v versus ε_a Plot of
CID Test Series V
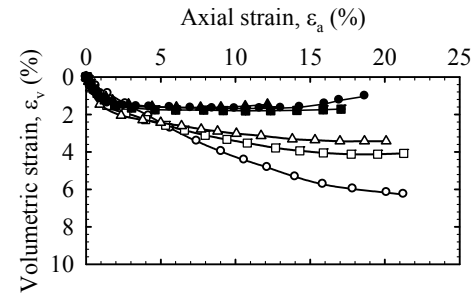
Figure 4.19 (b): ε_v versus ε_a Plot of
CK$_o$D Test Series VI
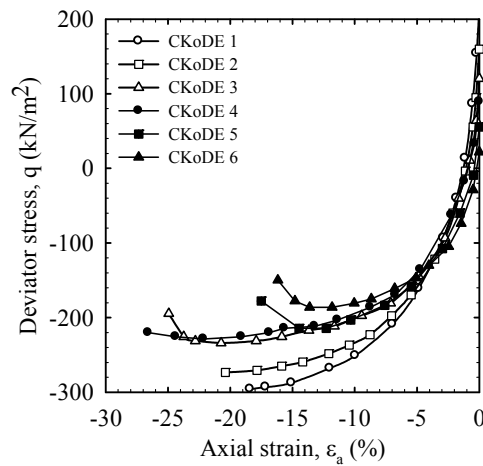
Figure 4.20 (a): q versus ε_a Plot of
CK$_o$DE Test Series VII

134
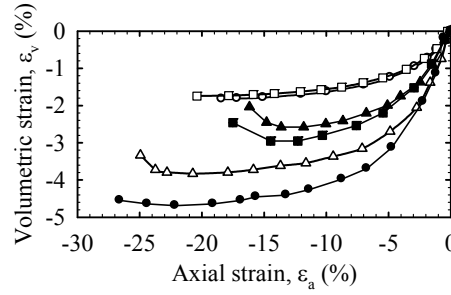
Figure 4.20 (b): ε_v versus ε_a Plot of
CK$_o$DE Test Series VII

4.7.5 Undrained Deformation Parameters of Lightly Overconsolidated Soft Clay

The undrained initial tangential modulus, $E_{u,i}$ and the failure factor R_f from the undrained test series II, III and IV (CIU, CK$_o$U and CK$_o$UE) were determined using the hyperbolic relationship (refer to Figure 4.4 and Eq.4.9) for all ranges of the OCR values. The tangent modulus, at 50 per cent shear strength, $E_{u,50}$, can be read directly from the (q, ε_a) curves by drawing a tangent from the origin through the point corresponding to 50 per cent shear strength on the (q, ε_a) curve.

The undrained tangent moduli ($E_{u,i}$, $E_{u,50}$) and the failure factor (R_f) from the three undrained test series (CIU, CK$_o$U and CK$_o$UE) are tabulated in Tables 4.16 to 4.18. The $E_{u,i}/E_{u,50}$ ratios were found to be consistent with the average values of 1.92, 2.35 and 2.52 for the CIU, CK$_o$U and CK$_o$UE series, respectively. The typical failure ratio (R_f) range, based on a variety of soil types of 0.75 to 1.0, was identified by Duncan and Chang (1970). Additionally, Brinkgreve (2002) suggested that the R_f of 0.9 be the default setting. In the current study, the average failure ratios from the undrained test series were in the order of 0.92, 0.97 and 0.87 for the CIU, CK$_o$U and CK$_o$UE series, respectively.

135

Table 4.16: Results from CIU Test Series II

Test type	OCR	$E_{u,i}$ (kN/m^2)	$E_{u,50}$ (kN/m^2)	$E_{u,i}/E_{u,50}$	q_f (kN/m^2)	q_{ult} (kN/m^2)	R_f
CIU 1	1	58824	29133	2.02	301	321	0.94
CIU 2	1.24	55546	27795	2.00	313	333	0.94
CIU 3	1.5	50042	26753	1.87	311	339	0.92
CIU 4	1.78	51282	27113	1.89	298	318	0.94
CIU 5	2.15	45455	22350	2.03	295	323	0.91
CIU 6	2.75	34483	20171	1.71	271	317	0.85

Table 4.17: Results from CK$_o$U Test Series III

Test type	OCR	$E_{u,i}$ (kN/m^2)	$E_{u,50}$ (kN/m^2)	$E_{u,i}/E_{u,50}$	q_f (kN/m^2)	q_{ult} (kN/m^2)	R_f
CK$_o$U 1	1	66653	38609	1.73	293	296	0.99
CK$_o$U 2	1.24	83321	51239	1.63	291	296	0.98
CK$_o$U 3	1.5	153846	49138	3.13	291	299	0.97
CK$_o$U 4	1.78	200104	67330	2.97	290	296	0.98
CK$_o$U 5	2.15	117647	50690	2.32	277	291	0.95
CK$_o$U 6	2.75	111098	51620	2.15	255	268	0.95

Table 4.18: Results from CK$_o$UE Test Series IV

Test type	OCR	$E_{u,i}$ (kN/m^2)	$E_{u,50}$ (kN/m^2)	$E_{u,i}/E_{u,50}$	q_f (kN/m^2)	q_{ult} (kN/m^2)	R_f
CK$_o$UE 1	1	29412	16550	1.78	-348	-417	0.83
CK$_o$UE 2	1.24	31250	11766	2.66	-350	-403	0.87
CK$_o$UE 3	1.5	30303	15585	1.94	-278	-346	0.80
CK$_o$UE 4	1.78	40022	13584	2.94	-318	-349	0.91
CK$_o$UE 5	2.15	28571	7733	3.69	-312	-345	0.91
CK$_o$UE 6	2.75	22219	10523	2.11	-320	-368	0.87

Figure 4.21 shows the (E_u/s_u, OCR) relationships resulting from the three triaxial undrained test series (CIU, CK$_o$U and CK$_o$UE), compared to the empirical chart based on the plate loading test results (Duncan and Buchignani, 1987) and the (E_u/s_u, OCR) relationships resulting from the direct simple shear (DSS) tests (Ladd *et al.*, 1977). The (E_u/s_u, OCR) relationship of the CIU, CK$_o$U and CK$_o$UE tests were obtained from $E_{u,50}$ of the aforementioned Bangkok soft clays data, with its plasticity index of 61. Similarly, the Bangkok clays with a lower I_p of 41 were tested using Direct Simple

Shear (DSS) test (Ladd *et al.*, 1977) at the ratio applied horizontal shear stress to the undrained shear strength (τ_h/s_u) of 1/3; the results were also plotted in Figure 4.21. According to Duncan and Buchignani's (1987) chart, the (E_u/s_u, OCR) relationship reduced as the soil plasticity index (I_p) increased. The relationship of the (E_u/s_u, OCR), based on the Cam Clay and the Modified Cam Clay models (Eq. 4.15 and 4.16) is also represented in this chart. As can be seen, both the (E_u/s_u, OCR) relationships from the CIU tests with $I_p = 61$, and from the DSS test with $I_p = 41$ coincide with Duncan and Buchignani's chart. In contrast to the E_u/s_u versus the OCR from the CIU tests, the relationships from the CK_oU and CK_oUE were higher and lower, respecitvely. They were also diverted from the $I_p > 50$ band. The reason of this diversion is not clear. Thus, it would be useful if more triaxial tests can be conducted to make comparison.
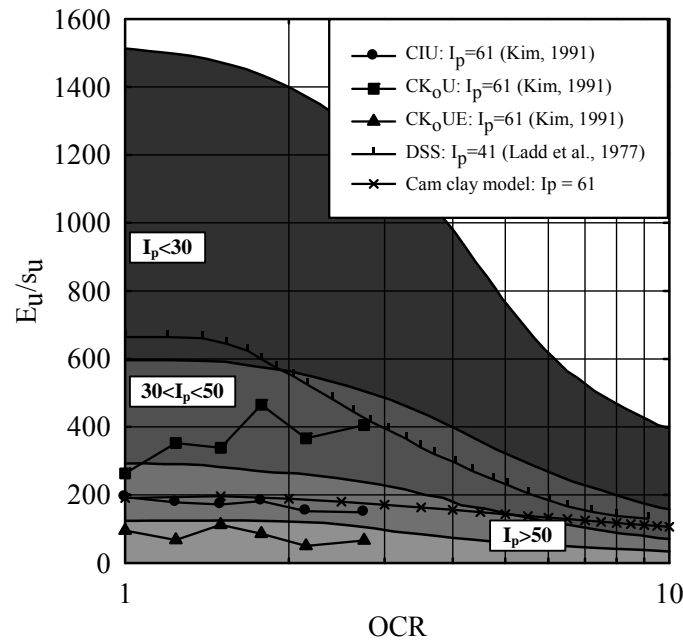
Figure 4.21: Normalised Undrained Modulus versus OCR,

(adapted from Duncan and Buchignani, 1987)

Crooks and Graham (1976) conducted a series of triaxial compression tests on lightly overconsolidated Belfast estuarine clay with I_p, that ranged from 22 to 57. Slightly higher average ratios of E_{50}/s_u of 500 and 300 were reported for the anisotropically and isotropically consolidated samples, respectively.

4.7.6 Drained Deformation Parameters of Lightly Overconsolidated Soft Clay

In line with the undrained test series, the drained initial tangential modulus, E'_i , drained tangential modulus at 50 per cent shear strength , E'_{50} ; with a failure factor R_f from the drained test series V, VI and VII (CID, CK_oD and CK_oDE) being determined in the same way as described in Section 4.7.5. Tables 4.19 to 4.21 list the results from drained test series (CID, CK_oD and CK_oDE), including the drained tangential moduli (E'_i , E'_{50}), and the failure ratio (R_f). In terms of the drained modulus and the OCR relationship, no definite conclusion can be drawn. The average ratios of E'_i / E'_{50} were slightly higher when compared to those of the undrained test series, with the values of 2.47, 3.20 and 2.39, for CID, CK_oD and CK_oDE, respectively. The average failure ratios (R_f) were 0.89, 0.96 and 0.87 for CID, CK_oD and CK_oDE, respectively

Table 4.19: Results from CID Test Series V

Test type	OCR	E'_i (kN/m^2)	E'_{50} (kN/m^2)	E'_i/E'_{50}	q_f (kN/m^2)	q_{ult} (kN/m^2)	R_f
CID 1	1	20021	5153	3.88	594	667	0.89
CID 2	1.24	23810	6816	3.49	539	595	0.91
CID 3	1.5	19231	8682	2.22	512	575	0.89
CID 4	1.78	19608	9208	2.13	482	538	0.90
CID 5	2.15	19231	11311	1.70	456	503	0.91
CID 6	2.75	18182	12995	1.40	378	435	0.87

Table 4.20: Results from CK_oD Test Series VI

Test type	OCR	E'_i (kN/m^2)	E'_{50} (kN/m^2)	E'_i/E'_{50}	q_f (kN/m^2)	q_{ult} (kN/m^2)	R_f
CK_oD 1	1	11107	1816	6.12	418	437	0.96
CK_oD 2	1.24	26316	8795	2.99	365	377	0.97
CK_oD 3	1.5	50068	16466	3.04	336	343	0.98
CK_oD 4	1.78	35714	15268	2.34	294	308	0.95
CK_oD 5	2.15	45458	18564	2.45	314	326	0.96
CK_oD 6	2.75	40025	17705	2.26	284	308	0.92

Table 4.21: Results from CK$_o$DE Test Series VII

Test type	OCR	E'_i (kN/m^2)	E'_{50} (kN/m^2)	E'_i/E'_{50}	q_f (kN/m^2)	q_{ult} (kN/m^2)	R_f
CK$_o$DE 1	1	27027	14056	1.92	-296	-356	0.83
CK$_o$DE 2	1.24	26316	10853	2.42	-273	-317	0.86
CK$_o$DE 3	1.5	25041	9108	2.74	-234	-259	0.91
CK$_o$DE 4	1.78	15385	6743	2.28	-228	-262	0.87
CK$_o$DE 5	2.15	18182	6377	2.85	-214	-250	0.86
CK$_o$DE 6	2.75	14286	6710	2.13	-186	-214	0.87

4.7.7 Basic Soil Properties of Soft and Stiff Clays in Bangkok Area

The following sections focus on the stress-strain characteristics of the soft and stiff clays. The drained and undrained reference moduli (E_i^{ref}, $E_{u,i}^{ref}$, E_{50}^{ref} and $E_{u,50}^{ref}$) were determined from four series of isotropically consolidated triaxial tests. Other Hyperbolic Soil Model and Hardening Soil Model parameters, such as the failure ratio (R_f) and the exponential power (m), were also interpreted using the graphical method outlined in Section 4.4.

All four test series were conducted on soft and stiff clay samples taken from the New Bangkok International Airport (Suvarnabhumi Airport) site. This location is also known as the Nong Ngoo Hao area. It is located in the lower part of the Chao Phraya Plain, approximately 30 km southeast of Bangkok. Generally, the soil profile consists of 4.5 m of weathered clay overlayed by 10 to 12 m of lightly consolidated and highly compressible soft clay. Below the soft clay layer, the stiff clay extends to a depth of approximately 10 m, under which lies alternate layers of sand and sandy clay. The basic properties of the clays are summarised in Table 4.22.

Table 4.22: Basic Engineering Properties of Weathered, Soft and Stiff Clays
(Balasubramaniam *et al.*, 1978)

Properties	Weathered clay	Soft clay	Stiff clay
Natural water content, w_n (%)	128 - 138	122 - 130	20 - 24
Natural voids ratio	3.71 - 4.01	3.11 - 3.64	1.10 - 1.30
Liquid limit, w_l (%)	123±2	118.5±1	46±2
Plastic limit, w_p (%)	41±2	43.1±0.3	19±2
Specific gravity (G_s)	2.73	2.75±0.1	2.74
Dry unit weight, γ (kN/m^3)	6	6.5	16
Degree of saturation (%)	93 - 97	98 - 100	94 - 100
Clay content (%)	69	64.3	34
Silt content (%)	23.5	31.7	43
Sand content (%)	7.5	4	23

4.7.8 Stress-strain Characteristics of Bangkok Soft Clay

Two series of isotropically consolidated triaxial compression tests, CIU and CID, were conducted by Chaudhry (1975). The soil samples were taken from a depth of 6.0 m below the ground surface. Confining pressures, σ'_3 from CIU (CID) S1 to CIU (CID) S5 were 138, 207, 276, 345 and 414 kN/m^2, respectively. The angle of the Internal Friction (ϕ') of the CIU and CID series were 27 and 23.6 degrees; whereas, the cohesion (c') was zero for both series. The drained strength parameters were also summarised in Table 4.23.

Table 4.23: Hardening Soil Model and Mohr Coulomb Model Parameters
from CID and CIU Series in Bangkok Soft Clay

Parameters		CID	CIU
Confining pressure (kN/m^2)		138 – 414	138 – 414
Initial	$E_i^{ref}, E_{u,i}^{ref}$ (kN/m^2)	1343	7690
	m	1.0	1.2
50 per cent	$E_{50}^{ref}, E_{u,50}^{ref}$ (kN/m^2)	690	4831
	m	1.1	1.0
	R_f	0.72	0.94
	ϕ'	23.6	27.0
	c' (kN/m^2)	0	0

Figure 4.22 (a and b) illustrate the (q, ε_a) and (u, ε_a) relationships for the CIU series. The deviator stress and excess pore pressures versus the axial strain relationships show typical normally to lightly overconslidated clay behaviour, where the deviator stress and excess pore pressure reaches their ultimate values at a relatively large strain. Moreover, all the excess pore pressure plots were located in the positive range. Table 4.24 summarises the deformation moduli and failure ratio resulting from the CIU series. It can be seen that both $E_{u,i}$ and $E_{u,50}$ increase with the confining pressures. The ratio of $E_{u,i}/E_{u,50}$ and R_f are, on the other hand, independent of the confining pressure. The average values of 1.87 and 0.94 were found for $E_{u,i}/E_{u,50}$ and R_f, respectively. These two values are consistence with the results of CIU, CK$_o$U and CK$_o$UE series on the lightly overconsolidated clays in Section 4.7.5. The reference moduli, $E_{u,i}^{ref}$, $E_{u,50}^{ref}$ and power m, were obtained from the double log scale plots in Figure 4.22 (c); they are also summarised in Table 4.23.
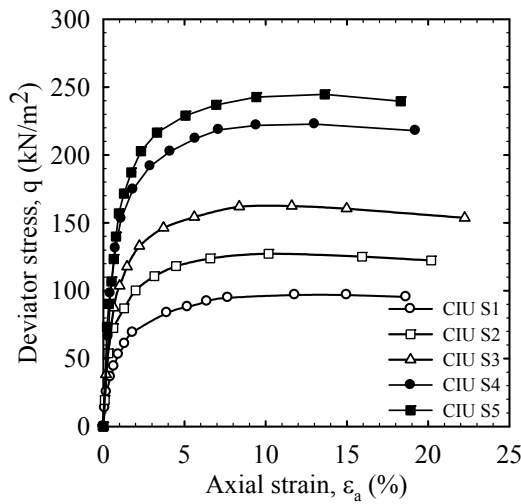
Figure 4.22 (a): Deviator Stress versus Axial Strain from CIU Series
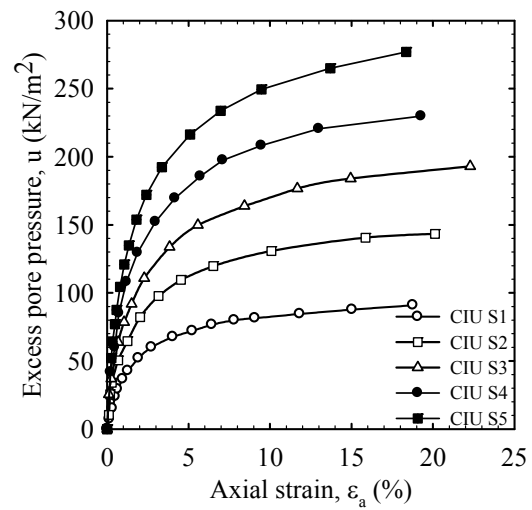
Figure 4.22 (b): Pore Pressure versus Axial Strain from CIU Series
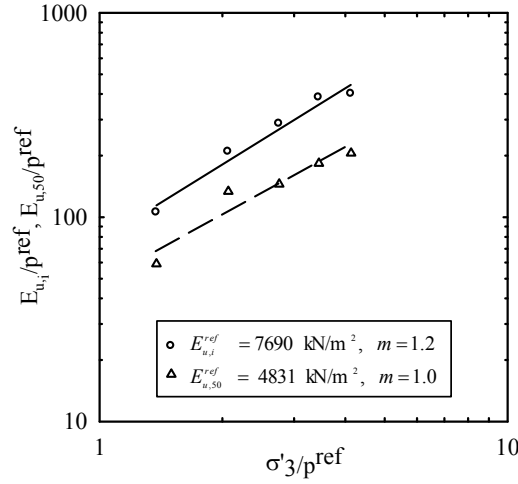
Figure 4.22 (c): Variation of $E_{u,i}$ and $E_{u,50}$
with Confining Pressure

Table 4.24: Deformation Moduli and Failure Ratio Resulting from CIU Series

Test type	σ'_3 (kN/m^2)	$E_{u,i}$ (kN/m^2)	$E_{u,50}$ (kN/m^2)	$E_{u,i}/E_{u,50}$	q_f (kN/m^2)	q_{ult} (kN/m^2)	R_f
CIU S1	138	10526	5898	1.78	97	105	0.92
CIU S2	207	20833	13355	1.56	127	135	0.94
CIU S3	276	28571	14497	1.97	162	172	0.94
CIU S4	345	38462	18305	2.10	223	235	0.95
CIU S5	414	40000	20564	1.95	245	257	0.95

The relationships of (q, ε_a) and (ε_v, ε_a) from the CID series are shown in Figure 4.23 (a and b). Table 4.25 summarises the deformation moduli and failure ratio resulting from the CID series. It can be seen that, during the application of the deviator stress, the volume of the soil specimen gradually consolidates (reduces in volume). The volumetric and axial strain curves of all the tests seem to coincide up to 10% axial strain, after that they tend to divert slightly. Similar to the CIU series, the E'_i and E'_{50} values increase with the confining pressure. The average ratio of E'_i/E'_{50} is 1.89, which is comparable to average $E_{u,i}/E_{u,50}$ of 1.87 from CIU series. The R_f ratio seems to be low with the value of 0.72. The variation of E'_i and E'_{50} with confining pressure is shown in Figure 4.23 (c). The reference moduli, E_i^{ref}, E_{50}^{ref} and power m, are summarised in Table 4.23.
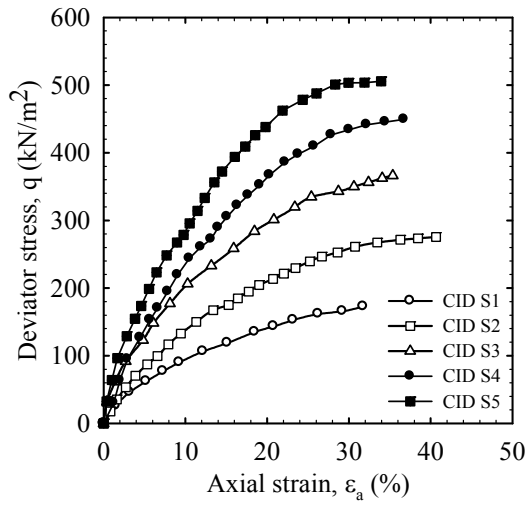
Figure 4.23 (a): Deviator Stress versus
Axial Strain from CID Series
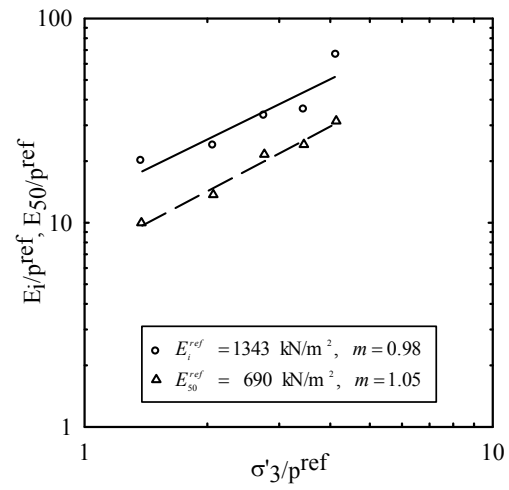
Figure 4.23 (c): Variation of E_i & E_{50}
with Confining Pressure
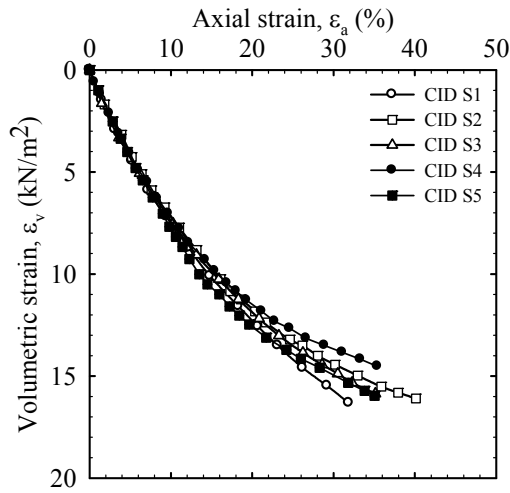
Figure 4.23 (b): Volumetric Strain versus
Axial Strain from CID Series

Table 4.25: Deformation Moduli and Failure Ratio Resulting from CID Series

Test type	σ'_3 (kN/m^2)	E'_i (kN/m^2)	E'_{50} (kN/m^2)	E'_i/E'_{50}	q_f (kN/m^2)	q_{ult} (kN/m^2)	R_f
CID S1	138	1953	997	1.96	173	238	0.73
CID S2	207	2375	1370	1.73	276	391	0.71
CID S3	276	3331	2157	1.54	366	515	0.71
CID S4	345	3571	2409	1.48	449	666	0.67
CID S5	414	6623	2409	2.75	506	667	0.76

4.7.9 Stress-strain Characteristics of Bangkok Stiff Clay

The two series of isotropically consolidated triaxial compression tests, CIU and CID, conducted by Hassan (1976) on stiff Bangkok clay, are re-interpreted in this section. The undisturbed soils sample was collected from a depth of 17.4 to 18 m below the ground surface. The pre-shear consolidation pressures ranged from 17 to 620 kN/m^2 and 34 to 552 kN/m^2, for the CIU and CID series, respectively. The angle of the Internal Friction (ϕ') of the CIU and CID series were 28.1 and 26.3 degrees; whereas, the values of cohesion (c') were 11.4 and 32.8 kN/m^2. The drained strength parameters are summarised in Table 4.26.

Table 4.26: Hardening Soil Model and Mohr-Coulomb Model Parameters
from CID and CIU Series in Bangkok Stiff Clay

Parameters		CID	CIU
Confining pressure (kN/m^2)		34 – 552	17 – 620
Initial	$E_i^{ref}, E_{u,i}^{ref}$ (kN/m^2)	29676	30109
	m	0.52	0.46
50 per cent	$E_{50}^{ref}, E_{u,50}^{ref}$ (kN/m^2)	14398	11104
	m	0.48	0.53
R_f		0.89	0.88
ϕ'		26.3	28.1
c' (kN/m^2)		32.8	11.4

Altogether nine CIU test results are shown in Figure 4.24. It can be seen from Figure 4.24 (a) that (q, ε_a) relationships, up to a pre-shear confining pressure of 138 kN/m^2 (CIU F1 to F3), exhibit no strain softening. From a level of confining pressure at 207 to 414 kN/m^2 (CIU F4 to F7), these clay samples behaved as heavily overconsolidated clays showing a clear peak deviator stress at a low axial strain, followed by a strain softening. Beyond the confining pressure of 552 kN/m^2 (CIU F8 and F9), these samples behaved as lightly overconsolidated clay. The relationships between the excess pore pressure and the axial strain are shown in Figure 4.24 (b). For all clay samples (CIU F1 to F9), the excess pore pressure increases as the deviator stress increases, until the peak values are reached at 1 to 4% axial strain, depending on the confining pressure. The peak excess pore pressure seems to be reached at a higher

axial strain as the confining pressure increases. As the sample is further sheared, the excess pore pressure gradually reduced to the minimum value, at approximately 12% axial strain. Only the first three samples (CIU F1 to F3) reached negative excess pore pressures.
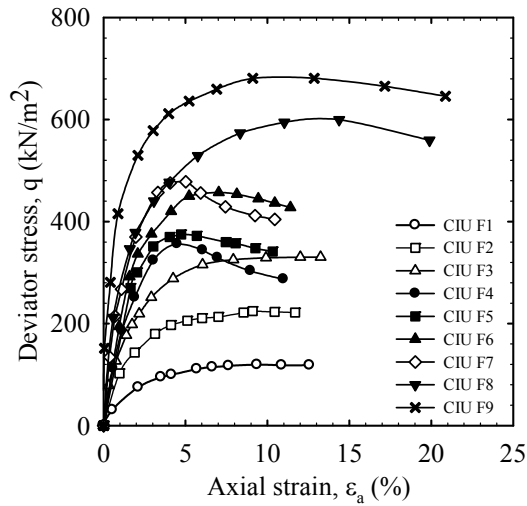
Figure 4.24 (a): Deviator Stress versus Axial Strain from CIU Series
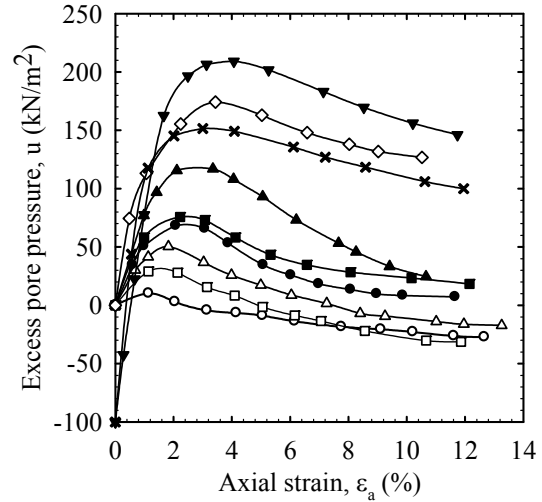
Figure 4.24 (b): Pore Pressure versus Axial Strain from CIU Series
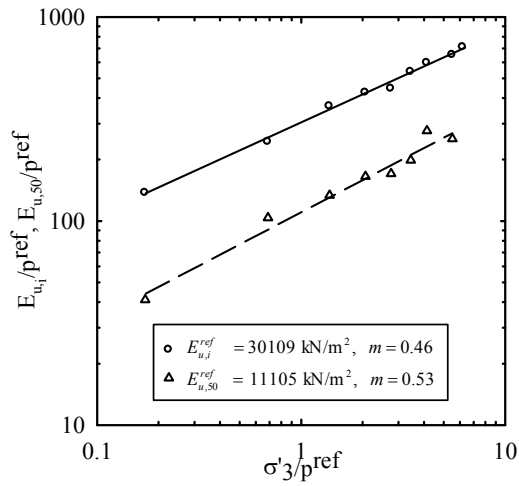
Figure 4.24 (c): Variation of $E_{u,i}$ and $E_{u,50}$ with Confining Pressure

Table 4.27 summarises the deformation moduli and the failure ratios resulting from the CIU series. As discussed in previous section, both $E_{u,i}$ and $E_{u,50}$ increase with increases in the pre-shear confining pressure. The $E_{u,i}/E_{u,50}$ ratios are fairly consistent, with an average value of 2.46. Failure ratio (R_f) also falls in a narrow range with an average value of 0.88. The double log scale plot of the normalised undrained moduli versus the normalised confining pressure is shown in Figure 4.24 (c). It can be clearly seen that the variations of both $E_{u,i}$ and $E_{u,50}$ with confining pressure are well explained by the hyperbolic law, as illustrated by linear relationships in the double log scale. The resulting reference moduli $E_{u,i}^{ref}$ and $E_{u,50}^{ref}$ are 30,109 and 11,105 kN/m^2, respectively. The exponential power m for both the initial and the 50 per cent moduli are approximately 0.5.

Table 4.27: Deformation Moduli and Failure Ratio Resulting from CIU Series

Test type	σ'_3 (kN/m^2)	$E_{u,i}$ (kN/m^2)	$E_{u,50}$ (kN/m^2)	$E_{u,i}/E_{u,50}$	q_f (kN/m^2)	q_{ult} (kN/m^2)	R_f
CIU F1	17	13699	4103	3.34	119	137	0.87
CIU F2	69	24331	10359	2.35	225	243	0.92
CIU F3	138	36364	13355	2.72	331	364	0.91
CIU F4	207	42463	16526	2.57	355	425	0.84
CIU F5	276	44385	17041	2.60	375	444	0.84
CIU F6	345	53619	19861	2.70	457	536	0.85
CIU F7	414	59365	27647	2.15	478	594	0.81
CIU F8	552	64882	25265	2.57	601	649	0.93
CIU F9	620	70821	61000	1.16	683	708	0.96

The deviator stress versus the axial strain relationships of the stiff clay CID test series are shown in Figure 4.25 (a). The pre-shear confining pressure of 34, 103, 414 and 552 kN/m^2 were adopted. None of the stiff clay samples demonstrated a well defined peak. However, samples CID F1 to F3 (with confining pressure of 34, 103 and 414) illustrate some degree of strain softening after the peak deviator stresses are reached at axial strain levels of 3 to 5%. The plot of the volumetric versus the axial strain can be seen in Figure 4.25 (b). The specimens with a confining pressure of 34 and 103 kN/m^2 (CID F1 and 2) start to dilate at about 1.2 and 3.5% axial strain. The specimen at 414 kN/m^2 confining pressure consolidates up to an axial strain level of 8%. After that, the volumetric strain seems to be constant with an increase in axial strain. The last

specimen with a confining pressure of 552 kN/m^2 consolidates up to 7% of the axial strain, and then it tends to dilate.
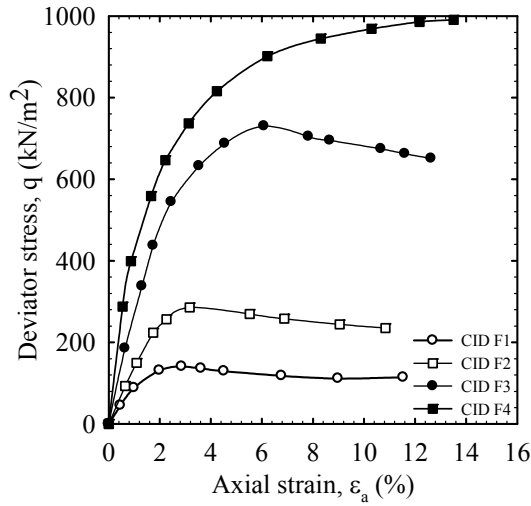
Figure 4.25 (a): Deviator Stress versus Axial Strain from CID Series
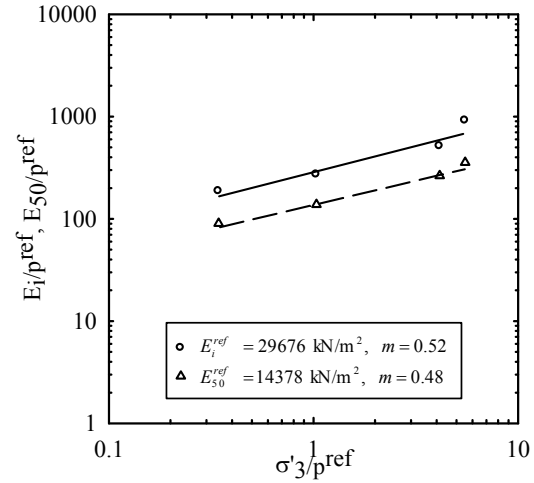
Figure 4.25 (c): Variation of E_i & E_{50} with Confining Pressure
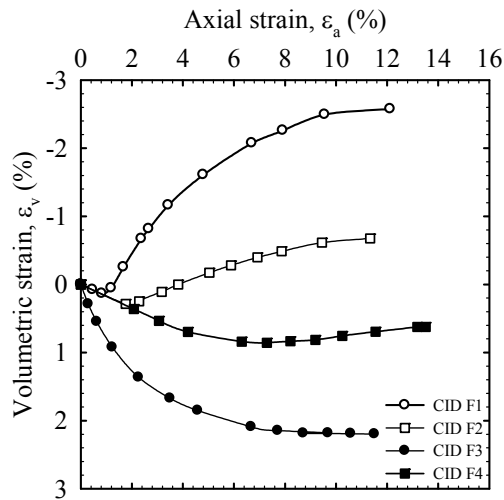
Figure 4.25 (b): Volumetric Strain versus Axial Strain from CID Series

Table 4.28 lists the drained moduli and the failure ratio at various confining pressures resulting from the CID series. Here, again, the E'_i and E'_{50} values tend to increase with the increase in the confining pressure. The ratios of E'_i/E'_{50} are fairly consistent, with an average of 2.12. The failure ratios (R_f) have an average of 0.89. Similar to the CIU series, both the initial and the 50 per cent drained moduli are plotted in the normalised

double log scale (Figure 4.25 (c)). The reference moduli E_i^{ref} and E_{50}^{ref} are found to be 29,676 and 14,378 kN/m^2, respectively The exponential power m for both cases is approximately equal to 0.5.

Table 4.28: Deformation Moduli and Failure Ratio Resulting from CID Series

Test type	σ'_3 (kN/m^2)	E'_i (kN/m^2)	E'_{50} (kN/m^2)	E'_i/E'_{50}	q_f (kN/m^2)	q_{ult} (kN/m^2)	R_f
CID F1	34	18519	9021	2.05	141	161	0.87
CID F2	103	27027	13799	1.96	286	328	0.87
CID F3	414	51073	26364	1.94	730	833	0.88
CID F4	552	90909	35639	2.55	991	1075	0.92

4.7.10 Discussion on Parameters m, R_f and E_i/E_{50} Ratios

The failure ratio (R_f), $E_{u,i}/E_{u,50}$ and E'_i/E'_{50}, from a study of lightly overconsolidated Bangkok soft clay (Section 4.7.5 to 4.7.6), are summarised in Table 4.29. Similarly, in Table 4.30, the parameters $E_{u,i}/E_{u,50}$, E'_i/E'_{50} and exponential power m (initial and 50 per cent), from Sections 4.7.8 to 4.7.9, are given. Duncan *et al.* (1980) reported the failure ratio of 0.7 to 0.9 from various types of soil. Wong and Broms (1989) stated that R_f in the Hyperbolic Soil Model governs the shape of the stress-strain curve. Thus, the soils with high R_f values exhibit plastic behaviour with failures at a large strain level; while the soils with a low R_f, on the other hand, exhibit brittle behaviour and are likely to fail at a low strain level. In the case of Bangkok soft and stiff clays, a failure ratio of 0.9 seems to be reasonable.

Table 4.29: Summary of R_f and E_i/E_{50} Ratios of

Lightly Overconsolidated Bangkok Soft Clay

Test type	OCR	R_f	$E_{u,i}/E_{u,50}$	E'_i/E'_{50}
CIU	1 – 2.75	0.92	1.92	-
CK$_o$U	1 – 2.75	0.97	2.35	-
CK$_o$UE	1 – 2.75	0.87	2.52	-
CIU	1 – 2.75	0.89	-	2.47
CK$_o$U	1 – 2.75	0.96	-	3.20
CK$_o$UE	1 – 2.75	0.87	-	2.39

Table 4.30: Summary of R_f, E_i/E_{50} Ratios and Power m

of Bangkok Soft and Stiff Clays

Test type	Soil type	R_f	$E_{u,i}/E_{u,50}$	E'_i/E'_{50}	m (Initial)	m (50%)
CIU	Soft clay	0.94	1.87	-	1.2	1.0
CID		0.72	-	1.89	1.0	1.0
CIU	Stiff clay	0.88	2.46	-	0.5	0.5
CID		0.89	-	2.12	0.5	0.5

The exponential power (m) varies from zero to unity. According to Janbu (1963), the m value of one represents normally consolidated clay. The value of zero, however, reveals perfectly elastic behaviour. For this reason the power m of 0.5 is suggested for medium dense sand. From the tables for lightly overconsolidated soft clay behaviour (Table 4.29), Bangkok Soft and Stiff Clay behaviour (Table 4.30), and power m from E_{oed}^{ref} modulus (Table 4.11), the exponential m of one is suitable for the Bangkok Soft Clay; whereas, the m of 0.5 to 0.6 should be adopted for medium stiff to hard clays. The ratios of E_i/E_{50}, in both the drained and undrained cases, are also reasonable, and so can be adopted as 2.0 to 2.5.

4.8 Determination of Drained Triaxial Modulus from Oedometer Test Results

4.8.1 Background

In geotechnical engineering practice, isotropically consolidated drained triaxial (CID) tests are seldom conducted on cohesive soil samples, due to their low permeability. Accordingly, Clough and Duncan (1969) developed a procedure to estimate the effective stress–strain hyperbolic parameters for clays, using the results of the consolidation and direct shear tests. Generally, the effective strength parameters, namely cohesion, c', and angle of internal friction, ϕ', are obtained from the direct shear tests, while a stress–strain relationship for the primary loading as derived from the results of the consolidation tests.

The following expression was proposed by Clough and Duncan (1969) to obtain the initial tangent modulus (E_i), from a known triaxial tangent modulus (E_t), for any load increment, as per Equation 4.17:

$$E_i = \frac{E_t}{\left(1 - \dfrac{R_f(1 - K_o)}{K_o\left(\tan^2(45 + \phi'/2) - 1\right)}\right)^2}$$

Eq. 4.17

where, K_o is the coefficient of earth pressure at rest. It should be noted that the effective cohesion of soil, c', is assumed to be zero. The triaxial tangent modulus at any load increment (E_t) can be calculated using the expression given by Change (1969), namely:

$$E_t = \frac{1 + e_o}{a_v}\left(1 - \frac{K_o^2}{(1 + K_o)}\right)$$

Eq. 4.18

where, e_o is the initial void ratio, and a_v is the coefficient of compressibility during primary loading. The term ($1 + e_o/a_v$) in Eq. 4.18 is equal to E_{oed}, therefore, by combining Eqs. 4.17 and 4.18, the initial tangent modulus (E'_i) can be computed.

Following the hyperbolic stress-strain curve, as shown, in Figure 4.4 above, the initial tangent modulus (E'_i) can be converted into the secant modulus, at 50 per cent shear strength (E'_{50}), using Eq. 4.10. The reference moduli, $E_{u,i}^{ref}$ and $E_{u,50}^{ref}$, and the exponential power, m, can be determined by plotting the double log scale plot of (E_i/p^{ref}, or E_{50u}/p^{ref} vs σ'_3/p^{ref}). The average value of σ'_3 during each load increment is obtained by multiplying the average vertical stress during the increment (from the oedometer test) by K_o.

Stark and Vettel (1991) compared the hyperbolic parameter values, obtained from the triaxial CID and oedometer tests, based on Clough and Duncan's (1969) method. The tested soil (the so called "slopewash" material, which is a medium to high plasticity clay (CL)) had a liquid and plastic limit of 40 and 20, respectively. The overconsolidation ratio ranged from 1.0 to 1.5. Various combinations of the moduli

(tangent and secant) and e_o (at the beginning of the test and the load increment, and the end of the load increment) from the oedometer tests were adapted to determine the modulus number, k (which gives E_i^{ref} by multiplying with p^{ref}) and the exponential power, m. At the same time, the strength parameters ϕ', c' and R_f were collected from direct shear tests. The authors concluded that the use of the results from the oedometer and direct shear tests will underestimate the modulus number, when compared to the results from the CID triaxial tests. As a consequence, it was determined that a factor of 1.6 – 2.2 should be used for multiplication depending, on the selected values of a_v and e_o.

4.8.2 Evaluation of Hardening Soil Model Parameters from CIU Triaxial and Oedometer Tests

The technique used for evaluating the hyperbolic stress–strain parameters has been summarised in the section above. Further, according to Clough and Duncan (1969), and Stark and Vettel (1991), the consolidation and direct shear test results are needed to obtain the hyperbolic stress–strain parameters. In the current study, the strength parameters ϕ', c' and R_f, from the CIU triaxial test, were used instead of those from the direct shear test. Hence, both results from the conventional consolidation and the constant rate of strain (CRS) tests were used to evaluate the constrained modulus, E_{oed}; subsequently, the parameters E_i and E_t can be obtained. The stiffness parameter, E_{50}^{ref}, necessary for the Hardening Soil Model analysis, was further derived from parameter E_i^{ref}. The details of this procedure and the results obtained are explained in the following subsections.

In the current study, the two consolidation tests (one conventional oedometer, OED, and one constant rate of strain, CRS) were conducted from undisturbed samples collected from the Bangkok-Chonburi new highway (BCNH), located approximately 6 km east of the new Bangkok International Airport. The test equipment and procedure used were in accordance with Seah and Koslanant (2000). Figure 4.26 shows the plots of effective vertical stress versus the vertical strain of both consolidation tests. Importantly, the oedometer virgin compression line (VCL) was

linear for all the applied stress range. The VCL of the CRS test gave, on the other hand, a linear trend up to an effective stress of 280 kN/m^2. After this level of stress, the VCL is diverted out, giving a bilinear relationship. The unloading curves from the OED and CRS tests are both linear. The reference constrained modulus (E_{oed}^{ref} and $E_{ur,oed}^{ref}$) and the Cam Clay parameters (λ^*, κ^*) are tabulated in Table 4.31.
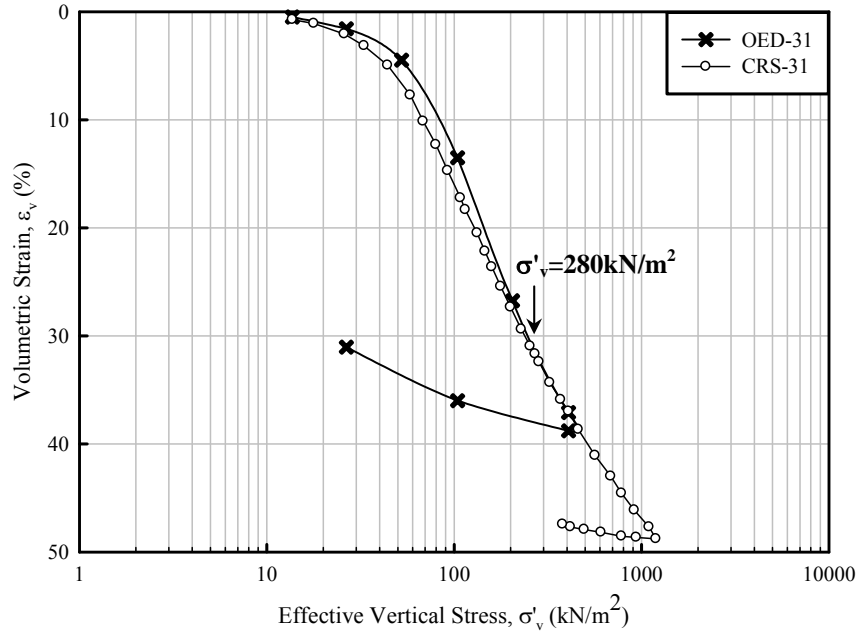
Figure 4.26: Oedometer and Constant Rate of Strain Consolidation Tests
(Bangkok Soft Clay at 6.5 m depth)

Table 4.31: Reference Constrained Moduli and Cam-Clay Parameters

Test	Loading		Un/re-loading		λ^*	κ^*	σ'_p
	E_{oed}^{ref}	m	$E_{ur,oed}^{ref}$	m			
	(kN/m^2)		(kN/m^2)				(kN/m^2)
OED	641	0.9	2864	1.4	0.163	0.028	53
CRS	628	1.0	1622	2.3	0.140	0.014	48

As can be seen from Figure 4.26 and Table 4.31, the loading parameters including, E_{oed}^{ref}, power m for loading, and λ^* are in good agreement for both the OED and CRS tests. However, only the results of the CRS test up to an effective stress of 280 kN/m^2 are used in calculating the compression parameters. The unloading parameters, on the other hand, differ by about a factor of two. This outcome is due to the fact that the unloading parameters are remarkably dependent on the level of stress

at the site where the unloading process has started. In this case, the unloading process begins at the stress level of 408 and 1194 kN/m^2 for the OED and CRS tests, respectively.

As summarised in Section 4.8.1, the effective Hardening Soil Model parameters can be obtained from the consolidation and direct shear test results. In this section, a similar procedure is followed; however the effective strength parameters from the direct shear have been replaced by those of from the CIU triaxial tests (see Section 4.7.8). Further, the loading consolidation tests results were adopted from the OED and CRS tests. A summary of the step involved in calculations (A to D) is given in the following:

A. Determine the values of the effective strength parameters (ϕ' and c') and failure stress ratio (R_f) from CIU triaxial tests (Table 4.23).

B. Determine the loading constrained modulus, E_{oed} at various levels of effective vertical stress from the consolidation tests.

C. Calculate E_t using Eq. 4.18, to be used in Eq. 4.17, for the E_i calculation. Parameters ϕ' and R_f in Eq. 4.17 are obtained from Step A. Hence, calculate E_{50} for all the values of E_i using Eq. 4.9.

D. Plot the variations of E_i and E_{50} with the confining pressure (see Figure 4.27). The values of the confining pressure, σ'_3, are the average of the confining pressure over each load increment of E_{oed} obtained in the consolidation tests. The confining pressure, σ'_3 from consolidation test, is estimated using the appropriate value of K_o.

It should be noted that the value of K_o remains unchanged in the loading condition along the normally consolidated line in the consolidation test. Therefore, it is reasonable to use one appropriate value of K_o to calculate the confining pressures in Step D above. In this analysis the K_o of Bangkok Soft Clay was assumed as 0.65.

The variation of E_i and E_{50} with the confining pressure, as obtained from the CIU triaxial and consolidation tests, are illustrated in Figure 4.27, while the results of E_i^{ref}, E_{50}^{ref} and m are listed in Table 4.32. The comparison from Table 4.23 reveals that

the reference moduli (E_i^{ref} and E_{50}^{ref}), resulting from the CIU and consolidation tests, underestimate the moduli from the CID tests by 17 and 11 per cent for E_i^{ref} and E_{50}^{ref}, respectively. Unlike the reference moduli, the exponential power m values are the same for both cases and are equal to unity.

$$E_i^{ref} = 1148 \text{ kN/m}^2, \quad m = 1.0$$
$$E_{50}^{ref} = 621 \text{ kN/m}^2, \quad m = 1.0$$
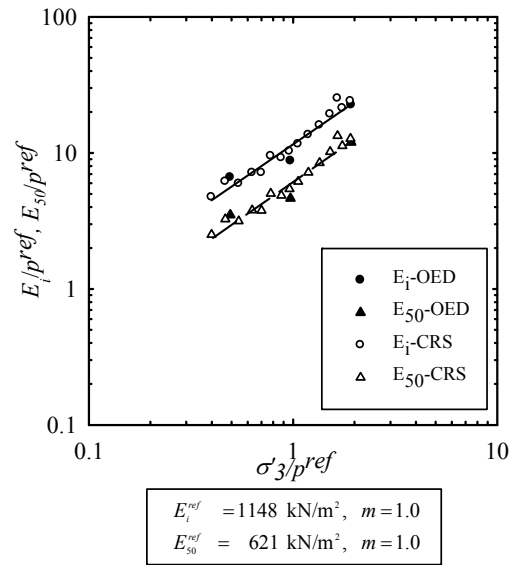
Figure 4.27: Variation of E_i and E_{50} with Confining Pressure
Resulting from Oedometer and CRS Tests

Table 4.32: Hardening Soil Model Parameters from CID and
CIU and Consolidation Tests

Parameters	Col. 1 Values from CID tests	Col. 2 Values from CIU & consolidation tests	Col. 3 Col. 1/Col. 3
Stress range (kN/m²)	138 – 414	40 – 192	–
E_i^{ref} (kN/m²)	1343	1148	1.17
E_{50}^{ref} (kN/m²)	690	621	1.11
m	1.0	1.0	1

4.9 Finite Element Modelling of Triaxial and Oedometer Tests and Soil Parameters Calibration

In this section, the undrained triaxial and oedometer tests are modelled using simplified axi-symmetric geometry. The parametric study of the Hardening Soil Model parameters, namely E_{50}^{ref}, E_{oed}^{ref}, E_{ur}^{ref}, m, R_f, K_o^{nc} and v_{ur}, are conducted to evaluate the effects of each parameter on the triaxial and oedometer relationships. Two series of undrained triaxial tests in soft and stiff clays were modelled; the Hardening Soil Model parameters were calibrated by means of curve fitting. The aim of this exercise was to find drained Hardening Soil Model parameters suitable for undrained materials (i.e. soft and stiff Bangkok clays).

4.9.1 Model Geometry of Triaxial and Oedometer Tests

The triaxial and oedometer tests were modelled by means of an axi-symmetric geometry of 1 m x 1 m unit dimensions (Figure 4.28). This unrealistically large dimension of the model did not influence the results, as the soil sample was set as a weightless material. The simplified geometry in the triaxial model represented one quarter of the soil sample. The deformations along the boundaries (line AC and CD) were kept free to allow for a smooth movement along the axes of symmetry, while the deformations perpendicular to the boundaries were fixed. Similar to the boundary condition of the triaxial test, boundaries AB and BD were free to move. The applied deviator stress and confining pressure were simulated as a distributed load system for A and B, respectively. Unlike the simplified geometry of the triaxial test, the oedometer geometry represented one half of the test specimen, as separated by the axis of symmetry (AC). The deformations perpendicular to the boundary lines, AC and BD, were fixed; however, the tangential deformations were free to move. Both the directions of the deformation were fixed for the bottom boundary CD. The effective vertical stress in the consolidation test was simulated as load system A.
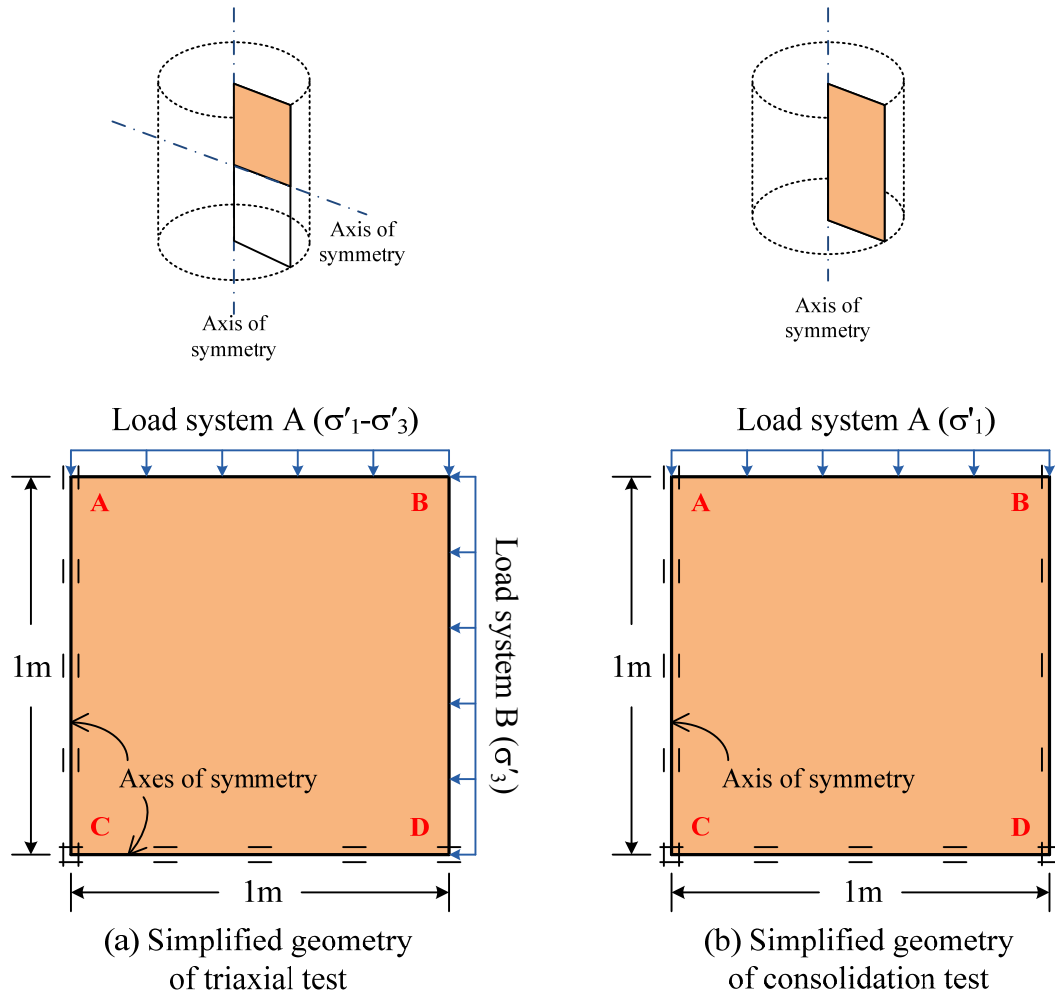
Figure 4.28: Simplified Geometries of Triaxial and Consolidation Tests

4.9.2 Parametric Study on Hardening Soil Model Parameters

A series of triaxial and oedometer tests were modelled according to the geometry described in the previous section. The Hardening Soil Model parameters in Table 4.33 were used as the control parameters. The reference pressure P^{ref} of 100 kN/m² was adopted. To simulate the isotropically consolidated triaxial test (CIU), the distributed load system A and B were applied equally, and was equal to 100 kN/m² (representing the confining pressure). After that, only the distributed load system A was increased until the soil model reached the failure point. The results were plotted as the deviator stress versus the axial strain (q versus ε_a), the excess pore pressure versus the axial strain (u versus ε_a), and the stress path (q versus p'). Load system A was used to simulate the applied vertical stress in oedometer tests. The loading and unloading vertical stresses were applied as 1, 200, 400, 50, 800, 1600 and 200 kN/m²,

respectively. The pre-consolidation pressure of 55 kN/m^2 was adopted for all the test models prior to the application of the loading and unloading vertical stresses. To study the effect of the different HS Model parameters (E_{50}^{ref} , E_{oed}^{ref} , E_{ur}^{ref} , m, R_f, K_o^{nc} and v_{ur}) on stress-strain and volume change behaviour, two different values (one higher and one lower than the controlled parameter) were applied to the model while other parameters were fixed.

Table 4.33: Hardening Soil Model Parameters Used as Controlled Parameters

ϕ' (°)	ψ' (°)	c' (kN/m^2)	E_{50}^{ref} (kN/m^2)	E_{oed}^{ref} (kN/m^2)	E_{ur}^{ref} (kN/m^2)	R_f	m	K_0^{nc}	v_{ur}
27	0	1	800	800	4000	0.9	1	0.55	0.2

Typical results of E_{50}^{ref} -parametric study are shown in Figure 4.29. The remaining results are illustrated in Appendix C. Table 4.34 summarises the effects of each parameter on the triaxial and oedometer relationships, namely, that parameters E_{oed}^{ref} , and K_o^{nc} have significant effects on the stress-strain relationships (q versus ε_a and u versus ε_a), as well as on the stress path (q versus p'). Parameter E_{50}^{ref} governs the triaxial stress-strain relationships, but has no effect on stress path. For ε_v vs log σ'_v the relationship in oedometer test, E_{oed}^{ref} , E_{ur}^{ref} , m and v_{ur}, are influencing factors, whereas E_{50}^{ref} , R_f and K_o^{nc} has little or no effects.
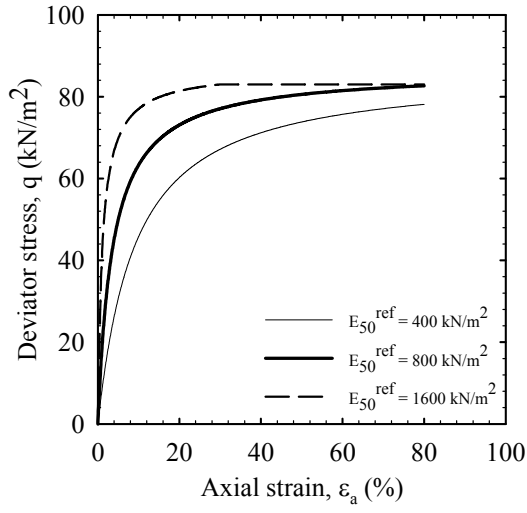
(a)
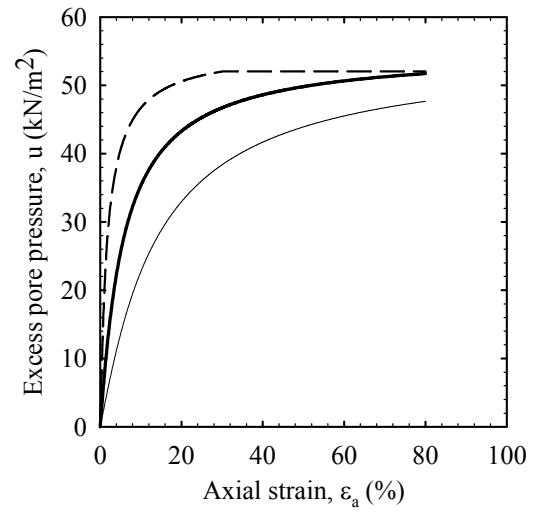
(b)
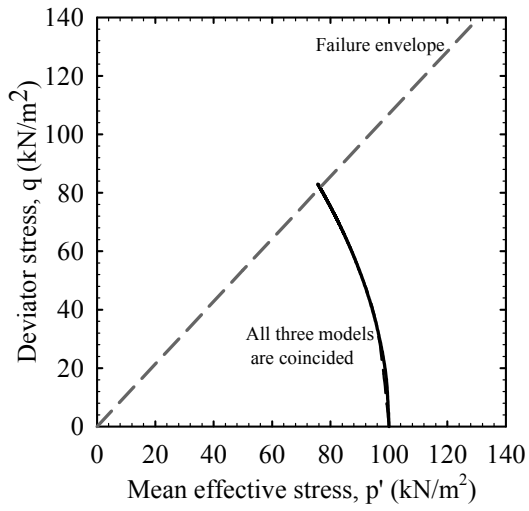
(c)
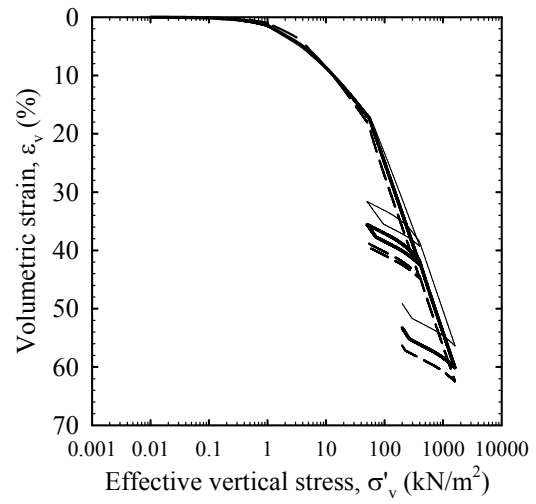
(d)

Figure 4.29: Parametric Study on E_{50}^{ref}

Table 4.34: Hardening Soil Model Parameters Affecting Triaxial and Oedometer Relationships

| Parameters | Important to | | | |
| | Triaxial | | | Oedometer |
	q - ε_a	u - ε_a	q - p'	ε_v - $\log \sigma'_v$
E_{50}^{ref}	V	V	N	L
E_{oed}^{ref}	V	V	V	V
E_{ur}^{ref}	V	V	V	V
m	L	L	L	V
R_f	L	L	N	N
K_0^{nc}	V	V	V	L
ν_{ur}	L	L	L	V

Note: V means Very important, L means Less important and N means Not important.

4.9.3 Hardening Soil Model Parameter Calibration for Bangkok Soft and Stiff Clays

A series of CIU tests on Bangkok soft clay (described in Section 4.8.1) was used in the Hardening Soil Model parameter calibration for this part of the study. However, for illustration purposes, only CIU S1, CIU S3 and CIU S5 (σ'_3 = 138, 276 and 414 kN/m^2) are presented. The drained strength and stiffness parameters are needed in the undrained modelling using the advanced soil model (i.e. HSM), as discussed in Section 4.1. Thus, the first attempt is to use drained stiffness parameters E_{50}^{ref} from the CID test series (see Section 4.7.8) and E_{oed}^{ref} and E_{ur}^{ref} from the oedometer test results (i.e. the average values from Table 4.31). These parameters are listed in Table 4.35. Note that, the reference pressure is kept as 100 kN/m^2 throughout the study. The results from Figure 4.30 reveal poor agreements among all the stress-strain and stress path relationships. In fact, with the input parameters from Table 4.35, the undrained shear strengths, calculated from Plaxis, vastly overestimated the values from the CIU test series for the entire range of confining pressures. There are two possible reasons for this outcome. Firstly, the assumption of adding bulk modulus of water, as used by the HSM in Plaxis (see Appendix A for detail), to convert the drained to the undrained modulus may not be appropriate. Secondly, the drained moduli from CID test series (from Table 4.35) may not be a representative set of the Bangkok soft clay. To overcome this problem, the input parameters were adjusted in order to obtain suitable

drained parameters to give the best fit results of the undrained stress-strain and stress path.

Table 4.35: HSM Input Parameters Based on CID and Oedometer Tests Results

ϕ' (°)	ψ' (°)	c' (kN/m²)	E_{50}^{ref} (kN/m²)	E_{oed}^{ref} (kN/m²)	E_{ur}^{ref} (kN/m²)	R_f	m	K_0^{nc}	υ_{ur}
27	0	1	690	635	2070	0.9	1	0.55	0.2
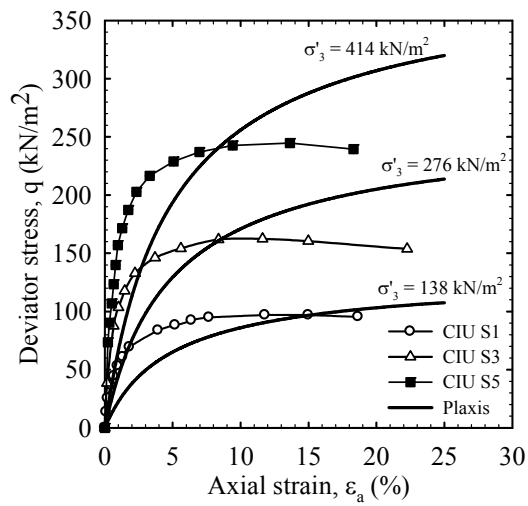
(a) Deviator Stress versus Axial Strain
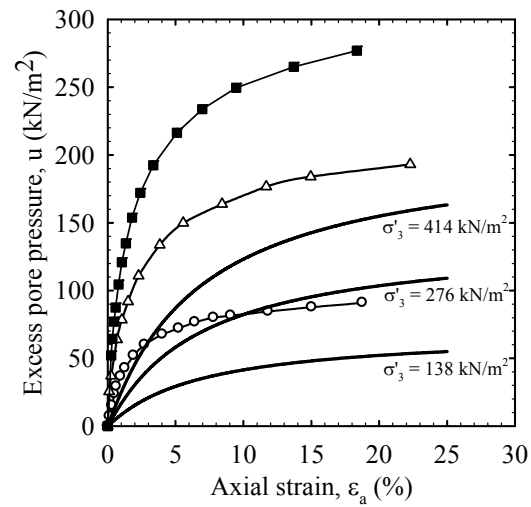
(b) Excess Pore Pressure versus Axial Strain
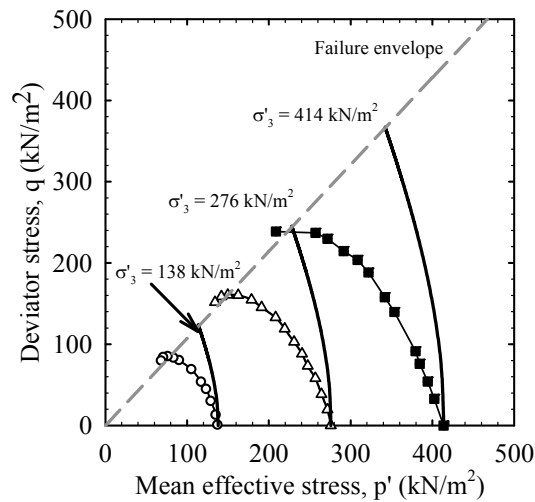
(c) Stress Path q versus p'

Figure 4.30: Bangkok Soft Clay CIU Test Results and Their Predictions from HSM (Using CID and Oedometer Tests Input Parameters)

160

The best fit input parameters are shown in Table 4.36, while the resulting stress-strain and stress path relationships are shown in Figure 4.31. In terms of the q veruss ε_a and u versus ε_a relationships at a relatively small strain (lower than 3%), the HS Model predictions agree reasonably well with the test results. However, the HS Model cannot predict the drop in the deviator stress, which represents a strain softening. Nevertheless, in terms of an effective stress path, the typical shape of the normally consolidated clay stress paths, and their undrained shear strength, are handled very well by the HS Model predictions.

Table 4.36: Calibrated HSM Parameters for Bangkok Soft Clay

ϕ' (°)	ψ' (°)	c' (kN/m²)	E_{50}^{ref} (kN/m²)	E_{oed}^{ref} (kN/m²)	E_{ur}^{ref} (kN/m²)	R_f	m	K_0^{nc}	υ_{ur}
27	0	1	800	850	8000	0.9	1	0.74	0.2

The HS Model calibration on the Bangkok stiff clay was conducted in a similar way to that used in the Bangkok soft clay. The test results from CIU F2, CIU F5 and CIU F7 (σ'_3 = 69, 276 and 414 kN/m²), from Section 4.7.9 above, were selected. The best fit HS Model parameters and their resulting predictions are illustrated in Table 4.37 and Figure 4.32, respectively. It is noteworthy that, even with the adjusted parameters, the HS Model cannot predict the drop in the deviator stress or the excess pore pressure, with reference to their ultimate values in q versus ε_a and u versus ε_a relationships. As a consequence, if a dilatancy angle of more than zero is introduced to the HS Model, some degree of drop in the excess pore pressure would be obtained. However, with the inclusion of dilatancy, the predicted q versus ε_a and stress path would be unrealistic (see Schweiger, 2002).

(a) Deviator Stress versus Axial Strain

(b) Excess Pore Pressure versus Axial Strain

(c) Stress Path q versus p'
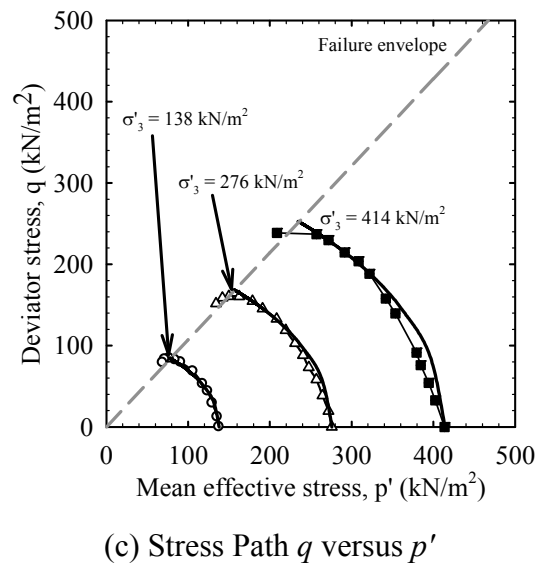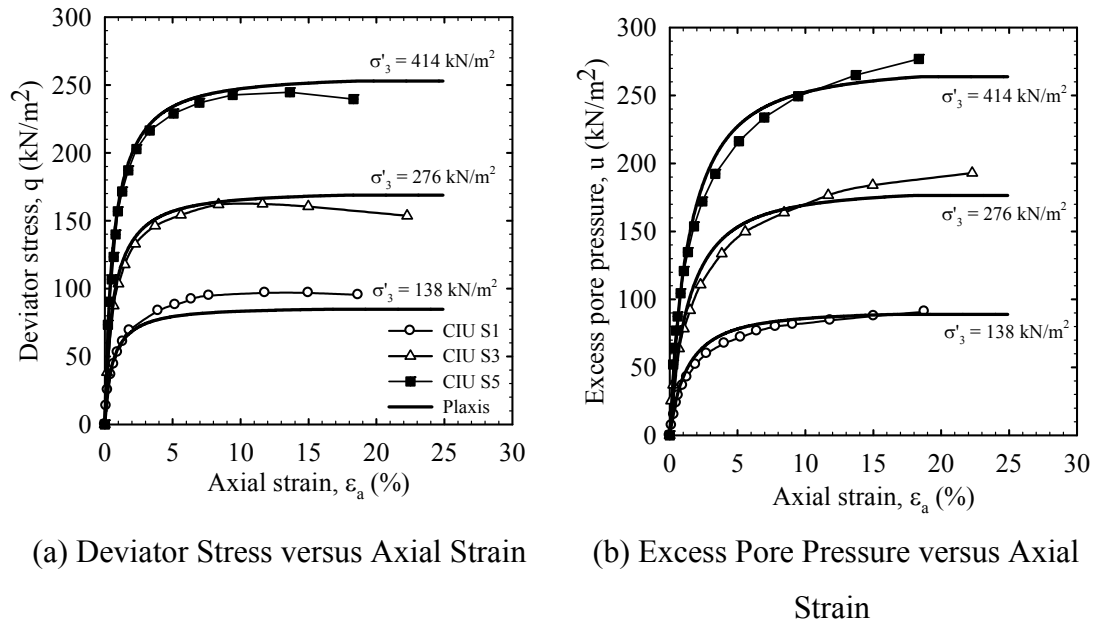
Figure 4.31: Bangkok Soft Clay CIU Test Results and Their Predictions from HSM (Using Best Fit Input Parameters)

Table 4.37: Calibrated HSM Parameters for Bangkok Stiff Clay

ϕ' (°)	ψ' (°)	c' (kN/m²)	E_{50}^{ref} (kN/m²)	E_{oed}^{ref} (kN/m²)	E_{ur}^{ref} (kN/m²)	R_f	m	K_0^{nc}	υ_{ur}
28	0	11.5	9500	12000	30000	0.9	1	0.5	0.2

(a) Deviator Stress versus Axial Strain

(b) Excess Pore Pressure versus Axial Strain

(c) Stress Path q versus p'
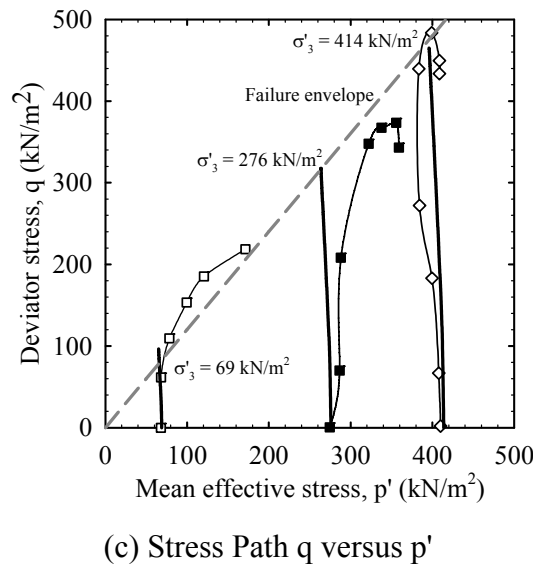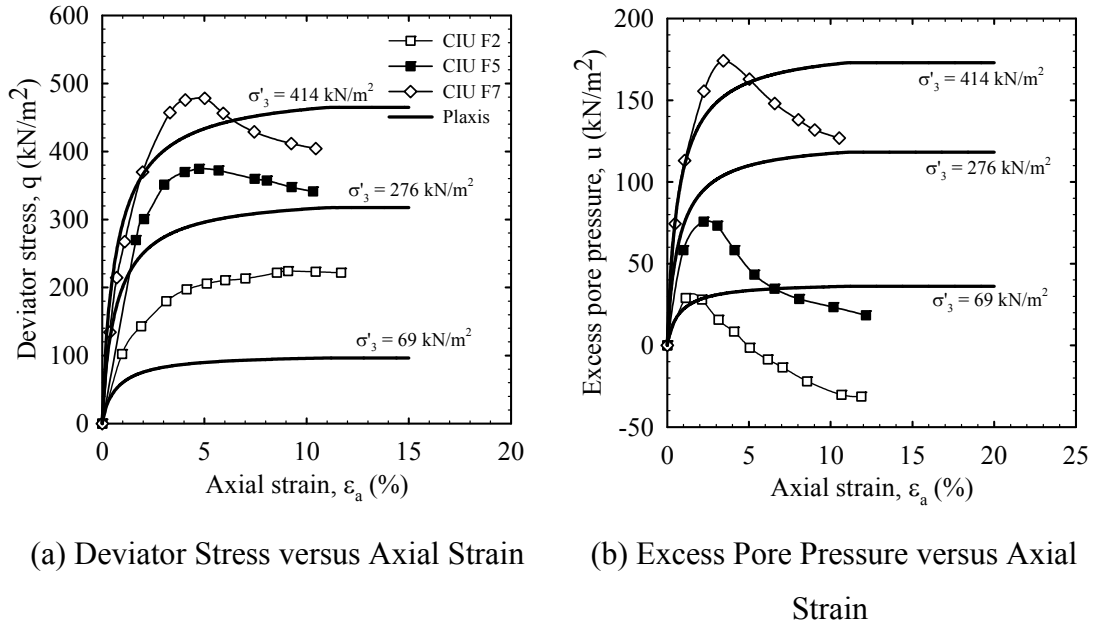
Figure 4.32: Bangkok Stiff Clay CIU Test Results and Their Predictions from HSM (Using Best Fit Input Parameters)

Further, from Figure 4.32 (c), the stress path q versus p' from the CIU tests, with a confining pressure of 69 kN/m^2, shows heavily overconsolidated clay behaviour; thus, where the stress paths reach failure on the failure envelopes (State Boundary Surface) on the dry side of the critical state line. These behaviour cannot be obtained from the HS Model predictions. The best estimation of the HS Model stress paths are the ones that are similar to the lightly overconsolidated clay, where the q versus p' stress path

163

goes vertically up to the failure envelope. Indeed, this lightly overconsolidated behaviour is more likely to be the case for the Bangkok stiff clay as the in-situ effective vertical stress at 18 m (where stiff clay samples were taken) is about 300 kN/m^2.

4.10 Concluding Remarks

The work contained in this chapter is in three major parts. The first one is related to undrained strength parameters of Bangkok Clays as interpreted from vane shear test (Bangkok Soft Clay) and CK$_o$U triaxial test (Stiff and Hard Clays). Path dependent drained strength parameters are also included in this section. The second part is the major one and it relates to interpretation of oedometer and triaxial deformation parameters for Hyperbolic and Hardening Soil Model analysis. Oedometer tests from Bangkok MRT Blue Line Extension project are used. Also, large amount of undrained and drained triaxial test series conducted at AIT under the supervision of Prof. Balasubramaniam (Chaudhry, 1975; Ahmed, 1975; Hassan, 1976; Kim, 1991; Gurung, 1992) are re-analysed. In the last part of this chapter, an attempt is made on 2D FE modelling of triaxial and oedometer tests using Plaxis. A series of parametric study is conducted to gain better understanding of the effects of input parameters. After that, soil model calibration is done by means of curve matching. The following concluding remarks can be made.

(1)   With the Mohr Coulomb Model undrained analyses in clays need the undrained strength. Undrained shear strength from field vane shear and CK$_o$U triaxial tests are utilised for soft to medium stiff and stiff to hard clays, respectively. Both field vane shear and CK$_o$U triaxial tests were conducted along the alignment of Bangkok MRT Blue Line Extension project. Correction factor of 0.8 according to the work of Bjerrum (1973) is applied to vane shear strength. The strength values are tabulated and presented as graphs.

Classical relations of undrained shear strength-effective stress ratio (s_u/σ'_{vo}) and plasticity index (I_p) are used from the relationships of Skempton and Henkel (1953), Osterman (1959), and Bjerrum and Simons (1960). An

alternative method to estimate s_u/σ'_{vo} ratio is to use the so called SHANSEP technique (Ladd, 1991) developed at MIT. Measured and predicted s_u/σ'_{vo} values are tabulated for soft to medium stiff clay as 0.26 to 0.36. The corresponding values for stiff to very stiff clay are in the range of 0.27 to 0.36. The corresponding values for very stiff to hard clays is only 0.22.

(2) **S**ummary tables of the drained strength parameters are also included. The ratio of triaxial compression to extension strength values are : 0.7, 0.74, 0.76, 0.77, 0.78, 0.8, 0.83, 0.89, 0.94, 1.1. The mean value is 0.83.

   (a) For Soft Bangkok Clay; average angle of internal friction at three depths of 2.5 to 4 m is 26 degrees and this reduced to 24 degrees at depths of 5.5 to 6 m.

   (b) For stiff clay at 16 m depth, the average angle of friction is 23 degrees and the average cohesion is 32 kN/m^2.

   (c) For hard clay at 39 to 43 m depth, the friction angle is 23.5 degrees and the cohesion is 42 kN/m^2.

(3) Values of the reference oedometer modulus are 962, 1,650, 4,689 and 3,947 kN/m^2 for soft, medium, stiff and hard clays, respectively. The corresponding values of the reference unloading/reloading oedometer modulus are 5,813, 5,394, 9,618 and 8,764 kN/m^2. An average range of reference unloading/reloading oedometer modulus to reference loading oedometer of 2 to 4 is obtained for soft clay. This ratio tends to reduce with depth. The lower value approximately 1.5 is found for hard clay. The values of OCR are also calculated from the estimated oedometer maximum past pressure. For soft clay layer, the OCR ranged from 1.1 to 1.8. Narrower range of 1.2 to 1.7 is obtained for medium stiff clay layer. At deeper depth, the OCR values of stiff to very stiff and hard clays are approximately equal to unity.

(4) The following equations can be used to estimate λ^* and E_{oed}^{ref} from I_l with reasonable R^2 of 0.8545 and 0.9311, respectively.

$$\lambda^* = 0.0239 \ln(I_l) + 0.117$$

$$E_{ref}^{oed} = 9238(I_l)^{-0.5643}$$

(5) One observation from the results of undrained triaxial test series (CIU, CK$_o$U and CK$_o$UE) is that, there is no definite trend of undrained moduli with OCR. The undrained moduli from CIU and CK$_o$UE test series give a decrease in values of undrained moduli with increasing OCR. Whereas, an increasing trend is found from the results of CK$_o$U series. The ranges of initial undrained modulus and undrained modulus at 50 per cent undrained strength for soft clay with OCR less than 2.75 are 34 to 59 MN/m^2 and 20 to 29 MN/m^2 for CIU series; 67 to 200 MN/m^2 and 39 to 67 MN/m^2 for CK$_o$U series and 22 to 40 MN/m^2 and 8 to 17 MN/m^2 for CK$_o$UE series. The ratios of $E_{u,i}/E_{u,50}$ are fairly consistence at 2 to 3 for all the undrained test series. This ratio can be used to estimate the initial undrained modulus, normally used in Duncan and Chang' (1970) model, to the undrained modulus at 50 per cent undrained strength of Mohr Coulomb Model and Hardening Soil Model in Plaxis analyses. Likewise, the failure ratio of 0.9 can serve as averaged value from all the undrained test series.

(6) For the range of OCR from 1.0 to 2.7, the normalised undrained modulus ratios (E_u/s_u) from CK$_o$U are highest followed by the ratios from CIU and CK$_o$UE series, respectively. The soil specimens tested in all undrained test series have the plasticity index of 61. When these ratios are compared with Duncan and Buchignani's (1976) graph, the E_u/s_u ratios from CIU series coincided with the band if $I_p > 50$. Furthermore, this E_u/s_u ratios are also coincided with the same ratios calculated by the Cam Clay based method. At the average value of OCR (say OCR = 1.6) of Bangkok Soft Clay, the E_u/s_u ratios of 200, 400 and 150 are obtained from CIU, CK$_o$U and CK$_o$UE test series, respectively. Note that various researchers (i.e. Teparaksa *et al.*, 1999; Phienwej and Gan, 2003; Phienwej, 2006 and Mirjalili, 2009, see Table 3.5 for details) reported a value of E_u/s_u ratio of 500 for Bangkok Soft Clay from diaphragm wall movement back-analyses. This value is somewhat closer to the E_u/s_u ratio obtained from CK$_o$U test series.

(7)   Similar to the conclusion from the undrained triaxial tests on lightly overconsolidated soft clay, there is no specific relationship between drained moduli and OCR. The ranges of initial drained modulus and drained modulus at 50 per cent ultimate strength for soft clay with OCR less than 2.75 are 18 to 24 MN/m^2 and 5 to 13 MN/m^2 for CIU series; 11 to 50 MN/m^2 and 1.8 to 19 MN/m^2 for CK$_o$U series and 14 to 27 MN/m^2 and 6.7 to 14 MN/m^2 for CK$_o$UE series. The same range of values of 2 to 3 (as compared with the undrained tests) is found for an approximate E'_i/E'_{50} ratios. Average failure ratio of 0.9 is once again observed from all the drained test series.

(8)   Two triaxial test series (CIU and CID) were conducted on Bangkok Soft Clay with a variation in confining pressure for each test. The confining pressure for both CIU and CID series range from 138 to 414 kN/m^2. For the CIU series, the initial undrained modulus and the undrained modulus at 50 per cent undrained strength range from 10.5 to 40 MN/m^2 and 5.9 to 20.5 MN/m^2, respectively. The $E_{u,i}/E_{u,50}$ and failure ratios of 2 and 0.9 are obtained. For the CID series, the initial drained modulus and the drained modulus at 50 per cent ultimate strength range from 2.0 to 6.6 MN/m^2 and 1.0 to 2.4 MN/m^2, respectively. The E'_i/E'_{50} ratio is approximately 2 with the failure ratio of 0.7. It is obvious that both undrained and drained moduli from triaxial tests increase with the increasing confining pressure. These increasing trends are shown by double log scale plots of normalised confining pressure versus normalised undrained and drained moduli. It was found that all test series have a highly linear relationships which confirmed the Equation 4.6 proposed by Janbu (1963). The exponential power (*m*) of approximately unity is observed for all cases (undrained and drained). The reference undrained and drained moduli (at reference pressure of 100 kN/m^2) are 7.7, 4.8, 1.3 and 0.7 MN/m^2 for the cases of $E_{u,i}^{ref}, E_{u,50}^{ref}, E_{i}^{ref}$ and E_{50}^{ref}, respectively. These reference moduli are readily to be used as input parameter in the Hardening Soil Model (HSM) and Hardening Soil Model with Small Strain Stiffness (HSS).

(9)   Similar to the triaxial test series conducted on Bangkok Soft Clay, two triaxial test series (CIU and CID) of Bangkok Stiff Clay were analysed. The confining

pressure of CIU and CID series range 17 to 620 kN/m^2 and 34 to 552 kN/m^2, respectively. For the CIU series, the initial undrained modulus and the undrained modulus at 50 per cent undrained strength ranged from 14 to 71 MN/m^2 and 4.1 to 61 MN/m^2, respectively. The $E_{u,i}/E_{u,50}$ and failure ratios of 2.5 and 0.9 are obtained. For the CID series, the initial drained modulus and the drained modulus at 50 per cent ultimate strength ranged from 19 to 91 MN/m^2 and 9 to 36 MN/m^2, respectively. The E'_i/E'_{50} ratio is approximately 2 with the failure ratio of 0.9. Here again, a set of linear relationships is observed from the normalised double log scale plots with the exponential power (m) of 0.5. The reference undrained and drained moduli (at reference pressure of 100 kN/m^2) are 30, 11, 29 and 14 MN/m^2 for the cases of $E_{u,i}^{ref}, E_{u,50}^{ref}, E_i^{ref}$ and E_{50}^{ref}, respectively.

(10) The indirect method to obtain drained reference modulus from oedometer test results (Stark and Vettle, 1991) is studied. It is shown that this method can be used to approximate the drained reference modulus in the absence of drained triaxial results. However, multiplication factor of 1.17 and 1.11 should be applied for the cases of E_i^{ref} and E_{50}^{ref}, respectively.

(11) Parametric study of seven Hardening Soil Model (HSM) parameters is conducted. Overview of their influences on standard undrained triaxial and oedometer behaviour is summarised in Table 4.34. The following conclusions are summarised based on the results of this analysis. The E_{50}^{ref} parameter governs mainly q-ε_a and u-ε_a behaviour in undrained triaxial tests. It has little to no effect on triaxial stress path and ε_v-logσ'_v oedometer in case of normally consolidated clay. Parameters E_{oed}^{ref}, E_{ur}^{ref} and K_o^{nc} are soil parameters used to control the cap and shear hardening surfaces in HSM. Therefore, they have high influence on both triaxial and oedometer behaviour. Failure ratio (R_f) and unloading-reloading Poisson's ratio (ν_{ur}) should be kept as 0.9 and 0.2 to retain realistic soil behaviour. Exponential power m of 1.0 is necessary in the case of normally consolidated clay.

(12) According to the study of Hardening Soil Model (HSM) parameter calibration, it is seen that the back-calculated drained moduli are needed in the Plaxis analysis of undrained materials (using Method D in Table 4.2 (b)). Two possible reasons of this phenomenon are as followings. First, the assumption of adding bulk modulus of water, as used by the HSM in Plaxis (see Appendix A for detail), to convert the drained to the undrained modulus may not be appropriate. Second, the drained moduli from CID test series may not be representative values of the Bangkok soft clay. Therefore, it is suggested that the process of parameter calibration (i.e. Section 4.9.3) is necessary for the Plaxis analysis of undrained materials using Method D.

CHAPTER 5

Geotechnical Parameters
Evaluated from Pressuremeter Test

5.1 Introduction

Soil parameter interpretations from pressuremeter tests are described in this chapter
with the emphasis on their application in finite element analyses. The vital idea is to
find an alternative source of soil parameters to be adapted in higher order soil models,
such as the Hardening Soil Model. An idea of determining the geotechnical
parameters at in-situ soil condition has led to the development of the pressuremeter
tests. The first documented evidence of a pressuremeter test was that presented by
Kögler in 1933. His method was to lower a balloon like device into the borehole and
inflating it to measure the deformation properties of the soil. A modern type of
pressuremeter known as the "Ménard Pressuremeter (MPM)", was developed at the
University of Illinois (Ménard, 1975). Since its first use in Chicago, MPM has
become one of the most widely used types of pressuremeter. Further, Ménard has also
developed a foundation design method based on this instrument. Conducting the
Ménard Pressuremeter test involves lowering a pressuremeter probe into a test pocket
that is slightly larger in diameter (see Figure 5.1 (a)). As a result, the test is normally

categorised as a pre-bored pressuremeter (PBP) type. In 1959, Fukuoka and Utsu (as cited in Menard (1975)) independently developed a device based on Kögler's method to determine the horizontal subgrade reaction coefficient, K in laterally loaded piles. This form of pressuremeter has then led to the development of the OYO Corporation device, called "Lateral Load Test". The lateral load test (LLT) pressuremeter shares a similar basic principle with the Ménard Pressuremeter, except that the LLT uses one monocell cylindrical probe instead the tricell system of Ménard Pressuremeter.
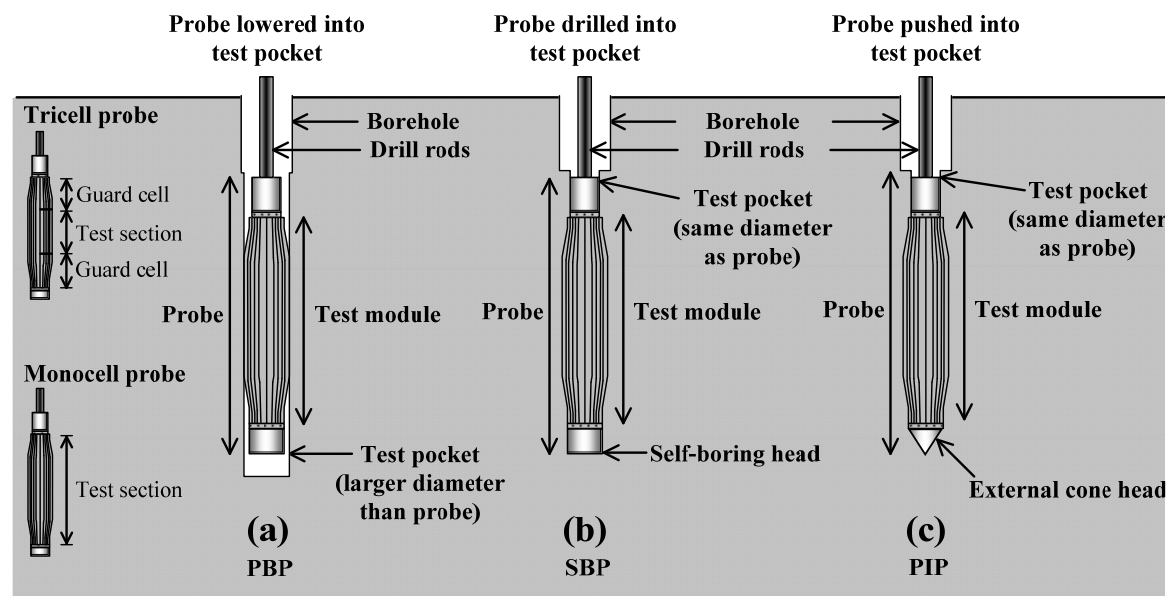
Figure 5.1: Pressuremeter Probes and Test Pockets of PBP, SBP and PIP
(Modified after Clarke, 1995)

The insertion of the pressuremeter probe in a pre-bored hole inevitably caused soil disturbance. To overcome this problem, the self – boring pressuremeters (SBP) were developed in both France and the United Kingdom (UK) (Jézéquel *et al.*, 1968; Baguelin *et al.*, 1972 and Wroth and Hughes, 1973). The SBP developed in the UK is known as the Cambridge pressuremeter or Camkometer, while the French version is known as Pressiometre Autoforeur (PAF). Figure 5.1 (b) shows the principle of the self-boring pressuremeter instruments.

The Pushed-in Pressuremeter (PIP) was primarily developed for use in offshore drilling; however, the recent version was designed for onshore use with cone trucks. If the pushed-in pressuremeter completely displaced the surrounding soil, it was known

as the Full Displacement Pressuremeter (FDP) or Cone Pressuremeter. Figure 5.1 (c) illustrates the probe components used in the Pushed-in Pressuremeter.

5.1.1 Test Procedure and Typical Test Results

The pressuremeter test can be divided into three phases, (see Figure 5.2 (a)). Phase I begins after the insertion of the pressuremeter probe. The applied effective pressure (p_e) starts from the origin at Point A and increases to Point C, where the membrane makes contact with the borehole side due to its expansion. At this stage, the pressuremeter membrane has no restraining pressure from the surrounding soil and tends to creep. The second phase, referred to as an elastic or pseudo-elastic phase, theoretically, has no excess pore pressure developing during the applied effective pressure from Point C to D, where the soil is behaving elastically. The time-dependent deformation, due to the dissipation of the excess pore pressure is, therefore, reasonably small and negligible. After the increase in the pressure has reached the soil strength, at pressure p_f, the excess pore pressure develops and creep will occur (Phase III). The plastic condition of the soil in Phase III continues with an increase in radius until a limit pressure, p_L is reached.
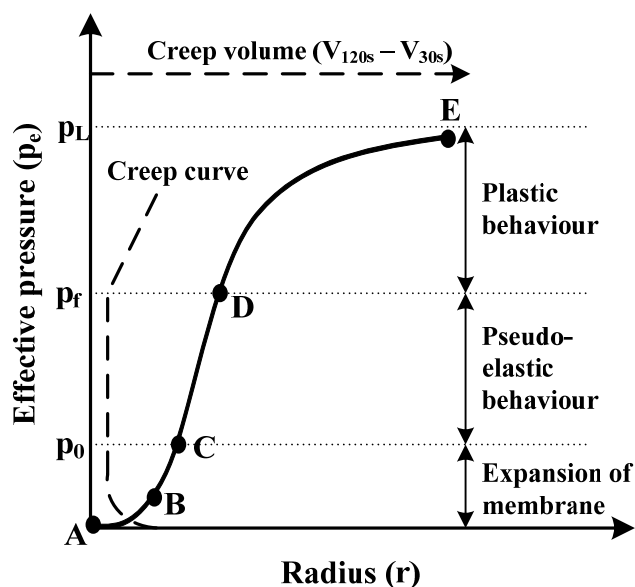
Figure 5.2 (a): Typical Result from Pressuremeter Test Plotted with Creep Curve (Mair and Wood, 1987)
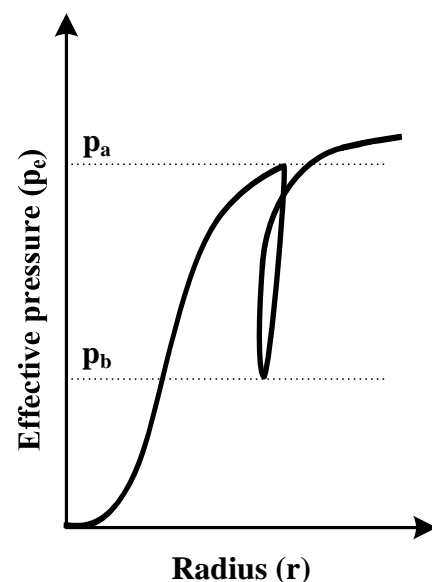
Figure 5.2 (b): Unloading/Reloading Loop from Pressuremeter Test

The results from the pressuremeter tests are normally represented by a plot of effective pressure (p_e) versus the radius of the probe (r), as illustrated in Figure 5.2 (a). The effective pressure (p_e) is the cell pressure corrected for rubber reaction and hydrostatic pressure. During the process of the pressuremeter test, equal pressure increments are applied in a number of steps. In each step, it is usual to maintain the pressure increment for approximately two minutes; the change in the membrane volume is recorded after 15, 30, 60 and 120 seconds.

The "Creep curve" is shown in Figure 5.2 (a) as a dashed line. This curve is constructed by plotting the change of injected volume between the 30 and 120 second readings against the corresponding pressure. The benefit of the creep curve is to aid in locating the position of pressure (p_i) necessary to achieve the initial contact between the probe cell and the borehole wall and the pressure (p_f) corresponding to the yielding pressure of the soil where the plastic strain occurs.

The installation of the pressuremeter probe can cause some degree of disturbance to the soil. There is also a question about how to locate the beginning point of the pseudo-elastic soil behaviour (or the beginning of the straight portion at Point C in Figure 5.2 (a)). Thus, an unloading/reloading loop, as shown in Figure 5.2 (b), is often added to the testing process. With this loop, the unloading/reloading shear modulus (G_{ur}) can be estimated (see Section 5.2.2 below). Wroth (1982) asserts that the pressure at the commencement of the unloading and reloading processes (p_a and p_b) should be as follow:

1. The pressure p_b should be equal to one half of the pressure p_a
2. In the case of clay soils, the difference between p_a and p_b should be lesser than two times the soil undrained shear strength.

5.1.2 Stress and Strain in Cavity Expansion Theory

An ideal pressuremeter test should occur without disturbance to the surrounding soil, the initial cavity pressure (p_i) would be equal to the in-situ total horizontal stress (σ_{ho}, p_o). The initial volume (V_o), of the cylindrical cavity can be calculated from the initial cavity radius (ρ_o) and the height of the pressuremeter cavity (h) (Figure 5.3 (a)). The cavity pressure (p), the cavity volume (V) and the cavity radius (ρ) are the measurements made during the test. In the case of an axial symmetry condition, the cavity height (h) is assumed to be high enough when compared to its diameter, so that all movements occur only in the radial direction (plane strain deformation and no vertical movement).
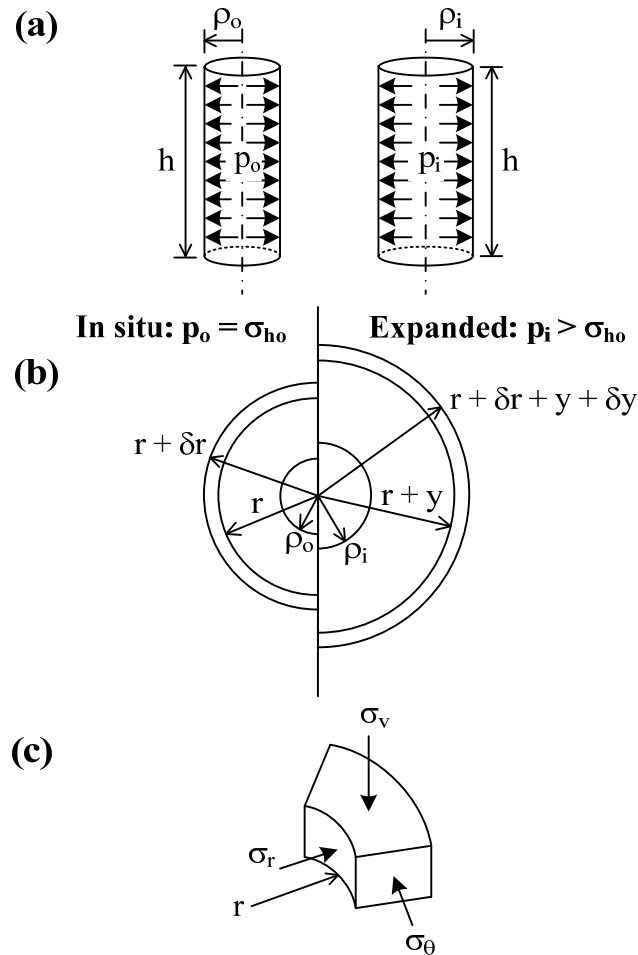
Figure 5.3: Definitions Used in the Analysis of Cylindrical Cavity Expansion Theory: (a) Expansion of a Cylindrical Cavity; (b) Expansion of an Element at Radius, r; (c) Stresses on an Element at Radius, r (Modified after Clarke, 1995)

An element of soil at the distance radius (r) and thickness (δ_r), measuring from centre of the cavity, is subjected to principal stresses σ_r, σ_θ and σ_v. According to Timoshenko and Goodier (1934), the equation of equilibrium, in terms of total stresses is:

$$\frac{d\sigma_r}{dr} + \frac{\sigma_r - \sigma_\theta}{r} = 0$$

Eq. 5.1

From Figure 5.3 (b), the in-situ soil element at p_o has an inner radius of r and a thickness of δ_r. This soil element expands due to the applied pressure, thus its inner radius and thickness increases to $r + y$ and $\delta_r + \delta_y$. The circumference of the soil circle of $2\pi r$ increases to $2\pi(r + y)$, and the tensile circumferential strain (ε_θ) is:

$$\varepsilon_\theta = \frac{y}{r}$$

Eq. 5.2

Since, the thickness of the soil element changes by δ_y, the radial strain, ε_r, is:

$$\varepsilon_r = \frac{\delta_y}{\delta_r}$$

Eq. 5.3

Typical results of the pressuremeter test are normally presented as a plot of pressure, p versus a cavity volume, V or change in volume, $\Delta V = V - V_o$. If the cavity radius, r, is measured, the circumferential strain at the cavity wall, known as the cavity strain, ε_c, is used instead of the cavity volume. The cavity strain is defined as:

$$\varepsilon_c = \frac{\rho - \rho_0}{\rho_0}$$

Eq. 5.4

The change of volume, ΔV, is related to the cavity strain by:

$$\frac{\Delta V}{V} = 1 - \frac{1}{(1 + \varepsilon_c)^2}$$

Eq. 5.5

5.2 Soil Parameters Obtained from the Interpretations of Pressuremeter Tests

The soil parameter interpretations from the LLT pressuremeter tests are discussed in this section, with an emphasis being placed on their application in the finite element analyses. The initiative is to find an alternative source of soil parameters that can be adapted in the higher order soil models, such as the Hardening Soil Model. Details of each method are summarised in subsequent sections.

5.2.1 Total Horizontal Stress and Coefficient of Earth Pressure at Rest

Soil movement prediction under working conditions, using finite element analyses, requires a realistic estimation of the in-situ stresses. Unlike the in-situ effective vertical stress (σ_{vo}), estimating the in-situ horizontal stress (σ_{ho}) is not straightforward. In engineering practice, in-situ horizontal stress is commonly obtained by the successive estimation of the coefficient of earth pressure at rest (K_o) using an empirical correlation. Various indirect laboratory techniques, i.e. preconsolidation pressure simulating method, consolidation under a constant stress ratio method, consolidation under zero lateral strain condition (Tantikom, 1982), were attempted. However, the pressuremeter is one of a few in-situ instruments that give the direct estimation of σ_{ho}.

The coefficient of earth pressure at rest (K_o), by definition, is equal to the ratio of the initial effective horizontal stress to the initial effective vertical stress. If the initial pore water pressure (u_o) is known (normally by mean of static pore water pressure), the coefficient of the earth pressure at rest (K_o) can be obtained from:

$$K_o = \frac{\sigma_{ho} - u_o}{\sigma_{vo} - u_o} \qquad \text{Eq. 5.6}$$

In the process of the pre-bored pressuremeter test, prior to drilling the borehole, the initial horizontal stress in the ground is taken as equal to the total horizontal stress at rest (σ_{ho}). As the borehole is drilled, the wall of the cylindrical cavity moves inward and the total horizontal stress decreases to about zero. After insertion of the pressuremeter probe, and as the probe is inflated in small pressure increments, the cylindrical cavity wall will move back to its original position corresponding to the total horizontal stress at rest. Baguelin *et al.* (1978) pointed that the pressure (p_o) at the start of the straight line portion of the pressuremeter curve (Point C in Figure 5.4), theoretically, should be equal to the total horizontal stress at rest (σ_{ho}). In practice, p_o is difficult to obtain as there are only a few points along the initial straight portion of the test curve. In contrast, Briaud (1992) suggested that the total horizontal stress at rest (σ_{ho}) should be located at the point of maximum curvature (Point B in Figure 5.4). During recompression process (path AB), the soil is in an overconsolidated state. After point B is reached, the soil will be stressed in virgin behaviour. In practice, the creep curve is normally drawn in assisting the selection of the initial pressure (p_i), as discussed in Section 5.1.1 and shown in Figure 5.2. This initial pressure is assumed to be equal to the in-situ total horizontal stress (σ_{ho}); this method is referred to as the "Creep Curve Method" in the current study.
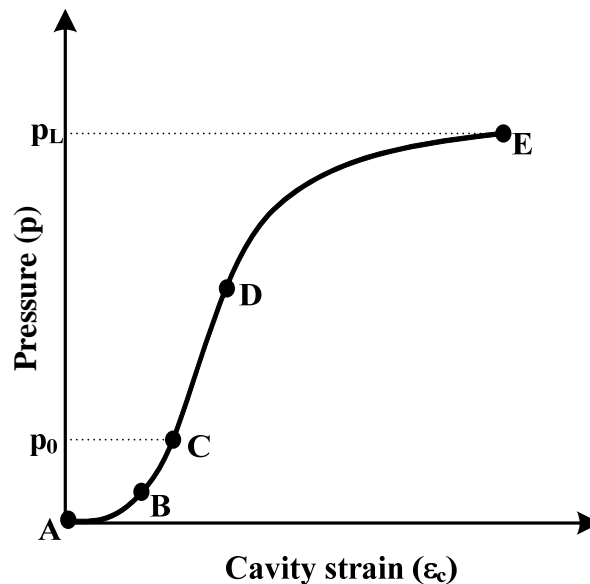
Figure 5.4: Obtaining Horizontal Pressure at Rest

Marsland and Randolph (1977) proposed an interactive procedure using effective pressure versus the cavity strain ($p - \varepsilon_c$) plot for the p_o determination. This method

was developed mainly for pressuremeter tests on stiff clay, which exhibit linear stress-strain behaviour until the peak strength is reached. The linear portion of the $p - \varepsilon_c$ plot should be terminated when the undrained shear strength of the soil is reached, i.e. the applied pressure is equal to p_o plus the soil undrained shear strength. The iteration process for this method is as follows (see Figure 5.5):

(1) Determine the initial estimate of the total horizontal stress (σ_{ho1}) from an assumed K_o and in situ pore water pressure;

(2) Obtain the volume V_o from the measured p versus V curve, corresponding to the cavity strain (ε_{o1});

(3) Plot a curve of p versus ln $\Delta V/V$ (where $\Delta V/V = \Delta V/(V_o+\Delta V)$). The peak value of the undrained shear strength, s_{u1} (i.e. Palmer's (1972) peak strength) is taken from this curve; and

(4) Proceed with the iteration process using other values of the total horizontal stress by repeating Steps 1 to 3, until Equation 5.7 is satisfied (see Figure 5.5 (b)).

$$p_y = \sigma_{ho} + s_u \qquad\qquad\qquad \text{Eq. 5.7}$$
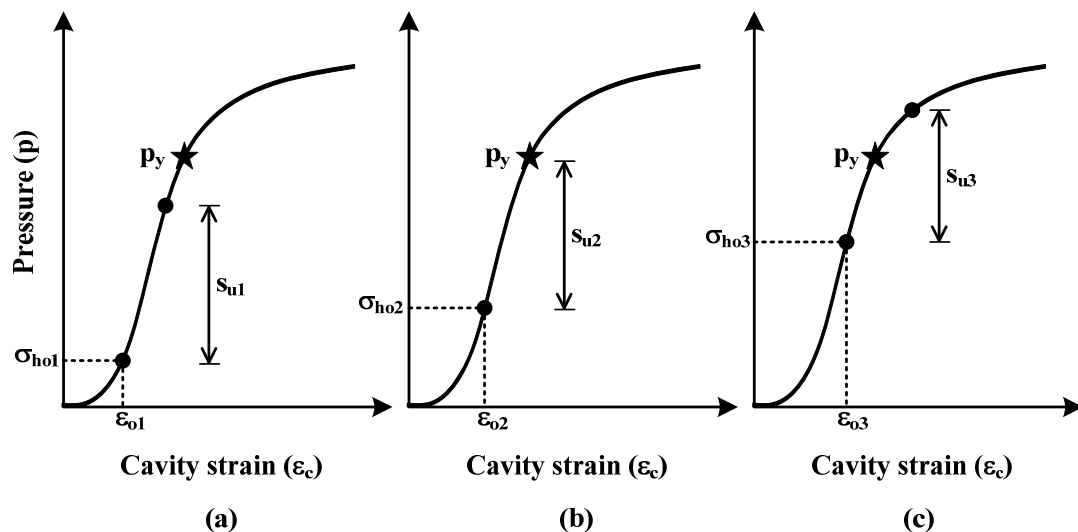
Figure 5.5: Iteration Process for Estimating the In-situ Horizontal Stress
(Marsland and Randolph, 1977)

178

Hawkins *et al.* (1990) modified the Marsland and Randolph (1977) method to determine the coefficient of earth pressure at rest. This method involves an iteration process similar to the Marsland and Randolph (1977) method. However, instead of using Palmer's (1972) peak strength, the undrained shear strength is obtained by forcing the p versus ε_c and p versus $\ln(\Delta V/V)$ diagrams to be mutually consistent during the soil elastic response (see Figure 5.6). The total horizontal stress from this method is achieved by following iteration steps from 1 to 3 above, however, the undrained shear strength of the soil from the slope of p versus $\ln(\Delta V/V)$ curve at the pressure equal to p_y is used This iteration process is repeated until Equation 5.8 is satisfied.

$$p - \sigma_{ho} = \frac{dp}{d[\ln(\Delta V / V)]}$$
Eq. 5.8
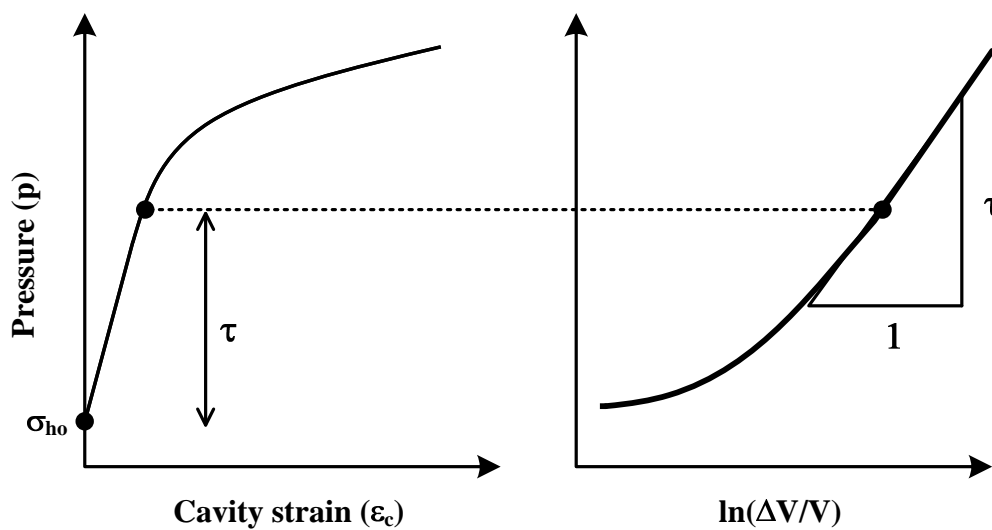
Figure 5.6: Diagram of Modified Marsland and Randolph Method
(Hawkins *et al.*, 1990)

5.2.2 Shear Modulus

Two shear moduli can be directly deduced from the pressuremeter test results. One is the initial shear modulus (G_i) and the other is the unloading/reloading shear modulus, (G_{ur}) (see Figure 5.7). These two moduli can be converted into initial and unloading/reloading pressuremeter moduli ($E_{p\ (i)}$ and $E_{p\ (ur)}$) using elasticity theory

179

with an assumed Poisson's ratio. According to Gibson and Anderson (1961), shear modulus from p versus ε_c and p versus V relations can be expressed as:

$$G = 0.5\left(\frac{\rho}{\rho_o}\right)\left(\frac{dp}{d\varepsilon_c}\right) \qquad \text{Eq.5.9}$$

$$G = V_m \frac{dp}{dV} \qquad \text{Eq.5.10}$$

where,

$\rho,\ \rho_o$ = radius of cavity, initial radius of cavity

dp = increment of applied pressure

$d\varepsilon_c$ = increment of cavity strain

V_m = average volume of cavity over the pressure increment dp

dV = increment in volume of cavity.
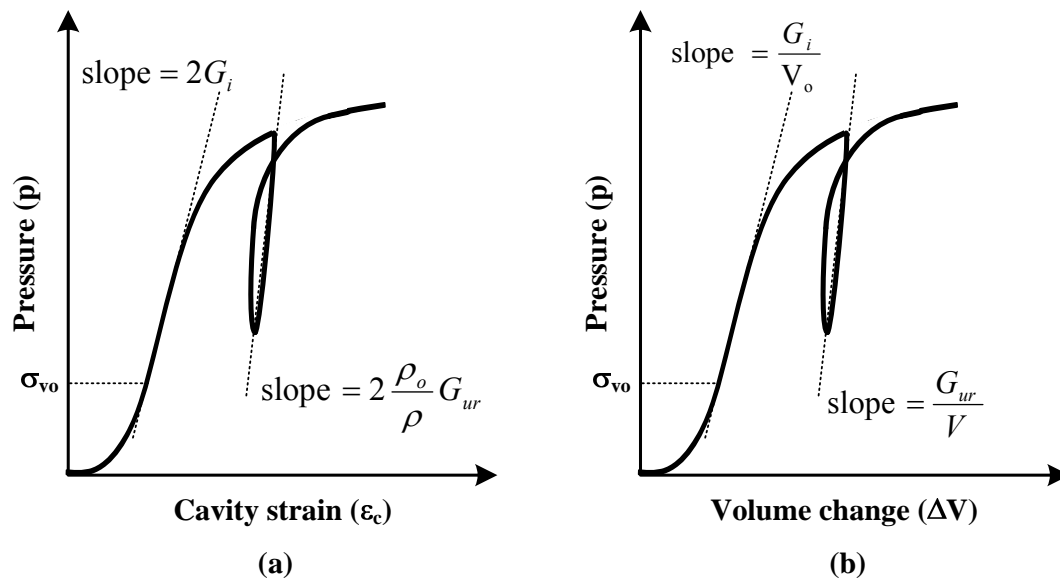
Figure 5.7: Determinations of Initial and Unloading/reloading Shear Moduli

The initial shear modulus (G_i) is taken from the initial part of the pressuremeter curve, starting from the pressure equal to the initial total horizontal stress (σ_{ho}). At this stage, when the level of strain is small, ρ_o is approximately equal to ρ, hence, the initial volume, $V_o \approx V$. Therefore, the initial shear modulus is given as:

$$G_i = 0.5 \left(\frac{dp}{d\varepsilon_c} \right)$$ Eq.5.11

$$G_i = V_o \frac{dp}{dV}$$ Eq.5.12

At the unloading/reloading loop in the pressuremeter test curve, the soil is assumed to behave elastically; as a result, the unloading/reloading shear modulus can be approximated as:

$$G_{ur} = 0.5 \left(\frac{dp}{d\varepsilon_c} \right)$$ Eq.5.13

$$G_{ur} = V \frac{dp}{dV}$$ Eq.5.14

5.2.3 Undrained Shear Strength

Unlike the horizontal stress and the shear modulus parameters, the shear strength of soils depends upon the drainage condition of the test. Baguelin *et al.* (1986) conducted a numerical study on the pore pressure generation around an expanding cavity utilising the Modified Cam Clay and elastic perfectly plastic soil models. The results revealed that soil permeability has an insignificant effect on the pressure-strain curve; hence, the effect on shear strength is negligible. Generally, the methods for the shear strength determinations can be divided into three categories, which are summarised in the following sections.

5.2.3.1 Undrained Shear Strength Estimated from General Analysis

The general analysis of the undrained plane-strain expansion of the cylindrical cavity in clay was developed by Palmer (1972). In this analysis, a complete stress-strain relationship can be deduced from the pressuremeter test curve. The only assumption made is that the soil deformation has no volume change under undrained conditions. The expression of the shear stress and cavity strain relationship is given as:

$$\tau = \frac{1}{2}\,\varepsilon_c\left(1+\varepsilon_c\right)\left(2+\varepsilon_c\right)\frac{dp}{d\varepsilon_c}$$ Eq.5.15

Equation 5.15 describes the complete shear stress–cavity strain relationship at the cavity wall. For a small strain, Equation 5.15 can be approximated as:

$$\tau = \varepsilon_c\,\frac{dp}{d\varepsilon_c}$$ Eq.5.16

Equation 5.16 can be re-written in terms of the volumetric strain as:

$$\tau = \frac{dp}{d\left[\ln\left(\Delta V / V\right)\right]}$$ Eq.5.17

Figure 5.8 (a and b) graphically illustrate Palmer's method. In Figure 5.8 (a), the shear stress (τ), at any level of cavity strain (ε_c), is obtained by projecting the tangent line to the pressure axis. Distance AB, which is the difference between the tangent line intersection (Point B) and the pressure at the strain level of interest (Point A), is equal to the shear strength. In the case of the pressure–volumetric strain plot (Figure 5.8 (b)), the shear strength at a particular cavity strain equals the slope of p versus $\ln(\Delta V/V)$ plot.
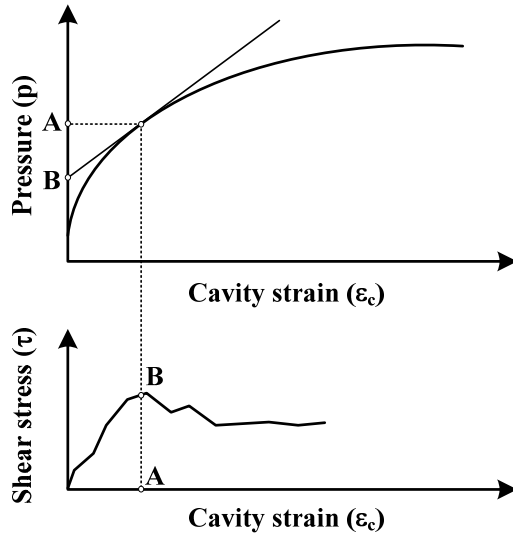
Figure 5.8 (a): Shear Strength
Determination from p-ε_c Curve
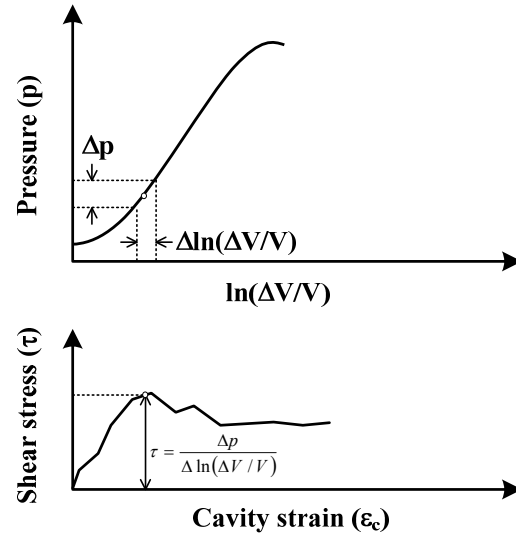
Figure 5.8 (b): Shear Strength
Determination from p-$\ln(\Delta V/V)$ Curve

5.2.3.2 Undrained Shear Strength Estimated from Linear Elastic Perfectly Plastic Soil

The undrained shear strength determination, based on elastic perfectly plastic soil
behaviour in undrained conditions, was developed by Gibson and Anderson (1961). If
the soil is assumed to behave in an elastic-perfectly plastic manner, and the probe is
inserted without any disturbance, then the initial cavity pressure should be the same as
the initial total horizontal stress (σ_{ho}). Figure 5.9 (a) shows the stress-strain
relationship of the elastic perfectly plastic ground, which will respond elastically until
the undrained shear strength of the soil is reached. At this stage, the small elastic
volumetric strain at the onset of yield is given as (Equation 5.19):

$$\frac{\Delta V}{V} = \frac{s_u}{G}$$

Eq.5.18

Further, according to Gibson and Anderson (1961), the pressure change during the
cavity expansion of elastic perfectly plastic soil is obtained by integrating Equation
5.17 with respect to $\ln(\Delta V/V)$, thus becoming Equation 5.19:

183

$$p - \sigma_h = s_u \left[1 + \ln\left(\frac{G}{s_u}\right) + \ln\left(\frac{\Delta V}{V}\right) \right] \qquad \text{Eq.5.19}$$

From Equation 5.19, a limit condition is reached when the value of $\Delta V/V$ is equal to one, and where the soil will deformed plastically. The pressure at this stage is referred to as limit pressure, p_L. Equation 5.19 can be reduced to Equation 5.20:

$$p_L - \sigma_h = s_u \left[1 + \ln\left(\frac{G}{s_u}\right) \right] \qquad \text{Eq.5.20}$$

By substituting Equations 5.17 and 5.18 into Equation 5.20, the response of the pressuremeter test in the plastic phase, where $\sigma_{ho} + s_u \leq p \leq p_L$ can be expressed as Equation 5.21:

$$p = p_L + s_u \ln\left(\frac{\Delta V}{V}\right) \qquad \text{Eq.5.21}$$

It can be seen from Equation 5.21 and Figure 5.9 (b) that the plot of pressure, p versus $\ln(\Delta V/V)$ should lie on a straight line in the plastic phase. Thus, the slope of this linear part is equal to the undrained shear strength, s_u, and the y-intercept is equal to the limit pressure, p_L, where $\Delta V = V$ or $\ln(\Delta V/V) = 0$.
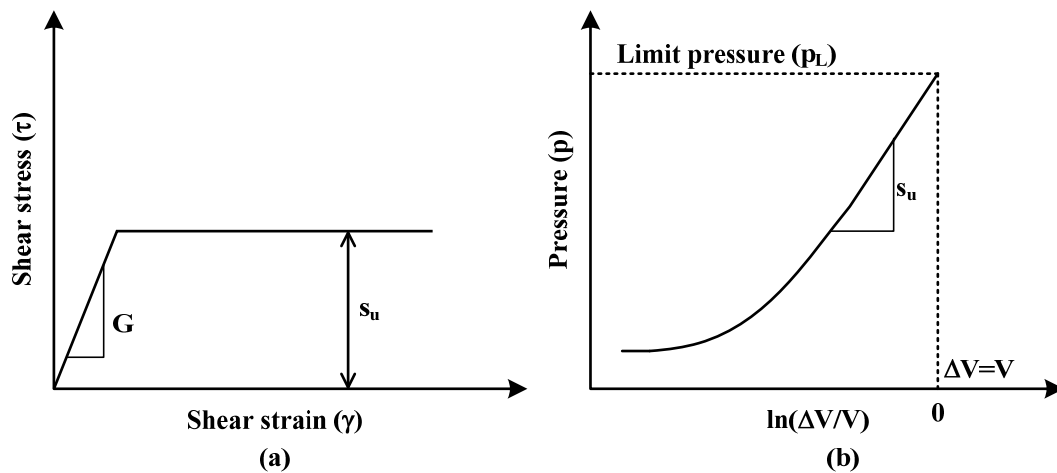
Figure 5.9: Determination of Undrained Shear Strength of
Elastic Perfectly Plastic Soil

5.2.3.3 Undrained Shear Strength Estimated from Limit Pressure

Following on from the analysis of the linear elastic perfectly plastic soil (Gibson and Anderson, 1961), Marsland and Randolph (1977) proposed methods for the shear strength determination from the limit pressure, p_L. In this method, the total horizontal stress (σ_{ho}), shear modulus (G), and limit pressure (p_L) are estimated from the test curve (see Sections 5.2.1, 5.2.2 and 5.2.3.2). Equation 5.20 can be rearranged as:

$$s_u = \frac{p_L - \sigma_{ho}}{1 + \ln\left(\dfrac{G}{s_u}\right)}$$

Eq.5.22

$$s_u = \frac{p_L - \sigma_{ho}}{N_p} = \frac{p_L^*}{N_p}$$

Eq.5.23

where,

p_L, p_L^* = limit pressure, net limit pressure

N_p = pressuremeter constant.

Parameters σ_{ho}, G and p_L are then substituted in Equation 5.22, with an assumed value of s_u in the terms of $1 + \ln (G/s_u)$. This s_u is then changed until the values in both terms are consistent. Alternatively, a so called "Pressuremeter constant, N_p" (Equation 5.23 can be used to estimate the undrained shear strength if the ratio of G/s_u is known. In this study G/s_u is found to be of the order of 150 and 300 for the Bangkok soft and stiff clays, respectively. These values correspond to the values of N_p of 6 and 6.7 for soft and stiff clays, respectively.

An alternative approach of shear strength determination from the limit pressure is to use empirical correlations. Various authors have conducted comprehensive studies on the correlation of the limit pressure and the undrained shear strength of clays (Lukas and LeClerc de Bussy, 1976; Baguelin *et al.* 1978; Bergado and Khaleque, 1986; Bergado *et al.*, 1986; Briaud, 1992). In general, the undrained shear strength from PMT is correlated with the vane shear strength in soft clay, and from the unconfined

compression or triaxial tests in stiff clay. Ménard (1975) proposed that the N_p parameter (Equation 5.23) can be taken as 5.5 for cohesive soil, regardless of the value of G/s_u. Bergado and Khaleque (1986), who studied the correlations of undrained shear strength from the field vane shear, s_{uv} with LLT limit pressure in Bangkok Soft Clay, found that these two parameters can be correlated as:

$$s_{uv} = \frac{p_L}{5.9}$$
Eq.5.24

It should be note that Equation 5.24 is based on the LLT test results in Bangkok soft clay, where its undrained shear strength and limit pressure are lower than 50 and 400 kN/m^2, respectively. Baguelin *et al.* (1978) identified a bi-linear relationship between the undrained shear strength and the net limit pressure. They proposed that the N_p of 5.5 (Equation 5.23) should be taken for clay with undrained shear strength less than 50 kN/m^2, and N_p of 10 for undrained shear strength less than 150 kN/m^2. Briaud (1992) extended this work and suggested a non-linear relationship between the undrained shear strength and the net limit pressure as:

$$s_u = 0.67 \, p_L^{*\,0.75}$$
Eq.5.25

where, both s_u and p_L are in kN/m^2.

5.2.3.4 Effects of Pressuremeter Geometry on Undrained Shear Strength

The undrained shear strength interpretation methods (as discussed in Section 5.2.3) are based on the theory of infinitely long cylindrical cavity expansion (one-dimensional cavity expansion theory). As a result, the effects of the 2D geometry of the pressuremeter are ignored; this leads to an overestimation of the shear strength parameter. Several researchers (i.e. Yu, 1990; Houlsby and Carter, 1993; Shuttle and Jefferies, 1995 and Yu *et al.*, 2005) have conducted parametric studies with the aid of the finite element analysis. The effects of the length to the diameter ratio L/D, the depth of penetration to the diameter ratio H/D, the rigidity index $I_r = G/s_u$, the types of soil models, the overconsolidation ratio OCR, the strain range over (which shear

strength is deduced), and the soil initial state of stress are included in the existing studies. The results were presented in terms of the correction factor (β) to be multiplied with the undrained shear strength derived from the infinitely long cylindrical cavity expansion. The results of this multiplication are called the true values of the undrained shear strength, which would have been measured if the pressuremeter was infinitely long.

Parametric studies using the Mohr Coulomb Model (Houlsby and Carter, 1993; Shuttle and Jefferies, 1995) revealed that the length to the diameter ratio L/D and the soil rigidity index $I_r = G/s_u$ are both significant factors affecting the correction factor (β). The effects of the depth of penetration to the diameter ratio H/D is minor and negligible. Similar parametric studies, using two critical state models were conducted by Yu *et al.* (2005). In the critical state models used in their analyses, the shear modulus (G) is assumed to be a linear function of the mean effective stress (p'); a constant Poisson's ratio is also assumed. When the shear modulus (G) changes with the mean effective stress (p'), the values of the shear modulus vary with the applied pressure (as the process of pressuremeter testing proceeds further in the finite element model). This variation is not applied when the shear modulus is assumed constant in the Mohr Coulomb Model. Hence, the effects of the rigidity index (G/s_u) on the correction factor (β), when the critical state models are used, are not meaningful. As a consequence, Yu *et al.* (2005) focused on the effect of the OCR , K_o and adopted soil models instead. The authors concluded that only the OCR had a significant effect on the overestimation of the undrained shear strength, while K_o and the adopted soil models were insignificant.

Tables 5.1 and 5.2 present a summary of the correction factor (β) for the Bangkok Soft Clay (BSC) and the First Stiff Clay (FSC) analyses, showing the results from the above mentioned parametric studies. It can be seen that all the analyses obtain a 10 – 25 per cent reduction of the undrained shear strength for both the LLT and SBP cases.

Table 5.1: Correction Factor from Mohr Coulomb Model Analysis

(at 2 to 5% Strain)

Authors	PMT	L/D	Soil model	Correction factor, β	
				BSC ($G/s_u = 150$)	FSC ($G/s_u = 300$)
Houlsby and Carter (1993)	LLT	8.57	MC	0.858	0.813
	SBP	6.02	MC	0.815	0.764
Shuttle and Jefferies (1995)	SBP	6.02	MC	0.910	0.875

Table 5.2: Correction Factor from Modified Cam Clay Model Analysis

(at 2 to 5% Strain)

Authors	PMT	L/D	Soil model	Correction factor, β	
				BSC (OCR = 1.5)	FSC (OCR = 1.6)
Yu *et al.* (2005)	LLT	8.57	MCC	0.891	0.896
	SBP	6.02	MCC	0.867	0.872

5.3 Soil Parameters Resulting from Pressuremeter Test in Bangkok Subsoils

This section summarise the pressuremeter tests previously conducted in the Bangkok areas. It involves both the pre-bored pressuremeter of the LLT type and the self-boring pressuremeter (SBP) of the Cambridge type. Details of both types of pressuremeter tests are presented in Table 5.3. In the early 1980s, the LLT tests were conducted, in the main, on Weathered clay, Bangkok Soft Clay and Stiff clay up 15 m deep at the Asian Institute of Technology campus. The classical cavity expansion theories, such as those of Gibson and Anderson (1961), and Palmer (1972), were utilised in the soil parameter interpretations. The results were compared and correlated with the in-situ vane shear test and the Cone Penetration Test (CPT). Bergado *et al.* (1986) summarised the LLT tests and related works undertaken at the AIT. They concluded that the undrained shear strength from the LLT tests (s_{up}) was 10 to 25 percent higher than the undrained shear strength from the vane shear (s_{uv}). The average relationship was given as:

$$s_{up} = 1.2 s_{uv} \qquad\qquad \text{Eq.5.26}$$

Table 5.3: Pressuremeter Tests Conducted in Bangkok Subsoils

| Type | Probe | | | Test location | Subsoils tested | Reference |
	Diameter (mm)	Length (mm)	*L/D*			
LLT	70	600	8.57	AIT campus	BSC, FSC	Huang (1980) Surya (1981) Begado *et al.* (1986)
SBP	83.1	500	6.02	Bangkok MRT Blue Line project	BSC, FSC, DS	Prust *et al.* (2005)
LLT	70	600	8.57	Bangkok MRT Blue Line Extension project	BSC, FSC	The current study

Note: BSC – Bangkok Soft Clay, FSC – First Stiff Clay and DS – Dense Sand

The self-boring pressuremeter test was first brought into Bangkok's engineering practice for the design of a subway station diaphragm wall in Bangkok's MRT Blue Line project (Prust *et al.*, 2005). A total of six SBP tests were conducted in Bangkok Soft Clay, First Stiff Clay and Dense Sand layers up to 40 m deep. Conventional site investigation programs were also employed, including wash-boring, vane shear test, SPT, and triaxial tests. The results of the SBP test interpretation were compared with those obtained from conventional methods (i.e. vane shear, triaxial tests, and empirical correlations), and the back-analysis of wall deflection. The results are summarised in Table 5.4:

Table 5.4: Comparisons of Soil Parameters from SBP, Conventional Investigations and Back-analysis Results (Prust *et al.*, 2005)

Soil layer	Conventional investigation	SBP	Back-analyses
	Earth pressure coefficient, K_o (-)		
BSC	0.75	0.1 to 0.3	0.75
FSC	0.4 to 1.0	0.2 to 1.4	0.65
DS	0.4	0.2 to 1.3	-
	Shear strength, s_u (kN/m^2)		
BSC	$s_u/\sigma'_{vo} = 0.35$	$s_u/\sigma'_{vo} = 0.45$	$s_u/\sigma'_{vo} = 0.45$
FSC	$s_u = 50 + 7.8z^*$	$s_u = 100 + 15.6z^*$	$s_u = 100 + 15.6z^*$
DS	$\phi' = 36^o$	$\phi' = 35 - 37^o$	$\phi' = 36^o$
	Stiffness ratio (E_u/s_u)		
BSC	$E_u = 400$ to $500s_u$	$E_u = 500s_u$ (Strain = 0.1 - 0.2%)	$E_u = 700s_u$
FSC	$E_u = 500s_u$ (above 18 m) $E_u = 1000s_u$ (below 18 m)	$E_u = 500s_u$ (above 18 m) $E_u = 1000s_u$ (below 18 m) (Strain = 0.05 to 0.1%)	$E_u = 1000s_u$
DS	$E'/N^\Delta = 0.8$ to 4.0	$E'/N^\Delta = 1.9$ to 7.9	-

Note: * Z is the depth below ground surface, $^\Delta$ N is SPT N value

The stiffness ratio (G/s_u) – shear strain relationship, resulting from the SBP tests, is shown in Figure 5.10. While the stiffness ratios of both BSC and FSC are not constant, the G/s_u ratio degrades with increasing shear strain level. Indeed, the typical range of the shear strain, resulting from the diaphragm wall movement, is from 0.1 to 0.2% and 0.05 to 0.1% for the Bangkok Soft Clay and First Stiff Clay, respectively (Teparaksa, 1999; Prust *et al.*, 2005). Similarly, the typical range of the shear strain of 0.05 to 0.2% was reported in a deep excavation case study in Taipei's silty clay (CL) with I_p = 20 (Ou *et al.*, 2000). In the case of the tunnel excavation, Mair (1993) suggested that the range of shear strain, induced by the tunnelling, should be in the order of 0.1 to 1 %. The shear strain ranges, as discussed above, and the ratios G/s_u and E_u/s_u

according to the SBP in the BSC and FSC for deep excavation and tunnelling, are broadly summarised in Table 5.5.
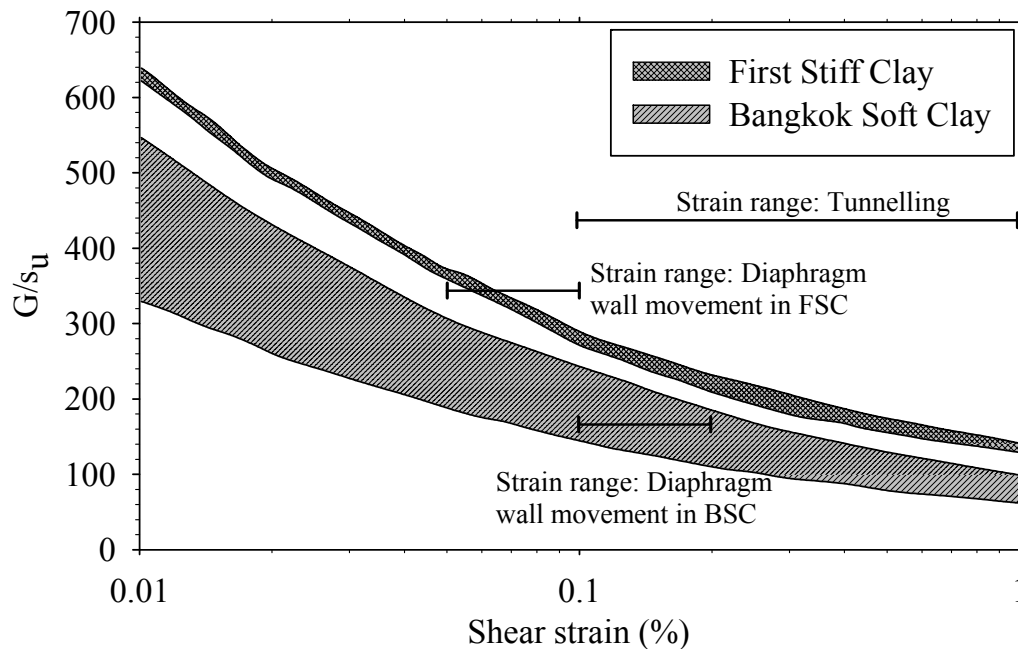
Figure 5.10: Variations of G/s_u with Shear Strain from SBP Tests in BSC and FSC (Modified After Prust *et al.*, 2005)

Table 5.5: Stiffness Ratios for Deep Excavation and Tunnelling Works

Stiffness ratio	Deep excavation		Tunnelling	
	BSC	FSC	BSC	FSC
G/s_u	100 - 250	250 - 350	65 - 250	130 - 350
E_u/s_u	300 - 750	750 - 1050	195 - 750	390 - 1050

5.4 LLT Test in Bangkok MRT Blue Line Extension Project (The Current Study)

In the current study, the Lateral Load Tests (LLT) were performed along the alignment of the Bangkok MRT Blue Line project. The OYO LLT pressuremeter model 4165 Type M, with a cell diameter of 70 mm and a length of 600 mm, was used. The schematic diagram of this LLT test is shown in Figure 5.11. Further details

of LLT pressuremeter were discussed in Section 5.1.1, above. Briefly, however, four LLT tests were conducted at each station location up to a depth of 24 m. The subsoils tested were Very Soft to Soft Bangkok Clays and Medium Stiff to Stiff Clays. Table 5.6 summarises the LLT tests locations in this study.
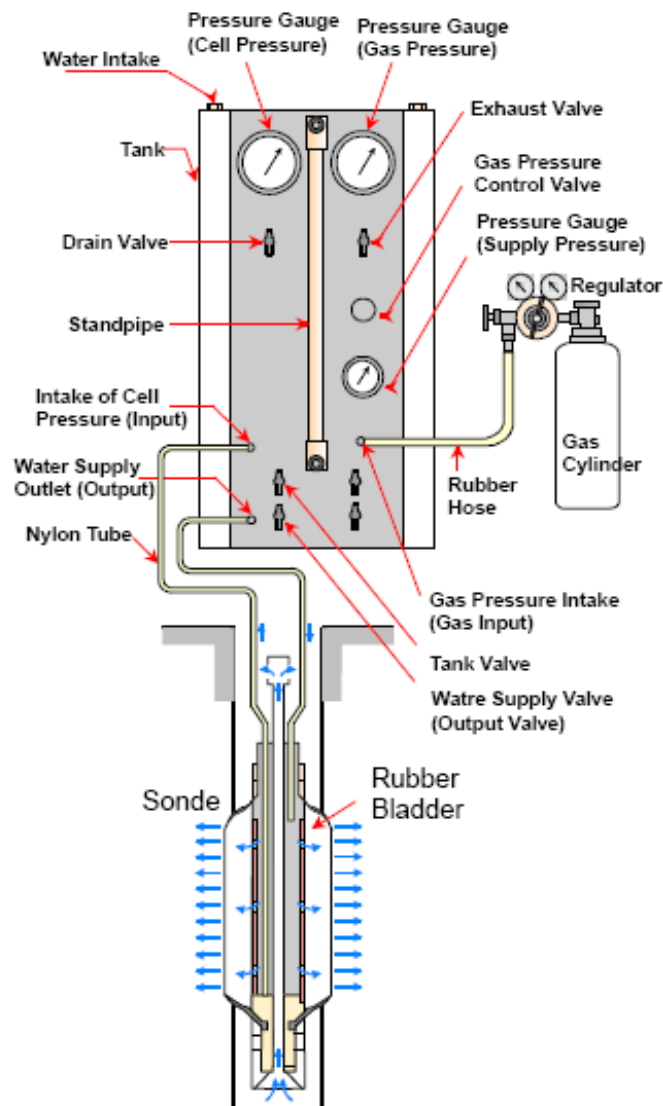
Figure 5.11: Schematic Diagram of LLT Pressuremeter

Table 5.6: Locations of LLT Tests

Station	Borehole	Chainage	Depth (m)	Soil type
Wat Mangkon Station	BS06	1+155	9	Soft clay
			13	Stiff clay
			16	Stiff clay
			21	Very stiff clay
Wang Burapha Station	BS09	2+010	6	Soft clay
			12	Medium stiff clay
			17	Very stiff clay
			22	Very stiff clay
Sanam Chai Station	BS12	2+890	10	Soft clay
			14	Medium stiff clay
			19	Very stiff clay
			24	Very stiff clay
Itsaraphap Station	BS18	4+503	8	Soft clay
			11	Soft clay
			16	Stiff clay
			20	Very stiff clay
Bang Wa Station	BS30-1	8+231	10	Soft clay
			15	Stiff clay
			19	Very stiff clay
			24	Stiff clay
Phet Kasem 48 Station	BS33-1	9+440	7	Soft clay
			11	Medium stiff clay
			16	Very stiff clay
			20	Very stiff clay

The wash boring method was used to advance the pre-borehole for the LLT tests. In 1980, Huang (1980) compared the LLT tests results performed in three borehole advancing methods, namely hand augering method, the thin-walled tube method, and the wash boring method. Huang concluded that the thin-walled tube method yielded

the best results, as tested in the Bangkok soft clay, followed by the wash boring and hand augering methods. In contrast, a subsequent work by Surya (1981) showed that the wash boring method performed well, especially in determining the pressuremeter modulus parameter, E_p even for the soft clay layer.

5.5 Effective Pressure versus Probe Radius and Creep Curve Resulting from LLT Tests

The results of the pressuremeter tests are generally plotted as effective pressure, p_e versus the radius of the probe, r or the change in the probe radius, Δr. A plot of effective pressure versus creep volume ($V_{120s} - V_{30s}$) or creep curve is normally included to aid the selection of the initial pressure, p_i and the yield pressure, p_f, as described in Section 5.1.2. Realistically, an ideal creep curve (as shown in Figure 5.2) can only be found in the tests conducted in stiff clays. Figure 5.12 (a to d) illustrate the pressuremeter test results in the Wang Burapha Station (BH09) location. The results of other locations can be found in Appendix C.
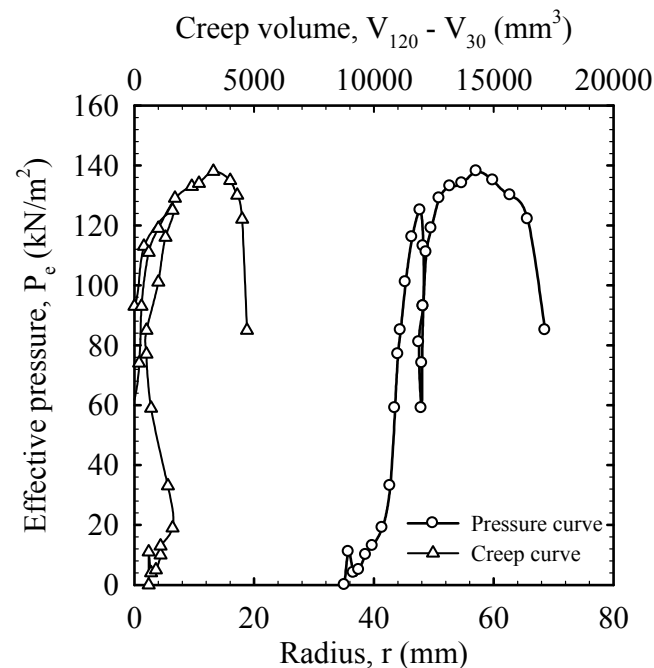
Figure 5.12 (a): Pressuremeter Test Result at Wang Burapha Station, BH09

(Soft Clay, Depth 6 m)
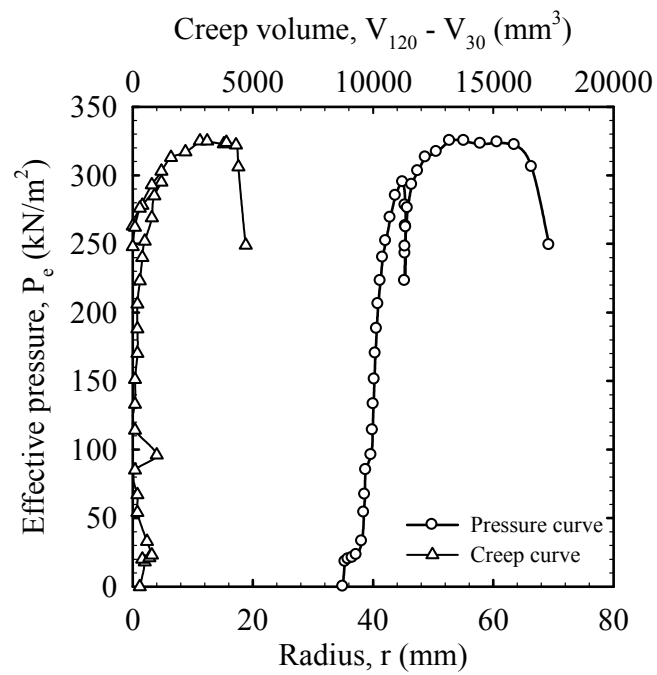
Figure 5.12 (b): Pressuremeter Test Result at Wang Burapha Station, BH09

(Medium Stiff Clay, Depth 12 m)
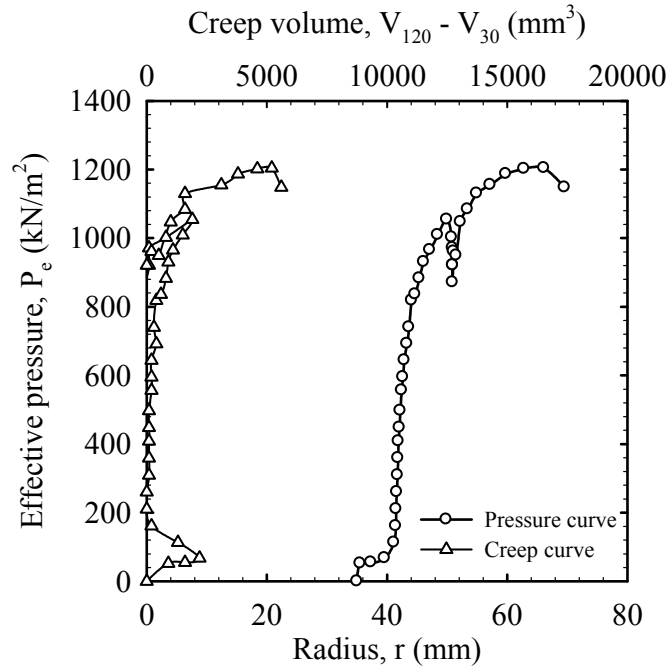
Figure 5.12 (c): Pressuremeter Test Result at Wang Burapha Station, BH09

(Very Stiff Clay, Depth 17 m)
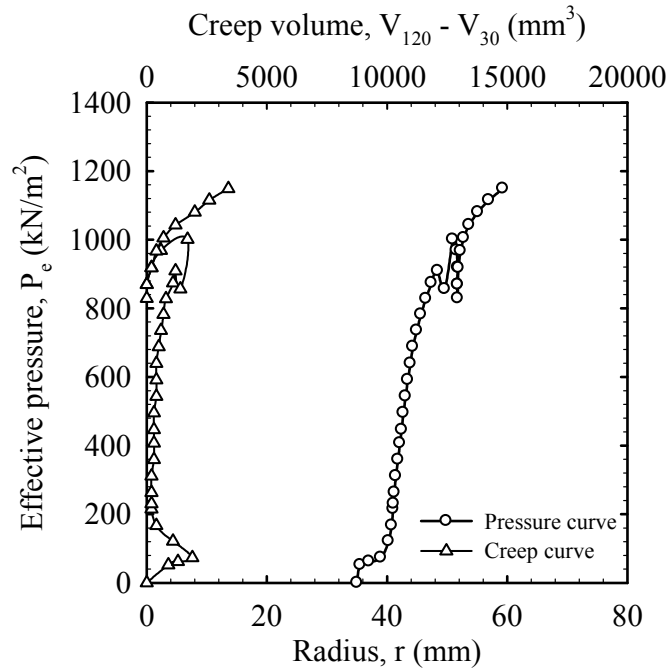
Figure 5.12 (d): Pressuremeter Test Result at Wang Burapha Station, BH09
(Very Stiff Clay, Depth 22 m)

5.6 Geotechnical Parameters Interpreted from LLT Tests

The geotechnical parameter interpretation from the LLT tests are summarised in Table 5.7 (a). These parameters include the total horizontal earth pressure (σ_{ho}, p_o), the yield pressure (p_y), the limit pressure (p_L), the initial and unloading/reloading pressuremeter modulus ($E_{p\ (i)}$, $E_{p\ (ur)}$), the undrained shear strength (s_u), and the pressuremeter constant (N_p). The total horizontal stress in Column 3 is calculated from Hawkins' *et al.* (1990) method, as it gives a more realistic K_o when compared to the creep curve and the Marsland and Randolph (1977) methods (further details of K_o interpretations are discussed in subsequent sections). The yield pressure (p_y), the limit pressure (p_L), the pressuremeter modulus (E_p), and the undrained shear strength (s_u) are determined as per the procedures explained in Sections 5.1 and 5.2. Note that the E_p parameters were calculated from the pressuremeter shear modulus (G) with an assumption of undrained elastic behaviour ($v = 0.5$).

Table 5.7 (a): Summary of Results from LLT Tests

1	2	3	4	5	6	7	8
Borehole	Depth (m)	p_o (kN/m^2)	p_y (kN/m^2)	p_L (kN/m^2)	$E_{p\,(i)}$ (MN/m^2)	$E_{p\,(ur)}$ (MN/m^2)	$\dfrac{E_{p(ur)}}{E_{p(i)}}$
BS-06	9	-	-	-	0.3	-	-
	13	154	247	367	1.2	-	-
	16	-	-	-	3.7	-	-
	21	-	-	-	18.7	141.3	7.54
BS-09	6	57	77	156	2.1	4.2	2.02
	12	145	188	367	5.6	6.6	1.18
	17	180	448	1347	30.7	34.2	1.11
	22	175	543	1370	12.8	44.7	3.48
BS-12	10	89	126	250	2.3	4.0	1.72
	14	189	260	463	6.8	7.1	1.04
	19	225	701	1967	26.1	52.5	2.01
	24	298	679	1483	11.0	20.9	1.90
BS-18	8	-	-	-	1.2	-	-
	11	-	-	-	0.6	-	11.63
	16	250	354	707	14.1	30.3	2.15
	20	321	516	1208	12.4	54.7	4.40
BS-30-1	10	-	155	408	2.4	8.3	3.44
	15	190	345	682	8.4	52.7	6.25
	19	210	505	1461	16.1	77.8	4.82
	24	349	555	1260	19.4	72.4	3.73
BS-33-1	7	65	80	146	2.1	4.5	2.11
	11	152	188	298	2.7	7.7	2.81
	16	200	490	1259	11.9	21.9	1.84
	20	365	660	1599	8.9	29.3	3.28

Table 5.7 (b): Summary of Results from LLT Tests (con't)

9	10	11	12	13	14	15
	s_u (kN/m^2)					N_p
Borehole	Palmer	Gibson and Anderson	$\dfrac{p_L - \sigma_{ho}}{1 + \ln\left(\dfrac{G_i}{s_u}\right)}$	$\dfrac{p_L - \sigma_{ho}}{1 + \ln\left(\dfrac{G_{ur}}{s_u}\right)}$	$\dfrac{p_L - \sigma_{ho}}{N_p}$	(from column 5)
BS-06	-	-	-	-	-	-
	-	-	84.0	-	35.5	-
	-	-	-	-	-	-
	-	-	-	-	-	-
BS-09	47.1	19.8	22.1	18.5	16.5	5.3
	70.5	43.1	47.7	45.6	37.1	4.9
	-	254.7	246.9	240.0	174.1	4.9
	427.5	367.2	337.6	231.3	178.3	5.2
BS-12	68.3	36.8	40.9	34.7	26.8	4.6
	148.8	67.3	59.0	58.3	45.7	4.7
	515.0	476.0	436.5	356.0	260.0	4.9
	504.0	381.1	355.9	281.7	176.9	4.2
BS-18	-	-	-	-	-	-
	-	-	-	-	-	-
	97.3	103.7	93.0	78.0	68.3	5.9
	349.0	193.7	227.2	153.5	132.4	5.8
BS-30-1	-	106.6	-	-	-	-
	143.3	133.7	117.9	76.4	81.9	6.4
	481.0	297.5	330.0	216.1	186.7	5.8
	450.0	206.4	204.5	149.8	136.0	6.1
BS-33-1	36.1	15.6	17.1	14.3	13.5	5.7
	55.6	35.3	33.9	26.0	24.3	5.6
	-	290.6	294.0	239.7	158.0	4.4
	-	286.4	415.2	268.4	184.1	4.6

Further results and discussions on the coefficient of earth pressure at rest, undrained shear strength, and pressure modulus are presented in Sections 5.6.1 to 5.6.3, respectively. These parameters, obtained from various interpretation methods, are compared, along with other laboratory and in-situ test results.

5.6.1 Total Horizontal Stress and Coefficient of Earth Pressure at Rest

The determination of the horizontal stress, σ_{ho} was conducted using three available methods: the creep curve, the Marsland and Randolph (1977), and the Hawkins *et al.* (1990) methods. After the values of the horizontal stress were obtained, the coefficient of the earth pressure at rest, K_o is calculated by:

$$K_o = \frac{\sigma'_{ho}}{\sigma'_{vo}} = \frac{\sigma_{ho} - u}{\sigma_{vo} - u} \qquad\qquad \text{Eq.5.27}$$

The piezometric pore water pressure of the Bangkok subsoils was not hydrostatic, due to extensive deep well pumping undertaken in the 1970s (see details in Chapter 3). Accordingly, the standpipe piezometer (on the land area) and the electric piezometer (under the river area) were employed to measure the piezometric pressure of Bangkok subsoils. Figure 5.13 shows the results of the measured piezometric pressure along the Bangkok Blue Line Extension project area. The ground water level (GWL) on the project site ranged from 1.0 to 1.5 m deep. This GWL was heavily influenced by the fluctuation of water in the canal system, especially in the rainy season. At the top of the first sand layer (approximately 21 to 25 m depth), the piezometric pressure approached a value of zero, indicating that there was a drawdown of water flow from the Bangkok soft clay and the first stiff clay layers to the first sand layer. Based on the above information on piezometric pressure and the drawdown water flow, an approximated piezometric line can be drawn (see Figure 5.13). This approximated line is used for the piezometric pressure, u (in Eq. 5.27) for K_o calculation.
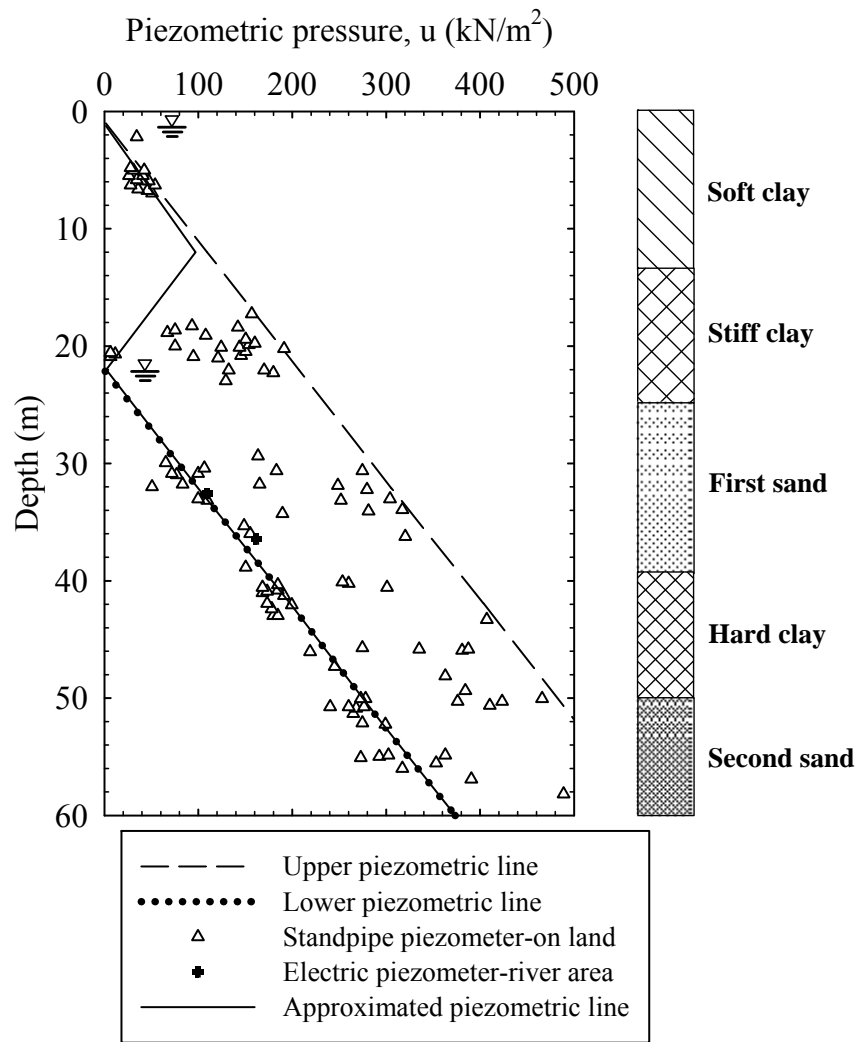
Figure 5.13: Piezometric Pressure of Bangkok Subsoils

The total horizontal stress and earth pressure coefficient (Figure 5.14) was obtained from the creep curve, Marsland and Randolph (1977), and Hawkins *et al.* (1990) methods. In soft clay layer, the interpretation of the total horizontal stress, using creep curve method, was not included. This action was taken as no clear Pseudo-elastic behaviour, such as represented in Figure 5.2, could be obtained. Both the Marsland and Randolph (1977), and Hawkins *et al.* (1990) methods gave very low values of the total horizontal stresses in the soft clay layer. Indeed, the total horizontal stresses obtained from the Marsland and Randolph (1977) method were lower than the piezometric pressure which, in turn, gave negative values for the earth pressure coefficient. Similarly, the total horizontal stress from the Hawkins *et al.* (1990) method was slightly higher than the piezometric pressure which gave an earth pressure coefficient of close to zero.
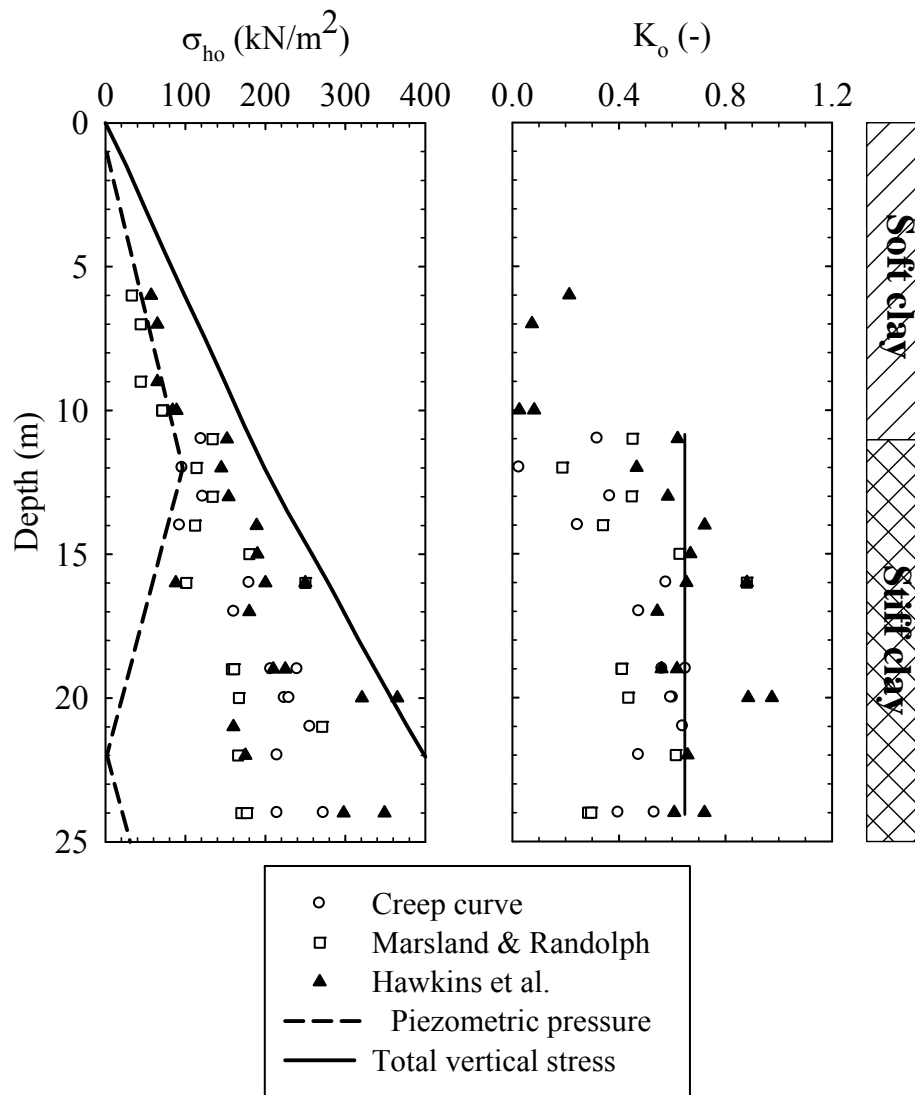
Figure 5.14: Total Horizontal Stress and Earth Pressure Coefficient from LLT Tests

Further, the earth pressure coefficient values in the stiff clay layer, calculated using the above three methods, fell in the range of 0.35 to 0.75. The creep curve, and Marsland and Randolph (197) methods yielded similar results, with the average K_o of 0.46 ± 0.18 and 0.45 ± 0.19, respectively. The Hawkins *et al.* (1990) method yielded an average value of K_o of 0.68 ± 0.14. Prust *et al.* (2005), in their interpretation of the K_o values resulting from self-boring pressuremeter tests, empirical correlations and finite element back-analysis (see Table 5.4), concluded that the values of K_o were 0.75 and 0.65 for the Bangkok Soft Clay and Bangkok Stiff Clay, respectively. Their K_o in stiff clay of 0.65 was somewhat close to the average value calculated by Hawkins *et al.*'s method of 0.68.

5.6.2 Undrained Shear Strength from LLT Tests

The undrained shear strength obtained from the peak strength (Palmer, 1972), elastic-perfectly plastic analysis (Gibson and Anderson, 1961), p_L with G_i, p_L with G_{ur} and p_L with N_p methods (Marsland and Randolph, 1977), are presented in Table 5.7 (b), Columns 10 to 14, respectively. The pressuremeter constant (N_p) adopted in Column 14 were 6 and 6.7 for soft to medium stiff (0 to 15 m depth) and stiff to very stiff clay (15 to 25 m depth), respectively.

The resulting undrained shear strength of Gibson and Anderson (1961), p_L with G_{ur} and G_L with N_p methods, were also compared with the vane shear strength in soft clay and the CK_oU undrained strength in stiff clay (see Figure 5.15). All the values of the field vane shear strength in the current study were factored by Bjerrum's (1972) correction factor.

The undrained shear strength in the Bangkok Soft Clay indicated a reasonable agreement among Gibson and Anderson (1961), p_L with G_i, p_L with G_{ur} and p_L with N_p methods with field vane shear strength. The trend of the undrained shear strength increased with depth, having the values of 15 to 60 kN/m^2 from depths of 5 to 13 m. The analysis of the Palmer method generally yielded higher values of the undrained shear strength compared to all the other methods. In the stiff clay layer, all the interpretation methods showed a relatively high degree of scatter. However, the tendencies of the undrained shear strength increased with depth, as shown by the solid lines in Figure 5.15. Further, the undrained shear strength from the Gibson and Anderson, p_L with G_i, p_L with G_{ur} and p_L with N_p methods were two, three and four times higher than the CK_oU triaxial undrained shear strength.
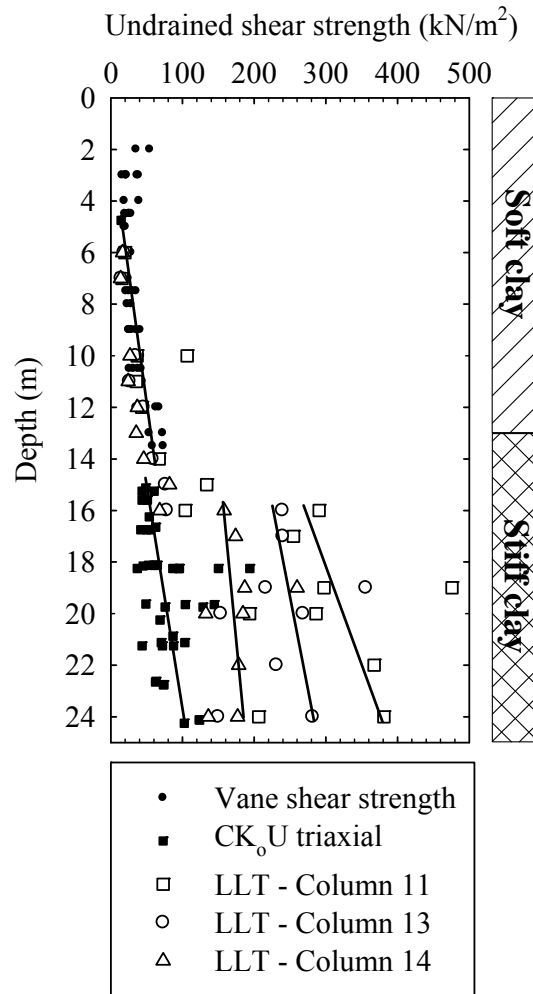
Figure 5.15: Comparison of Undrained Shear Strength from Vane Shear Test, CK_oU Triaxial Test and LLT Tests

As discussed in Section 5.2.3.4, the correction factor, due to pressuremeter geometry, would reduce the pressuremeter undrained shear strength by 10 to 25 per cent. In the case of the stiff clay, this correction factor would not bring the pressuremeter undrained shear strength close to the CK_oU triaxial strength. As a result, the empirical approaches were used to obtain the undrained shear strength from the pressuremeter limit pressure (p_L) and the net limit pressure (p_L^*). Figure 5.16 shows the plot of the undrained shear strength versus the limit pressure of both the soft and stiff clays.
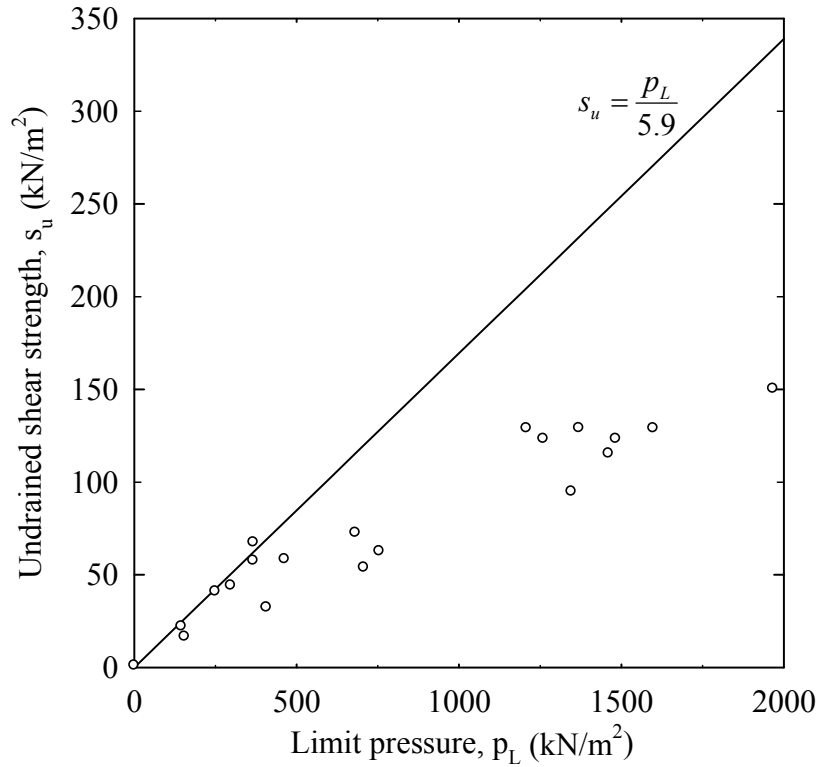
Figure 5.16: Correlation between Undrained Shear Strength and Limit Pressure

The empirical equation (Equation 5.24) from Bergado and Khaleque (1986) was also included. Note that the undrained shear strength in the soft clay (0 – 15 m depth) and in the stiff clay (15 – 25 m) was taken from the vane shear and the CK_oU triaxial undrained shear strength, respectively. It can be seen that Equation 5.24 agrees well with the (p_L-s_u) relationship up to the undrained shear strength of 70 kN/m². This agreement is reasonable as Equation 5.24 was calibrated with the vane shear strength in the soft clay layer. Equation 5.23 with N_p = 5.5 (as suggested by Ménard (1975)) and Eq. 5.25 as suggested by Briaud (1992) were compared with s_u versus p_L^* in Figure 5.17. The linear function of Equation 5.23 does not show a similar trend to that of the (p_L^*-s_u) relationship. Equation 5.25, however, gives a much better prediction when compared with Equation 5.23. Nevertheless, it seems to overestimate the undrained shear strength at a higher range of the net limit pressure. The best fit (dashed) line resulting from the regression analysis is also plotted in Figure 5.17. A reasonably high value of R^2 = 0.904 was obtained by the following equation:

$$s_u = 2.72 p_L^{*\,0.537}$$

where, both s_u and p_L^* are in kN/m^2.
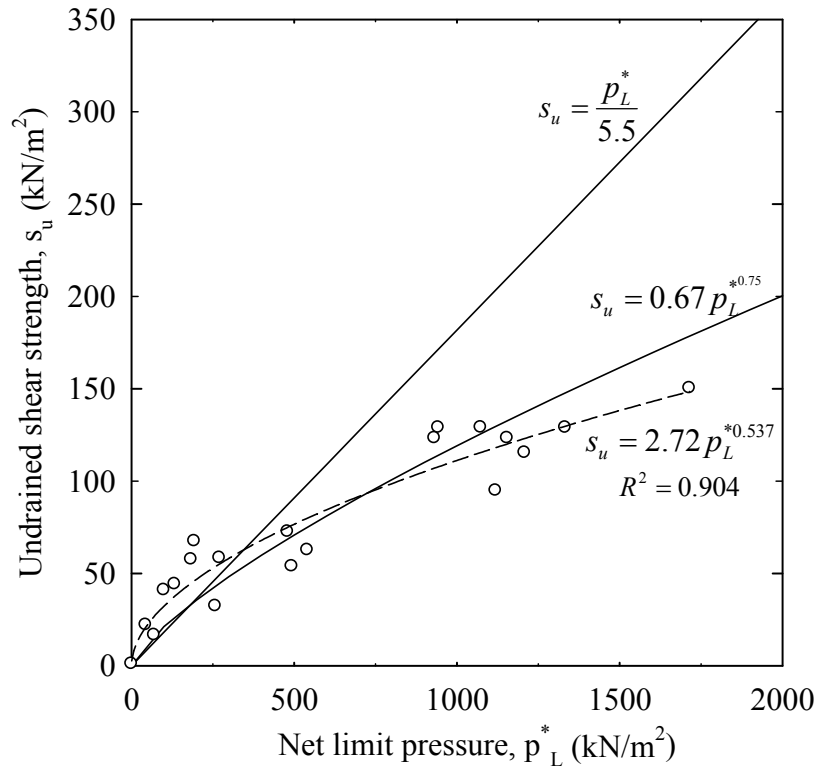
Figure 5.17: Correlations between Undrained Shear Strength and Net Limit Pressure

5.6.3 Soil Moduli from LLT Test

Following the procedures outlined in Section 5.2.2, the initial and unloading/reloading shear moduli were obtained from the pressuremeter curves. These two shear moduli were then converted to the initial and unloading/reloading pressuremeter moduli ($E_{p(i)}$ and $E_{p(ur)}$), using the elastic theory with the undrained Poisson's ratio of 0.5. The values of the pressuremeter moduli were determined from the initial (where $p_e = p_o$) and unloading/reloading curves (see Table 5.7 above), and were also plotted with depth (see Figure 5.18).
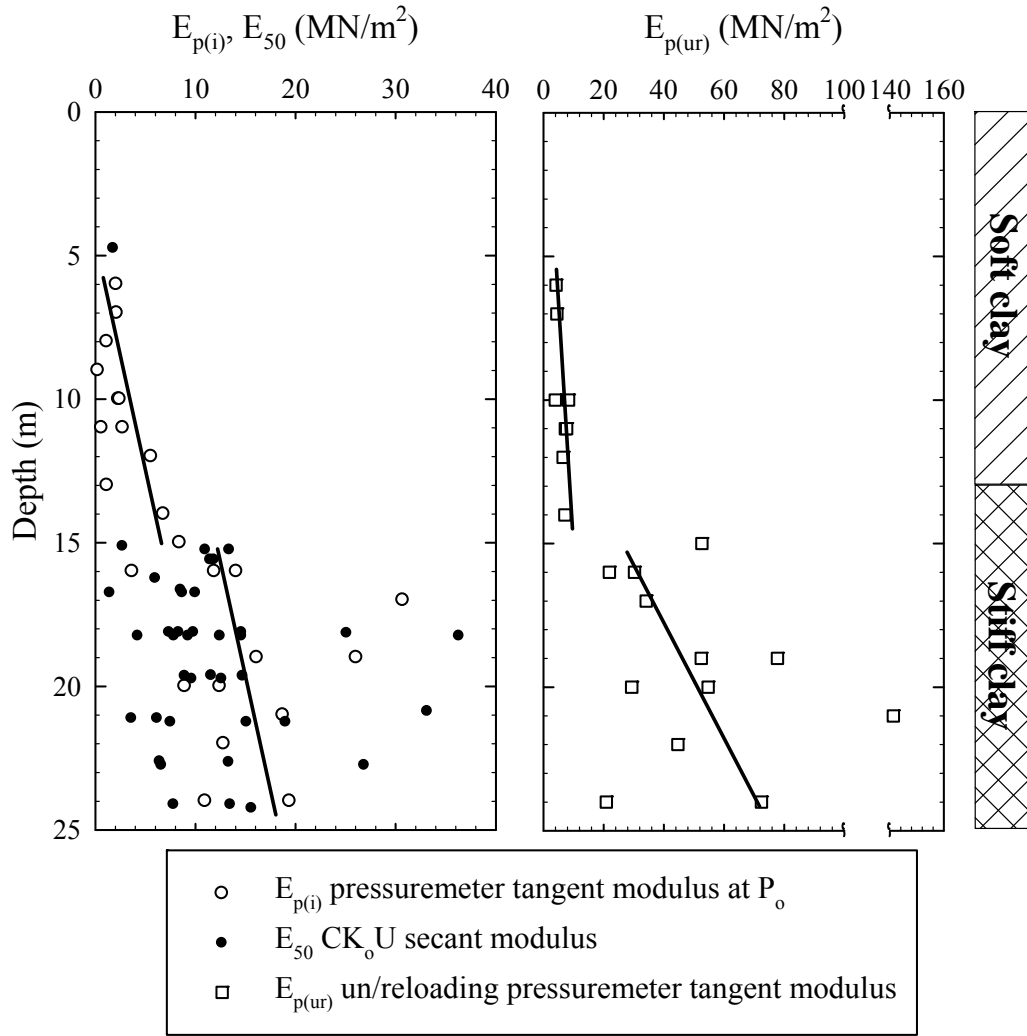
Figure 5.18: Comparisons of Initial and Unloading/reloading Pressuremeter Moduli from LLT and E_{50} from CK_oU Triaxial Tests

The tendencies of both the $E_{p(i)}$ and $E_{p(ur)}$ show an approximate linear increase with depth. However, the linear relationships are clearly separated between the soft and stiff clay layers. In general, the $E_{p(ur)}$ values are 2 and 3.5 times higher than the $E_{p(i)}$ in soft and stiff clays, respectively. When the $E_{p(i)}$ values are compared with the E_{50} obtained from the CK_oU triaxial tests, they seem to locate on the upper values of E_{50}. This outcome is possibly due to the lesser degree of soil disturbance caused by the LLT tests.

5.7 Concluding Remarks

The work reviewed in this chapter focused on the interpretation of geotechnical parameters from the LLT pressuremeter test in Bangkok Clays. Based on the studies conducted in this chapter, the following conclusions can be made:

(1) Three methods, namely the creep curve method, Marsland and Randolph's (1977) method, and Hawkins *et al.*'s (1990) method, are used to estimate the σ_{ho} (and, hence, the K_o) of Bangkok Clays. These methods provide the values of σ_{ho} close to the piezometric water pressure in the Bangkok Soft Clay layer. As a result, the calculated K_o values are negative or low values close to zero. One reason of for this result may be the high degree of disturbance while pre-boring the borehole in soft clay. In the case of stiff clay, the average K_o values of 0.46, 0.45 and 0.68 are calculated from the creep curve method, Marsland and Randolph's (1977) method, and Hawkins *et al.*'s (1990) method, respectively.

(2) The undrained shear strength of the Bangkok Soft Clay is estimated using Gibson and Anderson's (1961) method, and Marsland and Randolph's (1977) method (using p_L with G_i, p_L with G_{ur}, and p_L with $N_p = 6$); there is good agreement with the undrained shear strength from the vane shear test. The undrained shear strength tends to increase with depth, with the values of 15 to 60 kN/m^2 at depths of 5 to 13 m. In the case of the Bangkok Stiff Clay, the predicted undrained shear strength, using Gibson and Anderson's (1961) method, Marsland and Randolph's (1977) method (using p_L with G_i, p_L with G_{ur}, and p_L with $N_p = 6.7$), are two, three and four times greater than the values obtained from the CK$_o$U triaxial tests.

(3) The empirical relationship between the p_L and s_u (Equation 5.24) provides reasonable correlation within the Bangkok Soft Clay layer, with the undrained shear strength less than 70 kN/m^2 (corresponding to the limit pressure of 400 kN/m^2). The net limit pressure (p_L^*) correlates well with the undrained shear strength of both the Bangkok Soft and Stiff Clays. The proposed relationship

(Equation 5.28) can be used as the first approximation of the undrained shear strength.

(4) The values of the initial and unloading/reloading pressuremeter moduli, $E_{p(i)}$ and $E_{p(ur)}$, show the trends increasing with depth. The ratios of $E_{p(ur)}/E_{p(i)}$ are approximately 2 and 3.5 in the Bangkok Soft and Stiff Clays, respectively.

(5) The study in this chapter deals with three main geotechnical parameters namely, coefficient of earth pressure at rest (K_o), undrained shear strength (s_u) and pressuremeter moduli ($E_{p(i)}$ and $E_{p(ur)}$). In relation to the finite element analyses in subsequence chapters, the following conclusions are drawn.

(a) An average value of K_o of 0.68 ± 0.14, from Hawkins *et al.* (1990) method, can be used as an input parameter for stiff clay initial stresses calculation. None of the methods, studied in this chapter, give reasonable value of K_o for soft clay layer. Therefore, a value of 0.75 from literature (Prust *et al.*, 2005) is selected.

(b) In conducting the finite element analysis of undrained material with Method D (see Section 4.2 and Appendix A), it is necessary to ensure that the predicted undrained shear strength from adopted soil model does not exceed the field undrained shear strength. According to the results in this chapter, the correlations from the net limit pressure (p_L^*) provides reasonable values of the field undrained shear strength. As a result, Eqs.5.25 and 5.28 are suggested for both cases of Bangkok soft and stiff clays.

(c) The values of the pressuremeter tangent modulus at P_o ($E_{p(i)}$) are comparable with the E_{50} CK$_o$U secant modulus. Therefore, it maybe a better choice when it comes to the selection of stiffness modulus. However, care must be taken in term of the determination of P_o, where $E_{p(i)}$ is obtained.

CHAPTER 6

Small Strain Parameters of Bangkok Clays

6.1 Introduction

The material in this chapter is related to two small strain parameters, namely small strain shear modulus (G_{max}) and reference shear strain ($\gamma_{0.7}$) of Bangkok Clays. These two parameters are used to govern the small strain behaviour of soil in Hardening Soil Model with Small-Strain Stiffness (HSS). The area of research in small strain parameters of soils is new and not familiar to the researchers in Griffith University. For this reason, some basic concepts related to the subject are included herein. The first part of the chapter starts with a brief summary of the background knowledge of small strain stiffness, followed by the measurement methods (both in-situ and in laboratory). Next, the empirical methods for the determination of small strain shear modulus are reviewed. These methods are then verified with the small strain modulus being measured from the in-situ tests (down hole and seismic cone methods), and the laboratory tests (Bender

element test) in the Bangkok area. The small strain shear modulus (G_{max}) is also correlated with the pressuremeter parameters (i.e. limit pressure, p_L, and net limit pressure, p_L^*), as obtained from the studies referred to in Chapter 5. The second part of the chapter deals with the concept of the volumetric threshold shear strain (γ_{tv}) and its relationship with the reference shear strain parameter ($\gamma_{0.7}$). The two approaches, developed by Ishibashi and Zhang (1993), and Vucetic and Dobry (1991), are used to calculate the reference shear strain parameter ($\gamma_{0.7}$). The results of this calculation are then compared with the laboratory Bender element test results conducted in the Bangkok Soft Clay samples (Teachavorasinskun *et al.*, 2002a). The validation of the calculated $\gamma_{0.7}$ values for both the Bangkok Soft and Stiff Clays are conducted by means of deep excavation finite element back-analyses (presented in Chapter 7).

6.1.1 Background Knowledge of Small Strain Stiffness

Initial stiffness modulus is an important soil parameter relating to the predictions of the ground movements and field data interpretations. In soil dynamics, the small strain shear modulus (G_{max}) and the material damping ratio (D) are important parameters in the characterisation of the soil deposit, as a part of the ground motion analysis in earthquake engineering. Figure 6.1 shows a simplified framework of the stress–strain model in cyclic tests. This figure illustrates a simplified monotonic loading line *ac* (a backbone or skeleton curve), and a cyclic loop *abcd* (a hysteresis loop). A cyclic shear modulus (G) (sometimes referred to as the equivalent shear modulus (G_{eq})) is the slope of the skeleton curve. The amplitude of the shear stress (τ_a) and the shear strain (γ_a) are marked at point *a* in Figure 6.1, while the damping ratio (D) is also illustrated. In the static analysis, more attention is paid to the shear stiffness rather than the damping ratio. A stiffness degradation curve (Figure 6.2) is normally used to explain the shear stiffness for a wide range of shear strain. For example, the ground movements induced by the construction of the geotechnical structures, such as retaining walls, foundations and tunnels, relate to the shear strain at the small to large levels (see Figure 6.2). Atkinson and Sallfors (1989) categorised the strain levels into three groups: the Very Small Strain level, where the

stiffness modulus is constant in the elastic range; the Small Strain level, where the stiffness modulus varies non-linearly with the strain; and the Large Strain level, where the soil is close to failure and the soil stiffness is relatively small.
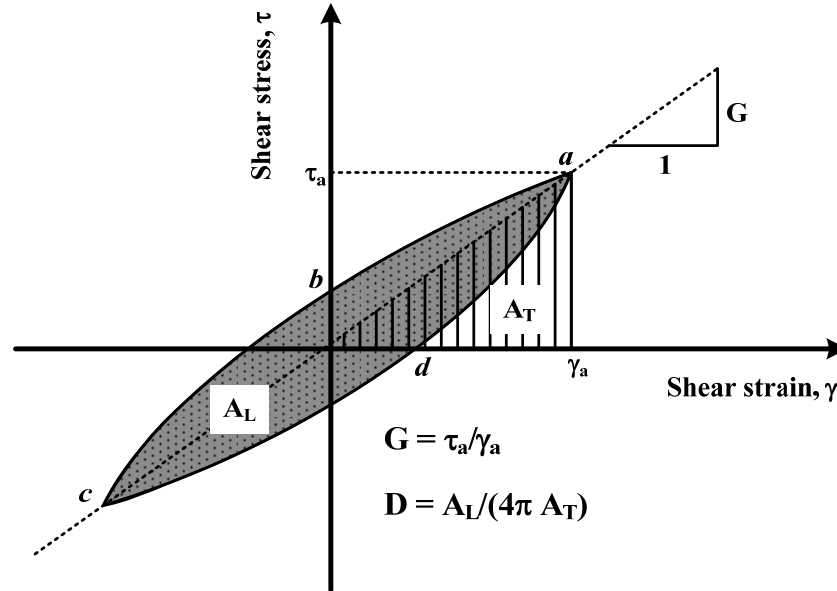
Figure 6.1: Determination of Shear Modulus and Damping Ratio
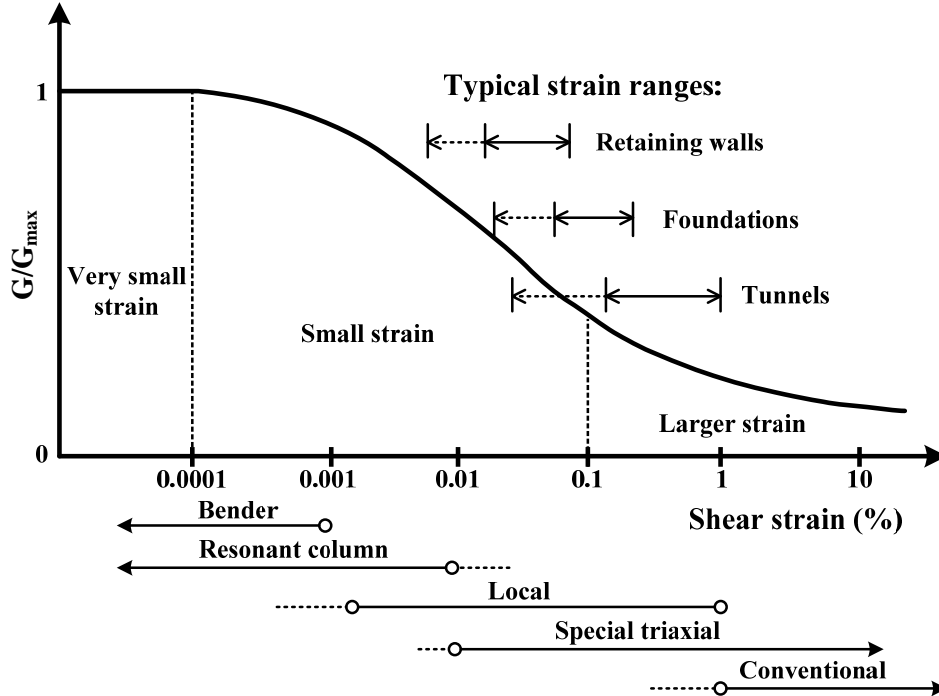
Figure 6.2: Normalised Stiffness Degradation Curve
(Modified after Atkinson and Sallfors, 1991; Mair, 1993)

6.1.2 Roles of Small Strain Parameter in Finite Element Analysis

The significance of small strain non-linear behaviour of soils in deep excavations was examined by Kung *et al.* (2009). Two soil models, namely the three-Surface Kinematic Hardening model, the 3-SKH model (Stallebrass and Taylor, 1997), and the Modified Cam Clay, MCC (Roscoe and Burland, 1968), were adopted. Comparisons of the diaphragm wall deflections and the ground surface settlements were observed from the field measurements, and were predicted from both models (see Figure 6.3). The small strain non-linear (3-SKH) model was used in the Type A analysis. For the Types B, C and D analyses, the MMC model was used, with the soil parameters being obtained from the laboratory Bender element tests (small strain parameters), the back-analysis of the wall deflection, and the back-analysis of the surface settlement, respectively. It can be seen that all attempts on the MCC model analyses (Type B, C and D) can not simultaneously capture both wall deflection and surface settlement in a single analysis. Furthermore, unlike the MCC model analyses, the 3-SKH model analysis yielded a realistic settlement profile when compared to the field observations. The settlement trough was steeper in the area close to the diaphragm wall (where the soils exhibited a large strain); and the trough was shallower in the area away far from the diaphragm wall (where the soils exhibited a small strain).
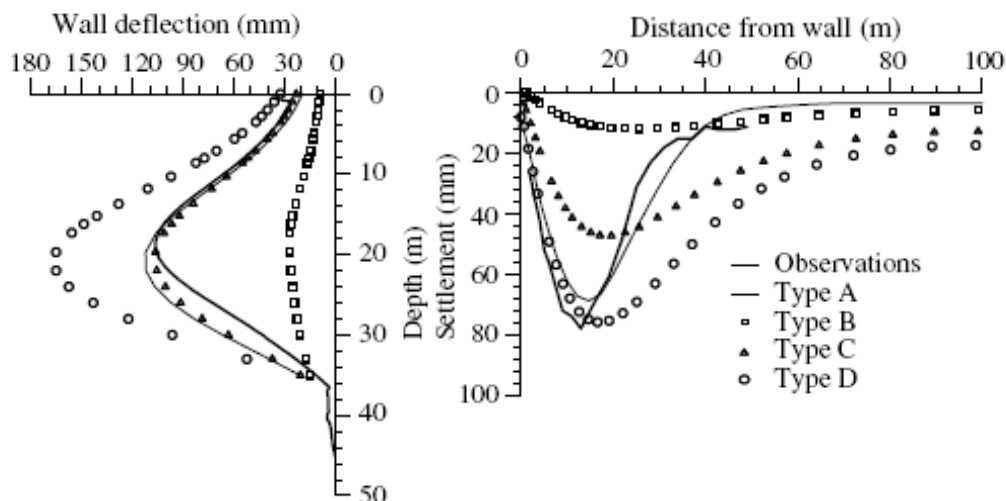
Figure 6.3: Prediction and Observation of Wall Deflections and Surface Settlements in TNEC Excavation Case (Kung *et al.*, 2009)

212

Similarly, in the case of the ground movements induced by tunnelling, the study by Addenbrooke *et al.* (1997) revealed that non-linear small strain stiffness models (referred to as AJ4i and AJ4ii in Figure 6.4) are necessary to achieve deeper surface settlement profiles that are closer to the field observations.
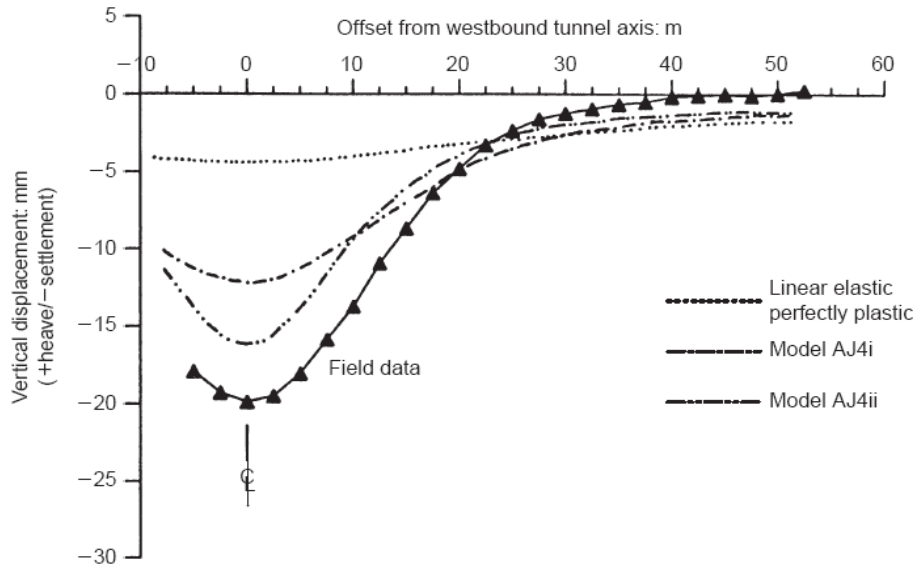
Figure 6.4: Prediction and Observation of Surface Settlement Profiles
(Addenbrooke *et al.*, 1997)

The above discussions demonstrate the significance of non-linear small strain stiffness in enhancing the predictive capabilities of finite element based models. The current in-depth study on the small strain parameters of Bangkok Clays is, presented below.

6.2 Measurements of Small Strain Stiffness

This section reviews the available methods (laboratory and in-situ) for measuring the pre-failure small strain stiffness of soils. Two distinctions were made in the laboratory static (direct) and dynamic (indirect) tests. The in-situ tests are, on the other hand, were classified as a dynamic analysis. For the static laboratory tests, special local stain gauges

were used (as is typical of such tests, to evaluate the soil stiffness at a small strain level (see Section 6.2.1). Dynamic exercises involved the determination of the dynamic properties of the soil, such as shear wave velocity (V_s) in the Bender element tests and resonant frequency of the soil sample in resonant column tests.

6.2.1 Laboratory Measurements of Small Strain Stiffness

6.2.1.1 Local Measurements

Conventional triaxial apparatus measures soil stiffness at a large strain of approximately 1%. Over the past years, an attempt has been made to improve the accuracy of the Linear Variable Differential Transformers (LVDT) to measure the local axial strain of the soil sample at a small strain level. In the early work of Jardine *et al.* (1984), the axial displacement gauges, developed by Burland and Symes (1982), were used to measure the undrained elastic modulus of the reconstituted clay (OCR = 1 to 8), at a level of axial strain equalling 0.05%. The resulting undrained elastic modulus, normalised with the undrained shear strength, was plotted with the axial strain in a log scale (Figure 6.5). The results showed that the stiffness, measured at a small strain level, was much higher than the values commonly obtained from conventional triaxial apparatus. In recent years, more precise versions of LVDTs were utilised with the computer controlled stress-path triaxial apparatus on resedimented Boston Blue Clay (Santagata, 1998; Santagata *et al.*, 2005). The undrained stiffness modulus at a very small strain level of 0.0001% was measured (see Figure 6.6). One of the advantages of this LVDT-based device is that the initial elastic modulus at a very small strain ($E_{u,max}$) is also captured from the test results. Thus, a full stiffness degradation curve was able to be acquired in one single test.
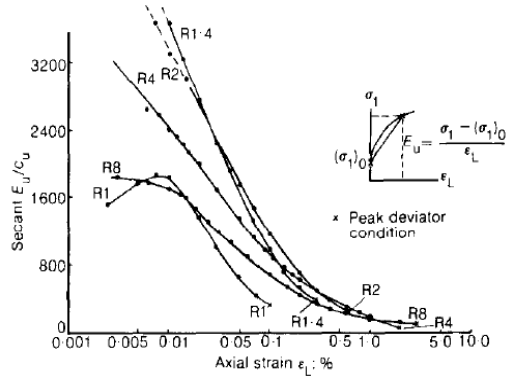
Figure 6.5: Normalised Undrained
Elastic Modulus at Small Strain
(Jardine *et al.*, 1984)
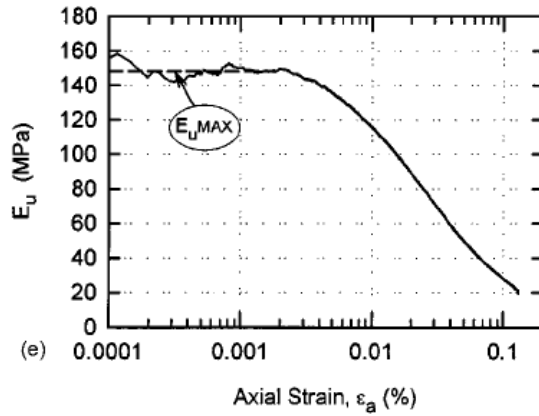
Figure 6.6: Undrained Elastic Modulus at
Very Small Strain
(Santagata *et al.*, 2005)

6.2.1.2 Resonant Column Test

The resonant column test was first developed in the 1930s. It, has been used worldwide because of its capability to obtain the shear modulus and because of the damping ratio associated with a low strain level of approximately 10^{-2}%; this level had been difficult to measure using the local strain gauges available during the 1960s to 1970s. The testing process involves applying a series of cyclic forces to soil specimens at various frequencies. The amplitude of the soil response at all magnitudes of the applied frequencies are recorded and plotted (as shown in Figure 6.7). The frequency corresponding to the peak amplitude from the accelerometer represents a theoretical value of the resonant (natural) frequency. At this point, the shear strain modulus (*G*) is obtained by:

$$G = \rho v_s^2 = \rho (2\pi L)^2 \left(\frac{f_n}{F} \right)^2 \qquad\qquad \text{Eq.6.1}$$

where,

ρ = Density of soil specimen

L = Length of specimen

215

f_n = Natural frequency

F = Frequency factor
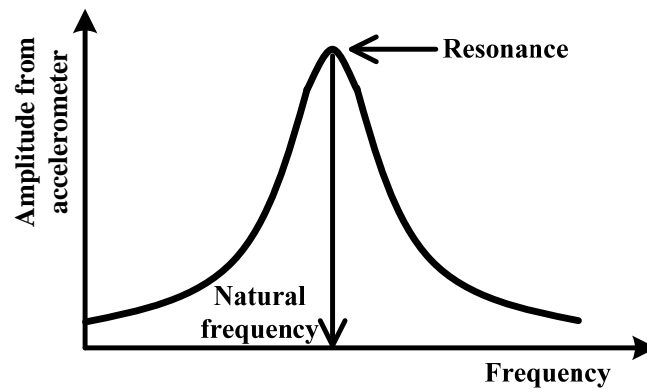
Figure 6.7: Idealised Frequency Response Curve in Resonant Column Test

The damping ratio can be acquired by observing the free-vibration curve. Towhata (2008) outlined two shortcomings of the resonant column test. First, the number of loading cycles experienced by the soil specimen in resonant column test is much higher than that from a real earthquake. Second, the high frequency of the shaking during the testing process dramatically reduces the permeability coefficient of the soil. In the case of a saturated sand specimen, liquefaction is likely.

6.2.1.3 Bender Element Test

The Bender elements are a set of electro-mechanical transducers that produce a high frequency shake (mechanical energy) and create S-wave propagation from one end of the soil specimen to the other. This mechanical energy, received from the far end of the specimen, is then converted to electrical energy to calculate the S-wave velocity using travel time and distance (Viggiani and Atkinson, 1995). Within this simple concept of the Bender element test, some uncertainties are encountered. For example, the travel distance of the S-wave cannot be clearly defined. The possible probabilities are the distance between the tips of the Bender element transducers or the full length of the soil

216

sample. Furthermore, the arrival times of the initial shaking and its peak are different. This makes the travel time of the S-wave uncertain (Towhata, 2008).

Regardless of such possible uncertainties, the Bender element test has advantages over other testing devices. For example, it is possible to equip the Bender element transducers with various types of standard laboratory equipment, i.e. the triaxial, direct shear and oedometer tests. Thus, the Bender element test can be performed under various soil laboratory conditions, such as during isotropic or K_o consolidations and during shearing, as well as on fully saturated soils.

The interpretation of the Bender element test results involves the calculation of the shear S-wave (shear wave) velocity (V_s) (see Equation 6.2):

$$V_s = \frac{L}{T}$$

Eq.6.2

where,

L = Length of specimen

T = Travel time of shear wave propagation

The initial shear modulus (G_{max}) is then calculated by:

$$G_{max} = \rho V_s^2$$

Eq.6.3

where,

ρ = Density of soil.

6.2.2 In-situ Measurements of Small Strain Stiffness

6.2.2.1 Down Hole Seismic Test

The down hole seismic test is one of the most commonly used techniques in engineering practice. It can provide a profile of small strain modulus versus depth. The test requires one borehole in which seismic receivers (accelerometers) are placed at desired depths, and a set of steel planks with dead weights and a hammer to artificially generate the S-wave propagation. The major shortcoming of the down hole seismic test is that the S-wave propagation generally travels from the source (at the ground surface) to the receivers at desired depths in the borehole. This S-wave is, therefore, travelling through multiple layers of soil and, thus, the resulting shear wave velocity is considered as an integration of the multi-layer soil property. By receiving measurements from different depths, it is, therefore, possible for the in-situ small strain stiffness of each soil layer to be back-calculated.

6.2.2.2 Cross Hole Seismic Test

In contrast to the down hole test, the cross hole test requires at least two boreholes, where an S-wave generator is placed in one hole and the receiver is mounted in the other. In this method of testing, the S-wave propagation is generated by either an explosive charge or a hammer blow. When the cross section distance between the two holes is known, the required travelling time of the S-wave can be recorded. Hence, the S-wave velocity (V_s) is calculated from Equation 6.2.

The cross hole test is considered as one of the most reliable techniques from which to determine the in-situ small strain stiffness, though also one of the most expensive methods. Thus, by having multiple boreholes, it is possible to monitor the travel time of the shear wave (hence shear wave velocity and shear modulus), as well as the decay of wave amplitude with distance. This decay can be directly related to the soil damping ratio. However, the S-wave sources generate insufficient energy to allow economical

borehole spacing (closely spaced boreholes are required). Additionally, the inclinometers are normally required for each borehole to identify the exact distance among the boreholes.

6.2.2.3 Seismic Cone Test

The seismic cone test is a hybrid test combining the original Cone Penetration Test (CPT) with the down hole seismic test. Normally the seismic cone test is pushed into the ground (where the CPT related quantities are measured), and penetration is stopped at 1 m intervals. During this pause, the S-wave propagation is generated in the similar manner as with the down hole seismic test (Section 6.2.2.1). The required travel time of the S-wave is recorded by the seismometer (receiver) attached with CPT equipment. It should be noted that the principle of cross hole seismic test can be applied if two or more sets of seismic cone tests are employed.

6.2.3 Empirical Correlations for Small Strain Stiffness

The small strain shear modulus, G_{max} (typically at $\gamma = 0.0001\%$), is most accurately determined by successive measurements of the shear wave velocity and the soil density, as described in the previous section. In the absence of a shear wave velocity measurement, the empirical correlations become a useful tool for the G_{max} estimation.

Based on the resonant column test on sand, Hardin and Richart (1963) proposed the following relationship:

$$G_{max} = A \cdot f(e) \cdot \left(\frac{p'}{p_r} \right)^m$$

Eq.6.4

where,
f(e) = void ratio function
p' = mean effective pressure = $(\sigma'_1 + \sigma'_2 + \sigma'_3)/3$

p_r = reference pressure

A & m = dimensionless constants depending on adopted p_r

With the void ratio function $f(e) = (2.17 - e^2)/(1+e)$ and p_r at the atmospheric pressure of 98.1 kN/m^2, the constants A and m were given as 6900 and 0.5, respectively.

Hardin and Black (1968) employed the vibration apparatus to measure the shear modulus on remoulded Kaolin clay ($I_p = 21$). Various initial conditions (isotropic and anisotropic) were utilised on the triaxial specimens, with the initial void ratios ranging from 0.76 to 0.9. Thus, the following equation has been proposed:

$$G_{max}\left(kN/m^2\right) = 3270 \cdot \frac{\left(2.973 - e^2\right)}{\left(1+e\right)} \cdot \left(\sigma_o'\right)^{0.5}$$

Eq.6.5

where,

σ_o' = ambient effective stress (kN/m^2)

The main shortcoming of the void ratio functions $f(e) = (2.17 - e^2)/(1+e)$ and $f(e) = (2.973 - e^2)/(1+e)$ is that $f(e)$ becomes negative where the void ratio exceeds 2.17 and 2.973, respectively. To overcome this limitation, an exponential form of $f(e) = e^{-\beta}$ was suggested by Jamiolkowski $et\ al.$ (1991). This void ratio function is also applicable for cemented and uncemented sands and gravels, as shown in the extensive study by Pestana and Salvati (2006). A generalised expression for G_{max}, taking into account, separately, the effects of the void ratio, OCR, the initial effective vertical and the horizontal stresses, was given by Jamiolkowski $et\ al.$ (1994) as:

$$G_{max} = S_{vh} \cdot f(e) \cdot OCR^k \cdot \sigma_r'^{(1-nh-nv)} \cdot \sigma_v'^{(nv)} \cdot \sigma_h'^{(nh)}$$

Eq.6.6

where,

S_{vh} = dimensionless material constant

σ_r = reference pressure

σ'_v & σ'_h = effective vertical and horizontal stresses

k, nv & nh = exponential constants

Importantly, the exponent (β) of 1.3 was found appropriate, having a wide range of soils. If f(e) = $e^{-1.3}$ is employed, the effect of OCR is ignored ($k = 0$), and the effects of effective vertical and horizontal stresses are assumed identical ($nv = nh$), while using the reference pressure of 1 kN/m^2, Equation 6.6 is reduced to:

$$G_{max} = S_{vh} \cdot e^{-1.3} \cdot \left(\sigma'_v \cdot \sigma'_h\right)^{nv}$$
Eq.6.7

Based on the seismic cone database in Japan and Europe, Shibuya and Tanaka (1996) conducted a number of statistical analyses. The soils tested covered a wide range of non-cemented materials with OCR; the plasticity index and the initial void ratio ranged from 1 to 2, 19 to 152 and 0.5 to 5, respectively. A simplified expression of G_{max} is given as:

$$G_{max}\left(kN/m^2\right) = 5000 e^{-1.5} \sigma_v'^{0.5}$$
Eq.6.8

From their equation, Shibuya and Tanaka (1996) concluded that the exponential constant, nv (as applying to σ'_v) of 0.5, was valid for un-cemented soft clay to dense sand. In contrast, the values of constants $A = 5000$ and $\beta = 1.5$ depended on soil type, particle size and shape, the degree of cementation, aging, etc. A more refined analysis (Shibuya, *et al.*, 1997) was conduced using a similar seismic survey database to that of Shibuya and Tanaka (1996). The results from the Bender element tests on reconstituted clay samples from eight sites were also included. The following expression for G_{max} estimation was given as:

$$G_{max}\left(kN/m^2\right) = A(1+e)^{-2.4} \sigma_v'^{0.5}$$
Eq.6.9

The values of the constant A, in Equation 6.9 from Shibuya *et al.*'s (1997) analysis, ranged from 10,700 to 30,800, with an average of 24,000. Further, the constant A seems

to increase as the clay becomes more aged and structured. Conversely, the term $(1 + e)^{-2.4}$ is independent, to varying degrees of the aging and soil structure.

An alternative way of correlating the parameter G_{max} in clays is to employ the undrained soil shear strength (s_u). Other researchers, for example, Ashford *et al.* (1996), and Likitlersuang and Kyaw (2010) have developed simple correlations of the shear wave velocity (V_s) and the undrained shear strength (s_u), based on reliable in-situ site investigations. Importantly, after the shear wave velocity and soil density (ρ) is estimated, the small strain stiffness (G_{max}) can be calculated using Equation 6.3.

A generalised shear wave velocity profile was developed by Ashford *et al.* (1996), who based their work on extensive seismic site investigations (see Figure 6.14 in Section 6.4.1). The proposed generalised profile was constructed from an extensive data set of empirical correlations (nine sites) and the down hole seismic method (four sites) across the Bangkok area. The simple correlation between the shear wave velocity (V_s in m/s) and the undrained shear strength (s_u in kN/m^2) for the Bangkok soft clay is given as:

$$V_s(m/s) = 23 s_u^{0.475}$$

Eq.6.10

A similar study was recently conducted on the V_s - s_u correlation for Bangkok subsoils (Likitlersuang and Kyaw, 2010). The shear wave velocity data were obtained from the down hole and MASW methods conducted at three Bangkok sites. Two correlations were proposed, being based on the down hole and MASW data, respectively:

$$V_s(m/s) = 187 \left(\frac{s_u}{p_r} \right)^{0.372}$$

Eq.6.11

$$V_s(m/s) = 228 \left(\frac{s_u}{p_r} \right)^{0.51}$$

Eq.6.12

Likitlersuang and Kyaw (2010) also compared their $V_s - s_u$ correlations (Equations 6.11 and 6.12) with Eq. 6.10 from the work of Ashford *et al.* (1996). Likitlersuang and Kyaw found that Equations 6.11 and 6.12 seem to give the lower and upper bound values for shear wave velocity, while Equation 6.10 gives the average values.

6.3 Threshold Shear Strain of Soils

6.3.1 Concepts of Threshold Shear Strain

The concept of the threshold shear strains was elucidated by Vucetic (1994). From an extensive laboratory test database, two types of threshold shear strains (linear threshold shear strain (γ_{tl}) and volumetric threshold shear strain (γ_{tv})) were introduced (Figure 6.8). These threshold shear strains represent the boundaries of the fundamental cyclic behaviours of soils at very small, small and medium to large strain level. The soils at strain level below the linear threshold shear strain behave as linear elastic materials. Between γ_{tl} and γ_{tv}, the soils commence to exhibit non-linear behaviour, but remain largely recoverable (elastic), since the microstructure of the soils remains unchanged. Beyond γ_{tv}, the soils become heavily non-linear and in-elastic materials. In other words, the soil microstructure changes irreversibly when the shear strain exceeds the volumetric threshold shear strain (γ_{tv}).
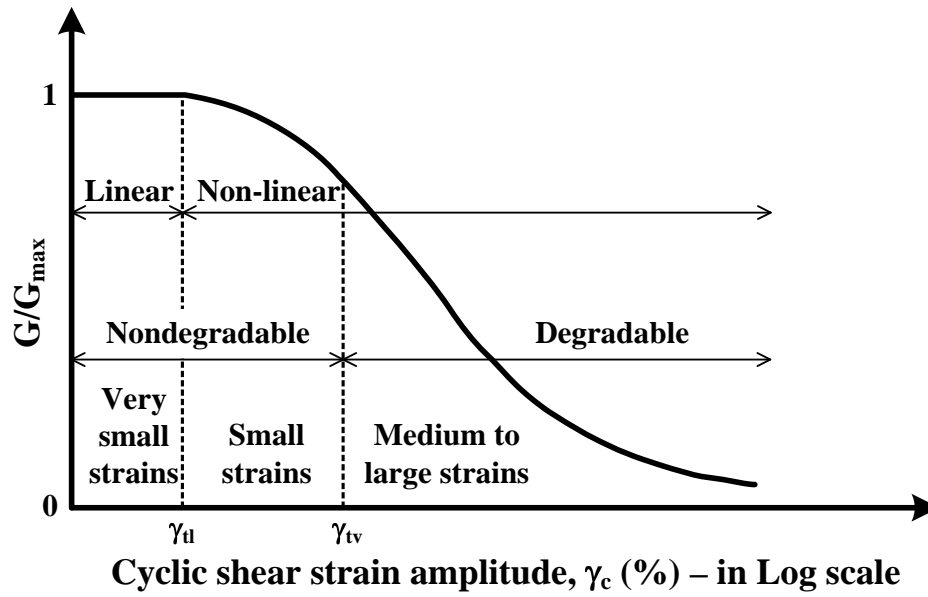
Figure 6.8: Normalised Stiffness Degradation Curve for Fully Saturated Soils

(Vucetic, 1994)

Under triaxial test conditions (drained and undrained), the volumetric threshold shear strains (γ_{tv}) have slightly different meanings in sandy and clayey soils. Indeed, Youd (1972) pointed out that the sands under cyclic loading always contract, regardless of their relative density, unless the maximum density is reached. Thus, γ_{tv} for sand cyclically sheared in a drained condition corresponds to the cyclic shear strain at the start of the settlement or where the positive volumetric strain (ε_v) commences to develop. In the case of an undrained cyclic test in clay, the positive pore pressure (Δu) always develops in normally consolidated (NC) clays. It is, however, not the case in the overconsolidated (OC) clays, where the pore pressure tends to be negative. Vucetic (1994) identified that γ_{tv} remains unique in both NC and OC clays, where the positive and negative pore pressure starts to develop in contrast to the positive volumetric strain in sands. This work was based on the study by Matasovic and Vucetic (1992),. It should also be noted that γ_{tv} seems to have a negligible effect with increasing OCR. From a practical point of view, the threshold shear strain is also defined as the beginning point of significant stiffness degradation.

224

Further, from various laboratory test results on both sandy and clayey soils, Vucetic (1994) proposed a model of volumetric cyclic threshold shear strain increasing with soil plasticity index, as shown in Figure 6.9. This model was later confirmed and refined by Hsu and Vucetic (2004). Within their study, all the test results of the sandy soils were referred to as non-plastic. These values are included in Figure 6.9 in the bottom range, where the plasticity index (y-axis) equals to zero.
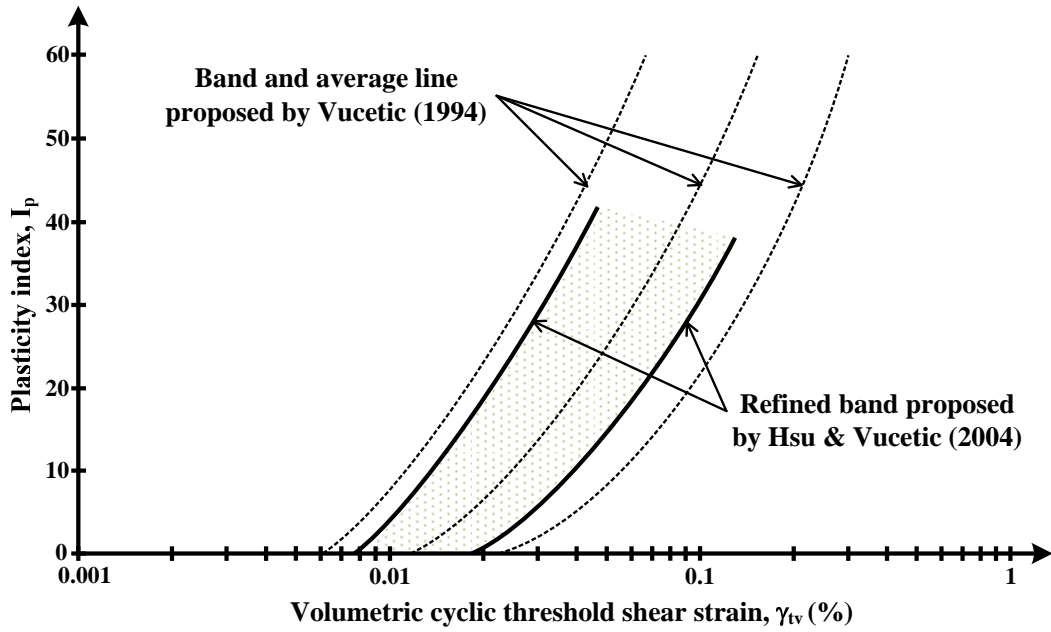
Figure 6.9: Effect of Plasticity Index (I_p) on Volumetric Cyclic Threshold Shear Strain (γ_{tv}), (Hsu and Vucetic, 2004)

Importantly, the normalised shear strain degradation curves tend to move up and to the right as soil plasticity index increase (Vucetic and Dobry, 1991; Vucetic, 1994) (see Figure 6.10). When the volumetric cyclic threshold shear strains from Figure 6.9 were plotted in the normalised degradation curves of Vucetic and Dobry (1991), the bands of γ_{tv} from both Vucetic (1994) and Hsu and Vucetic (2004) were approximately horizontal (see Figure 6.10). This means that, regardless of the soil type, the secant shear modulus decreases by the same proportion before the cyclic threshold shear strain is reached. The average lines of γ_{tv} proposed by Vucetic (1994) and the one calculated from Hsu and Vucetic (2004) refined the band to correspond with the values for G/G_{max} of 0.65 and

0.67, respectively. Based on this concept, Santos and Correia (2000) proposed a reference threshold shear strain ($\gamma_{0.7}$), defined as the shear strain at G/G_{max} of 0.7 within the normalised shear modulus degradation curves. This $\gamma_{0.7}$ was later utilised in the Hardening Soil Model with Small Strain Stiffness, and the HSS Model (Benz, 2006) in the Plaxis program.
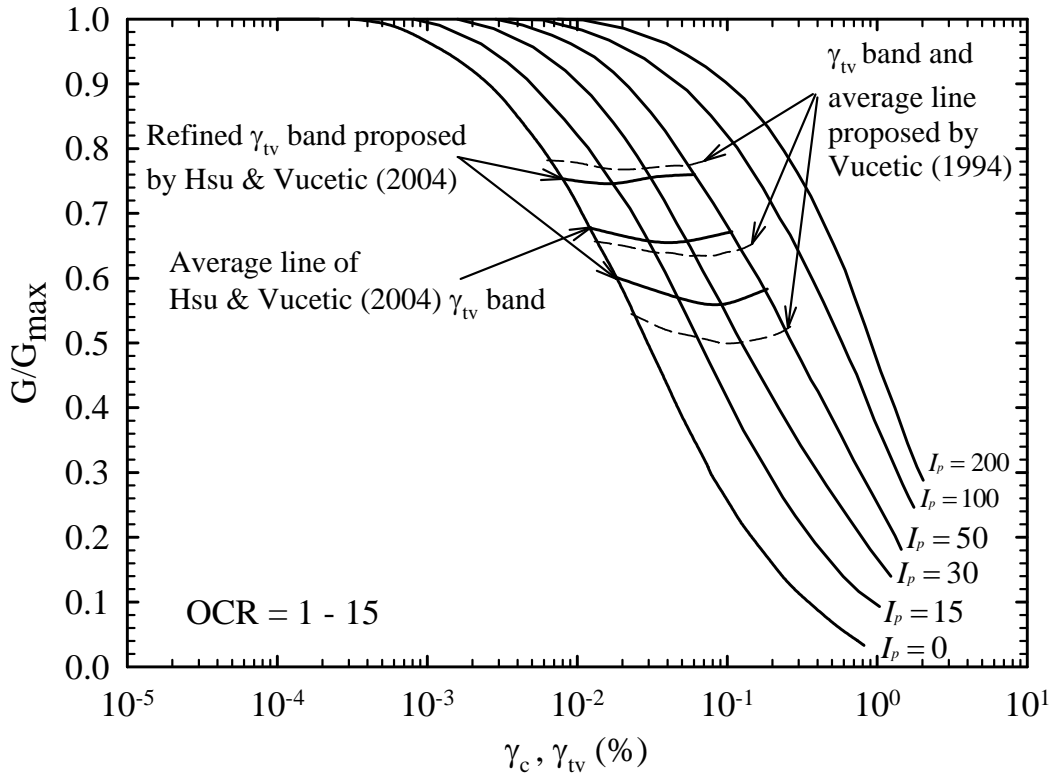
Figure 6.10: Relation between Normalised Modulus Degradation Curves and γ_{tv}
(Modified from Vucetic and Dobry (1991), Vucetic (1994))

6.3.2 Calculation Methods of $\gamma_{0.7}$ Parameter

The concept of the threshold shear strain (γ_{tv}) and ($\gamma_{0.7}$) the parameter is closely related (see discussion in the previous section). This ($\gamma_{0.7}$) parameter is regarded as a soil parameter, which is also needed as an input parameter in the HSS Model. Two methods of calculation, which allow the ($\gamma_{0.7}$) parameter to be calculated, are considered in this

section. The first method is based on the stiffness degradation model (as shown in Figure 6.10) (Vucetic and Dobry, 1991; Vucetic, 1994). In this model, the full stiffness degradation curves of the soils range from non-plastic material with I_p of 0 (sandy soil) to high plasticity soil with I_p of 200. The ($\gamma_{0.7}$) parameter, which is the value of the shear strain where G/G_{max} reduces to 70 per cent of its initial value, can readily been seen from the proposed model. The values of ($\gamma_{0.7}$) parameter from the Vucetic and Dobry (1991) model can be linearly correlated with the plasticity index, as shown in Figure 6.11. The following equation, obtained from the best fit linear function, is used in ($\gamma_{0.7}$) parameter calculation for this study.

$$\gamma_{0.7} = 0.0021 I_p - 0.0055$$
Eq.6.13
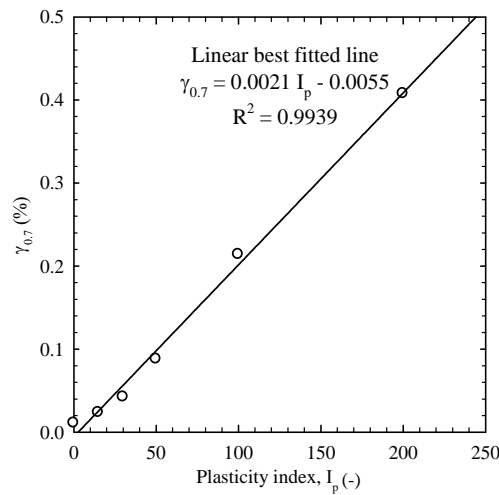
Figure 6.11: Linear Correlation between $\gamma_{0.7}$ and I_p

(Based on Vucetic and Dobry,1991)

A slightly more rigorous method for the stiffness degradation curve was proposed by Ishibashi and Zhang in 1993. Unlike the Vucetic and Dobry (1991) method, the Ishibashi and Zhang (1993) method takes into account the effects of both the mean effective confining stress (p' or σ'_{mo}) and the soil plasticity index (I_p) on the stiffness degradation curves. The major differences between these methods are discussed more in Ishibashi (1992).

227

The Ishibashi and Zhang (1993) stiffness degradation curves are given in mathematical form as:

$$\frac{G}{G_{max}} = K(\gamma, I_p) \cdot (\sigma'_{mo})^{\tilde{m}(\gamma, I_p)}$$

Eq.6.14

$$K(\gamma, I_p) = 0.5 \left[1 + \tanh \left\{ \ln \left(\frac{0.000102 + n(I_p)}{\gamma} \right)^{0.492} \right\} \right]$$

Eq.6.15

$$n(I_p) = \begin{cases} 0.0 & \text{for} \quad I_p = 0 & \text{(sandy soils)} \\ 3.37 \times 10^{-6} \cdot I_p^{1.404} & \text{for} \quad 0 < I_p \leq 15 & \text{(low plastic soils)} \\ 7.0 \times 10^{-7} \cdot I_p^{1.976} & \text{for} \quad 15 < I_p \leq 70 & \text{(medium plastic soils)} \\ 2.7 \times 10^{-5} \cdot I_p^{1.115} & \text{for} \quad I_p > 70 & \text{(high plastic soils)} \end{cases}$$

Eq.6.16

$$\tilde{m}(\gamma, I_p) = 0.272 \left[1 - \tanh \left\{ \ln \left(\frac{0.000556}{\gamma} \right)^{0.4} \right\} \right] e^{-0.0145 I_p^{1.3}}$$

Eq.6.17

The mean in-situ effective confining stress (p' or σ'_{mo}) is calculated using the cross-anisotropic (or transverse-anisotropic) concept, where the effective horizontal stresses are the same in all directions, but they are different from the effective vertical stress. This concept can be applied in level ground conditions. Equation 6.18 defines the mean effective confining stress, as follows:

$$\sigma'_{mo} = \left(\frac{1 + 2K_o}{3} \right) \cdot \sigma'_{vo}$$

Eq.6.18

where,

σ'_{mo} = Mean effective confining stress

σ'_{vo} = Effective vertical stress

K_o = Coefficient of earth pressure at rest

Figure 6.12 shows the variations of $\gamma_{0.7}$ with the range of I_p from 0 to 200 and σ'_{mo} from 1 to 600 kN/m^2, as calculated from Ishibashi and Zhang's (1993) method. The variation of $\gamma_{0.7}$ with I_p from Vucetic and Dobry (1991) is also included for a better comparison. From Ishibashi and Zhang (1993) method, the calculated values of $\gamma_{0.7}$ are affected by the mean effective confining stress, especially for non-plastic and low plasticity soils. Basically, $\gamma_{0.7}$ tends to increase with the increasing mean effective stress. After the plasticity index of soils goes beyond 100, the effect of the mean effective confining stress seems to become insignificant and negligible. It is interesting to see that the values of $\gamma_{0.7}$ from Vucetic and Dobry's (1991) model are nearly identical to those values of Ishibashi and Zhang (1993) with σ'_{mo} of 20 kN/m^2.

The comparison of the volumetric cyclic threshold shear strain (γ_{tv}) and the parameter ($\gamma_{0.7}$) is shown in Figure 6.12. The band of (γ_{tv}) and its average line, proposed by Vucetic (1994), and the refined band, proposed by Hsu and Vucetic (2004), are plotted with the calculated lines of Ishibashi and Zhang's (1993) σ'_{mo} with of 1 and 600 kN/m^2. Similar trends of γ_{tv} and $\gamma_{0.7}$, increasing with the plasticity index, are observed for both parameters. In particular, both bands of γ_{tv} are located within the calculated band of Ishibashi and Zhang (1993) for both the non-plastic soils and the soils with a plasticity index less than 70. This observation can further consolidate the concept of using parameter ($\gamma_{0.7}$) in preference to the volumetric cyclic threshold shear strain (γ_{tv}) (see Figure 6.13).
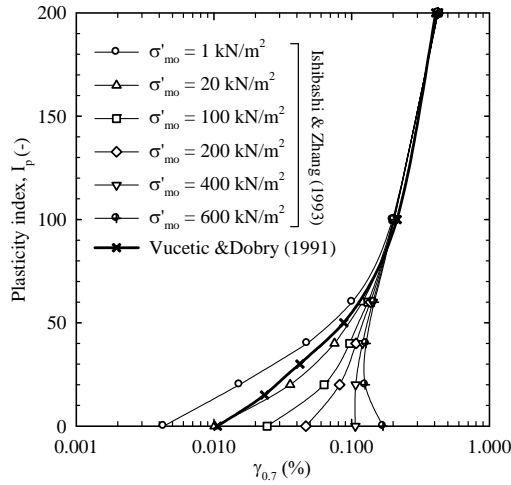
Figure 6.12: Comparison of $\gamma_{0.7}$
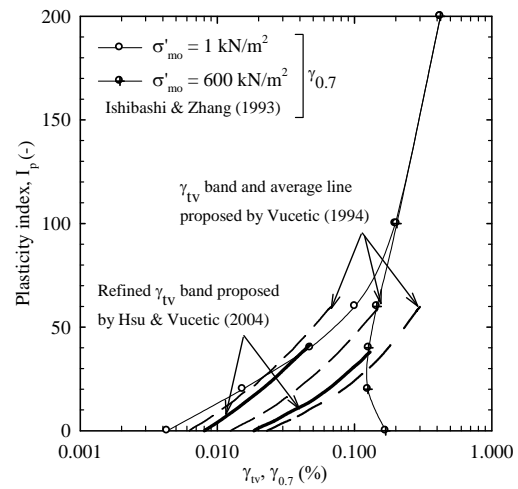
Figure 6.13: Comparison of $\gamma_{0.7}$ and γ_{tv} Bands

6.4 G_{max} and $\gamma_{0.7}$ of Bangkok Clays

The knowledge of small strain nonlinear behaviour was studied comprehensively in the pioneer works of Hardin and Drnevich (1972). Since a large amount of research has been undertaken; the practical applications of the results in relation to small strain stiffness and nonlinear soil behaviour have become standard in many countries. In Thailand, on the other hand, the concept is still very new and confined to a few groups of researchers. The following section, therefore, provides a brief overview of the literature related to the small strain parameters of Bangkok subsoils. The section also examines the empirical correlations of small strain stiffness to identify the most suitable for practical use. The parameter $\gamma_{0.7}$, as closely related to the volumetric threshold shear strain (γ_{tv}), is also studied. Additionally, both the parameters (G_{max} and $\gamma_{0.7}$) have been adopted in a practical case study of the Bangkok MRT station excavation (see Chapter 7).

6.4.1 Small Strain Stiffness of Bangkok Clays

Prior to the detailed study of the G_{max} parameter in Bangkok subsoils, it is important to identify the locations at which this study will be centred. As discussed in Chapter 3, the Bangkok MRT Blue Line project consists of two sections (i.e. North and South sections, see Figure 3.1). The extension (in the design stage) continues from the southern end of the existing project. In terms of the soil profiles from both the MRT projects, the Bangkok subsoils are fairly uniform in thickness and parameter wise. In term of the G_{max} parameter, its uniformity is shown in Figure 6.14. This figure presents a typical soil profile of the Bangkok MRT project, its basic moisture content, and Atterberg limits, as well as the G_{max} parameter from the Suthisan site (Dong, 1998; Theramast, 1998), the Chulalongkorn university site (Warnitchai *et al.*, 1996), and the generalised data for the six sites in Bangkok (Ashford *et al.*, 1996). The Suthisan site is located close to the Suthisan (MRT) station in the northern section of the Bangkok MRT Blue Line. Two parallel studies, related to the small strain behaviour of soils, were conducted. The Dong (1998) study concentrated on the in-situ measurement aspects and Theramast (1998) study used the laboratory Bender element test. Importantly, the values of G_{max}, as shown in Figure 6.14, were calculated from the measured shear wave velocity (V_s) and the soil density ($\rho_s = 1.6$ and 1.8 Mg/m^3 for soft and stiff clays, respectively). Similarly, the G_{max} values were calculated in the same way at the Chulalongkorn university site. This site is located close to the Samyan (southern section) MRT station and is regarded as the Bangkok MRT Blue Line South parameters. The values of G_{max} from the northern and southern sections are fairly similar, especially for the soft clay layer. The generalised data from Ashford *et al.* (1996) also falls into a narrow band. Indeed, the trends of the G_{max} values increase with depth in both the soft and stiff clays. However, the magnitudes of G_{max} are significantly higher in the stiff clay layers.
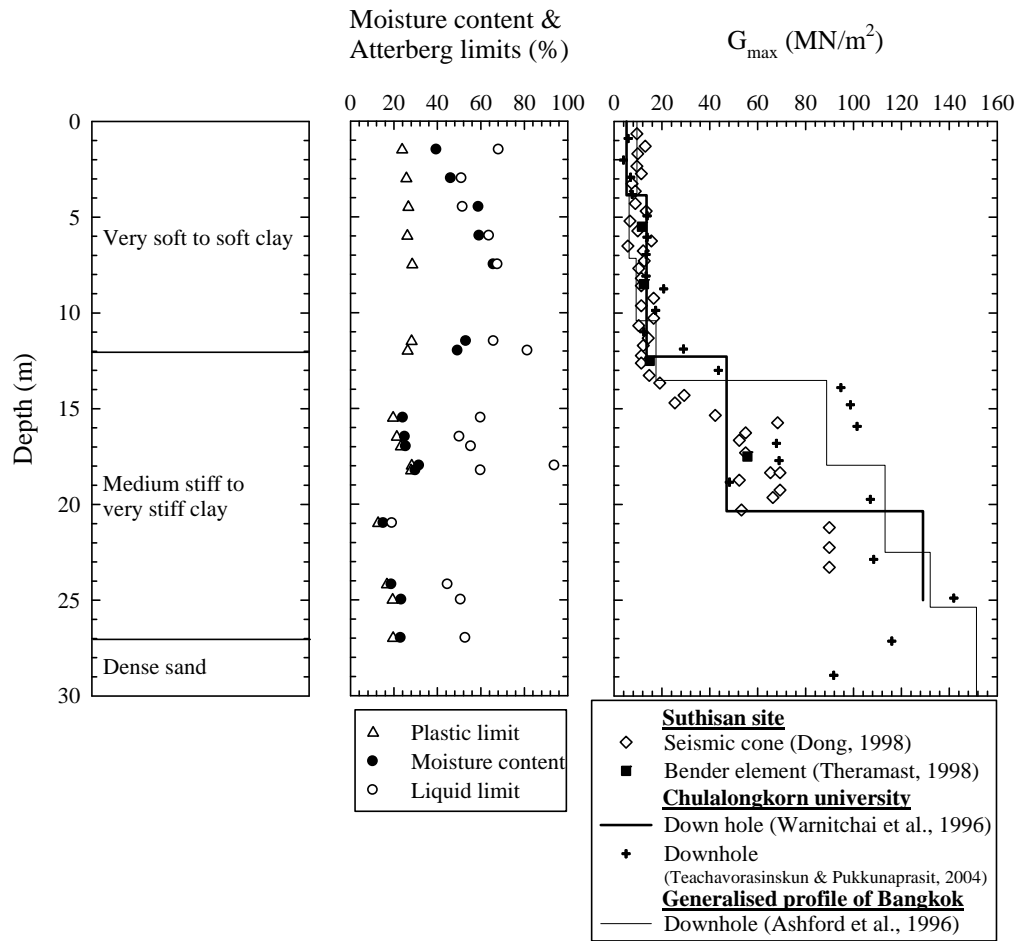
Figure 6.14: Comparison of G_{max} from Laboratory and In-situ Tests in Bangkok Area

The empirical correlations for the small strain stiffness (G_{max}), as reviewed in Section 6.2.3, are applied to the Bangkok subsoils. For the methods proposed by Hardin and Black (1968), Shibuya and Tanaka (1996), and Shibuya $et.al.$ (1997), the void ratio (e_o) and the in-situ stresses (σ'_v and σ'_{mo}) are essential. The void ratio values are calculated from the natural moisture content (w_n), as depicted in Figure 6.15. The approximated drawdown piezometric line (see Figure 5.13) was used in the in-situ stress calculation. Equation 6.5 was applied using the Hardin and Black (1969) method, while Equations 6.8 and 6.9 were used with constant A parameters of 5000 and 24000, as recommended by the Shibuya and Tanaka (1996), and Shibuya $et\ al.$ (1997) methods. Interesting all three methods gave similar results for the soft clay layer. In general, the predicted values lie on the upper range, or slightly overpredict, the measured values. In stiff clay, the predictions

of Shibuya *et al.* (1997) are at two times the measurements, whereas, the predictions of Shibuya and Tanaka (1996), and Hardin and Black (1969) are approximately three times the measured values.

From Shibuya and Tanaka's (1996), and Shibuya *et al.*'s (1997) research, the constant *A*, in Eqs. 6.8 and 6.9, is dependent on the soil types, structure and ageing effects. For this reason, in the current study, this parameter was adjusted to obtain suitable values for the Bangkok Soft and Stiff Clays. The results of the best fit parameter are illustrated in Figure 6.16. Best fit constant parameters *A* as adopted are tabulated in Table 6.1.
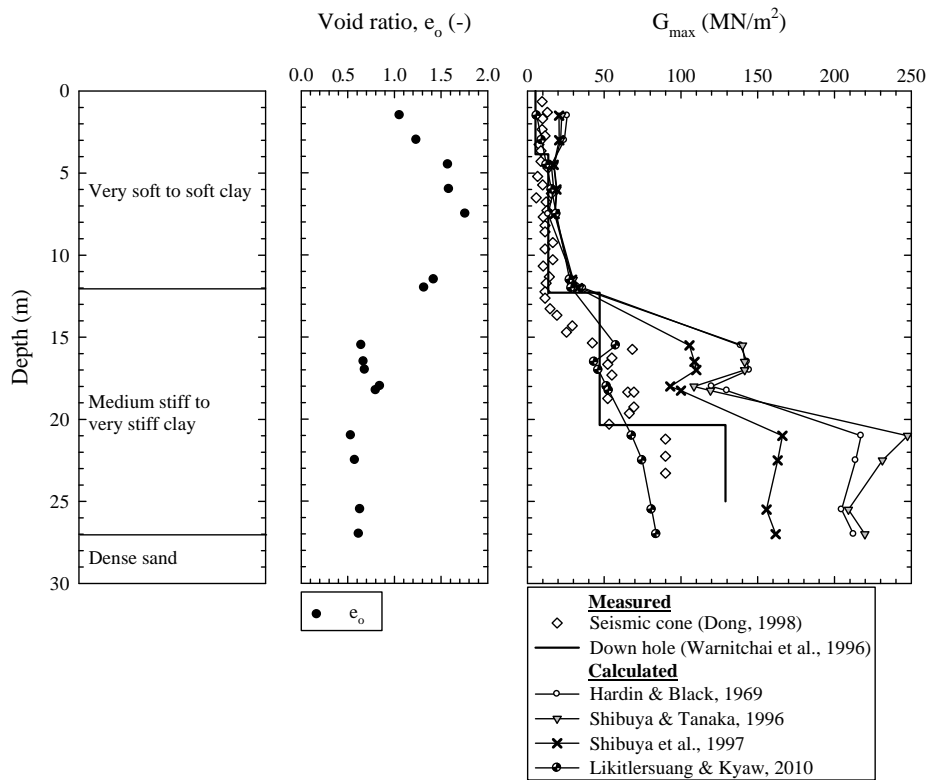
Figure 6.15: Measured and Predicted *G*_{max} of Bangkok Clays
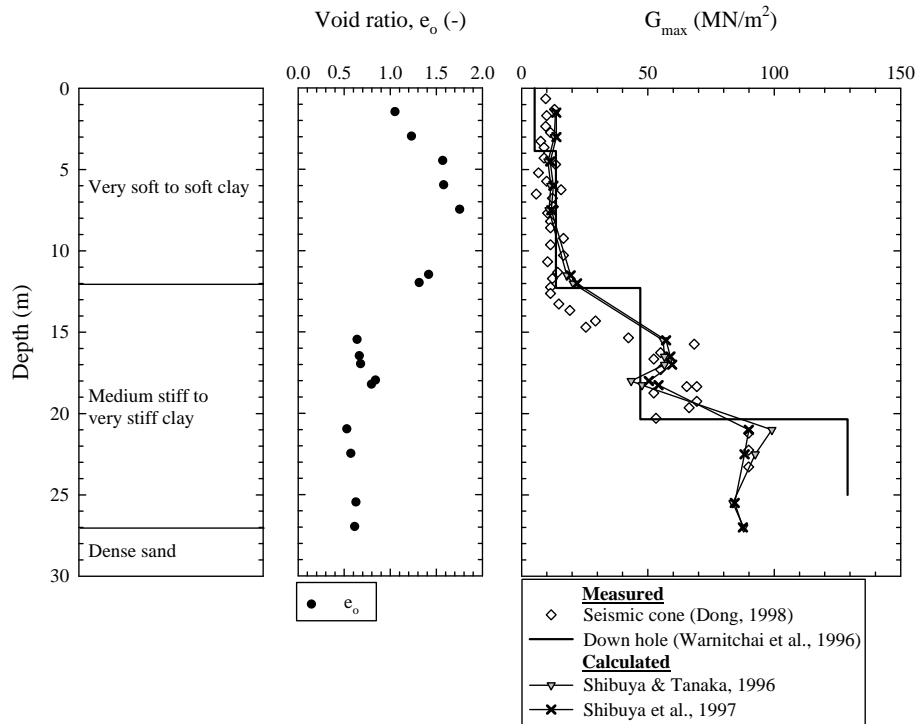
Figure 6.16: Predicted Values of G_{max} Resulting from Best Fit Constant A Parameter

Table 6.1: Best Fit Values of Constant Parameter A for Bangkok Soft and Stiff Clays

Soil type	Constant parameter A	
	Eq. 6.8	Eq. 6.9
Soft clay	3000	16000
Stiff clay	2000	13000

An alternative way to obtain the G_{max} is to use the shear wave velocity (V_s) and undrained shear strength (s_u) correlation. Equation 6.12, from Likitlersuang and Kyaw (2010), was selected as it gave a close approximation of V_s compared to the measured values. The undrained shear strength of Bangkok Soft and Stiff Clays is calculated from the s_u/σ'_{vo} ratios of 0.33 and 0.2. These two ratios were verified earlier with the undrained shear strength from the in-situ vane shear and the undrained triaxial tests in Section 4.3.1. The G_{max} values of the soft and stiff clays, as calculated from the correlated shear wave velocity and the soil density, are plotted in Figure 6.15. The predicted G_{max} gives the

same trend as the measured values. These simple correlations, therefore, can be used as the first approximation when only the in-situ vertical effective stress is known.

The last section on the G_{max} parameter on the Bangkok Clays relates to the correlations between the G_{max} and the limit and net limit pressure (p_L and p_L^*) from the LLT pressuremeter tests. Chapter 5 showed that p_L and p_L^* can be reasonably correlated with the undrained shear strength of Bangkok Clays. As illustrated in Figure 6.17, pressuremeter p_L and p_L^* of the Bangkok Soft and Stiff Clays, when plotted with depth, provide a similar trend when compared with the G_{max} values. Indeed, they are in excellent agreement with the simple linear correlations, as follows:

$$G_{max} = 50 \cdot p_L \qquad\qquad\qquad \text{Eq.6.19}$$

$$G_{max} = 80 \cdot p_L^* \qquad\qquad\qquad \text{Eq.6.20}$$
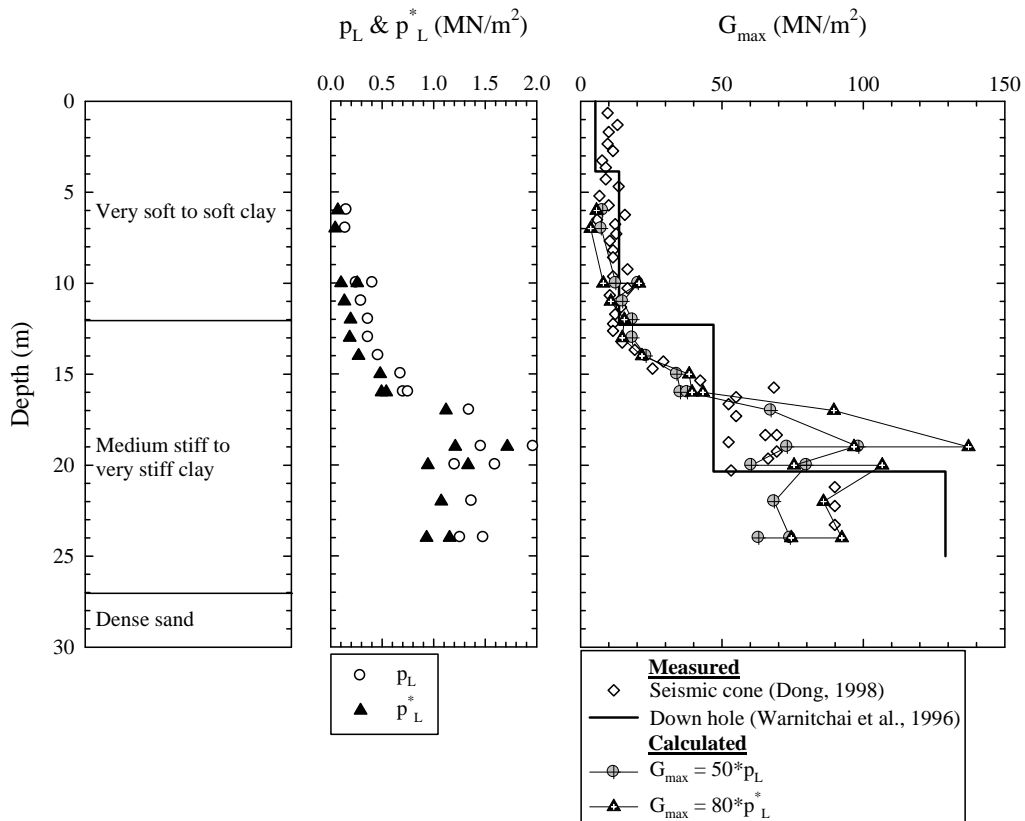
Figure 6.17: Correlations of G_{max} from p_L and p_L^*

235

Further, Equations 6.19 and 6.20 can be treated as a simple rule of thumb, in practice, when the results from the pressuremeter tests are available.

6.4.2 Parameter $\gamma_{0.7}$ of Bangkok Clays

A brief summary of the parameter $\gamma_{0.7}$, and the available methods to calculate the parameter were discussed in Section 6.3. Unlike the small strain stiffness (G_{max}), the knowledge of $\gamma_{0.7}$ on Bangkok Clays is very limited. To obtain the measured values of $\gamma_{0.7}$, one needs to first know the values of the G_{max}, and then measure the shear modulus (G) at a small level of shear strain amplitude (say 10^{-4}%) to a large strain level. Next, the normalised stiffness degradation curve can be constructed and the $\gamma_{0.7}$ can be read from the curve. An example of such normalised stiffness degradation curves was shown in the study by Teachavorasinskun *et al.* (2002a). They conducted a series of cyclic triaxial tests on Bangkok Soft Clay using the LVDT apparatus to measure the load displacement at a small strain level of 0.01%. The results from two sites were chosen (the Chulalongkorn University (CU) site and the Mahidol University (MU) site, located in the centre of Bangkok close to the alignment of Bangkok MRT Blue Line South project). The plasticity index of soil samples were 30 and 40 for the CU and MU sites, respectively. Figure 6.18 shows the normalised G/G_{max} curves resulting from the cyclic triaxial tests at 50, 150 and 250 kN/m^2 for the confining pressure (σ'_c). Importantly, the G_{max} used in this normalised curve was taken from the down hole seismic test for the CU site and from the Hardin and Black (1968) correlation for the MU site. According to Teachavorasinskun *et al.* (2002a), the stiffness degradation curves fell within the ranges of plasticity index similar to those reported by Vucetic and Dobry (1991). However, the effects of the different load frequencies (at 0.1 and 1.0 Hz) were insignificant. Further, the parameter $\gamma_{0.7}$, read directly from Figure 6.18, is approximately 0.03 – 0.07 %. These ranges of values correspond to $\gamma_{0.7}$ of the Bangkok Soft Clay with I_p of 30 - 40 and with the confining pressure of 50 - 250 kN/m^2.
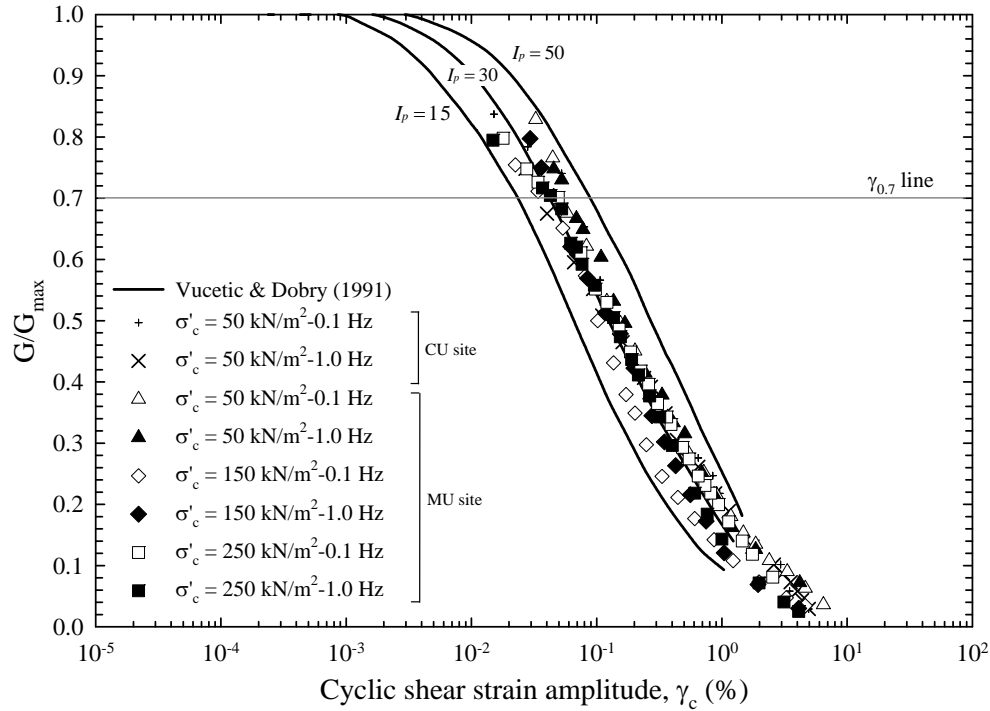
Figure 6.18: Stiffness Reduction Curves and $\gamma_{0.7}$ of Bangkok Soft Clay
(after Teachavorasinskul *et al.*, 2002)

Teachavorasinskun *et al.* (2002b) also conducted a series of cyclic triaxial tests on the Bangkok Soft Clay at the CU site. The applied load frequency of this series was 0.00025 and 0.1 Hz. The soil samples had I_p of 40 and the confining pressure ranged from 50 to 100 kN/m^2. The authors reported that the excess pore pressure started to built up at the level of the axial strain (ε_a) of 0.02 – 0.2%, which corresponds to the cyclic shear strain amplitude (γ_c) of 0.03 – 0.3 %. The levels of the shear strain amplitude, where the soil commences to behave non-linearly and irrecoverably, refer to the cyclic threshold shear strain (γ_{tv}). In the case of clayey soils, γ_{tv} is taken as the shear strain amplitude where the excess pore pressure starts to develop. The concept of using $\gamma_{0.7}$ is closely related to γ_{tv}, as discussed in Section 6.3. The ranges of $\gamma_{0.7}$ and γ_{tv} of Bangkok Soft Clay also coincided with the levels of 0.03 – 0.07 and 0.03 – 0.3 %, respectively.

The two methods which allowed for the calculation of $\gamma_{0.7}$ (Vucetic and Dobry, 1991; Ishibashi and Zhang, 1993) are discussed in this section, with an emphasis on their application to Bangkok Clays. The Vucetic and Dobry (1991) method utilises only the

237

plasticity index to determine $\gamma_{0.7}$ from their stress reduction curves (Figure 6.10), while Ishibashi and Zhang (1993) take the influence of both the plasticity index and the effective mean confining stress into their calculations. Comparisons of $\gamma_{0.7}$, calculated from both methods, are compared in Figure 6.12, above. These calculated values are replotted with the measured $\gamma_{0.7}$ of the Bangkok Soft Clay in Figure 6.19. The Vucetic and Dobry (1991) method gave results within the range of the measured $\gamma_{0.7}$. Ishibashi and Zhang's (1993) method also exhibited good agreement when the lower values of the effective mean stress are applied. Slightly overpredicted values of $\gamma_{0.7}$ are observed when the effective mean stress exceeds 200 kN/m^2. The ranges of $\gamma_{0.7}$ of 0.03 – 0.07 % were obtained from a soil sample with I_p of 35 – 40 and an effective confining pressure of 50 – 250 kN/m^2.
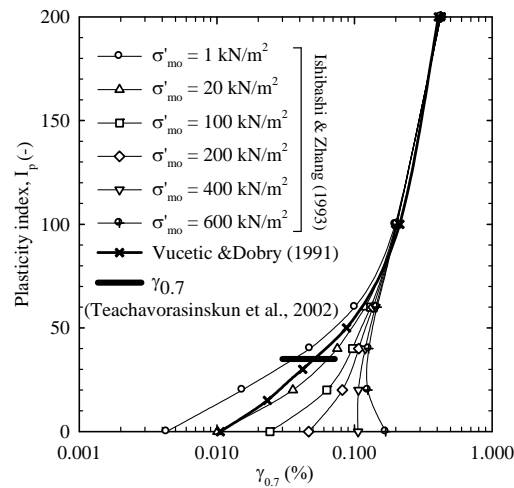
Figure 6.19: Comparison of Measured and Computed $\gamma_{0.7}$ of Bangkok Soft Clay

With the average values of the plasticity index and the effective mean stress of the Bangkok Soft and Stiff Clays, $\gamma_{0.7}$ is computed using both Vucetic and Dobry (1991) and the Ishibashi and Zhang (1993) methods, as shown in Figure 6.20. Both methods provide close approximations of $\gamma_{0.7}$ within the very soft to soft clay layers, up to the depth of 12 m. These values of $\gamma_{0.7}$ are also confined within the ranges of $\gamma_{0.7}$ and γ_{tv} of the Bangkok Soft Clay of 0.03 – 0.07 and 0.03 – 0.3 %, as observed in the literature. On the other hand, the values of $\gamma_{0.7}$ from both methods gave different trends in the medium stiff to

very stiff clays, at a depth of 12 to 27 m. The Ishibashi and Zhang (1993) method calculated an approximate constant $\gamma_{0.7}$ of 0.1% along the stiff clays, while the Vucetic and Dobry (1991) method gave a trend of $\gamma_{0.7}$ reducing with depth, and values ranging from 0.06 to 0.02 %. Unlike the case of the Bangkok Soft Clay, there was no comparable information from the laboratory $\gamma_{0.7}$ of the stiff clays. Nevertheless, the computed values of $\gamma_{0.7}$ will be used in a finite element analysis study of the MRT station excavations in Chapter 7. Verifications of $\gamma_{0.7}$ in both the soft and stiff clays will then be undertaken using parameter back-calculations.
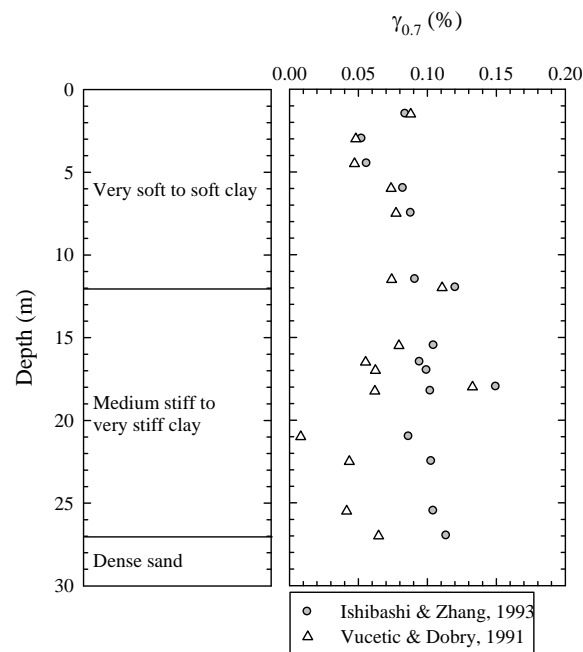
Figure 6.20: Computed $\gamma_{0.7}$ of Bangkok Clays

6.5   Concluding Remarks

In early parts of this chapter, the basic knowledge and measurement methods for small strain shear stiffness are summarised. Then, two small strain parameters of Bangkok Clay (namely small strain shear stiffness (G_{max}) and reference shear strain ($\gamma_{0.7}$)) are studied. For the small strain shear stiffness of Bangkok Clays, the following conclusions can be drawn:

(1) G_{max} of the Bangkok Clays is fairly uniform across all areas of the Bangkok MRT Blue Line Projects, as well across other parts mentioned in this study. The values of the G_{max} tend to increase with depth with a clear distinction between the soft and stiff clays.

(2) All empirical equations estimated reasonable values of the G_{max}. However, their constant parameters needed to be calibrated.

(3) Simple correlations between the G_{max} and the LLT pressuremeter parameters are proposed. Basically, the G_{max} values in both the soft and stiff clays are approximately equal to 50 and 80 times that of the limit pressure (p_L) and the net limit pressure (p_L^*), respectively.

Similarly, conclusions from the studies of $\gamma_{0.7}$ can be summarised as:

(1) The concept of using the reference shear strain ($\gamma_{0.7}$) for its close relationship to the volumetric threshold shear strain (γ_{tv}) is confirmed. For this reason, $\gamma_{0.7}$ should be considered as a soil parameter.

(2) In the case of the Bangkok Soft Clay, the $\gamma_{0.7}$ values, predicted from Ishibashi and Zhang (1993), and Vucetic and Dobry (1991) are nearly identical. Their predictions are also comparable with the measured values from the laboratory tests. However, for the stiff clays, the predictions from both methods do not agree. As a consequence, the predicted values of both the soft and stiff clays will be verified using the back-calculated methods in the next chapter.

CHAPTER 7

Diaphragm Wall Deflections and Ground Settlements Induced by MRT Station Excavations

7.1 Introduction

This chapter presents a study of the movements of the diaphragm wall and the ground surface settlements induced by the Mass Rapid Transit (MRT) station excavations. During the study, more attention was paid to the practically oriented aspects so that the outcomes would assist practicing engineers. The chapter also presents the empirical and numerical analyses related to the assessment of the wall movements and ground surface settlements. The relationships between the maximum lateral wall deflections (δ_{hm}) and the maximum ground surface settlements (δ_{vm}) are also studied. This approach is adopted for the verification of the suitability of the empirical methods to predict ground surface settlements induced by excavations in the Bangkok subsoils. In respect to the numerical aspects, four soil models were employed: Mohr Coulomb Model, Soft Soil Model,

Hardening Soil Model, and Harden Soil Model with Small Strain Stiffness (HSS) (a summary of each model is given in Chapter 2). The performances of these models are examined in terms of D-wall movements and ground surface settlement predictions. Extensive studies of the geotechnical parameters were conducted using both laboratory and in-situ testing (see Chapters 4, 5 and 6). The soil parameters from these studies were used as the input parameters in the four constitutive models. The materials contained in Sections 7.1 and 7.2 as presented here and not in Chapter 2 as these materials are needed in the on-going presentations of the results.

7.1.1 Types of Retaining Wall Movements and Ground Surface Settlements

Broadly speaking, the types or patterns of retaining wall movements are governed by many factors, such as the type of subsoil encountered, the support system of the retaining wall (i.e. braced or anchored), the quality of the workmanship, etc. These patterns of wall movements can be categorised as cantilever and deep inward or braced excavations (see Figure 7.1). At the initial stage of excavation or when the encountered soil is predominantly sandy, a cantilever type of movement tends to occur. As excavation proceeds further and especially in soft soils, deep inward movement is more likely to be encountered.
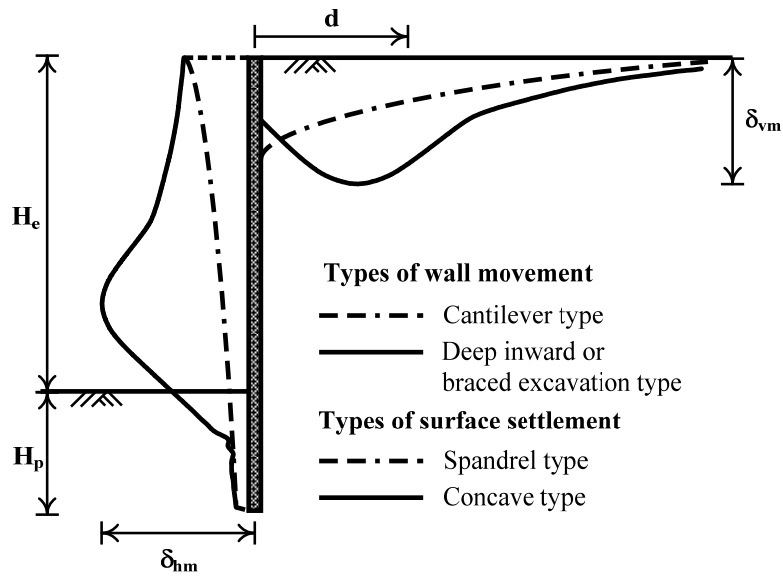
Figure 7.1: Types of Wall Movement and Ground Surface Settlement

Further, the ground surface settlement induced by the excavations can be divided into two groups. According to Hsieh and Ou (1998) these are: (i) the spandrel type, in which the maximum surface settlement locates near the wall; and (ii) the concave type, in which the maximum surface settlement occurs at a distance away from the wall. Ou (2006) pointed out that the magnitude and the shape of the retaining wall movements, as the excavation progresses, are the major factors governing the shape and type of ground surface settlements. Generally, the spandrel surface settlement profile is likely to occur with the cantilever pattern of wall movements, while the concave surface settlement profile is likely to occur with a deep inward movement pattern. Indeed, Hsieh and Ou (1998) also proposed a simplified method to justify the type of surface settlements. This method is summarised in three points below:

(1) The area enclosed by the cantilever wall movement, at the first stage of excavation, and the cantilever component of the wall movement, at the final stage of excavation, are estimated; they are denoted as A_{c1} and A_{c2} in Figure 7.2. The higher magnitude of these two areas is considered to be the dominant cantilever component area (A_c).

243

(2) The area enclosed by the deep inward movement component, at final excavation stage (A_s), is estimated by subtracting the entire area of the final stage wall movement curve from A_{c2}.

(3) Finally, if the area A_s is greater than or equal to 1.6 A_c, then a concave type of settlement profile should be employed; otherwise, the surface settlement will be a spandrel shape.
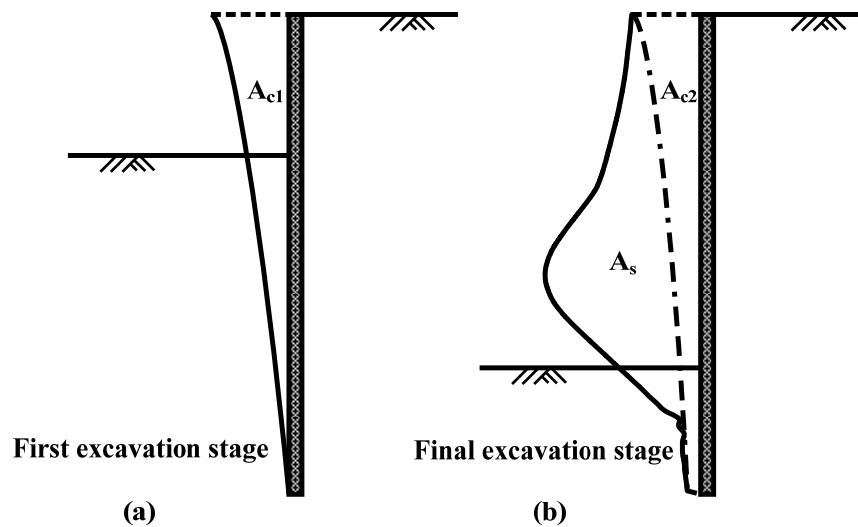
Figure 7.2: Area of Cantilever and Deep Inward Components (Hsieh and Ou, 1998)

7.2 Empirical Methods for Excavation Induced Ground Movement Predictions

The first empirically based method to predict ground settlement, induced by excavation, was proposed by Peck (1969). Using a monitoring database of case histories from Chicago and Oslo, Peck established a relationship between the ground surface settlements, the soil types, the excavated depths, and the workmanship quality. The

monitoring data were obtained, in the main, from steel sheet piles or soldier piles; these piles are quite different to those used in more recent construction methods (i.e. diaphragm wall with braced or anchored supports). Indeed, Ou (2006) stated that Peck's method may not necessarily be applicable to all excavation types. For ground surface settlements, induced by excavation, Bowles (1986) proposed an estimation procedure. To estimate the ground surface settlement curve this procedure utilised the area enclosed by the lateral wall deflection envelope , resulting from the finite element or beam on elastic soil layer analysis, the angle of internal friction of soil (ϕ') and the excavation width and depth. The major shortcoming of this method was the estimated ground surface settlement curve, which always yielded a spandrel surface settlement type. As a consequence, a concave-like settlement curve cannot be predicted using the Bowles's method.

Similar to Peck's (1969) method, Clough and O'Rourke (1990) proposed a more refined set of surface settlement envelopes induced by an excavation. The shape and magnitude of the surface settlement envelopes depend on the type of soil, the excavation depth and the maximum wall deflection. In the case of sand and stiff clay, the triangular shape surface settlement envelopes were adopted (as shown in Figure 7.3 (a and b)). With a triangular shaped surface settlement, the maximum surface settlement is located close to the wall. The distinction between the sand and stiff to very stiff clay is made by the length of the influence zone of $2H_e$ and $3H_e$, respectively. For the soft to medium stiff clay, a trapezoidal diagram is used; it differs from those observed in the cases of sand and stiff clays. This difference occurs because the soft to medium stiff clays have two influencing zones. The first zone has a rectangular shape and extends, from the wall, to a distance of $0.7H_e$. Beyond this point, the second zone of settlement envelope extends; it has a triangular shape similar to those for the sand and stiff clay cases. This zone ends at the distance of $2H_e$.
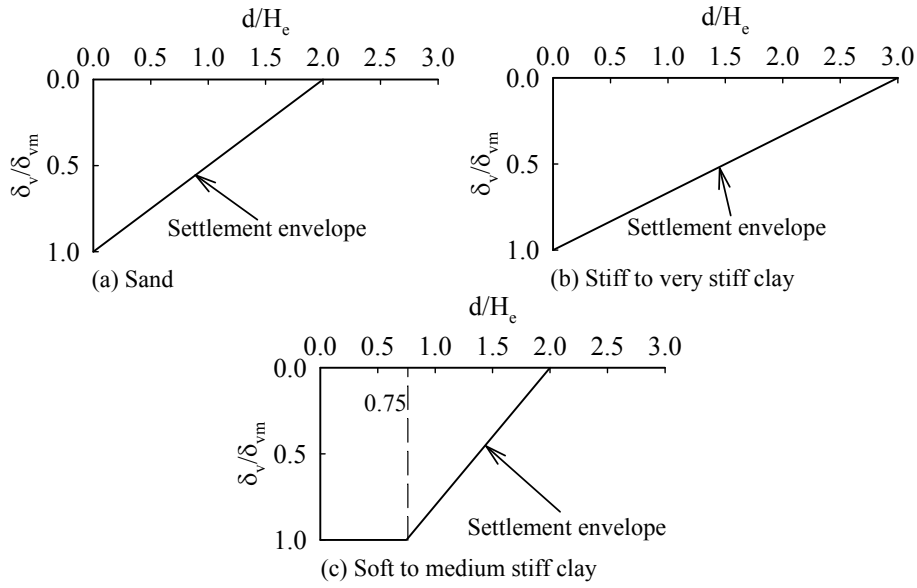
Note: d = distance from the wall; H_e = length of excavation;
δ_v = surface settlement at distance (d); δ_{vm} = maximum surface settlement

Figure 7.3: Estimation of Ground Surface Settlement (Clough and O'Rourke, 1990)

Hsieh and Ou (1998) further refined Clough and O'Rourke's (1990) method by introducing two zones of influence, namely the Primary Influence Zone (PIZ) and the Secondary Influence Zone (SIZ). The depth of the excavation (H_e) was kept as the primary parameter to predict the length of each zone. As a result, the surface settlement within the PIZ is larger when compared to that in the SIZ. The PIZ extends from the wall up to the length of $2H_e$, while the SIZ continues from the length of $2H_e$ to 4 H_e. As a consequence, for the spandrel settlement profile, a bi-linear relationship was proposed. First, the larger surface settlement in the PIZ is predicted using Equation 7.1. Then, Equation 7.2 is used to estimate the smaller surface settlement in the SIZ.

$$\delta_v = \left(-0.636\sqrt{\frac{d}{H_e}} + 1 \right)\delta_{vm} \text{, if d/H}_e \leq 2; \text{ and} \qquad \text{Eq.7.1}$$

246

$$\delta_v = \left(-0.171\sqrt{\frac{d}{H_e}} + 0.342\right)\delta_{vm}, \text{ if } 2 < d/H_e \leq 4 \qquad \text{Eq.7.2}$$

where, δ_v and δ_{vm} are the surface settlement and the maximum surface settlement for the soil at distance d form the wall. For a concave settlement profile prediction, the diagram in Figure 7.4 was proposed. This diagram can be regarded as a refinement of Figure 7.3 (c) (Clough and O'Rourke, 1990). The major differences between the two figures are the shape of the surface settlement within the PIZ (the area from the wall to distance $4H_e$) and the inclusion of the surface settlement in the SIZ (line cd in Figure 7.4).
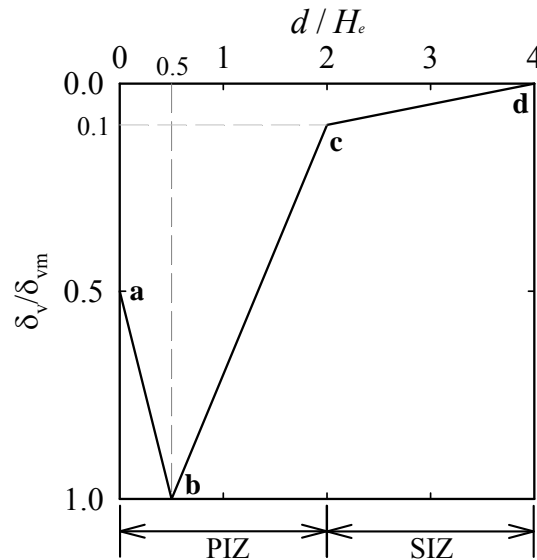
Figure 7.4: Estimation of Ground Concave Surface Settlement (Hsieh and Ou, 1998)

Unlike Peck (1969), and Clough and O'Rourke (1990), where the shapes of the surface settlements are distinguished primarily by soil types, Hsieh and Ou (1998) classified the shapes of the surface settlement as spandrel and concave settlement profiles. This method is explained above in Section 7.1.

The empirical methods of Peck (1969), Clough and O'Rourke (1990), and Hsieh and Ou (1998), as summarised above, utilised the excavation depth (H_e) as a normalised parameter to the distance from the retaining wall (d). In other words, the shape and the

magnitude predicted by the above methods depend primarily on H_e. Ou and Hsieh (2000) method takes into account the width of excavation (B), the depth to hard stratum (H_g), and the excavation depth (H_e) to identify the shape of the ground surface settlement. These two surface settlement patterns (i.e. spandrel and concave) are considered, which continues the author's earlier method published in 1998. Figure 7.5 (a and b) show the surface settlement pattern using the revamped method.
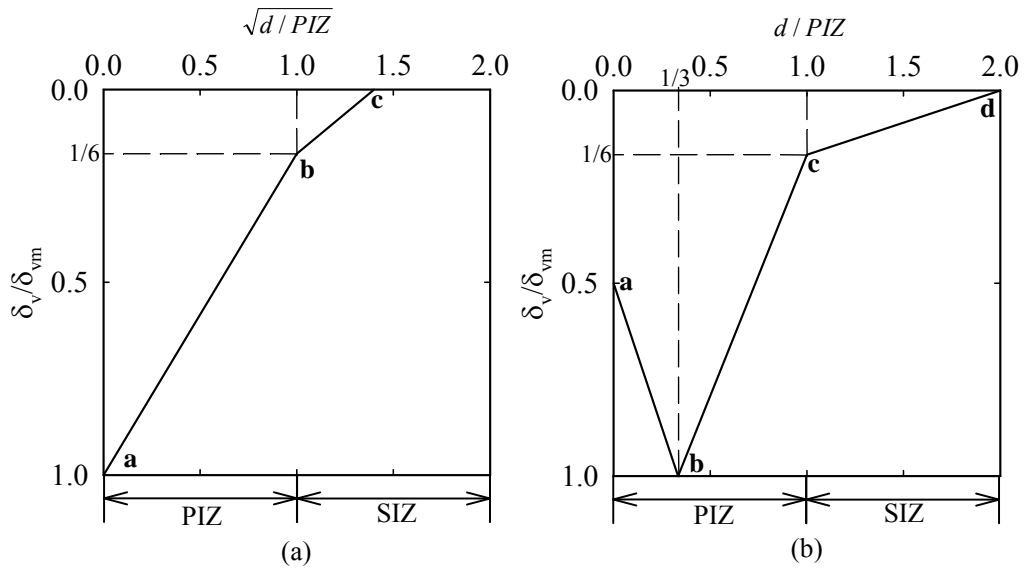
Figure 7.5: Estimation of Surface Settlement (a) Spandrel Type,
(b) Concave Type (Ou and Hsieh, 2000)

Instead of using H_e as normalised parameter, the length of the Primary Influence Zone (PIZ) is used. The parameter PIZ can be estimated as:

(1) When the hard stratum is at a greater depth, free earth support is considered. With this method, both the wall and the soil at the bottom of wall are allowed to move. The length of the Primary Influence Zone is denoted as PIZ_1, and equals the lower value between $2H_e$ and H_g, where H_e and H_g are the excavation depth and the depth to the hard stratum, respectively.

(2) However, when the potential basal heave failure is considered, the length of the potential failure zone (PIZ_2) is the lowest value between the excavation width (B) and the depth of soft soil encountered (H_f).

(3) Both PIZ_1 and PIZ_2 are possible potential failure zones; therefore the length of the Primary Influence Zone is the largest of them.

Three empirical methods (Clough and O'Rourke, 1990; Hsieh and Ou, 1998 and Ou and Hsieh, 2000) share the same normalised ratio of δ_v/δ_{vm} to predict the magnitude of the settlement at any distance d. This means that successive estimations of the maximum vertical movement (δ_{vm}) are necessary prior to the ground surface settlement prediction. In their methods, Peck (1969), and Clough and O'Rourke (1990) correlated the maximum surface settlement with the excavation depth (H_e). In his later work, Ou (2006) stated that the excavation depth was not the only parameter affecting the surface settlement. He also pointed out that, from his observations, the factors affecting the wall movement also influenced the ground surface settlement. Based on case histories from San Francisco, Oslo and Chicago (Mana and Clough, 1981), and from Taipei, Ou *et al.* (1993) concluded that, in most cases, the ratio of the maximum surface settlement to the maximum wall movement (δ_{vm}/δ_{hm}) fell into a range of 0.5 to 0.7. The lower limit of 0.5 represents the findings from most excavation cases in sandy soils, whereas the excavations in clays tend to give the δ_{vm}/δ_{hm} ratio, which is close to the upper limit. However, in some cases, where the excavations were conducted in very soft soil, δ_{vm}/δ_{hm} ratios larger than unity are also observed. Interestingly, the line of $\delta_{vm} = 0.7\ \delta_{hm}$ in Figure 7.6 has been shifted slightly to $\delta_{vm} = 0.75\ \delta_{hm}$ (Ou, 2006).
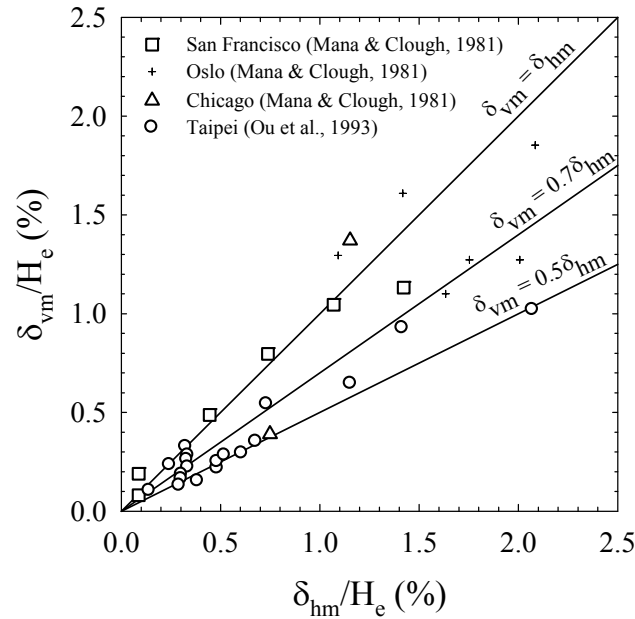
Figure 7.6: Maximum Ground Surface Settlement and Lateral Wall Deflection

(After Ou *et al.*, 1993)

7.3   MRT Subway Station Case Studies

7.3.1 Sukhumvit Station

The Sukhumvit Station is located underneath Asok Road, next to the Sukhumvit - Asok Roads Intersection (Figure 7.7). The station box is surrounded, in the main, by commercial (3 to 4 stories) and residential buildings. The soil profile consists of 2 to 3 m of made ground (MG), underlain by approximately 9 m of normally consolidated Bangkok Soft Clay (BSC), with a vane shear strength of about 20 kN/m^2. The undrained shear strength of this layer tends to increase with depth from the level below 7 m. Beneath the BSC layer, there is 2 m of Medium Clay (MC), with a vane shear strength of more than 60 kN/m^2. A thin, but continuous, medium dense Clayey Sand (CS) of 1.5 m is sandwiched between the First and Second Stiff Clays (1st SC and 2nd SC), with thicknesses of 6 m and 4 m, respectively. At the depth of 23 to 40 m, the Hard Clay (HC) layer (SPT N values of 30 to 40), with some sand lenses, is found. This HC layer is then

underlain by the Dense Sand (DS) layer, up to 60 m deep. The ground water level at this location was found at 1.5 m below the ground surface. A schematic diagram of the Sukhumvit Station soil profile is shown in Figure 7.8. This soil profile is also adopted as the soil profile model in the finite element analysis presented in the following sections. Note that the soil profile model in Figure 7.8 is developed base on a synthesis series of 4 boreholes, located between the Station 16 + 800 to 17 + 500 (see Figure 3.14).
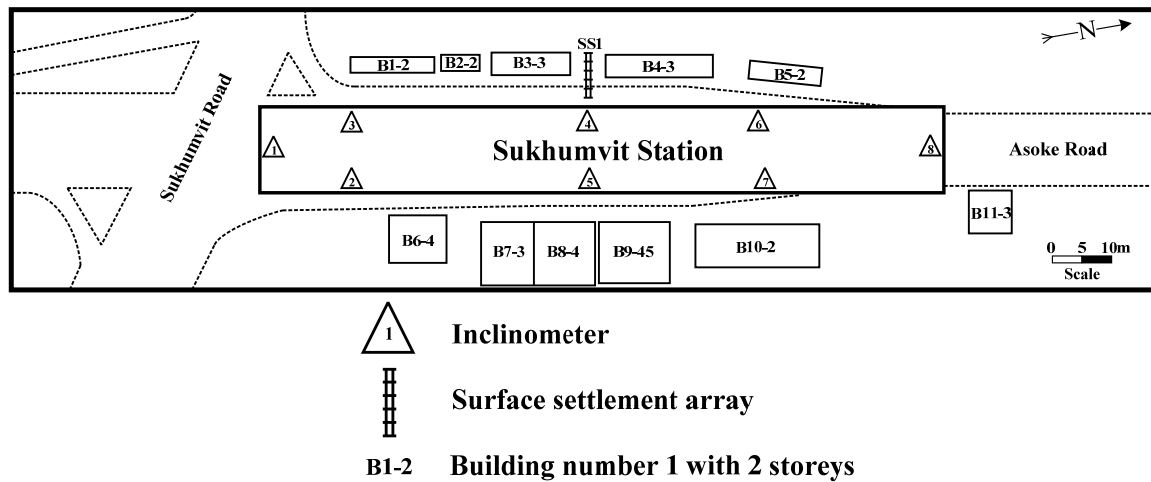
Figure 7.7: Plan View of Sukhumvit Station and Its Instrumentations
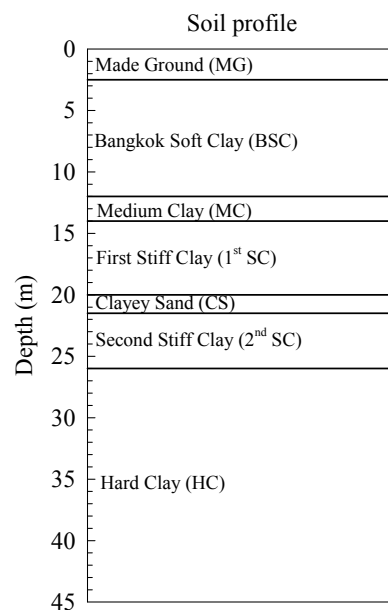
Figure 7.8: Soil Profile at Sukhumvit Station Location

251

The Sukhumvit Station was constructed using the top down construction method, with a configuration of the centre platform type. The station box had the width, length and depth of 23 × 200 × 21 m. The reinforced concrete diaphragm walls (D-wall) were 1 m thick and 27.9 m deep; they were used for earth-retaining and permanent structures in the station. The 1 m thick concrete slabs of the first, second and third slabs (Roof, Access and Concourse levels) and the 1.8 m thick base slab were the primary braced support system for the D-walls. Figures 7.7 and 7.9 show the plan view and the cross section geometry of the Sukhumvit Station. The construction sequences adopted in the station box construction simulation are summarised in Table 7.1.
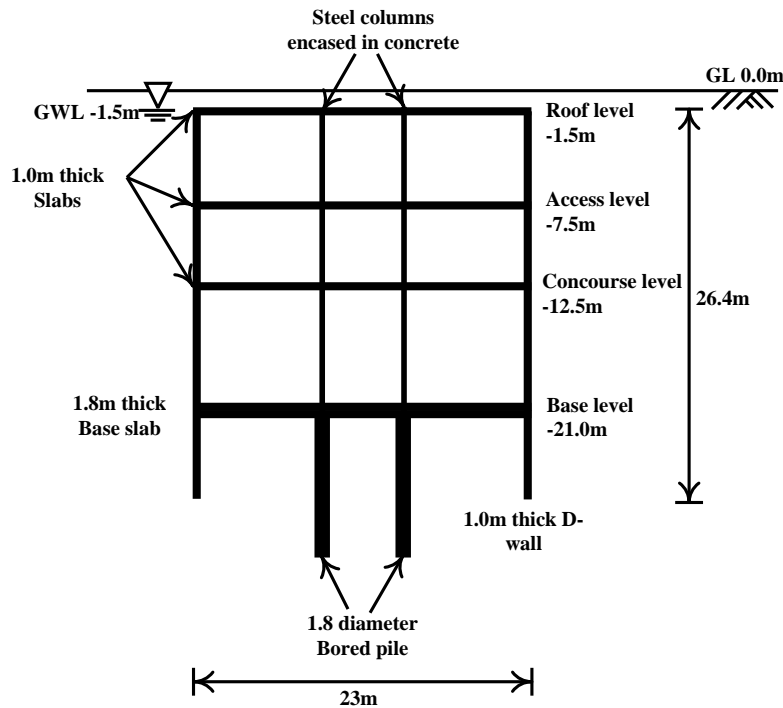
Figure 7.9: Geometry of Sukhumvit Station

Table 7.1: Construction Sequences of Sukhumvit Station (Hooi, 2003)

Stage	Construction activities
1	Construction of diaphragm walls
2	Construction of bored piles
3	Installation of steel columns, which were plunged into the top of bored piles to form pin piles
4	Pre-excavation and placement of temporary steel decking supported by pin piles for traffic diversion
5	Excavation to level of underside of temporary prop and installation of temporary prop, if necessary
6	Excavation to level of underside of roof slab and construction of permanent concrete roof slab
7	Removal of temporary prop, if needed
8	Excavation to level of underside of second slab level
9	Construction of second concrete slab
10	Stage 8 and 9 were repeated for third and fourth (base) slab
11	Plunged steel columns were encased in concrete
12	Construction of internal structures including platforms, lift shafts, staircases, etc.
13	Electrical and mechanical installations followed by architectural finishing
14	Backfill roof slab and finial road reinstatement

Extensive instrumentation programs were adopted to monitor the deflection of the diaphragm wall and the ground settlement induced by deep excavations. The instrumentation included inclinometers installed in the D-wall, inclinometers combined with extensometers, surface settlement points, and surface settlement arrays. The building settlement points tilt and crack meters were also installed to ensure that any damage to the adjacent buildings was kept within the design limitations. The instruments, which are of most interest in this study, are depicted in Figure 7.7 above. These instruments comprise of eight sets of inclinometers installed in the D-wall at various locations and one set of surface settlement arrays (SS1). The surface settlement (SS1) selection for this location was chosen because the surface settlement array (SS1) was located in a bare area

253

between buildings B3 and B4. Thus, the surface settlement measured from the SS1 could be considered as close to a greenfield condition. Moreover, the location of the SS1 was in the middle of the North-South length of the Sukhumvit Station, where the effects of the corners were expected to be minimised. For this reason, the inclinometer number 4 (IN4) will also be used to compare the 2D finite element studies.

7.3.2 Diaphragm Wall Movements Induced by Excavations

The field observations from the inclinometers revealed that the cantilever pattern developed after the first excavation stage. As the excavation proceeded to a greater depth, the D-wall showed braced excavation patterns with a bulge in the first stiff clay layer. A similar trend was reported in the literature when the diaphragm wall behaviour was induced by a deep excavation in the soft ground (the top-down excavation in Taipei) (Ou *et al.*, 1993), and the bottom-up excavation in Singapore (Lee *et al.*, 1998). Figure 7.10 shows the four stages of the diaphragm wall movements from inclinometers 4, 6 and 8 (IN4, 6 and 8). These inclinometers were located approximately 95, 45 and 11 m from the nearest corner of the excavation box. As can be seen from Figure 7.10, a significant corner effect occurred on the short side of the excavation box; the maximum wall deflection of IN8 was reduced by half compared to IN4. In contrast, the wall movements of IN6 at all stages only showed a slight reduction (less than 15%) compared to the movements of IN4. This evidence confirms the studies of Ou and Chiou (1993), and Wong and Patron (1993), who drew similar conclusions regarding the effect of the corner, namely that it was significant up to a distance equal to or less than the excavation depth. At the Sukhumvit Station box, the excavation depth in stage 4 was 21 m. Figure 7.11 illustrates the maximum wall movements after the stage 4 excavation for all eight inclinometers. It also shows that the corner effect, along both long sides (East: IN2, 5, 7 and West: IN3, 4, 6), is relatively small compared to that of the short sides (North: IN8 and South: IN1).
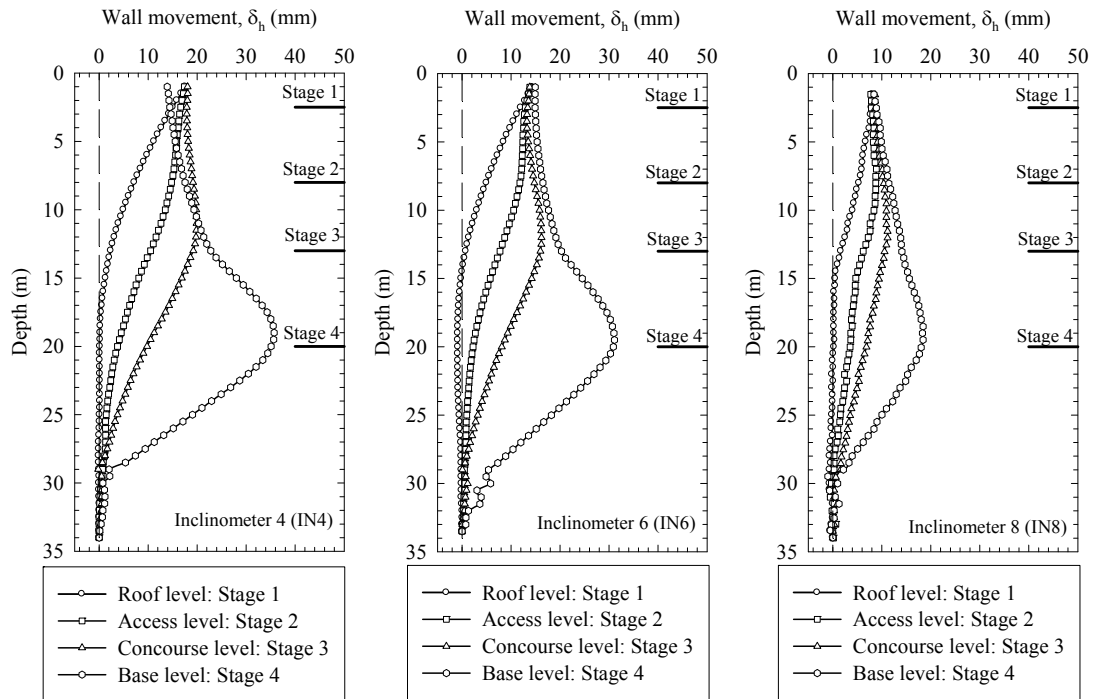
Figure 7.10: Horizontal Movement of Diaphragm Wall from Inclinometers 4, 6 and 8

Figure 7.11: Maximum Horizontal Movement of D-Wall (After Stage 4 Excavation)

The increase in the maximum wall movement, after the stage 4 excavation for all eight inclinometers is shown in Figure 7.12. The relationship between the maximum wall movement and the distance to the nearest corner is approximately linear (with some degree of scatter). A similar tendency was reported by Lee *et al.* (1998).
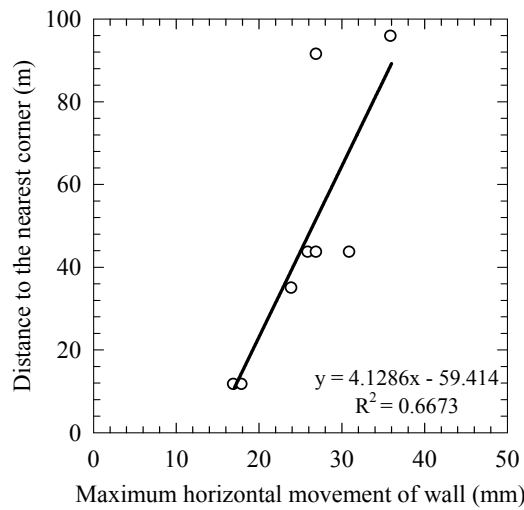
Figure 7.12: General Trend of Maximum Horizontal Movement of Wall and
Distance to the Nearest Corner

7.3.3 Relationships between Maximum Lateral Wall Deflections and Maximum Surface Settlements

Prior to the surface settlement profile predictions being obtained, successive estimations of the maximum vertical surface settlement (δ_{vm}) are required. A δ_{vm}/δ_{hm} ratio of 0.5 to 0.75 was suggested by Ou (2006) for soil conditions ranging from sandy to clayey soils. This ratio can also be extended to 1.0 in cases where the excavation occurs in very soft soil conditions.

The four MRT stations (Hua Lamphong (S1), Sirikit Centre (S6), Sukhumvit (S7) and Petchaburi (S8)). from the Bangkok MRT Blue Line South project, provided reliable field measurements, and so were used to validate the concept of empirically relating the maximum surface settlements to the maximum wall deflections. For stations S6 to S8, four excavation stages were conducted. Only three excavation stages were applied at station S1. The details for the station dimensions, final excavation depths, and diaphragm wall lengths are given in Table 3.2 (Chapter 3). The excavation depths for each stage are presented in Table 7.2. All four stations encountered similar soil conditions, as shown in

Figure 3.14 (Chapter 3). Figure 7.13 (a) shows the normalised maximum surface settlement versus the normalised wall deflection from the four Bangkok MRT subway station excavations. The data from all stages are plotted together in this figure.

Table 7.2: Summary of Stage Construction Excavation Depth
(Stations S1, S6, S7 and S8)

Station	Excavation depth below ground surface (m)			
	Stage 1	Stage 2	Stage 3	Stage 4
Hua Lamphong (S1)	2.9	8.0	15.5	-
Sirikit Centre (S6)	3.7	10.8	16.3	23.6
Sukhumvit (S7)	2.6	7.8	13.3	20.9
Phetchaburi (S8)	4.0	9.3	14.8	22.4

(a)   (b)
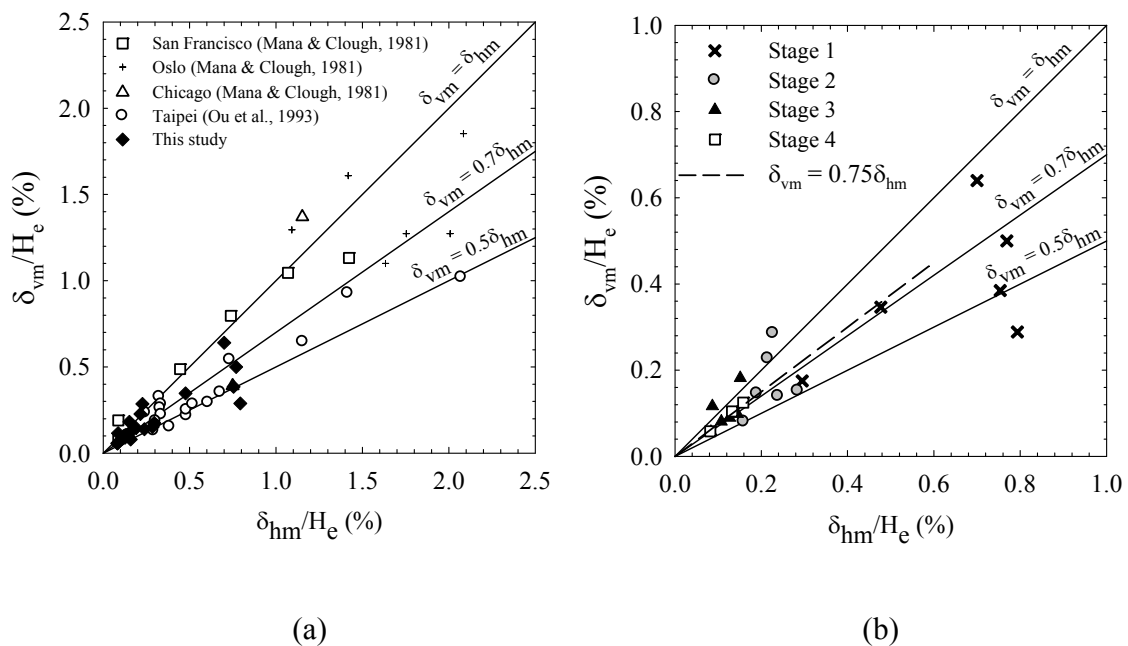
Figure 7.13: Maximum Lateral Wall Deflection and Maximum Surface Settlement

The normalised data from the literature (Mana and Clough, 1981; Ou *et al.*, 1993) are also plotted to enhance the comparison. According to Figure 7.13 (a), the following can be observed. First, both the maximum surface settlement and the lateral wall deflection

from the Bangkok case studies are less than one per cent of their excavation depth (H_e). These values are much smaller when compared to the case studies of 1981; these percentages ranged from 1 to 2.5 per cent. The data points from excavations in Taipei (from 1993), are scattered between the two. Thus, it can be stated that the general trend of both the wall movement and the ground surface settlement reduce as newer and more advanced excavating techniques become available. The second observation comes from Figure 7.13 (b), where only the data from the four subway stations are presented in a larger scale plot. The data from the stage 1 excavation shows that the wall deflections are cantilevered and the excavation depth is shallow. Further, a higher percentage of wall movement and ground surface settlement is exhibited in comparison to the deep inward movement observed in stages 2, 3 and 4. The third observation indicates that the majority of the data, especially from stages 2 to 4, have δ_{vm}/δ_{hm} ratios that agree well with the recommendations of Ou *et al.* (1993) and Ou (2006). Further, in relation to the movements at the final stage, a δ_{vm}/δ_{hm} ratio of 0.75 gives a reasonable agreement for the Bangkok MRT case studies. The fourth confirms a similar finding to that of the case studies from Oslo, Chicago and San Francisco (Mana and Clough, 1981), namely that the four data points lie above the $\delta_{vm} = \delta_{hm}$ line, indicating the case of the excavation in very soft clay. Some data points from stages 2 and 3 are also located above the $\delta_{vm} = \delta_{hm}$ line.

7.3.4 Ground Surface Settlements Induced by Excavations

The empirical methods for the surface settlement estimation, as described in Section 7.2 (Clough and O'Rourke, 1990; Hsieh and Ou, 1998; Ou and Hsieh, 2000), are presented in this section. The predicted settlement profiles are compared with the surface settlement from the settlement array (SS1). The width of the settlement envelope from Clough and O'Rourke (1990), and the width of Primary Influence Zone (PIZ) from Hsieh and Ou (1998), are both equal to $2H_e$. Ou and Hsieh (2000), on the other hand, take into account the location of the hard stratum in calculating the width of the PIZ. Thus, from the Sukhumvit Station soil profile, a Hard Clay layer can be taken as a hard stratum and, therefore, the depth to the hard stratum (H_g) would be 26.5 m. Nevertheless, the field measurements at a number of locations indicated that the toe of the diaphragm wall,

embedded in Hard Clay layer, had moved. Thus, a "kick-in" failure is presumed to have occurred. Hence, the Dense Sand below the Hard Clay layer should be treated as a hard stratum. If this is the case, then the width of the PIZ, calculated from Hsieh and Ou (1998), is also equal to $2H_e$. Further, the maximum surface settlement (δ_{vm}) for all three methods is estimated by correlating them with the maximum lateral wall deflection (δ_{hm}). The δ_{vm}/δ_{hm} ratio of 0.75, as discussed in the previous section, is adopted.

Figure 7.14 compares the measured and calculated ground surface settlement at the Sukhumvit Station. All three empirical methods exhibit similar surface settlement envelopes, and are also in good agreement with the field measurements. However, one exception is that, the Clough and O'Rourke (1990) method cannot predict the surface settlement in the Secondary Influence Zone (SIZ). Additionally, the field surface settlements did not appear to extend far enough from the wall to enable the measurement of the surface settlement in the SIZ. As a result, the findings from the further studies on surface settlements, using finite element analysis, will be compared with both the field measurements (within PIZ) and the predicted surface settlement envelope from the empirical estimation (within SIZ).
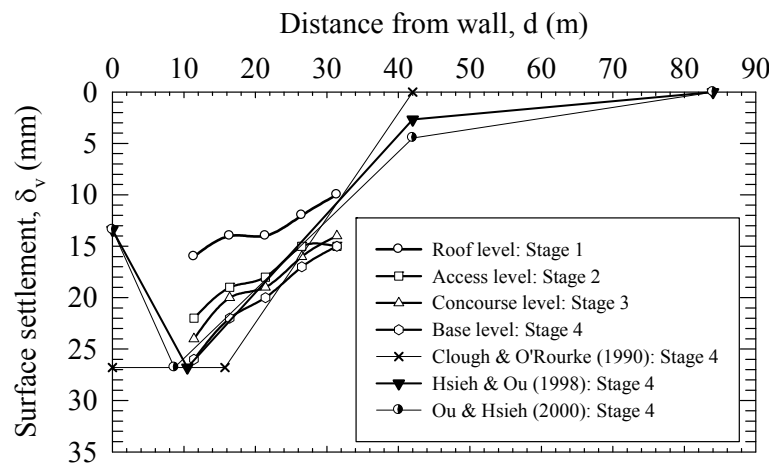
Figure 7.14: Comparison between Measured and Predicted Surface Settlements

7.4 Finite Element Analysis of Sukhumvit Station

When constructing deep excavation projects in urban environments, the major concerns are the deflection of the supporting system (i.e. diaphragm wall, sheet pile, etc.) and the associated ground movement. A number of researchers (Finno and Harahap, 1991; Ng, 1992; Whittle *et al.*, 1993) have conducted finite element analyses of deep excavation problems for a few decades. As a result, it appears that the diaphragm wall movements can be predicted with good accuracy, especially if the representative constitutive models and the geotechnical parameters are adopted with appropriate construction procedures.

The 2D plane strain finite analysis approach, using Plaxis v.9 software, was adopted in this study. As the ratio of the length (*L*) to width (*B*) of Sukhumvit Station box was high (*L/B* = 8.7), the 3D effect along the long sides of the station (see Figure 7.7) was small, thus the 2D plane strain approach was considered appropriate. Only the right half of the station box (at the cross section of IN4 and IN5) was modelled because the station configuration was symmetric. A seven-layer soil profile (as shown in Figure 7.8) was adopted. Importantly, four soil models (Mohr-Column Model (MCM), Soft Soil Model (SSM), Hardening Soil Model (HSM) and Hardening Soil Model with Small-Strain Stiffness (HSS)) were used to evaluate their performances in deep excavation modelling. All soil layers were modelled using the 15 - node elements. For the structural components (i.e. diaphragm wall, platform and base slab, column and pile), the non - volume plate elements were used. The stiffness of the concrete was reduced by 20 per cent to take into account the possibility of cracking. Table 7.3 presents the input parameters for the structural components.

Table 7.3: Input Parameters for Structure Components

Parameter	Diaphragm wall (1 m thickness)	Platform slab (1 m thickness)	Base slab (1.8 m thickness)
Axial stiffness, EA (MN/m)	28000	28000	50400
Flexural rigidity, EI (MN/m^2/m)	2333	2333	13608
Weight, w (kN/m^2)	16.5	25	45
Poisson ratio, ν'	0.15	0.15	0.15

Table 7.3 (con't): Input Parameters for Structure Elements

Parameter	Column (0.8 m dia. @ 11.4 spacing)	Pile (1.8 m dia. @ 11.4 m spacing)
Axial stiffness, EA (MN/m)	1712	3852
Flexural rigidity, EI (MN/m^2/m)	91.3	1040
Weight, w (kN/m^2)	25	25
Poisson ratio, ν'	0.15	0.15

7.4.1 Effect of Mesh Refinement

Prior to the study on the soil constitutive models, it was decided to clarify the effect of the mesh refinement on the finite element model constructed. The finite element models and their mesh generation are shown in Figures 7.15 and 7.16. The model in Figure 7.15 has an average element size of 2.53 m and a total element number of 649. A finer mesh generation was adopted in the model (as shown in Figure 7.16), with an average mesh size of 1.42 m and a total of 2054 elements. Both models were initially analysed using the same soil and structure component parameters. The Hardening Soil Model was used for all the layers. The predicted lateral wall movements and the ground surface settlements in Figure 7.17 reveal the almost identical wall movement profiles and surface settlement envelopes from both models. For this reason, only the model with 649 elements was considered to be sufficient for the analysis.
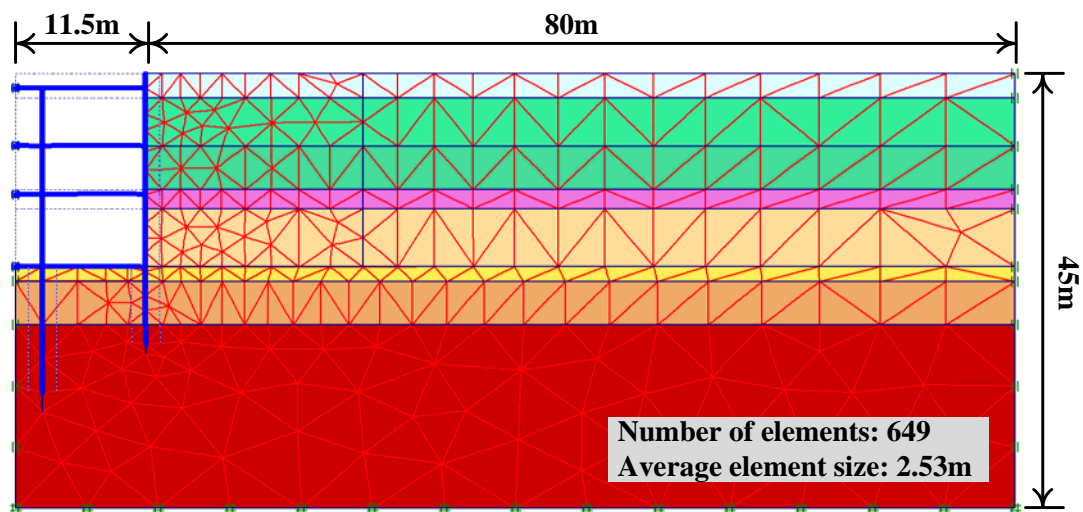
Figure 7.15: Finite Element Model and Mesh Generation (649 elements)
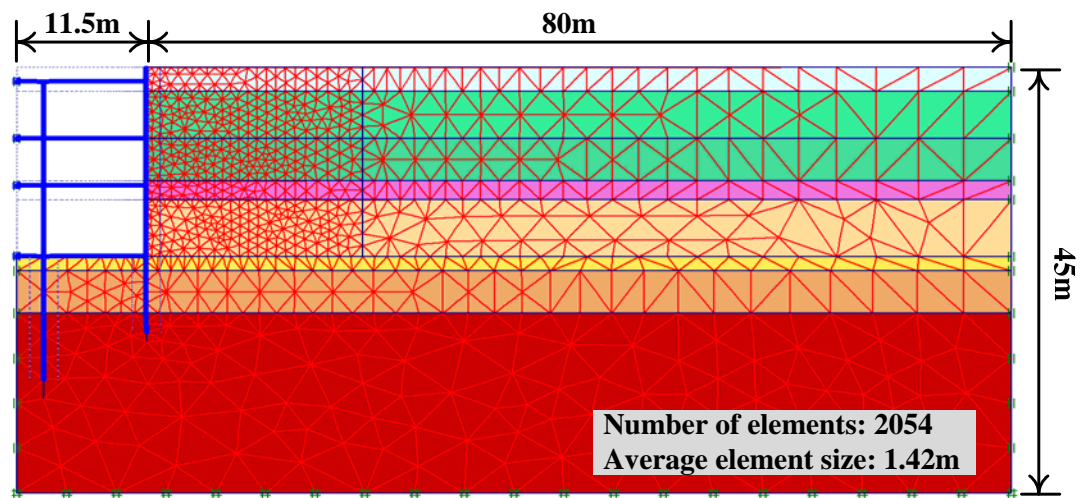
Figure 7.16: Finite Element Model and Mesh Generation (2054 elements)
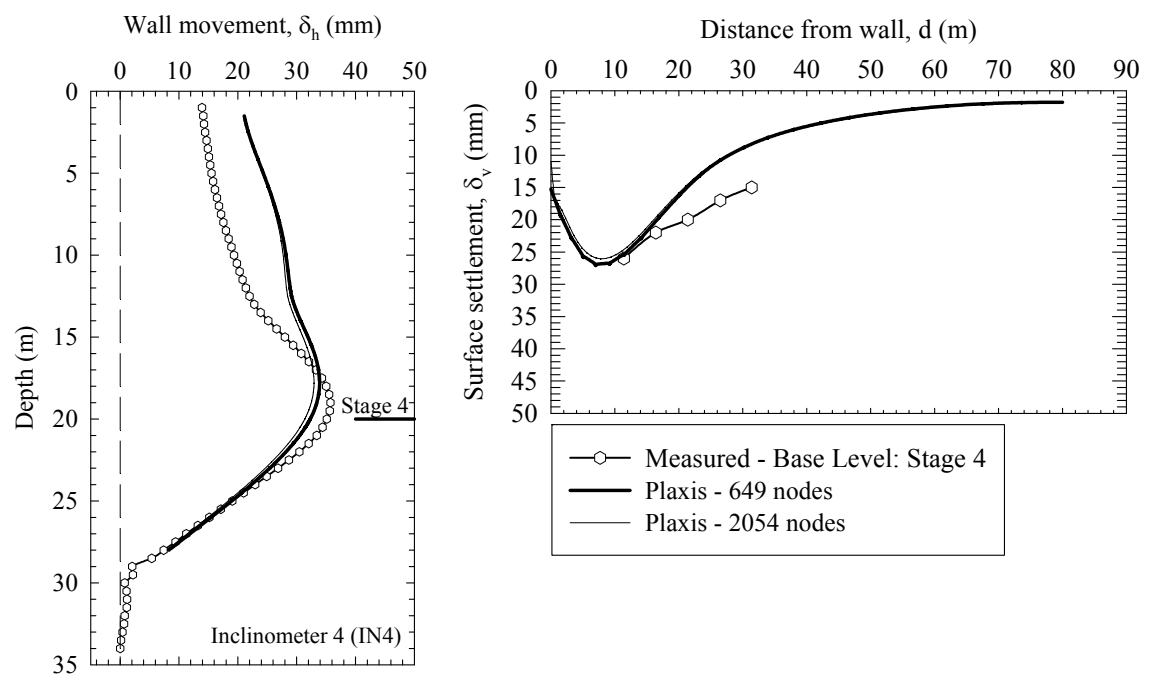
Figure 7.17: Comparison of Finite Element

7.4.2 Effect of Initial Pore Water Pressure (Drawdown and Hydrostatic)

As the pore water pressure in the Bangkok area is not hydrostatic, due to the effect of deep well pumping. More detailed pore water pressure conditions were given in Section 3.3.2). To investigate the effect of the initial pore water pressure condition in the finite element modelling, two analyses were conducted. The first applied a drawdown pore water pressure profile, while the second assumed a hydrostatic pore water pressure. The ground water level was set at 2.0 m below the ground surface. Figure 7.18 depicts the drawdown and hydrostatic pore water profiles generated by Plaxis. In a similar manner to the mesh refinement effect study, the all soil parameters, structure element parameters, number of elements in the model were kept the same for both analyses. Only the initial pore water pressure was changed to fit the conditions described.
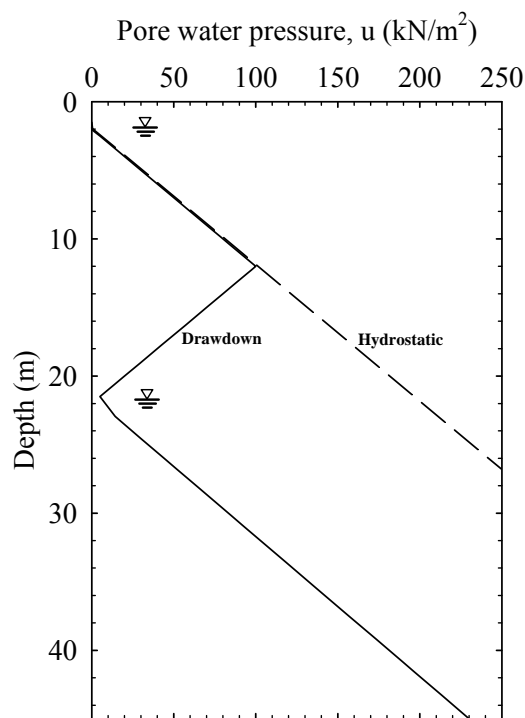
Figure 7.18: Hydrostatic and Drawdown Pore Water Pressure

The results of the finite element analyses, with drawdown and hydrostatic pore water pressure conditions, are shown in Figure 7.19. For both the maximum lateral wall movement and the maximum surface settlement, the hydrostatic case prediction was two times higher than the corresponding field measurements. The drawdown case seems to give a reasonable agreement, especially for the peak values. More importantly, at the toe of diaphragm wall, the lateral wall movement from the hydrostatic case was nearly three times the values indicated by the inclinometer. This outcome shows a high degree of instability for the diaphragm wall, which did not occur on site. It is, therefore, concluded that a realistic drawdown pore water pressure is necessary for a finite element analysis in the Bangkok area. This drawdown pore water pressure can be then applied to all the analyses in the following sections.
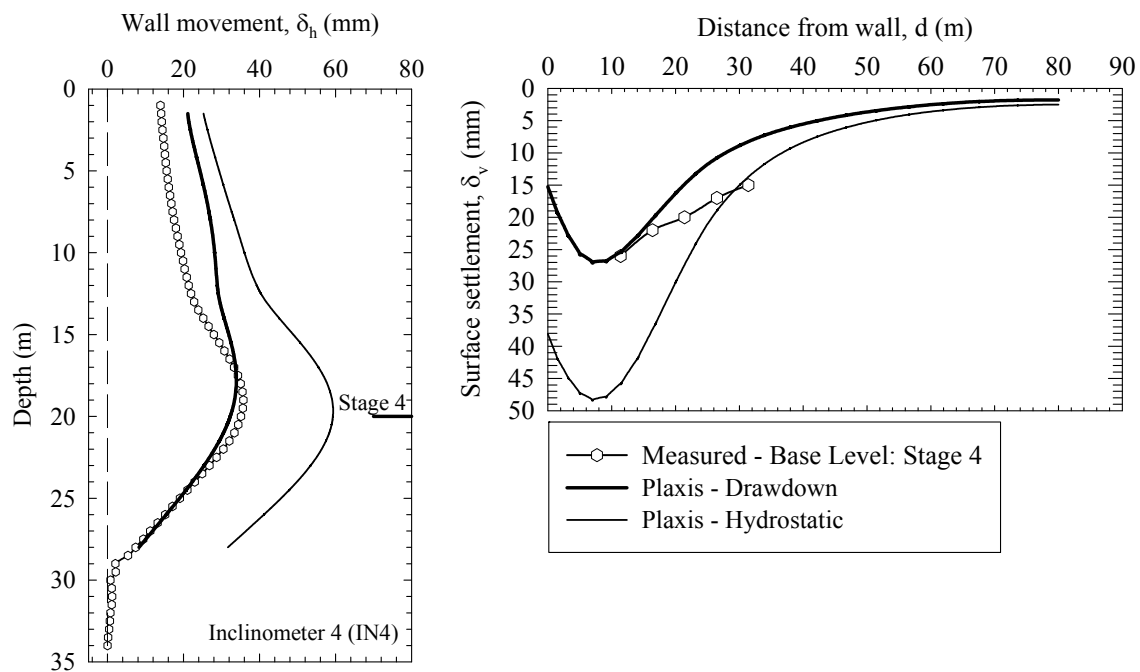
Figure 7.19: Comparison of Finite Element Predictions
from Drawdown and Hydrostatic Cases

7.4.3 Results and Discussions from Mohr Coulomb Model (MCM) Analysis

The concept of the total stress analysis ($\phi' = 0$) with the Mohr Coulomb Model (MCM) for clayey soils has been widely used in geotechnical engineering practice. One of the major advantages of this concept is that the soil parameters are easy to obtain, as only undrained shear strength (s_u) and undrained elastic modulus (E_u) are needed for the rapid loading conditions. Details of the total stress analysis for undrained materials (Method C) are given in Appendix A. The undrained shear strength of the Bangkok subsoils vane shear triaxial tests (see Chapter 4) will be used to govern the strength of the Bangkok Soft Clay (BSC), Medium Clay (MC), 1st Stiff Clay (1st SC), 2nd Stiff Clay (2nd SC), and Hard Clay (HC). Back analyses of the deep excavation problems in Bangkok subsoils (Teparaksa, *et al.* 1999; Phienwej and Gan, 2003) have shown that the E_u/s_u ratios of 500 and 1000 to 2000 give a reasonable agreement between the measured and the predicted wall movements. In the current study, E_u/s_u of 500 was adopted in the BSC, MC, 1st SC. Higher values of $E_u/s_u = 600$ and 1000 were used for the 2nd SC and HC. These values of E_u/s_u were selected based on the literatures (as mentioned above) and the relationships among E_u/s_u, OCR and I_p in Figure 4.13. The MG and CS layers were modelled with the drained analysis. Their drained moduli were estimated from the SPT N values from the adjacent boreholes. Table 7.4 summarises the parameters used in the MCM analysis.

Table 7.4: Parameters for Mohr Coulomb Model (MCM) Analysis

Layer	Soil type	Depth (m)	γ_b (kN/m^3)	E_u (MN/m^2)	E' (MN/m^2)	v_u	v'	Analysis type
1	MG	0 – 2.5	18	-	8	-	0.3	D
2a	BSC 1	2.5 – 7.5	16.5	10	-	0.495	-	UD-C
2b	BSC 2	7.5 – 12	16.5	20.5	-	0.495	-	UD-C
3	MC	12 – 14	17.5	27.5	-	0.495	-	UD-C
4	1[st]SC	14 – 20	19.5	40	-	0.495	-	UD-C
5	CS	20 – 21.5	19	-	53	-	0.25	D
6	2[nd]SC	21.5 – 26	20	72	-	0.495	-	UD-C
7	HC	26 – 45	20	240	-	0.495	-	UD-C

Table 7.4 (con't): Parameters for Mohr Coulomb Model (MCM) Analysis

Layer	Soil type	Depth (m)	s_u (kN/m^2)	ϕ' (degrees)	c' (kN/m^2)
1	MG	0 – 2.5	-	25	1
2a	BSC 1	2.5 – 7.5	20	-	-
2b	BSC 2	7.5 – 12	39	-	-
3	MC	12 – 14	55	-	-
4	1stSC	14 – 20	80	-	-
5	CS	20 – 21.5	-	27	1
6	2ndSC	21.5 – 26	120	-	-
7	HC	26 – 45	240	-	-

Figure 7.20 shows the measured and predicted lateral wall movement and ground surface settlement for the Sukhumvit Station box excavation using MCM. The ground surface settlement predicted by Hsieh and Ou (1998) at the stage 4 excavation was also included for comparison. The predictions given by the MCM analysis slightly under-predict the lateral wall movements at all stages of the excavation. The maximum lateral movement of the wall at the final excavation stage is about 15% lower that the measured value. Contrary to the lateral movement, the MCM analysis shows a much shallower and wider surface settlement profile, when compared to the field measurement and empirical prediction. The predicted maximum surface settlement at the final excavation stage was less than one half of the field measurement. Similar trends in surface settlement profiles of the MCM prediction of surface settlements were found in the literature (Kung *et al.*, 2009; Schweiger, 2009).

It should be pointed out that wider settlement envelopes, as predicted by the MCM, lead to the overprediction of the surface settlements in the Secondary Influence Zone (SIZ). Nevertheless, a flatter settlement envelope is expected to lead to less predicted differential settlements for the buildings located at the transition of the PIZ and SIZ.

Figure 7.20: Measured and Predicted Lateral Wall Movement and Surface Settlement
(MCM Analysis)

7.4.4 Results and Discussions from Soft Soil Model (SSM) Analysis

The Soft Soil Model (SSM) was modified from the Modified Cam Clay (MCC) Model.
The two main modifications were the use of Mohr Coulomb failure criteria and an
improvement in the volumetric yield surface. Parameters λ^* and κ^*, as used in the MCC,
remain the same in the SSM. Further, two additional parameters, namely v_{ur} and K_o^{nc},
were introduced. The influences of both the parameters on the triaxial (q versus ε_a, q
versus p') and the oedometer (ε_v versus log p') behaviour, resulting from the parametric
study, were discussed in Section 4.10.2. Table 7.5 presents the parameters from the SSM
analysis for the BSC, MC, 1stSC, 2ndSC and HC layers. The Hardening Soil Model
(HSM) was applied to the MG and CS layers instead of the SSM. The Cam Clay Model,
which forms the basis of the MCC and SSM models, was developed specially to simulate
the soft clay behaviour. Therefore, the SSM is not suitable for the MG and CS layers.
Also, soil movements owing to excavation of the MG and CS layers are relatively small
compared to the BSC, 1stSC and 2ndSC layers. Consequently, using the HSM instead of
the SSM in the MG and CS layers will have a negligible influence on this analysis.

268

Parameters λ^* and κ^* (see Table 7.5) were obtained from the consolidation characteristics of the Bangkok clays (identified in Section 4.5). Hence, ν_{ur} and K_o^{nc} are set according to the results of the parametric studies mentioned earlier.

Table 7.5: Parameters for Soft Soil Model (SSM) Analysis

Layer	Soil type	Depth (m)	λ^*	κ^*	ν_{ur}	K_o^{nc}
1	MG	0 – 2.5		HSM		
2	BSC	2.5 – 12	0.12	0.02	0.2	0.7
3	MC	12 – 14	0.1	0.009	0.2	0.6
4	1stSC	14 – 20	0.045	0.009	0.2	0.5
5	CS	20 – 21.5		HSM		
6	2ndSC	21.5 – 26	0.045	0.009	0.2	0.5
7	HC	26 – 45	0.006	0.0009	0.2	0.5

Note:
1. Strength parameters, ϕ' and c' and bulk unit weight for SSM analysis are the same as those of HSM analysis
2. HSM is used for Made Ground and Clayey Sand layers

The predicted lateral wall movement profiles and surface settlement envelopes were predicted from SSM analysis are shown in Figure 7.21. Further, these predicted lateral wall movements at stage 1 to 3 are fairly close to the field measurements. The maximum lateral wall movement at the final stage underpredicted, slightly, the measured values by approximately 15 % (similar to MCM predictions). In terms of the ground surface settlement predictions, the SSM gave better trends for the settlement envelope compared to the MCM. Nevertheless, the same general trend of shallower and wider settlement envelopes was observed.
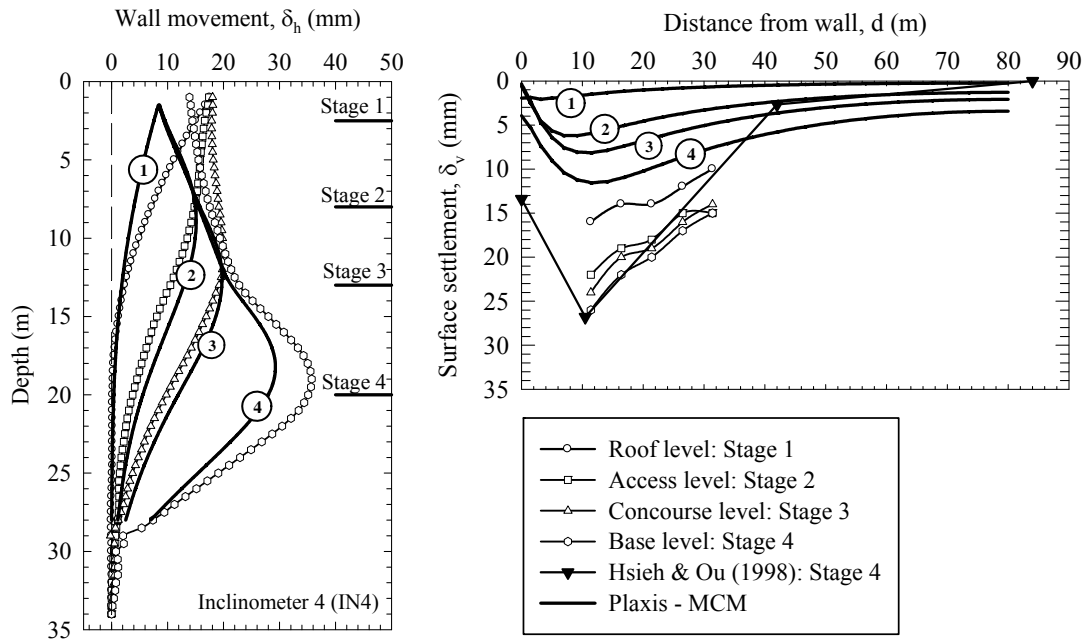
Figure 7.21: Measured and Predicted Lateral Wall Movement and Surface Settlement (SSM Analysis)

7.4.5 Results and Discussions from Hardening Soil Model (HSM) Analysis

This section presents an overview of the results and discussions for the HSM analysis. The strength and stiffness parameters are used as inputs for the HSM (see extensive discussion in Chapter 4). The input parameters listed in Table 7.6 are the results of the parametric studies and the undrained triaxial test series back-calculations. More specifically, the following procedure is adopted.

(a) The E_{50}^{ref} used in the analyses of drained materials (MG and CS) is estimated from SPT N values of adjacent boreholes. The ratios of $E_{oed}^{ref} = E_{50}^{ref}$ and $E_{ur}^{ref} = 3 E_{50}^{ref}$ were suggested by Brinkgreve (2002).

(b) For BSC, MC, 1st SC, 2ndSC and HC, the procedure of triaxial and oedometer modelling of Section 4.9 are adopted. The CIU triaxial and oedometer tests results from the samples taken from adjacent boreholes were used in stiffness moduli back-calculation.

(c) The parameters υ_{ur}, m and R_f were kept as 0.2, 1 and 0.9, respectively. These values were suggested in Section 4.10.

Table 7.6: Parameters for Hardening Soil Model (HSM) Analysis

Layer	Soil type	Depth (m)	γ_b (kN/m^3)	E_{50}^{ref} (MN/m^2)	E_{oed}^{ref} (MN/m^2)	E_{ur}^{ref} (MN/m^2)	Analysis type
1	MG	0 – 2.5	18	45.6	45.6	136.8	D
2	BSC	2.5 – 12	16.5	0.8	0.85	8.0	UD
3	MC	12 – 14	17.5	1.65	1.65	5.4	UD
4	1stSC	14 – 20	19.5	8.5	9.0	30.0	UD
5	CS	20 – 21.5	19	38.0	38.0	115.0	D
6	2ndSC	21.5 – 26	20	8.5	9.0	30.0	UD
7	HC	26 – 45	20	30.0	30.0	120.0	UD

Table 7.6(con't): Parameters for Hardening Soil Model (HSM) Analysis

Layer	Soil type	ϕ' (degrees)	c' (kN/m^2)	v_{ur}	m	K_o^{nc}	R_f
1	MG	25	1	0.2	1	0.58	0.9
2	BSC	23	1	0.2	1	0.7	0.9
3	MC	25	10	0.2	1	0.6	0.9
4	1stSC	26	25	0.2	1	0.5	0.9
5	CS	27	1	0.2	0.5	0.55	0.9
6	2ndSC	26	25	0.2	1	0.5	0.9
7	HC	24	40	0.2	1	0.5	0.9

Figure 7.22 compares the measured lateral wall movement and the ground surface settlement with those predicted by the HSM. The predicted lateral wall movements at all excavation stages within the BSC layer (2.5 to 12 m depth) were slightly higher than the field measurements. This overestimation extends further into the deeper layers for the excavation stages 1 to 3. The maximum lateral movement in the last excavation stage (located in 1st and 2nd SC layers) agrees well with the measured values. In the case of the ground surface settlement comparison, the HSM predicted better settlement envelopes compared to those predicted by the MCM and SSM. However, the settlements within the SIZ were still slightly larger than the predictions using the Hsieh and Ou (1998) method.
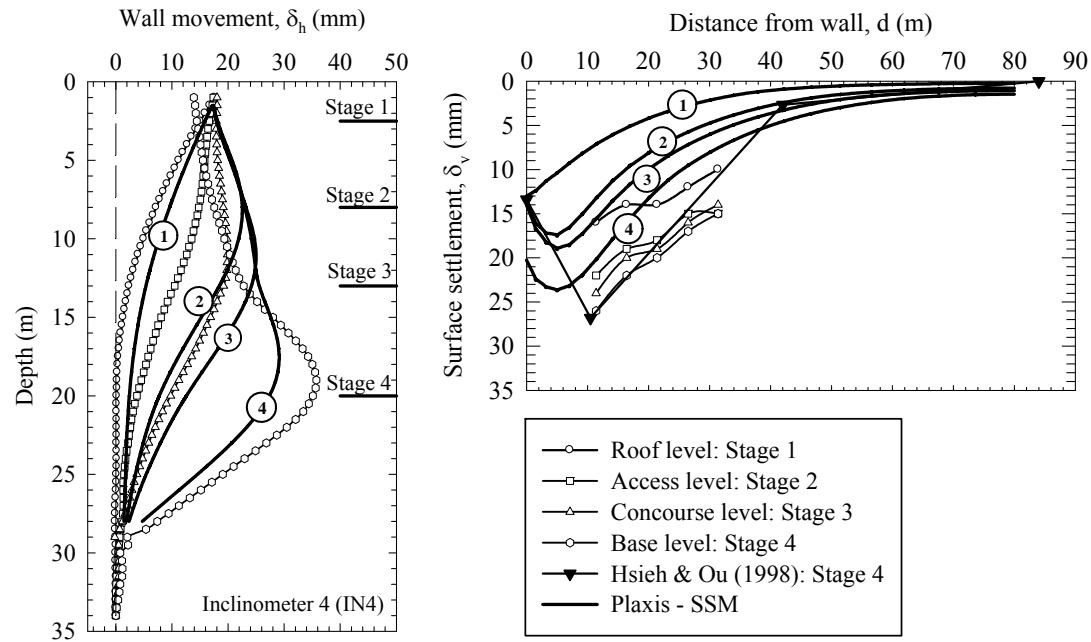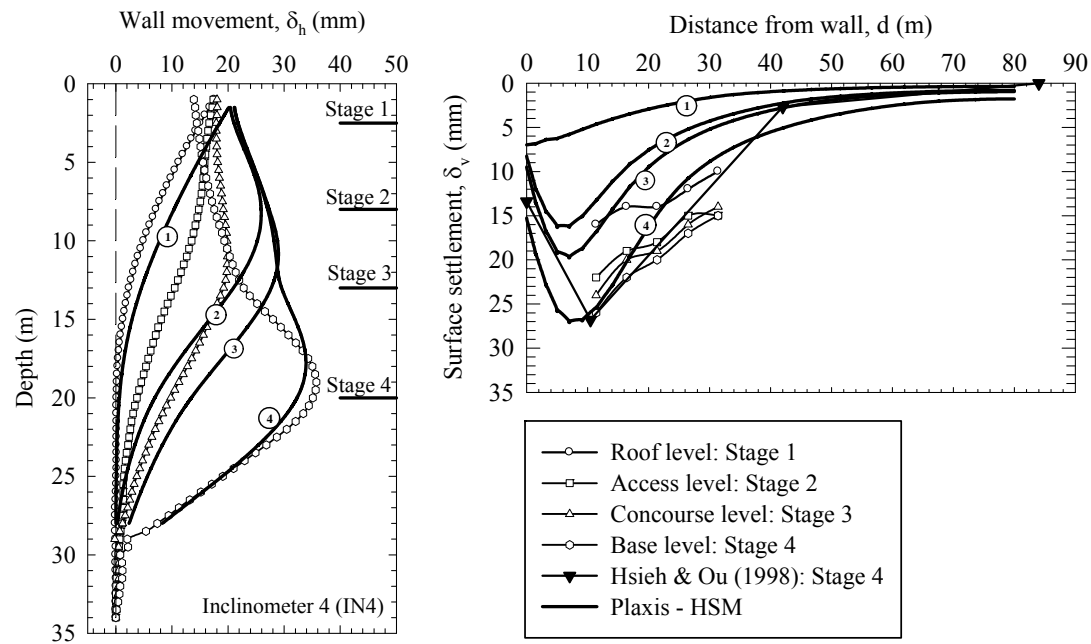
Figure 7.22: Measured and Predicted Lateral Wall Movement and Surface Settlement (HSM Analysis)

7.4.6 Results and Discussions from Hardening Soil Model with Small-Strain Stiffness (HSS) Analysis

The Hardening Soil Model with Small-Strain Stiffness (HSS) is a modification of the Hardening Soil Model, incorporating the small strain stiffness of soils. Two additional parameters, namely the small strain shear modulus (G_{max}) and the reference shear strain, where $G = 0.7G_{max}$ ($\gamma_{0.7}$), are utilised to govern the soil stiffness at a small strain level. The input parameters for the HSM, as presented in Table 7.6 above, remain the same for the HSS analysis in this section. Knowledge about the small strain parameters for the MG, SC and HC layers is very limited. Additionally, the expected soil movements arising from these layers are small in comparison to the BSC, MC, 1stSC and 2ndSC layers. Therefore, the HSM is used in the MG, CS and HC layers. The HSS is applied to the predominant layers, i.e. BSC, MC, 1st SC and 2nd SC layers.

The detailed studies of the small strain parameters, G_{max} and $\gamma_{0.7}$ of the Bangkok Clays were described in Chapter 6. The shear modulus at a small strain (G_{max}) was obtained from both the in-situ tests (down hole and seismic cone tests) and the laboratory tests (Bender element test). Hence, parameter G_{max} is considered to be reliable and is selected straight from the test results, as listed in Table 7.7. Parameter $\gamma_{0.7}$ is, on the other hand considered to have more variation. The two empirically based methods (Ishibashi and Zhang, 1993; Vucetic and Dobry, 1991) are used to calculate $\gamma_{0.7}$ of the Bangkok Clays (Figure 7.23). Both methods estimated similar results for the Bangkok Soft Clay layer, which also coincide with the Bender element tests in the Bangkok Soft Clay (Teachavorasinskul *et al.*, 2002a). The two sets of Hardening Soil Models with Small Strain Stiffness analyses (HSS 1 and HSS 2) are considered herein. For the HSS 1 analysis, the average values of $\gamma_{0.7}$ for BSC and MC layers from both the work of Ishibashi and Zhang (1993), and Vucetic and Dobry (1991) are used (see Figure 7.23).

Table 7.7: Parameters for Hardening Soil Model with Small Strain Stiffness
(HSS 1 and 2) Analyses

Layer	Soil type	Depth (m)	G_{max} (MN/m^2)	$\gamma_{0.7}$ (%) for HSS 1	$\gamma_{0.7}$ (%) for HSS 2
1	MG	0 – 2.5		HSM	
2a	BSC 1	2.5 – 7.5	7	0.056	0.056
2b	BSC 2	7.5 – 12	10	0.08	0.08
3	MC	12 – 14	12	0.09	0.09
4	1stSC	14 – 20	30	0.1	0.002
5	CS	20 – 21.5		HSM	
6	2ndSC	21.5 – 26	50	0.1	0.002
7	HC	26 – 45		HSM	

Note:
1. Strength parameters, ϕ' and c' and bulk unit weight for HSS analysis are the same as those of HSM analysis
2. HSM is used for Made Ground, Clayey Sand and Hard Clay layers
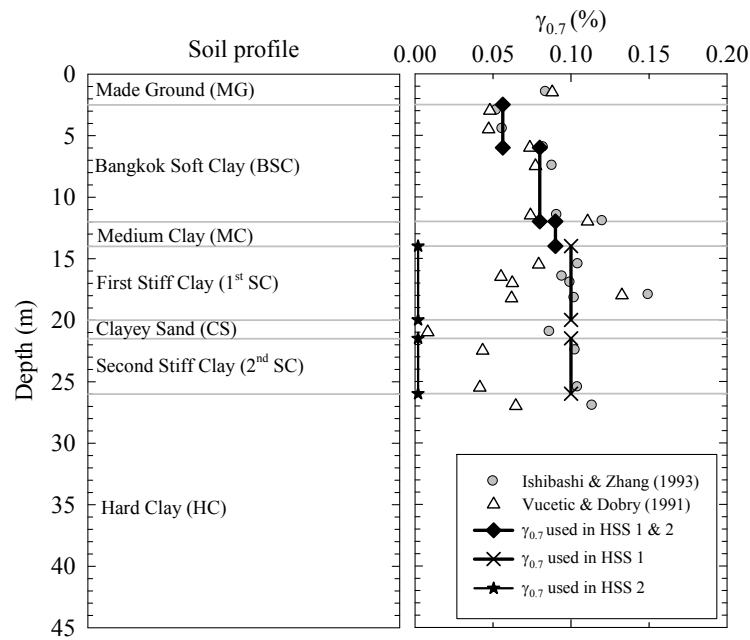
Figure 7.23: Parameter $\gamma_{0.7}$ as Used in HSS 1 and HSS 2 Models

The results from the HSS 1 analysis are shown in Figure 7.24. The HSS 1 analysis improved the lateral wall movement prediction, when compared to those predicted by the HSM for all excavation stages in the BSC and MC layers. The predictions about the deeper layers (1st SC, CS and 2nd SC) were, however, much smaller than in the HSM analysis. Indeed, the predicted maximum lateral wall movement was only one half of the measured magnitudes. The corresponding surface settlements were also underpredicted by the HSS 1 analysis. This outcome confirmed that the parameters ($\gamma_{0.7}$) calculated by Ishibashi and Zhang's (1993), and Vucetic and Dobry's (1991) methods for the BSC and MC layers are valid. However, this conclusion was not true for the Stiff Clay layers. As previously mentioned in Chapter 6, there is no information on the laboratory $\gamma_{0.7}$ available in the case Bangkok Stiff Clay. If one has a detailed look at the values of G_{max} values (Figure 6.14) of 1st SC and 2nd SC layers, a greater degree of variation, compare to that of in BSC, can be observed. This creates more variability on the analysis adopted. Therefore, it is suggested that more refined analysis would be appropriate before any definite conclusion can be made on the values of small strain stiffness of Bangkok Stiff

Clay, especially when a better set of laboratory and field data is available. For the purpose of this study, it was decided that a back fitted value of $\gamma_{0.7}$ should be adopted.

In the second HSS analysis (HSS 2), only the parameter $\gamma_{0.7}$ in the 1st SC and 2nd SC was adjusted to obtain the best fit results. The best fit value of $\gamma_{0.7}$ for both layers was obtained as 0.002 % (see also Table 7.7 and Figure 7.23). The predictions of the wall movements and the surface settlements, obtained by the HSS 2 analysis, are depicted in Figure 7.25. As far as the results in the final stage are concerned, both the predicted lateral wall movement and the surface settlement agree well with the measured data.
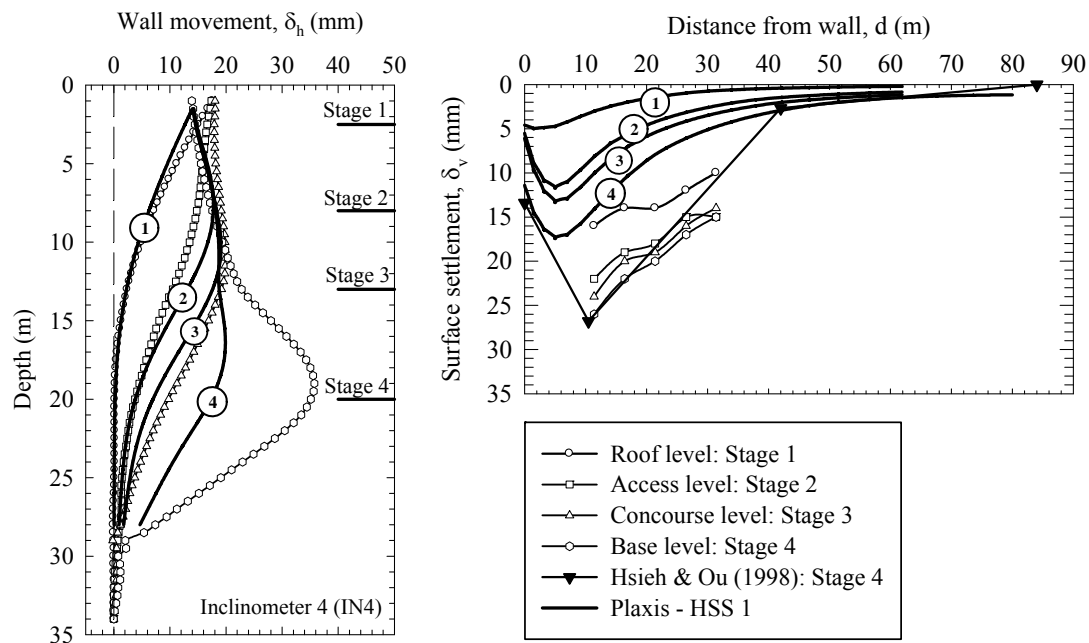
Figure 7.24: Measured and Predicted Lateral Wall Movement and Surface Settlement (HSS 1 Analysis)
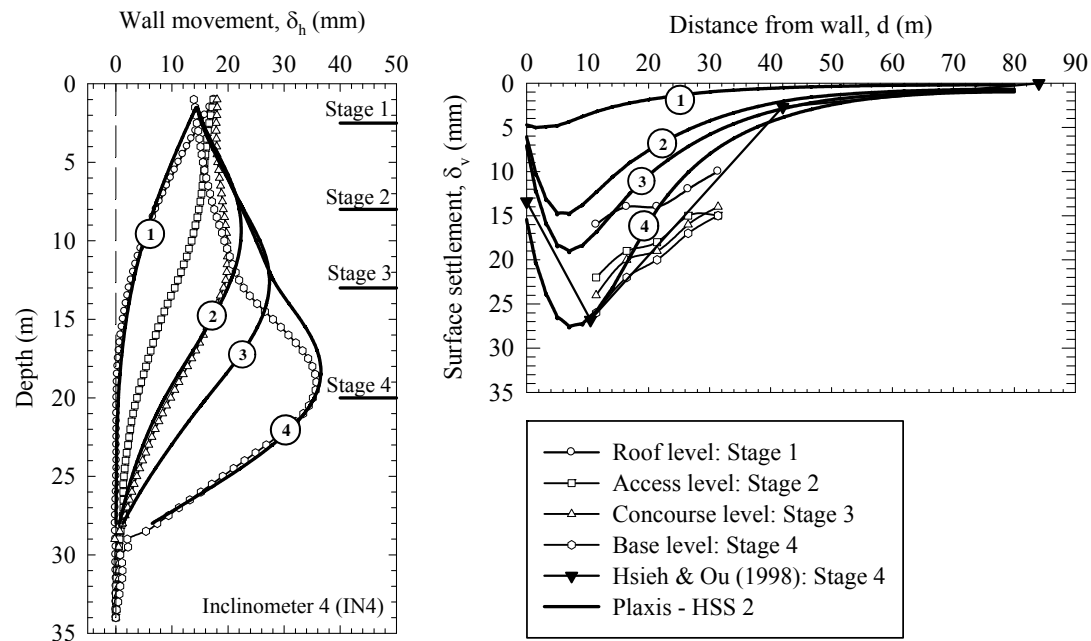
Figure 7.25: Measured and Predicted Lateral Wall Movement and Surface Settlement
(HSS 2 Analysis)

7.4.7 Comparisons of D-wall Movements and Ground Settlements for Each Construction Stage

The results from the MCM, SSM, HSM and HSS 2 analyses (in Section 7.4.3 to 7.4.6) are compared according to the stage construction in this section. Figures 7.26 to 7.29 show the measured and predicted lateral wall movements and surface settlements arising from excavation stage 1 to 4, respectively. As far as the wall movements after the first stage construction are concerned, the SSM, HSM and HSS 2 provide reasonably good predictions compared to the measured data, while the MCM give a slight underpredicted movement. The surface settlement profiles, of all four analyses, are smaller than the field measurements. The maximum surface settlements from the largest to smallest are in the following order: the SSM, HSM, HSS 2 and MCM. The same trends of the predicted wall movements and ground surface settlements are obtained from stage 2 and 3 analyses. The predicted wall movements from the SSM, HSM and HSS 2 analyses are of the same in their magnitudes. Their predictions agree with the measurements at the top part of the D-wall but slightly overpredicted the wall movements from the depth of excavation to the

lower end of D-wall. The MCM prediction is, on the other hand, well matches with the measurements at the depth of excavation. However, the MCM analysis gives smaller prediction at the top part of the D-wall. The predicted surface settlements at stage 2 and 3 from the SSM, HSM and HSS 2 analyses are nearly identical. The shapes of their predicted settlement profiles are much steeper than that of the MCM analysis. For the fourth stage of excavation, all the four models give generally good predictions of wall movements. However, the HSS 2 analysis shows the best prediction of maximum wall movement compared to the field data. For the surface settlements, the HSM and HSS 2 show nearly identical settlement profiles. Their results, at the final stage, are also agreeing with the field data. The MCM's settlement profile is much shallower and wider than the measured surface settlement. Its maximum surface settlement is lesser than half of the measured data. The settlement prediction from the SSM lies between the results of the MCM and HSM analyses.
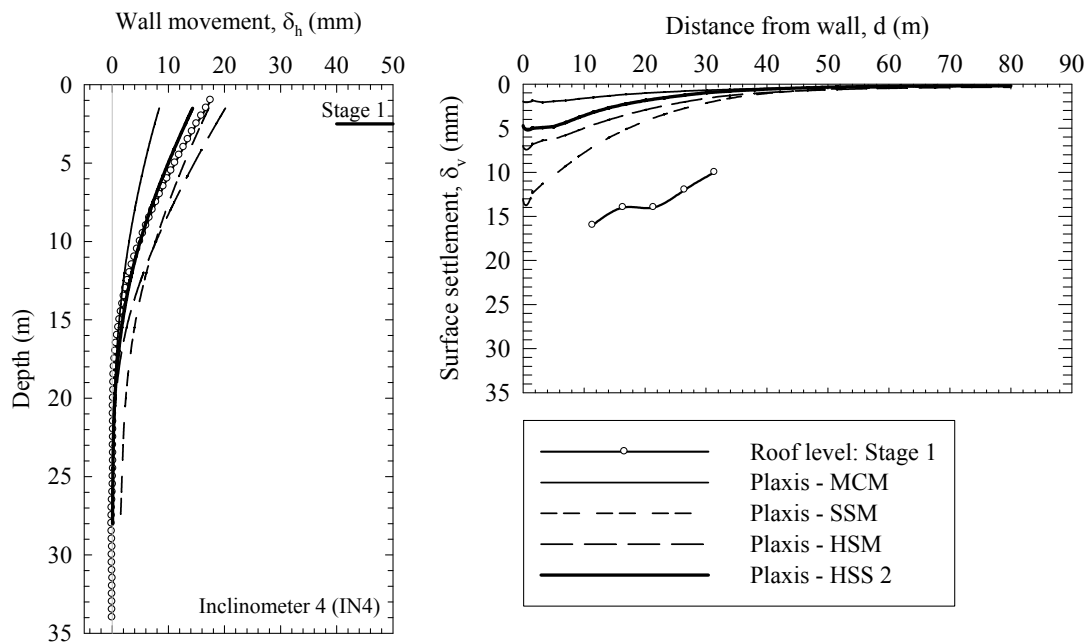
Figure 7.26: Measured and Predicted Lateral Wall Movement and Surface Settlement
(Comparison of MCM, SSM, HSM and HSS 2: Stage 1)
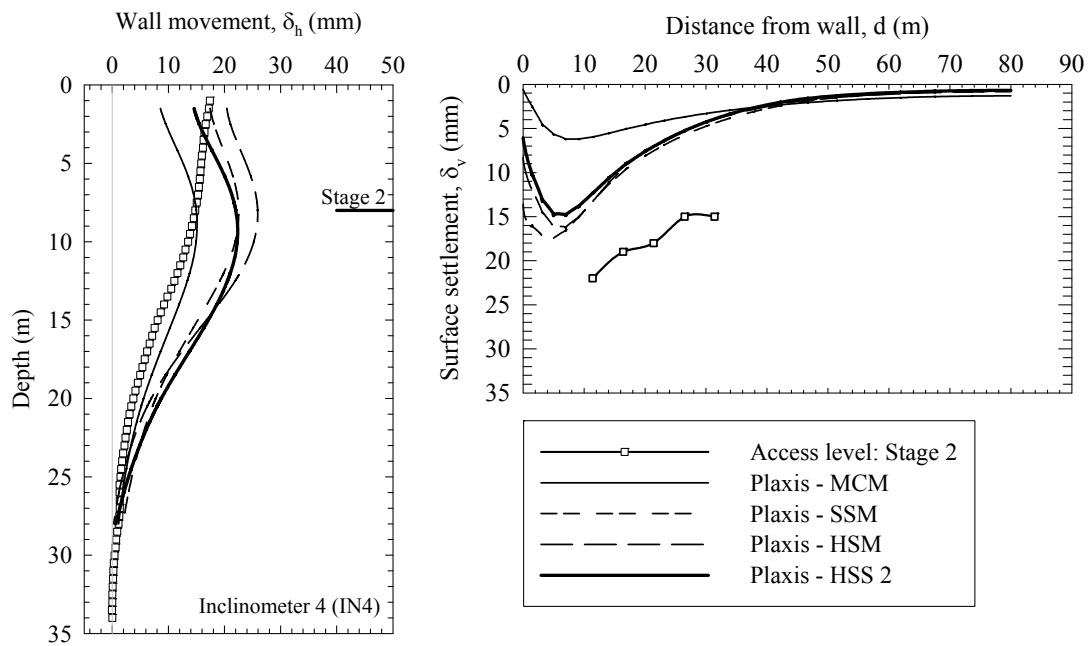
Figure 7.27: Measured and Predicted Lateral Wall Movement and Surface Settlement
(Comparison of MCM, SSM, HSM and HSS 2: Stage 2)
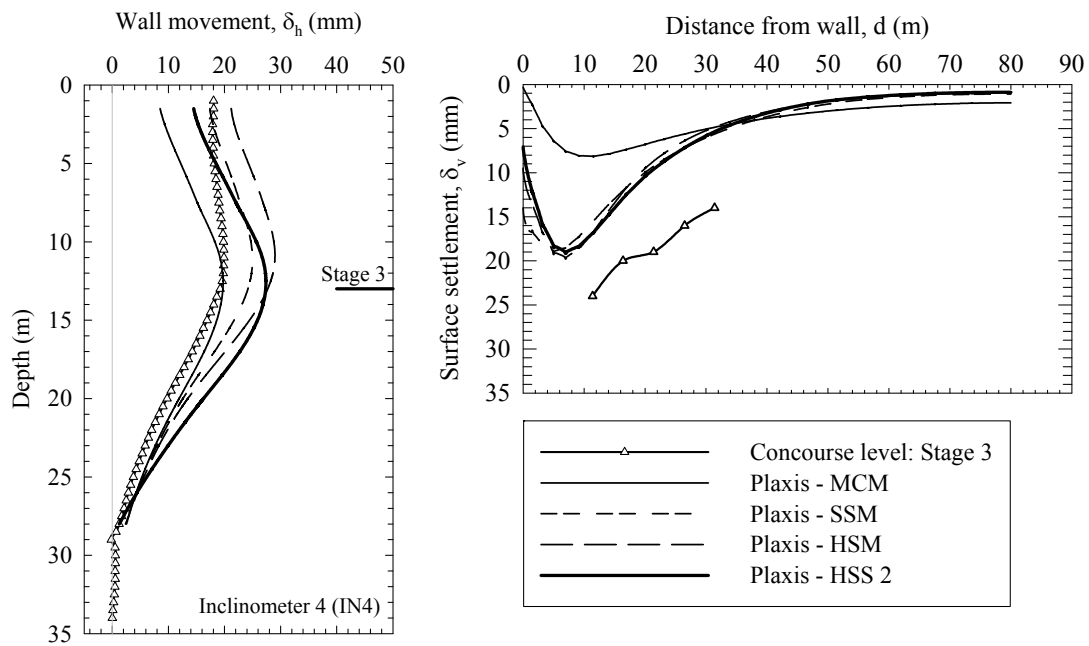
Figure 7.28: Measured and Predicted Lateral Wall Movement and Surface Settlement
(Comparison of MCM, SSM, HSM and HSS 2: Stage 3)
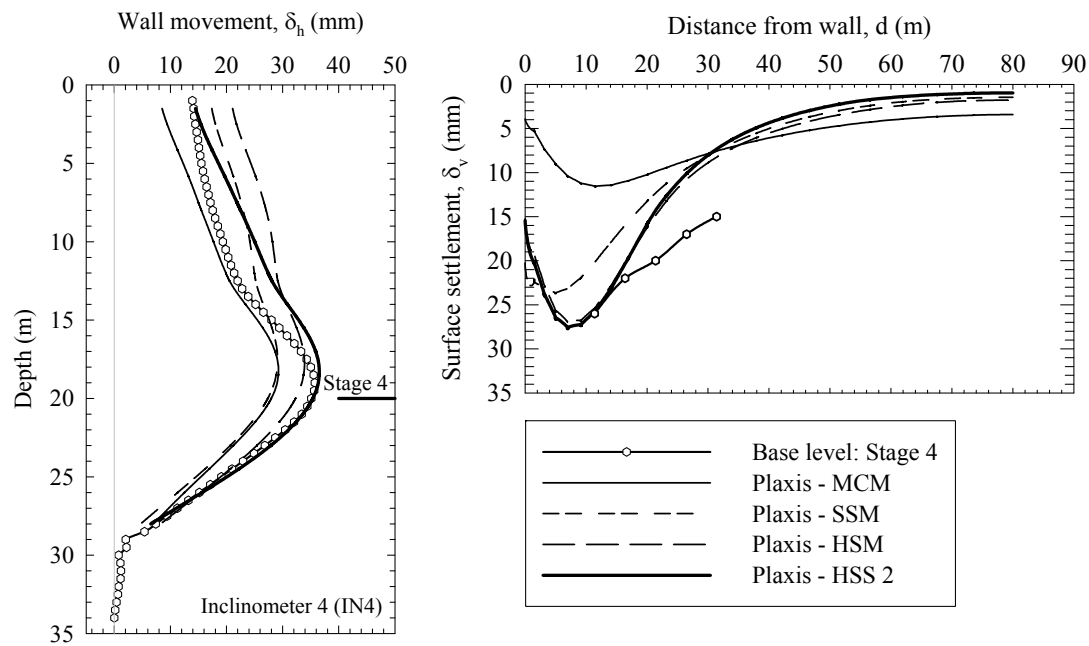
Figure 7.29: Measured and Predicted Lateral Wall Movement and Surface Settlement
(Comparison of MCM, SSM, HSM and HSS 2: Stage 4)

7.4.8 Comparisons of Axial Force, Shear Force and Bending Moment from MCM, SSM, HSM and HSS 2 Analyses

The diaphragm wall axial and shear force, and the bending moment, from the final excavation stage of the four analyses, are compared in Figure 7.30. In general, there was no significant difference. Indeed, the maximum differences of the structure forces and the bending moments among all four analyses was less than 10 per cent.
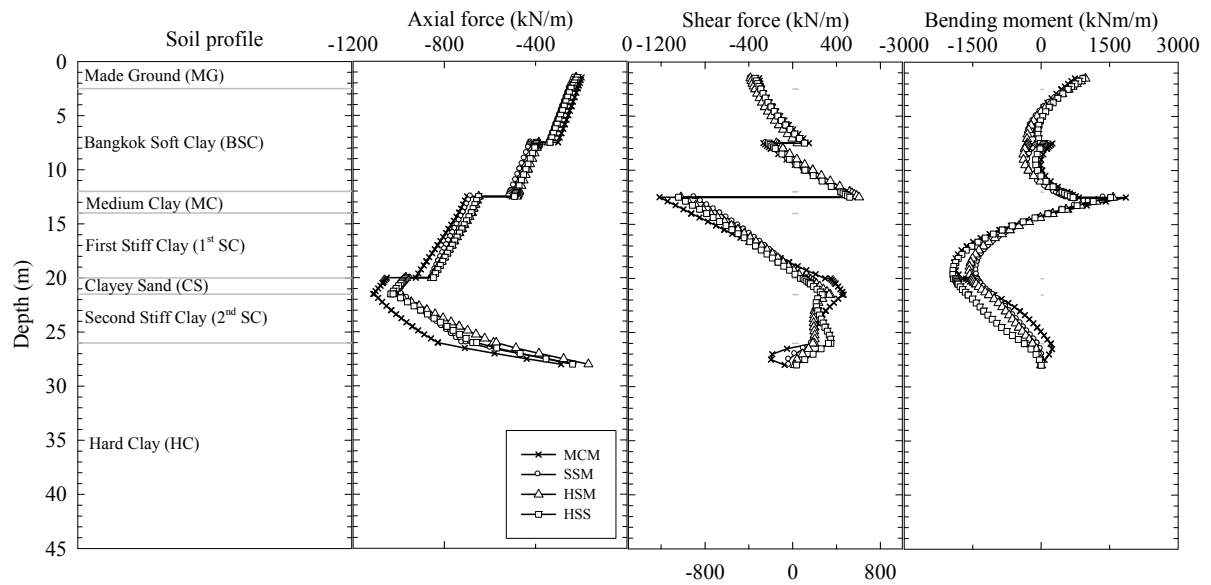
Figure 7.30: Comparisons of Axial Force, Shear Force and Bending Moment
from MCM, SSM, HSM and HSS 2 Analyses

7.5 Concluding Remarks

This chapter investigates the behaviour of D-wall movement and ground surface settlement by means of empirical and numerical analyses. Subway station excavations of Bangkok MRT Blue Line project were used as a case study. Important points based on the results of this study are summarised as follows.

(1) Inclinometer measurements from Sukhumvit Station showed that 3D effects on the long sides of D-wall are small compared to the ones from short sides. This evidence confirmed other studies on 3D effects of deep excavations (Ou and Chiou, 1993; Wong and Patron, 1993).

(2) The relationship between maximum lateral wall movements and maximum ground surface settlements agreed well with the data published in the literature. The ratio of δ_{vm}/δ_{hm} of 0.75 gave the average trend of Bangkok MRT station

excavations especially when the movements at the last excavation stage are considered.

(3) Predicted surface settlement profiles coincided with the observed data within the Primary Influence Zone. However, ground surface settlement measurements did not extend far enough to make comparison in the Secondary Influence Zone.

(4) No significant effect on both wall movement and surface settlement is observed from two finite element models with different average element sizes. In contrast, considerable differences are found from finite element analyses with hydrostatic and drawdown pore water conditions. The case of more realistic drawdown pore pressure predicted closer lateral wall movement and ground surface settlement compared to field observations.

(5) In general, better lateral wall movement and ground surface settlement are obtained from higher degrees of sophistication of constitutive models in the following order, i.e. MCM, SSM, HSM and HSS. Nonetheless, no salient differences between the results of axial forces, shear force and bending moment predictions are observed.

(6) Back-calculated E_u/s_u ratios from literatures can be used reasonably for lateral movement prediction with MCM. However, accurate ground surface settlements were not obtained.

(7) SSM and HSM analyses with soil parameters interpreted from laboratory and in-situ tests (studies from Chapter 4 and 5), provided good agreement with lateral wall movement and surface settlement field observations.

(8) Results from HSS analysis confirmed the values of $\gamma_{0.7}$ in BSC as predicted by Ishibashi and Zhang (1993) and Vucetic and Dobry (1991). In the case of stiff

clay, however, a back-calculated $\gamma_{0.7}$ of 0.002% is necessary for better lateral wall movement and surface settlement predictions.

(9) As a consequence of the study in this chapter, it can be stated that no matter what analysis or numerical method is employed, it need not necessarily give a good prediction of ground movements unless the relevant parameters are selected. In the case of the FEM, a suitable simulation process is adopted.

CHAPTER 8

Ground Settlements Induced by MRT Tunnel Excavations

8.1 Introduction

The research work, presented in this chapter in three parts, examined analytical and numerical methods for predicting ground movement induced by Mass Rapid Transit (MRT) tunnel excavations. Similar to the analyses in the previous chapter (on diaphragm wall deflection and ground settlement induced by MRT station excavations), the results from various analytical and numerical methods are compared with the field measurements. The first part of the research addresses the three analytical solutions (Verruijt and Booker, 1996; Loganathan and Poulos, 1998; Bobet, 2001) for ground movement owing to tunnelling operations. The analysis includes both the single and twin tunnel configurations. The second part involves the 2D plane stain finite element analysis of the shield tunnel. As the soil behaviour, induced by the tunnelling, is heavily

influenced by the 3D effect, the 2D plane strain methods required a number of assumptions to govern the missing third dimension. Once again, three, 2D finite element methods (the contraction method, the stress reduction method, and the modified grout pressure method) are used. The findings for the ground movements using these methods are also compared with the measured settlement profiles. The third part involves the preliminary design of the "Combined Cut-and-Cover and New Austrian Tunnelling Methods (NATM)" for the MRT station excavation. As the name implies, the finite element model of this station consists of a cut-and-cover station box with an extension of two tunnels constructed using the NATM technique. Since this station is in the design stage, the results from the finite element analysis can only be compared with the results from a simplified solution.

8.2 Analytical Computations for Shield Tunnelling

As noted above, three analytical methods are adopted (Verruijt and Booker, 1996; Loganathan and Poulos, 1998; Bobet, 2001) for eight different sections of the tunnelling. The section selection was based on the geometries of the section and the position of the tunnels. Section CS-8 (Phra Ram 9 to Phetchaburi stations) was chosen to represent the side-by-side twin tunnel, located mainly in the stiff clay layer; Section 26-001 (Lat Phrao to Ratchada stations) is selected to represent the side-by-side twin tunnel, located partly in the soft clay layer and partly in the stiff clay layer; Section 23-001 (Pracharat Bumphen to Thiam Ruam Mit stations) and 6D (Sirikit to Sukhumvit stations) were chosen for the side-by-side twin tunnel, partly located in the dense sand layer and partly in the overlying stiff clay layer; Section 7C (Sukhumvit to Phetchaburi stations) was assessed for the side-by-side tunnel, partly located in the clayey sand layer and in the stiff clay layer; and, lastly, Sections CS-2A-1 (Silom to Samyan stations), CS-3 (Lumphini to Silom stations) and 4C (Lumphini to Bon Kai stations) were chosen as the stack tunnels, located in soft clay, stiff clay and dense sand layers. The gap parameter (see Chapter 2 for details) of Lee *et al.* (1992) is adopted in the surface settlement calculations for all three

analytical methods. Their suggestion to use 10 per cent of the physical gap is also followed.

The eight sections chosen for the study cover all cases for the different locations of tunnels and their relative positions side-by-side or stacked one above the other. The results obtained from these solutions are presented in the following sections. Both the single tunnel and the twin tunnel behaviour in these selected sections are assessed.

8.2.1 Calculation of Soil Parameters for Analytical Computations

The assumption of the soil behaviour in the analysis is homogeneous; hence the equivalent homogeneous strength and stiffness parameters are evaluated, as follows.

The typical example for Section 23-001 is given below:

$$s_u = \frac{(1 \times 40) + (14 \times 30) + (9 \times 138.2) + (1.8 \times 0)}{1 + 14 + 9 + 1.8} \approx 66 \, \text{kN/m}^2$$

$$E_u = \frac{(1 \times 13.5) + (14 \times 8.9) + (9 \times 47) + (1.8 \times 0)}{1 + 14 + 9 + 1.8} \approx 22 \, \text{MN/m}^2$$

Similar calculations were conducted for all values of the soil properties; these are summarised in Table 8.1. The details of the soil profiles are presented in Figures 8.1 (a) to (h). The abbreviation SB, in the results, represents the "South Bound tunnel", while NB represents the "North Bound tunnel". These notations are applied to all the results contained in this chapter.

Table 8.1: Calculated Soil Parameters for Each Section

Sections	γ (kN/m^3)	s_u (kN/m^2)	E_u (MN/m^2)
26-001	17.7	58.8	19.1
23-001	18.3	66	21.75
CS-8	17.7	56.1	18.71
6D	18.7	70	25.28
7C	18.3	58.2	24.3
CS-3			
NB	17.6	60	18.93
SB	18.9	86.8	19.8
CS-2A-1			
NB	17.9	60.3	18.37
SB	18.7	87.2	36.8
CS-4C			
NB	17.7	56.2	18.45
SB	18.9	69.3	23.44
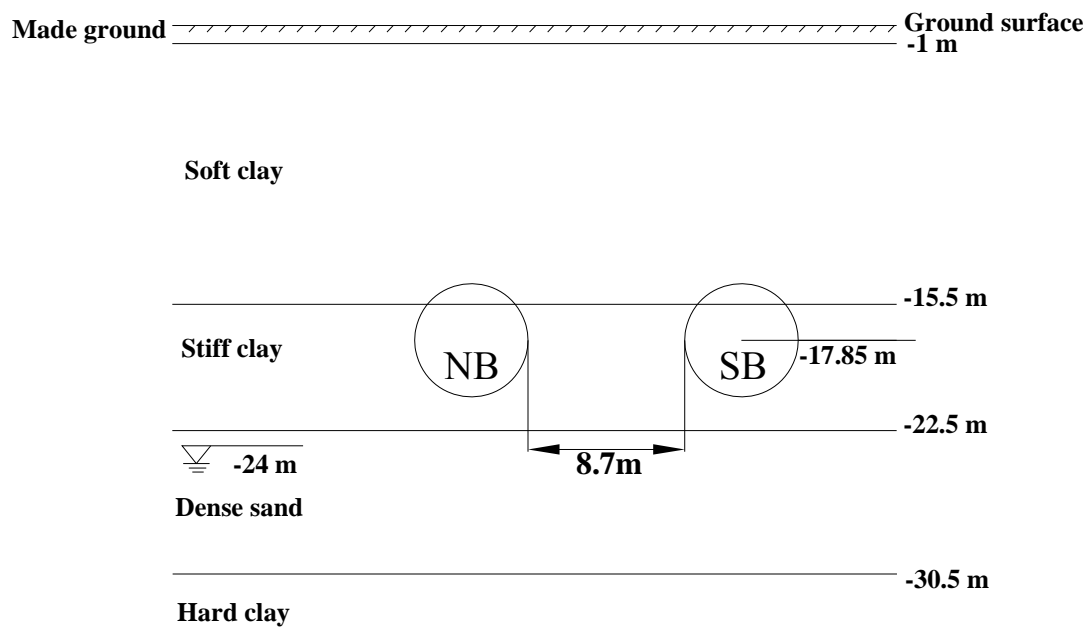
Figure 8.1 (a): Soil Profile of Section 26-001 (Ratchada to Lad Phrao)

Ground surface

Made ground /// -1 m

Soft clay

-15 m

Stiff clay

NB   SB

-22.65 m

-24 m ▽   -24 m

Dense sand

9 m

-30 m
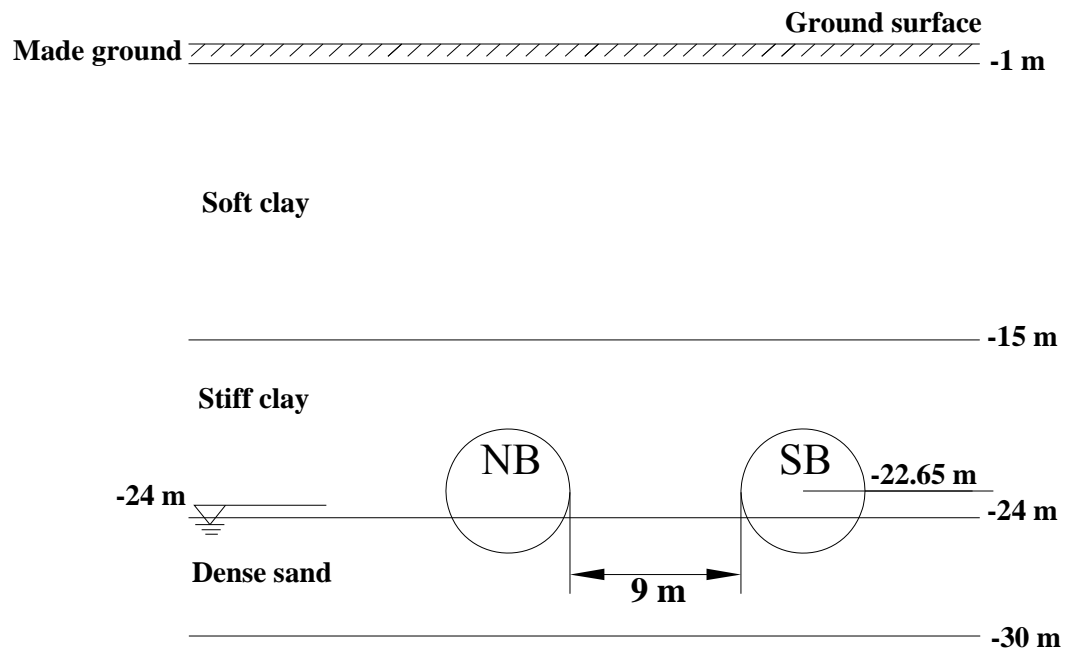
Figure 8.1 (b): Soil Profile of Section 23-001

(Thiam Ruam Mit to Pracharat Bumphen)

Ground surface

Made ground ///

-2 m

Soft clay

-14.8 m

Medium clay   -16.1 m

Stiff clay   NB   SB   -17.5 m

-21.6 m

-24 m ▽   8.7m

Hard clay

-29 m
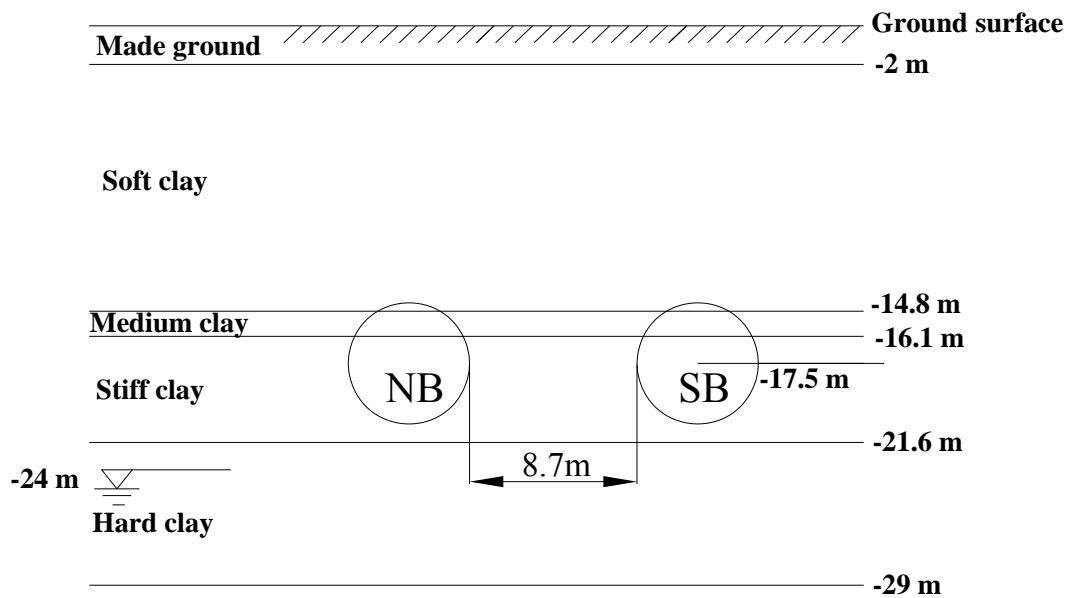
Figure 8.1 (c): Soil Profile of Section CS-8 (Petchaburi to Rama 9)

287

Made ground
Ground surface
-2.5 m

Soft clay

-12 m
Medium clay
-14 m

Stiff clay

-24 m
-23.15 m
-24 m
NB
7 m
SB
Dense sand

-30 m

Hard clay

-40 m
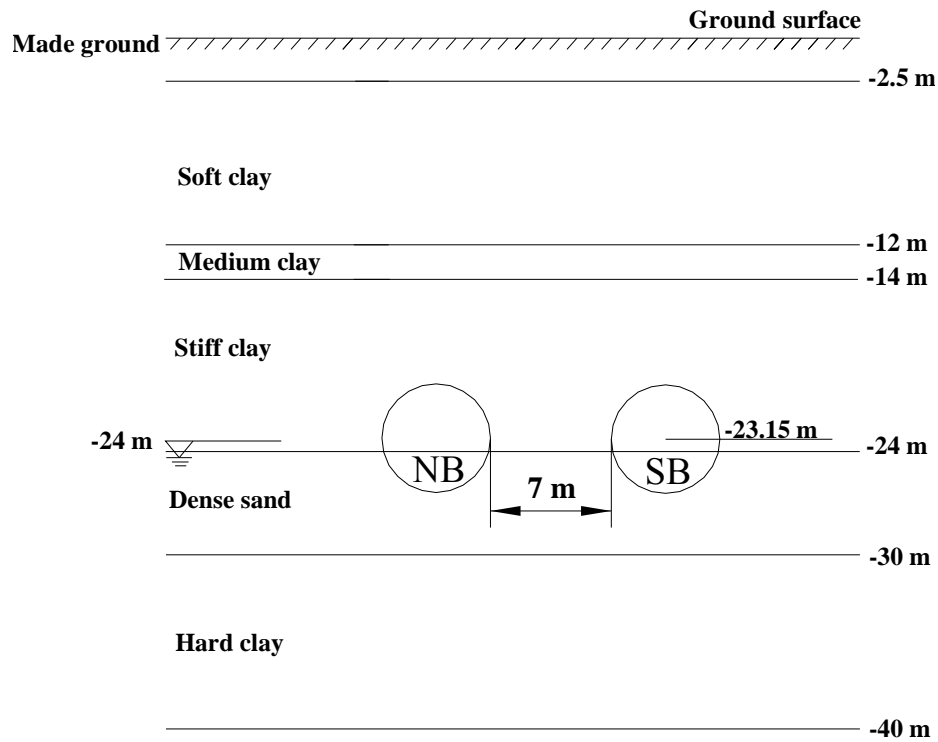
Figure 8.1 (d): Soil Profile of Section 6D (Sirikit to Sukhumvit)

Made ground
Ground surface
-2 m

Soft clay

-12 m
Medium clay
-14 m

Stiff clay

Hard clay
-19 m
-20 m
-21.15 m
Stiff clay
NB
4 m
SB
-24 m
Stiff clay

-29 m

Hard clay

-40 m
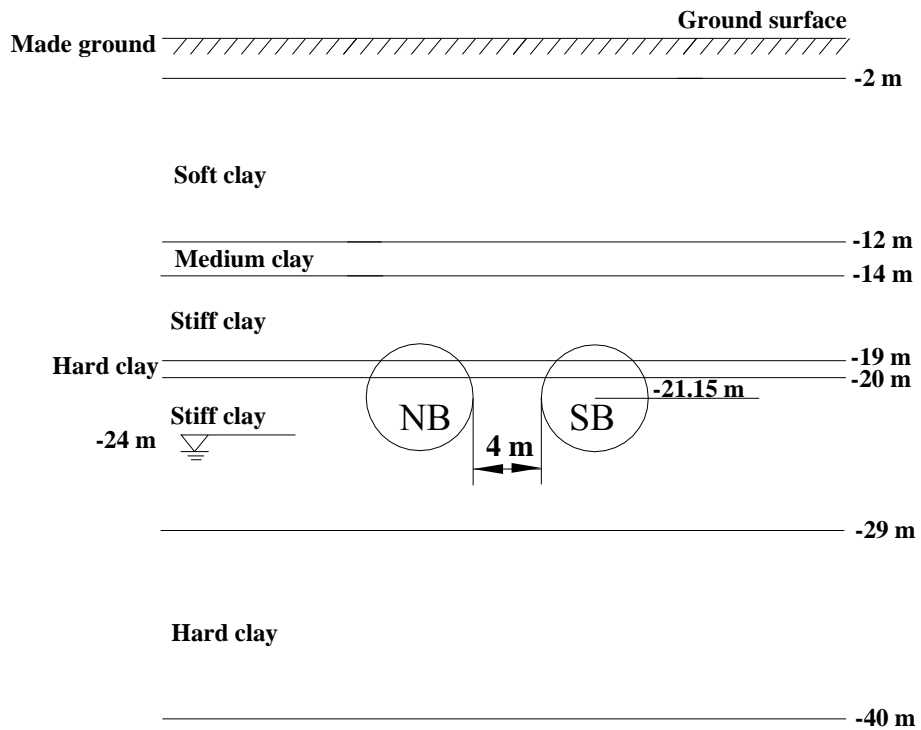
Figure 8.1 (e): Soil Profile of Section 7C (Sukhumvit to Phetchaburi)

288

Made ground

Ground surface
-1.5 m

Soft clay

-11.5 m

Medium clay

-13 m

NB -14.15 m

Stiff clay

-22 m

∇ -24 m

Dense sand

SB -26.95 m

-33 m

Hard clay
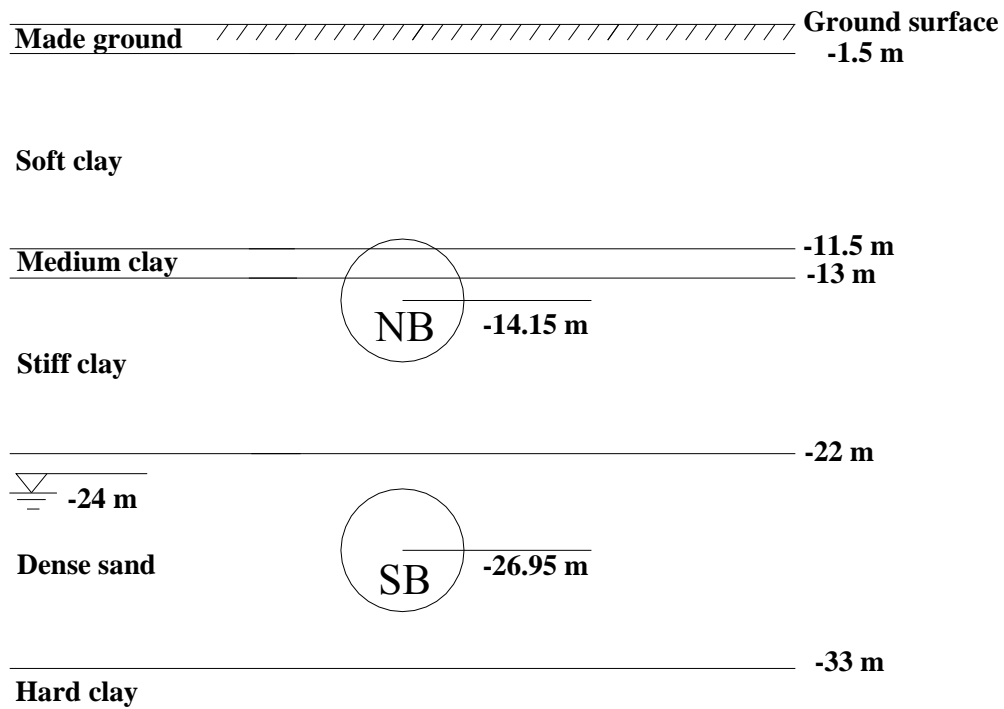
Figure 8.1 (f): Soil Profile of Section CS-3 (Silom to Lumphini)

Made ground

Ground surface
-2 m

Soft clay

-10.9 m

Medium clay

-12.7 m

NB -13.65 m

Stiff clay

-19.4 m

Sandy clay

-22.9 m

∇ -24 m

Clayey sand

SB -25.95 m

-29.9 m

Hard clay
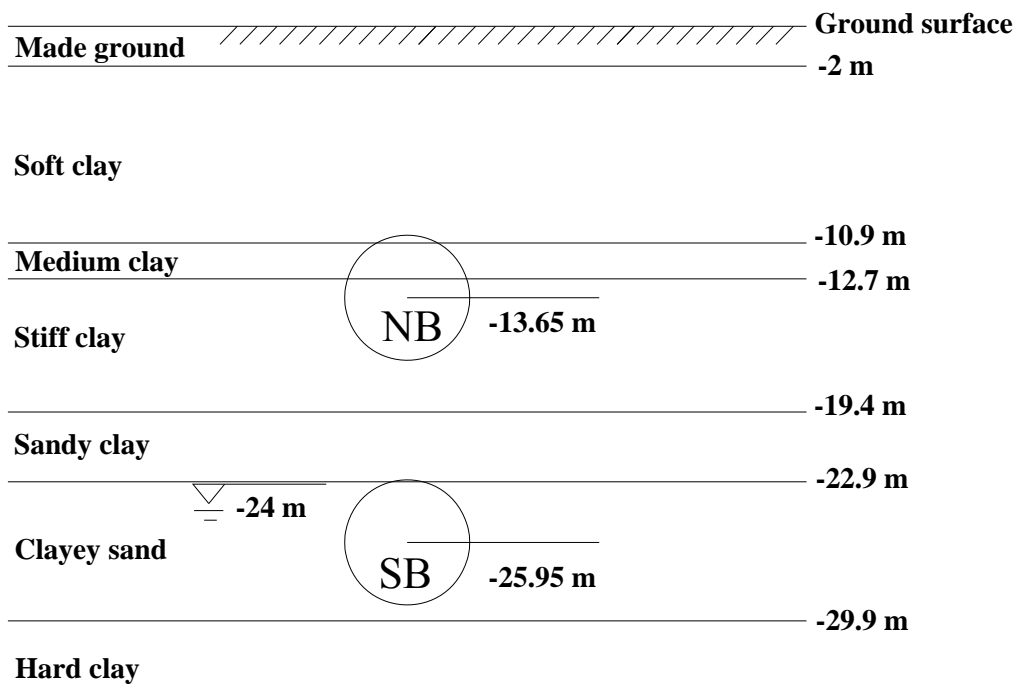
Figure 8.1 (g): Soil Profile of Section CS-2A-1 (Sam Yan to Silom)
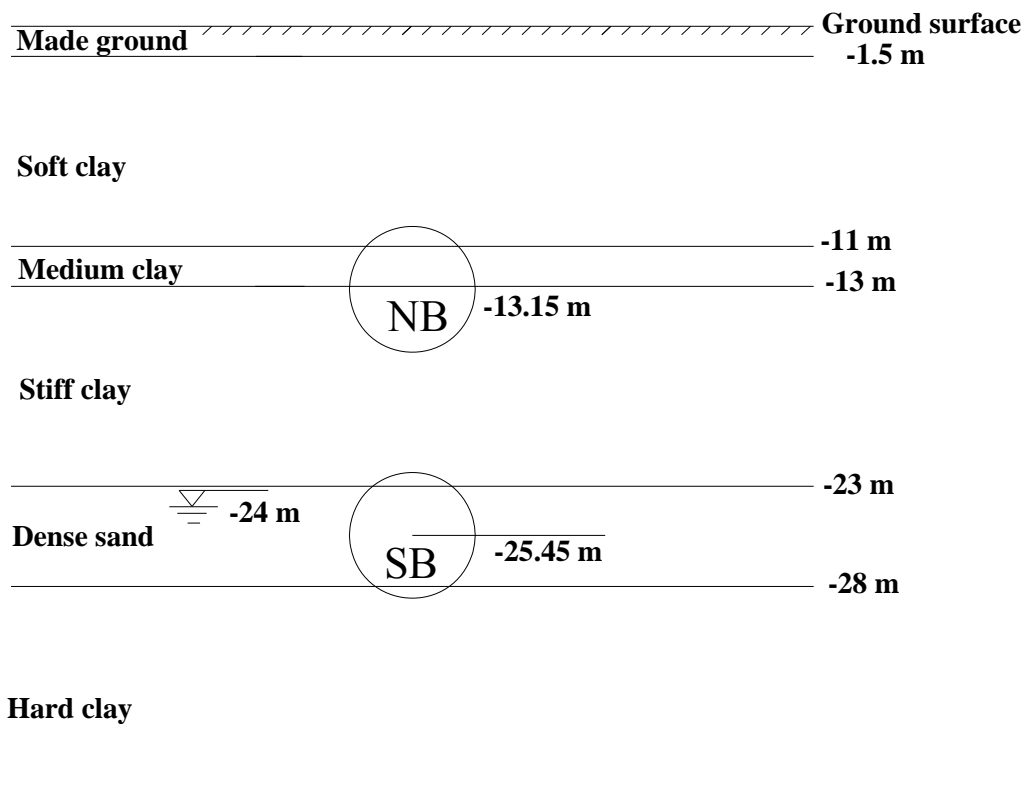
Figure 8.1 (h): Soil Profile of Section CS-4C (Lumphini to Bon Kai)

Figure 8.1 (a) to (h): Soil Profiles for Selected Sections

8.2.2 Single Tunnel Behaviour

Single tunnel behaviour is first examined in this study using three different approaches. Results from the three analytical methods as well as the field observation are shown in Figures 8.2 (a) to (e). As can be seen from the figures, Verruijt and Booker (1996) solution basically gives widest settlement trough while Bobet (2001) gives the narrowest bowl of settlement.

Figure 8.2 (a): Single Tunnel Behaviour Using Different Analytical Approaches:

Section 26-001-SB (Lat Phrao to Ratchada)

Figure 8.2 (b): Single Tunnel Behaviour Using Different Analytical Approaches

Section 23-001-SB (Pracharat Bumphen to Thiam Ruam Mit)

291
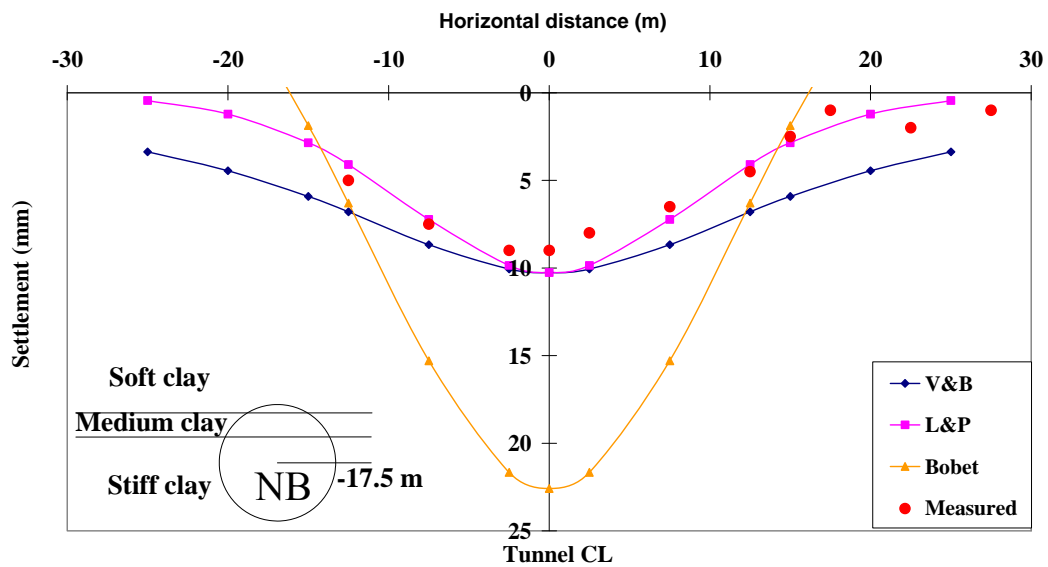
Figure 8.2 (c) Single Tunnel Behaviour Using Different Analytical Approaches: Section CS-8-NB (Phra Ram 9 to Phetchaburi)
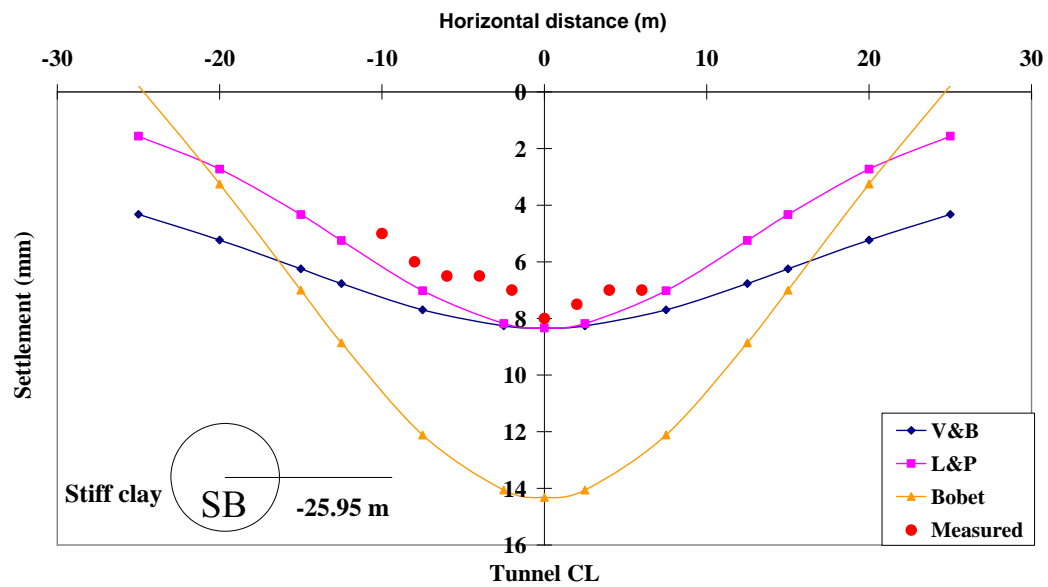
Figure 8.2 (d): Single Tunnel Behaviour Using Different Analytical Approaches: Section CS-2A-1-SB (Silom to Samyan)
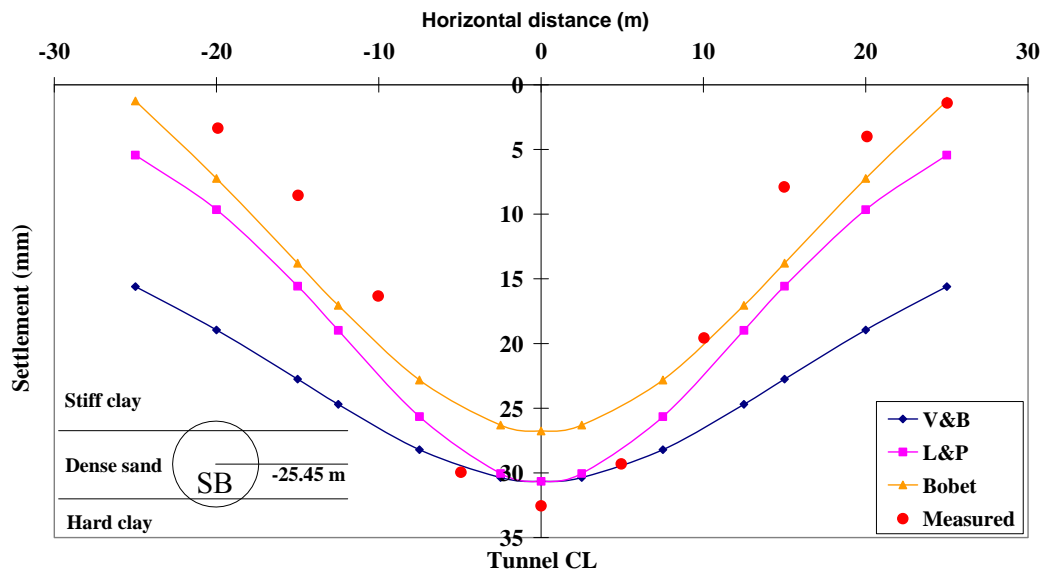
Figure 8.2(e): Single Tunnel Behaviour Using Different Analytical Approaches:
CS-4C-SB (Lumphini to Bon Kai)

Figure 8.2 (a) to (e): Single Tunnel Behaviour Using Different Analytical Approaches for
Selected Sections

From these comprehensive analyses, it can be noted that Bobet's solution underpredicted the settlement in Sections 26-001-NB, 23-001-SB and CS-4C-SB; and over-predicted Sections CS-8-NB and CS-2A-1-SB. It is interesting to note that Bobet's solution over-predict the settlement when measurement is small (say 8-15 mm) and under-predict the field measurement when the settlement is large (say larger than 35 mm). As settlement is controlled mainly by the gap parameter, it is clear that Bobet's solution performs better when larger gap parameters are adopted.

Verruijt and Booker (1996) and Loganathan and Poulos (1998) gave similar settlement predictions with maximum surface settlement, while Verruijt and Booker (1996) forecasts wider settlement trough in all cases. The solution from Loganathan and Poulos (1998) gives reasonably good predictions for all five cases both in maximum settlement and

293

settlement shape. It should be noted that the Loganathan and Poulos (1998) method predicted the measured settlements both when they are low and when they are high.

8.2.3 Twin Tunnel Behaviour

Twin tunnel behaviour will now be discussed from the closed form analysis. The detail predictions are shown in Figures 8.3 (a) to (h). It should be noted that the same gap parameter is used for both tunnels. It is obvious the Verruijt and Booker (1996), Loganathan and Poulos (1998) and Bobet (2001) methods give different width of settlement trough in descending order, which follows the same trend of the single tunnel behaviour presented in the earlier section.
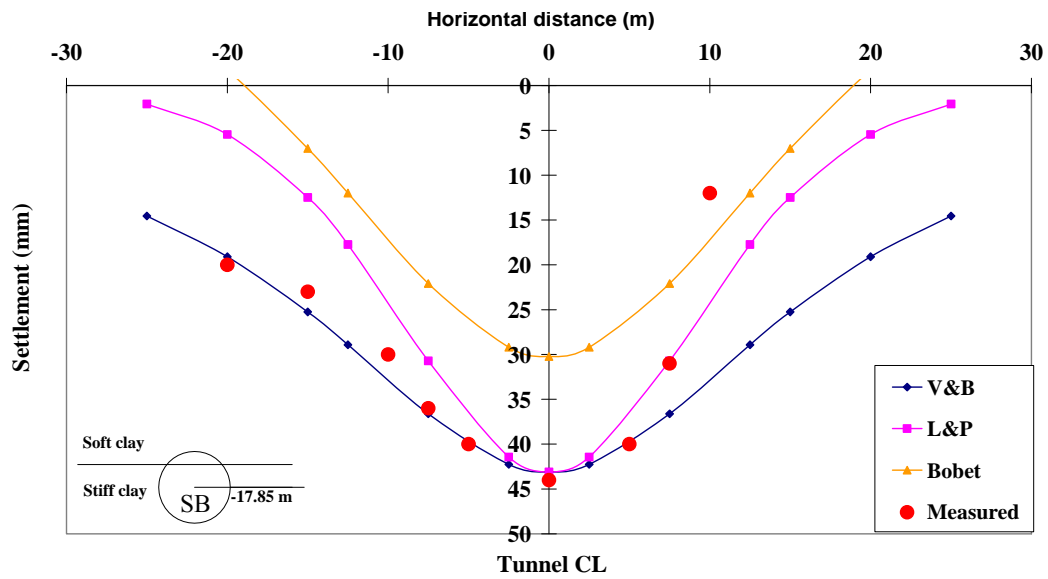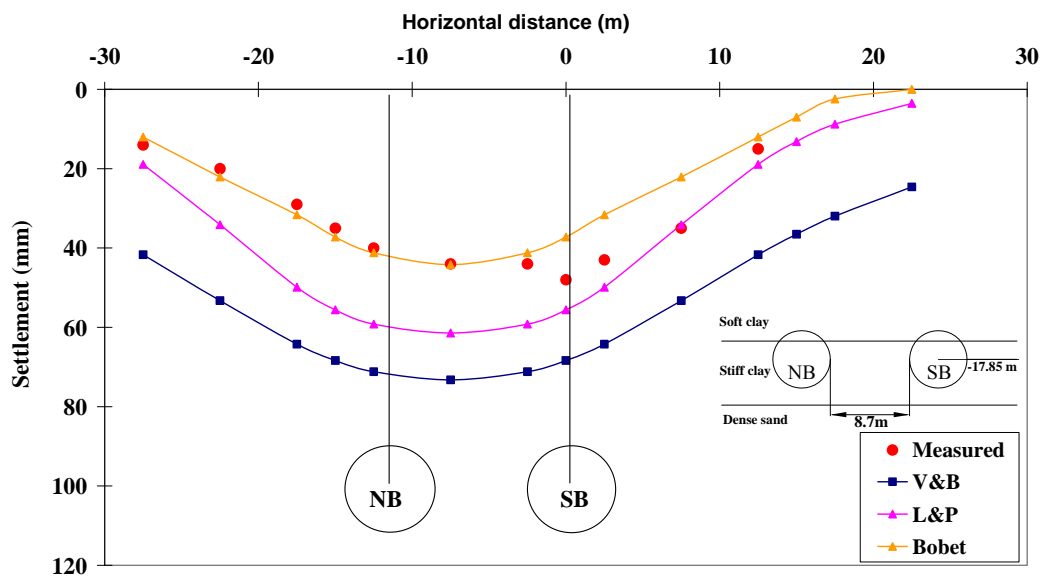

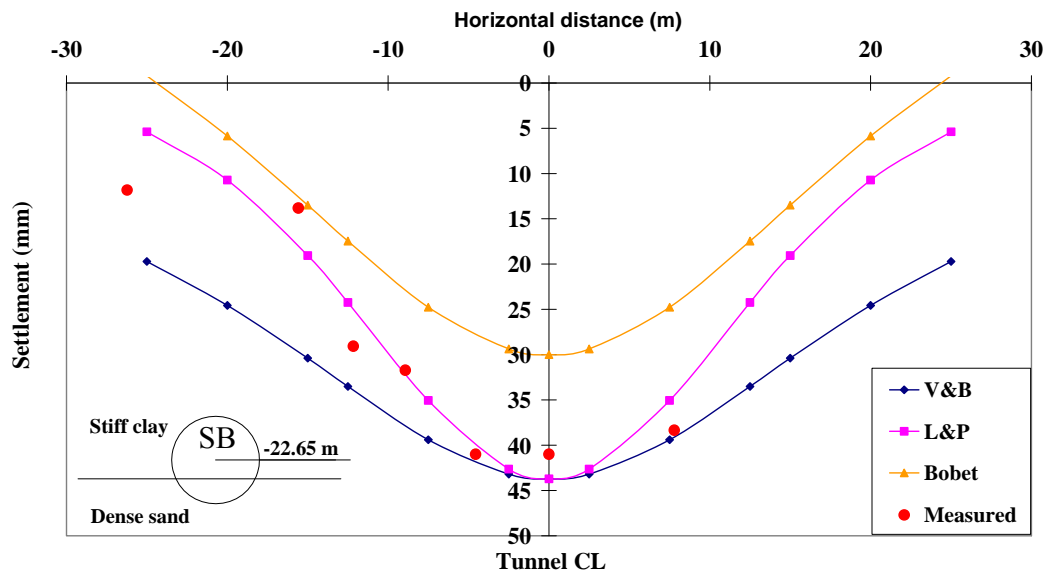Figure 8.3 (a): Twin Tunnel Behaviour Using Different Analytical Methods: Section 26-001 (Lat Phrao to Ratchada)
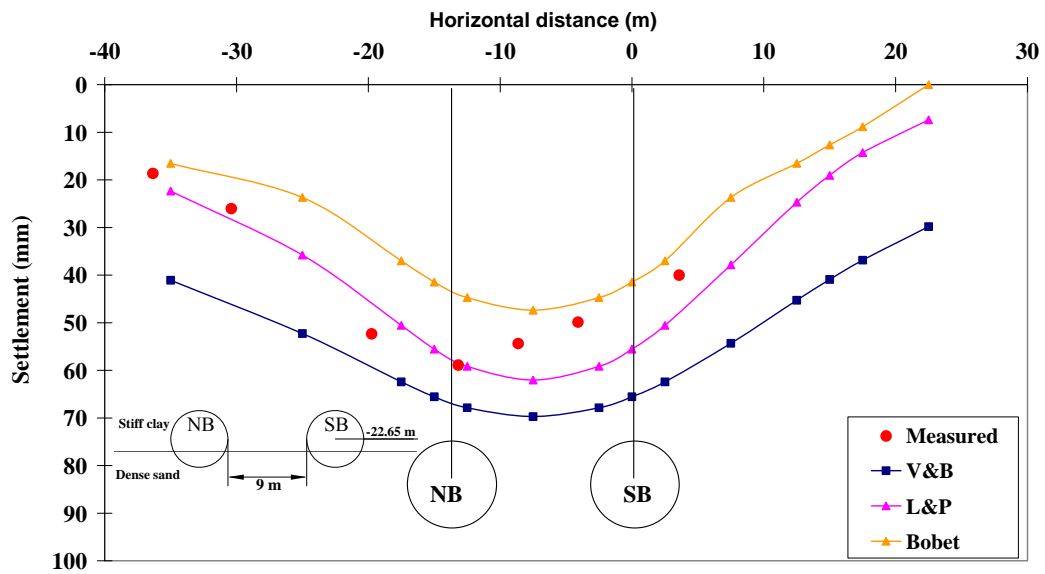
Figure 8.3 (b): Twin Tunnel Behaviour Using Different Analytical Methods:
Section 23-001 (Pracharat Bumphen to Thiam Ruam Mit)
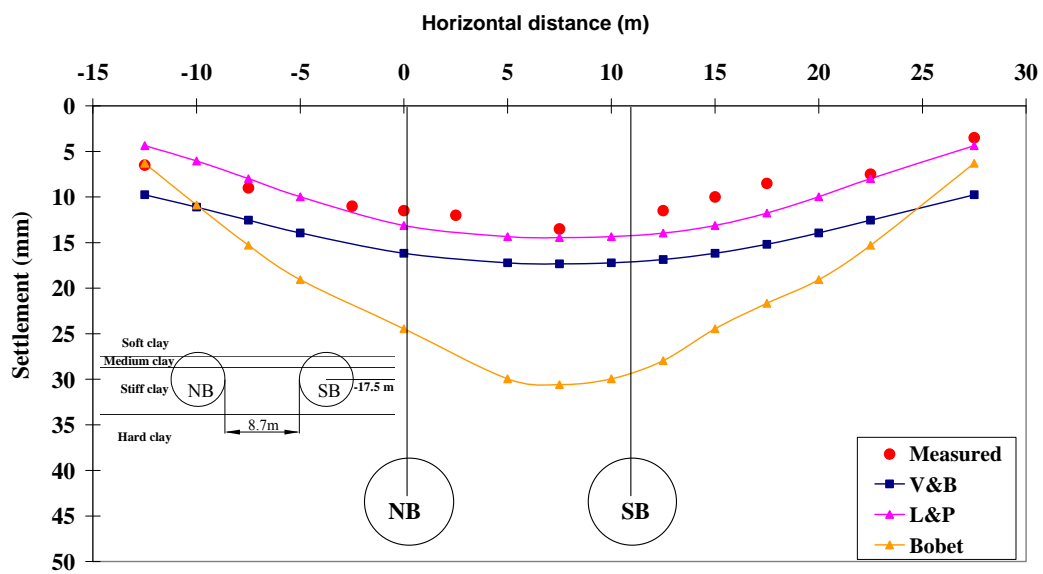
Figure 8.3 (c): Twin Tunnel Behaviour Using Different Analytical Methods:
Section CS-8 (Phra Ram 9 to Phetchaburi)

295
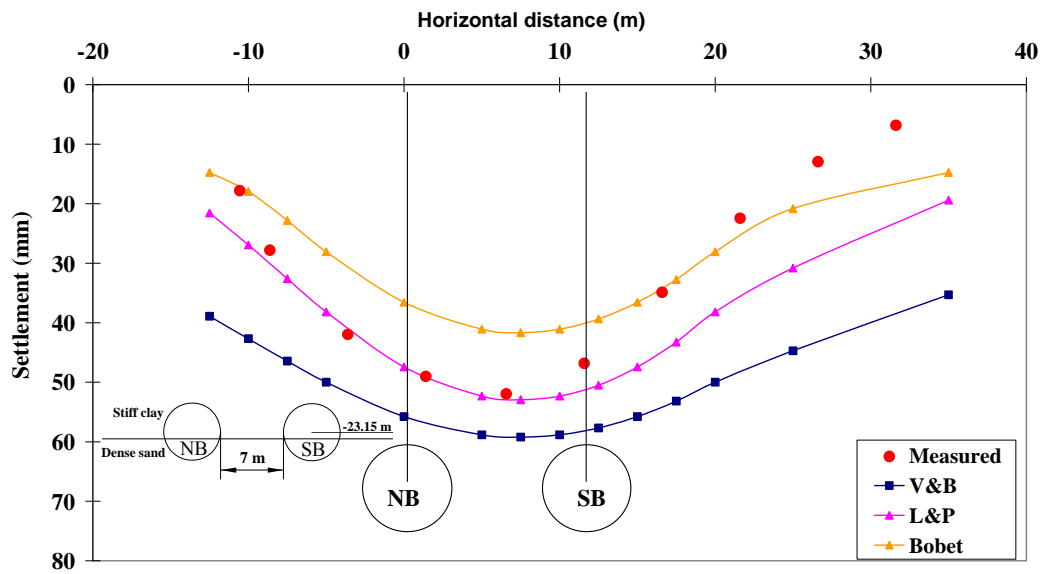
Figure 8.3 (d): Twin Tunnel Behaviour Using Different Analytical Methods:
Section 6D (Sirikit to Sukhumvit)
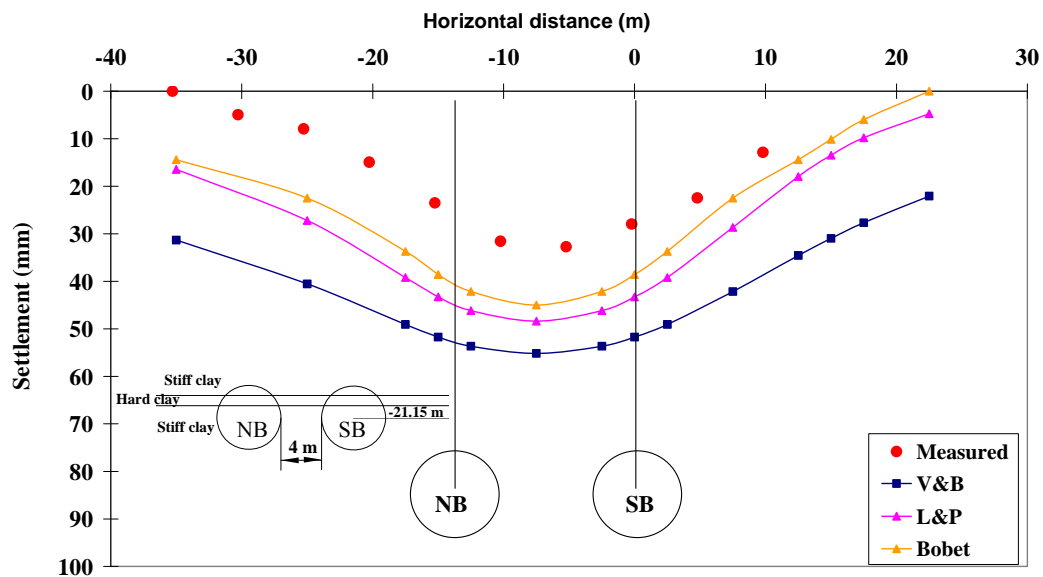
Figure 8.3 (e): Twin Tunnel Behaviour Using Different Analytical Methods:
Section 7C (Sukhumvit to Phetchaburi)
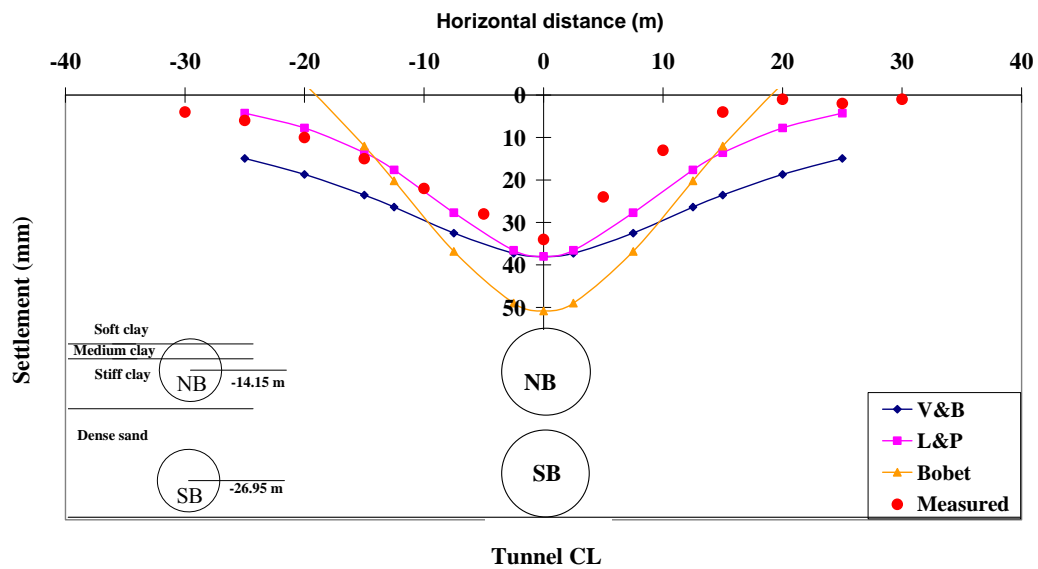
Figure 8.3 (f): Twin Tunnel Behaviour Using Different Analytical Methods:
Section CS-3 (Lumphini to Silom)
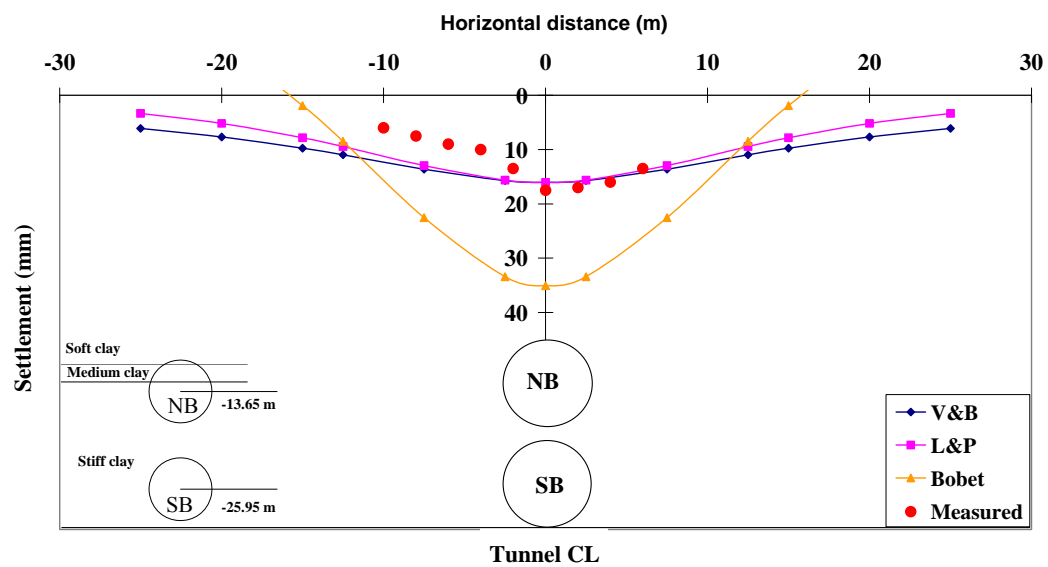
Figure 8.3 (g): Twin Tunnel Behaviour Using Different Analytical Methods:
Section CS-2A-1 (Silom to Samyan)
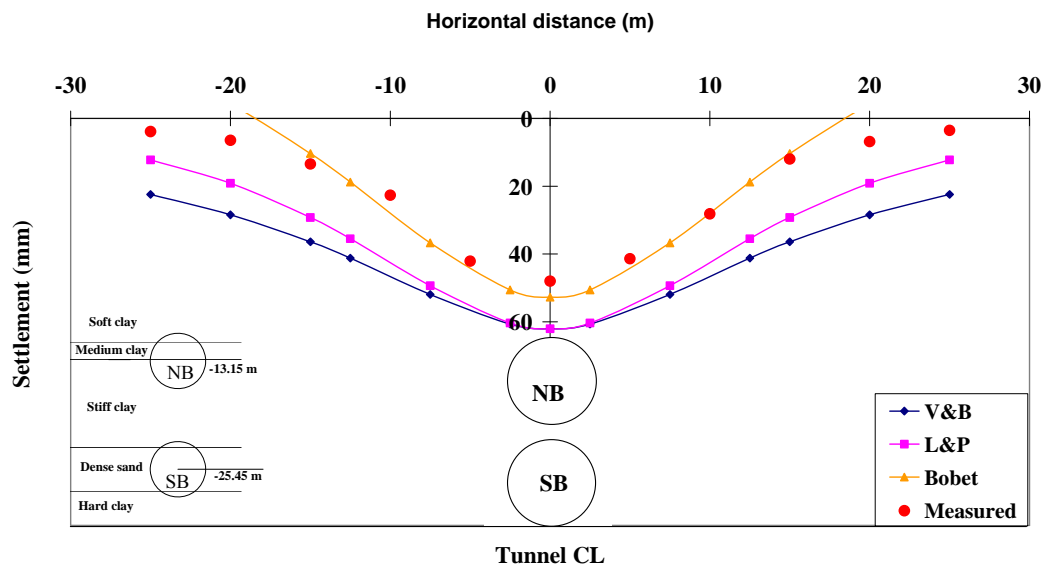
Figure 8.3 (h): Twin Tunnel Behaviour Using Different Analytical Methods:
Section CS-4C (Lumphini to Bon Kai)

Figure 8.3 (a) to (h): Twin Tunnel Behaviour Using Different Analytical Approaches for
Selected Sections

As can be seen from Figures 8.3 (a) to (h):, the Bobet (2001) method predicts reasonably
well in Sections 26-001 and CS-4C. In Sections 23-001, 6D and 7C, it under-predicts the
settlement; meanwhile it overpredicts the values in Sections CS-8B, CS-3B and CS-2A-1.
The same trend from Bobet's (2001) method was noted in the single tunnel prediction.
The Verruijt and Booker (1996) method gave a similar, but larger, settlement trough than
the Loganathan and Poulos (1998) method, in the case of the twin tunnels. Apparently the
two methods do not give the same values for the maximum settlement; these results differ
from the behaviour exhibited in the single tunnel case. However, in all the cases, the
Verruijt and Booker (1996) method overpredicted the settlements in comparison to the
field measurements, while the predicted trough could not match the observation. The
Loganathan and Poulos (1998) solution seems to have given the best performance in the
twin tunnel cases. Nevertheless, it overpredicted the settlement in Sections 26-001 and

7C, while it matched the measurement in the other sections. Thus the Loganathan and Poulos (1998) method gave the best prediction in both single and twin tunnel behaviours.

8.3 Finite Element Analysis for Shield Tunnelling

8.3.1 Dimensions of 2D and 3D Mesh Generations

In undertaking the 2D finite element modelling a sufficient mesh dimension is required. This process avoids the influence of the finite element modelling (herein, tunnelling) at the boundary of the mesh model. A range of criteria are adopted in the literatures; for example, Bliehm (2001) suggested that the mesh dimensions should be chosen so that the strains, perpendicular to the mesh boundaries, are less than 0.005% after the tunnels have been constructed. The mesh dimensions adopted in this study are those of Moller (2006), who limited the maximum primary stresses rotation to less than 2.5 degrees at the bottom boundary. At the left and right boundaries, the maximum vertical strain is kept to a value less than 1% of the maximum vertical strain at the centreline. The results of his finite element study with the Hardening Soil Model showed that the distance from the tunnel crown to the bottom boundary (h) should be at least 2.2 times the tunnel diameter. This criterion is restricted to cases where the tunnel diameter ranged from 4 to 12 m. The width of the mesh generation is suggested as:

$$w = 2D\left(1 + \frac{H}{D}\right)$$ Eq.8.1

where, $\qquad$ w = width of mesh generation

H = distance from ground surface to tunnel crown

D = tunnel diameter.

In a case of 3D mesh generation, Moller (2006) recommended that a smaller distance from the tunnel crown to the bottom boundary (h) of 1.45D could be used. The width of

the mesh dimension is kept the same as in Eq. 8.1. In terms of mesh length (l), the following equation was suggested:

$$l = D\left(13 + \frac{11}{3} + \frac{H}{D}\right)$$ Eq.8.2

8.3.2 Tunnelling Process Modelling in 2D Finite Element Analysis

The tunnel excavation techniques involve the 3D phenomena. Both the open and closed face simulations in the 2D plane-strain finite element analysis required a number of assumptions to govern the missing dimension. Different approaches were proposed in the literature (Rowe et al., 1983; Swaboda, 1979; Panet and Guenot, 1982; Vermeer and Brinkgreve, 1993; Addenbrooke, 1996; Mollor, 2006). They are summarised and discussed further in this section; however, the focus here is on their advantages and disadvantages in relation to the prediction of the ground movements, complexity and reliability of the required parameter(s) and their influence on the lining forces.

8.3.2.1 Gap Method

The Gap method was first introduced by Rowe *et al.* (1983). Later it was refined and formulated by Lee *et al.* (1992). This Gap method allows all three major components of ground loss, owing to tunnelling (Face loss, Shield loss and Tail loss) to be taken into consideration separately. The "Gap parameters (g)", as explained in Chapter 2, was required prior to the analytical or numerical analyses. The parameter consists of three components, namely the parameter related to 3D movement in the front of tunnel face (U^*_{3D}), the workmanship parameter (ω), and the physical gap parameter (G_p). The first parameter (U^*_{3D}) was estimated on the basis of the 3D elastoplastic undrained finite element analysis results; the second, workmanship, parameter (ω) governs the loss of ground over the shield. (It can be estimated with a known pitching angle or it can be empirically correlated with the physical gap (G_p)). The third parameter, the physical gap, is basically the difference between the outer diameters of the shield and the lining. (In the

modern shield tunnelling techniques, this physical gap is normally filled with grouting materials to minimise the tail loss. Lee *et al.* (1992) suggested that, if the grouting is injected into the tailpiece voids, G_p can be reduced to zero, depending on the efficiency of working process.)

8.3.2.2 Stiffness Reduction Method (α - Method)

The stiffness reduction method takes into account the 3D nature of ground displacement due to tunnelling, by reducing the stiffness of the soil to be excavated and allowing the ground to deform to a new equilibrium, prior to the liner installation. This α – method (also called the progressive softening or stiffness reduction method) was originally developed by Swoboda (1979) to simulate the construction process of the New Austrian Tunnelling Method (NATM). The schematic diagrams of the calculation phases in the stiffness reduction method are shown in Figure 8.4. In the initial phase, the ground inside and outside the excavated zones are having the same initial stiffness of E_o. The initial support pressure at the tunnel cross section boundary equals to p_o.,while the tunnel excavation is simulated by applying a stiffness reduction factor (α) to E_o. This reduction factor ranges from zero to unity. At the calculation stage, the reduced support pressure p_α has a value less than p_o. Thus, the surrounding soils are allowed to move towards the tunnel boundary. In the last stage, the soil cluster inside the tunnel boundary is deactivated and the tunnel lining is activated. The support pressure (p_α) is now zero and the load from the surrounding soils are taken by the tunnel lining.
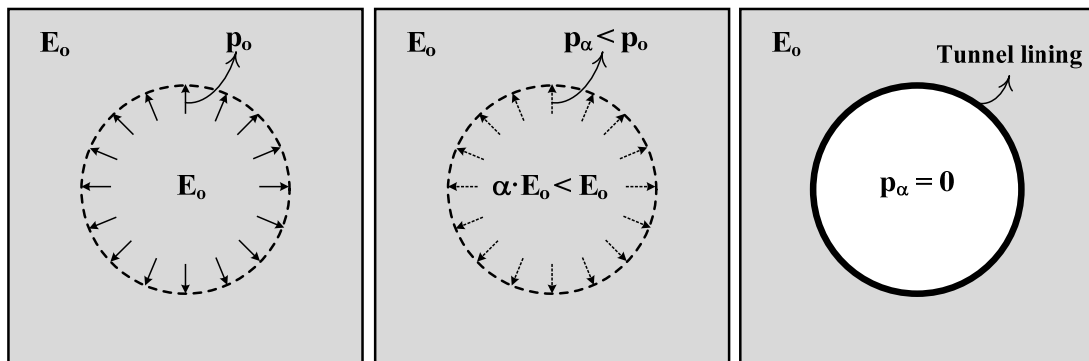
Figure 8.4: Calculation Phases in Stiffness Reduction Method

The application of the stiffness reduction method on the NATM tunnel allows the tunnel cross section to be partially deactivated (according to the construction sequence). Different values of α can also be applied to each part of the tunnel cross section. It should be noted that this method was left out in the currrent study for two reasons. First, the stiffness reduction factor (α), which applys to E_o, is often obtained from back-analysis results. This process is relatively simple when the soil constitutive model, with one stiffness modulus (for instance, Mohr Coulomb Model), is adopted. On the other hand, if an advanced soil model, which requires more than one stiffness moduli, is used, finding a suitable value for α may be somewhat cumbersome. Second, based on the back-analysis results of the Heathrow Express Trial Tunnel Type-2 (Karakus, 2007), the stiffness reduction method is more sensitive to the selection of the element type used to model the tunnel lining compared to the other methods (i.e. the stress reduction and hypothetical modulus of elasticity methods).

8.3.2.3 Stress Reduction Method (β or λ – Method)

The stress reduction method, also known as the convergence-confinement method (β or λ – methods) was introduced by Panet and Guenot (1982). The method uses an "unloading factor (β)" to take into account the 3D tunnelling effects in the 2D plain strain analysis. Figure 8.5 shows the calculation phases of this method. Similar to the stiffness reduction method, the first calculation phase has the initial support pressure (p_o) acting on the tunnel periphery (equilibrium stage). This p_o reduces to p_β ($p_\beta = p_o \cdot \beta$; $0 < \beta < 1$) in the second calculation phase to allow the surrounding soil to deform. In the final phase, the soil cluster inside the tunnel periphery is deactivated, while the tunnel lining is activated in the same way as the stiffness reduction method.
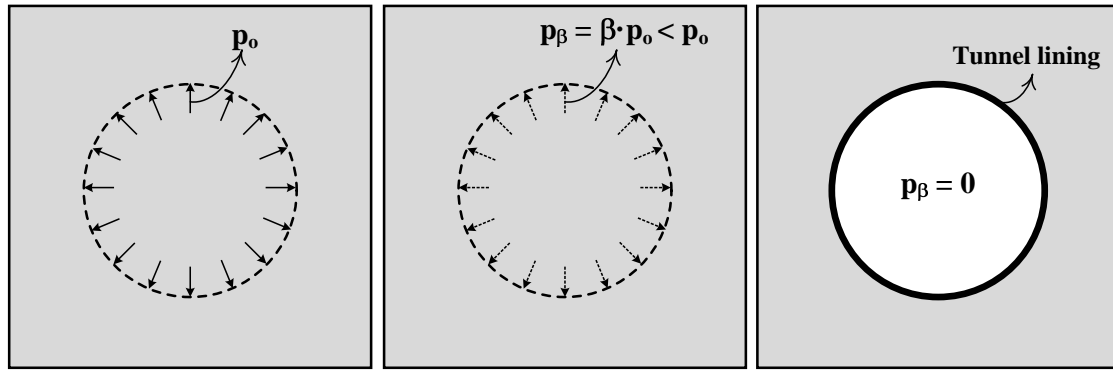
Figure 8.5: Calculation Phases in Stress Reduction Method

Kim *et al.* (2006) proposed a method to estimate the unloading factor (β) in linear elastic and cohesionless ground for both open and closed face tunnels. The values of the unloading factor depend on three parameters, namely, the coefficient of the earth pressure at rest (K_o), the angle of the internal friction (ϕ'), and the ratio of the support delay length or round length (L_{exc}) to the tunnel diameter (D). It was found that the L_{exc}/D ratio has the most influence on the magnitude of the unloading factor. In the case of the open face tunnel the values of the unloading factor ranged from 0.45 to 0.70 (with $0.6 \leq K_o \leq 1.0$, $20 \leq \phi' \leq 40$ and $0 < L_{exc}/D \leq 1.0$). A similar range of unloading factors,, 0.5 to 0.7, was suggested by Moller (2006), for a conservative approach to the estimation of the structure forces. However, the lower β-values from 0.3 to 0.4 were required to match the measured settlement profiles from this back-analysis study. The summary reveals that the unloading factor varies over a large range in the case of the open face tunnel. There are, in fact, other factors (i.e. construction sequences, delayed period prior to lining installation, pattern of tunnel face advance) that contribute to the settlement of the ground induced by the open face tunnel excavation. These effects have been studied numerically (Karakus and Fowell, 2003; Karakus and Fowell, 2005). As a rule-of-thumb in engineering practice, a lower range of β-values leads to a smaller support pressure on the tunnel periphery and, thus, a larger ground movement and lesser forces on the tunnel lining. On the other hand, the higher β-values lead to a smaller ground movement and higher structure forces.

A much narrower band of 0.72 to 0.78 was found for the unloading factor (β) in the close face tunnel (Kim *et al.*, 2006). Note that this small variation was obtained from the assumption of the liner elastic and stable ground conditions. It will be shown later, from the current study, that the values of the unloading factor is a significant factor for the settlement computations and can be varied in a larger range, according to the shield tunnelling factors (i.e. face pressure, penetration rate, grout pressure).

8.3.2.4 Contraction Method

Vermeer and Brinkgreve (1993) proposed a 2D plain strain finite element method, namely the contraction method, for ground movement computation owing to tunnelling. This method involves two calculation steps (see Figure 8.6). The first calculation step starts by deactivating the soil cluster within the tunnel periphery. The tunnel lining is also activated. The tunnel lining is allowed to move upward due to the removal of the excavated soils. In the second calculation step, the tunnel lining is stepwise uniformly contracted until the pre-assigned contraction ratio is reached. Importantly, this contraction ratio should be the same as the volume loss ratio (see also Section 2.1.1) in the undrained condition.
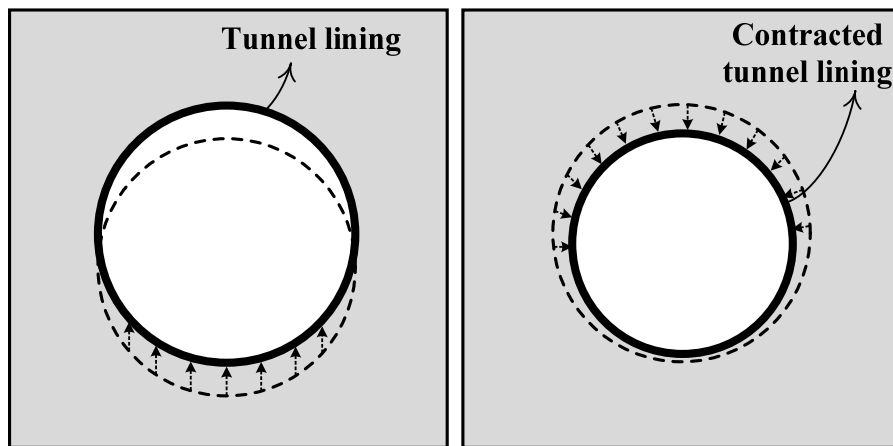
Figure 8.6: Calculation Phases in Contraction Method

8.3.2.5 Volume Loss Control Method

Addenbrooke (1996) and Addenbrooke *et al.* (1997) developed a 2D finite element method for ground movement induced by shield tunnelling. The method combined the reduced support stress at the tunnel periphery, from the stress reduction method, with the control of the ground loss by prescribing the volume loss ratio. This combination was necessary as shield tunnelling is often controlled by the volume loss ratio, while the value of the unloading factor is uncertain. The calculation steps for this method involved a series stepwise reduction of support pressure. After each pressure reduction, the ground loss was calculated, with the calculation process ceasing when the calculated ground loss matches the prescribed value.

8.3.2.6 Grout Pressure Method

The grout pressure method (Moller, 2006; Moller and Vermeer, 2008) utilises the "Gap element" to simulate the physical gap (i.e. the gap created as a result of the larger diameter of the shield compared to the tunnel lining), as well as the grout pressure. This gap element is an interface element with the actual thickness of the physical gap. Figure 8.7 illustrates the finite element installation procedure of the grout pressure method. This method is modelled by a radial pressure, which hydrostatically increases with the depth, according to a prescribed grout unit weight. One advantage of the grout pressure method over the others is that the heaving type of ground movement profile can also be predicted, if the applied grout pressure is higher relative to the total over burden pressure above the tunnel crown. The prediction becomes critical for shield tunnelling at a shallow depth in an urban area, especially as the shield operator tends to use high face pressure to minimise the surface settlement. At the same time, the face pressure should also be limited by a low total over the burden pressure at a shallow depth.
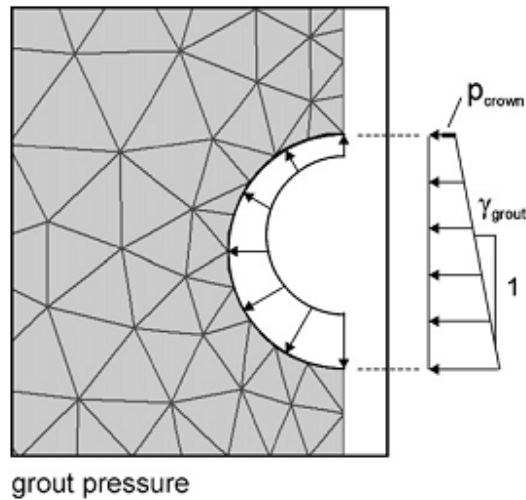
grout pressure

Figure 8.7: Finite Element Procedure for Shield Tunnelling: Grout Pressure Method
(after Moller and Vermeer, 2008)

8.3.2.7 Modified Grout Pressure Method

All the 2D finite element methods summarised above, with the exception of the stiffness reduction method, have been adopted for closed face (or shield) tunnelling. Only the gap method allows all three components involved in the ground loss owing to shield tunnelling (i.e. face loss, shield loss and tail loss) to be taken, individually, into consideration. In contrast, the other methods combine all the settlement components together, while the shape and the magnitude of the settlement profile are controlled by one parameter (i.e. the unloading factor, contraction ratio, volume loss ratio and grout pressure). The importance of the gap method lies in its control of the tail loss component, which considers the physical gap between the shield and tunnel lining. As discussed earlier, this physical gap is filled with grout material, therefore, only part of the physical gap should be used (Lee *et al.*, 1992).

Within this study, the grout pressure method was modified so that the different settlement components could be computed separately. The modified method used three calculation phases (see Figure 8.8). In the first phase, the soil cluster inside the Tunnel Boring Machine (TBM) was deactivated. Simultaneously, the face pressure was applied to an

entire area of the TBM cross section. This pressure represents the slurry pressure inside the TBM chamber, which increases linearly with depth at a gradient equal to the unit weight of the slurry (γ_s). The tunnel lining, as modelled by the plate element, was activated in the second calculation phase. The area surrounding the tunnel lining representing the physical gap was then filled with fresh grout, and the grout pressure was applied to the physical gap area. The grout pressure was selected in accordance with the applied grout pressure at the tail of the TBM. The unit weight of grout (γ_g) can be used as an increment of the grout pressure. Importantly, the continuum element was used to model the grout material. Further, the cluster inside tunnel lining was set as a dry cluster. In the last phase, the grout pressure was removed, with the physical gap area being replaced by the harden grout material.
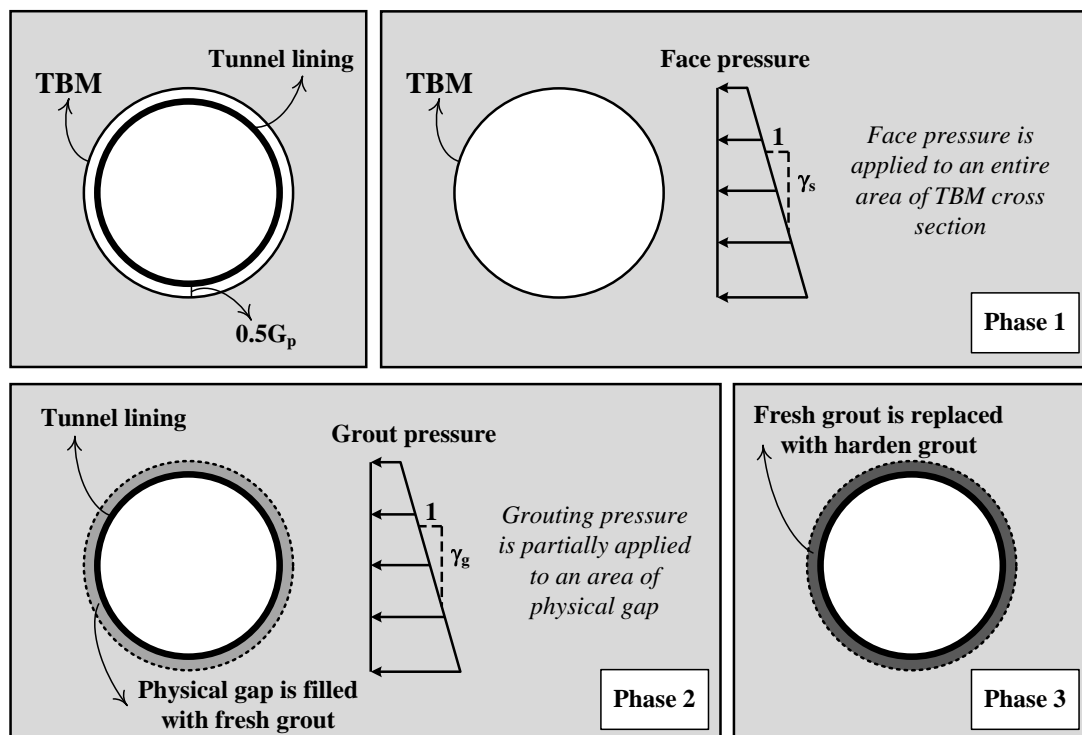

Figure 8.8: Calculation Phases in Modified Grout Pressure Method

The advantages of separating the face pressure and the grout pressure into a two phase calculation are: first, the face loss component can be controlled separately by the applied face pressure. The benefit of being able to predict the heaving type of soil movement

profile, similar to the grout pressure method, is retained. Second, the tail loss can be restricted by the actual physical gap. Moreover, the area of the physical gap can be either contracted or expanded, depending on the applied grout pressure. One limitation of this method is that the shield loss component is ignored. This shield loss component is important as it is created by the applied pitching angle of the TBM (as the TBM is normally moved in a slightly upward angle), and the overcutting of the TBM when the tunnel alignment is curved. As a result, the modified method may be restricted to a straight alignment shield tunnelling simulation. Alternatively, expanding the area of the physical gap, to one slightly larger than the difference between the TBM and the tunnel lining diameters, may produce a large pitching angle or may involve excessive overcutting.

8.3.3 Finite Element Analysis of the Bangkok MRT Blue Line Project

The three, 2D finite element methods selected here, namely the contraction method, the stress reduction method, and the modified grout pressure method, are used to model the shield tunnelling of the Bangkok MRT Blue Line project. The general geological conditions of this project were discussed in Chapter 3. Figure 3.1 shows the locations of the MRT stations and the tunnel alignments of the Bangkok MRT Blue Line project. Seven sections (as presented in Table 8.2), selected for the case studies, were twin tunnels with a side-by-side pattern. The selection of the sections was based on the attempt to cover various combinations of soil profiles and shield operation factors encountered in engineering practice. For example, the tunnel cross section was located entirely in stiff clay, or partially stiff clay, and clayey sand. In term of the shield operation factors, four factors (face pressure, penetration rate, grout pressure and percentage of grout filling) were the most influential in relation to shield tunnelling. If sufficiently high levels of face pressure, grout pressure, and percentage grout filling are combined with a fast penetration rate, the resulting surface settlement can be limited to an order of 10 to 15 mm. In contrast, if one or more shield operation factors fail to reach the required magnitude, a higher magnitude for the surface settlement is expected. The soil profiles for all the sections, as adopted in finite element analysis, are illustrated in Figure 8.9.

Table 8.2: Location of the Studied Sections

Section		Location
A	23-AR-001	Thiam Ruam Mit - Phacharat Bumphen
A	23-G3-007-019	Thiam Ruam Mit - Phacharat Bumphen
B	26-AR-001	Ratchada - Lat Phrao
C	CS-8B	Phra Ram 9 - Phetchaburi
C	CS-8D	Phra Ram 9 - Phetchaburi
D	SS-5T-52e-s	Sirikit - Bon Kai
D	SS-5T-22e-o	Sirikit - Bon Kai

A brief summary of the shield tunnelling parameters and the subsoil conditions encountered during the project is presented below; this summary is also given in Table 8.3.

1. *Section A: 23-AR-001*

   The twin tunnels of this section are located entirely in stiff clay layer. A low face pressure of 40 to 80 kN/m^2 was applied with a high penetration rate of 30 to 60 mm/min, a high grout pressure of 250 to 300 kN/m^2, and a high percentage of grout filling of 120% for both tunnels (i.e. Northbound-NB and Southbound-SB). The maximum surface settlement after both shields had passed was about 60 mm.

2. *Section A: 23-G3-007-019*

   The twin tunnels of this section are located partially in the stiff clay and partially in the clayey sand layers. A low face pressure of 40 kN/m^2 was applied to the SB tunnel, while a higher face pressure of 80 kN/m^2 was applied to the NB tunnel. Additionally, a high penetration rate of 30 to 40 mm/min, a high grout pressure of 250 to 350 kN/m^2, and high percentage of grout filling of 100 to 150% were applied for both the NB and SB tunnels. The maximum surface settlement after both shields had passed was about 45 mm.
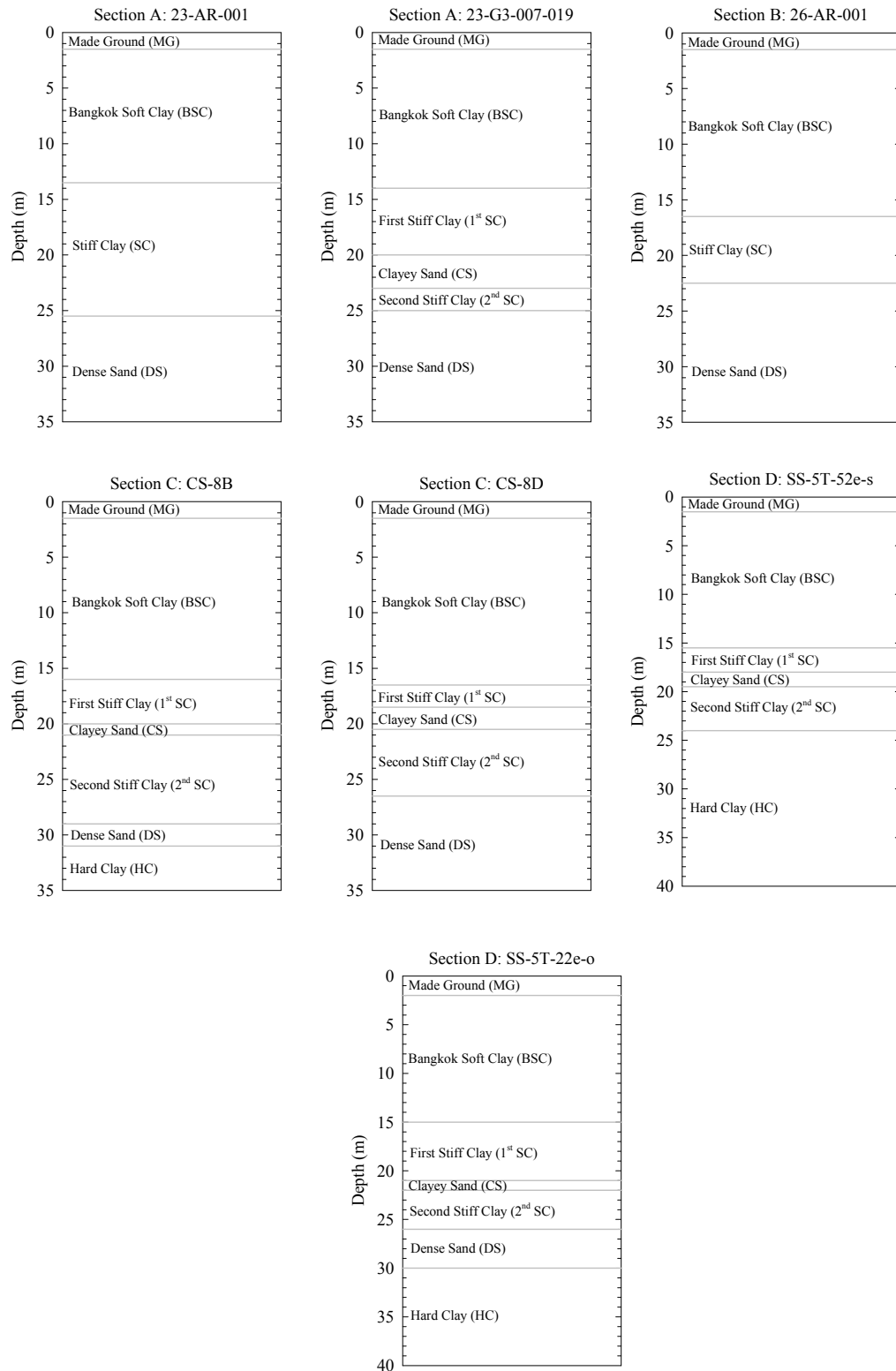
Figure 8.9: Soil Profiles of Studied Sections

3. *Section B: 26-AR-001*

The twin tunnels of this section are located partially in the soft clay and partially in the stiff clay layers. A high face pressure of 130 to 180 kN/m^2 was applied with a low penetration rate of 3 to 15 mm/min, and a high percentage of grout filling of 100 to 120% for both the NB and SB tunnels. A low grout pressure of 100 kN/m^2 was applied to the SB tunnel, while a higher grout pressure of 170 kN/m^2 was used in the NB tunnel. The maximum surface settlement after both shields had passed was about 50 mm.

4. *Section C: CS-8B*

The twin tunnels of this section are located partially in stiff clay and partially in clayey sand layers. A high face pressure of 150 to 200 kN/m^2 was applied to both the SB and NB tunnels along with a high penetration rate of 50 mm/min, a high grout pressure of 200 kN/m^2, and a high percentage of grout filling of 140 to 150%. The maximum surface settlement after both shields had passed was about 10 mm.

5. *Section C: CS-8D*

The twin tunnels of this section are located partially in the stiff clay and partially in the clayey sand layers. A high face pressure of 150 to 200 kN/m^2 was applied to both the SB and NB tunnels, along with a high penetration rate of 50 mm/min, a high grout pressure of 150 to 200 kN/m^2, and a high percentage of grout filling of 130 to 140%. The maximum surface settlement after both shields had passed was about 12 mm.

6. *Section D: SS-5T-52e-s*

The twin tunnels of this section are located partially in the stiff clay and partially in the hard clay layers. A high face pressure of 170 kN/m^2 was applied to both the SB and NB tunnels, along with a penetration rate of 25 mm/min, a high grout pressure of 250 to 400 kN/m^2, and a high percentage of grout filling of 150%. The maximum surface settlement after both shields had passed was about 25 mm.

7. *Section D: SS-5T-22e-o*

The twin tunnels of this section are located partially in the stiff clay and partially in the dense sand layers. A high face pressure of 200 to 250 kN/m^2 was applied to both the SB and NB tunnels, along with a high penetration rate of 35 to 40 mm/min, a high grout pressure of 400 kN/m^2, and a high percentage of grout filling of 140 to 150%. The maximum surface settlement after both shields had passed was about 10 mm.

Table 8.3 (a): Summary of Shield Tunnelling Parameters and Subsoil Conditions

	Section	Face pressure, p_F (kN/m^2)		Grout pressure (kN/m^2)		Penetration rate (mm/min)	
		SB	NB	SB	NB	SB	NB
A	23-AR-001	40-80	40-80	250-300	250-300	30-60	30-60
A	23-G3-007-019	40	80	250-350	350-350	30-40	30-40
B	26-AR-001	130-180	130-180	100	170	3-15	3-15
C	CS-8B	150-200	150-200	200	200	50	50
C	CS-8D	150-200	150-200	150-200	150-200	50	50
D	SS-5T-52e-s	170	170	250-400	250-400	25	25
D	SS-5T-22e-o	200-250	200-250	400	400	35-40	35-40

Table 8.3 (b): Summary of Shield Tunnelling Parameters and Subsoil Conditions (cont'd)

	Section	Percentage of grout filling (%)		Subsoils condition encountered
		SB	NB	Both SB and NB
A	23-AR-001	120	120	Stiff clay
A	23-G3-007-019	100-150	100-150	Stiff clay, clayey sand
B	26-AR-001	100-120	100-120	Soft clay, stiff clay
C	CS-8B	140-150	140-150	Stiff clay, clayey sand
C	CS-8D	130140	130-140	Stiff clay, clayey sand
D	SS-5T-52e-s	150	150	Stiff clay, hard clay
D	SS-5T-22e-o	140-150	140-150	Stiff clay, dense sand

Based on the above brief summary of all seven cases, it can be concluded that, regardless of the soil conditions encountered, the ground settlement owing to shield tunnelling is largely influenced by the shield operation factors (i.e. face pressure, penetration rate, grout pressure and percentage of grout filling).

The soil constitutive model adopted herein was the Hardening Soil Model (HSM). The input parameters of the HSM finite element analysis study (in Chapter 7, from Table 7.6) were retained. The tunnel lining was modelled using the plate element with $EA = 8000$ MN/m and $EI = 56$ MNm^2/m. For the modified grout pressure method, the grout material, which fills the physical gap, was modelled by a linear elastic continuum element. The elastic modulus of the grout was assumed as 7.5 and 15 MN/m^2 for the fresh and hardened grouts, respectively. Figure 8.10 depicts the finite element mesh generation of Section D: SS-5T22e-o. The lateral movements were restricted on the left and right boundaries, and both the lateral and vertical movements were restricted on the bottom boundary. The geometry of the model mesh generation was selected so that the conditions (as discussed in Section 8.3.1) were satisfied. For the finite element model shown in Figure 8.10, the number of elements is 1670 with an average element size of 1.55 m. The finer mesh size was created on the middle area, which extends at least two times the tunnel's diameter from both sides of the tunnel inverse. The drawdown pore water pressure (see Figure 7.18) was adopted for all the studied models.
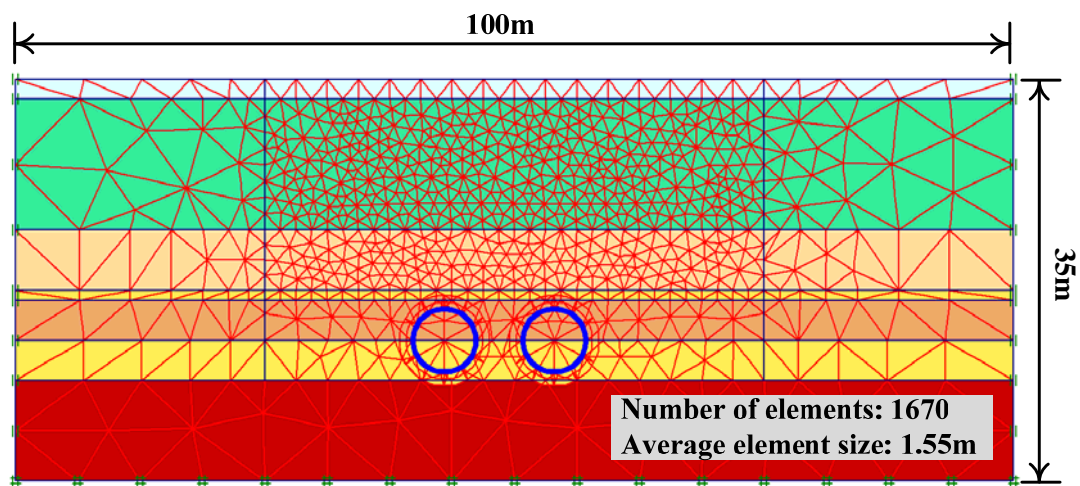

Figure 8.10: Finite Element Model and Mesh Generation (Section D: SS-5T-22e-o)

8.3.3.1 Results and Discussions from the Contraction Method

The contraction method was used in the first set of the analysis. The calculation steps involved the two-phase calculation, as detailed in Section 8.3.2.4. The values of prescribed contraction ratio were chosen so that the predicted maximum settlement matched with the measured one. The results of the contraction method back-analysis are highlighted in Figures 8.11 (a) to 8.11 (g). In general, the soil profiles, estimated from the contraction method along with the Hardening Soil Model, agree well with the measured profiles. The back-calculated percentage of the contraction for each tunnel is also shown in Figures 8.11 (a) to 8.11 (g), and listed in Table 8.4. The percentage of the contraction required to match the measured settlement profiles range from the values of 0.22 to 3.6. As one would expect, the larger percentage of the contraction was needed in the case of the higher maximum surface settlement.

Figure 8.11 (a): Results from Contraction Method Back-analysis (Section A: 23-AR-001)

314

Figure 8.11 (b): Results from Contraction Method Back-analysis
(Section A: 23-B3-007-019)

Figure 8.11 (c): Results from Contraction Method Back-analysis (Section B: 26-AR-001)

315

Figure 8.11 (d): Results from Contraction Method Back-analysis (Section C: CS-8B)

Figure 8.11 (e): Results from Contraction Method Back-analysis (Section C: CS-8D)

Figure 8.11 (f): Results from Contraction Method Back-analysis
(Section D: SS-5T-52e-s)
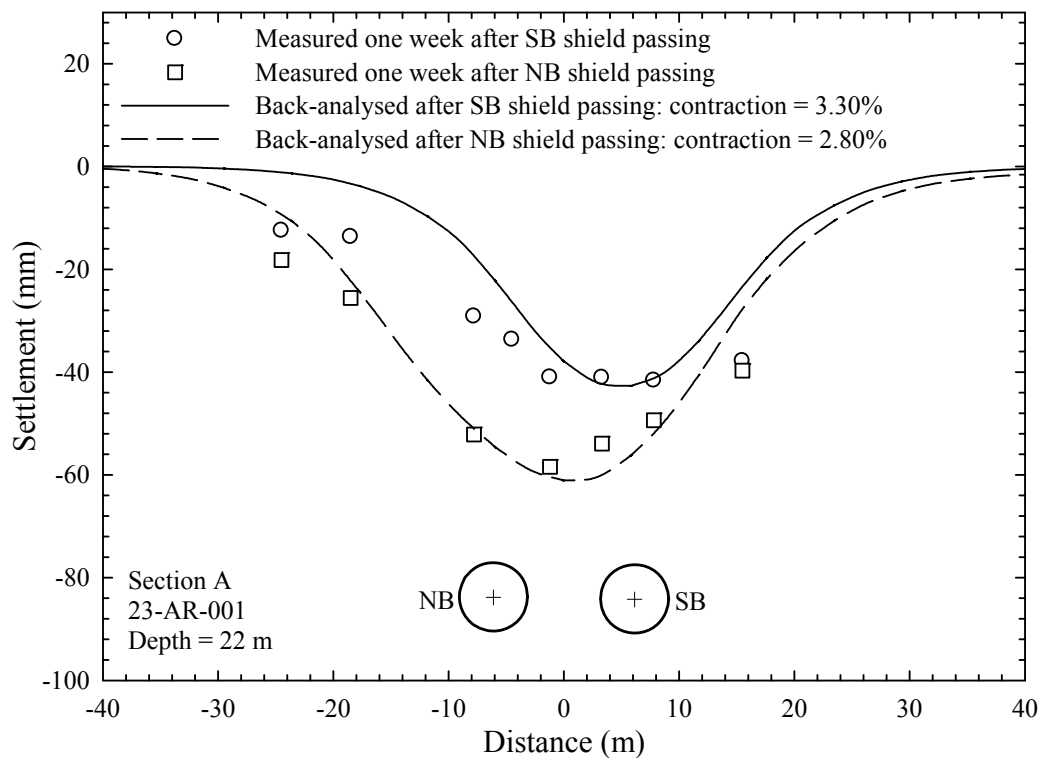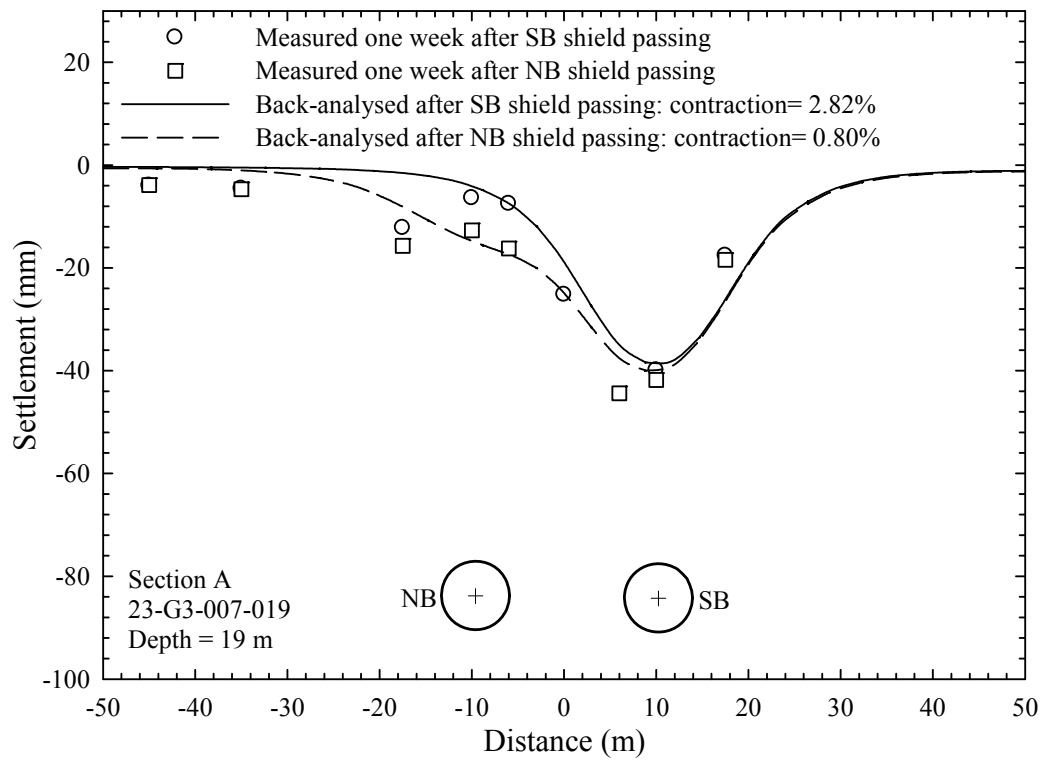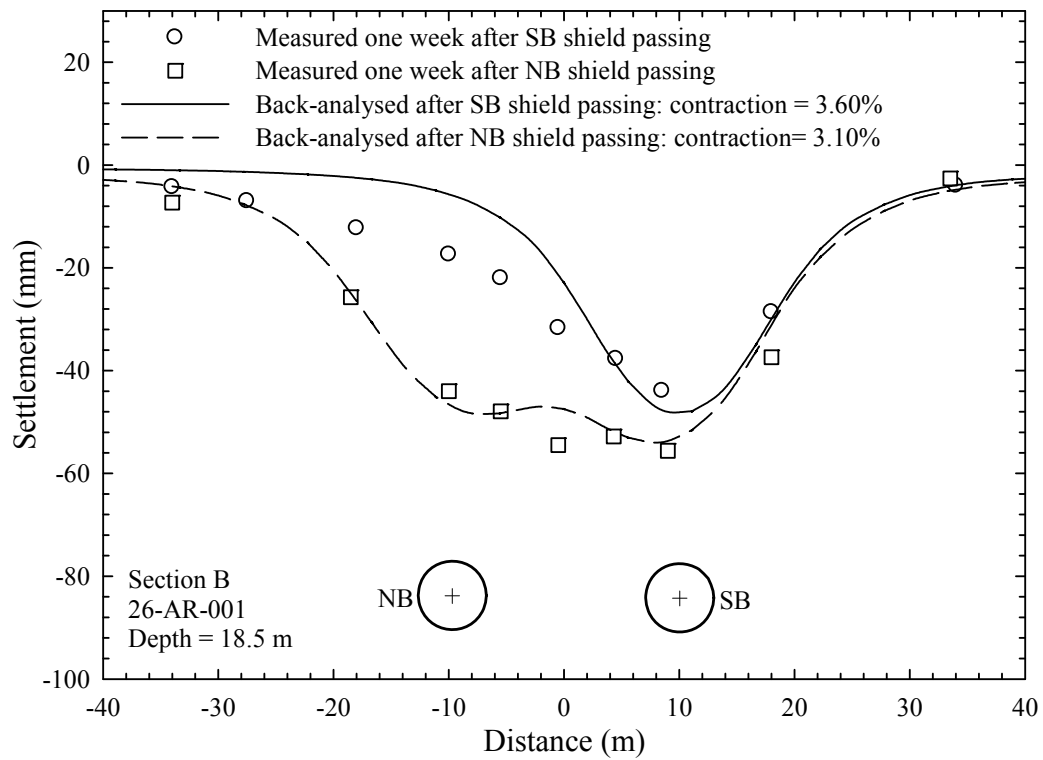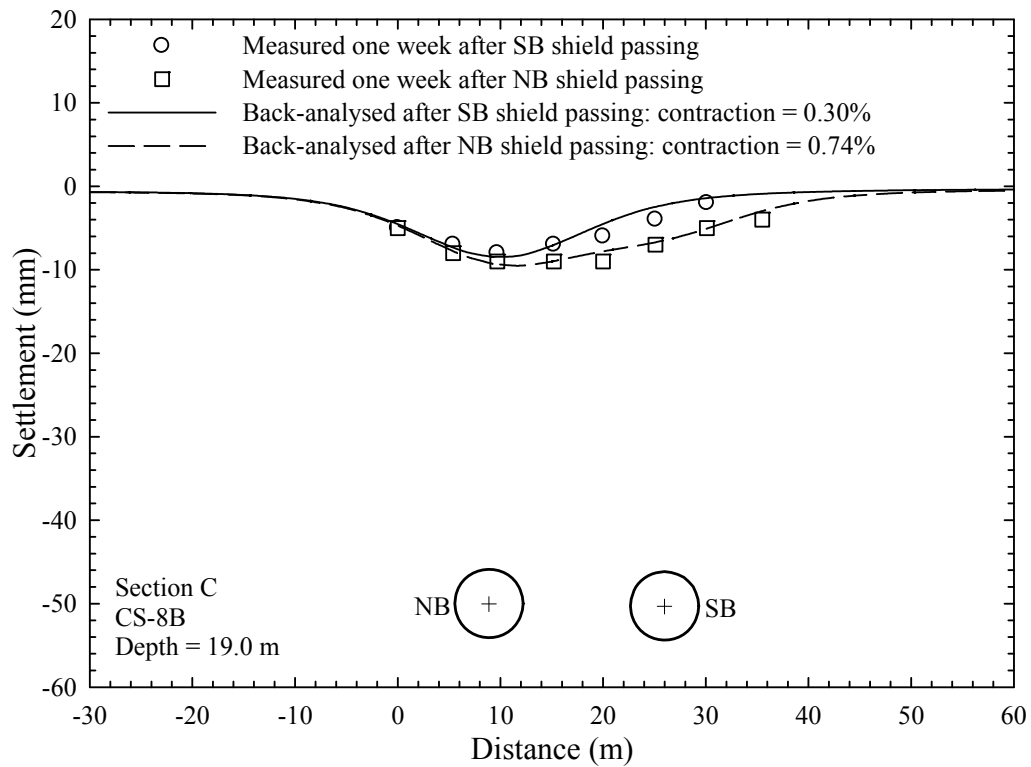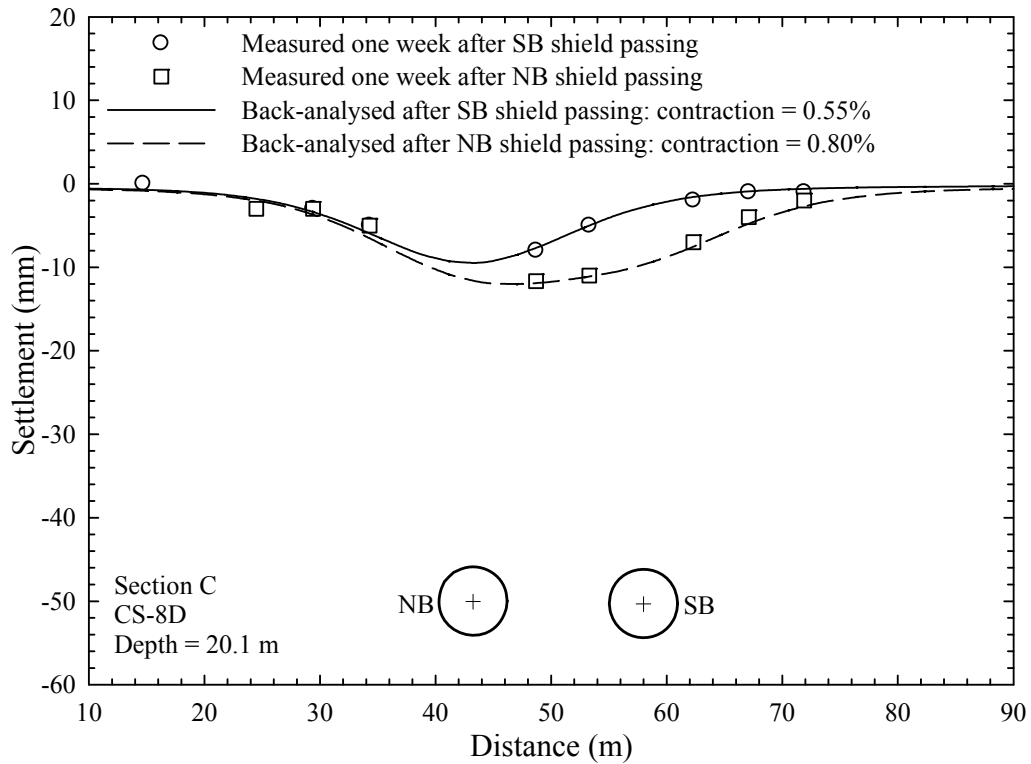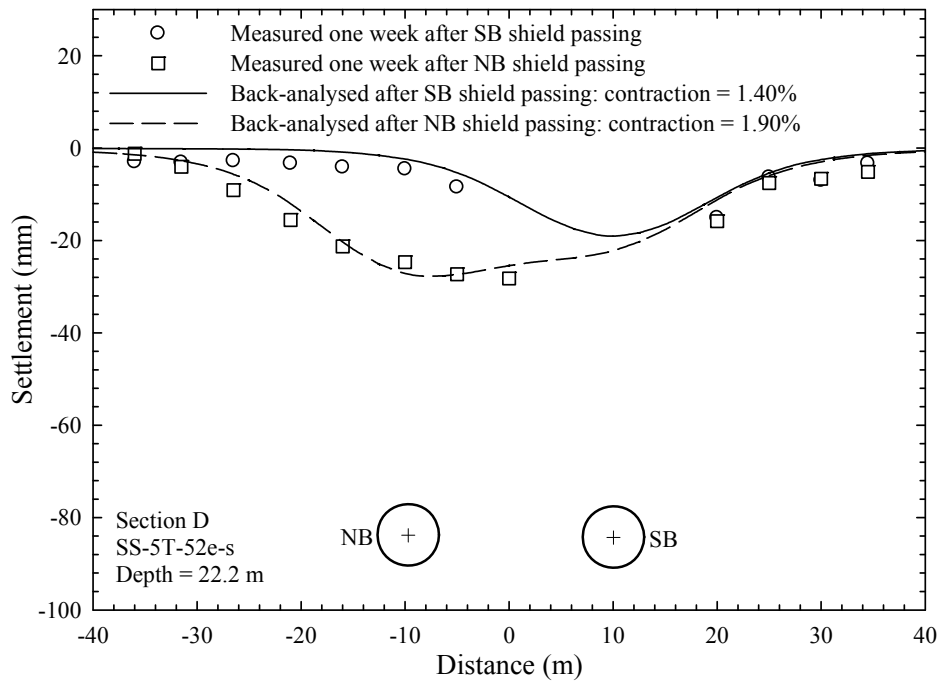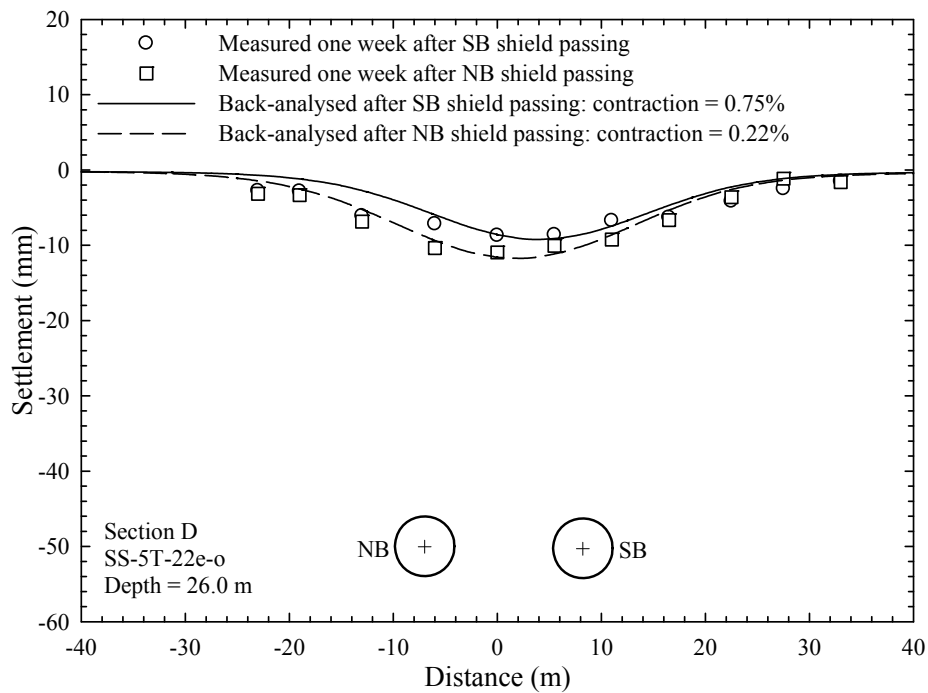

Figure 8.11 (g): Results from Contraction Method Back-analysis
(Section D: SS-5T-22e-o)

Figure 8.11: Results from Contraction Method Back-analysis

317

Table 8.4: Volume Loss from Superposition Technique and FEM Back-analysis and Stress Reduction Factor from FEM Back-analysis

	Section	V_L (%) from Superposition technique		Contraction (%) from FEM back-analysis		β from FEM back-analysis	
		SB	NB	SB	NB	SB	NB
A	23-AR-001	4.86	1.67	3.30	2.80	0.40	0.45
A	23-G3-007-019	2.78	0.62	2.82	0.80	0.41	0.70
B	26-AR-001	4.41	2.67	3.60	3.10	0.53	0.62
C	CS-8B	0.27	0.74	0.30	0.74	0.84	0.72
C	CS-8D	0.43	0.69	0.55	0.82	0.76	0.71
D	SS-5T-52e-s	1.69	1.99	1.40	1.90	0.46	0.40
D	SS-5T-22e-o	0.92	0.22	0.75	0.22	0.59	0.80

Another comparison was made between the back-analysed percentage of volume loss (V_L) and the percentage of the contraction. By using the Gaussian curve (Peck, 1969) to match the measured settlement, the trough width parameter (i) and the maximum surface settlement ($\delta_{v,max}$) were obtained. For the second tunnel in the side-by-side pattern, the superposition technique (Suwansawat and Einstein, 2007) was used for i and $\delta_{v,max}$ estimation (see discussion on this technique in Chapter 3). The back-analysed i and $\delta_{v,max}$ are listed in Table 8.5. The percentage of the volume loss, listed in Table 8.4, was calculated using Equation 2.3. The back-analysed percentage of the volume loss and contraction are in good agreement. However, in the finite element calculations, the material of all the dominant clay layers was set as undrained. This means that the area enclosed by the computed surface settlement profiles and the contracted area of the tunnel lining are the same (i.e. no volume loss). Thus, the percentage of the volume loss and the contraction are comparable.

Table 8.5: Summary of Trough Width Parameter (i) and Maximum Surface Settlement ($\delta_{v,max}$) from Superposition Technique (Suwansawat and Einstein, 2007)

Section	1st tunnel excavated	i (m)		$\delta_{v,max}$ (mm)	
		SB	NB	SB	NB
A	23-AR-001	SB	15	9	42.0	24.0
A	23-G3-007-019	SB	9	10	40.0	8.0
B	26-AR-001	SB	13	13	43.9	26.6
C	CS-8B	NB	10	12	3.5	8.0
C	CS-8D	NB	9	10	6.2	9.0
D	SS-5T-52e-s	SB	13	13	17.0	20.0
D	SS-5T-22e-o	SB	14	9	8.6	3.2

8.3.3.2 Results and Discussions from the Stress Reduction Method

Similar to the study of the contraction method in previous section, a series of finite element back-analyses was conducted with the stress reduction method. Apart from the difference in the shield tunnel installation technique (i.e. the contraction ratio and stress reduction methods), all the other conditions in the finite element computation were kept the same, namely, the initial stress calculation, the soil constitutive, and the parameters used, the model geometry, and the mesh generation, etc. The values of the unloading factor (β) were selected so that the computed settlements matched the field measurements. The results from the stress reduction method back-analyses are presented in Figures 8.12 (a) to 8.12 (g). The fitted unloading factors are also shown in the figures, as well as being listed in Table 8.4. It is seen that the lower values of unloading factor lead to a higher prediction of surface settlements and vice versa. This higher settlement causes by a higher degree of stress release as less support pressure is calculated from lower value of unloading factor.

Figure 8.12 (a): Results from Stress Reduction Method Back-analysis
(Section A: 23-AR-001)

Figure 8.12 (b): Results from Stress Reduction Method Back-analysis
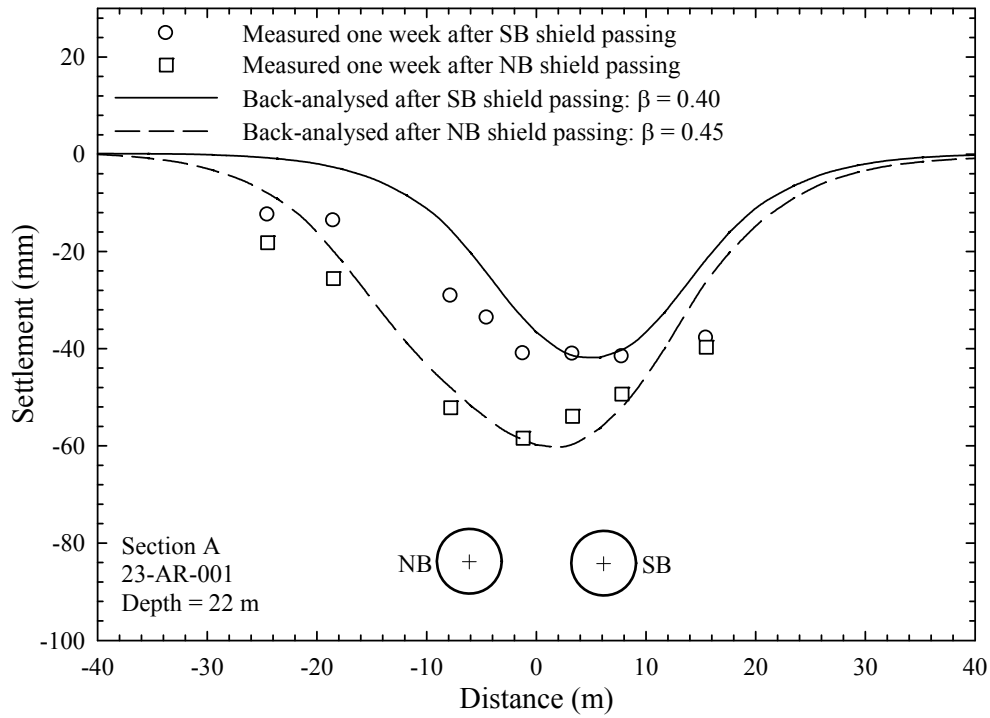(Section A:23-G3-007-019)

Figure 8.12 (c): Results from Stress Reduction Method Back-analysis
(Section B: 26-AR-001)
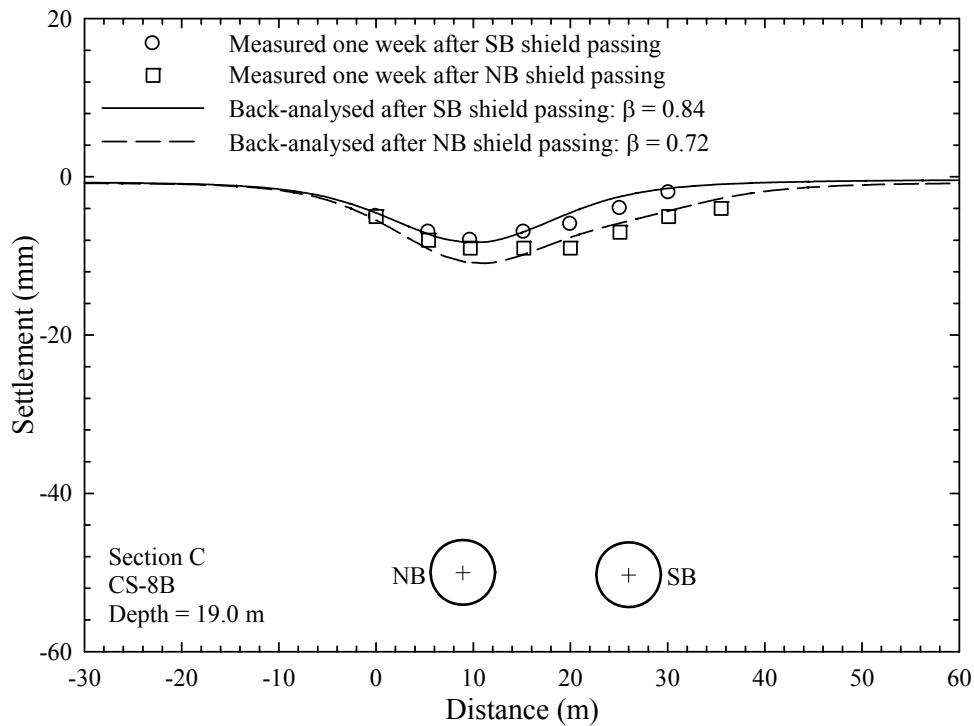
Figure 8.12 (d): Results from Stress Reduction Method Back-analysis (Section C: CS-8B)

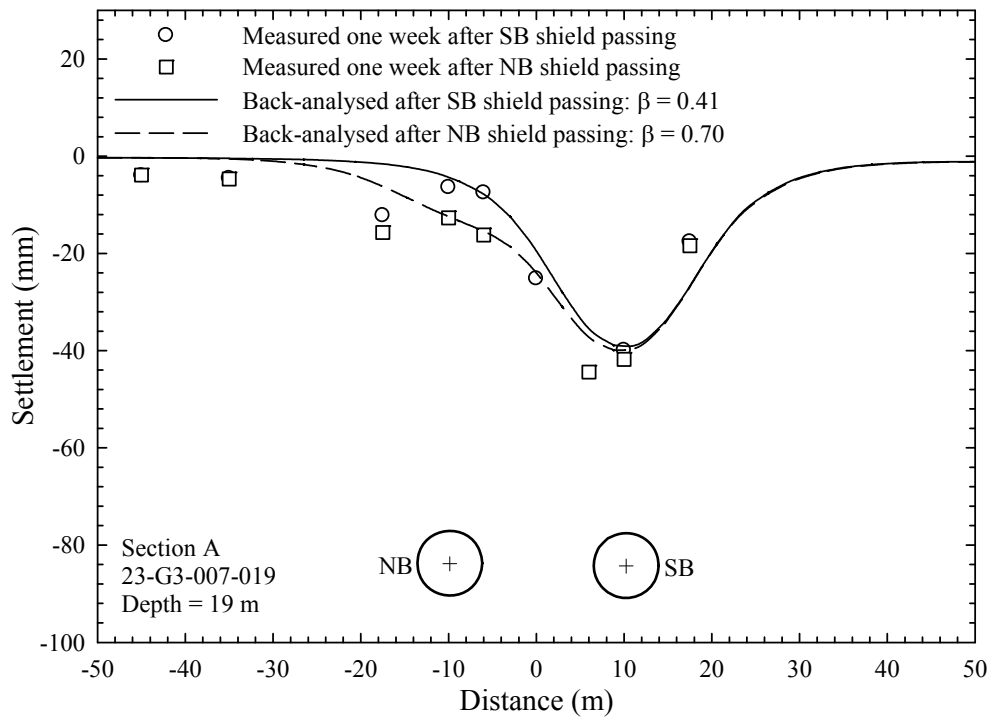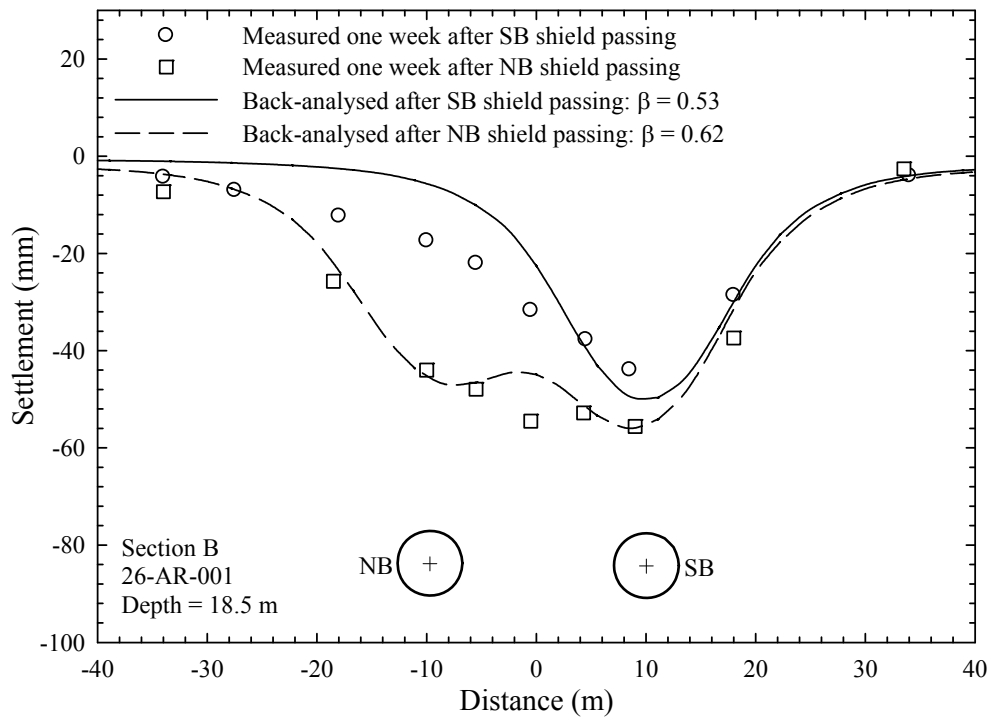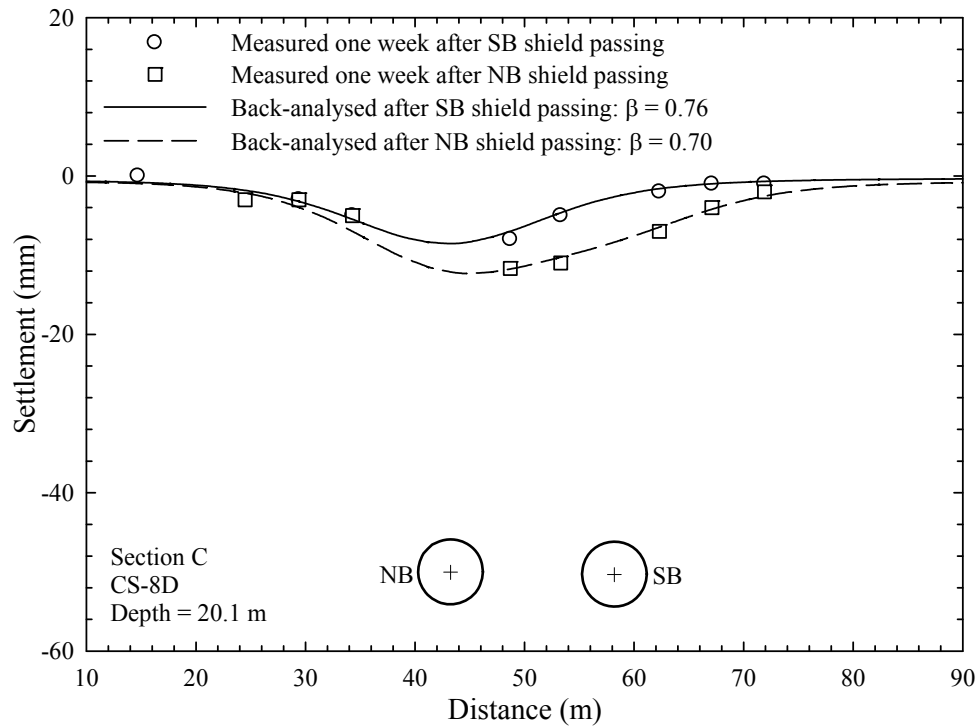Figure 8.12 (e): Results from Stress Reduction Method Back-analysis (Section C: CS-8D)
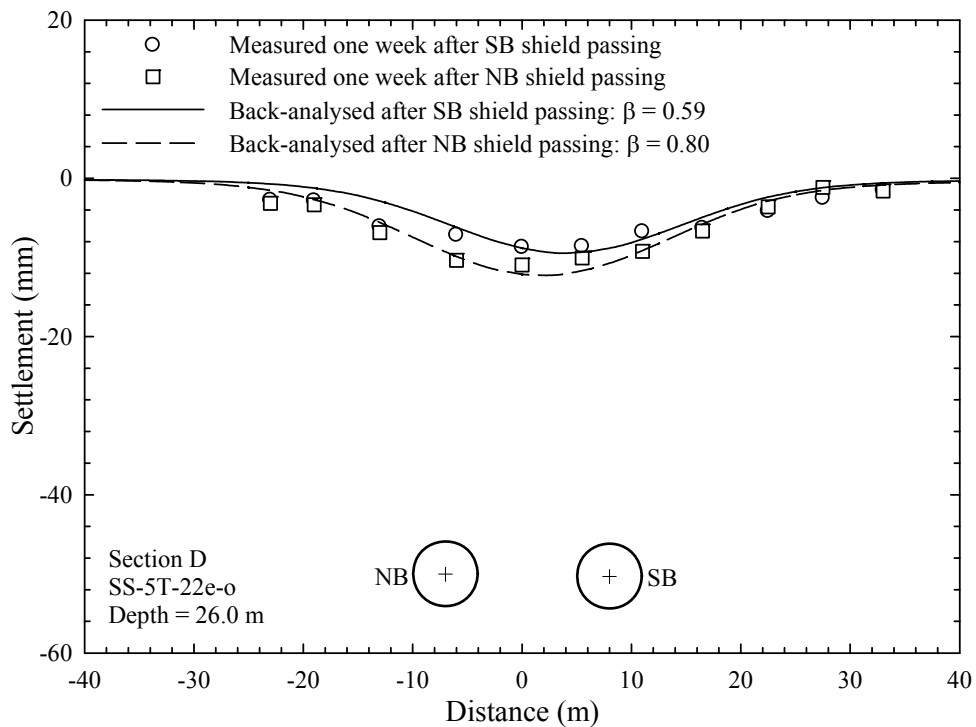
Figure 8.12 (f): Results from Stress Reduction Method Back-analysis
(Section D: SS-5T-52e-s)
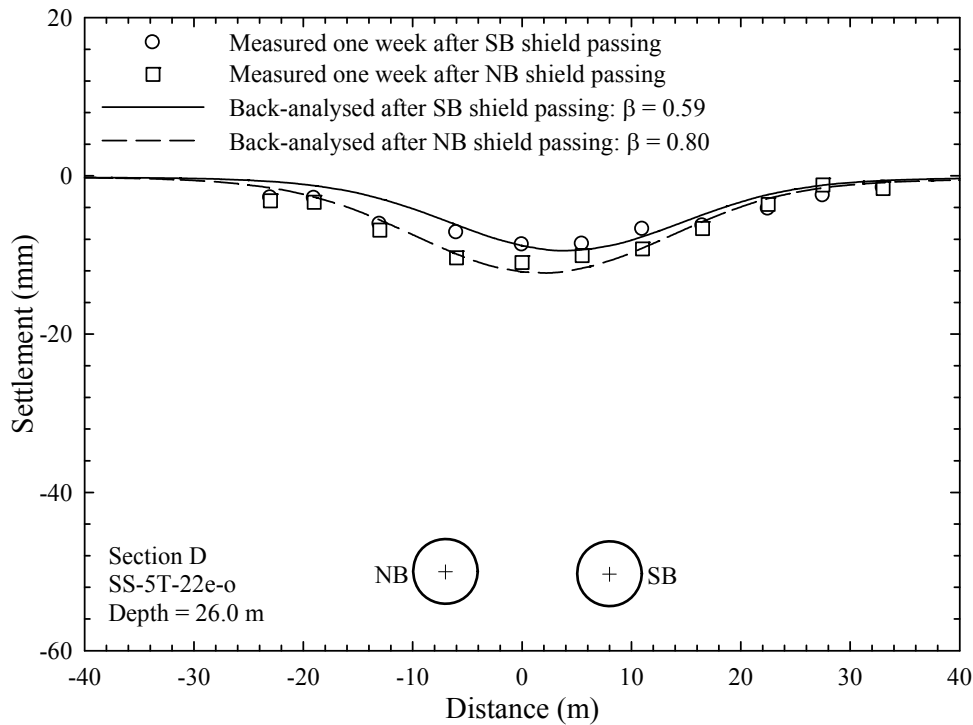
Figure 8.12 (g): Results from Stress Reduction Method Back-analysis
(Section D: SS-5T-22e-o)

Figure 8.12: Results from Stress Reduction Method Back-analysis

The back-analysed values of the unloading factor and the percentage of the contraction are plotted in Figure 8.13. A fairly good correlation was obtained between the percentage of contraction and the stress reduction ratio factor, with R^2 of 0.877. However, the two data points, the results from the SB and NB tunnels of Section B: 26-AR-001, were excluded in the regression analysis. The volume loss for the SB and NB tunnels was high with V_L = 4.41 and 2.67 per cent, respectively. As discussed earlier in Section 8.3.3, a high face pressure of 130 to 180 kN/m^2 and the percentage of the grout filling of 120 % were used in this section. As a consequence, the causes of the high volume loss, and thus the large settlement, were from the very low applied penetration rate of 3 to 15 mm/min and the moderately low grout pressure of 100 kN/m^2. According to Suwansawat (2002),a low penetration rate was adopted in this location as a result of the inexperienced tunnel crews who used the muck pumping technique. With this low penetration rate, the assumptions of the back-analysis using the stress reduction method may not be valid. The

323

first assumption rested on the condition being undrained. However, a low penetration rate, as small as 3 mm/min, may cause the surrounding soil to be partially drained. Nevertheless, the settlement predictions from the stress reduction method agree well with the field measurement data (Figure 8.12 (c)). Indeed, the back-analysed unloading factor (β) may not represent the stress release due to the tunnel excavation.
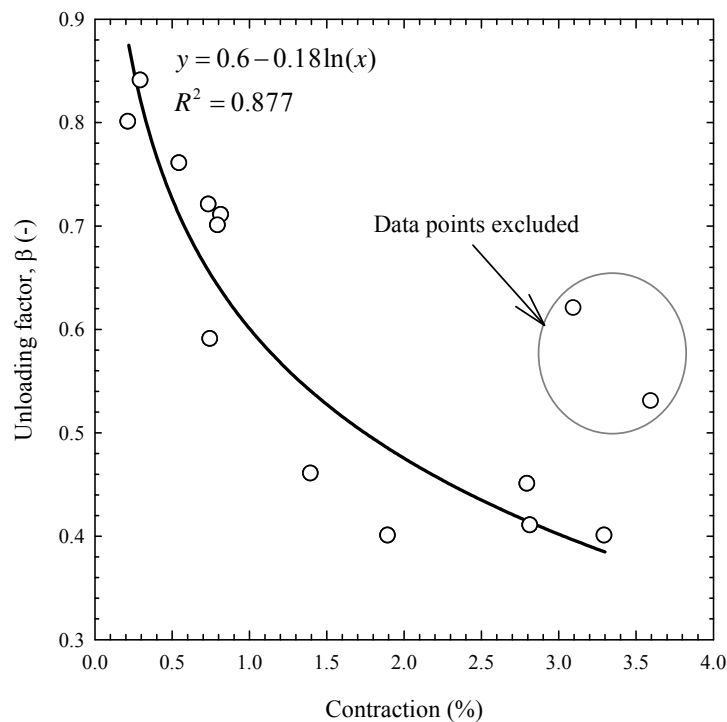
Figure 8.13: Relationship between Percentage of Contraction and Unloading Factor

In engineering practice, the ground settlement owing to the shield tunnelling is often limited by the percentage of the volume loss. One possible practical application of the correlation, presented in Figure 8.13, is that the unloading factor, to be used in a finite element analysis, can be estimated from the prescribed percentage of the volume loss (or the percentage of contraction). Even so, it should be kept in mind that an additional settlement, caused by a low applied penetration rate, will not be predicted from the estimated unloading factor (see Figure 8.13).

8.3.3.3 Results and Discussions from the Modified Grout Pressure Method

The last method considered herein is the modified grout pressure method. It is a three step calculation (described in Section 8.3.2.7), which is applied to the finite element analyses. Similar to the contraction ratio and the stress reduction methods, it involves a series of finite element analyses being undertaken for the seven twin tunnel excavation cases. In the modified grout method, the face and grout pressures were modelled by an applied pressure which increased linearly with depth. The unit weight of the slurry and grout material were assumed to be 12 and 15 kN/m^2, respectively. In the first attempt, the average face and grout pressures, as measured from the earth pressure chamber and the shield tail, were used as the face and grout pressures at the mid point of the TBM. The average measured face and grout pressures, as used in the first attempt of the analysis, are listed in Table 8.6. These face and grout pressure were averaged from highly fluctuating data. As a consequence, using the measured face and grout pressures gave an over-prediction of the ground settlement, when compared to the field measurements. Furthermore, using the very low face pressures of 45 and 40 kN/m^2 for the two cases of Section A has led to an unstable (near failure) analysis. It is obvious that a higher magnitude of face pressure was needed to achieve a reasonable settlement prediction. This is perhaps understandable, because the face pressure is a measurement of the slurry pressure inside the chamber. However, a total support pressure consists of a face pressure, support from the arched soil in front of the TBM and, perhaps, a support from the TBM rotating blades.

In the second attempt, it was decided that a series of back-analyses, similar to those of the contraction method and the stress reduction methods, should be performed. The values of the average measured grout pressure were used in these analyses, as the variation of the grout pressure was less than the face pressure. The results of the finite element back-calculations are shown in Figures 8.14 (a) to 8.14 (g) and listed in Table 8.7. In general, the predictions of the surface settlement agree well with the field measurements. The ratios of the back-calculated and measured face pressure were calculated for comparison. This ratio varied in a wide range from 1.03 to 4.38. Nevertheless, if the low face pressure

sections (Section A: 23-AR-001 and 23-G3-007-019) are excluded, this range is reduced to 1.03 to 1.46, with an average value of 1.22.

Table 8.6: Measured Face and Grout Pressures in the Studied Sections
(Suwansawat, 2002)

	Section	1st tunnel excavated	Measured face pressure (kN/m²)		Measured grout pressure (kN/m²)	
			SB	NB	SB	NB
A	23-AR-001	SB	45	70	250	250
A	23-G3-007-019	SB	40	80	300	350
B	26-AR-001	SB	140	170	100	220
C	CS-8B	NB	190	170	200	200
C	CS-8D	NB	190	200	200	150
D	SS-5T-52e-s	SB	175	170	250	400
D	SS-5T-22e-o	SB	225	250	380	410

Figure 8.14 (a): Results from Modified Grout Pressure Method Back-analysis
(Section A: 23-AR-001)

Figure 8.14 (b): Results from Modified Grout Pressure Method Back-analysis
(Section A:23-G3-007-019)

Figure 8.14 (c): Results from Modified Grout Pressure Method Back-analysis
(Section B: 26-AR-001)

327

Figure 8.14 (d): Results from Modified Grout Pressure Method Back-analysis (Section C: CS-8B)
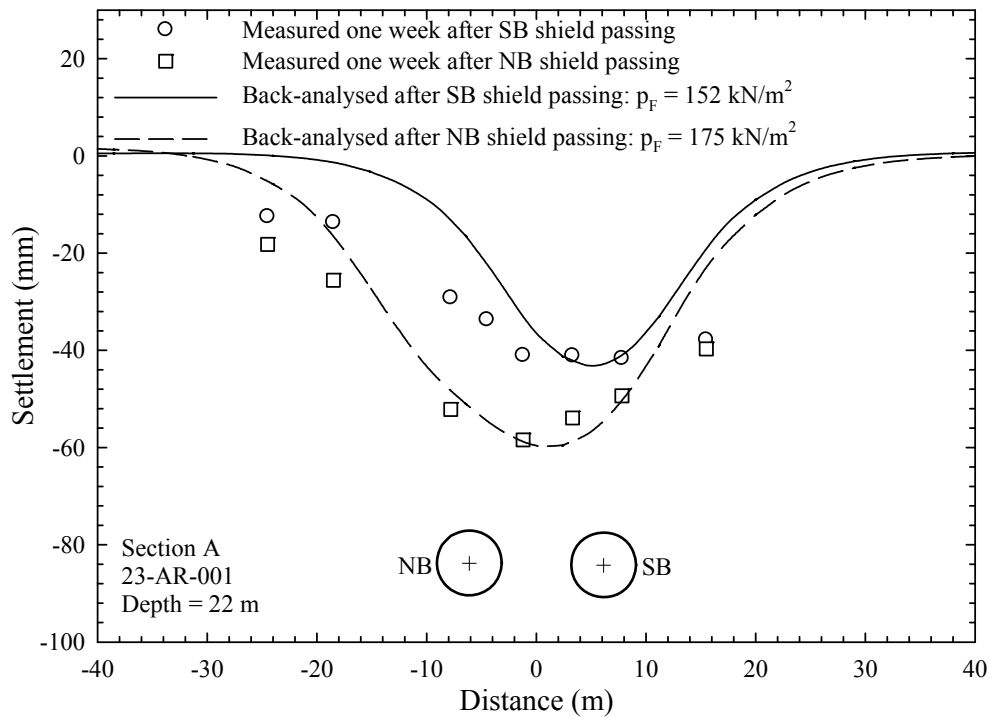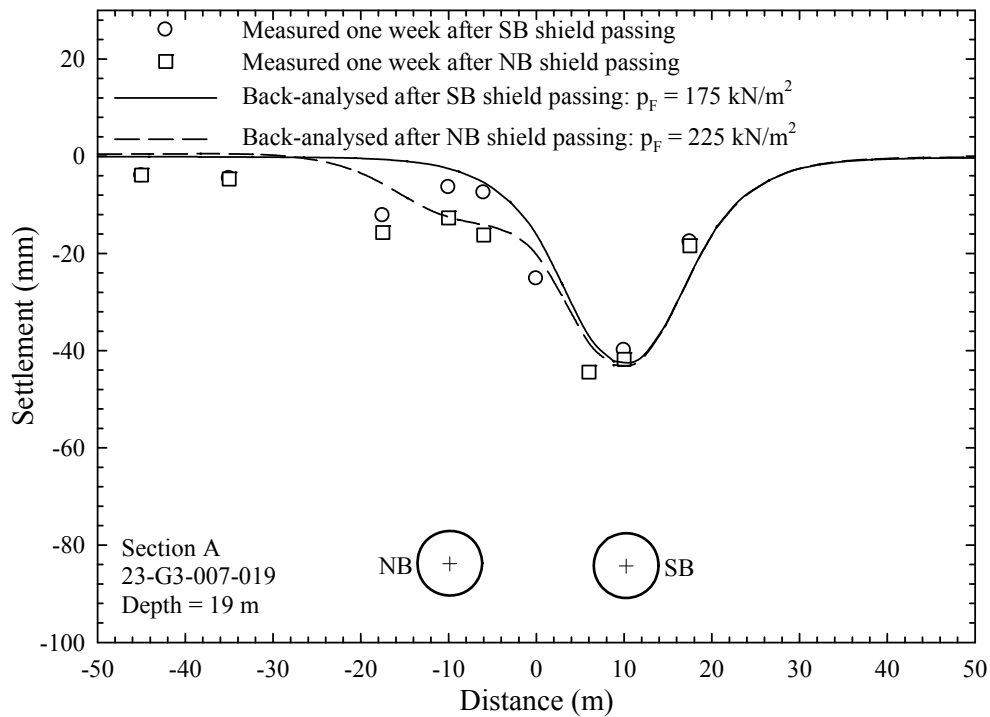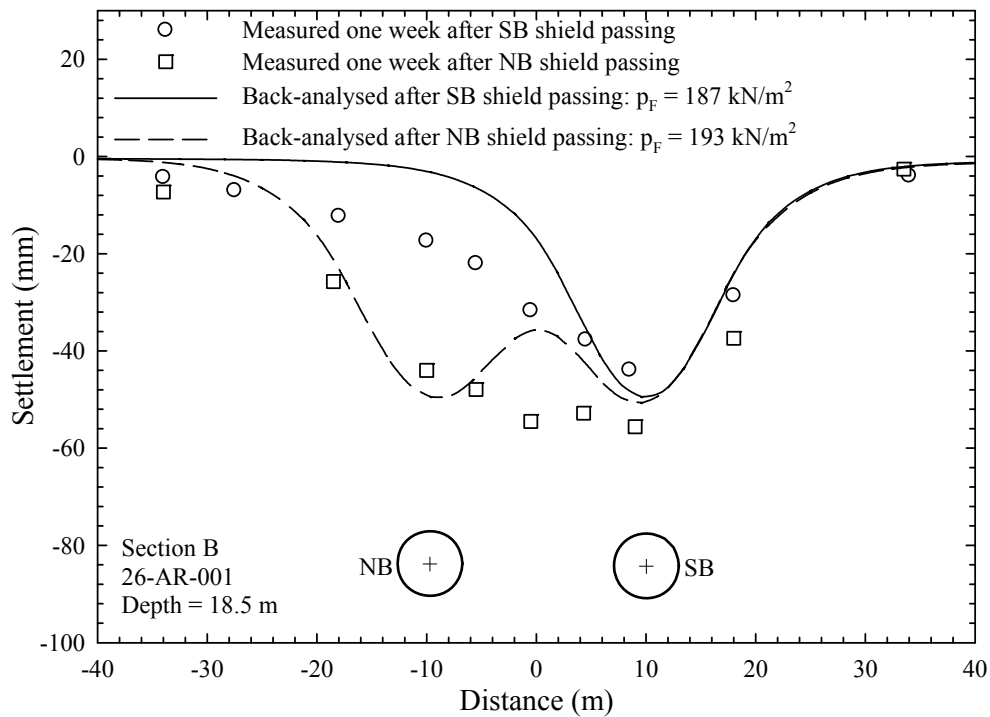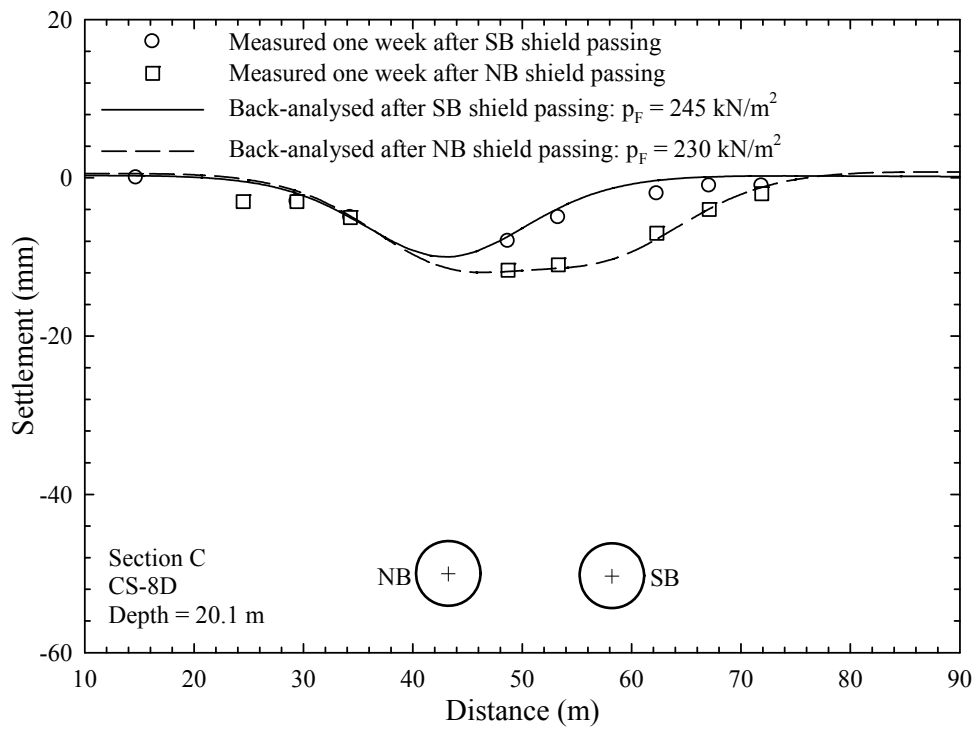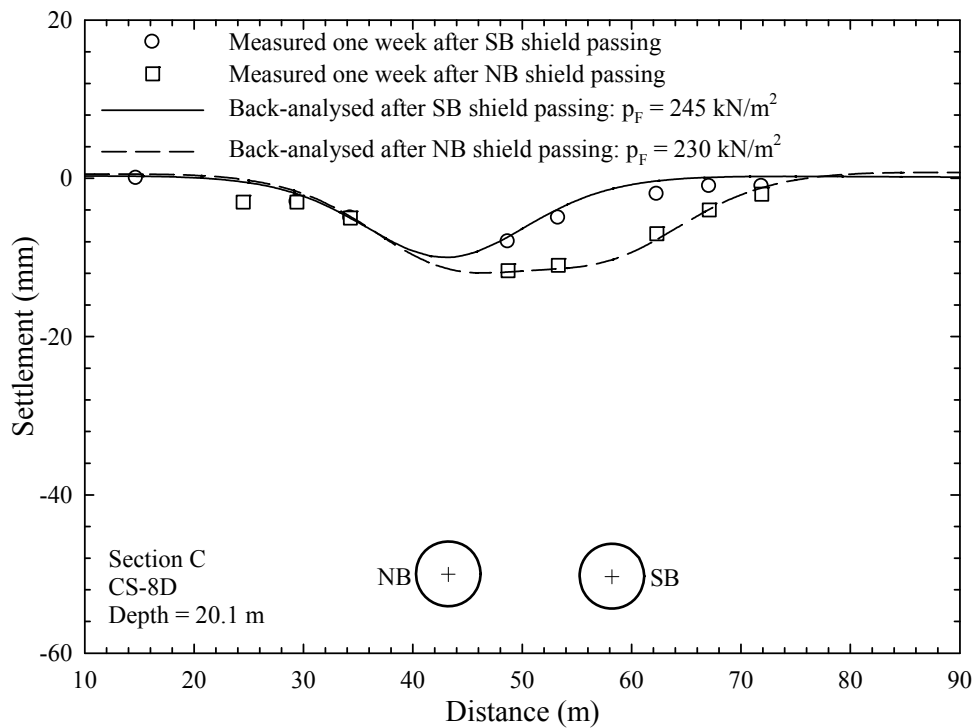

Figure 8.14 (e): Results from Modified Grout Pressure Method Back-analysis (Section C: CS-8D)
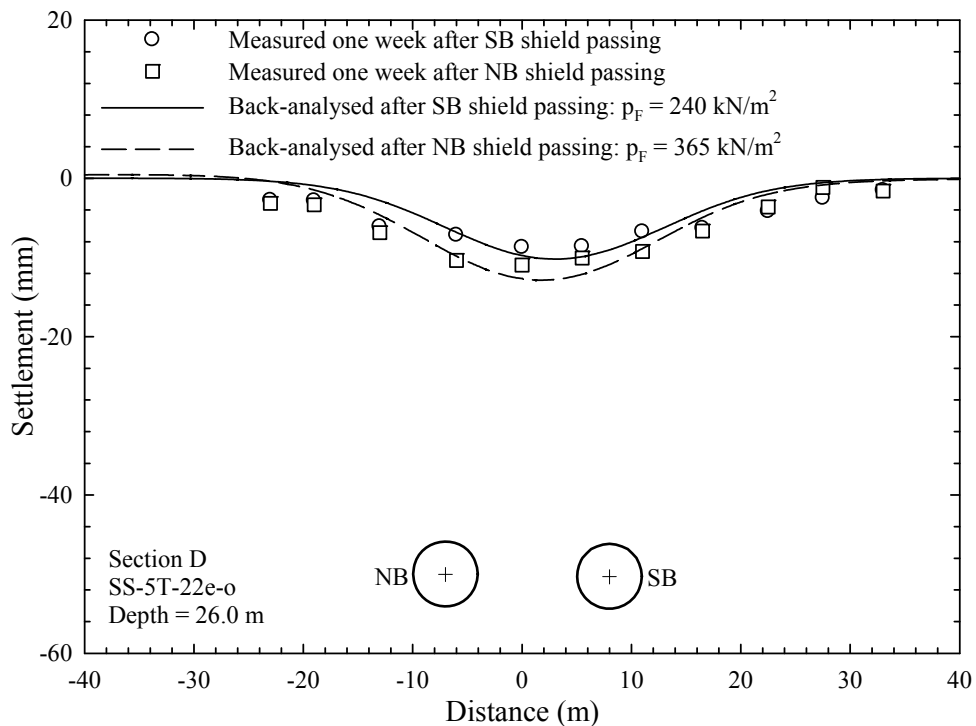
Figure 8.14 (f): Results from Modified Grout Pressure Method Back-analysis
(Section D: SS-5T-52e-s)
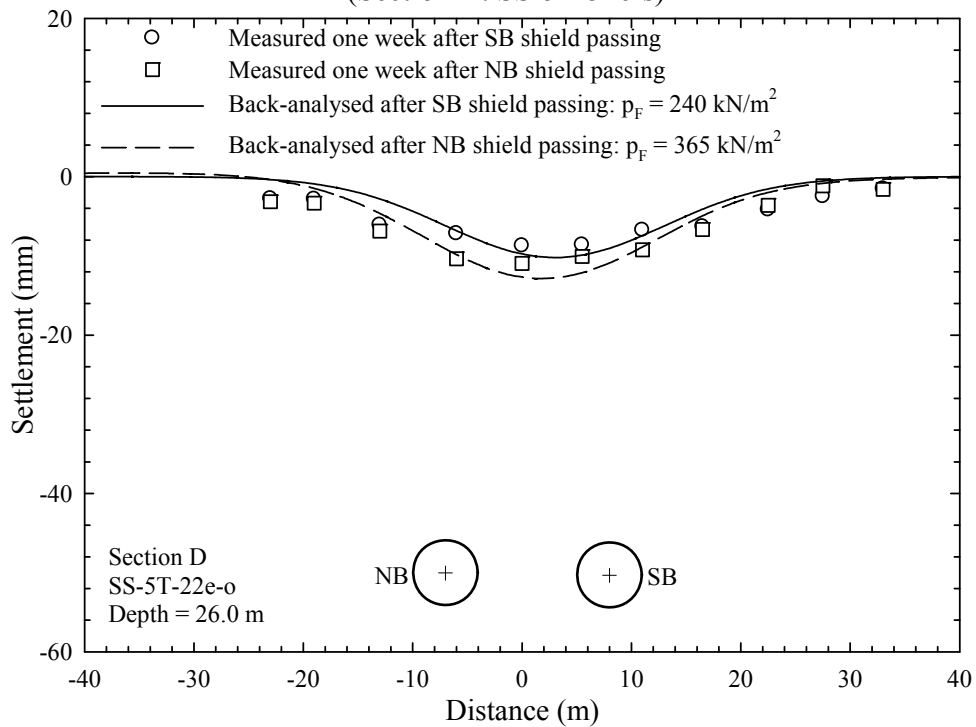
Figure 8.14 (g): Results from Modified Grout Pressure Method Back-analysis
(Section D: SS-5T-22e-o)

Figure 8.14: Results from Modified Grout Pressure Method Back-analysis

Table 8.7: Back-calculated Face Pressure in the Studied Sections

Section	1st tunnel excavated	Back-calculated face pressure (kN/m^2)		Ratio of back-calculated/measured face pressure	
		SB	NB	SB	NB
A	23-AR-001	SB	152	175	3.38	2.50
A	23-G3-007-019	SB	175	225	4.38	2.81
B	26-AR-001	SB	187	193	1.34	1.14
C	CS-8B	NB	250	235	1.32	1.38
C	CS-8D	NB	245	230	1.29	1.15
D	SS-5T-52e-s	SB	185	175	1.06	1.03
D	SS-5T-22e-o	SB	240	365	1.07	1.46

From the current study, and for a practical engineering application, it appears that establishing a relationship among all the three 2D finite element methods is worthwhile. The back-calculated unloading factor was plotted with the ratio of the face pressure and the total vertical stress (p_F/σ_v). As one may expect, most of the data points were located close to the $p_F/\sigma_v = \beta$ line (Figure 8.15). This correlation between β and p_F/σ_v in a close face tunnel is comparable to the correlation between the unloading factor (β) and the delay support length (or round length). With a plot of the percentage contraction versus the unloading factor on the side, an inter-correlations among the three methods can be formed. For example, if the ground settlement is limited at 1 per cent of the volume loss, the percentage of the contraction of the tunnel lining is approximately the same in the undrained condition. From Figure 8.15, the unloading factor (β) reads as 0.6, which also corresponds to the face pressure (p_F) of $0.6\sigma_v$. However, if this face pressure is applied as slurry pressure inside the TBM chamber, the surface settlement would be less than the finite element prediction. In relation to the assumptions adopted in the finite element analyses, Figure 8.15 should be employed in the cases where the TBM is operated with a high penetration rate, but with no excessive use of the copy cutter.
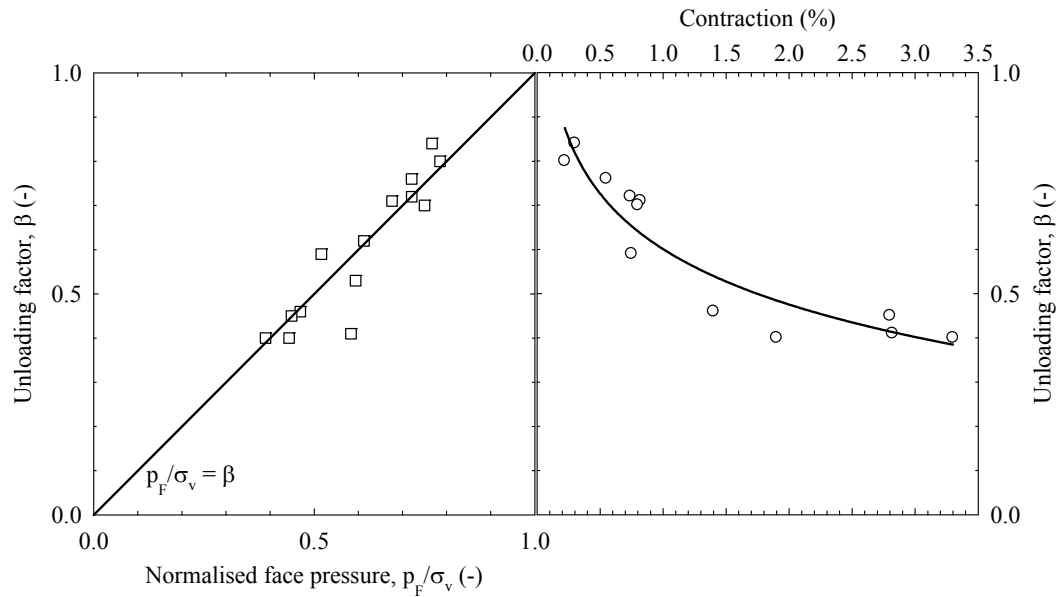
Figure 8.15: Relationships of Contraction, Stress Reduction
and Modified Grout Pressure Methods

8.3.3.4 Comparisons of Three 2D Finite Element Methods

This section compares the predictions of the contraction method, the stress reduction method and the modified grout pressure method. Section A: 23-AR-001 was selected for this comparison. Figure 8.16 presents the predicted surface settlement from all three methods; the shape of the predicted settlement profiles is the same. The modified grout pressure method provides a slightly steeper settlement trough, followed by the stress reduction method and the contraction method. The next comparison focused on the tunnel lining. The maximum lining deformation, maximum bending moment, maximum shear force, and maximum axial force from the three methods are listed in Table 8.8. The maximum magnitudes of the lining deformation, the bending moment and the structure forces are comparable. However, the shape of the bending moment and the shear force in the diagrams is not the same. There are also some dissimilarities in terms of the deformed shape of the tunnel lining, as shown in Figures 8.17 (a) to 8.17 (c). The contraction method predicts a contracted shape of the tunnel lining with a uniform oval shape, while deformed tunnel lining shapes of the stress reduction and modified grout pressure methods are similar. A close look at the data reveals that the modified grout pressure

331

method allows more local movement at the crown and less movement at the inverse of the tunnel lining.
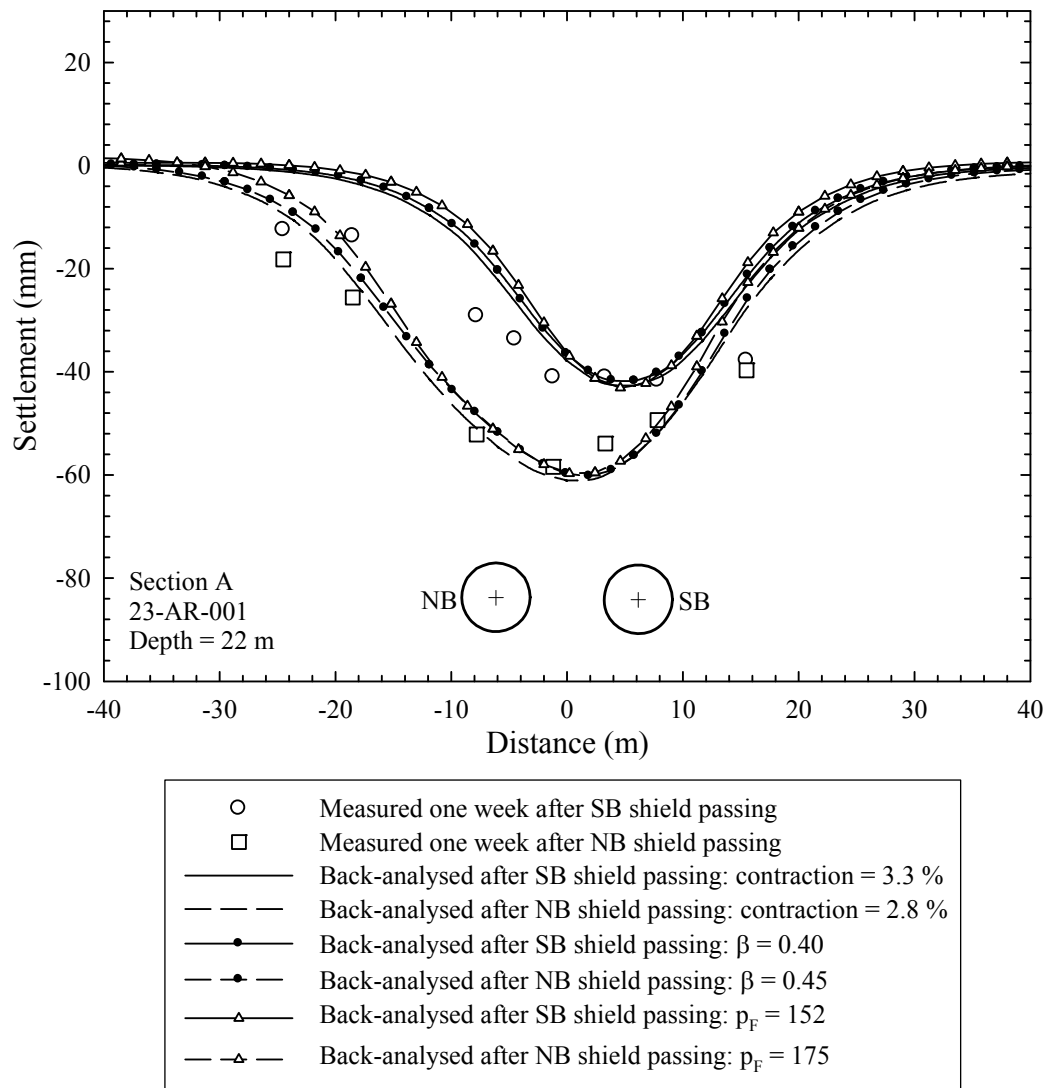
Figure 8.16: Comparison of Measured and Predicted Surface Settlements
(Section A: 23-AR-001)

Table 8.8: Lining Deformation and Lining Forces (Section A: 23-AR-001)

Lining deformation and forces	Contraction ratio		Stress reduction		Modified grout pressure	
	SB	NB	SB	NB	SB	NB
Maximum lining deformation (mm)	104.3	89.2	102	88.3	103.3	92.2
Maximum bending moment (kNm/m)	-94.5	-78.5	-64.6	-63.5	-76.1	-80
Maximum shear force (kN/m)	-60.8	52.3	45.34	43.7	-52.2	-51.8
Maximum axial force (kN/m)	-425.2	-534.6	-534.5	-653.3	-527.1	-594.3
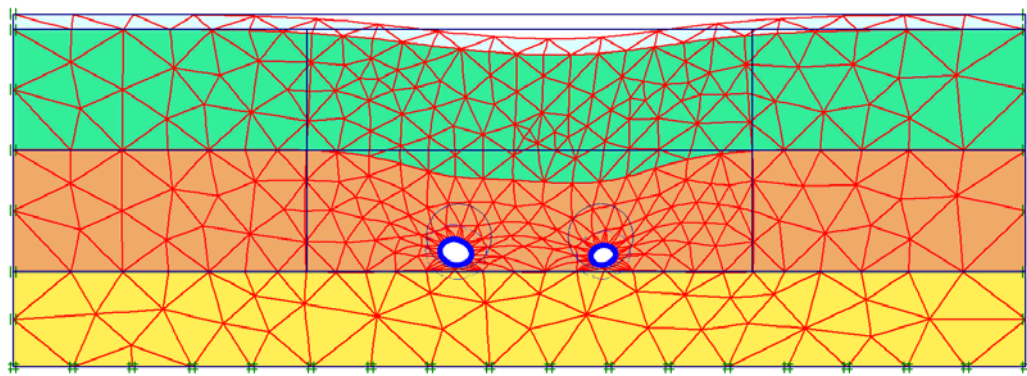
Figure 8.17 (a): Deformed Finite Element Mesh from Contraction Method
(Scaled up 40 times)
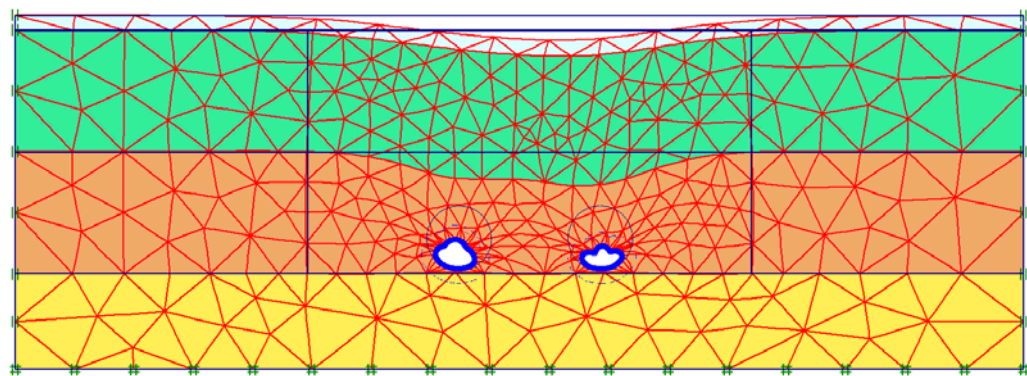
Figure 8.17 (b): Deformed Finite Element Mesh from Stress Reduction Method
(Scaled up 40 times)
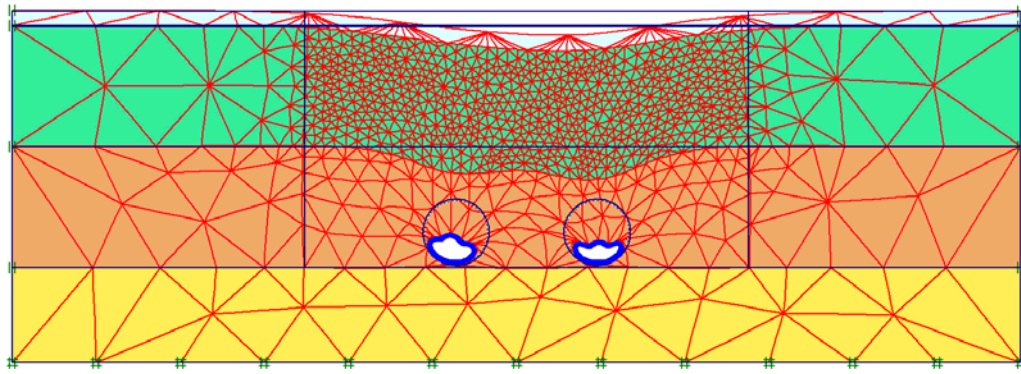
Figure 8.17 (c): Deformed Finite Element Mesh from Modified Grout Pressure Method
(Scaled up 40 times)

8.4 Finite Element Analysis of the Combined Cut-and-Cover and New Austrian Tunnelling Methods for MRT Station

This section focuses on the ground and wall movements in an excavation using a combined cut-and-cover method and New Austrian Tunnelling Method (NATM) for a MRT station. A two dimensional finite element analysis was employed. The MRT station (Wang Burapha) is a part of the Bangkok Blue Line Extension project, which is currently in the design stage. Importantly, the analysis described in this section was conducted as part of the preliminary design of the Bangkok MRT Blue Line Extension project (at an early stage in the author's study). The soil parameters used in this analysis were different from the more refined set of parameters used in Chapter 7 and in the first part of Chapter 8. Indeed, it was the author's interest in this new construction technique that the study was undertaken into ground and wall movements during the planned construction.

The main aim of this section of the study was to evaluate the behaviour of the ground and concrete wall movements induced by the construction of a station. The details of the station location, cross-section dimension used in the finite element analysis, and the subsoil condition were addressed in Chapter 3. Below are the steps adopted in this study:

334

(1) The Hardening Soil Model was used for all the soil layers. The soil parameters were obtained from the results of the unconsolidated undrained triaxial tests and the site investigation of the project feasibility study.

(2) The finite element modelling was undertaken according to the construction sequences (which involved the cut-and-cover excavation of the station box, followed by the NATM enlargement excavation).

(3) Comparisons were made of the ground surface settlements during the cut-and-cover excavation of the station box, as given by the finite element analysis, and predicted by the simplified method proposed by Ou and Hsieh (2000).

(4) Finally, the NATM enlargement from the side of the cut-and-cover excavation box was analysed. The results obtained are discussed below.

The construction sequences of the Wang Burapha station can be summarised as:

(1) The demolition of an existing four storey building in the cut-and-cover box construction area;

(2) The construction of the 1.2-m and 1.0-m-wide diaphragm walls on the left and right hand sides of the cut-and-cover excavation, respectively. The diaphragm walls are to be installed down to the Very Dense Sand layer at a depth of 42.4 m;

(3) The excavation of the box using 3.0-m-deep excavation steps to the base slab level at a depth of 32 m. Each excavation step will be followed immediately by the installation of temporary steel struts at 4.5 m horizontal spacing. Soil improvement in the area of the upper NATM will be constructed in this construction step;

(4) The installation of 2.0 m thick base slab;

(5) The soil improvement of the Dense Sand layer in the area below the base slab and underneath the area of the lower tunnel; An enlargement of the excavation of the station to encompass two vertically stacked bored tunnels using the NATM technique. Each of the circular enlargements is to be made at a diameter of 12.4 m. The lower tunnel is to be excavated first.

Figure 8.18 shows the Wang Burapha Station cross section. For both the lower and upper NATM tunnels, the excavation cross section was divided into two main sections, E-S 2 and E-S 3, and each section was divided into a further three sub-sections, as illustrated in Figure 8.19. The construction sequences of the lower and upper tunnels were the same and they followed the numerical and alphabetical order from E-S 2A to E-S 3C, respectively. After the lower NATM tunnel construction was completed, the permanent 1.0 m thick platforms could be constructed using the bottom up method, followed by the removal of the temporary steel struts; this process is also applicable in the construction of upper tunnel.
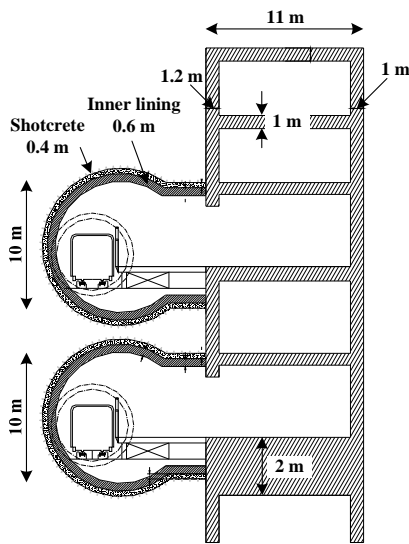
Figure 8.18: Wang Burapha Station (CS-A)   Figure 8.19: NATM Construction Sequences
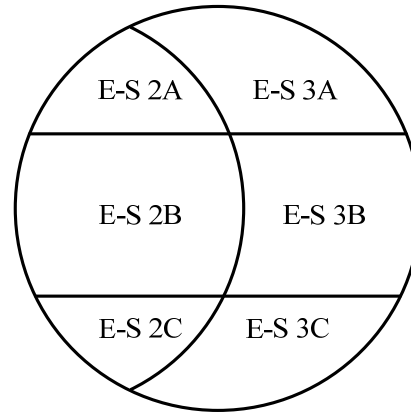
8.4.1 Finite Element Modelling

Due to the asymmetrical shape of the Wang Burapha Station cross section, the selected cross section CS-A (Figure 8.18) was modelled in full geometry. The drawdown pore water pressure was assumed, with the upper ground water level being at 1.2 m below the ground surface. All the soil layers, as shown in Figure 8.20, were modelled with the Hardening Soil Model. The input parameters are given in Table 8.9. The area of improved soil was modelled using the Mohr Coulomb Model (the input parameters are listed in Table 8.10). The existing four storey buildings and roads were considered as

336

distributed load of 50 and 16.7 kN/m^2, respectively. For the area of the pile foundation of the buildings, an approximate method (Fleming *et al.*, 1985) was used to obtain the combined axial stiffness of the piles and soil. The diaphragm wall and slab were modelled using the plate elements, whilst the spring and tunnel elements were selected for the strut and the NATM excavation lining, respectively. The 2D plane strain model and the mesh generation are depicted in Figure 8.20. The model consists of 3086, 15-noded triangular elements. The input parameters of the diaphragm walls, base slab, platform slabs, tensile pile, temporary struts and shotcrete are listed in Tables 8.11 to 8.14. Further, the stress reduction method (*β*-method) was used to simulate the 3D effect on the NATM tunnelling. The unloading factor (*β*) of 0.35 (Moller, 2006) was selected according to the design round length of 1.0 m.
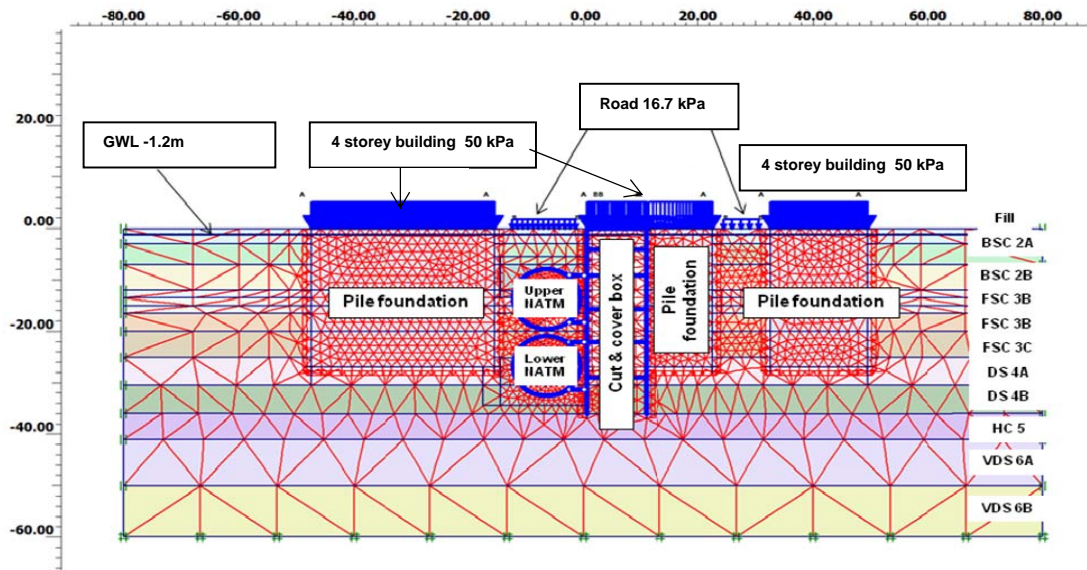
Figure 8.20: Geometry and Finite Element Mesh of Wang Burapha Station

Table 8.9: Soil Parameters – Wang Burapha Station

Type of soil	Depth (m)	Unit weight (kN/m³)	E_{50}^{ref} E_{oed}^{ref} E_{ur}^{ref} (MN/m²)	ν_{ur}	p^{ref} (kN/m²)	Power m	ϕ'/ψ (°)	c' (kN/m²)	K_0^{nc}	OCR
Fill 1	0.0 to 3.0	18.0	5 5 25	0.2	8.1	0.5	25/0	0.0	0.58	1.0
BSC 2A	3.0 to 7.0	16.0	6.5 6.5 65	0.2	34.7	1.0	23/0	16.7	0.61	2.5
BSC 2B	7.0 to 12.0	16.0	7.5 7.5 60	0.2	50.1	1.0	23/0	20.3	0.61	2.0
BSC 2C	12.0 to 13.5	16.0	9 9 72	0.2	66.9	1.0	23/0	26.8	0.61	2.0
FSC 3A	13.5 to 16.5	16.0	10 10 100	0.2	70.0	0.85	26/0	40.0	0.56	1.65
FSC 3B	16.5 to 20.0	17.0	12 12 120	0.2	93.6	0.85	26/0	45.0	0.56	1.65
FSC 3C	20.0 to 25.0	17.5	15 15 150	0.2	123.9	0.85	26/0	52.0	0.56	1.65
DS 4A	25.0 to 30.5	17.5	37 29.6 90	0.2	100.0	0.5	41/7	0.0	0.34	1.7
DS 4B	30.5 to 36.0	17.5	37 29.6 90	0.2	100.0	0.5	41/7	0.0	0.34	1.7
HC 5	36.0 to 41.0	18.0	19 19 190	0.2	203.2	0.8	23/0	68.0	0.61	1.0
VDS 6A	41.0 to 50.0	17.5	37 29.6 90	0.2	100.0	0.5	41/14	0.0	0.34	1.7
VDS 6B	50.0 to 70.0	17.5	37 29.6 90	0.2	100.0	0.5	41/14	0.0	0.34	1.7

Table 8.10: Input Parameters – Improved Soil

Parameter	Soil Improvement - MC
Elastic modulus (MN/m^2)	100
Poisson Ratio, ν	0.25
Friction Angle, ϕ' (°)	35
Cohesion, c' (kN/m^2)	200
Material type	Non-porous

Table 8.11: Input Parameters – Diaphragm Walls

Parameter	Diaphragm wall d = 1.2 m	Diaphragm wall d = 1.0 m
Elastic modulus of concrete, E_c (MN/m²)	24400 (reduced 20% due to cracking and shrinkage)	
Axial stiffness, EA (MN/m)	29280	24400
Flexural rigidity, EI (MNm²/m)	3514	2033
Weight, w (kN/m²)	19.2	16.0
Poisson ratio, ν	0.2	0.2

Table 8.12: Input Parameters – Slabs and Storey Columns

Parameter	Base slab d = 2.0 m	Platform slabs d = 1.0 m	Storey columns d = 0.8 m every 11.4 m
Elastic modulus of concrete, E_c (MN/m²)	24400 (reduced 20% due to cracking and shrinkage)		
Axial stiffness, EA (MN/m)	48800	24400	1712
Flexural rigidity, EI (MNm²/m)	16267	2033	91
Weight, w (kN/m²)	32	25	25
Poisson ratio, ν	0.2	0.2	0.2

Table 8.13: Input Parameters – Tensile Pile and Temporary Strut

Parameter	Tensile pile d = 1.8 m every 11.4 m	Temporary struts every 4.5 m longitudinal
Axial stiffness EA (MN/m)	1675	4440

Table 8.14: Input Parameters – NATM Tunnel Lining

Parameter	Shotcrete lining green / fully hardened $d = 0.4$ m	Temporary shotcrete lining green / fully hardened $d = 0.35$ m	Final lining $d = 0.6$ m	Combined Shotcrete / final lining $d = 1.0$ m
Elastic modulus of concrete, E_c (MN/m²)	7.5 / 15	7.5 / 15	24.4	20.6
Axial stiffness, EA (MN/m)	3000 / 6000	2625 / 5250	14640	20640
Flexural rigidity, EI (MNm²/m)	40 / 80	26.8 / 53.6	439	1720
Weight, w (kN/m²)	6.4	5.6	9.6	16.0
Poisson ratio, v	0.2	0.2	0.2	0.2

8.4.2 Simulating the Construction Process

The construction process of both the cut-and-cover box and the NATM tunnels were divided into a number of calculation steps. However, only four salient steps (9, 14, 28 and 40) were used in this study (see Table 8.15). Steps 9 and 14 represent the calculation steps, after the cut-and-cover station box has been excavated to a half and a full depth. Steps 28 and 40 are undertaken following the completion of the lower and upper NATM tunnels, respectively.

Table 8.15: Summary of Calculation Steps

Calculation Steps	Descriptions
Step 9	- Excavation depth is at 15 m
Step 14	- Excavation depth is at 32 m
Step 28	- After lower NATM tunnel is constructed
Step 40	- After both lower and upper NATM tunnels are constructed

8.4.3 Calculation Results

8.4.3.1 Results after Construction of Cut-and-Cover Station Box

Ou and Hsieh (2000) developed a simplified calculation method, based on the shape or type of the ground surface settlements observed from many deep excavation case histories (for a detailed discussion see Section 7.2). The ground surface settlements, calculated from the finite element analysis at excavation depths of 15 and 32 m, were compared with the simplified method predictions (Figure 8.21 and 8.22). These comparisons revealed a reasonably good agreement in the Primary Influence Zone (PIZ) for both location and magnitude of maximum settlement. The location of the PIZ did not change as the excavation increased. In an area of the Secondary Influence Zone (SIZ), the results from the finite element analysis seem to be greater.
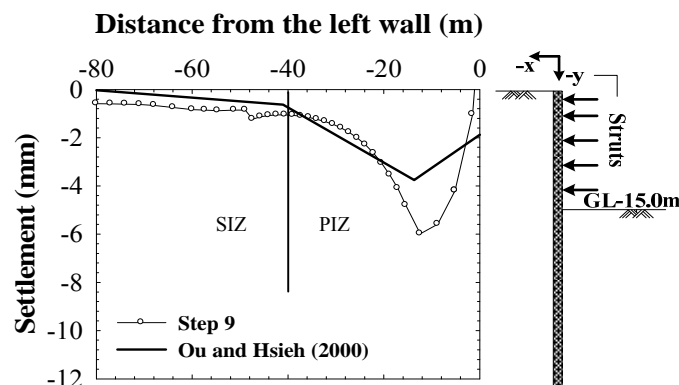

Figure 8.21: Comparison between Finite Element Analysis and Simplified Method
(Step 9 at 15 m excavation depth)
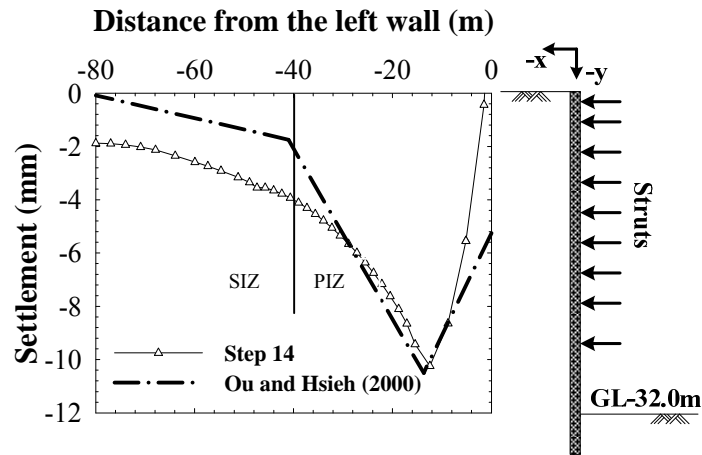
Figure 8.22: Comparison between Finite Element Analysis and Simplified Method
(Step 14 at 32 m Excavation Depth)

8.4.3.2 Results after Construction of NATM Tunnels

All four steps of the calculation (according to Table 8.15) from the finite element analysis are shown below: for the lateral wall displacement and ground surface settlement at the left wall see Figure 8.23 and at the right wall see Figure 8.24. The maximum ground surface settlement and lateral wall displacement increased with the excavation depth (from Steps 9 to p 14; see Figure 8.23). However, after the lower and upper NATM tunnels were constructed (Steps 28 and 40), the maximum wall displacement reduced from its peak value of 21 mm to 14 mm. The stress release, due to the NATM tunnels excavation, caused the tip of the left diaphragm wall to move toward the retained area. In addition, the maximum ground surface settlement increased to 21 and 31 mm after the construction of the lower and upper NATM tunnels, respectively. In Figure 8.24, the right wall shows a continuous movement into the excavated area as further construction steps are applied. Further, the magnitudes of the right wall movement are higher than the ones on left wall, due to the smaller size of the diaphragm wall. In contrast, the settlements behind the right wall were relatively small (maximum settlement of 7 mm). It appears that this difference resulted from the stiffer material modulus, as an approximation method to combine the pile and soil stiffness was adopted.

342
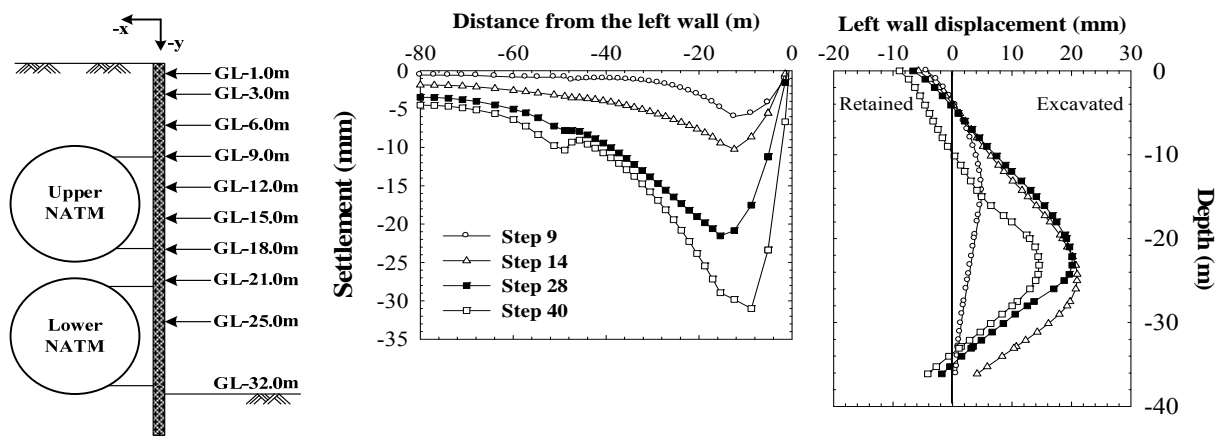
Figure 8.23: Ground Settlements and Wall Displacements on the Left Side
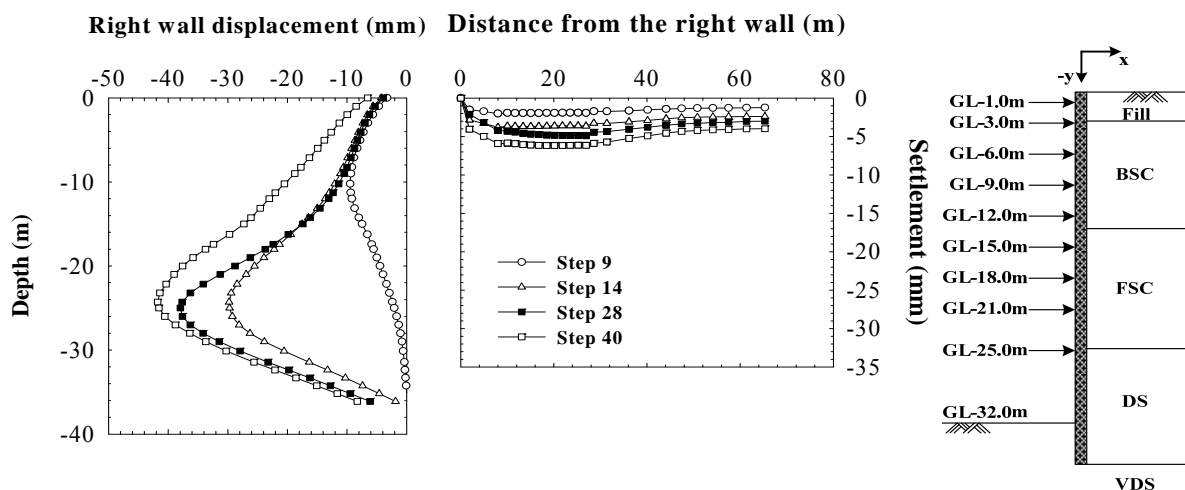
Figure 8.24: Ground Settlements and Wall Displacements on the Right Side

8.5 Concluding Remarks

The results from the analytical and numerical studies on ground movements associated with the MRT tunnel excavations are summarised in this section. In the first part of the study, analytical computations for the shield tunnelling were conducted using three methods (Verruijt and Booker, 1996; Loganathan and Poulos, 1998; and Bobet, 2001).

343

These three methods shared the same assumption regarding ground loss as was made for the gap parameter method (put what the assumption was). A total of eight twin tunnel cross sections (five side-by-side and three stack tunnels) were analysed. The Loganathan and Poulos (1998) method provided the best performance in terms of the ground surface settlement prediction, when compared with the field measurements. One possible reason for this outcome was the more realistic assumption of an oval shaped ground loss, used in Loganathan and Poulos' method, compared to a uniform shape of the other two methods.

The second part of this study focused on the 2D finite element analysis of the shield tunnelling. The stiffness reduction method was left out of the study, since it was considered inappropriate when using a higher order constitutive model. A total of three methods (contraction method, stress reduction method and modified grout method) were used to model the 3D effects of tunnelling in the 2D finite element analysis. All the clay layers (Bangkok Soft Clay, First and Second Stiff Clay and Hard Clay) within the selected soil profiles were modelled as undrained. This approach was taken because the resulting ground movements were compared with the after construction (short term) field measurements. The seven cross sections with a side-by-side configuration were selected for this analysis. The following conclusions were drawn from the studies:

(1) The back-calculated percentage of contraction from the numerical analysis and the back-calculated percentage of the volume loss from the Gaussian curve and the superposition technique were comparable. This finding was logical as the contracted volume of the tunnel lining should be equal to the volume loss arising from the surface settlement curve in an undrained condition. A range of values from 0.22 to 4.86 and 0.22 to 3.60 were obtained for the percentage of volume loss and contraction, respectively.

(2) The back-calculated unloading factor of the studied sections ranged from 0.40 to 0.84. When the shield tunnel was operating in under perfect conditions (high face pressure, high penetration rate, high grout pressure and high percentage of grout

344

filling), Figure 8.13 could be used to correlate the unloading factor and the percentage of contraction.

(3) The values of the back-calculated face pressure were higher than the measured one with the ratio of back-calculated/measured being 1.03 to 4.38. The higher back-calculated face pressure probably resulted because the actual supporting pressure consisted of the slurry pressure inside the shield chamber, the soil arching in front of the shield, and some supports from the shield element (i.e. shield blades).

(4) All three methods provided a sensible degree of matching for the predicted surface settlement profiles. They were also very similar in shape to the surface settlement profiles; they also had similar values to the structure forces.

(5) The relationships among the three back-calculated parameters (percentage of contraction, unloading factor, and normalised face pressure) were established. Figure 8.15 can be used to approximate the values of the unloading factor or the face pressure with a given percentage of contraction or volume loss, and vice versa.

The final part of this study dealt with a newly designed subway station construction approach, the "Cut-and-cover and New Austrian Tunnelling Method (NATM). Based on the analysis results, the following conclusions can be drawn:

(1) For the construction of a cut-and-cover box, the ground settlements behind the diaphragm wall (as obtained from the 2D finite element analysis using a non-linear elasto-plastic HS model) agree well with that in the PIZ zone predicted by the simplified method of Ou and Hsien (2000). However, the settlements in the SIZ zone did not match well.

(2) The stress release, due to the NATM excavation enlargement of the cut-and-cover box, caused the near wall of the box to move outward to the NATM excavated area. As a result, the maximum wall displacement was reduced.

(3) In contrast to the wall deflection, the ground surface settlements above the NATM tunnel excavation substantially increased after the completion of the NATM tunnel excavations.

(4) The approximated stiffness modulus of the pile and soil results was unrealistic, as indicating from a very small settlement behind the right wall. To obtain better soil behaviour in such an area, 3D finite element analysis is recommended.

CHAPTER 9

Concluding Remarks and Recommendations

9.1 Introduction

The completed Bangkok MRT Blue Line and its extension project gave a unique opportunity in this Doctoral research to study the ground response in terms of deformation during deep excavations and tunnelling works in Bangkok subsoils. The tunnel alignment, which is 22 km in length, included 18 underground cut and cover subway stations, and was divided into two major alignments; named as the North and the South Alignments. The stations are up to 230 m long and approximately 25 m wide, and are excavated up to a depth of 25 m to 30 m below the ground surface. The station perimeter was constructed of diaphragm walls, 1.0 – 1.2 m thick and up to 30 – 35 m deep. The tunnel lining is of twin bored single-track tunnels. Each tube has an outer diameter of 6.3 m, with an inner diameter of 5.7 m of concrete segmental lining.

Field exploration and laboratory tests show that the Bangkok subsoils, down to a maximum depth of approximately 60 to 65 m, can be divided into seven distinct layers: Weathered Crust and Backfill Material; Very Soft to Soft Bangkok Clay; Medium Stiff Clay; Stiff to Hard Clay; Medium Dense to Very Dense Sand; Very Stiff to Hard Clay; and Very Dense Sand.

In addition to the critical literature review performed, this research work is essentially in three parts on detail studies of: (1) The strength and deformation characteristics of the Bangkok subsoils as determined from laboratory tests (mainly oedometer and triaxial tests); in-situ field tests such as vane tests and LLT and self boring pressuremeters; and both laboratory and field tests to determine the small strain behaviour. (2) The defections of the retaining wall of the excavations and the ground surface settlements and (3) the ground surface settlements during tunnelling works with earth pressure balanced shield machines. At the end of each chapter in Chapters 2 to 8, a set of comprehensive conclusions and concluding remarks are presented. In addition, the major conclusions are also presented below under three sub-sections: (1) Geotechnical parameters of Bangkok subsoils; (2) Ground deformations induced during deep excavations; and (3) Ground deformations induced during earth pressure balanced shield tunnelling.

9.2 Geotechnical Parameters of Bangkok Subsoils

In this section concluding remarks are presented for (1) Geotechnical parameters from laboratory tests; (2) Geotechnical parameters from LLT pressuremeter tests; and (3) Small strain parameters for Bangkok subsoils.

9.2.1 Geotechnical Parameters from Laboratory Tests

(i)   Based on the results of field vane shear test (in soft to medium stiff clays) and CK_oU triaxial tests (in stiff to hard clays), strength ratios (s_u/σ'_{vo}) of 0.26 to 0.36

are obtained for soft to medium stiff clay; 0.27 to 0.36 for stiff to very stiff clays and 0.22 for hard clays.

(ii) The drained values of the angle of internal friction of Bangkok Soft Clay are 26 degrees at 2.5 to 6 m; 24 degrees at 5.5 to 6 m. For stiff clay at 16 m depth, the average angle of friction is 23 degrees and the average cohesion is 32 kN/m^2. For hard clay at 39 to 43 m depth, the friction angle is 23.5 degrees and the cohesion is 42 kN/m^2.

(iii) Values of the reference oedometer modulus are 962, 1650, 4689 and 3947 kN/m^2 for soft, medium, stiff and hard clays, respectively. The corresponding values of the reference unloading/reloading oedometer modulus are 5813, 5394, 9618 and 8764 kN/m^2. An average range of the ratio of the reference unloading/reloading oedometer modulus to the reference oedometer modulus during loading is 2 to for soft clay. This ratio tends to reduce with depth. The lowest value is approximately 1.5 for hard clay.

(iv) Based on the results from both laboratory triaxial tests and finite element parametric studies, a failure ratio R_f of 0.9 should be adopted in the use of the Hardening Soil Model.

(v) The validity of Janbu's exponential law (Janbu, 1963) on Bangkok Clays is confirmed from the results of oedometer and triaxial tests. The exponential power m is 1 from both oedometer and triaxial test series on Bangkok Soft Clay. This value reduced to 0.5 to 0.6 in the case of stiff to hard clays.

(vi) The parametric study of on Hardening Soil Model (HSM) parameters shows that the E_{50}^{ref} parameter governs mainly the q-ε_a and u-ε_a relationships in undrained triaxial tests and has little to no effect on the triaxial stress paths and the (ε_v - log σ'_v) relationships. The parameters E_{oed}^{ref}, E_{ur}^{ref} and K_o^{nc} are soil parameters used to control the cap and shear hardening surfaces in HSM. Therefore, they have high influence in the soil behaviour under both the triaxial and oedometer stress conditions. The Failure ratio (R_f) and unloading-reloading Poisson's ratio (ν_{ur}) should be kept as 0.9 and 0.2 to retain realistic soil behaviour. Exponential power m of 1.0 is necessary in the case of normally consolidated clay.

349

9.2.2 Geotechnical Parameters from LLT Pressuremeter Tests

(i)   The coefficient of earth pressure at rest K_o for Bangkok Soft Clay cannot be determined reliably using the LLT pressuremeter. For stiff clay, the average K_o values are found to be 0.46, 0.45 and 0.68 with the use of the Creep Curve Method, the Marsland and Randolph's Method and Hawkins *et al.*'s Method respectively.

(ii) The undrained shear strength of Soft Clay as estimated from Gibson & Anderson's (1961) Method and Marsland & Randolph's (1977) Method (using p_L with G_i, p_L with G_{ur}, and p_L with $N_p = 6$) are in good agreement with the undrained shear strength as determined from vane shear tests. . In the case of Stiff Clay, the undrained shear strength predicted from the Gibson & Anderson's (1961) Method, and Marsland & Randolph's (1977) Method (using p_L with G_i, p_L with G_{ur}, and p_L with $N_p = 6.7$) are an order two to four times higher than the values obtained from CK$_o$U triaxial tests.

(iii) The net limit pressure (p^*_L) is well correlated with the undrained shear strength for both Soft and Stiff Clays. The correlation proposed in this thesis can be used as a first approximation for the determination of the undrained shear strength.

9.2.3 Small Strain Parameters for Bangkok Sub-soils

(i)   The maximum shear modulus of Bangkok subsoils is fairly uniform throughout the areas studied in this thesis. The *A* parameter values of 3000 and 2000 are needed in Shibuya and Tanaka's (1996) method for soft and stiff clays to get better predicted values of the maximum shear modulus. The corresponding values are 16000 and 13000 for soft and stiff when the equation of Shibuya *et al.*'s (1997) is used.

(ii) The maximum shear modulus as obtained from the seismic cone and the down hole seismic methods are found to be 50 and 80 times higher than the LLT pressuremeter limit pressure and net limit pressure, respectively.

(iii) The parameter $\gamma_{0.7}$ of Soft Clay as obtained from the cyclic triaxial tests (Teachavorasinskun *et al.*, 2002a) is of the order of 0.03 – 0.07 %. No information is yet available on this parameter for stiff clay.

(iv) Ishibashi and Zhang (1993) and Vucetic and Dobry (1991) methods predict nearly identical values of $\gamma_{0.7}$ for Soft Clay. Their predictions also agreed well with the results from cyclic triaxial tests.

9.3 Ground Deformations Induced during Deep Excavations

(i) Based on the review of the quality of field measurements (wall deflections and ground surface settlements), in 18 subway stations , the Sukhumvit Station is selected as the best one to perform a detail 2D finite element analysis using Plaxis. Four soil constitutive models (i.e. Mohr Coulomb Model, Soft Soil Model, Hardening Soil Model and Hardening Soil Model with Small Strain Stiffness) are used in the analysis. The seven-layer soil profile model as established from the geotechnical parameters was also used in this analysis.

(ii) The Results from the inclinometer readings of Sukhumvit Station showed a significant 3D (or corner) effects of the diaphragm wall movements. The relationship between the maximum horizontal wall movement and the distance to the nearest corner is approximately linear.

(iii) The ratio of the maximum ground surface settlement to the maximum horizontal wall movement is 0.75 as measured from four deep excavations. This ratio lies within the range as reported in the literature (Mana and Clough, 1981; Ou *et al.*, 1993).

(iv) Three empirical methods (i.e. Clough and O'Rourke, 1990; Hsieh and Ou, 1998; Ou and Hsieh, 2000) are adopted for surface settlement computations. It was found that all three methods provide similar magnitude of maximum surface settlement, which agrees well with the measured data. However, only the methods of Hsieh and Ou (1998) and Ou and Hsieh (2000) predicted well, the surface settlements in the Primary and Secondary Influence Zones.

(v)   The lateral wall movements and the surface settlements predicted are very sensitive to the type of constitutive soil models used in the 2D Plaxis analysis: i.e. Mohr Coulomb Model, Soft Soil Model, Hardening Soil Model and Hardening Soil Model with Small Strain Stiffness. Realistic values are obtained when the constitutive models are sophisticated and the accuracy is increased with the Soft Soil Model than with the Mohr Coulomb Model; also with the Hardening Soil Model with Small Strain Stiffness than with Soft Soil Model.

(vi)   The axial force, shear force and bending moment distributions from the Plaxis analyses are not sensitive to the type of soil model used in the analyses.

(vii)   Back-calculated E_u/s_u ratios from the literature can be used for the prediction of the lateral movement of the retaining walls with Mohr Coulomb Model. However, accurate ground surface settlements cannot be obtained. For Soft Soil Model and Hardening Soil Model analyses, the soil parameters interpreted from laboratory best fitted parameters (i.e. Figure 4.31) and in-situ tests (studies from Chapter 5) are sufficient to obtain overall trends of lateral wall movements and surface settlements.

(viii) Both the Hardening Soil Model and Hardening Soil Model with Small Strain Stiffness gave good predictions of wall movement at the final stage. They also provided reasonable wall movement predictions of cantilever mode at the first excavation stage. However, an slightly over-predictions of the deep inward component in the second and third stages of excavation.

(ix)   Results from the Hardening Soil Model with Small Strain analysis confirmed the values of $\gamma_{0.7}$ in soft clay as predicted by Ishibashi and Zhang (1993) and Vucetic and Dobry (1991) methods. However, a lower value of $\gamma_{0.7}$ of 0.002% is necessary for better lateral wall movement and surface settlement predictions in stiff clay layer.

9.4 Ground Deformations Induced during Earth Pressure Balanced Shield Tunnelling

(i)   With the aim to find the best analytical method to predict the ground surface settlement induced by shield tunnelling, three analytical methods (i.e. Verruijt and Booker, 1996; Loganathan and Poulos, 1998; Bobet 2001) are examined in this study. Eight twin tunnels cross sections, which consist of both side-by-side and stack configurations, are selected. These sections cover various conditions of subsoils in which the shields located during the tunnelling works. It is found that the Loganathan and Poulos (1998) Method gave the best prediction of ground surface settlements induced by shield tunnelling compared to the other two analytical methods.

(ii)   A total of 21 (7 locations with three methods of analysis in each case) twin side-by-side shield tunnelling cases are analysed with 2D finite element method. Three, 2D approaches for shield tunnel modelling, namely the contraction method, the stress reduction method and the modified grout pressure method are used. All analyses are conducted using Hardening Soil Model.

(iii)   Back-calculated percentage of contraction from numerical analysis and the back-calculated percentage of volume loss from Gaussian curve and super position techniques are comparable. Values of 0.22 to 4.86 and 0.22 to 3.60 are obtained for the percentage of volume loss and contraction, respectively.

(iv)   Back-calculated unloading factor of the studied sections range from 0.40 to 0.84. Figure 8.13 can be used to estimate the unloading factor from the percentage of contraction in the case of shield tunnel operating in perfect condition (i.e. the Tunnel Boring Machine operates with high face pressure, high grout pressure, high penetration rate and high percentage of grout filling).

(v)   Back-calculated face pressures from the modified grout pressure method are higher than the measured values and the corresponding ratio is in the range of 1.03 – 4.38. The higher back-calculated face pressure resulted because the actual supporting pressure consisted of the slurry pressure inside the shield

353

chamber, the soil arching in front of the shield and some supports from the shield element (i.e. shield blades).

(vi) Inter-relationships among the contraction ratio, which is comparable to the volume loss ratio in the undrained condition, the unloading factor and the normalised face pressure are established. These relationships in Figure 8.15 can be used to approximate the values of unloading factor or face pressure with a given percentage of contraction or volume loss and vice versa.

(vii) In the Blue Line Extension Project currently under design at the Wang Burapha Station a 2D plane strain finite element analysis is performed method with the Hardening Soil Model. The cut and cover and New Austrian Tunnelling methods (NATM) are adopted as a combination in this new construction technique recommended in the design. For the analysis of cut-and-cover station box, the ground settlements behind the diaphragm wall as obtained from the 2D finite element analysis using Hardening Soil Model agree well with that in Primary Influence Zone predicted by simplified method of Ou and Hsieh (2000). However, the settlements in the Secondary Influence Zone are not well matched.

(viii) In the analyses performed during the design stage, the stress release due to NATM excavation enlargement of the cut and cover box causes the near wall of the box to move outward to the NATM excavated area. As a result, the maximum wall displacement predicted is reduced. Contrary to the predicted wall deflection, the predicted ground surface settlements above the proposed NATM tunnel excavation substantially increased as indicated by the results from the analyses for the stage after the completion of the NATM tunnels excavation.

9.5 Recommendations for Future Research

To further enhance the work presented in this research, the following recommendations are suggested.

(i) In this study, the unloading modulus is obtained from oedometer test (oedometer unloading modulus) and finite element back-analysis (triaxial unloading modulus). To further confirm the validity of the unloading modulus of Bangkok subsoils, a series of triaxial (undrained and drained tests) with the unloading/reloading loop should be conducted. This will make a direct comparison on the unloading parameters from triaxial tests and finite element back-calculated values.

The current study helped to gain a better understanding of ground movement mechanisms as induced by deep excavations and shield tunnelling. The geotechnical aspects covered herein are more likely to benefit the practicing engineers. The results from finite element analyses of both deep excavation and shield tunnelling reveal that the Hardening Soil Model (HSM) has its potential in predicting the ground deformations. Extensive data from oedometer and triaxial tests are analysed to obtain the input parameters of the HSM. One major advantage of the HSM over the basic Mohr Coulomb Model (MCM) is that distinction can be made between the modulus of loading and unloading.

(ii) It is unfortunate that the long term field measurements are not available from the Bangkok MRT Blue Line project. In the presence of such long term measurements, the consolidation parameters can be back-analysed by means of a coupled undrained and consolidation analyses in the Plaxis program. Alternatively, drained analysis can also be conducted for comparison.

(iii) On the New Austrian Tunnelling Method (NATM) section of the current design station (Bangkok MRT Blue Line Extension), more finite element analyses need to be conducted to study the following: (a) the effect of

construction sequences on the associated ground movements; (b) the effective delay length or round length to be adopted in the construction phase; and (c) the zones where ground improvements to be adopted and if so, the suitable type of ground improvement techniques which result in acceptable ground movements.

REFERENCES

Addenbrooke, T. I. (1996) *Numerical analysis of tunnelling in stiff clay*. Doctoral Thesis, Imperial College. London, University of London.

Addenbrooke, T. I., Potts, D. M., and Puzrin, A. M. (1997) The influence of pre-failure soil stiffness on the numerical analysis of tunnel construction. *Geotechnique,* 47, 693-712.

AFTES (2000) New recommendations on choosing mechanized tunnelling techniques. French tunnelling and underground engineering association.

Ahmed, M. A. (1975) *Stress-strain behaviour and strength characteristics of stiff Nong Ngoo Hao Clay during extension tests under undrained conditions.* Masters Thesis, Asian Institute of Technology, Bangkok.

Al-Tabbaa, A., and Wood, D. M. (1989) An experimentally based "bubble" model for clay. *In: Proceedings of the International Conference on Numerical Models in Geomechanics NUMOG 3*, (edt. Pietruszczak and Pande), A.A. Balkema, 91 – 99.

Ashford, S. A., Jakrapiyanum, W., and Lukkanaprasit, P. (1996) Amplification of earthquake ground motions in Bangkok, Asian Instititive of Technology research report, submitted to the Public Works Department, Thailand.

Atkinson, J., Richardson, D., and Robinson, P.J. (1987) Compression and extension of K_o normally consolidated kaolin clay. *Journal of Geotechnical Engineering Division, ASCE,* 113, 1468 – 1482.

Atkinson, J.H., and Sallfors, G. (1991) Experimental determination of soil properties. *In Proc. 10th ECSMFE, Florence*, Vol 3, 915 – 956.

Attewell, P. B. (1978) Ground movements caused by tunnelling in soil. *In: Proceeding of International Conference on Large Movements and Structures* (ed. Geddes, J. D.), Pentech Press, London, 812 – 948.

Attewell, P. B., and Farmer, J. W. (1974) Ground deformations resulting from shield tunnelling in London Clay. *Canadian Geotechnical Journal,* 11, 380 – 395.

Baguelin, F., Frank, R. A., and Nahra, R. (1986) A theoretical study of pore pressure generation and dissipation around the pressuremeter. *In: Proceedings of the 2nd Int. Symp. Pressuremeter Marine Appl.*, Texam, USA, 169 – 186.

Baguelin, F., Jezequel, J. F., Le Mee, E., and Le Mehaute, A. (1972) Expansion of cylindrical probes in cohesive soils, *Journal of Soil Mechanics and Foundations Division, ASCE,* 98(SM11), 129 - 142.

Baguelin, F., Jezequel, J. F., and Shield, D.H. (1978) *The pressuremeter and foundation engineering.* Trans Tech Publications.

Balasubramaniam, A. S., Bergado, D. T., Chai, J. C., and Sutabutr, T. (1994) Deformation analysis of deep excavation on Bangkok subsoil, *In: Proceedings of the 13th International Conference on Soil Mechanics and Foundation Engineering.* New Delhi, India, 909 – 914.

Balasubramaniam, A. S., and Chaudhry, A.R. (1978) Deformation and strength characteristics of Soft Bangkok Clay. *Journal of Geotechnical Engineering Division, ASCE,* 104, 1153 - 1167.

Balasubramaniam, A. S., Oh, E.Y.N., Bolton, M.W., Bergado, D.T., and Phienwej, N. (2005) Deep-well pumping in the Bangkok Plain and its influence on ground improvement development with surcharge and vertical drains. Institution of Civil Engineers, London, *Ground Improvement,* 9, 149 - 162.

Balasubramaniam, A. S., and Uddin, W. (1977) Deformation characteristics of weathered Bangkok Clay in triaxial extension. *Geotechnique,* 27, 75 – 92.

Balasubramaniam, A. S., Zue-Ming, H., Uddin, W., Chaudhry, A.R., and Li, Y.G. (1978) Critical state parameters and peak stress envelops for Bangkok Clays. *Quaternary Journal of Engineering Geology,* 11, 219 - 232.

Bergado, D. T., Balasubramaniam, A.S., Fannin, R.J., and Holtz, R.D. (2002) Prefabricated vertical drain (PVD) in soft Bangkok clay: a case study of the new Bangkok International Airport Project. *Canadian Geotechnical Journal,* 39, 304 – 315.

Bergado, D. T., and Khaledque, M.A. (1986) Correlations of LLT pressuremeter, vane and Dutch cone, test in Bangkok marine clay, Thailand, *In: Proceedings of the International Symposium on Pressuremeter and Its Marine Application*, Texam, USA, ASTM STP 950, 339 -353.

Bergado, D. T., Khaledque, M.A., Neeyapan, R., and Chang, C.C. (1986) Correlations of in situ tests in Bangkok subsoils, *Geotechnical Engineering*, 17(1), 1 – 3.

Benz, T. (2006) *Small-strain stiffness of soils and its numerical consequences*. Doctoral Thesis, Institute of Geotechnical Engineering, University of Stuttgart, Stuttgart.

Bjerrum, L. (1973) Problems of soil mechanics and construction on soft clays. *Proceedings of the 8th International Conference on Soil Mechanics and Foundation Engineering.* Moscow, Russia.

Bjerrum, L., and Simons, N.E. (1960) Comparison of shear strength characteristics of normally consolidated clays. *In: Proceedings of Research Conference on Shear Strength of Cohesive Soils*, Boulder, Colorado. 771 - 724.

Bliehm, C. (2001) *Advances in geotechnical engineering and tunnelling.* 3D Finite Element Calculation in Tunnelling, Number 4, Logos, Berlin.

Bloodworth, A.G. (2002) *Three-dimensional analysis of tunnelling effects on structures to develop design methods*. Doctoral Thesis, University of Oxford, UK..

BMTDC (2002) Geotechnical investigation report, feasibility study, detailed design and tender document preparation for the remaining extensions and new routes.

Bobet, A. (2001) Analytical solutions for shallow tunnels in saturated ground. *Journal of Engineering Mechanics,* 127, 1258 - 1266.

Bolton, M. D. (1986) The strength and dilatancy of sands. Geotechnique, 36(1), 65 – 78.

Bower, K. H. (1997) *An appraisal of the New Austrian Tunnelling Method in soil and weak rock*. Leeds, University of Leeds.

Bowles, J. E. (1986) *Foundation analysis and design*, McGraw-Hill, New York.

Briaud, J. L. (1992) *The pressuremeter.* A.A. Balkema, Netherlands.

Brinkgreve, R.B.L. (2002) Plaxis 2D – version 8 manuals. A.A. Balkema, Netherlands.

Burland, J. B. (1989) Small is beautiful - the stiffness at small strains. *Canadian Geotechnical Journal,* 26**,** 499 – 516.

Burland, J. B., and Kalra, J.C. (1989) Queen Elizabeth II Conference Centre: geotechnical aspects. *Proc. Instn, Civ, Engrs*., 80(1), 1479-1503

Burland, J. B., Symes, M. J. (1982) A simple axial displacement gauge for use in the triaxial apparatus. Geotechnique, 32, 62 – 65.

Chaiseri, A. and Parkinson, M. (1989) Design and performance monitoring of a diaphragm wall for 6-level excavation in Bangkok. *EIT Annual Meeting, Theme: New Technology in Engineering*, EIT, Bangkok.

Chanchaya, C. (2000) *Analysis of movements in Bangkok subsoils due to subway tunnelling by the soil modelling method.* Masters Thesis, Chulalongkorn University, Bangkok.

Chang, C. Y. (1969) *Finite element analyses of soil movements caused by deep excavation and dewatering. Doctoral Thesis*, University of California, Berkeley.

Chaudhry, A. R. (1975) *Effects of applied stress path on the stress-strain behaviour and strength characteristics of soft Nong Ngoo Hao Clay.* Masters Thesis, Asian Institute of Technology, Bangkok.

Chou, W., and Bobet, A. (2002) Predictions of ground deformations in shallow tunnels in clay. *Tunnelling and Underground Space Technology,* 17, 3 – 19.

Clark, B. G. (1995) *Pressuremeter in geotechnical design*. Blackie Academic, London.

Clough, G. W., and Duncan, J. M. (1969) Finite element analyses of Port Allen and Old River Locks. Report No. TE69-3, University of California, Berkeley, 265.

Clough, G. W., and Leca, E. (1993) EPB shield tunnelling in mixed face conditions. *Journal of Geotechnical Engineering,* 119, 1640 – 1656.

Clough, G. W., and O'Rourke, T. D. (1990) Construction-induced movements of in situ walls, Design and performance of earth retaining structure, ASCE special publication, 25, 439 – 470.

Cording, E.J., Hansmire, W.H. (1975) Displacements around soft ground tunnels – General report. *In: 5th Pan American Conference on Soil Mechanics and Foundation Engineering*, Buenos Aires, Session 4, 571-632.

Cox, J. B. (1968) A review of the engineering characteristic of the recent marine clays in Southeast Asia. Bangkok, Thailand: Asian Institute of Technology.

Crooks, J. H., and Graham, J. (1976): Geotechnical properties of the Belfast estuarine deposit. *Geotechnique,* 26, 293 - 315.

Darendeli, M. B. (2001) *Development of a new family of normalised modulus reduction and material damping curves*. Doctoral Thesis, University of Texas at Austin, Texas.

Ding, W. Q., Yue, Z. Q., Tham, L. G., Zhu, H. H., Lee, C. F., and Hashimoto, T. (2004) analysis of shield tunnel. *International Journal for Numerical and Analytical Methods in Geomechanics,* 28, 57-91.

Dong, N. P. (1998) *In-situ investigation of soft and stiff clay in Bangkok*. Masters Thesis, Asian Institute of Technology, Bangkok.

Du, P. M. (2003) *Predictions of ground movements due to tunnelling of Bangkok sewer and MRT Blue Line by analytical methods and 2D FEM*. Masters Thesis. Asian Institute of Technology, Bangkok.

Duncan, J. M., and Buchignani, A.L. (1976) An engineering manual for settlement studies. University of California Berkeley. Need location

Duncan, J. M., Byrne, P., Wong, K.S., and Mabry, P. (1980) Strength, stress-strain and bulk modulus parameters for finite element analysis of stresses and movements in soil masses. In: (Fourth Edition ed.), Report No. UCB/GT/80-01, University of California Berkley.

Duncan, J. M., and Change, C.Y. (1970) Nonlinear analysis of stress in soils. *Journal of Soil Mechanics and Foundations Division, ASCE,* 96, 1629 - 1653.

EFNARC (2005) Specification and guidelines for the use of specialist products for Mechanised Tunnelling (TBM) in soft ground and hard rock. European Federation of Producers and Contractors of Specialist Products for Structures.

Einstein, H.H., and Schwartz, C.W. (1979) Simplified analysis for tunnel supports. *Journal of Geotechnical Engineering Division*, *ASCE*, 105(4), 499-518.

Finno, R. J., and Clough, G. W. (1985) Evaluation of soil response to EPB shield tunnelling. *Journal of Geotechnical Engineering,* 111, 155-173.

Finno, R. J., and Harahap, I. S. (1991) Finite element analysis of HDR-4 excavation, *Journal of Geotechnical Engineering, ASCE*, 117(10), 1590 – 1609.

Fleming, W. G. K., Weltman, A. J., Randolph, M. F., and Elson, W. K. (1985) *Piling engineering*. Blackie A & P, London.

Gan, C. H. (1997) *Review and analysis of ground movements of braced excavations in Bangkok subsoil using diaphragm walls*. Masters Thesis. Asian Institute of Technology, Bangkok.

Gens, A. (1995) General report: Prediction, performance and design. *Int. Symp. on pre-failure deformation characteristic of geomaterials*. 1233-1247, Balkema, Rotterdam.

Gibson, R. E., and Anderson, W. F. (1961), In situ measurement of soil properties with the pressuremeter, *Civ. Engng Publications Works and Rev*., 56, 615 – 618.

Gonzalez, C., and Sagaseta, C. (2001) Patterns of soil deformations around tunnels. application to the extension of Madrid Metro. *Computers and Geotechnics,* 28, 445-468.

Gurung, S. B. (1992) *Yielding of soft Bangkok Clay below the state boundary surface under compression condition*. Masters Thesis, Asian Institute of Technology, Bangkok.

Hardin, B. O., and Black, W. L. (1968) Vibration modulus of normally consolidated clays. *Journal of Geotechnical Engineer Division, ASCE,* 94(SM2), 353 – 369.

Hardin, B. O., and Drnevich, V. P. (1972) Shear modulus and damping in soils: design equations and curves. *Journal of Soil Mechanics and Foundations Division, ASCE*, 98(SM7), 667 – 692.

Hardin, B. O., and Richart, F. E. (1963) Elastic wave velocities in granular soils. *Journal of Soil Mechanics and Foundations Division, ASCE,* 89(SM1), 33 – 65.

Hassan, Z. (1976) *Stress-strain behaviour and shear strength characteristics of stiff Bangkok Clays.* Masters Thesis, Asian Institute of Technology, Bangkok.

Hawkins, P.G., Mair, R.J., Mathieson, W.G. and Muir Wood, D. (1990) Pressuremeter measurement of total horizontal stress in stiff clay, *In: Proceeding of the 3rd International Symposium on pressuremeter*. Oxford, 321 – 330.

Hong, C. P. (2005) *Three dimensional analysis of ground movement in EPB shield in Bangkok*. Masters Thesis, Asian Institute of Technology, Bangkok.

Hooi, Y. K. (2003) *Ground movements associated with station excavation of the first Bangkok MRT subway.* Masters Thesis, Asian Institute of Technology, Bangkok.

Houlsby, G. T., and Carter, J. P. (1993) The effects of pressuremeter geometry on the results of tests in clay. *Geotechnique*, 43(4), 567 – 576.

Hsieh, P.G., and Ou, C.Y. (1998) Shape of ground surface settlement profiles caused by excavation, *Canadian Geotechnical Journal*, 35(6), 1004 – 1017.

Hsu, C. C., and Vucetic, M. (2004) Threshold shear strain for cyclic pore-water pressure in cohesive soils. *Journal of Geotechnical and Geoenvironmental Engineering*, 132(10), 1325 – 1335.

Huang, W. F. (1980) *LLT pressuremeter test in Bangkok Clay*. Masters Thesis, Asian Institute of Technology, Bangkok.

Ishibashi, I. (1992) Discussion to: Effect of soil plasticity on cyclic response, by Vucetic M. and Dobry R., *Journal of Geotechnical Engineering, ASCE*, 118(5), 830 – 832.

Ishibashi, I., and Zhang, X. (1993) Unified dynamic shear moduli and damping ratios of sand and clay. *Soils and Foundations*, 33(1), 182 – 191.

ITA/AITES (2007) Settlements induced by tunnelling in soft ground. *Tunnelling and Underground Space Technology*, 22, 119-149.

Jamiolkowski, M., Lancellotta, R., and Lo Presti, D. C. F. (1994), Remarks on the stiffness at small strains of six Italian clays. *Pre-failure Deformation of Geomaterials*, Shibuya, S., Mitachi, T. and Miura, S. (eds.), A.A. Balkema, Vol. 2, 817 – 836.

Jamiolkowski, M., Leroueil, S., and Presti, D. C. F. (1991) Design parameter from theory and practice. *In: Proceeding of the International Conference on Geotechnical Engineering for Coastal Development* (Geo-coast' 91), Yokohama, Vol. 2, 877 – 891.

Janbu, N. (1963) Soil compressibility as determined by oedometer and triaxial test. *In: Proceedings of the European Conference on Soil Mechanics and Foundation Engineering*, 19 - 25.

Jardine, R. J., Potts, D. M., Fourie, A. B., and Burland, J. B. (1986) Studies of the influence of non-linear stress-strain characteristics in soil-structure interaction. *Geotechnique*, 36(3), 377 – 396.

Jardine, R. J., Symes, M. J., and Burland, J. B. (1984) The measurement of soil stiffness in the triaxial apparatus. *Geotechnique*, 34(3), 323 – 340.

Jezequel, J. F., Lemasson, H., and Touze, J. (1968) Le pressiometre Louis Menard quelques problemes de mise en oeuvre et leur influence sur les valeurs pressiometriques, *Bull. De Liaison du LCPC*, 32, 97 – 120.

Karakus, M. (2007) Appraising the methods accounting for 3D tunnelling effects in 2D plane strain FE analysis. *Tunnelling and Underground Space Technology*, 22, 47 – 56.

Karakus, M., and Fowell, R. J. (2003) Effects of different tunnel face advance excavation on the settlement by FEM. *Tunnelling and Underground Space Technology,* 18, 513-523.

Karakus, M., and Fowell, R. J. (2005) Back analysis for tunnelling induced ground movements and stress redistribution. *Tunnelling and Underground Space Technology,* 20, 514-524.

Karakus, M., and Fowell, R. J. (2006) 2-D and 3-D finite element analyses for the settlement due to soft ground tunnelling *Tunnelling and Underground Space Technology,* 21, 392-.

Kim, S. R. (1991) *Stress-strain behaviour and strength characteristics of lightly overconsolidated clay.* Doctoral Thesis, Asian Institute of Technology, Bangkok.

Kim, H.J., Eisenstein, Z., Chae, B.G. and Jeong, C.H. (2006) Estimates of stress reduction factors for the tunnel design. *Tunnelling and Underground Space Technology*, 21, 451.

Kimura, T., and Mair, R. J. (1981) Centrifugal testing of model tunnels in Soft Clay. *In: Proceeding of the 10th International Conference on Soil Mechanics and Foundations Engineering.* Stockholm, Vol. 1, 319 – 322.

Komiya, K., Soga, K., Akagi, H., Hagiwara, T., and Bolton, M. D. (1999) Finite element modelling of excavation and advancement processes of a shield tunnelling machine. *Soils and Foundations,* 39, 37-52.

Kondner, R. L. (1963) Hyperbolic stress-strain response cohesive soils. *Journal of Soil Mechanics and Foundations Division, ASCE,* 89, 115 - 143.

Kulhawy, F. H., and Mayne, P.H. (1990) Manual on estimating soil properties for foundation design. Electric Power Research Institute (EPRI). New York.

Kung, G. T., Ou, C. Y., and Juang, C. H. (2009) Modelling small-strain behaviour of Taipei clays for finite element analysis of braced excavations. *Computer and Geotechnics*, 36, 304 – 319.

Ladd, C. C. (1991) Stability evaluation during stage construction: 22nd Terzaghi Lecture. *Journal of Geotechnical Engineering, ASCE,* 117, 537 - 615.

Ladd, C. C., Foott, R., Ishihara, K., Schlosser, F., and Poulous, H.G. (1977) Stress-deformation and strength characteristics. *In: Proceedings of the 9th International Conference on Soil Mechanics and Foundation Engineering*, Tokyo. 421 - 494.

Leblais, Y., and Bochon, A. (1991) Villejust tunnel: slurry shield effects on soils and lining behaviour and comments on monitoring requirement. *Tunnelling' 91*, London, 65-77.

Lee, F. H., Yong, K. Y., Quan, K. C., and Chee, K. T. (1998) Effect of corners in strutted excavation: field monitoring and case histories, *Journal of Geotechnical and Geoenvironmental Engineering*, 124(4), 339 – 349.

Lee, K. M., and Rowe, R. K. (1989) Deformations caused by surface loading and tunnelling: the role of elastic anisotropy. *Geotechnique,* 39, 125-140.

Lee, K. M., Rowe, R. K., and Lo, K. Y. (1992) Subsidence owing to tunnelling. I: estimating the gap parameter. *Canadian Geotechnical Journal*, 29, 929 – 940.

Lee, I.M., Nam, S.W., and Ahn, J.H. (2003) Effect of seepage forces on tunnel face stability. *Canadian Geotechnical Journal,* 40(2), 342-350.

Likitlersuang, S., and Kyaw, K. (2010) A unified correlation for shear wave velocity of Bangkok subsoil. *In: Proceeding of the 17th Southeast Asian Geotechnical Conference*, Taipei, Vol.1, 431 – 435.

Lim, A., Ou, C. Y., and Hsieh, P. G. (2010) Evaluation of clay constitutive models for analysis of deep excavation under undrained conditions. *Journal of GeoEngineering*, 5(1), 9 – 20.

Litwinsizyn, J. (1956) Application of the equation of stochastic processes to mechanics of loose bodie. *Arch. Mech. Stosow*, Vol. 8, 396 – 411.

Lo, K. Y., and Rowe, R. K. (1982) *Prediction of ground subsidence due to tunnelling in clays*. Res. Report. GEOT-10-82, Faculty of Engineering Science, University of Western Ontario, London.

Loganathan, N., and Poulos, H. G. (1998) Analytical prediction for tunnelling-induced ground movements in clays. *Journal of Geotechnical and Geoenvironmental Engineering,* 124, 846 – 856.

Lukas, G. L., and LeClerc de Bussy, B. (1976) Pressuremeter and laboratory test correlations for clays, *Journal of Geotechnical Engineer Division, ASCE*, 102(GT9), 954 – 963.

Mair, R. J. (1993) Unwin memorial lecture 1992 development in geotechnical engineering research: application to tunnels and deep excavation. *In: Proceedings of Instn Civ. Engng. 1993,* 93, Feb. 27 – 41.

Mair, R. J., and Taylor, R. N. (1997) Bore tunnelling in the urban environment. Theme Lection, Plenary Session 4, *In: Proceedings of the 14th International Conference of Soil Mechanics and Foundation Engineering*, Hamburg, Vol. 4, 2353 – 2385.

Mair, R. J., and Wood, D. M. (1987) *Pressuremeter testing – methods and interpretation*, Butterworth.

Mana, A. I., and Clough, G. W. (1981) Prediction of movements for braced cut in clay, *Journal Geotechnical Engineering Division, ASCE*, 107(6), 759 – 777.

Marsland, A. and Randolph, M. F. (1977) Comparisons on the results from pressuremeter tests and large in-situ plate tests in London clay, *Geotechnique*, 27(2), 217 – 243.

Matasovic, N., and Vucetic, M (1992) A pore pressure model for cyclic straining of clay. *Soils and Foundations*, 32(3), 156 – 173.

Mayne, P.W., and Swanson, P.G. (1981) The critical state pore pressure parameter from consolidated-undrained shear tests. *Laboratory shear strength of soil (STP 740), ASTM*, Philadelphia, 410 – 430.

Menard, L. (1975) The Menard pressuremeter: interpretation and application of the pressuremeter test results to foundation design, *Sols-Soils*, 26.

Mirjalili, R. (2009) *Performance of deep excavations in MRT stations: Bangkok MRT as a case study.* Masters Thesis, Griffith University, Gold Coast.

Moller, S. C. (2006) *Tunnel induced settlements and structural forces in linings.* Doctoral Thesis, University of Stuttgart, Stuttgart.

Moller, S. C., and Vermeer, P. A. (2008) On numerical simulation of tunnel installation. *Tunnelling and Underground Space Technology*, 23, 461 – 475.

New, B. M., and Bowers, K. H. (1993) Ground movement model validation at the Heathrow Express Trial Tunnel. *Tunnelling'94*, IMM, London, 301 – 329.

Ng, C. W. W. W. (1992) *An evaluation of soil-structure interaction associated with a multi-propped excavation.* Doctoral Thesis, University of Bristol, UK.

Nguyen, A. D. (1999) *Updating and analysis of Bangkok land subsidence caused by deep well pumping with emphasis on shallow soil settlement.* Masters Thesis, Asian Institute of Technology, Bangkok.

Nordal, S. (1989) A Coulombian soil model applied to an offshore platform. *In: Proceedings of the 20th Inter. Conf. on Soil Mechanics and Foundation Engineering,* Rio de Janeiro, Vol.1, 471 – 474.

Nordal, S. (1999) Present of Plaxis. *Beyond 2000 in Computational Geotechnics - 10 Years of PLAXIS International.* Balkema, Rotterdam, 45 – 54.

Nyren, R. J. (1998) *Field measurements above twin tunnels in London clay.* Doctoral Thesis, Imperial College. London, University of London.

O'Reilly, M. P., and New, B. M. (1982) Settlement above tunnels in the United Kingdom – their magnitude and prediction. *Tunnelling' 82*, London, 231 – 241.

Osterman, J. (1959) Notes on the shearing resistance of soft clays. Stockholm: *Acta Polytechnica Scandinavica*. Civil Engineering a Build Construction Service. No. 2.

Ou, C. Y. (2006) *Deep excavation: theory and practice*. Taylor & Francis, London, U K.

Ou, C. Y., and Chiou, D. C. (1993) Three-dimensional finite element analysis of deep excavation. *In: Proceeding of the 11th Southeast Asian Geotechnical Conference*, Kuala Lumpur, 769 – 774.

Ou, C. Y., and Hsieh, P. G. (2000) Prediction of ground surface settlement induced by deep excavation, Geotechnical Research Report No. GT200008, Department of Construction Engineering National Taiwan University of Science and Technology, Taipei.

Ou, C. Y., Hsieh, P. G., and Chiou, D. C. (1993) Characteristics of ground surface settlement during excavation, *Canadian Geotechnical Journal*, 30, 758 – 767.

Ou, C. Y., Shiau, B. Y., and Wang, I. W. (2000) Three-dimensional deformation behaviour of TNEC excavation case history. *Canadian Geotechnical Journal*, 37(2), 438 – 448.

Palmer, A. C. (1972) Undrained plane-strain expansion of a cylindrical cavity in clay: a simple interpretation of the pressuremeter test, *Geotechnique*, 2(3), 451 – 457.

Panet, M. and Guenot, A. (1982) Analysis of convergence behind the face of tunnel. *Tunnelling' 82*, The Institution of Mining and Metallurgy, London, 197 – 204.

Parry, R. H. G. (1960) Triaxial compression and extension tests on remoulded saturated clay. *Geotechnique,* 10, 166 - 180.

Parry, R. H. G., and Nadarajah, V. (1973) Observations on laboratory prepared, lightly overconsolidated specimens of kaolin. *Geotechnique,* 24, 345 - 358.

Parry, R. H. G., and Nadarajah, V. (1974) Anisotropy in a natural soft clayey silt. *Engineering Geology,* 8, 287 - 309.

Peck, R. B. (1969) Deep Excavations and Tunnelling in Soft Ground. *In: Proceeding of the 7th International Conference on Soil Mechanics and Foundations Engineering.* Mexico City, State of the Art Volume, 225 - 290.

Pestana, J. M., and Salvati, L. A. (2006) Small-strain behaviour of granular soils. 1: Model for cemented and uncemented sands and gravels. *Journal of Geotechnical and Geoenvironmental Engineering*, 132(8), 1071 – 1081.

Phienwej, N. (1997) Tunnelling for Bangkok subway projects. *Proceedings of World Tunnel Congress'97,* Tunnels for people, Vienna, Austria, 337 – 342.

Phienwej, N. (2008) Ground movement in station excavations of Bangkok first MRT. *In: Proceedings of the 6th International Symposium (IS-Shanghai 2008)*, Shanghai, China, 181 – 186.

Phienwej, N. (2009) Ground movement in station excavations of Bangkok first MRT. *Geotechnical Aspects of Underground Construction in Soft Ground*. Taylor and Francis, London.

Phienwej, N., and Gan, C. H. (2003) Characteristics of ground movement in deep excavations with concrete diaphragm walls in Bangkok soils and their prediction, *Journal of the Southeast Asian Geotechnical Society*, 34(3), 167 – 175.

Phienwej, N., Giao, P.H., and Natalaya, P. (2006) Land subsidence in Bangkok, Thailand. *Engineering Geology,* 82, 187 - 201.

Phienwej, N., Sirivachiraporn, A., Timpong, S., Tavaranum, S. & Suwansawat, S. (2006) Characteristics of ground movements from shield tunnelling of the first Bangkok subway line. *In:International Symposium on Underground Excavation and Tunnelling.* Bangkok, Thailand, 319 – 330.

Pianchareon, C. (1976) Ground water and land subsidence in Bangkok, Thailand. *Proceedings of the Second International Symposium on Land Subsidence.* Anaheim, California.

Pott, D.M. (1976) Behaviour of lined and unlined tunnels in sand. Doctoral Thesis, *University of Cambridge*, London.

Potts, D. M., and Zdravkovic, L. (2001) *Finite element analysis in geotechnical engineering: theory and application,* , Thomas Telford, London.

Prust, R. E., Davies, J., and Shuang, H. (2005) Pressuremeter investigation for Mass Rapid Transit in Bangkok, Thailand. *Journal of the Transportation Research Board.* 1928, 207 – 217.

Roscoe, K. H., and Burland, J. B. (1968) On the generalised stress-strain behaviour of wet clay. *Engineering Plasticity*, Cambridge: Cambridge University Press, New York, 535 - 609.

Rowe, R. K., and Kack, G. J. (1983) A theoretical examination of the settlements induced by tunnelling: four case histories. *Canadian Geotechnical Journal,* 20, 299-314.

Rowe, R. K., and Lee, K. M. (1992) Subsidence owing to tunnelling. II: evaluation of a prediction technique. *Canadian Geotechnical Journal*, 29, 941-954.

Rowe, R. K., Lo, K. Y., and Kack, G. J. (1983) A method of estimating surface settlement above tunnel constructed in soft ground. *Canadian Geotechnical Journal,* 20, 11-22.

Sagaseta, C. (1987) Analysis of undrained soil deformation due to ground loss. *Geotechnique,* 37, 301-320.

Santagata, M. (1998) *Factors affecting the initial stiffness and stiffness degradation of cohesive soils*. Doctoral Thesis, Massachusetts Institute of Technology, Cambridge, Mass.

Santagata, M., Germaine, J. T., and Ladd, C. C. (2005) Factors affecting the initial stiffness of cohesive soils. *Journal of Geotechnical and Geoenvironmental Engineering*, 131(4), 430 – 441.

Santos, J. A., and Correia, A. G. (2001) Reference threshold shear strain of soil. Its application to obtain a unique strain-dependent shear modulus curve for soil. *In: Proceedings of the 15th International Conference on Soil Mechanics and Geotechnical Engineering*, Vol. 1, Istanbul, A.A. Balkema, 267 – 270.

Schanz, T., Vermeer, P.A., and Bonnier, P.G. (1999) The hardening soil model: Formulation and verification. *Beyond 2000 in Computational Geotechnics.* Rotterdam. Taylor & Francis.

Schroeder, F. C. (2002) *The Influence of Bored Piles on Existing Tunnels.* Doctoral Thesis, Imperial College. London, University of London.

Schweiger, H. F. (2002) Some remarks on pore pressure parameter A and B in undrained analyses with the Hardening Soil Model. *Plaxis Bulletin,* 12, 6 - 9.

Schweiger, H. F. (2009) Influence of constitutive model and EC7 design approach in FEM analysis of deep excavations. *In: Proceeding of ISSMGE Int. Seminar on Deep Excavations and Retaining Structures*, Budapest, 99 – 114.

Seah, T. H., and Koslanant, S. (2000) Anisotropic consolidation behaviour of soft Bangkok clay. Geotechnical Testing Journal, 26(3), 1 – 11.

Shibuya, S., Hwang, S. C., and Mitachi, T. (1997) Elastic shear modulus of soft clays from shear wave velocity measurement. *Geotechnique*, 47(3), 593 – 601.

Shibuya, S., and Tanaka, H. (1996) Estimate of elastic shear modulus in Holocene soil deposits. *Soils and Foundations*, 36(4), 45 – 55.

Shuttle, D.A., and Jefferues, M.G. (1995) A practical geometry correction for interpreting pressuremeter tests in clay. *Géotechnique* 45(3), 549 – 554.

Skempton, A.W. (1954) The pore-pressure coefficients A and B. *Geotechnique*, 4, 143-147

Skempton, A. W., and Henkel, D.J. (1953) The Post-Glacial Clays of the Thames Estuary at Tilbury and Shellhaven. *In: Proceedings of the 3rd International Conference on Soil Mechanics and Foundation Engineering*, Switzerland. 302.

Soos Von, P. (2001) *Properties of soil and rock* (in German), Grundbautaschenbuch, Vol. 1, 6th Ed., Ernst & Son, Berlin, 117 – 201.

Stallebrass, S. E., and Taylor, R. N. (1997) The development and evaluation of the constitutive model for the prediction of ground movements in overconsolidation clay. *Geotechnique*, 47(2), 235 – 253.

Stark, T. D., and Vettel, J. J. (1991) Effective stress hyperbolic stress-strain parameters of clay. *Geotechnical Testing Journal*, 14(2), 146 – 156.

Surarak, C., Horny, U., Suwansawat, S., Phienwej, N., Oh, E., and Balasubramaniam, A. S. (2007) Numerical analysis of the combined cut and cover and New Austrian Tunnelling Methods for MRT station in Bangkok subsoils. *In: International Symposium on Tunnelling for Urban Development (IS-Pattaya 2007).* Pattaya City, Thailand, 116 – 132.

Surya, I. (1981) *Application of the LLT pressuremeter test to soil engineering problems in Bangkok Clay.* Masters Thesis, Asian Institute of Technology, Bangkok.

Suwansawat, S. (2002) *Earth Pressure Balance (EPB) shield tunnelling in Bangkok: ground response and prediction of surface settlements using artificial neural networks.* Doctoral Thesis, Massachusetts Institute of Technology.

Suwansawat, S., Chaiwonglek, C., and Horny, U. (2007) Design aspects of NATM and cut and cover underground stations for the Bangkok MRTA Blue Line Extension. *In: International Symposium on Tunnelling for Urban Development (IS-Pattaya 2007).* Pattaya City, Thailand, 64 – 75.

Suwansawat, S., and Einstein, H. H. (2007) Describing settlement troughs over twin tunnels using a Superposition Technique. *Journal of Geotechnical and Geoenvironmental Engineering,* 133**,** 445-468.

Swoboda, G. (1979) Finite element analysis of the New Austrian Tunnelling Method (NATM). *In: Proceedings of the 3rd International Conference on Numerical Methods in Geomechanic.* Aachen, Germany, A.A.Balkema, 604 – 618.

Swoboda, G., and Abu-Krisha, A. (1999) Three-dimensional numerical modelling for TBM tunnelling in consolidated clay. *Tunnelling and Underground Space Technology*, 14(3), 327 – 333.

Tantikom, S. (1982) *K_o measurements on Bangkok clay.* Masters Thesis, Asian Institute of Technology, Bangkok.

Taparaksa, W. (1999) Principal and application of instrumentation on the first MRTA subway in Bangkok. *In: Proceedings of the 5th International Conference on Field Measurement in Geomechanics*, Balkema, Rotterdam.

Tavaranum, S. (2004) *Analysis of subsurface ground movements induced by EPB shield tunnelling in the Bangkok MRT Blue Line project.* Masters Thesis, Asian Institute of Technology, Bangkok.

Teachavorasinskun, S., and Lukkunaprasit, P. (2004) A simple correlation for shear wave velocity of soft Bangkok clays. *Geotechnique*, 54, 323 – 326.

Teachavorasinskun, S., Thongchim, P., and Lukkunaprasit, P. (2002a) Shear modulus and damping of soft Bangkok clays. *Canadian Geotechnical Journal*, 39, 1201 – 1208.

Teachavorasinskun, S., Thongchim, P., and Lukkunaprasit, P. (2002b) Stress rate effect on the stiffness of a soft clay from cyclic, compression and extension triaxial tests. *Geotechnique*, 52(1), 51 – 54.

Theramast, N. (1998) *Characterisation of pseudo-elastic shear modulus and shear strength of Bangkok clay*. Masters Thesis, Asian Institute of Technology, Bangkok.

Timoshenko, S. P., and Goodier, J. N. (1934) *Theory of elasticity*, McGraw-Hill, New York.

Timpong, S. (2002) *Analysis of ground movements in Bangkok MRT Blue Line project*. Master Thesis, Asian Institute of Technology.

Towhata, I. (2008) *Geotechnical earthquake engineering*. Springer, Tokyo.

Vermeer, P. A. (1978) A double hardening model for sand. *Geotechnique*, 28(4), 413 – 433.

Vermeer, P.A. and Brinkgreve, R. (1993) *Plaxis version 5 manual*. Rotterdam, A.A. Balkema.

Verruijt, A., and Booker, J. R. (1996) Surface settlements due to deformation of a tunnel in an elastic half plane. *Geotechnique,* 46, 753-756.

Viggiani, G., and Atkinson, J. H. (1995) Stiffness of fine-grained soil at very small strains. *Geotechnique*, 45(2), 249 – 265.

Vucetic, M. (1994) Cyclic threshold shear strains in soils. *Journal of Geotechnical Engineering*, 120(12), 2208 – 2228.

Vucetic, M., and Dobry, R. (1991) Effect of soil plasticity on cyclic response. *Journal of Geotechnical Engineering, ASCE*, 117(1), 89 – 107.

Warnitchai, P., Sangarayakul, C., and Ashford, S. A. (1996) Seismic hazard in Bangkok due to long-distance earthquakes. *In: Proceedings of the 12th World Conference on Earthquake Engineering*, Madrid, A.A. Balkema, 2145 – 2153.

Whittle, A. J., Hashash, Y. M. A., and Whitman, R. V. (1993) Analysis of a deep excavation in Boston, *Journal of Geotechnical Engineering, ASCE*, 119(1), 69 – 90.

Whittle, A. J., and Kavvadas, M. J. (1994) Formulation of MIT-E3 constitutive model for overconsolidated clays. *Journal of Geotechnical Engineering, ASCE*, 120(1), 173 – 198.

Wong, K. S., and Broms, B.B. (1989) Lateral wall deflections of braced excavations in clay. *Journal of Geotechnical Engineering, ASCE,* 115, 853 - 870.

Wong, L. W., and Patron, B. C. (1993) Settlement induced by deep excavations in Taipei. *In: Proceedings of the 11ᵗʰ Southeast Geotechnical Conference*, Kuala Lumpur, 787 – 791.

Wongsaroj, J. (2005) *Three-dimensional finite element analysis of short and long-term ground response to open-face tunnelling in stiff clay.* Doctoral Thesis, University of Cambridge.

Wood, D.M. (1995) Kinematic hardening model for structure soil. *In: Proceedings of the International Conference on Numerical Models in Geomechanics NUMOG 5*, (edt. Pande and Pietruszczak), A.A. Balkema, 83 – 88.

Wroth, C. P. (1982) British experience with the self-boring pressuremeter, *In: Proceedings of International Symposium on Pressuremeter and Its Marine Applications*, Paris, 143 – 164.

Wroth, C. P., and Hughes, J. (1973) An instrument for the in-situ measurement of the properties of soft clay. *In: Proceedings of the International Conference on Soil Mechanics and Foundation Engineering,* Moscow.

Wroth, C. P., Randolph, M. F., Houlsby, G. T., and Fahey, M. (1979) A review of the engineering properties of soils with particular reference to the shear modulus. *CUED/D-Soils TR75*, Cambridge University.

Youd, L. T. (1972) Compaction of sands by repeated shear straining. *Journal of Soil Mechanics and Foundation Engineering Division, ASCE*, 98(7), 709 – 725.

Yu, H. S. (1990) *Cavity expansion theory and its application to the analysis of pressuremters*. Doctoral Thesis, University of Oxford.

Yu, H. S., Charles, M. T., and Khong, C. D. (2005) Analysis of pressuremeter geometry effects in clay using critical state models. *International Journal for Numerical and Analytical Methods in Geomechanics*, 29, 845 – 859.

APPENDIX A

Drained and Undrained Modelling in Finite Element Analysis

A1 Introduction

Numerical analyses of undrained materials are complex and therefore, require an understanding in calculation methods and constitutive models. Advantages and limitations of available undrained analysis methods in Plaxis software are summarised and discussed herein. Majority of literature materials reviewed in this section are obtained from a lecture series given at Griffith University in 2008. The invited lecturers were Prof. Schweiger, H.F., Prof. Gens, A., Dr. Broere W. and Dennis W.

A2 Drained and Undrained Modelling in Finite Element Analysis

In conducting a finite element analysis, care much be taken to the drained and undrained behaviour of the modelled soils. In case of high permeability material such as sand, appropriate type of analysis is drained analysis. There is no complication in

carrying out drained analysis for drained material due to the fact that only effective strength and stiffness parameters should be adopted in conjunction with drained material setting. This drained analysis is applicable for both basic Mohr Coulomb Model (MCM) and advanced models, such as Hardening Soil (HSM) and Soft Soil (SSM) Models. Modelling of undrained material, i.e. clayey types of soil, is on the other hand more complex. Brief summary of drained and undrained analyses is given below.

Drained analysis:

- Applicable for modelling the behaviour of high permeability (sandy) materials or low permeability (clayey) materials in case of low rate of loading.
- Short term behaviour is not of interest for the problem considered.
- No excess pore pressure is generated.

Undrained analysis:

- Applicable only for modelling the behaviour of low permeability (clayey) materials with a high rate of loading.
- Short term behaviour is to be accessed.
- Excess pore pressure is fully generated.

Various FE analysis methods are available for undrained behaviour modelling. Selection of effective and total stress parameters should be made together with the type of soil model used prior to the modelling process. Basically, there are four methods available in Plaxis, namely Method A, B, C and D. Methods A, B and C are used in combination with Mohr-Coulomb (MC) soil model. While, Method D is used in advanced soil models, such as hardening soil (HS) and soft soil (SS) models. Details of each method are given in the following sections and are summarised in Table A1.

Table A1: Summary of Analyses for Undrained Materials

Method	Material type	Material model	Computed stresses	Parameters Stiffness	Parameters Strength
A	Undrained (MC)	Mohr-Coulomb	Effective stress & pore pressure	Effective (E', ν')	Effective (ϕ', c')
B	Undrained (MC)	Mohr-Coulomb	Effective stress & pore pressure	Effective (E', ν')	Total (ϕ_u, c_u)
C1	Non-porous (MC)	Mohr-Coulomb	Total stress	Total (E_u, ν_u)	Total (ϕ_u, c_u)
C2	Drained (MC)	Mohr-Coulomb	Total stress	Total (E_u, ν_u)	Total (ϕ_u, c_u)
D	Undrained (MCC, SS, HS, HSS)	Hardening Soil or Soft Soil	Effective stress & pore pressure	Effective parameters depending on soil model selected	

NOTE: MC = Mohr-Coulomb Model, MCC = Modified Cam Clay Model, SS = Soft Soil Model, HS = Hardening Soil Model and HSS = Hardening Soil Model with Small Strain

When material type is set to "undrained" (Methods A, B and D), Plaxis automatically adds bulk modulus of water, K_w/n to the bulk modulus of soil skeleton, K' and distinguishes between total stresses, effective stresses and excess pore pressures:

Total stress:
$$\Delta\sigma = K_u \Delta\varepsilon_v \qquad \text{Eq. A1}$$

Effective stress:
$$\Delta\sigma' = (1-B)\Delta\sigma = K'\Delta\varepsilon_v \qquad \text{Eq. A2}$$

Excess pore pressure:
$$\Delta u = B\Delta\sigma = \frac{K_w}{n}\Delta\varepsilon_v \qquad \text{Eq. A3}$$

Excess pore pressure (triaxial): $\Delta u = B(\Delta\sigma_3 + A(\Delta\sigma_1 - \Delta\sigma_3))$ Eq. A4

where, $\Delta\sigma$, $\Delta\sigma'$ and Δu are changes in total stress, effective stress and pore pressure, respectively. A & B are the Skempton's parameters (Skempton, 1954). Skempton A-parameter is not a soil parameter. In fact, its value depends on calculated stress path resulting from constitutive model used. Parametric study by Schweiger (2002) revealed that Mohr-Coulomb soil model with non-dilation yielded a value of A-parameter of 1/3. This is identical to its values of isotropic elastic model. For Hardening soil model, A-parameter is not constant but increases with the applied deviatoric loading. A value of approximately 0.44 at failure is obtained for a particular parameter set applied in his study.

K_u in Eq. B3 is the total (undrained) bulk modulus:

$$K_u = K' + \frac{K_w}{n} \qquad \text{Eq. A5}$$

$$K_u = \frac{E_u}{3(1-2\upsilon_u)} = \frac{2G(1+\nu_u)}{3(1-2\upsilon_u)} = \frac{E'(1+\nu_u)}{3(1-2\upsilon_u)(1+\nu')} \qquad \text{Eq. A6}$$

where, E_u and E' are undrained and drained elastic moduli. G is shear modulus. ν_u and ν' are undrained and drained Poisson's ratios. Calculation of effective stress and excess pore pressure (Eqs. A2 & A3) involves Skempton B-parameter, which can be approximated by:

$$B = \frac{1}{1 + \frac{n}{K_w}K'} \qquad \text{Eq. A7}$$

According to Eq. B7, Skempton B-parameter approaches unity when bulk modulus of water, K_w/n is very high compare to the bulk modulus of soil skeleton, K'. In reality, a high realistic bulk modulus of water may cause numerical problems in the calculation, therefore Plaxis utilises slightly lower number of bulk modulus of water as calculated by the following process. First bulk modulus of soil skeleton, K' is estimated from the input drained elastic modulus, E':

$$K' = \frac{E'}{3(1-2\upsilon')} \qquad \text{Eq. A8}$$

Then, estimates total (undrained) bulk modulus, K_u from Eq. B6. Please note that Plaxis uses value of 0.495 for undrained Poisson's ratio as default setting. Finally, Skempton B-parameter is obtained from Eq. A6. Following this process, Skempton B-parameter will depend only on the value of drained Poisson's ratio. For undrained behaviour, drained Poisson's ratio should be smaller than 0.35, as using higher values would lead to an unrealistically low Skemption B-parameter.

A3 Advantages and Limitations of Method A, B, C and D

Figure A1 illustrates typical total stress path (TSP) and effective stress paths (ESP) resulting form isotropically consolidated undrained triaxial test of normally consolidated clay. Stress paths OA, OB, OC and OD in Figure A1 (a to d) are the calculated results of Method A, B, C and D, respectively. Details of each method are summarised below.

A3.1 Method A

Method A utilises both effective stress and stiffness parameters to model undrained behaviour of soils. The constitutive model used is Mohr-Coulomb model. As shown in Figure A1 (a), effective stress path (ESP) predicted by Mohr-Coulomb model rose up vertically until failure envelop is reached (stress path OA). This stress path is unlikely to be identical to the real stress path especially in case of normally consolidated clay. As a result, calculated pore water pressure is also unlikely to be correct. Furthermore, undrained shear strength predicted by Method A (Point A) may exceed the undrained shear strength as followed by triaxial effective stress path. Due to the unreliability of both soil strength and pore water pressure calculation, this method should generally be avoided.

A3.2 Method B

Similar to Method A, effective stiffness parameters and Mohr-Coulomb model are used in Method B. However, the failure criterion is governed by an input total strength parameter, i.e. $\phi_u = o$ and $c = c_u$. Calculated stress path from Method B is identical to that of from Method A (stress path OB), therefore calculated pore water pressure should be ignored. For this reason, Method B should not be followed by consolidation analyses. It should be note that if Hardening Soil model is selected in Method B, the stiffness moduli will be no longer stress-dependent and the model exhibits no compression hardening. Conversely, the model retains its separation of loading and unloading-reloading moduli and shear hardening.

A3.3 Method C1

Method C1 is a total stress approach. It adopts both undrained strength and undrained stiffness parameters. Material type of Method C1 is set to "Non-porous" which means neither initial nor excess pore pressure will be taken into account. The disadvantage of this approach is that no distinction is made between effective stress and pore water pressure. Hence, all calculated stresses are total stress and pore water pressures are equal to zero.

A3.4 Method C2

Method C2 is identical to Method C1 except the material type is set to "Drained". Major distinction between Method C1 and C2 is that Method C2 carries over the initial pore water pressure to the analysis. Nevertheless, there is no change of pore water pressure computed afterward.

A3.5 Method D

Input parameters of Method D for both stiffness and strength parameters are the same as Method A. Only diversion from these two methods is Method A utilises a more sophisticated advanced model (such as Hardening Soil or Soft Soil models). Undrained shear strength computed form this method depends on the accuracy of effective stress part as obtained from the advanced model used (stress path OD in Figure A1 (d)).
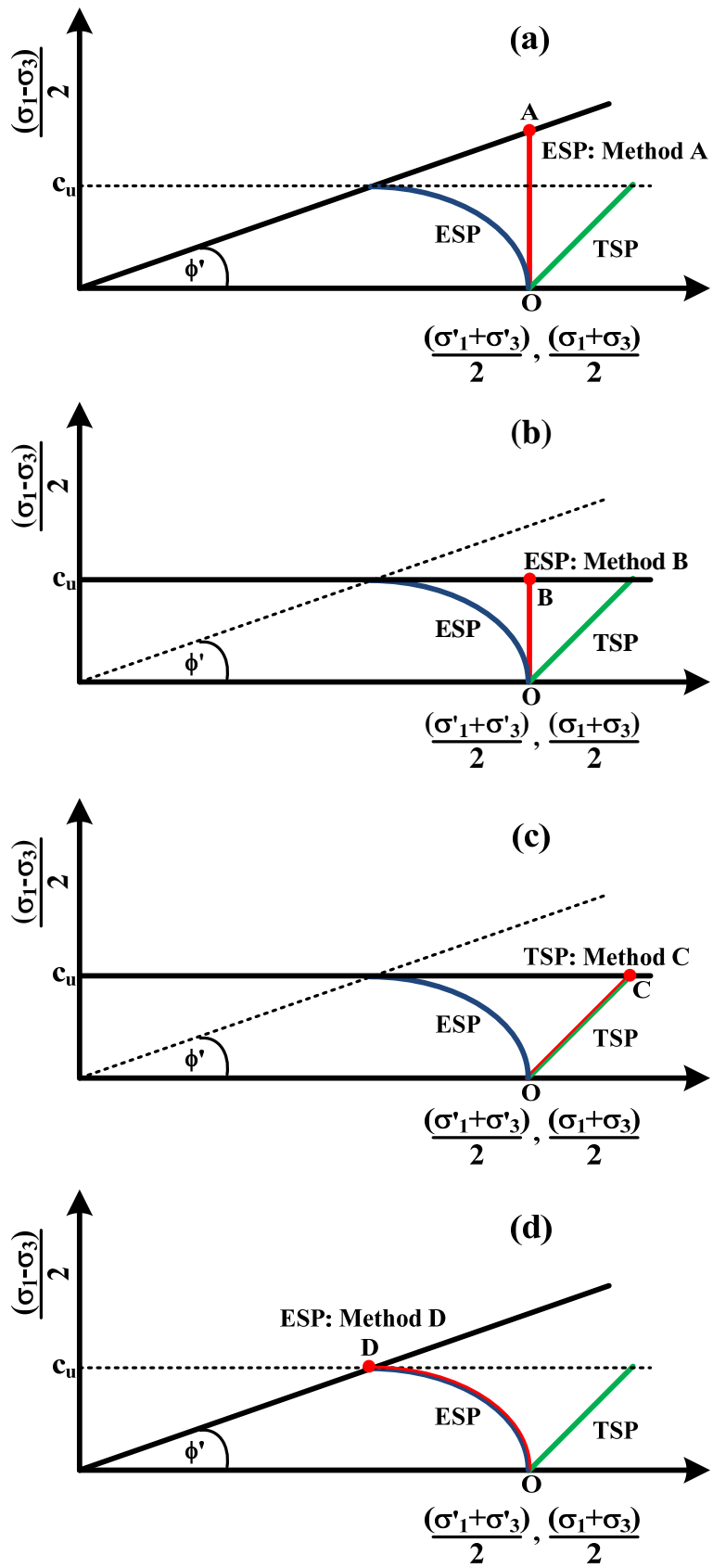
Figure A1: Calculated Stress Paths Resulting from Methods A, B, C and D

APPENDIX B

Parametric Study on

Hardening Soil Model Parameters

(a)

(b)

(c)

(d)
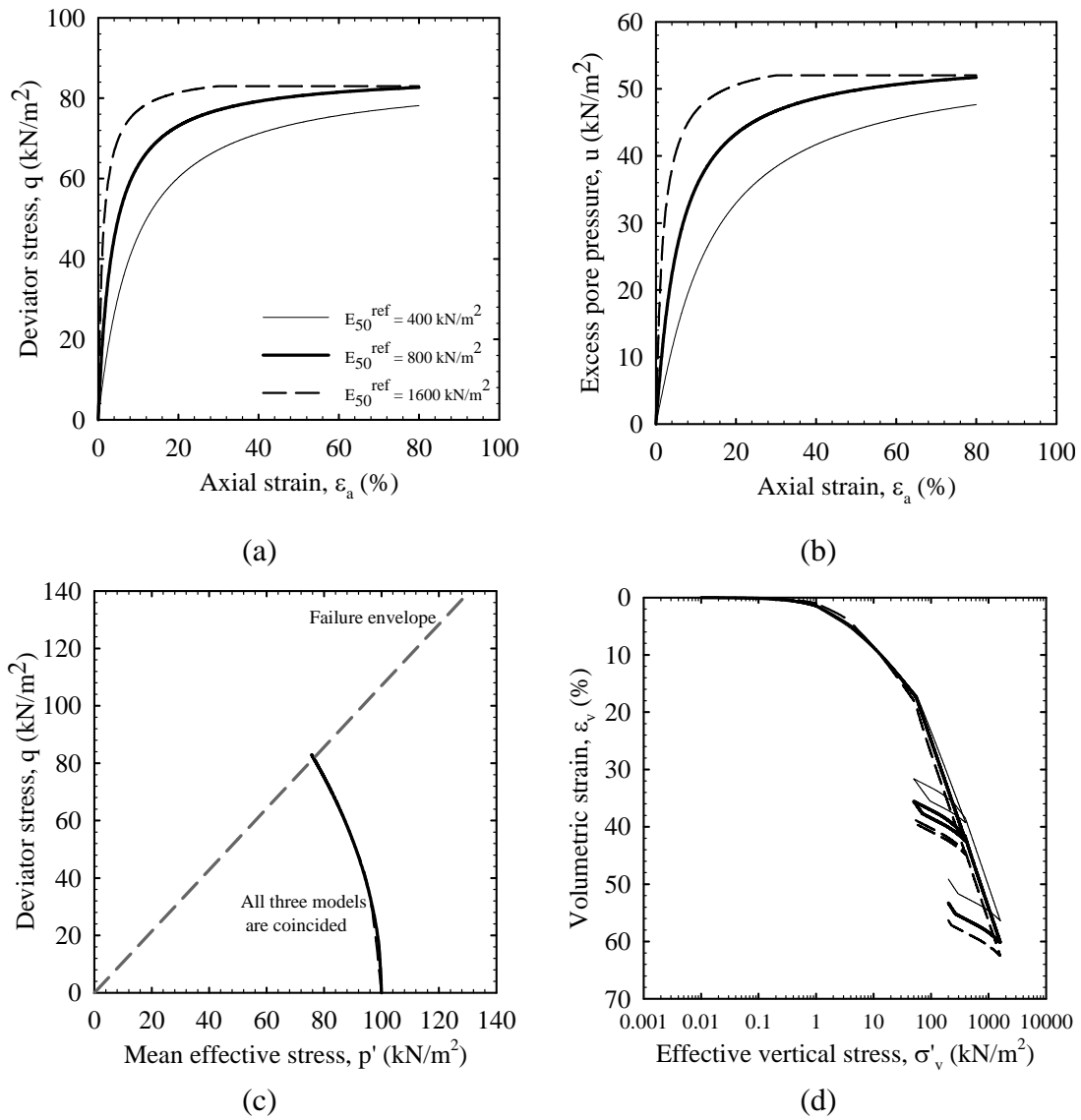
Figure B1: Parametric Study on E_{50}^{ref}
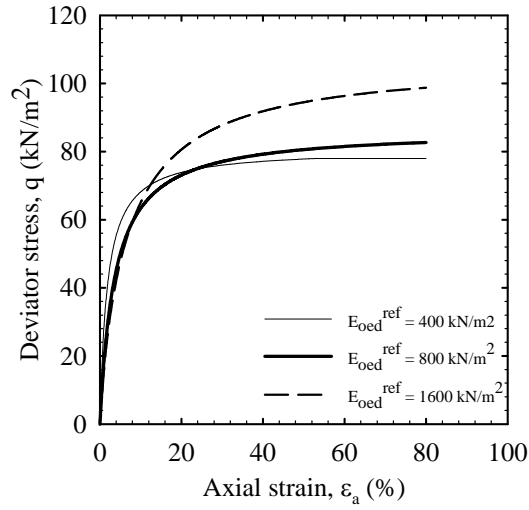
(a)
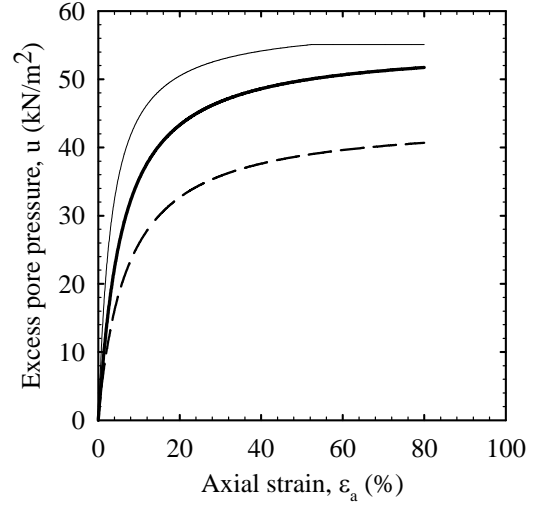
(b)
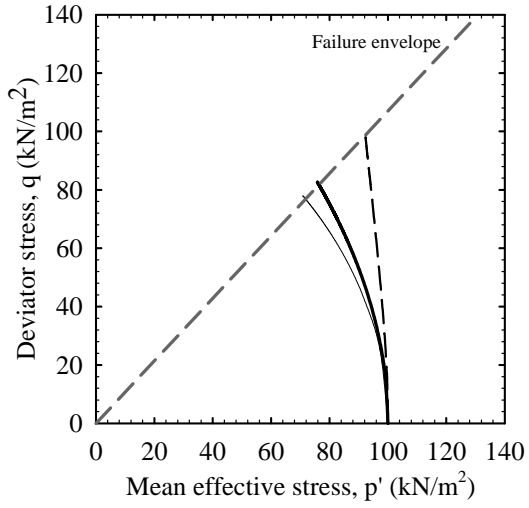
(c)
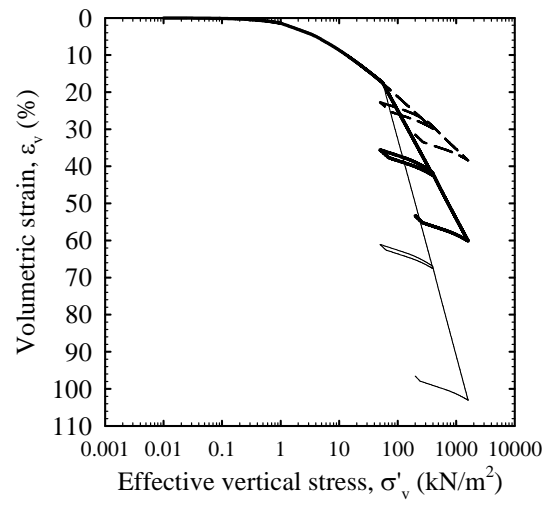
(d)

Figure B2: Parametric Study on E_{oed}^{ref}

381

(a)

(b)

(c)

(d)
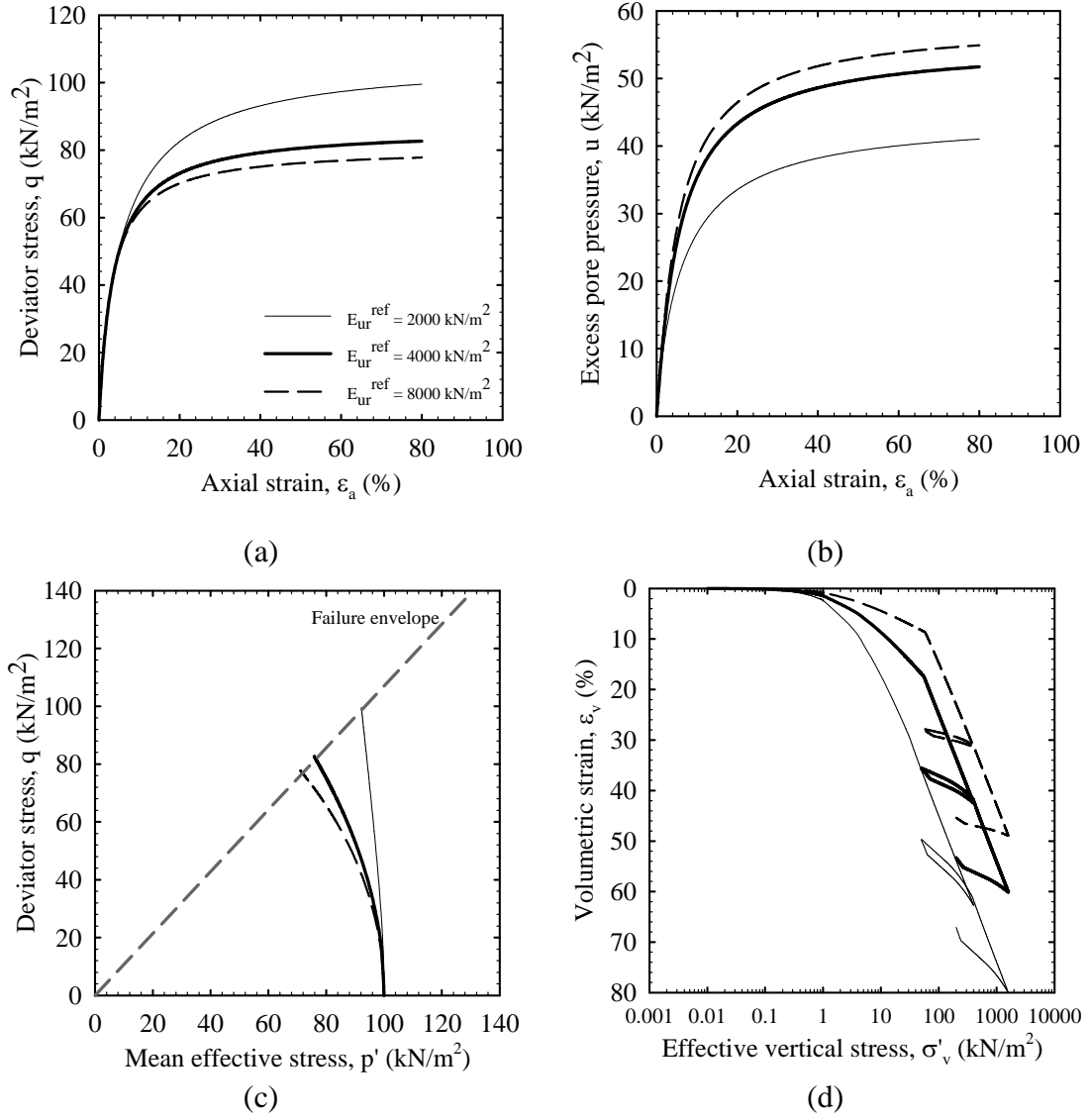
Figure B3: Parametric Study on E_{ur}^{ref}
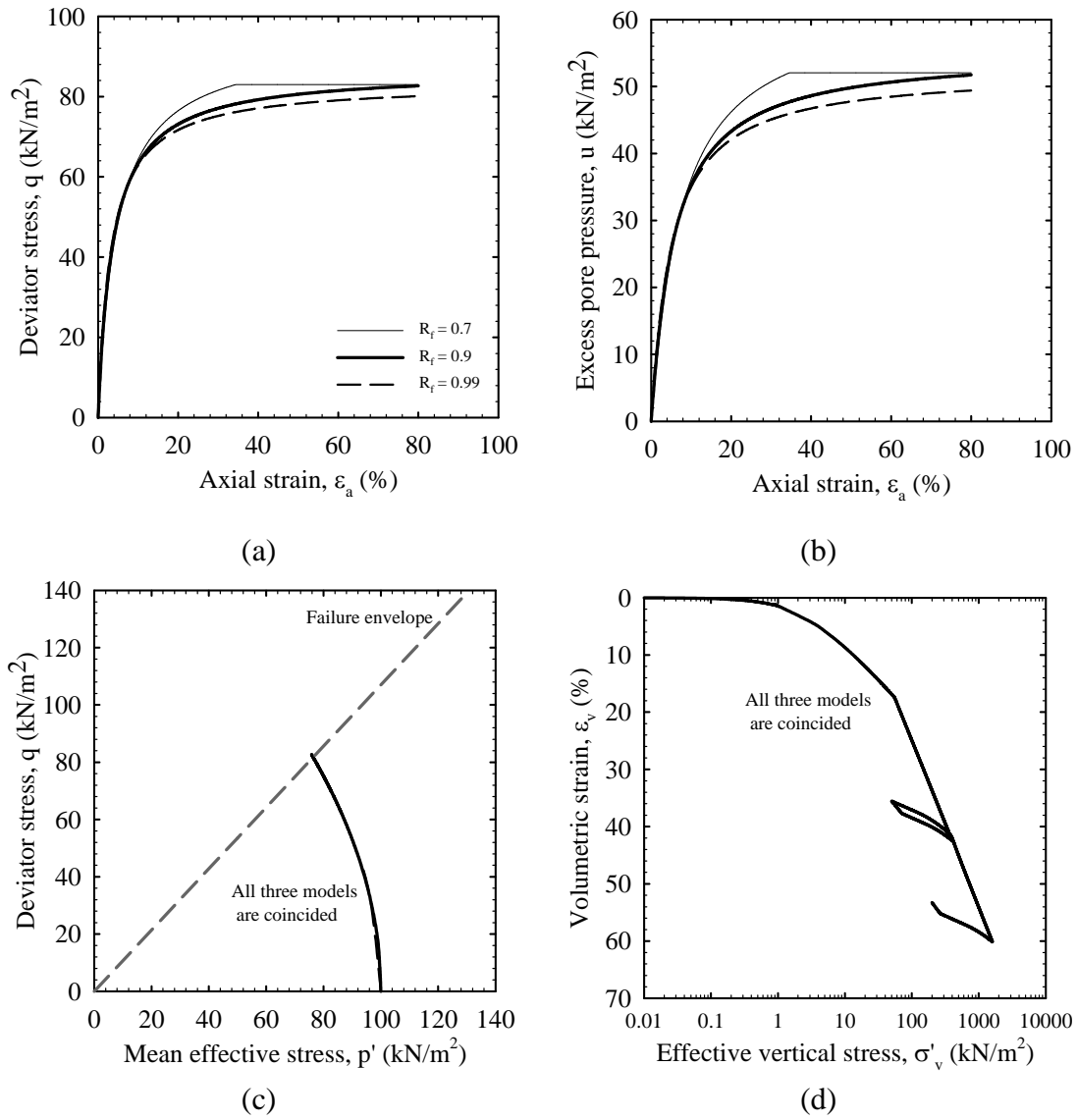
Figure B4: Parametric Study on R_f
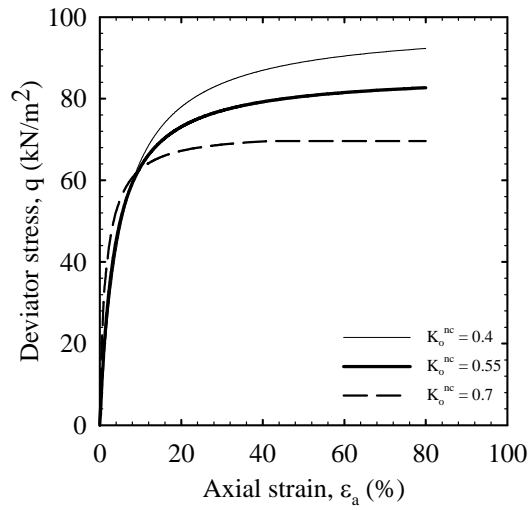
(a)
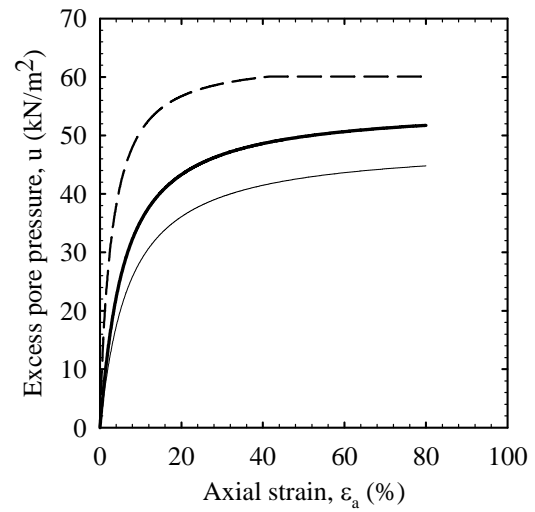
(b)
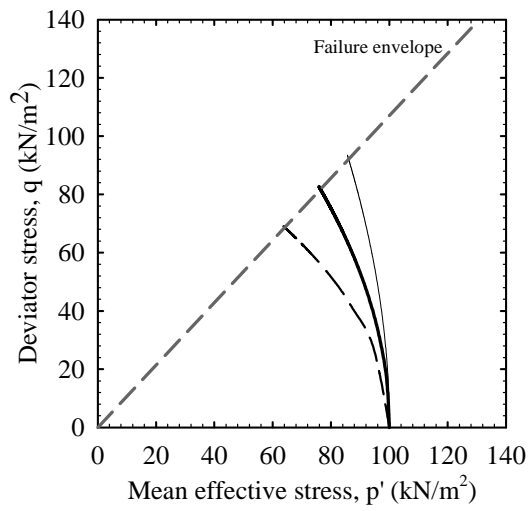
(c)
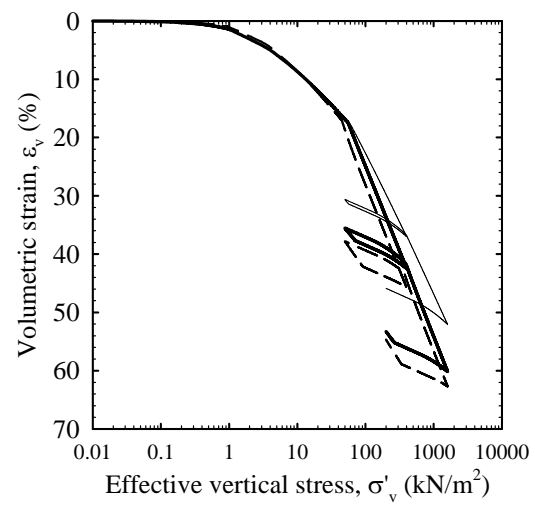
(d)

Figure B5: Parametric Study on K_0^{nc}

384

(a)

(b)

(c)

(d)
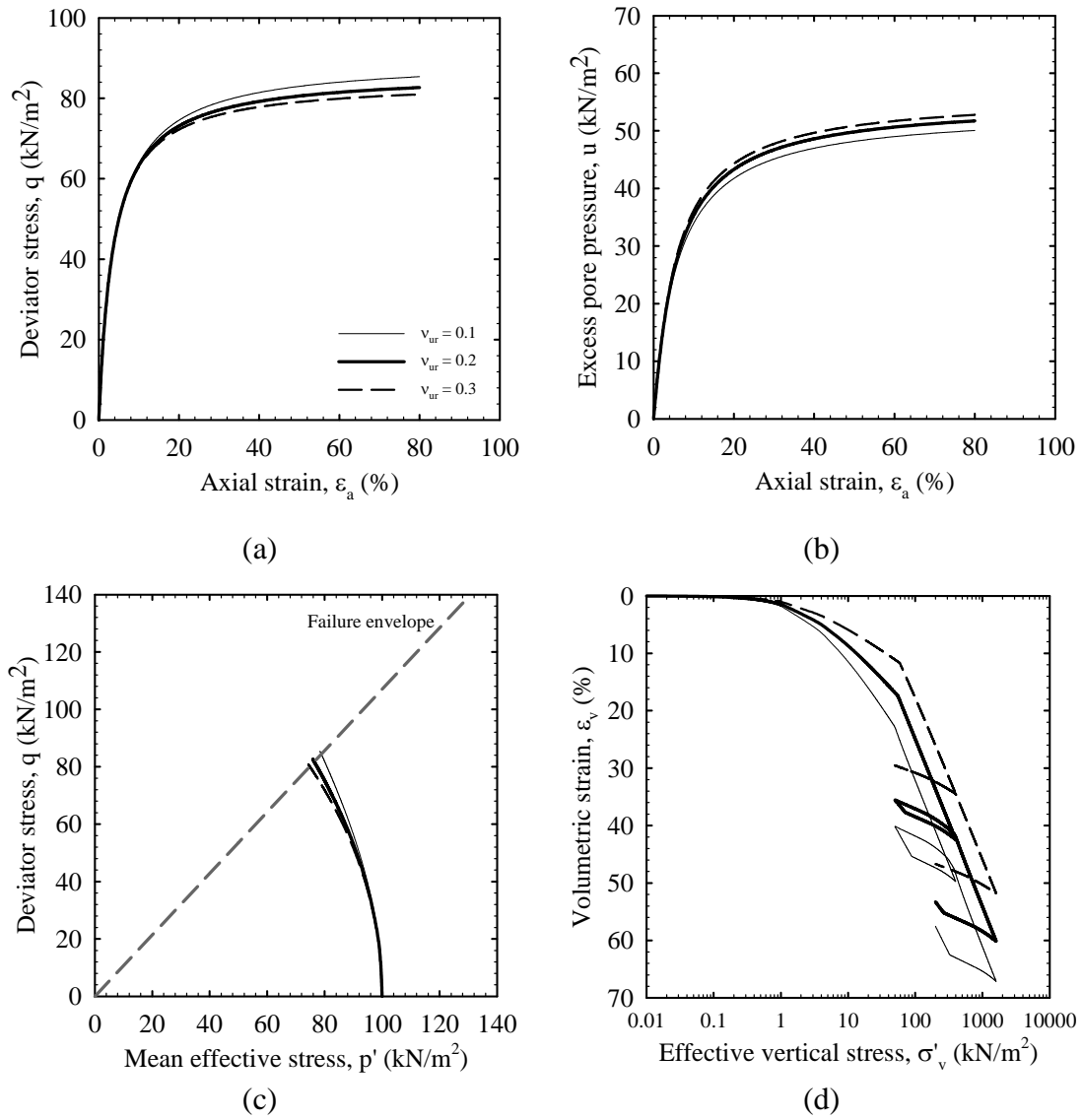
Figure B6: Parametric Study on ν_{ur}

385
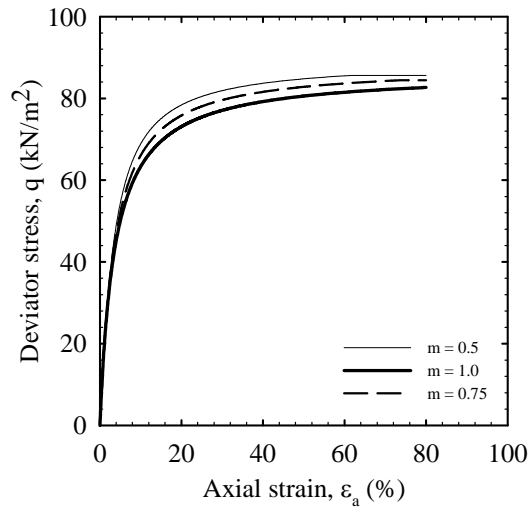
(a)
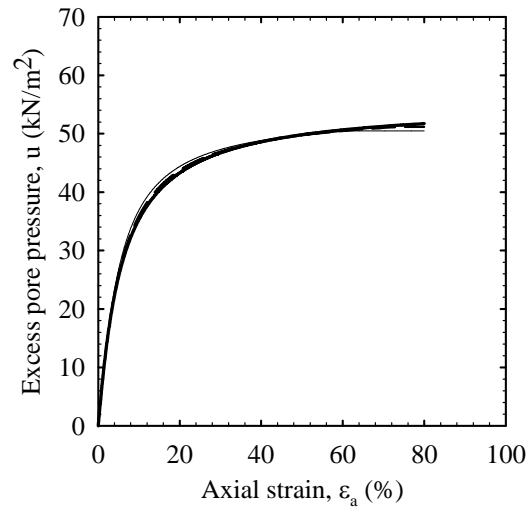
(b)
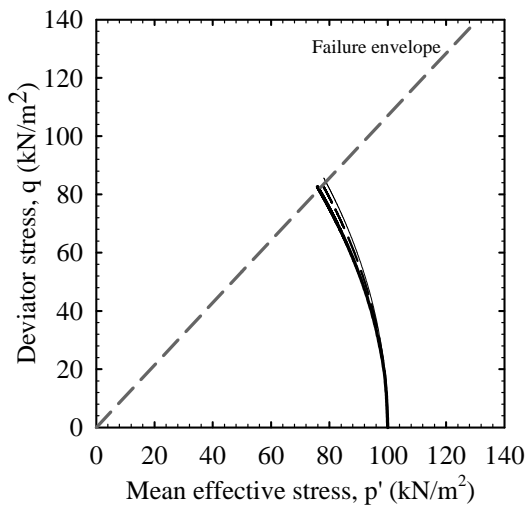
(c)
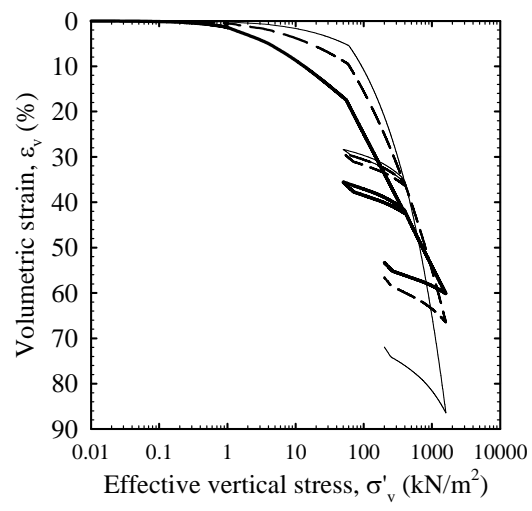
(d)

Figure B7: Parametric Study on *m*
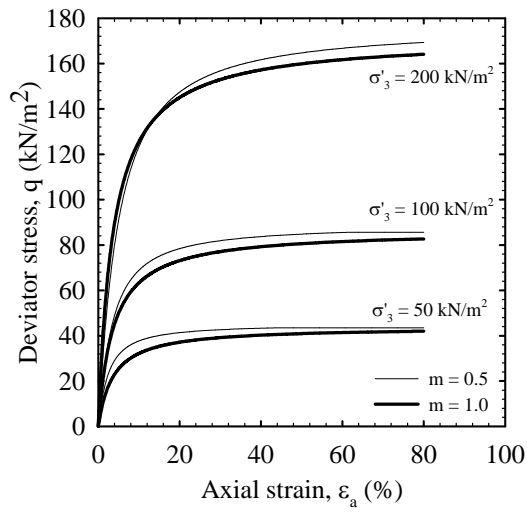
(e)
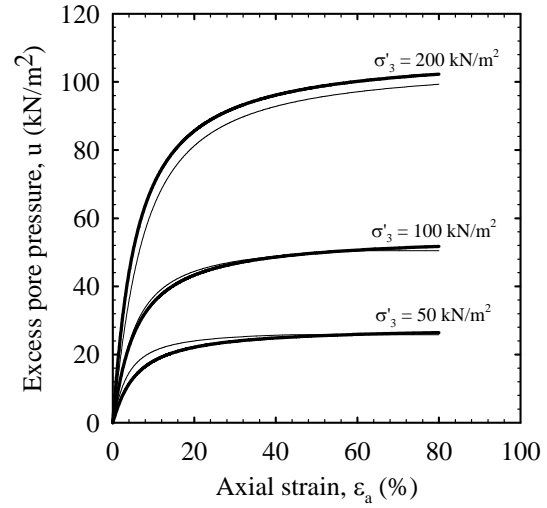
(f)
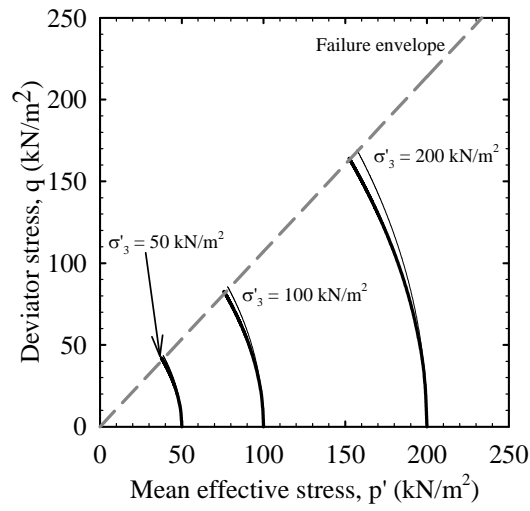
(g)

Figure B7: Parametric Study on *m* (cont'd)

APPENDIX C

Results from LLT

Pressuremeter Tests
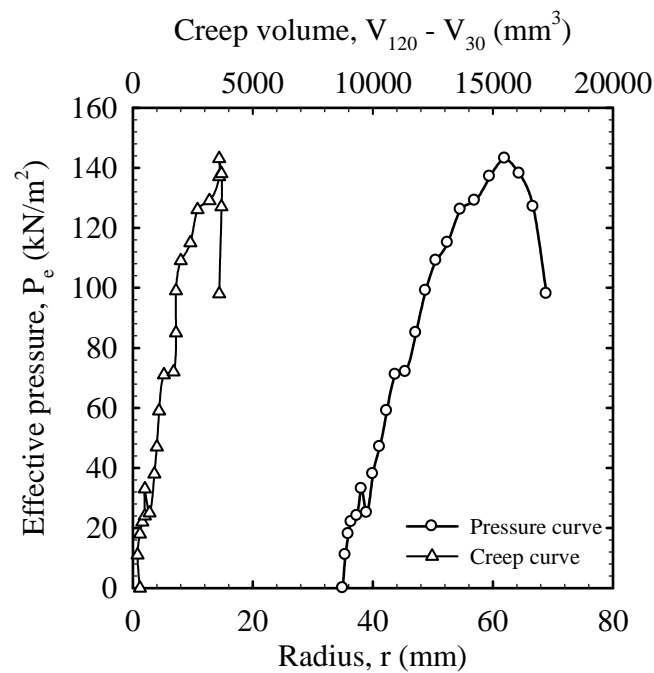
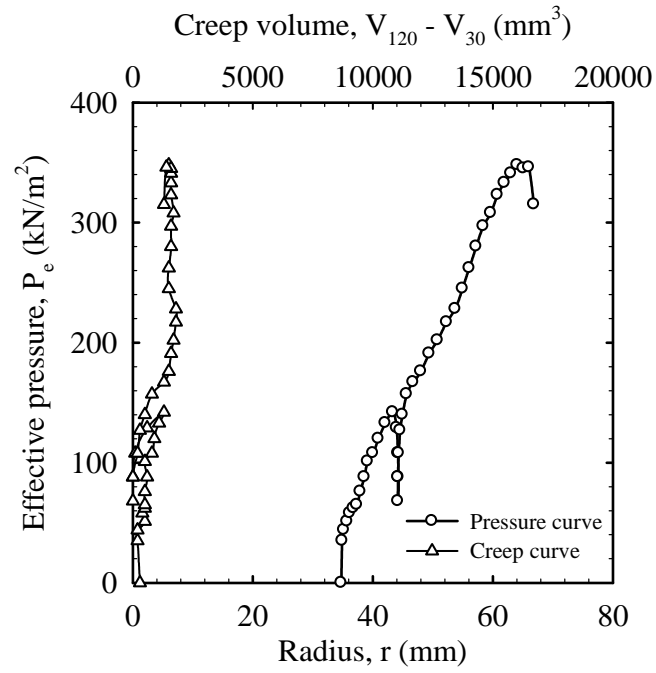Figure C1 (a): Pressuremeter Test Results at Wat Mangkon Station, BH06

(Soft Clay, depth 9m)
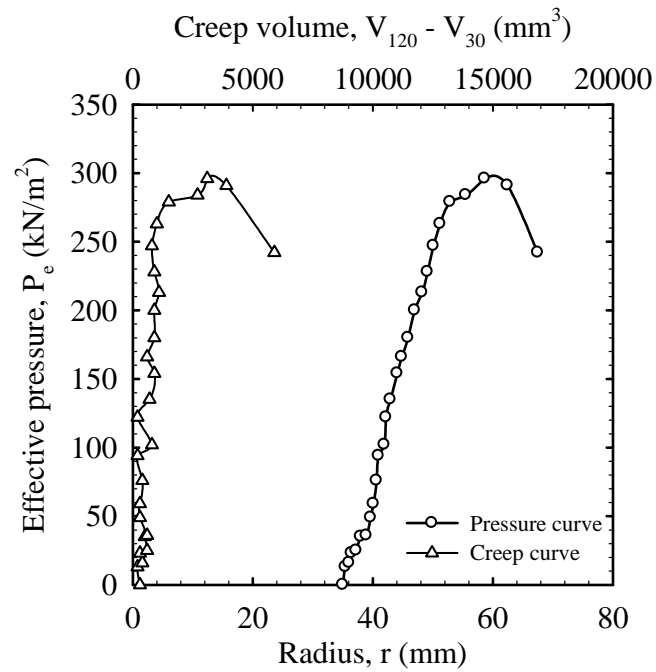
Figure C1 (b): Pressuremeter Test Results at Wat Mangkon Station, BH06

(Stiff Clay, depth 13m)
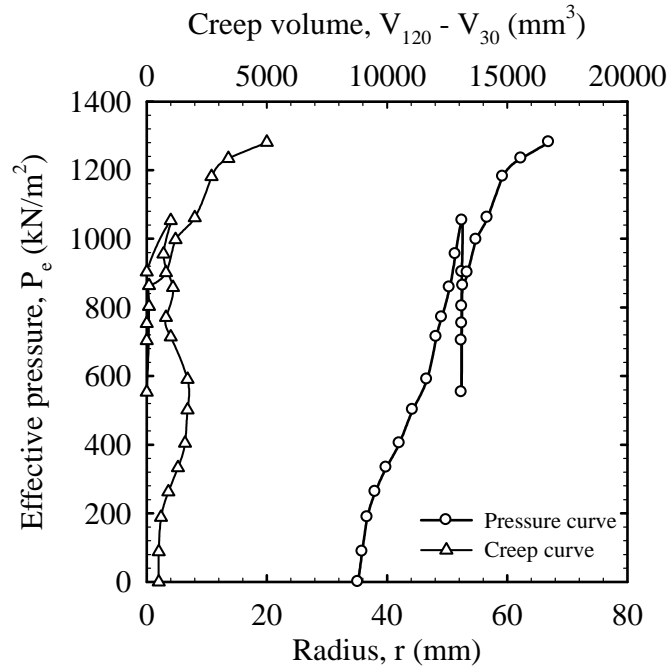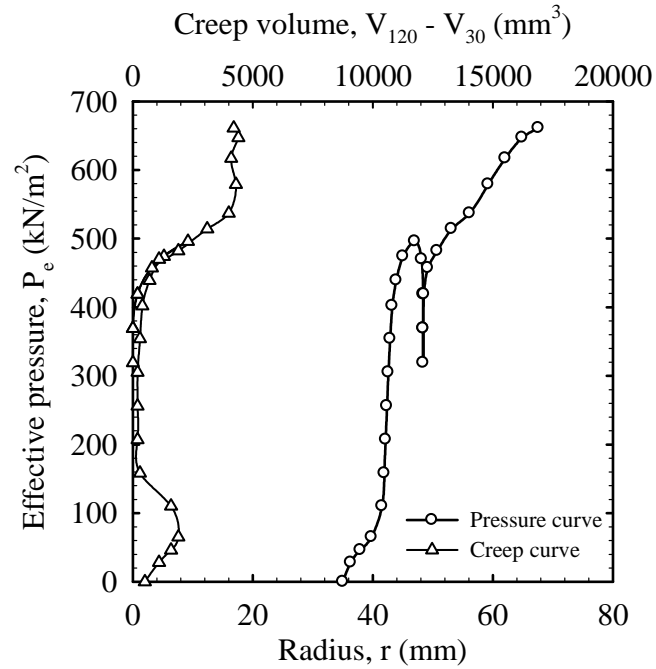

Figure C1 (c): Pressuremeter Test Results at Wat Mangkon Station, BH06

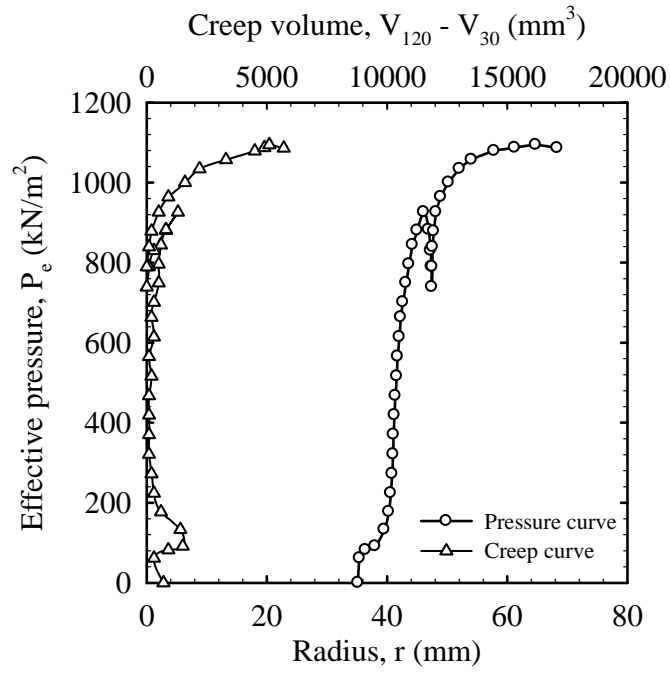(Stiff Clay, depth 16m)
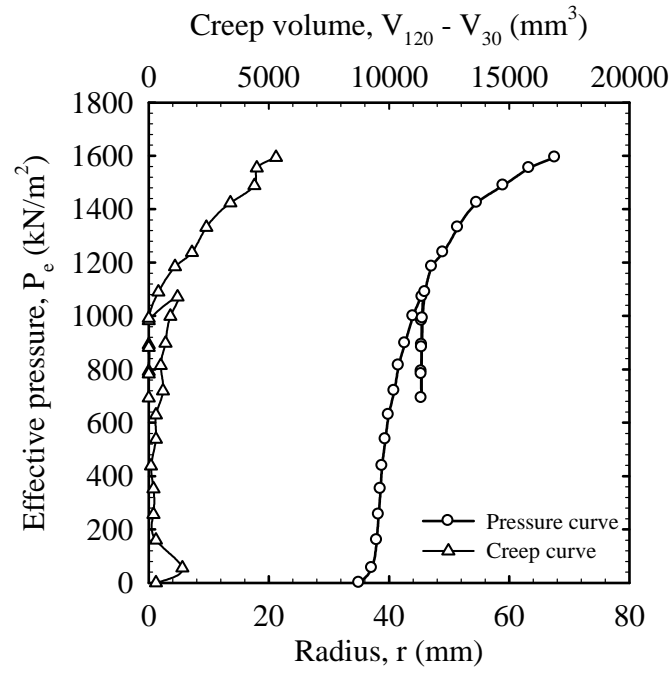
Figure C1 (d): Pressuremeter Test Results at Wat Mangkon Station, BH06

(Very Stiff Clay, depth 21m)
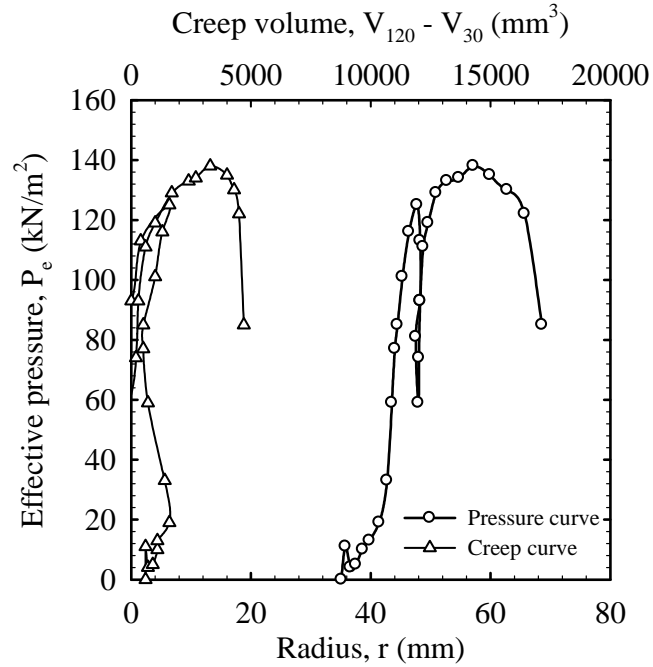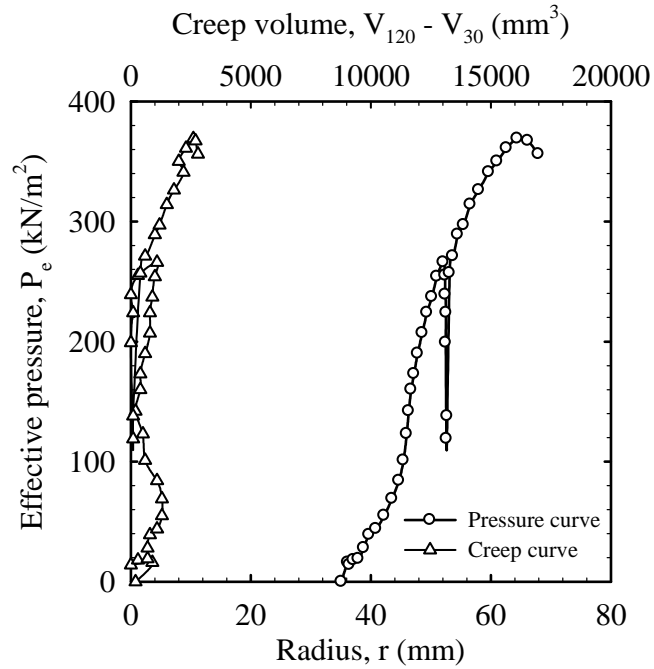

Figure C2 (a): Pressuremeter Test Results at Wang Burapha Station, BH09

(Soft Clay, depth 6m)
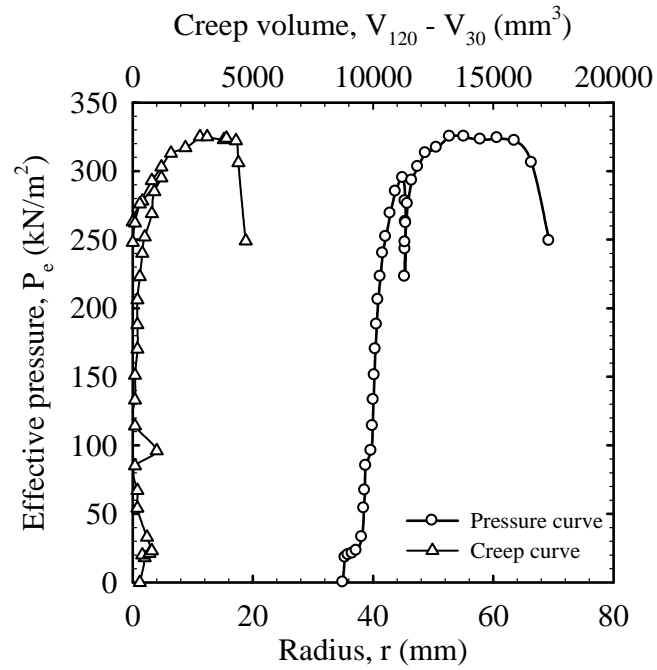
Figure C2 (b): Pressuremeter Test Results at Wang Burapha Station, BH09

(Medium Stiff Clay, depth 12m)
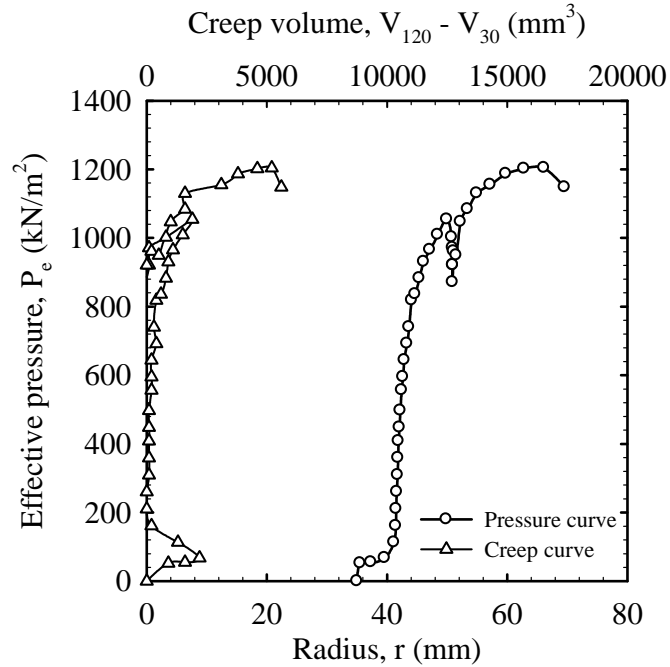
Figure C2 (c): Pressuremeter Test Results at Wang Burapha Station, BH09

(Very Stiff Clay, depth 17m)
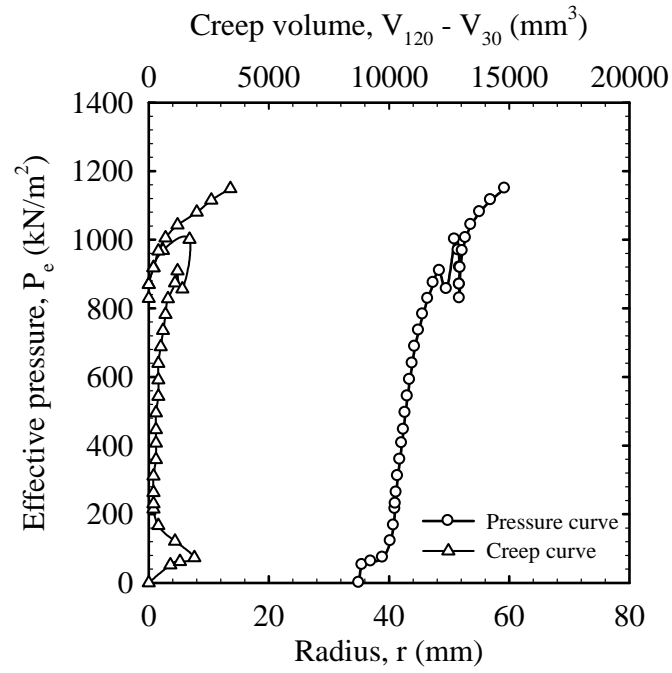
Figure C2 (d): Pressuremeter Test Results at Wang Burapha Station, BH09

(Very Stiff Clay, depth 22m)
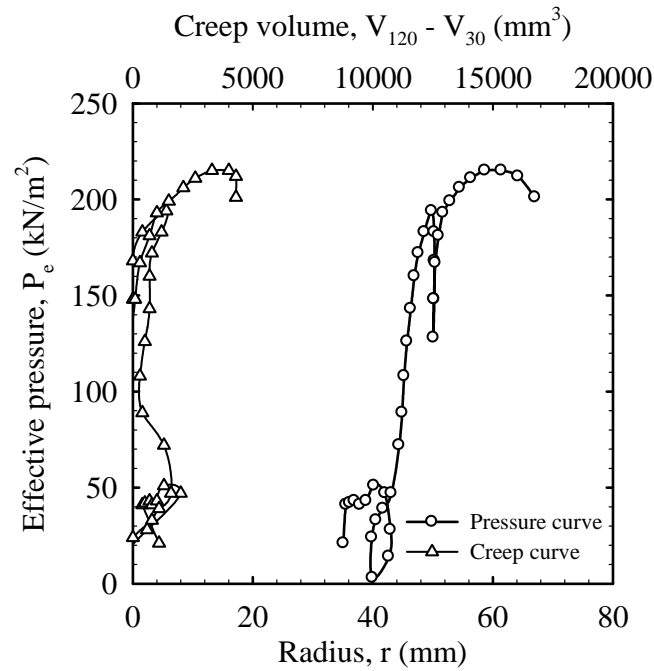
Figure C3 (a): Pressuremeter Test Results at Sanam Chai Station, BH12

(Soft Clay, depth 10m)
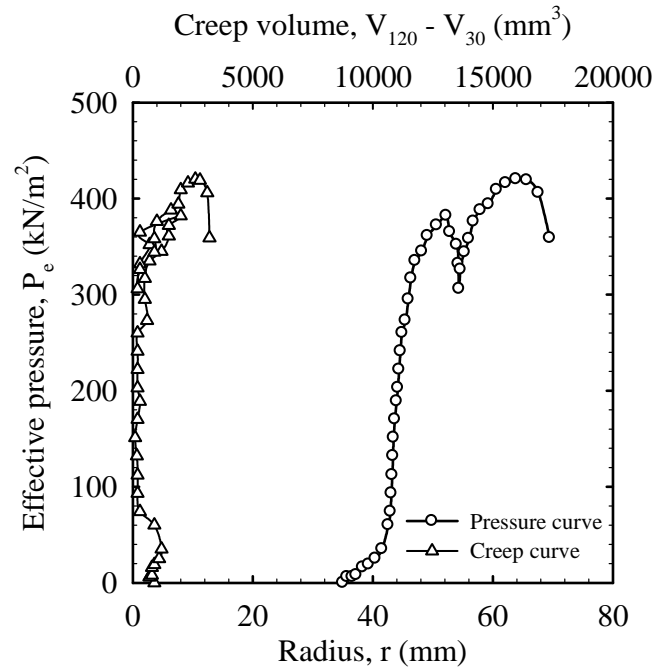
Figure C3 (b): Pressuremeter Test Results at Sanam Chai Station, BH12
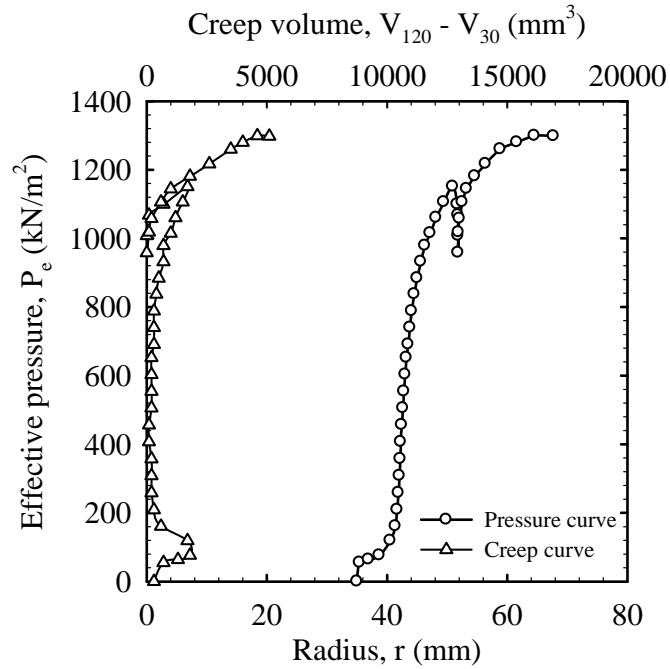
(Medium Stiff Clay, depth 14m)
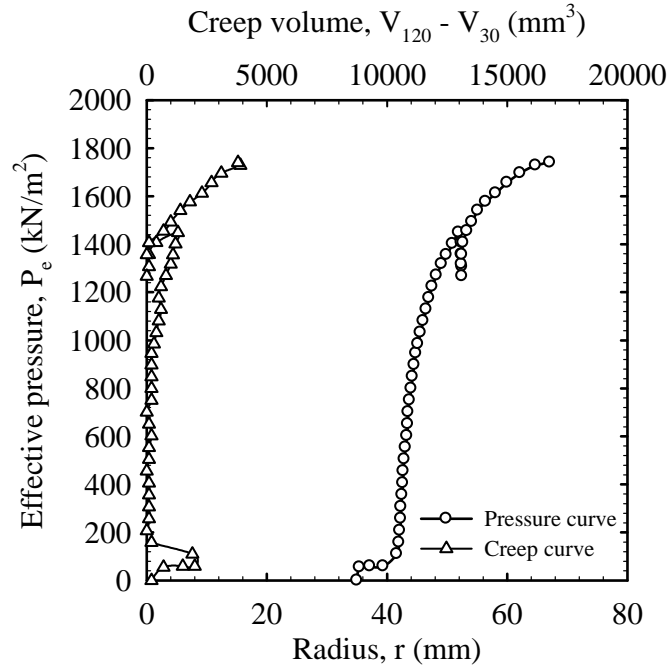
Figure C3 (c): Pressuremeter Test Results at Sanam Chai Station, BH12
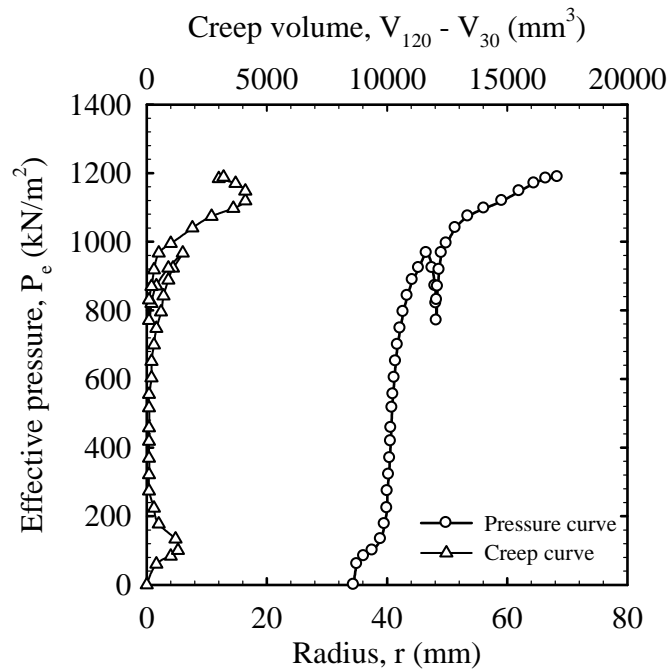
(Very Stiff Clay, depth 19m)
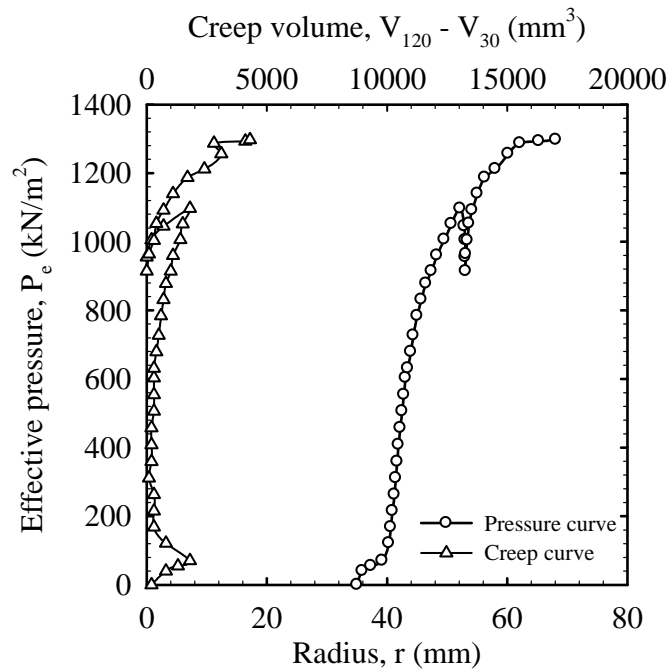
Figure C3 (d): Pressuremeter Test Results at Sanam Chai Station, BH12

(Very Stiff Clay, depth 24m)
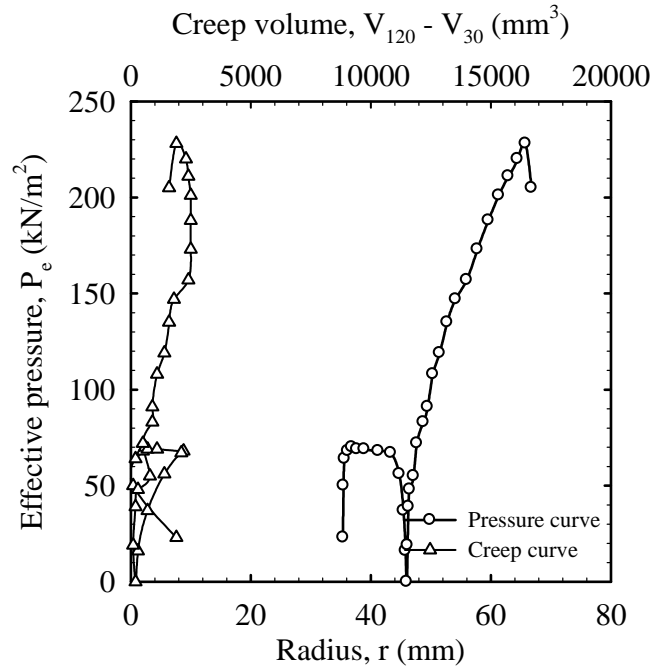
Figure C4 (a): Pressuremeter Test Results at Isaraphap Station, BH18

(Soft Clay, depth 8m)

Figure C4 (b): Pressuremeter Test Results at Isaraphap Station, BH18

(Soft Clay, depth 11m)

Figure C4 (c): Pressuremeter Test Results at Isaraphap Station, BH18

(Stiff Clay, depth 16m)

Figure C4 (d): Pressuremeter Test Results at Isaraphap Station, BH18

(Very Stiff Clay, depth 20m)

Figure C5 (a): Pressuremeter Test Results at Bang Wa Station, BH30-1

(Soft Clay, depth 10m)
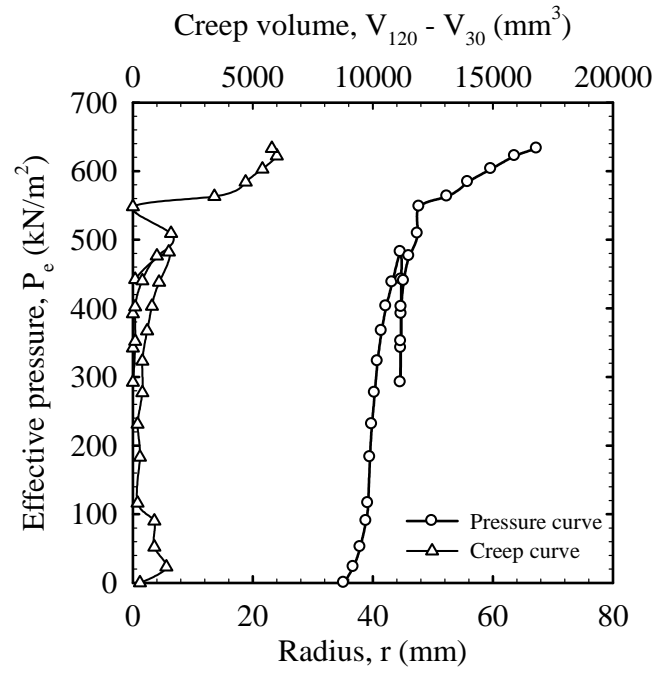
Figure C5 (b): Pressuremeter Test Results at Bang Wa Station, BH30-1

(Stiff Clay, depth 15m)

Figure C5 (c): Pressuremeter Test Results at Bang Wa Station, BH30-1
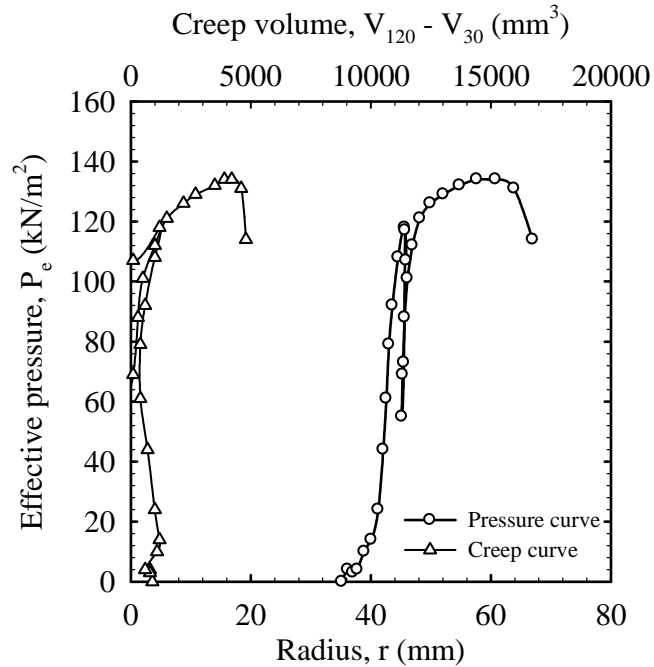
(Very Stiff Clay, depth 19m)

Figure C5 (d): Pressuremeter Test Results at Bang Wa Station, BH30-1

(Stiff Clay, depth 24m)

Figure C6 (a): Pressuremeter Test Results at Phet Kasem 48 Station, BH33-1
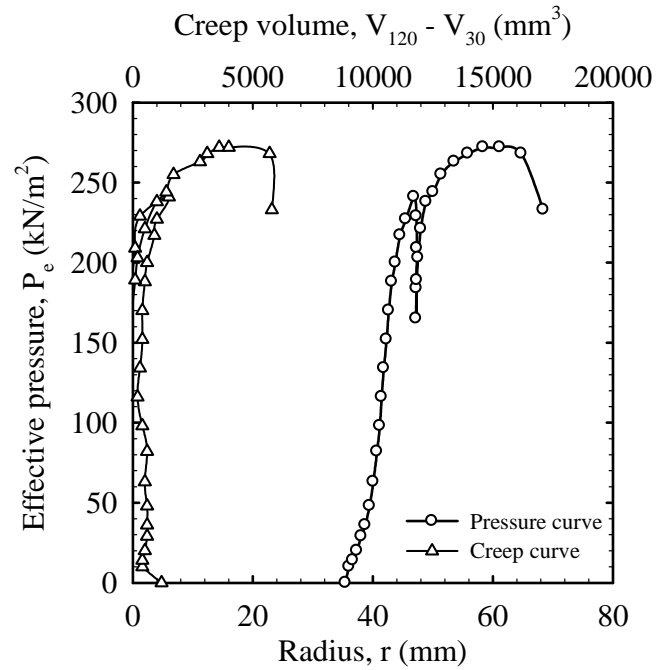
(Soft Clay, depth 7m)

Figure C6 (b): Pressuremeter Test Results at Phet Kasem 48 Station, BH33-1
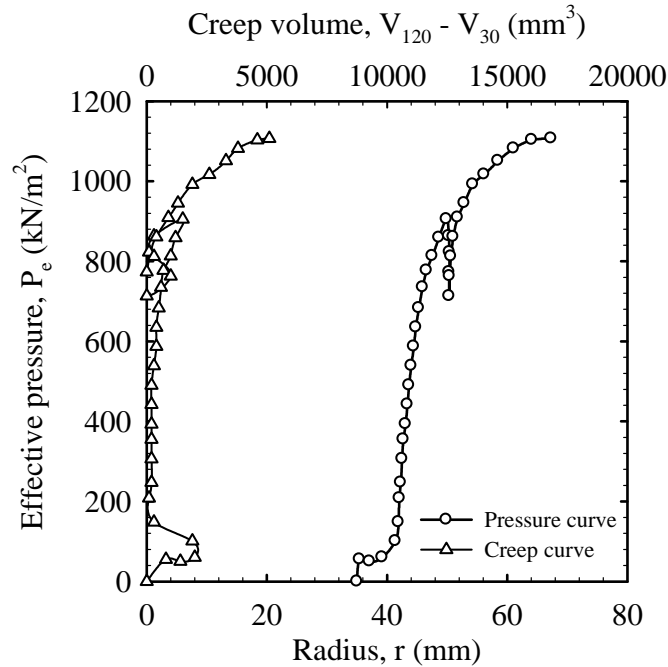
(Medium Stiff Clay, depth 11m)

Figure C6 (c): Pressuremeter Test Results at Phet Kasem 48 Station, BH33-1
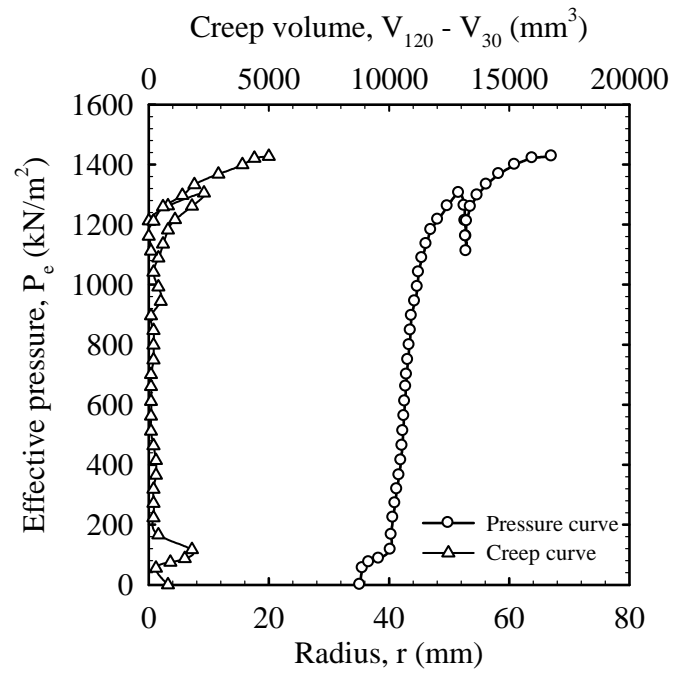
(Very Stiff Clay, depth 16m)

Figure C6 (d): Pressuremeter Test Results at Phet Kasem 48 Station, BH33-1

(Very Stiff Clay, depth 20m)